

STRESS-STRAIN BEHAVIOUR AND STRENGTH CHARACTERISTICS OF LIGHTLY OVERCONSOLIDATED CLAYS

by

SEUNG RYULL KIM

A dissertation submitted in partial fulfillment of the
requirements for the Degree of Doctor of Engineering.

Examination Committee:	Prof. A. S. Balasubramaniam	(Chairman)
	Dr. Yusuke Honjo	(Co-chairman)
	Prof. Pisidhi Karasudhi	
	Dr. Dennes T. Bergado	
	Dr. Noppadol Phien-wej	
External Examiner:	Prof. J. B. Burland	

SEUNG RYULL KIM

Nationality	:	Korean
Previous Degree	:	B.S. Civil Engineering (Hanyang University)
		Seoul, Korea
		Master of Engineering (Asian Institute of Technology)
		Bangkok, Thailand
Scholarship Donor	:	The Government of Japan

Asian Institute of Technology
Bangkok, Thailand
1991

ACKNOWLEDGMENTS

"The fear of the Lord is the beginning of knowledge" (Proverbs 1:7a).

The author wishes to express his profound gratitude to his advisor Prof. A. S. Balasubramaniam for his unfailing guidance, invaluable suggestions, criticisms and encouragement. Without Prof. A. S. Balasubramaniam's unstinted help in both academic and personal concerns throughout the years of the author's graduate studies at the Asian Institute of Technology, this dissertation work could not have been completed. He is also very grateful to his co-advisor, Dr. Yusuke Honjo for his useful advice and encouragement. Sincere thanks and appreciation are due to Prof. Pisidhi Karasudhi, Dr. Dennes. T. Bergado and Dr. Noppadol Phien-wej for their helpful and valuable suggestions, and for serving as members of his examination committee.

The author is grateful to Prof. J. B. Burland of the Imperial College of Science, Technology and Medicine for sharing his views and comments on this study as an external examiner. A note of appreciation is also extended to Prof. Yudhbir for his encouragement and interest in this study.

The author thankfully acknowledges the scholarship grant provided by the Government of Japan which made possible the completion of his doctoral programme at the Asian Institute of Technology. He would like to express his appreciation to the secretaries in the Division of Geotechnical and Transportation Engineering, Mrs. Vatinee and Mrs. Uraiwan for their kind help. Thanks are also due to the soil laboratory staff, especially Mr. Sataporn, for providing the author with the necessary facilities needed in conducting the experiments.

Sincere thanks and appreciation are due to his brothers and sisters at the AIT Christian Fellowship, especially brother Yian Kwan Ang, for their prayers and encouragement throughout his period of study. A word of thanks also goes to his friends, Dr. V. Udomchoke, Dr. B. R. Buensuceso, Mr. J. C. Chai, and Mr. R. Shivashankar for sharing the burden together in times of need.

A very special debt of deep gratitude is offered to his parents and parents-in-law for their unceasing prayers, love and encouragement. The author also greatly acknowledges the financial and moral assistance provided by his brother Mr. Man Yeon Kim.

Finally to his beloved wife Young Hee for her constant love, prayers, encouragement and many sacrifices. His beloved children, Bo Keum and Dong Won, are a source of strength. It is to his beloved wife, Young Hee, that this piece of work is lovingly dedicated.

ABSTRACT

The path dependent stress-strain behaviour and strength characteristics of Soft Bangkok clay in the normally and overconsolidated states are studied both under isotropic and K_0 pre-shear consolidation conditions in compression and in extension. The experimental programme included triaxial consolidation and swelling tests (both isotropic and K_0 -consolidation and swelling) as well as four series of undrained triaxial tests (three of them are in compression and one in extension) and ten series of drained tests. Following the Hvorslev approach, the initial pre-shear void ratio of all the samples is kept constant to about 1.16.

The review of the literature is presented in two chapters, one emphasizing the K_0 -consolidated behaviour of clays and the other on the Critical State stress-strain theories both with 'associated' and 'non-associated' flow rules. Critical comments are made at the end of each chapter.

The undrained behaviour of the Soft Bangkok clay is described in one chapter where all the test data are presented in a suitable form for evaluation of undrained soil parameters. In a broad sense, the data confirm the unique State Boundary Surface, the associated Critical State Line and the Hvorslev failure envelope. They also confirm the existence of a set of constant q yield loci for undrained distortional strains within the State Boundary Surface and on the wet side. A radial fan of undrained shear strain contours is obtained on the dry side. Pore pressure-stress ratio relationships are established to determine the undrained stress path and the excess pore pressure. Volumetric yield points constituting the volumetric yield locus which lie on the State Boundary Surface are determined for the samples when the stress states reach the State Boundary Surface.

The drained behaviour of the Soft Bangkok clay is then introduced in the following chapter. The drained behaviour also confirms a unique State Boundary Surface with the associated Critical State Line and the Hvorslev failure envelope. The region within the State Boundary Surface is divided into three zones based on plastic volumetric yielding. In one zone, the volumetric strain is purely elastic and is close to the isotropic axis. In the second zone on the wet side, compressive plastic volumetric strains take place, while in the third zone dilational plastic volumetric strains occur. A flow rule is then established which will merge with the flow rule of the Modified Cam Clay Theory of ROSCOE and BURLAND (1968) for stress states on the State Boundary Surface and which shows a reduction in the plastic dilatancy ratio with a decrease in the mean normal stress at any one stress ratio.

Comparisons of the experimental observations with predictions from the Critical State theories reveal that the Revised Cam Clay Theory of ROSCOE and BURLAND (1968) makes successful predictions for stress states on the State Boundary Surface, while Pender's Model

(PENDER, 1977, 1978) gives approximate predictions for stress states within the State Boundary Surface. Dafalias' Model (DAFALIAS, 1987) is found to be more suitable for the anisotropic stress-strain behaviour when the stress states lie on the State Boundary Surface.

For the region inside the State Boundary Surface, a Cam Clay (SCHOFIELD and WROTH, 1968) type of yield locus is established to calculate plastic volumetric strains on the wet side of the Critical State. The plastic volumetric strain so obtained is used with the flow rule established to determine the plastic shear strains due to volumetric yielding inside the State Boundary Surface. The contribution from the constant q yield loci is then added to make the full value of the plastic shear strains on the wet side of the Critical State. On the dry side, however, the plastic volumetric strains are obtained from a set of dilational volumetric yield loci. These yield loci, when combined with the flow rule (as established for the wet side but with a negative magnitude), enable the distortional strains due to dilational plastic volumetric strains. The undrained shear strain increments on the dry side as determined from the radial fan of constant shear strain contours are then added to the distortional strain increment obtained from the volumetric yield loci to make the full value of the shear strain increments.

Finally, comparisons are made within the State Boundary Surface for the pore pressures and strains from the Author's Model with the experimental observations.

TABLE OF CONTENTS

CHAPTER	TITLE	Page
	Title Page	i
	Acknowledgments	ii
	Abstract	iii
	Table of Contents	v
	List of Notations	xiii
	List of Tables	xvii
	List of Figures	xviii
I	INTRODUCTION	1
1.1	General Background	1
1.2	Scope and Objectives of Study	2
1.3	Organization of the Dissertation	3
II	REVIEW OF THE BEHAVIOUR OF CLAYS UNDER ANISOTROPIC STRESS CONDITIONS	5
2.1	Introduction	5
2.2	Coefficient of Earth Pressure at Rest (K_0)	6
2.2.1	General	6
2.2.2	Prediction of K_0	7
2.3	Behaviour of Normally Consolidated Clays	8
2.3.1	Undrained Stress Paths	8
2.3.2	Deviator Stress-Strain Relationships	10
2.3.3	Pore Pressure-Strain Relationships	10
2.3.4	Strength Characteristics	13
2.3.5	Shear Strain Contours	17
2.4	Behaviour of Overconsolidated Clays	18
2.4.1	Undrained Stress Paths	18
2.4.2	Stress-Strain Relationships	20
2.4.3	Pore Pressure-Strain Relationships	21
2.4.4	Strength Characteristics	24
2.4.5	Shear Strain Contours	26
2.5	Yield Locus of Natural Clays	28
2.5.1	Evidence of Yielding on Natural Clays	28
2.5.2	Techniques for Estimation of Yield Locus	29
2.5.3	Geometric Properties of Yield Locus	29
2.5.4	Direction of Plastic Strain Increment Vectors and the Yield Locus	31

CHAPTER	TITLE	Page
2.6	Anisotropic Elasticity of Natural Clays	31
2.7	Time-dependent Behaviour of Natural Clays	32
2.8	Concluding Remarks and Comments	33
2.8.1	Behaviour of Resedimented Specimens of Kaolin	33
2.8.2	Behaviour of Remoulded and Natural Clays	33
III	REVIEW OF THE STRESS-STRAIN THEORIES AS BASED ON THE CRITICAL STATE CONCEPTS	35
3.1	Introduction	35
3.2	State Boundary Surface and Critical State Line	36
3.3	Incremental Stress-Strain Theory (ROSCOE and POOROOSHASB, 1963) for Normally Consolidated Clays	36
3.4	Cambridge Stress-Strain Theories for Wet Clays Based on the Critical State Concept	38
3.4.1	General	38
3.4.2	Cam Clay Theory (ROSCOE et. al., 1963)	38
3.4.3	Modified Cam Clay Theory (BURLAND, 1965)	40
3.4.4	Revised Theory (ROSCOE & BURLAND, 1968)	41
3.4.5	Summary of the Stress-Stress Theories of the Cambridge Groups	42
3.5	PENDER's Model (1977, 1978)	42
3.5.1	General	42
3.5.2	Assumptions and Hypotheses	43
3.5.3	Overconsolidated Behaviour	45
3.5.4	Normally Consolidated Behaviour	45
3.5.5	Summary of PENDER's Model	46
3.6	DAFALIAS' Model (1987)	46
3.6.1	Summary of DAFALIAS' Model	48
3.7	Some Formulations of Anisotropic Behaviour of Clays	48
3.8	Concluding Remarks and Comments	50
IV	EXPERIMENTAL INVESTIGATIONS	51
4.1	Introduction	51
4.2	Sampling	51
4.3	Description of Apparatus	51
4.3.1	Triaxial Cells	52
4.3.2	Loading Device	52
4.3.3	Measurement of Strains and Pore Pressures	52

CHAPTER	TITLE	Page
4.4	Calibrations	53
4.4.1	Proving Rings	53
4.4.2	Pressure Gages and Pore Pressure Transducers	53
4.4.3	Frictional Resistance and Upthrust of Loading Ram	53
4.5	Laboratory Testing Programme	54
4.5.1	Triaxial Consolidation Tests	54
4.5.2	Triaxial Test Series	55
4.6	Triaxial Testing Procedures	58
4.6.1	Preparation and Setting-up of Specimens	59
4.6.2	Saturation of Specimens	59
4.6.3	Consolidation of Specimens	60
4.6.4	Overconsolidated Specimens	61
4.6.5	Shearing of Specimens	61
4.7	End of Test Procedures	62
4.8	Processing of Test Data	63
4.8.1	Calculation of Stress and Strain	63
4.8.2	Corrections made on the Results	64
V	UNDRAINED BEHAVIOUR OF CLAYS	66
5.1	Introduction	66
5.2	Index Properties of Clay	66
5.3	Consolidation Characteristics of Clay	67
5.3.1	Void Ratio-Pressure Relationships	67
5.3.2	Swelling Characteristics	68
5.3.3	Experimental Determination of K_o swelling Line	69
5.3.4	Coefficient of Earth Pressure, K_o	69
5.4	Undrained Behaviour of Normally Consolidated Samples	70
5.4.1	Introduction	70
5.4.2	Undrained Behaviour under Isotropic Conditions	70
5.4.2.1	Undrained Stress Paths	71
5.4.2.2	Stress-Strain Relationships	71
5.4.2.3	Excess Pore Pressure-Strain Relationships	71
5.4.2.4	Strength Characteristics	72
5.4.3	Undrained Behaviour under K_o -Conditions	73
5.4.3.1	Undrained Stress Paths	73
5.4.3.2	Stress-Strain Relationships	74
5.4.3.3	Stress Ratio-Strain Relationships	75
5.4.3.4	Excess Pore Pressures	75
5.4.3.5	Strength Characteristics	76

CHAPTER	TITLE	Page
5.5	Comparison of Isotropically and K_0 -normally Consolidated Samples in Triaxial Compression	77
5.5.1	Introduction	77
5.5.2	Undrained Stress Paths	77
5.5.3	Stress-Strain Relationships	78
5.5.4	Stress Ratio-Strain Relationships	78
5.5.5	Excess Pore Pressure-Strain Relationships	79
5.5.6	Excess Pore Pressure-Stress Ratio Relationships	79
5.6	Undrained Behaviour of Overconsolidated Samples under Isotropic Pre-shear Conditions	80
5.6.1	Introduction	80
5.6.2	Undrained Stress Paths	81
5.6.3	Stress-Strain Relationships	82
5.6.4	Pore Pressure-Strain Relationships	82
5.6.5	Normalized Pore Pressure-Stress Ratio Relationships	82
5.6.6	Pore Pressure Parameter A_f	84
5.6.7	Volumetric Yielding Inside the State Boundary Surface	84
5.6.8	Shear Strength of Overconsolidated Samples	85
5.6.9	Void Ratio-Stress Relationships at the Critical State and Failure	85
5.6.10	Shear Strain Contours	86
5.7	Undrained Behaviour of Overconsolidated Samples under K_0 Pre-shear Conditions	87
5.7.1	Introduction	87
5.7.2	Undrained Stress Paths	88
5.7.3	Stress-Strain Relationships	90
5.7.4	Excess Pore Pressure Characteristics	91
5.7.5	Excess Pore Pressure-Stress Ratio Relationships	92
5.7.6	Yield Envelope, Critical State and Hvorslev Envelope	93
5.7.7	Undrained Strength Characteristics	94
5.7.8	Stress Ratio-Shear Strain Relationships	94
5.8	Summary of Undrained Behaviour	94
VI	DRAINED BEHAVIOUR OF CLAYS	101
6.1	Introduction	101
6.2	Isotropically Consolidated Drained Tests (CID Tests)	101
6.2.1	Effective Stress Paths	101
6.2.2	Stress-Strain Relationships	102
6.2.3	Constant Shear Strain Contours	103
6.2.4	Normalized (q/p_e , p/p_e) Plot	104
6.2.5	Deviator Stress-Volumetric Strain Relationships	104

CHAPTER	TITLE	Page
6.2.6	Stress Ratio-Strain Relationships	104
6.2.7	Plastic Volumetric Strains Within and Outside the State Boundary Surface (SBS)	104
6.3	Conventional Drained Tests on K_0 Consolidated Samples	105
6.3.1	Effective Stress Paths	105
6.3.2	Stress-Strain Relationships	106
6.3.3	Volumetric Strain-Shear Strain Relationships	106
6.3.4	Stress Ratio-Shear Strain Relationships	107
6.3.5	Volumetric Strains	107
6.4	Conventional Drained Tests on Anisotropically Consolidated Samples (CAD Tests)	108
6.4.1	Effective Stress Paths	108
6.4.2	Stress-Strain Relationships	108
6.4.3	Mean Normal Stress-Volumetric Strain Relationships	108
6.4.4	Volumetric Strain-Shear Strain Relationships	108
6.4.5	Stress Ratio-Shear Strain Relationships	109
6.4.6	Normalized (q/p_e , p/p_e) Plot	109
6.4.7	Volumetric Strains	109
6.5	Constant p Compression Tests on K_0 Consolidated Samples	109
6.5.1	Effective Stress Paths	109
6.5.2	Stress-Strain Relationships	110
6.5.3	Stress Ratio-Shear Strain Relationships	110
6.5.4	Volumetric Strain-Shear Strain Relationships	111
6.5.5	Normalized (q/p_e , p/p_e) Plot	111
6.5.6	Volumetric Strains	111
6.6	Unloading Compression Tests (CK_0DU Tests)	112
6.6.1	Effective Stress Paths	112
6.6.2	Stress-Strain Relationships	112
6.6.3	Volumetric Strain-Shear Strain Relationships	112
6.6.4	Stress Ratio-Shear Strain Relationships	113
6.6.5	Normalized (q/p_e , p/p_e) Plot	113
6.6.6	Volumetric Strains	113
6.7	Constant q Unloading Tests (CK_0QU Tests)	113
6.7.1	Effective Stress Paths	114
6.7.2	Stress Ratio-Shear Strain Relationships	114
6.7.3	Volumetric Strains	114
6.7.4	Normalized (q/p_e , p/p_e) Plot	115
6.7.5	(e_f , $\ln p$) Plot	115
6.8	Conventional Drained Extension Tests (CK_0DE Tests)	115
6.8.1	Deviator Stress-Shear Strain Relationships	115
6.8.2	Volumetric Strains	115
6.8.3	Normalized (q/p_e , p/p_e) Plot	116
6.9	Constant p Extension Tests (CK_0PE Tests)	116

CHAPTER	TITLE	Page
6.9.1	Effective Stress Paths	116
6.9.2	Shear Strains	116
6.9.3	Volumetric Strains	117
6.9.4	Normalized (q/p_e , p/p_e) Plot	117
6.10	Strength Envelope and Yield Locus from Drained Tests	117
6.10.1	Strength Envelope	117
6.10.2	(Δe_f , p_f) Relationships	118
6.10.3	Yielding from Drained Tests on K_o -consolidated Samples	118
6.10.4	Shear Strain Contours	119
6.11	Summary of Drained Behaviour	119
VII	CRITICAL STATE MODELS AND THEIR COMPARISONS WITH THE EXPERIMENTAL OBSERVATIONS	123
7.1	Introduction	123
7.2	Comparisons of Undrained Behaviour of Normally Consolidated Clays Sheared from Isotropic Pre-shear Stress Conditions	124
7.2.1	Effective Stress Paths in Compression	124
7.2.2	Stress-Strain Relationships	125
7.2.3	Stress Ratio-Shear Strain Relationships	125
7.2.4	Excess Pore Pressures	125
7.3	Comparisons of Undrained Behaviour of Normally Consolidated Clays under K_o Pre-shear Stress Conditions	126
7.3.1	Incremental Form of Stress-Strain Relationships (Dafalias' Model, 1987)	126
7.3.2	Extended Form of Modified Cam Clay Theory (ATKINSON et al., 1987)	127
7.3.3	Effective Stress Paths	128
7.3.4	Stress-Strain Relationships	129
7.3.5	Stress Ratio-Shear Strain Relationships	129
7.3.6	Excess Pore Pressure	130
7.4	Variation of Parameter α in Dafalias' Model (1987)	130
7.5	Comparisons of Undrained Behaviour of Overconsolidated Clays as Sheared from Isotropic Pre-shear Stress Conditions	130
7.5.1	Effective Stress Paths	131
7.5.2	Stress-Strain Relationships	131
7.5.3	Excess Pore Pressures	131
7.6	Comparisons of Undrained Behaviour of Overconsolidated Samples Sheared from K_o Pre-shear Stress Conditions	132
7.6.1	Triaxial Compressions	132
7.6.2	Triaxial Extension	133

CHAPTER	TITLE	Page
7.7	Summary of the Model Predictions for the Undrained Behaviour	133
7.7.1	Normally Consolidated Behaviour	133
7.7.2	Overconsolidated Behaviour	133
7.8	Comparisons of Drained Behaviour of Normally Consolidated Clays Sheared from Isotropic Pre-shear Stress Conditions	134
7.8.1	Stress-Strain Relationships	134
7.8.2	Stress Ratio-Strain Relationships	134
7.8.3	Plastic Shear Strain-Plastic Volumetric Strain Relationships	134
7.9	Comparisons of Drained Behaviour of Normally Consolidated Clays Sheared from K_0 Pre-shear Stress Conditions	135
7.9.1	Triaxial Compression	135
7.9.2	Triaxial Extension	135
7.10	Comparisons of Drained Behaviour of Overconsolidated Clays Sheared from Isotropic Pre-shear Stress Conditions	136
7.11	Comparisons of Drained Behaviour of Overconsolidated Clays Sheared from K_0 Pre-shear Stress Conditions	137
7.11.1	Conventional Drained Compression Tests (CK_0D)	137
7.11.2	Constant p Compression Tests (CK_0PC Tests)	137
7.11.3	Unloading Compression Tests (CK_0DU Tests)	138
7.11.4	Constant q Unloading Tests (CK_0QU Tests)	138
7.11.5	Conventional Drained Extension Tests (CK_0DE)	139
7.11.6	Constant p Extension Tests (CK_0PE Tests)	139
7.12	Summary of the Predictions for the Drained Behaviour	140
7.12.1	Normally Consolidated Behaviour	140
7.12.2	Overconsolidated Behaviour	140
7.13	Evaluation of PENDER's Assumption on the Plastic Strain Increment Ratio	140
7.14	A Conceptual Modification of Pender's Model	142
7.14.1	For the Isotropically Consolidated Samples	142
7.14.2	For the K_0 -overconsolidated Samples	143
7.15	Concluding Remarks and Comments of the Model Evaluations	144
VIII	FORMULATION OF STRESS-STRAIN BEHAVIOUR BELOW THE STATE BOUNDARY SURFACE	146
8.1	Introduction	146
8.2	Formulation of Volumetric Yield Loci Inside the SBS	147

CHAPTER	TITLE	Page
8.2.1	Simplified Plastic Volumetric Strain Contours Inside the SBS	147
8.2.2	Stress-Strain Behaviour in Zone I to Zone IV	148
8.2.3	Plastic Strain Increment Ratio	151
8.2.4	Plastic Strain Increment Ratios Inside the SBS from CID Test	152
8.2.5	Plastic Strain Increment Ratios Inside the SBS from K_0 Tests	154
8.2.6	Simplified (ϵ, η) Relationship within the SBS	154
8.2.7	Derivation of the Volumetric Yield Loci within the SBS	156
8.3	Prediction of Strains using Author's Model for Lightly Overconsolidated Clays	157
8.3.1	Undrained Behaviour	157
8.3.2	Drained Behaviour in the Wet Zone	158
8.3.3	Drained Behaviour in the Dry Zone	159
8.4	Concluding Remarks and Comments	160
IX	CONCLUSIONS	163
	REFERENCES	170
	TABLES	177
	FIGURES	178

LIST OF NOTATIONS

A	pore pressure parameter (SKEMPTON, 1954)
A	a coefficient to distinguish loading compression and loading extension in the model of PENDER (1978)
A	area of sample at each stage of loading
A_o	area of sample prior to shearing
A_f	pore pressure parameter A at failure
A_r	area ratio during swelling process (A/A_s)
A_s	area of sample prior to swelling
c	cohesion intercept (shear strength parameter)
\bar{c}_e	Hvorslev true cohesion
C	slope of the ($u/p_o, \eta$) relationship (for an isotropically consolidated sample in the normally consolidated state)
C	constant for the Author's Model
C_1	slope of the first linear segment in the ($u/p_o, \eta$) relationship for an overconsolidated sample
C_2	slope of the second linear segment in the ($u/p_o, \eta$) relationship for an overconsolidated sample
$\left \frac{dq}{dp} \right $	stress ratio increment during swelling process
dW	dissipated energy per unit volume of soil
$d\epsilon_{sp}$	increment of plastic shear strain
$d\epsilon_{ve}$	increment of elastic volumetric strain
$d\epsilon_{vp}$	increment of plastic volumetric strain
$\frac{d\epsilon_{vp}}{d\epsilon_{sp}}$	plastic strain increment ratio
$d\left(\frac{d\epsilon_{vp}}{d\epsilon_{sp}}\right)_\eta$	increment of plastic strain increment ratio at stress ratio η inside the state boundary surface
$d\left(\frac{p}{p_e}\right)_\eta$	difference of p/p_e at stress ratio η (the Author's Model)
$d\epsilon_{ij}$	plastic strain increment tensor
$d\sigma_{ij}$	stress increment tensor
$e (e_o)$	void (initial) ratio

Δe_f	change in void ratio at failure
e_{K_0}	initial void ratio under K_0 consolidation
f	yield function (Pender's Model, 1978)
g	plastic potential function (Pender's Model, 1978)
h	hardening function (Pender's Model, 1978)
I_p	plasticity index
K_0	coefficient of earth pressure at rest
K_{on}	coefficient of earth pressure at rest for a K_0 -normally consolidated sample
M	slope of the critical state line in the (q, p) plot
$(M)_{ci}$	slopes of the critical state line in the (q, p) plot for isotropically and K_0 -consolidated samples during undrained compression
$(M)_{ck}$	
$(M)_{pi}$	slope of the failure line corresponding to the peak deviator stress in the (q, p) plot for isotropically consolidated samples during undrained compression tests
$(M)_{ek}$	slope of the critical state line in the (q, p) plot for K_0 -consolidated samples during undrained extension tests
M_r	compression modulus of the rubber membrane
OCR	overconsolidation ratio
p	mean normal stress $(\bar{\sigma}_1 + 2\bar{\sigma}_3) / 3$
p_α	value of p corresponding to α -parameter in the yield locus (Dafalias' Model, 1987)
p_c	preconsolidation stress
p_{cs}	value of p corresponding to the critical state (Pender's Model, 1978)
p_{cs}^*	value of p corresponding to the peak deviator stress
p_e	equivalent stress (value of p at the point on the normally consolidation line at the same void ratio)
p_f	value of p corresponding to peak deviator stress of normally consolidated samples sheared from isotropic stress (HANDALI, 1986)
p_f	value of p at failure
p_i	initial mean normal stress in the HANDALI's pore pressure formulation (1986)
p_{max}	maximum past consolidation pressure
p_o	pre-shear consolidation stress
p_{on}	pre-shear consolidation stress for isotropically consolidated sample in the normally consolidated state
p_t	transition point in the $(e, \ln p)$ plot in the normally consolidated state
q	deviator stress $(\bar{\sigma}_1 - \bar{\sigma}_3)$
q_{max}	maximum deviator stress

q_o	value of q corresponding to the pre-shear consolidation stress
$(q_o)_{\max}$	value of q corresponding to preconsolidation pressure p_{\max} for K_o -overconsolidated samples
S_{ij}	deviator stress tensor
s_{uc}	undrained shear strength at the critical state during compression test
s_{ue}	undrained shear strength at the critical state during extension test
s_{up}	peak undrained strength during compression test
u	pore pressure
α	dimensionless parameter as a measure of C_i defined by HANDALI (1986)
β	dimensionless parameter as a measure of p_i defined by HANDALI (1986)
β^*	parameter for yield locus inside the state boundary surface and on the wet side of the critical state (the Author's Model)
$\Delta p, \Delta q$	increment of p and q , respectively
Δu	increment of pore pressure
ϵ_s	shear strain
ϵ_v	volumetric strain
η	stress ratio (q/p)
η_o	pre-shear stress ratio
η_k	stress ratio corresponding to the K_o -consolidation
η_t	stress ratio corresponding to the transition point of the bilinear ($u/p_o, \eta$) relationship
\exists	gradient of the simplified ($\frac{de_{vp}}{de_{sp}}, p/p_e$) relationship (the Author's Model)
κ	gradient of swelling line in ($e, \ln p$) plot
λ	gradient of isotropic and anisotropic consolidation of normally consolidated samples in the ($e, \ln p$) plot
λ_{oc}	gradient of consolidation in Zone II inside the state boundary surface (the Author's Model)
Λ	$1 - \kappa/\lambda$
ψ	plastic strain increment ratio
$\bar{\sigma}_1, \bar{\sigma}_3$	principal effective stresses
σ_{am}	axial stress taken by rubber membrane
$\bar{\sigma}_{vo}$	pre-shear vertical stress

$\bar{\sigma}_{vm}$	pre-consolidation vertical stress
$\bar{\phi}$	angle of internal friction
$\Phi^*(\eta)$	increment of plastic shear strain as a function of η inside the state boundary surface and on the wet side
$\Phi^{**}(\eta)$	increment of shear strain as a function of η inside the state boundary surface and on the dry side
ζ	p/p_e for the stress states on the state boundary surface from the Modified Cam Clay Theory

CSL : Critical State Line
 SBS : State Boundary Surface
 ISB2 : Zone II inside the state boundary surface
 ISB4 : Zone IV inside the state boundary surface
 OSB : outside the state boundary surface

LIST OF TABLES

Table No.	Title	Page
Table 4.1	Triaxial Consolidation Test	55
Table 4.2	Stress Conditions for Normally and Overconsolidated Samples in the q-p Stress Space	178
Table 4.3	Test Conditions and Test Names with Test Series	57
Table 5.1	Index Properties	67
Table 5.2	Comparison of Undrained Strength Ratios	73
Table 5.3	OCR Values from Different Definitions	89

LIST OF FIGURES

- Fig. 2.1a Typical Undrained Paths and $(u/p_o, \eta)$ plot for Overconsolidated Samples (After HANDALI, 1986)
- Fig. 2.1b (α, β) Plot for Isotropically Consolidated Samples and Anisotropically Consolidated Samples (After HANDALI, 1986)
- Fig. 2.2 Stress Paths and Strain Contours for Undrained Triaxial Tests on Kaolin (After WROTH and LOUDON, 1967)
- Fig. 2.3 Measured Yield Envelope for Natural Plastic Winnipeg Clay Showing Graphically Constructed V Traces and the Shape of the State Boundary Surface (After GRAHAM et al., 1988)
- Fig. 3.1 Three Dimensional Presentation of the State Boundary Surface and the Critical State Line
- Fig. 3.2 Volumetric and Constant-q Yield Loci of ROSCOE and BURLAND (1968)
- Fig. 3.3 Direction of Plastic Strain Increment Vectors (After PENDER, 1978)
- Fig. 3.4 Parabolic Undrained Stress Path for Various OCR Values (After PENDER, 1978)
- Fig. 3.5 Schematic Diagram of the Anisotropic Yield Locus (After, DAFALIAS, 1987)
- Fig. 3.6 Anisotropic State Boundary Surface (After STIPHO, 1982)
- Fig. 4.1 Schematic Diagram of Consolidation Process
- Fig. 4.2 Initial Stress Points of Test Series I, II & III
- Fig. 4.3 Typical Stress Paths followed in this Investigation of the Behaviour of Lightly Overconsolidated Clay (Test Series, I)
- Fig. 5. 1 Typical Consolidation and Swelling Curves
- Fig. 5. 2 Variation of Cross-Sectional Area in Swelling Process
- Fig. 5. 3a Relationship between K_o and OCR
- Fig. 5. 3b Relationship between Normalized K_o and OCR
- Fig. 5. 4 Undrained Stress Paths of Normally Consolidated Samples at Different Isotropic Stresses
- Fig. 5. 5 Normalized Undrained Stress Paths of Normally Consolidated Samples under Isotropic Stress
- Fig. 5. 6 (q, ϵ_s) Plot for Normally Consolidated Samples under Isotropic Stress
- Fig. 5. 7 $(q/p_o, \epsilon_s)$ Plot for Normally Consolidated Samples under Isotropic Stress
- Fig. 5. 8 $(u/p_o, \epsilon_s)$ Plot for Normally Consolidated Samples under Isotropic Stress
- Fig. 5. 9 $(u/p_o, \eta)$ Plot for Normally Consolidated Samples under Isotropic Stress
- Fig. 5.10 Undrained Stress Paths of K_o -normally Consolidated Samples in Triaxial Compression
- Fig. 5.11 Undrained Stress Paths of K_o -normally Consolidated Sample both in Triaxial Compression and Extension
- Fig. 5.12 Normalized Undrained Stress Paths of K_o -normally Consolidated Sample both in Triaxial Compression and Extension

- Fig. 5.13 ($q/p_o, \epsilon_s$) Plot for K_o -normally Consolidated Samples both in Triaxial Compression and Extension
- Fig. 5.14 (η, ϵ_s) Plot for Normally Consolidated Sample under K_o and Isotropic Stresses
- Fig. 5.15 ($u/p_o, \epsilon_s$) Plot for K_o -normally Consolidated Samples both in Triaxial Compression and Extension
- Fig. 5.16 ($u/p_o, \eta$) Plot for K_o -normally Consolidated Samples both in Triaxial Compression and Extension
- Fig. 5.17 Undrained Stress Paths of K_o and Isotropically Consolidated Samples
- Fig. 5.18 (q, ϵ_s) Plot for K_o and Isotropically Consolidated Samples
- Fig. 5.19 (η, ϵ_s) Plot for K_o and Isotropically Consolidated Samples
- Fig. 5.20 (u, ϵ_s) Plot for K_o and Isotropically Consolidated Samples
- Fig. 5.21 ($u/p_o, \eta$) Plot for K_o and Isotropically Consolidated Samples beyond K_o State
- Fig. 5.22 ($u/p_{on}, \eta$) Plot for K_o and Isotropically Consolidated Samples beyond K_o State
- Fig. 5.23 ($u/p_{on}, \eta$) Plot for K_o and Isotropically Consolidated Samples
- Fig. 5.24 Undrained Stress Paths of Overconsolidated Samples from CIU Tests
- Fig. 5.25 (q, p) Plot for CIU Tests with Results Obtained by WROTH and LOUDON (1967)
- Fig. 5.26 ($p/p_e, q/p_e$) Plot for CIU Tests with Results Obtained by WROTH and LOUDON (1967)
- Fig. 5.27 (q, ϵ_s) Plot for Overconsolidated Samples from CIU Tests
- Fig. 5.28 (u, ϵ_s) Plot for Overconsolidated Samples from CIU Tests
- Fig. 5.29 ($u/p_o, \eta$) Plot for Overconsolidated Samples from CIU Tests
- Fig. 5.30 ($u/p_o, \eta$) Plot for Overconsolidated Samples under Isotropic Stress (After WROTH and LOUDON, 1967)
- Fig. 5.31 ($u/p_{on}, \eta$) Plot for Overconsolidated Samples from CIU tests
- Fig. 5.32 ($u/p_{on}, \eta$) Plot for Overconsolidated Samples under Isotropic Stress (After WROTH and LOUDON, 1967)
- Fig. 5.33a Variation of η_t with OCR in the ($u/p_o, \eta$) Relationship from CIU Tests (Wet Zone)
- Fig. 5.33b Variation of C_1 with OCR in the ($u/p_o, \eta$) Relationship from CIU Tests (Wet Zone)
- Fig. 5.34a Variation of η_t with OCR in the ($u/p_o, \eta$) Relationship from CIU Tests
- Fig. 5.34b Variation of C_1 with OCR in the ($u/p_o, \eta$) Relationship from CIU Tests
- Fig. 5.35a Variation of η_t with OCR in the ($u/p_{on}, \eta$) Relationship from CIU Tests
- Fig. 5.35b Variation of C_1 with OCR in the ($u/p_{on}, \eta$) Relationship from CIU Tests
- Fig. 5.36 Variation of A_f with OCR for the Overconsolidated Samples from CIU Tests
- Fig. 5.37 Failure and Yield Points of the Overconsolidated Samples from CIU Tests

- Fig. 5.38 Variation of Undrained Strength Ratio with OCR for Overconsolidated Samples from CIU Tests
- Fig. 5.39a Critical State Line Corresponding to q_{\max} Conditions from CIU Tests
- Fig. 5.39b Critical State Line Corresponding to the $(\bar{\sigma}_1'/\bar{\sigma}_3')_{\max}$ Conditions from CIU Tests
- Fig. 5.39c Critical State Lines Corresponding to the Different Criteria
- Fig. 5.40 Shear Strain Contours of Overconsolidated Samples from CIU Tests
- Fig. 5.41 Simplified Shear Strain Contours for Overconsolidated Samples from CIU Tests
- Fig. 5.42 (η, ϵ_s) Relationship for Overconsolidated Samples from Strain Contours of Fig. 5.40
- Fig. 5.43 Schematic Diagram of Sample Preparation for the Test Series I
- Fig. 5.44 Correlation between Two Types of OCR Values
- Fig. 5.45 Undrained Stress Paths for K_o -overconsolidated Samples from CK_oU & CK_oUE Tests
- Fig. 5.46 Schematic Diagram for Determining the OCR Values for the Samples in the Test Series I based on the Isotropic Stresses
- Fig. 5.47 OCR Values for the Samples in the Test Series I based on the Isotropic Stresses
- Fig. 5.48 Undrained Stress Paths for K_o -overconsolidated Samples from CK_oU & CAU Tests
- Fig. 5.49 Schematic Diagram for the Estimation of the Shear Strains of CK_oU & CAU Tests from the Constant q -yield Loci of the Isotropically Consolidated Samples
- Fig. 5.50a An Illustration of the Estimation of the Shear Strains in the CK_oU Test from the Constant q -yield Loci of the CIU Tests (Wet Zone)
- Fig. 5.50b An Illustration of the Estimation of the Shear Strains in the CK_oU Test from the Constant q -yield Loci of the CIU Tests (Dry Zone)
- Fig. 5.51 Comparisons of (q, ϵ_s) Relationship between the CK_oU Tests and the Estimated Ones from the Constant q -yield Loci of CIU Tests; (a) OCR = 1.24; (b) OCR = 1.50; (c) OCR = 1.78
- Fig. 5.52 Comparisons of (q, ϵ_s) Relationship between the CK_oU Tests and the Estimated Ones from the Constant q -yield Loci of CIU Tests; (a) OCR = 2.15; (b) OCR = 2.75
- Fig. 5.53 (q, ϵ_s) Plot for K_o -overconsolidated Samples from CK_oU Tests
- Fig. 5.54 (q, ϵ_s) Plot of K_o -overconsolidated Samples from CK_oU Tests for the Stress Ratios greater than η_k
- Fig. 5.55 (q, ϵ_s) Plot of K_o -overconsolidated Samples from CK_oU Tests for the Deviator Stress greater than the Past Maximum Deviator Stress, $(q_o)_{\max}$
- Fig. 5.56 (q, ϵ_s) Plot for Anisotropically Overconsolidated Samples from CAU Tests
- Fig. 5.57 (q, ϵ_s) Plot for K_o -overconsolidated Samples from CK_oUE Tests
- Fig. 5.58 (u, ϵ_s) Plot for K_o -overconsolidated Samples from CK_oU Tests
- Fig. 5.59 (u, ϵ_s) Plot for Anisotropically Overconsolidated Samples from CAU Tests

- Fig. 5.60 (u, ϵ_s) Plot for K_o -overconsolidated Samples from CK_oUE Tests
- Fig. 5.61 Variation of A_f with OCR for the Overconsolidated Samples
- Fig. 5.62 $(u/p_o, \eta)$ Plot for K_o -overconsolidated Samples from CK_oU Tests
- Fig. 5.63 Simplified $(u/p_o, \eta)$ Relationship for K_o -overconsolidated Samples from CK_oU Tests (Wet Zone)
- Fig. 5.64 Simplified $(u/p_o, \eta)$ Relationship for K_o -overconsolidated Samples from CK_oU Tests (Dry Zone)
- Fig. 5.65 Simplified $(u/p_o, \eta)$ Relationship for Anisotropically Consolidated Samples from CAU Tests
- Fig. 5.66 $(u/p_o, \eta)$ Relationship for K_o -overconsolidated Samples from CK_oUE Tests
- Fig. 5.67 Failure Points from the Undrained Compression Tests
(Test Series I, II & III)
- Fig. 5.68 Volumetric Yield Points from the Undrained Compression Tests
(Test Series I, II & III)
- Fig. 5.69 Strength Ratios and OCR from Undrained Tests
(Test Series I, II & III)
- Fig. 5.70 Normalized Strength Ratios and OCR from Undrained Tests
(Test Series I, II & III)
- Fig. 5.71a Pre-shear Stresses and q_{max} Points with the Maximum Past Pressures for CK_oU Tests
- Fig. 5.71b Critical State Line Corresponding to the $(\bar{\sigma}_1'/\bar{\sigma}_3')_{max}$ Conditions from CK_oU Tests
- Fig. 5.72 (η, ϵ_s) Relationship for K_o -overconsolidated Samples from CK_oU Tests
- Fig. 5.73 (η, ϵ_s) Relationship for Anisotropically Overconsolidated Samples from CAU Tests
- Fig. 5.74 (η, ϵ_s) Relationship for K_o -overconsolidated Samples from CK_oUE Tests
- Fig. 6.1 Typical Drained Stress Paths and Test Names of K_o -overconsolidated Samples (Test Series I)
- Fig. 6.2 Drained Stress Paths from CID Tests
- Fig. 6.3 (q, ϵ_s) Plot from CID Tests
- Fig. 6.4 (p, ϵ_v) Plot from CID Tests
- Fig. 6.5 Shear Strain Contours within the State Boundary Surface from CIU & CID Tests
- Fig. 6.6 $(\epsilon_{vp}, \epsilon_s)$ Plot from CID Tests
- Fig. 6.7 Direction of the Plastic Stain Increment Vectors from CID Tests
- Fig. 6.8 $(q/p_e, p/p_e)$ Plot from CID Tests
- Fig. 6.9 (q, ϵ_v) Plot from CID Tests
- Fig. 6.10 (η, ϵ_s) Plot from CID Tests
- Fig. 6.11 (η, ϵ_v) Plot from CID Tests
- Fig. 6.12 (η, ϵ_{vp}) Plot from CID Tests

Fig. 6.13	Relationships between η and Positive Plastic Volumetric Strains from CID Tests
Fig. 6.14	Zero Plastic Volumetric Strain and Yield Points from CID and CK _o D Tests
Fig. 6.15	Volumetric Yield Loci and Stress Paths for CK _o D Samples
Fig. 6.16	Drained Stress Paths from CK _o D Tests with Undrained Stress Paths of K _o -normally Consolidated Samples
Fig. 6.17	(q , ϵ_s) Plot from CK _o D Tests
Fig. 6.18	(p , ϵ_v) Plot from CK _o D Tests
Fig. 6.19a	(ϵ_v , ϵ_s) Plot from CK _o D Tests (Wet Zone)
Fig. 6.19b	(ϵ_v , ϵ_s) Plot from CK _o D Tests (Dry Zone)
Fig. 6.19c	(ϵ_{vp} , ϵ_s) Plot from CK _o D Tests
Fig. 6.20	(η , ϵ_s) Plot from CK _o D Tests
Fig. 6.21	(q/p_e , p/p_e) Plot from CK _o D Tests
Fig. 6.22	(η , ϵ_v) Plot from CK _o D Tests
Fig. 6.23	(q , ϵ_v) Plot from CK _o D Tests
Fig. 6.24	(η , ϵ_{vp}) Plot from CK _o D1 and CK _o D2 Samples
Fig. 6.25	(q , ϵ_{vp}) Plot from CK _o D1 and CK _o D2 Samples
Fig. 6.26	(ϵ_{vp} , p) Plot from CK _o D Tests
Fig. 6.27	Volumetric Yield Loci and Stress Paths for CAD Samples
Fig. 6.28	(q , ϵ_s) Plot from CAD Tests
Fig. 6.29	(ϵ_v , p) Plot from CAD Tests
Fig. 6.30a	(ϵ_v , ϵ_s) Plot from CAD Tests (Wet Zone)
Fig. 6.30b	(ϵ_v , ϵ_s) Plot from CAD Tests (Dry Zone)
Fig. 6.30c	(ϵ_{vp} , ϵ_s) Plot from CAD Tests
Fig. 6.31	(η , ϵ_s) Plot from CAD Tests
Fig. 6.32	(q/p_e , p/p_e) Plot from CAD Tests
Fig. 6.33	(q , ϵ_v) Plot from CAD Tests
Fig. 6.34a	(η , ϵ_v) Plot from CAD Tests
Fig. 6.34b	(η , ϵ_{vp}) Plot from CAD1 and CAD2 Samples
Fig. 6.35	Volumetric Yield Loci and Stress Paths for CK _o PC Samples
Fig. 6.36	(q , ϵ_s) Plot from CK _o PC Tests
Fig. 6.37	Deviator Stress Increment and Shear Strain Relationships from CK _o PC Tests
Fig. 6.38	(η , ϵ_s) Plot from CK _o PC Tests
Fig. 6.39	(ϵ_{vp} , ϵ_s) Plot from CK _o PC Tests
Fig. 6.40	(q/p_e , p/p_e) Plot from CK _o PC Tests

Fig. 6.41	(q , ϵ_v) Plot from CK _o PC Tests
Fig. 6.42	(η , ϵ_v) Plot from CK _o PC Tests
Fig. 6.43	Plastic Volumetric Strain Contours from CK _o PC Tests
Fig. 6.44	Volumetric Yield Loci and Stress Paths for CK _o DU Tests
Fig. 6.45	(q , ϵ_s) Plot from CK _o DU Tests
Fig. 6.46	Deviator Stress Increment and Shear Strain Relationship from CK _o DU Tests
Fig. 6.46a	(ϵ_v , ϵ_s) Plot from CK _o DU Tests
Fig. 6.46b	(ϵ_{ve} , ϵ_s) Plot from CK _o DU Tests
Fig. 6.46c	(ϵ_{vp} , ϵ_s) Plot from CK _o DU Tests
Fig. 6.47	(η , ϵ_s) Plot from CK _o DU Tests
Fig. 6.48	(q/p_e , p/p_e) Plot from CK _o DU Tests
Fig. 6.49	(η , ϵ_v) Plot from CK _o DU Tests
Fig. 6.50	(q , ϵ_v) Plot from CK _o DU Tests
Fig. 6.51	(η , ϵ_{vp}) Plot from CK _o DU Tests
Fig. 6.52	(q , ϵ_{vp}) Plot from CK _o DU Tests
Fig. 6.53	(ϵ_{vp} , p) Plot from CK _o DU Tests
Fig. 6.54	Plastic Volumetric Strain Contours from CK _o DU Tests
Fig. 6.55	Drained Stress Paths from CK _o QU Tests
Fig. 6.56	(η , ϵ_s) Plot from CK _o QU Tests
Fig. 6.57	(ϵ_v , p) Plot from CK _o QU Tests
Fig. 6.58	(ϵ_{vp} , p) Plot from CK _o QU Tests
Fig. 6.59	(ϵ_v , ϵ_s) Plot from CK _o QU Tests
Fig. 6.60	(ϵ_{vp} , ϵ_s) Plot from CK _o QU Tests
Fig. 6.61	(η , ϵ_v) Plot from CK _o QU Tests
Fig. 6.62	(ϵ_{vp} , p) Plot from CK _o QU Tests
Fig. 6.63	(η , ϵ_{vp}) Plot from CK _o QU Tests
Fig. 6.64	Plastic Volumetric Strain Contours from CK _o QU Tests
Fig. 6.65	(q/p_e , p/p_e) Plot from CK _o QU Tests
Fig. 6.66	(e , $\ln p$) Plot from CK _o QU Tests
Fig. 6.67	Drained Stress Paths from CK _o DE Tests
Fig. 6.68	(q , ϵ_s) Plot from CK _o DE Tests
Fig. 6.69	(η , ϵ_s) Plot from CK _o DE Tests
Fig. 6.70	(ϵ_v , p) Plot from CK _o DE Tests

- Fig. 6.71a (ϵ_v, ϵ_s) Plot from CK_o DE Tests (Wet Zone)
- Fig. 6.71b (ϵ_v, ϵ_s) Plot from CK_o DE Tests (Dry Zone)
- Fig. 6.72 ($\epsilon_{vp}, \epsilon_s$) Plot from CK_o DE Tests
- Fig. 6.73 (η, ϵ_v) Plot from CK_o DE Tests
- Fig. 6.74 (q, ϵ_v) Plot from CK_o DE Tests
- Fig. 6.75 (η, ϵ_{vp}) Plot from CK_o DE Tests
- Fig. 6.76 (q, ϵ_{vp}) Plot from CK_o DE Tests
- Fig. 6.77 Plastic Volumetric Strain Contours from CK_o DE Tests
- Fig. 6.78 ($q/p_e, p/p_e$) Plot from CK_o DE Tests
- Fig. 6.79 Drained Stress Path from CK_o PE Tests
- Fig. 6.80 (q, ϵ_s) Plot from CK_o PE Tests
- Fig. 6.81 (η, ϵ_s) Plot from CK_o PE Tests
- Fig. 6.82 (q, ϵ_v) Plot from CK_o PE Tests
- Fig. 6.83 (η, ϵ_v) Plot from CK_o PE Tests
- Fig. 6.84 Plastic Volumetric Strain Contours from CK_o PE Tests
- Fig. 6.85 ($q/p_e, p/p_e$) Plot from CK_o PE Tests
- Fig. 8.86a Failure Envelope from Drained Tests on K_o Consolidated Samples in the Compression Side
- Fig. 6.86b Failure Points from Drained Tests in the ($q/p_e, p/p_e$) Plot
- Fig. 6.87 Strength Envelope and Stress Paths in the (q, p) Plot
- Fig. 6.88 State Boundary Surface and Failure Points from Drained and Undrained Tests (Test Series I, II & III) in the (q, p) Plot
- Fig. 6.89 ($\Delta e_f, p_f$) Plot from Drained Tests
- Fig. 6.90 ($\Delta e_f, \ln(p_f/p_e)$) Plot from Drained Tests
- Fig. 6.91 Volumetric Yield Points from Drained and Undrained Tests on K_o Consolidated Samples in the (q, p) Plot
- Fig. 6.92 Volumetric Yield Zone from Drained and Undrained Tests on K_o Consolidated Samples in the (q, p) Plot
- Fig. 6.93 Volumetric Yield Locus from Drained and Undrained Tests on K_o Consolidated Samples in the ($q/p_e, p/p_e$) Plot
- Fig. 6.94 State Boundary Surface and Elastic Zone for K_o Consolidated Samples in the ($q/p_e, p/p_e$) Plot
- Fig. 6.95 Shear Strain Contours from Drained Tests on K_o Consolidated Samples in the (q, p) Plot
- Fig. 7.1 ($q/p_o, p/p_o$) Plot for Isotropically Normally Consolidated Samples Compared with the Model Predictions (Critical State)
- Fig. 7.2 ($q/p_o, p/p_o$) Plot for CIU1 Sample Compared with the Model Predictions (Peak Stress State)

- Fig. 7.3 $(q/p_o, \epsilon_s)$ Plot for CIU1 Sample Compared with the Model Predictions (Critical State)
- Fig. 7.4 $(q/p_o, \epsilon_s)$ Plot for CIU1 Sample Compared with the Model Predictions (Peak Stress State)
- Fig. 7.5 (η, ϵ_s) Plot for CIU1 Sample Compared with the Model Predictions (Critical State)
- Fig. 7.6 (η, ϵ_s) Plot for CIU1 Sample Compared with the Model Predictions (Peak Stress State)
- Fig. 7.7 $(u/p_o, \eta)$ Plot for CIU1 Sample Compared with the Model Predictions (Critical State)
- Fig. 7.8 $(u/p_o, \eta)$ Plot for CIU1 Sample (Peak Stress State)
- Fig. 7.9 (q, p) Plot for K_o -normally Consolidated Samples Compared with Predictions from Pender's Model (Critical State)
- Fig. 7.10 (q, ϵ_s) Plot for K_o -normally Consolidated Samples Compared with the Model Predictions (Critical State)
- Fig. 7.10a (q, ϵ_s) Plot for CK_oU1 Sample Compared with the Model Predictions in Compression Conditions
- Fig. 7.10b (q, ϵ_s) Plot for CK_oUE1 Sample Compared with the Model Predictions in Compression Conditions
- Fig. 7.11 (q, ϵ_s) Plot for K_o -normally Consolidated Samples Compared with the Model Predictions (Peak Stress State)
- Fig. 7.12 (η, ϵ_s) Plot for CK_oU1 Sample Compared with the Model Predictions
- Fig. 7.13 (η, ϵ_s) Plot for CK_oUE1 Sample Compared with the Model Predictions
- Fig. 7.14 (u, ϵ_s) Plot for CK_oU1 Sample Compared with the Model Predictions
- Fig. 7.15 (u, ϵ_s) Plot for CK_oUE1 Sample Compared with the Model Predictions
- Fig. 7.16 Variations of Dafalias' α -parameter with the Stress Ratio for K_o -normally Consolidated Samples
- Fig. 7.17 Variations of Dafalias' α -parameter with the Stress Ratio for K_o -overconsolidated Samples
- Fig. 7.18 (q, p) Plot for Isotropically Overconsolidated Samples Compared with the Predictions from Pender's Model (Critical State)
- Fig. 7.19 (q, p) Plot for Isotropically Overconsolidated Samples Compared with the Predictions from Pender's Model (Peak Stress State)
- Fig. 7.20 (q, ϵ_s) Plot for Isotropically Overconsolidated Samples Compared with the Predictions from Pender's Model (Critical State)
- Fig. 7.21 (q, ϵ_s) Plot for Isotropically Overconsolidated Samples Compared with the Predictions from Pender's Model (Peak Stress State)
- Fig. 7.22 (u, ϵ_s) Plot for Isotropically Overconsolidated Samples Compared with the Predictions from Pender's Model (Critical State)

- Fig. 7.23 (u, ϵ_s) Plot for Isotropically Overconsolidated Samples Compared with the Predictions from Pender's Model (Peak Stress State)
- Fig. 7.24 (q, p) Plot for K_o -overconsolidated Samples Compared with the Predictions from Pender's Model (Critical State)
- Fig. 7.25 (q, ϵ_s) Plot for K_o -overconsolidated Samples Compared with the Predictions from Pender's Model (Critical State)
- Fig. 7.26 (q, ϵ_s) Plot for K_o -overconsolidated Samples Compared with the Predictions from Pender's Model (Peak Stress State)
- Fig. 7.27 (η, ϵ_s) Plot for K_o -overconsolidated Samples Compared with the Predictions from Pender's Model (Critical & Peak Stress State)
- Fig. 7.28 (u, ϵ_s) Plot for K_o -overconsolidated Samples Compared with the Predictions from Pender's Model (Critical State)
- Fig. 7.29 (u, ϵ_s) Plot for K_o -overconsolidated Samples Compared with the Predictions from Pender's Model (Peak Stress State)
- Fig. 7.30 (q, p) Plot for K_o -overconsolidated Samples both in Compression and in Extension Conditions Compared with the Predictions from Pender's Model (Peak Stress State)
- Fig. 7.31 (q, ϵ_s) Plot for K_o -overconsolidated Samples in Extension Conditions Compared with the Predictions from the Pender's Model
- Fig. 7.32 (u, ϵ_s) Plot for K_o -overconsolidated Samples in Extension Conditions Compared with the Predictions from Pender's Model
- Fig. 7.33 (q, ϵ_s) Plot for CID1 Sample Compared with the Model Predictions
- Fig. 7.34 (q, ϵ_v) Plot for CID1 Sample Compared with the Model Predictions
- Fig. 7.35 (η, ϵ_s) Plot for CID1 Sample Compared with the Model Predictions
- Fig. 7.36 (η, ϵ_v) Plot for CID1 Sample Compared with the Model Predictions
- Fig. 7.37 $(\epsilon_{vp}, \epsilon_{sp})$ Plot for CID1 Sample Compared with the Model Predictions
- Fig. 7.38 (q, ϵ_s) Plot for CK_oD1 Sample Compared with the Model Predictions
- Fig. 7.39 (q, ϵ_v) Plot for CK_oD1 Sample Compared with the Model Predictions
- Fig. 7.40 (η, ϵ_s) Plot for CK_oD1 Sample Compared with the Model Predictions
- Fig. 7.41 (η, ϵ_v) Plot for CK_oD1 Sample Compared with the Model Predictions
- Fig. 7.42 $(\epsilon_{vp}, \epsilon_{sp})$ Plot for CK_oD1 Sample Compared with the Model Predictions
- Fig. 7.43 (q, ϵ_s) Plot for CK_oDE1 Sample Compared with the Model Predictions
- Fig. 7.44 (η, ϵ_s) Plot for CK_oDE1 Sample Compared with the Model Predictions
- Fig. 7.45 (η, ϵ_v) Plot for CK_oDE1 Sample Compared with the Model Predictions
- Fig. 7.46 (q, ϵ_s) Plot for Isotropically Overconsolidated Samples Compared with the Model Predictions

- Fig. 7.47 (ϵ_v, p) Plot for Isotropically Overconsolidated Samples Compared with the Model Predictions
- Fig. 7.48 (η, ϵ_s) Plot for Isotropically Overconsolidated Samples Compared with the Model Predictions
- Fig. 7.49 (η, ϵ_v) Plot for Isotropically Overconsolidated Samples Compared with the Model Predictions
- Fig. 7.50 (q, ϵ_s) Plot for CK_oD Samples Compared with the Model Predictions
- Fig. 7.51 (q, ϵ_v) Plot for CK_oD Samples Compared with the Model Predictions
- Fig. 7.52 (η, ϵ_s) Plot for CK_oD Samples Compared with the Model Predictions
- Fig. 7.53 (η, ϵ_v) Plot for CK_oD Samples Compared with the Model Predictions
- Fig. 7.54 (q, ϵ_s) Plot for CK_oPC Samples Compared with the Model Predictions
- Fig. 7.55 (q, ϵ_v) Plot for CK_oPC Samples Compared with the Model Predictions
- Fig. 7.56 (η, ϵ_s) Plot for CK_oPC Samples Compared with the Model Predictions
- Fig. 7.57 (η, ϵ_v) Plot for CK_oPC Samples Compared with the Model Predictions
- Fig. 7.58 (q, ϵ_s) Plot for CK_oDU Samples Compared with the Model Predictions
- Fig. 7.59 (q, ϵ_v) Plot for CK_oDU Samples Compared with the Model Predictions
- Fig. 7.60 (η, ϵ_s) Plot for CK_oDU Samples Compared with the Model Predictions
- Fig. 7.61 (η, ϵ_v) Plot for CK_oDU Samples Compared with the Model Predictions
- Fig. 7.62 (ϵ_v, p) Plot for CK_oQU Samples Compared with the Model Predictions
- Fig. 7.63 (η, ϵ_s) Plot for CK_oQU Samples Compared with the Model Predictions
- Fig. 7.64 (η, ϵ_v) Plot for CK_oQU Samples Compared with the Model Predictions
- Fig. 7.65 (q, ϵ_s) Plot for CK_oDE Samples Compared with the Model Predictions
- Fig. 7.66 (q, ϵ_v) Plot for CK_oDE Samples Compared with the Model Predictions
- Fig. 7.67 (η, ϵ_s) Plot for CK_oDE Samples Compared with the Model Predictions
- Fig. 7.68 (η, ϵ_v) Plot for CK_oDE Samples Compared with the Model Predictions
- Fig. 7.69 (q, ϵ_s) Plot for CK_oPE Samples Compared with the Model Predictions
- Fig. 7.70 (q, ϵ_v) Plot for CK_oPE Samples Compared with the Model Predictions
- Fig. 7.71 (η, ϵ_s) Plot for CK_oPE Samples Compared with the Model Predictions
- Fig. 7.72 (η, ϵ_v) Plot for CK_oPE Samples Compared with the Model Predictions
- Fig. 7.73 Variations of the $(d\epsilon_{sp}/d\epsilon_{vp})$ along the CID1 Path Compared with the Predictions from Pender's Model (Wet Zone)
- Fig. 7.74 Variations of the $(d\epsilon_{sp}/d\epsilon_{vp})$ along the CID3 Path Compared with the Predictions from Pender's Model (Wet Zone)

- Fig. 7.75 Variations of the $(d\epsilon_{sp}/d\epsilon_{vp})$ along the CID4 Path Compared with the Predictions from Pender's Model (Dry Zone)
- Fig. 7.76 Variations of the $(d\epsilon_{sp}/d\epsilon_{vp})$ along the CID6 Path Compared with the Predictions from Pender's Model (Dry Zone)
- Fig. 7.77 Variations of the $(d\epsilon_{sp}/d\epsilon_{vp})$ along the CK₀D1 Path Compared with the Predictions from Pender's Model (Wet Zone)
- Fig. 7.78 Variations of the $(d\epsilon_{sp}/d\epsilon_{vp})$ along the CK₀D6 Path Compared with the Predictions from Pender's Model (Dry Zone)
- Fig. 7.79 (q, ϵ_s) Plot for Isotropically Overconsolidated Samples Compared with the Predictions from Pender's Model with Some Modifications
- Fig. 7.80 Shear Strain Contours and Undrained Stress Paths for the Isotropically Overconsolidated Samples Predicted from Pender's Model with some Modifications
- Fig. 7.81 (q, p) Plot from Pender's Model with and without Shifted Initial Stress Points
- Fig. 7.82 (q, p) Plot for K₀-overconsolidated Samples Compared with the Predictions from Pender's Model with Shifted Initial Stress Points
- Fig. 7.83 (q, ϵ_s) Plot for K₀-overconsolidated Samples Compared with the Predictions from Pender's Model with and without Shifted Initial Stress Points (Wet Zone)
- Fig. 7.84 (q, ϵ_s) Plot for K₀-overconsolidated Samples Compared with the Predictions from Pender's Model with and without Shifted Initial Stress Points (Dry Zone)
- Fig. 7.85 (u, ϵ_s) Plot for K₀-overconsolidated Samples Compared with the Predictions from Pender's Model with and without Shifted Initial Stress Points (Wet Zone)
- Fig. 7.86 (u, ϵ_s) Plot for K₀-overconsolidated Samples Compared with the Predictions from Pender's Model with and without Shifted Initial Stress Points (Dry Zone)
- Fig. 8.1a Plastic Volumetric Strains within the State Boundary Surface from CID Tests
- Fig. 8.1b Plastic Volumetric Strain Contours within the State Boundary Surface
- Fig. 8.2 Simplified Plastic Volumetric Strain Contours within the State Boundary Surface and the Strain Zones
- Fig. 8.3 Constant Stress Ratio Lines and Normalized Drained Stress Paths from CID Tests
- Fig. 8.4 Typical Shear Strain Contours within the State Boundary Surface and the Corresponding Stress Path
- Fig. 8.5 Variation of the Dilatancy Ratio with the Mean Normal Stress on the Constant Stress Ratio Lines from CID Tests
- Fig. 8.6 Simplified $(\frac{d\epsilon_{vp}}{d\epsilon_{sp}}, \frac{p}{p_e})$ Relationship on the Constant Stress Ratio Lines from CID Tests
- Fig. 8.7 Gradient of the $(\frac{d\epsilon_{vp}}{d\epsilon_{sp}}, \frac{p}{p_e})$ Relationship with the Stress Ratio from CID Tests
- Fig. 8.8 p/p_e at Zero Dilatancy Ratio on the Particular Stress Ratio Line from CID Tests
- Fig. 8.9a Simplified $(\frac{d\epsilon_{vp}}{d\epsilon_{sp}}, \frac{p}{p_e})$ Relationship on the Constant Stress Ratio Lines from K₀ Compression Tests

- Fig. 8.9b Gradient of the $(\frac{d\epsilon_{vp}}{d\epsilon_{sp}}, \frac{p}{p_e})$ Relationship with the Stress Ratio from CID and K_0 Compression Tests
- Fig. 8.10 $(\frac{d\epsilon_{vp}}{d\epsilon_{sp}}, \frac{p}{p_e})$ Relationship on the Constant Stress Ratio Lines from K_0 Compression Tests
- Fig. 8.11 Simplified $(\frac{d\epsilon_{vp}}{d\epsilon_{sp}}, \frac{p}{p_e})$ Relationship on the Constant Stress Ratio Lines from K_0 Extension Tests
- Fig. 8.12 $(\frac{d\epsilon_{vp}}{d\epsilon_{sp}}, \frac{p}{p_e})$ Relationship on the Constant Stress Ratio Lines from K_0 Extension Tests
- Fig. 8.13 p/p_e at Zero Dilatancy Ratio on the Particular Stress Ratio Line from K_0 Extension Tests
- Fig. 8.14 Gradient of the $(\frac{d\epsilon_{vp}}{d\epsilon_{sp}}, \frac{p}{p_e})$ Relationship with the Stress Ratio from CID, K_0 Compression and K_0 Extension Tests
- Fig. 8.15 Variation of the $(\frac{d\epsilon_{vp}}{d\epsilon_{sp}}, \frac{p}{p_e})$ Plot with the Stress Ratio within the State Boundary Surface
- Fig. 8.15a Direction of Plastic Strain Increment Vectors and Their Locations within the State Boundary Surface
- Fig. 8.16 Simplified Plastic Volumetric Strain Contours within the State Boundary Surface from CID Tests (Wet Zone)
- Fig. 8.17 Schematic Diagram for the Plastic Volume Change during Conventional Drained Compression and the Definition of λ_{oc}
- Fig. 8.18 OCR- C_1 - η_i Relationship from CID Samples on the Wet Zone
- Fig. 8.19 Simplified Stress-Strain Relationship for the Samples on the Wet Zone
- Fig. 8.20 Comparisons between the Predicted Undrained Stress Paths and the Experimental Observations from CIU Tests
- Fig. 8.21 Schematic Diagram for the Calculation of the Plastic Strains within the State Boundary Surface (Wet Zone)
- Fig. 8.22a (q, ϵ_s) Plot for CID2 Sample Compared with the Model Predictions
- Fig. 8.22b (q, ϵ_v) Plot for CID2 Sample Compared with the Model Predictions
- Fig. 8.23a (η, ϵ_s) Plot for CID2 Sample Compared with the Model Predictions
- Fig. 8.23b (η, ϵ_v) Plot for CID2 Sample Compared with the Model Predictions
- Fig. 8.24a (q, ϵ_s) Plot for CID3 Sample Compared with the Model Predictions
- Fig. 8.24b (q, ϵ_v) Plot for CID3 Sample Compared with the Model Predictions
- Fig. 8.25a (η, ϵ_s) Plot for CID3 Sample Compared with the Model Predictions
- Fig. 8.25b (η, ϵ_v) Plot for CID3 Sample Compared with the Model Predictions

- Fig. 8.26a (q, ϵ_s) Plot for CID4 Sample Compared with the Model Predictions
- Fig. 8.26b (q, ϵ_v) Plot for CID4 Sample Compared with the Model Predictions
- Fig. 8.27a (η, ϵ_s) Plot for CID4 Sample Compared with the Model Predictions
- Fig. 8.27b (η, ϵ_v) Plot for CID4 Sample Compared with the Model Predictions
- Fig. 8.28a (q, ϵ_s) Plot for CID5 Sample Compared with the Model Predictions
- Fig. 8.28b (q, ϵ_v) Plot for CID5 Sample Compared with the Model Predictions
- Fig. 8.29a (η, ϵ_s) Plot for CID5 Sample Compared with the Model Predictions
- Fig. 8.29b (η, ϵ_v) Plot for CID5 Sample Compared with the Model Predictions
- Fig. 8.30 Simplified Strain Contours on the Dry Zone and Typical Stress Paths Sheared from the Isotropic Pre-shear Conditions for the Model Comparisons
- Fig. 8.31 Simplified Strain Contours on the Dry Zone and Typical Stress Paths Sheared from the K_0 Pre-shear Conditions for the Model Comparisons
- Fig. 8.32a (q, ϵ_s) Plot for the Constant p Compression Test Sheared from Isotropic Pre-shear Condition Compared with the Model Predictions (Dry Zone)
- Fig. 8.32b (q, ϵ_v) Plot for the Constant p Compression Test Sheared from Isotropic Pre-shear Condition Compared with the Model Predictions (Dry Zone)
- Fig. 8.33a (q, ϵ_s) Plot for the Unloading Compression Test Sheared from Isotropic Pre-shear Condition Compared with the Model Predictions (Dry Zone)
- Fig. 8.33b (q, ϵ_v) Plot for the Unloading Compression Test Sheared from Isotropic Pre-shear Condition Compared with the Model Predictions (Dry Zone)
- Fig. 8.34a (q, ϵ_s) Plot for the Unloading Compression Test Sheared from K_0 Pre-shear Condition Compared with the Model Predictions (Dry Zone)
- Fig. 8.34b (q, ϵ_v) Plot for the Unloading Compression Test Sheared from K_0 Pre-shear Condition Compared with the Model Predictions (Dry Zone)
- Fig. 8.35a (q, ϵ_s) Plot for the Constant p Compression Test Sheared from K_0 Pre-shear Condition Compared with the Model Predictions (Dry Zone)
- Fig. 8.35b (q, ϵ_v) Plot for the Constant p Compression Test Sheared from K_0 Pre-shear Condition Compared with the Model Predictions (Dry Zone)
- Fig. 8.36a (q, ϵ_s) Plot for the Conventional Compression Test Sheared from K_0 Pre-shear Condition Compared with the Model Predictions (Dry Zone)
- Fig. 8.36b (q, ϵ_v) Plot for the Conventional Compression Test Sheared from K_0 Pre-shear Condition Compared with the Model Predictions (Dry Zone)

I INTRODUCTION

1.1 General Background

With the extensive use of computer software in the analysis of geotechnical problems, the use of stress path dependent soil properties becomes more and more a convenience in current geotechnical engineering practice. Also computer controlled stress path dependent tests can now be carried out in many geotechnical laboratories. These trends help in the use of realistic soil parameters for the numerical analysis of many geotechnical problems.

This dissertation is thus aimed to study the path dependent behaviour of lightly overconsolidated clays wherein the state paths lie below the State Boundary Surface (see ROSCOE, SCHOFIELD and WROTH, 1958). For normally consolidated clays when the stress paths are such that their states lie on the State Boundary Surface, successful stress-strain theories have been developed based on the Critical State Concepts. These theories namely, the Cam Clay Theory (ROSCOE, SCHOFIELD and THURAIRAJAH, 1963; SCHOFIELD and WROTH, 1968) and the Modified Cam Clay Theory (ROSCOE and BURLAND, 1968) are found to capture most of the behaviour of undrained and drained specimens sheared from isotropic stress states and in compression with a monotonically increasing stress ratio. The Modified Theory in particular with the use of both the volumetric and constant q yield loci makes excellent predictions of K_o , the pore pressure development and the stress-strain behaviour of Bangkok clay when tested in the normally consolidated state (see BALASUBRAMANIAM et al., 1977). In the use of the Revised Theory of ROSCOE and BURLAND (1968) for stress conditions within the State Boundary Surface, only elastic volumetric strain is assumed to take place. The elastic distortional strain within the State Boundary Surface is neglected and the plastic distortional strain is taken as contributed by a set of constant deviator stress yield loci on the wet side of the Critical State and a set of constant stress ratio lines on the dry side of the Critical State. Such a contribution on the distortional strains within the State Boundary Surface especially under undrained conditions arose from the experimental study of WROTH and LOUDON (1967) and was originally analyzed in the form of a constant deviator stress yield loci by ROSCOE and BURLAND (1968). Subsequent research work including that of BALASUBRAMANIAM (1969) and researchers at AIT have confirmed the concept of constant deviator stress yield loci within the State Boundary Surface on the wet side of the Critical State.

In this dissertation, two aspects of the behaviour of natural clays which tend to deviate from the simple stress-strain behaviour as predicted by the Cam Clay Theory and the Revised Theory are explored in detail. The first aspect relates to the in-situ stress conditions which are anisotropic in the field and for most clays the coefficient of earth pressure at rest, K_o , is less than one. The stress-strain behaviour of K_o consolidated samples, both undisturbed and laboratory prepared ones, were studied in detail by many researchers, however, their results are often reported

in a confusing manner, at times to agree with the behaviour of isotropically consolidated specimens but for the most part disagree. In attempting to carry out such a task, when comparing the behaviour of anisotropically consolidated samples (including K_0 consolidation) and the isotropically consolidated samples, often the constraints of time and the investigator's interest inevitably brought either an incomplete treatment of the topic or a higher degree of imbalance in making the comparisons. A comprehensive study on natural clays, especially with a narrow range of overconsolidation ratios and various applied stress paths has not yet been spotted by the Author. One of the aims of this dissertation is to make an attempt to study the K_0 consolidated behaviour of lightly overconsolidated Bangkok clay under a variety of applied stress path conditions to obtain the realistic stress-strain behaviour and then wherever possible to make comparisons with the behaviour as exhibited by isotropically consolidated samples. The data so obtained would also be useful in the numerical analysis of various types of loading conditions on soft clays.

The second aspect of the dissertation relates to a detailed investigation of the behaviour of Soft Bangkok clay for stress paths which lie below the State Boundary Surface and to an examination of how plastic volumetric dilation and compression can take place inside the State Boundary Surface and their relative magnitude for the counterpart behaviour when the stress state lies on the State Boundary Surface. Such an investigation is also extended to the plastic dilatancy ratio (i.e., the ratio of the plastic volumetric strain to distortional strain) where a positive dilatancy ratio (expansive plastic volumetric strain) is obtained on the dry side of the Critical State and a negative dilatancy ratio (positive volumetric strain) is observed on the wet side of the Critical State. These investigations will then offer the usefulness of the idea of 'associated or non-associated flow rules' which are often used extensively in the elasto-plastic behaviour of soils.

1.2 Scope and Objective of Study

An attempt is made to formulate the stress-strain behaviour and strength characteristics of lightly overconsolidated Bangkok clay under the isotropic and K_0 consolidation conditions. Experimental observations on the wet side of the Critical State and in compression are rather comprehensive, while on the dry side of the Critical State and in the extension phase only limited investigation is carried out. The Critical State Concepts are used as a framework in this study because these concepts appeal to only a few well-known soil parameters instead of depending on a large number of empirical constants. Comprehensive triaxial tests were carried out on undisturbed samples of Soft Bangkok clay.

Generally, the stress-strain models to describe the behaviour of soils are developed based on several assumptions and hypotheses in conjunction with well-known concepts in the theory of plasticity. The models developed by the Cambridge Group (e.g., Cam Clay and Modified Cam Clay Theories) are based on energy balance equations and the normality condition. Recently, the energy balance equation was modified by DAFALIAS (1987) in order to describe the behaviour of normally consolidated clays under anisotropic stress conditions. The above

mentioned theories used the normality concept and the energy balance equation to obtain a set of volumetric yield loci. The shifting of these yield loci generates plastic volumetric strain, and associated with the plastic volumetric strain is the distortional strains obeying the energy balance criterion. Such volumetric yield loci lie on the State Boundary Surface (SBS) and below the SBS only the Revised Theory accepts distortional yielding as per the contribution from the constant deviator stress yield loci. The volumetric strain below the State Boundary Surface is assumed to be elastic and the elastic distortional strain is neglected. A unified stress-strain model for both the overconsolidated and normally consolidated clay behaviour was proposed by PENDER (1977) based on a non-associated flow rule with many empirical assumptions based on experimental observations; however, many of these ideas retained the original Critical State Concepts. The current research of the Author complements the above works in incorporating subsets of volumetric yield loci within the State Boundary Surface in such a manner that the yielding is compressive on the wet side and dilatant on the dry side. Also an attempt will be made to describe the plastic dilatancy ratio associated with the volumetric yielding inside the State Boundary Surface both on the wet and dry sides of the Critical State. The prediction of strains and pore pressures from Author's simplified model will then be compared with other predictions as well as the experimental observations.

1.3 Organization of the Dissertation

Following the introductory chapter which describes the aim and scope of the work in relation to the current status on the understanding of the stress-strain behaviour of soft clays, Chapters II and III are devoted to a review of the literature associated with the Author's work. Chapter II is a review of the behaviour of clays under anisotropic stress conditions and includes sub-sections on K_0 , behaviour of normally and overconsolidated clays, yield loci and anisotropic elasticity. Chapter III is entirely devoted to a review of the Critical State stress-strain theories. It deals with the Critical State Concepts, the philosophy behind the Incremental Stress-Strain Theory of ROSCOE and POOROOSHASB (1963), the Cam Clay Theory (ROSCOE, SCHOFIELD and THURAIRAJAH, 1963; SCHOFIELD and WROTH, 1968) and the Modified Cam Clay Theory (ROSCOE and BURLAND, 1968) as theories based on an 'associated flow rule'. Pender's Theory is then reviewed as a theory based on a 'non-associated flow rule' retaining the Critical State framework. Finally, Dafalias' Model for anisotropic behaviour of clay is also reviewed as an extension of the Modified Cam Clay Theory.

Chapter IV describes the experimental programme and the testing procedures. Four series of triaxial tests were conducted in undrained conditions, three of them were under compression and one under extension conditions. The undrained compression tests were under CIU, CK_0U and CAU conditions, respectively. The undrained extension tests were of the CK_0UE type. All the undrained compression tests were of the loading type with constant cell pressure, while the undrained extension tests were of the unloading type with constant radial stress. Ten series of drained tests were conducted. One was CID type and this was followed by CAD and CK_0D tests. Constant p drained tests from the K_0 conditions were carried out under compression and extension conditions. Constant q drained tests were conducted from K_0 conditions with the mean normal

stress p decreasing and the mean normal stress p increasing. From the K_0 conditions, compression unloading tests and extension unloading tests were also carried out. Each series of undrained and drained tests included a normally consolidated sample and samples with four to five different overconsolidation ratios mostly in the lightly overconsolidated range. All samples were of the same pre-shear void ratio.

Chapter V presents the results and discussions pertinent to the undrained behaviour of the normally consolidated and overconsolidated samples as tested from isotropic and K_0 conditions both in compression and in extension. The interpretation of the data relates to the stress paths, the pore pressure development, the stress - strain behaviour, the shear strain contours and the strength and water content relationships.

Chapter VI contains the results and discussion of the data from the ten series of drained tests. Considerable efforts have been made in the interpretation of each of these series of drained tests and in the estimation of the volumetric yield loci which lie on the State Boundary Surface as well as below the State Boundary Surface. Plastic dilatancy ratios are also determined on the wet and dry side of the Critical State under compression conditions. Failure envelopes, Critical State Line and water content-strength relationships are also presented. As stated before, a novel feature of the results presented in Chapters V and VI is that all samples have approximately the same pre-shear void ratio.

In Chapter VII, the stress-strain theories based on the Critical State Concepts are critically evaluated by comparing the predictions with the experimental observations for both normally and overconsolidated states under undrained and drained conditions.

Finally, in Chapter VIII, the salient aspects of the stress-strain behaviour in Chapters V and VI are presented in a simplified model which supports the Critical State Concepts both in compression and in extension, the Hvorslev failure envelopes, the adaptation of the volumetric yield loci lying on the State Boundary Surface and the set of constant deviator stress yield loci for the prediction of strains in stress paths which lie on the State Boundary Surface with increasing stress ratio. Within the State Boundary Surface, the zones in which plastic volumetric compression and dilation take place are identified and the plastic dilatancy ratios are established. Chapter VIII also contains a proposed model by the Author for the determination of strains and pore pressures for various types of applied stress paths within the State Boundary Surface. Comparisons of the predictions from the Author's Model are made with the experimental observations and those from Pender's Model.

Concluding remarks are made at the end of each chapter, and an overall conclusion is also made in Chapter IX.

II REVIEW OF THE BEHAVIOUR OF CLAYS UNDER ANISOTROPIC STRESS CONDITIONS

2.1 Introduction

The Critical State Concept and the associated stress-strain theories attempt to capture as much as possible the behaviour exhibited by artificially sedimented, remoulded and undisturbed specimens of clay, while the hypothesis and assumptions are based on proven and accepted trends in the experimental observations both in the laboratory and in the field. The earlier emphasis was, therefore, on verifying the concepts and ideas based on resedimented samples of Kaolin which exhibit little secondary consolidation or time effects as well as on studying the compression behaviour as sheared from isotropic stress conditions. Such an emphasis was made because the experimental errors and limitations associated with the triaxial apparatus enable the compression test data to be analyzed more reliably than the extension test data in which non-uniformity of stresses and reorientation of principal stress take place after consolidation and during shear. Therefore, the basic Critical State ideas simplify that the extension behaviour is similar to that in compression and that time effects are not significant. Thus, these theories predict the behaviour of isotropically and anisotropically consolidated specimens to be the same (irrespective of their pre-shear mode of consolidation) and to depend only on the subsequent applied stress paths. Also when specimens are sheared from the isotropic or anisotropic initial state, the behaviour in compression and extension are expected to be identical.

Since these developments, two major points have received intense investigation. The first is the behaviour of natural clays which have a time effect (in the sense that when two samples are isotropically and anisotropically consolidated, the pre-shear consolidation time has a substantial effect during subsequent shearing). If such a phenomenon occurs, then, the state of a normally consolidated specimen with prolonged time can move inside the State Boundary Surface and thereby, become an apparently overconsolidated specimen. The second refers to the development of an anisotropic clay structure either due to the mode of deposition or to the subsequent shear after consolidation. The research work reported in the literature often becomes confusing when it is difficult to identify the two phenomena mentioned above or even their combined effects. Furthermore, these studies are at times carried out on deposits of clay which have special properties such as those of sensitive clay or cemented clay. These contributions, when considered without taking into account their special mode of deposition, further add to the confusion. Moreover, some of this research work seems, at least implicitly, to be conducted with a negative view to challenge the simple Critical State Concepts (which do expect such deviations) rather than to help in modifying the ideas to accept such perturbations.

As such the literature reviewed in this chapter at times tends to make contradictory comments when considered without taking account of special considerations with regard to the mineralogy, sensitivity or special features such as cementing action. The work of some researchers features extensively in this chapter and this may perhaps give the impression that

these effects are not yet appreciated by those who advocate the simplified concepts for the understanding of the major part of the behaviour of normally consolidated and overconsolidated clays.

The material contained in this chapter deals with the coefficient of earth pressure at rest as related to the preparation of undisturbed samples in the laboratory under K_0 conditions. It then describes the behaviour of normally consolidated clay both under isotropic and K_0 pre-shear consolidation conditions. A similar coverage is then made of the overconsolidated clays. Finally, the chapter ends with the topics of yield loci for natural clays, directions of plastic strain increment vectors, and anisotropic elastic behaviour.

The selection of the material presented in this chapter is perhaps somewhat deliberate in the sense that it covers the behaviour of resedimented laboratory specimens (the work of PARRY and NADARAJAH, 1973), the behaviour of laboratory and undisturbed specimens of clays (LADD et al., 1977, and the work on Bangkok clays) and the behaviour of Canadian clays, both cemented and uncemented (VAID and CAMPANELLA, 1974; TAVENAS and LEROUÉIL, 1977; LEROUÉIL et al., 1979; GRAHAM et al., 1983, 1988). Also, the extensive interpretations made by MAYNE (1985) and MAYNE and STEWART (1988) are reviewed. Adequate coverage is given to the research work of these authors and to their contributions. Critical concluding comments are made at the end of the chapter.

2.2 Coefficient of Earth Pressure at Rest (K_0)

2.2.1 General

The coefficient of earth pressure (K_0) is defined as the ratio of the effective horizontal to the effective vertical stress under a condition of zero lateral strain. It is an essential parameter not only in reconstructing the in-situ stress state, but also in the design and the analysis of many practical engineering problems. K_0 is not readily amenable to theoretical formulation in terms of other soil parameters, and it is generally defined through measurements. The value of K_0 is known to be dependent upon the soil type and the stress history (BISHOP and HENKEL, 1957; BROOKER and IRELAND, 1965).

The techniques proposed in determining K_0 can be broadly grouped into two types: one is a direct measurement method with an aid of instruments in the laboratory (AL-HUSSAINI, 1981) and field, and the other is an indirect estimation from the empirical formulation in terms of various soil parameters. The second of the above techniques was reviewed by ABDELHAMID and KRIZEK (1976) and JAMIOLKOWSKI et al. (1985), respectively. However, it is important to note that each technique has its own limitations, hence there is no satisfactory method to determine the value of K_0 for soils. For normally consolidated clay, the method suggested by POULOS and DAVIS (1972) is widely used in many laboratories.

2.2.2 Prediction of K_0

Several theoretical and empirical relationships for K_0 have been proposed by many researchers (JAKY, 1944; ROWE, 1957; FRASER, 1957; BROOKER and IRELAND, 1965). Probably the simplest and most widely known relationship of K_0 for the normally consolidated state is :

$$K_0 \cong 1 - \sin \bar{\phi} \quad \dots(2.1)$$

in which $\bar{\phi}$ is the effective frictional angle. The confirmation of Eqn. 2.1, which is quoted as JAKY's expression, has been provided by results obtained from the sophisticated K_0 -test (AL-HUSSAINI, 1981), and by statistic analysis based on numerous experimental data from a variety of sources (MAYNE and KULHAWY, 1982).

Some empirical expressions have been suggested in relating K_0 with overconsolidation ratio during the unloading phase. These expressions have been reviewed by MAYNE and KULHAWY (1982). The simplest relationship proposed is that by SCHMIDT (1966) for K_0 (O.C) during primary unloading as :

$$\frac{K_0(O.C)}{K_0(N.C)} = (OCR)^\alpha \quad \dots(2.2)$$

in which α is a constant for a particular soil. ALPAN (1967) and SCHMERTMANN (1975) recommended the value of α as 0.4-0.5 and 0.42, respectively. LADD et al. (1977) showed that the value of α varies from about 0.42 for low plasticity clays to about 0.32 for high plasticity clays. GRAHAM et al. (1988), however, argued that K_0 in clays may not be solely a function of OCR, but depends on post-depositional straining.

By reviewing laboratory data from over 170 different soils, MAYNE and KULHAWY (1982) established the equation of K_0 in a more general form as :

$$K_0 = (1 - \sin \bar{\phi})^{\sin \bar{\phi}} \quad \dots(2.3)$$

For lightly overconsolidated soils, the value of K_0 in the field for which the overconsolidation ratio will be commonly between 1 and 2.5, may be expected to range from about 0.6 for a normally consolidated clay with low plasticity to nearly unity for a clay with high plasticity.

However, there is some experimental evidence which suggest that during secondary consolidation the value of K_o remains approximately constant. This indicates that the value of K_o for overconsolidated clay is not necessarily greater than the normally consolidated value provided the overconsolidation is not due to stress release. JAMIOLKOWSKI et al. (1985) also postulated that K_o for cemented deposits may well remain nearly the same as the value for the normally consolidated clay, while the mechanical representation of overconsolidation in the laboratory increases the in-situ K_o if the overconsolidation is due to stress release.

CHANG (1973) conducted tests on naturally deposited soft clay taken from the AIT Campus at a depth of 5.5 meter. The measured K_o -value was 0.63. CHAIYADHUMA (1974) performed K_o tests on undisturbed samples taken from the same depth at the Nong Ngoo Hao site situated about 28 km southeast of Bangkok. The K_o value was about 0.63.

2.3 Behaviour of Normally Consolidated Clays

2.3.1 Undrained Stress Paths

(1) **Triaxial Compression** - The concepts of the Critical State Soil Mechanics require that the states of the normally consolidated clay under anisotropic stresses should lie on the State Boundary Surface of the normally consolidated clay under isotropic stress conditions (SCHOFFIELD and WROTH, 1968; ROSCOE and BURLAND, 1968). Thus, the undrained stress path of anisotropically consolidated specimens was assumed to follow the State Boundary Surface of the isotropically consolidated clay, hence it reaches the same Critical State as a normally consolidated clay could reach under isotropic conditions at the same water content.

PARRY and NADARAJAH (1973) have shown, through a series of tests run on reconstituted specimens of kaolin, that the undrained stress paths of normally consolidated specimen under K_o -stress condition show a pronounced bullet nose (p' decreasing rapidly as q increases in magnitude) at its intersection with the K_o -consolidation line. However, the clear evidence that the effective stress path should be drawn with pointed apices at their intersection with K_o -line have not been provided by subsequent investigators. Several investigators (LADD, 1965; RUJIRAAPA, 1971; CHAIYADHUMA, 1974; LEROUEIL et al., 1979; KOUTSOFTAS, 1981; HIGHT et al., 1987; ATKINSON et al., 1987) rather showed from their experiments that the effective stress paths for the K_o -consolidated undrained clay in triaxial compression rose almost vertically up to certain levels of deviator stress. Once yielding has taken place, specimens experienced a significant strain-softening. VAID and CAMPANELLA (1974) postulated that the undrained stress paths of K_o -normally consolidated natural clay in the triaxial compression, both in loading and in extension conditions, appeared to be identical in the $(p/p_o, q/q_o)$ plot.

(2) **Triaxial Extension** - The Critical State Theories would imply that the shape of undrained stress path of the isotropically normally consolidated clay in extension is similar to the mirror image of that in compression about the p -axis. This aspect was experimentally supported by subsequent investigators. TAMPUBOLON (1981) added to the evidence of the above

behaviour by comparing his extension test results and compression results obtained by ALI (1981) on soft Bangkok clays. It was further revealed that the undrained stress paths in extension were approximately identical both in the unloading extension and in the loading extension (BALASUBRAMANIAM and UDDIN, 1977; MITACHI and KITAGO, 1979; TAMPUBOLON, 1981). MITACHI and KITAGO (1979) also reported that this behaviour was found for the K_0 -normally consolidated clay.

On the contrary, usually the K_0 -normally consolidated clay showed remarkably different behaviour from that of isotropically consolidated clay. KOUTSOFTAS (1981) presented data to show that the undrained stress path of K_0 -consolidated clay in extension exhibited a drastic reduction in the effective mean normal stress, which obviously resulted in low strength. Subsequently, the undrained stress path of normally consolidated clay in extension was approximately parallel to the drained unloading extension stress path. However, the excess pore pressure was expected to remain negative throughout the shearing. HIGHT et al. (1987) found similar undrained stress paths from the test run on K_0 -normally reconstituted clays (Lower Cromer Till, London clay and Magnus clay). They further mentioned that the effective stress paths in triaxial extension are much dependent on plasticity (stress paths swing to the right with increasing plasticity index resulting in higher strength). It is interesting, however, to note that some of the effective stress paths (with $I_p = 47, 53\%$) move nearly parallel to the q -axis at the early stage of unloading.

ATKINSON et al. (1987) illustrated that the effective stress path of K_0 -normally consolidated clay in extension test is almost parallel to the q -axis up to the p -axis ($\eta = 0$) and then it tends to move towards the origin without a significant reduction in mean effective normal stress. Furthermore, K_0 -extension tests on the reconsolidated Bangkok clay under consolidation stresses far in excess of the in-situ stresses (TAMPUBOLON, 1981; WIJEYAKULASURIYA, 1986) demonstrated that the undrained stress paths swing to the right more than those reported by ATKINSON et al. (1987). Consequently, the undrained stress paths of K_0 -normally consolidated clay in extension did not deviate much from the direction parallel to the q -axis until failure.

It is generally accepted that the undrained stress paths of normally consolidated specimens under isotropic stress have a symmetry about the p -axis for compression and extension tests even though there were contradicting findings (e.g., MITACHI and KITAGO, 1979). However, in the case of K_0 -consolidated specimens, the symmetry appears to be shifted to the K_0 -line. Obviously, this behaviour deviates from the idea of the Critical State Theories. Such deviation can arise due to secondary consolidation and time effects among other factors, which relates to initial shear to reach the K_0 conditions.

2.3.2 Deviator Stress-Strain Relationships

LADD (1965) observed that the anisotropically consolidated samples showed much lower strain at failure as contrast to that of the isotropically consolidated specimens. A significant softening was also noticed at strains beyond yielding. Subsequent research works done by other investigators illustrated similar trends.

PARRY and NADARAJAH (1973) have shown that the change in q from the start of the test to failure during the triaxial compression was very small compared with the initial deviator stress, and these too occurred mostly within 1% of axial strain. They also observed that the increment of deviator stress at 1% of deviator strain was much greater in extension than in compression for the normally consolidated specimen sheared from anisotropic stress conditions. This indicated that for K_0 -normally consolidated specimens, the stiffness was much higher in extension than in compression. In contrast to the anisotropic specimen, the deviator stress increments at $\epsilon_s = 1\%$ for isotropic specimens were equal both in compression and in extension. VAID and CAMPANELLA (1974) have also shown that the strain to peak deviator stress was much less in compression than in extension. The softening in compression was more pronounced for the anisotropically consolidated specimen than for the isotropically consolidated one under the same vertical consolidation pressure. Similarly, WIJEYAKULASURIYA (1986) observed that the softening was more pronounced for anisotropically consolidated specimens. Furthermore, these samples also failed at a lower strain level of 4%, while isotropically consolidated specimen failed at much higher strains. However, no softening was observed in extension conditions. Further, the principal effective stress ratio reached the same limiting values indicating a loss of anisotropy in the K_0 -consolidated specimens at large strains.

CROOKS and GRAHAM (1976) pointed out that samples consolidated anisotropically to axial stress well in excess of the preconsolidation pressure, p'_{max} , reached maximum deviator stress at less than 1% axial strain. On the contrary, samples which had been normally consolidated under isotropic stress conditions showed much higher strain at the maximum deviator stress.

It can be concluded that the anisotropically consolidated clay fails at small strain in triaxial compression, generally being in the order of 1% axial strain. Also strain softening is commonly exhibited in the anisotropically consolidated clay specimens.

2.3.3 Pore Pressure-Strain Relationships

It is generally known that the pore pressure generated during undrained shear is not a unique property of the soil, but it depends on the applied stress increments. The pore pressure can be split into two components, namely the shear induced pore pressure and the pore pressure due to the increase in the applied mean normal stress.

LADD (1965) illustrated that the normally consolidated clay under anisotropic stress conditions showed a lower pore pressure parameter, A , at small strains but a higher one at larger strains. This observation indicated the vertical rise-up of the undrained stress path at the initial loading stage followed by a drastic softening. The total amount of excess pore pressure, Δu , is reduced when it was compared with that of isotropically consolidated specimens, since a large portion of the stress difference was applied prior to the undrained shear due to anisotropic consolidation. CROOKS and GRAHAM (1976) have also shown that the isotropic consolidation resulted in higher values of A_f than those obtained from K_o -consolidated specimens. They employed an alternative parameter, $m = \Delta u / \Delta \sigma_{oct}$, which has been used for the prediction of the pore pressure by CLAUSEN (1969) and showed that the average value of the parameter, m , for the normally consolidated specimen under either anisotropic or isotropic consolidation was well in excess of unity, while m for the specimen consolidated to the approximate field stress state was close to unity. The value of m was also affected by the rate of strain during shear. On the contrary, PARRY and NADARAJAH (1973) noticed a sharp rise of pore pressure (significant decrease in p') during shearing on the K_o -normally consolidated specimens, and the pore pressure continually increased up to failure. They also stated that the normally consolidated specimen under K_o -conditions has a high degree of instability in undrained compression, and hence the high magnitude of the pore pressure parameter at failure, $A_f = 3.60$, compared with other specimens.

VAID and CAMPENELLA (1974) concluded that the maximum value of shear induced pore pressure was approximately the same for all types of tests regardless of stress paths, i.e., the pore pressure responses were primarily associated with the magnitude of the change in total mean normal stress.

HANDALI (1986) and BALASUBRAMANIAM et al. (1989) demonstrated that a linear relationship existed between the pore pressure, u , and the stress ratio, η , for normally consolidated clay under isotropic stress conditions, although some deviations in the early stage of the test were noticed. These authors showed that this linear relationship was valid even beyond the maximum deviator stress, and can be normalized with respect to the corresponding pre-shear consolidation stress, giving a unique curve. HANDALI (1986) confirmed this relationship by replotting the existing data on Bangkok clay. The existence of this linear variation of pore pressure versus stress ratio relationship was further confirmed from the data on other clays such as Drammen clay, Halloysite, Kaolin, Grundite clay, Lagunillas clay, and Boston Blue clay. From this relationship, he introduced a pore pressure parameter C , which denoted the slope of the $(u/p_o, \eta)$ line, as an alternative to Skempton's A -parameter during undrained shear. HANDALI (1986) emphasized that C can be considered as a material property dependent on $\bar{\phi}$, while A -value depends on the level of deviator stress. HANDALI (1986) further demonstrated that this parameter C can be successfully used for the formulation of the undrained stress path of normally consolidated clay under the conventional triaxial compression conditions. It was also pointed out, however, that the gradient of the linear variation was somewhat dependent on the rate of strain during undrained shearing.

In the case of the normally consolidated clay under an anisotropic stress condition, the $(u/p_o, \eta)$ relationship appeared to be bi-linear having a well defined transition point between two linear sections. The gradient of the first linear portion was dependent on the initial effective mean normal stress p_i (i.e., pre-shear consolidation stress), while the gradient of the second linear section was equal to that of isotropically consolidated samples. p_o used for the normalization was the magnitude of the consolidation stress corresponding to the stress on the isotropic consolidation line at the same void ratio. The normally consolidated clay under anisotropic stress conditions generally shows a significant strain-softening, and hence the same gradient of the second linear section as that of the isotropically consolidated sample is questionable. The relationships for normally and overconsolidated samples observed by HANDALI (1986) will be reviewed in Section 2.4.3

The undrained stress paths of K_o -normally consolidated clay in extension by KOUT-SOFTAS (1981) and HIGHT et al. (1987) clearly indicated that the development of excess pore pressure was relatively low until the major principal stress was rotated to the horizontal direction. However, they were expected to remain negative up to nearly the failure state. A different behaviour in which the excess pore pressure was continually increasing negatively was also reported (TAMPUBOLON, 1981; WIJEYAKULASURIYA, 1986) from the experimental data on Bangkok clay. Comparisons of the pore pressure response between compression and extension conditions are limited.

An equation for the pore pressure parameter A_f for the normally consolidated clay under isotropic stress conditions can be derived with the aid of the Critical State Soil Mechanics as :

$$A_f = \frac{1}{M} \left(\frac{1}{r} \right)^{-\Lambda} + \frac{M}{3} - 1 \quad \dots(2.4)$$

where, M : the slope of the Critical State Line in the (q, p) plot
 Λ : $(\lambda - \kappa) / \lambda$
 r : the spacing ratio ($r = 2$ for the Modified Cam Clay Model)

The values of r and Λ may depend on the type of clay. However, they result in merely scaling the ordinate axis appropriately, i.e., the shape of the curve would remain unchanged. MAYNE and STEWART (1988) proposed an equation of A_f as a function of overconsolidation ratio for the K_o -consolidated clays. For the normally consolidated state, by taking $OCR = 1.0$ and cohesion intercept $c = 0$, it reduces to :

$$A_f = \frac{1 - \sin \bar{\phi}}{\sin \bar{\phi}} \quad \dots(2.5)$$

This equation indicates that the A_f for the particular soil under K_o -normally consolidated state is constant. FEDERICO (1990) argued that the predictive accuracy of Eqn. 2.5 was very poor when its prediction was compared with the experimental data of SIVAKUGAN et al. (1988).

2.3.4 Strength Characteristics

(1) **Undrained Compression** - Some researchers (LADD, 1965; PARRY and NADARAJAH, 1973; VAID and CAMPANELLA, 1974; CROOKS and GRAHAM, 1976) have concluded that the normally consolidated clays under K_o and isotropic stress conditions have practically the same undrained strength ratio, $s_{uc}/\sqrt{\sigma_{vo}}$, in triaxial compression. LADD (1965) specified the variation of the undrained strength ratio as $\pm 15\%$. He mentioned, however, that it can be highly dependent on the type of total stress system applied during shear, hence the common assumption that the in-situ undrained strength is a constant along a curved failure surface is questionable. CROOKS and GRAHAM (1976) noticed that the isotropic consolidation generally resulted in slightly higher undrained strength ratio at the same vertical consolidation pressure. They explained that it probably resulted from less water content in isotropic specimens caused by the higher mean normal consolidation pressure.

Subsequent studies (MITACHI and KITAGO, 1979; NAKASE and KAMEI, 1983) suggested that the undrained strength ratio, $s_{uc}/\sqrt{\sigma_{vo}}$, was smaller for K_o -consolidated specimens compared with that of the isotropic ones. MAYNE (1985) found the general trend from a review of over 40 different clays consolidated under both isotropic and anisotropic conditions that the undrained strength ratio, $s_{uc}/\sqrt{\sigma_{vo}}$, for normally consolidated clays under anisotropic conditions averaged about 87% of the value for the isotropic specimens. WIJEYAKULASURIYA (1986) also found a similar value from the tests on undisturbed Bangkok clay, in which the undrained strength ratio under K_o condition was around 86% that of under isotropic conditions.

Related to strength parameters, LADD (1965) showed in the compression tests that $\bar{\phi}$ at maximum stress difference tends to decrease for K_o specimens, while $\bar{\phi}$ at maximum obliquity remained unchanged. This perhaps indicates that the frictional resistance is mobilized after elimination of anisotropy at large strains. MAYNE (1985) also reported the same trend. However, he concluded that the overall stress anisotropy appeared to have little effect on $\bar{\phi}$ ($\bar{\phi}$ from anisotropic tests was an average 97% of the value determined from isotropic tests for both compression and extension).

(2) **Undrained Extension** - LADD (1965) observed that the K_o -normally consolidated clay under extension conditions may have only half the undrained strength of identical specimens failed by compression. PARRY and NADARAJAH (1973) also reported that undrained strength ratio in extension conditions, $s_{ue}/\sqrt{\sigma_{vo}}$, for anisotropic specimens to be lower than that for other

types of tests. They attributed this lower value to the stress reversal during shear. The value of $\bar{\phi}$ for extension tests was observed to be markedly higher than the value of $\bar{\phi}$ for K_0 and isotropic compression or isotropic extension tests which are more or less comparable.

VAID and CAMPANELLA (1974) observed that the value of undrained strength ratio, $s_{ue}/\sqrt{\sigma_{vo}}$, under K_0 -triaxial extension was considerably lower than that for compression (about 63%). They reported, however, that the effective internal friction angle, $\bar{\phi}$, corresponding to the maximum principal effective stress ratio in extension was slightly greater (of the order of 3°) than in compression. MITACHI and KITAGO (1979) in their study on K_0 -consolidated remoulded clays also observed that $s_{ue}/\sqrt{\sigma_{vo}}$ for anisotropic samples were considerably lower than that for isotropic samples and hence $\bar{\phi}$ at peak deviator stress. NAKASE and KAMEI (1983) showed similar behaviour of K_0 -consolidated sandy clay. MAYNE (1985) quantitatively showed that anisotropic normalized strengths in triaxial extension averaged to about 60% of the isotropic strength for normally consolidated clays. Consequently, the isotropic extension tests seriously overestimate the anisotropic undrained strength of soft clays. Furthermore, studies which focused on the undrained behaviour of undisturbed Bangkok clay under extension conditions (TAMPUBOLON, 1981; WIJEYAKULASURIYA, 1986) also showed that $s_{ue}/\sqrt{\sigma_{vo}}$ for anisotropically consolidated samples were about 34% - 40% less when compared with those of the isotropically consolidated samples.

(3) Undrained Compression and Extension- The undrained strength characteristics of isotropically and K_0 -normally consolidated clay both in triaxial compression and in extension were reviewed by MITACHI and KITAGO (1979). They provided comparisons to indicate clearly that the compression resulted in a higher undrained strength ratio, $s_{uc}/\sqrt{\sigma_{vo}}$, than the extension irrespective of the initial consolidation stress. This trend was more prominent for the K_0 -consolidated clays. They also pointed out that the plasticity index played a more significant role in strength anisotropy than the stress system during shear. Generally, these differences of undrained strength ratio in compression and in extension were reduced with the increase in plasticity index, and approached to an identical value with increasing plasticity index. On the other hand, the effective friction angle, $\bar{\phi}$, in extension was slightly higher than those in compression, although half of the reviewed data showed nearly equal values in both stress systems.

TAMPUBOLON (1981) and HIGHT et al. (1987) reported a similar strength anisotropy, i.e., the compression resulted in a slightly higher strength than in extension for the isotropically and K_0 -consolidated clay, respectively. However, MITACHI and KITAGO (1979) and WIJEYAKULASURIYA (1986) observed a contradicting behaviour to the above statements from the isotropic and K_0 -consolidated compression and extension tests respectively. They observed rather a higher undrained strength in extension.

(4) Prediction of Strength - LADD (1965) stressed that the effects of K_0 -consolidation cannot be predicted from the results of isotropic tests, because the tests follow two different stress paths. However, the practical advantages of isotropic tests make it highly desirable to be able to accurately estimate the K_0 -consolidated undrained shear strength directly from isotropic

test results. Some recent research works revealed that a reasonably good estimation of K_0 -strength may be obtained from an isotropic test run on the same soil. Predictions of undrained strength ratio under triaxial compression will be briefly described below.

SKEMPTON (1957) suggested the equation of undrained strength ratio correlated with the plasticity index as follows :

$$\frac{s_{uc}}{\bar{\sigma}_{vo}} = 0.11 + 0.0037 I_p \quad \dots(2.6)$$

WROTH (1984) suggested the use of $\bar{\phi}$ instead of I_p even though $\bar{\phi}$ can be expected to depend on I_p . ATKINSON and BRANSBY (1978) showed that the undrained strength ratio, $s_{uc}/\bar{\sigma}_{vo}$, of normally consolidated clay is constant for any particular clay by assuming geometrically similar stress paths under undrained conditions and constant K_0 .

MAYNE (1980) reviewed the data from a total of 96 documented and published works found in the geotechnical literature and then compared observed soil behaviour under undrained conditions with predictions using the Critical State Concepts. He proposed Eqn. 2.7 for the normally consolidated clay and remarked that the prediction with Critical State Theory appears exceptionally good and on the conservative side.

$$\left(\frac{s_{uc}}{\bar{\sigma}_{vo}} \right) (N.C)_{experimental} = \alpha \left(\frac{s_{uc}}{\bar{\sigma}_{vo}} \right) (N.C)_{predicted} \quad \dots(2.7)$$

where α is a parameter obtained from the linear regression analysis on experimental data and the predicted value by theory. α is 1.123 and 1.076 for the isotropic stress conditions and the anisotropic stress conditions, respectively.

WROTH (1984) derived an expression for the prediction of undrained strength ratio by the Critical State Soil Mechanics. The undrained strength ratio of normally consolidated clays for triaxial compression under isotropic stress conditions is given as :

$$\frac{s_{uc}}{\bar{\sigma}_{vo}} = \frac{M}{2} \left(\frac{1}{r} \right)^\lambda \quad \dots(2.8)$$

where, M : the slope of the Critical State Line in the (q, p) plot
 r : the spacing ratio ($r = 2$ for the Modified Cam Clay Model)
 Λ : $(\lambda - \kappa) / \lambda$

WROTH (1984) suggested 2 and 0.8 as the reasonable approximate values of r and Λ , respectively. He extended this equation for the K_o -consolidated stress history and suggested the equation as :

$$\left(\frac{s_{uc}}{\sigma_{vo}} \right)_{K_o} \cong \frac{\sin \bar{\phi}}{2a} \left(\frac{a^2 + 1}{2} \right)^\Lambda \quad \dots(2.9)$$

$$\text{where, } a = \frac{3 - \sin \bar{\phi}}{2(3 - 2 \sin \bar{\phi})}$$

It is assumed in the derivation of Eqn. 2.9 that the State Boundary Surface is formed by the elliptical yield surface of Modified Cam Clay Theory, and the normally consolidated state and the anisotropic consolidation states lie on the same State Boundary Surface as for the isotropically consolidated samples. Thus, it is assumed that failure in both stress systems will occur at the Critical State with the same undrained strength as a normally consolidated specimen under isotropic stress at the same water content. However, because the initial stress states are different, the actual value of the undrained strength ratio for the anisotropic specimen will not be the same, and will depend on the shape of the State Boundary Surface as well as on the value of K_o .

MAYNE (1985) expressed the undrained strength ratio of normally consolidated clay from anisotropic and isotropic stress states under triaxial compression as:

$$\left(\frac{s_{uc}}{\sigma_{vo}} \right)_{anisotropic} = 0.88 \left(\frac{s_{uc}}{\sigma_{vo}} \right)_{isotropic} \quad \dots(2.10)$$

MAYNE (1985) also added that the data from the overconsolidated samples also showed the same relationship. He expressed the relationship between the normally consolidated strength ratio and the effective stress friction angle as:

$$\left(\frac{s_{uc}}{\sigma_{vo}} \right)_{isotropic} = 0.75 \sin \bar{\phi} \quad \dots(2.11)$$

$$\left(\frac{s_{uc}}{\bar{\sigma}_{vo}} \right)_{anisotropic} = 0.67 \sin \bar{\phi} \quad \dots(2.12)$$

SIVAKUGAN et al. (1988) derived the strength ratio between K_o -consolidated and isotropically consolidated clay from the Critical State Eqns. 2.8, 2.9 as :

$$\frac{(s_{uc}/\bar{\sigma}_{vo})_{K_o}}{(s_{uc}/\bar{\sigma}_{vo})_{isotropic}} = \frac{3 - 2 \sin \bar{\phi}}{3} (1 + a^2)^A \quad \dots(2.13)$$

He also proposed a similar relationship using Skempton's pore pressure parameter A and K_o as:

$$\frac{(s_{uc}/\bar{\sigma}_{vo})_{K_o}}{(s_{uc}/\bar{\sigma}_{vo})_{isotropic}} = \frac{K_o + 2(1 - K_o)}{K_o + 2(1 - K_o)} \frac{A_{f,i}}{A_{f,K_o}} \{A_{f,K_o} (1 - K_o) + K_o\} \quad \dots(2.14)$$

where, $A_{f,i}$: A parameter at failure for isotropic test
 A_{f,K_o} : A parameter at failure for anisotropic test
 K_o : coefficient of earth pressure at rest

He argued that using the Skempton's A parameter seems to be philosophically more appropriate to develop strength predictions based on triaxial tests rather than taking from time consuming consolidation tests. It was further shown that Eqn. 2.14 gives more realistic predictions than the values obtained with the Critical State Concepts.

2.3.5 Shear Strain Contours

ROSCOE and POOROOSHASB (1963) showed, from the experimental observations on Weald clay and London clay, that the constant shear strain contours are linear and passed through the origin, when they are superimposed on the effective stress paths. This ensured a unique normalizable relationship between stress ratio, η , and the shear strain ϵ_s . Subsequently, BALASUBRAMANIAM (1969, 1973) demonstrated that the load increment size and the magnitude of isotropic pre-shear stress did not have any effect on the (η , ϵ_s) relationships. LADD (1964) and LAMBE (1964) also showed similar plot which was earlier presented by ROSCOE and POOROOSHASB (1963) for 'Simple clay' and Boston Blue clay, respectively.

MITCHELL (1970) showed from isotropically consolidated triaxial compression tests that the undrained shear strain contours of normally consolidated clay formed a 'fan' of straight lines extending back to the origin of coordinates.

The research work done on the normally consolidated Bangkok clay confirmed the normalizable nature of the (η, ϵ_s) relationship (both in triaxial compression and in extension) under isotropic and K_0 -consolidation. CHAUDHRY (1975) found similar shear strain contours, during the undrained compression tests, to those reported by previous investigators. He further showed that these trends were also seen in the compression tests on the K_0 -normally consolidated samples by replotting the data from CHAIYADHUMA (1974). It was further shown that these contours of constant shear strain are straight lines and pass through the origin in the (q, p) plot in the case of fully drained triaxial compression tests. BALASUBRAMANIAM and UDDIN (1977) reported similar behaviour during triaxial undrained extension tests on normally consolidated specimens under isotropic pre-shear conditions.

2.4 Behaviour of Overconsolidated Clays

2.4.1 Undrained Stress Paths

The data on the behaviour of lightly overconsolidated clays sheared from K_0 conditions are somewhat limited. Most of the data reported on overconsolidated clays are concerned with the isotropic pre-shear conditions. Therefore, some aspects of the behaviour of overconsolidated clay under isotropic pre-shear conditions are also reviewed briefly in this section.

(1) **Overconsolidated Samples under Isotropic Stresses** - WROTH and LOUDON (1967) conducted a series of triaxial tests on sedimented and then overconsolidated Kaolin under isotropic pre-shear conditions. They demonstrated that the undrained stress paths for the normally consolidated samples formed a part of the boundary to the possible states of stress that can be experienced by such samples. Also, the undrained stress paths within the State Boundary Surface rose nearly vertical until they approached the State Boundary Surface and then reached the Critical State. The Critical State Soil Mechanics, which deals with the behaviour of soil sheared from an initially spherical stress condition, imply that the undrained stress paths of an overconsolidated clay will reach the same point at the Critical State Line as a normally consolidated sample with the same water content (SCHOFIELD and WROTH, 1968). This idea was not fully supported by the experimental data on overconsolidated clays. MITCHELL (1970) rather observed that the effective stress paths of cemented clay tested from isotropic stress conditions within a yield curve reached a portion of the failure envelope parallel to the p -axis and deviating from the Critical State Line.

YUDHBIR and VARADARAJAN (1974) carried out triaxial tests on reconstituted clay under normally and overconsolidated pre-shear isotropic conditions to study the effect of overconsolidation ratio on the stress-strain-pore pressure response. They found a range of critical

overconsolidation ratio (about 2.5 - 4.5) for which the pore pressure parameter A is strain independent. The effective stress path of the sample, therefore, in this case is linear and can be determined once the A value is known.

(2) **Overconsolidated Samples under K_o -conditions** - PARRY and NADARAJAH (1973) reported data from stress-controlled tests on remoulded Spestone Kaolin which were normally or lightly overconsolidated both under K_o and isotropic stress conditions. They demonstrated that the stress paths of specimens having the same overconsolidation ratios but different maximum consolidation pressures were geometrically similar. They also showed that for the K_o -consolidated specimen with an overconsolidation ratio of 2.6, when subsequently swelled back to isotropic stress states prior to shear, generated a substantially vertical undrained stress path in the (q, p) plot both in compression and in extension. The intermediate stress paths were transitional. They also showed that the stress paths within the State Boundary Surface were vertical (more pronounced for the anisotropic specimens) until they meet the yield surface. On reaching the volumetric yield curve, the stress path sharply bent and showed a distinct tendency to follow the yield curve. Thus, these authors pointed out how faithful the elasto-plastic behaviour of remoulded clay is as subjected to the basic idea of Cam Clay Model proposed by ROSCOE et al. (1963).

KOUTSOFTAS (1981) presented data on triaxial compression and extension tests under K_o -condition with overconsolidation ratios of 1, 2, 4 and 11. It was illustrated that the shape of the effective stress path changed from concave towards the origin of the (q, p) plot to convex as the overconsolidation ratio was increased. The undrained stress paths of the samples having overconsolidation ratios greater than 2.0 in triaxial compression tend to convex towards the origin, i.e., p' increases continuously during shear. Although the gradual transition of undrained stress paths, especially for those with an overconsolidation ratio less than two, was not made, the overconsolidated samples in compression showed a significant increase in the average effective stress, while the normally consolidated sample showed a large strain-softening behaviour. The increase in effective stress became more pronounced as the overconsolidation ratio was increased. The samples tested in triaxial extension, however, showed a reduction in effective stress, particularly significant for the normally consolidated samples. As the overconsolidation ratio increased, the reduction in effective stress became smaller. Eventually at an overconsolidation ratio greater than two, there was an increase in effective stress. Recently, HIGHT et al. (1987) presented the patterns of behaviour displayed by an overconsolidated young clay sample in triaxial compression and in extension. The overall shapes of the undrained stress paths of these overconsolidated samples were remarkably similar to those obtained by KOUTSOFTAS (1981). PENDER (1978) presented a formulation of this trend by assuming the parabolic undrained stress paths within the State Boundary Surface, i.e., for the overconsolidated behaviour of clays.

2.4.2 Stress-Strain Relationships

The remoulded clays and normally consolidated clays clearly demonstrate the nonlinearity of clay behaviour. On the contrary, it was reported that most natural clays were often stiffer and showed more linear behaviour in a certain range of loading. PARRY and NADARAJAH (1973) demonstrated that the stiffness (i.e., deviator stress increment Δq for a given strain $\epsilon_1 = 1\%$) of remoulded clay specimens with the isotropic consolidation was nearly the same in compression as it was in extension during the early stage of undrained loading. However, for K_0 -consolidated specimens, the stiffness was much higher in extension (more than five times) than in compression for the normally consolidated clay, but the trend was reversed for the lightly overconsolidated clay.

CROOK and GRAHAM (1976) showed that the stress-strain behaviour of samples consolidated isotropically under pressures less than the maximum past pressure, even at a stress below the overburden pressure, has no sharp break in p'_{\max} between the low compressibility and the high compressibility behaviour while those under anisotropic conditions exhibited a distinct change of rate when axial stresses exceeded p'_{\max} . It was also found that the samples which had been consolidated isotropically to stresses either above or below p'_{\max} showed much higher strains at maximum deviator stresses than those observed from the anisotropically consolidated samples.

KOUTSOFTAS (1981) conducted several triaxial compression and extension tests on the normally and overconsolidated samples under K_0 -conditions. These data revealed the anisotropy of K_0 -consolidated samples in many ways; (i) the samples in compression failed at very low axial strains especially at low overconsolidation ratios; (ii) the failure strains increased with increasing overconsolidation ratios; (iii) for those samples tested in extension, failure took place at larger strains; (iv) overconsolidated samples also showed strain-softening in compression, although those were not as pronounced as for normally consolidated samples. (v) On the contrary, the extension test specimens showed no tendency for strain-softening. KOUTSOFTAS (1981) also showed that the undrained secant moduli from compression tests were two to three times greater than the modulus determined from extension tests at corresponding incremental shear stress levels and overconsolidation ratios. The secant moduli were determined at an incremental shear stress level of one half the value at failure.

HIGHT et al. (1987) found similar stress-strain characteristics of K_0 -overconsolidated samples as presented by KOUTSOFTAS (1981). These authors found that stress-strain relationships were non-linear at all overconsolidation ratios and the lightly overconsolidated clay showed strain-softening in compression. As the overconsolidation ratio was increased, however, this softening behaviour was reduced and the strain mobilized at the peak strength increased. On the contrary, no samples with an overconsolidation ratio ranging from 1 to 8 showed strain-softening in extension tests. Generally, the secant moduli in compression decreased with increasing shear strains. The reduction in stiffness was more pronounced for strains less than 0.15%. Although the stress-strain characteristics for overconsolidation ratios of 1 and 1.5 were stiffer and similar in form, a continuous decrease in stiffness was observed with increasing

overconsolidation ratios from 2 to 10. In extension tests, the stiffness was initially high, especially for lightly overconsolidated samples ($OCR = 1$ and 2). For higher overconsolidation ratios, the stiffness in extension was considerably lower than the counterpart values in compression.

2.4.3 Pore Pressure-Strain Relationships

Previous research has shown that the pore pressure parameter at failure, A_f , decreased as the overconsolidation ratio is increased, and eventually the variation of A_f is significantly smaller at higher overconsolidation ratios as compared with its variation at low overconsolidation values. It was also noted that the value of A_f was generally dependent not only on the type of clay and its overconsolidation ratio, but also on the applied stress systems.

PARRY and NADARAJAH (1973) reported the results from a series of triaxial compression and extension tests on normally and lightly overconsolidated kaolin clay sheared both from isotropic and K_o -conditions. The relationship between A_f and the overconsolidation ratio for the isotropically consolidated samples both in compression and in extension was almost identical over the range of overconsolidation ratio close to 2.6. Up to an overconsolidation ratio of 1.25 the A_f values from the K_o -compression tests were much higher than those from the isotropic compression and extension tests, while A_f in K_o -extension was slightly less than those in both type of tests under isotropic conditions. For overconsolidation ratios higher than 1.25, the value of A_f from the K_o -compression test drop quickly to a constant value of 0.3. For overconsolidation ratios of 2.0 or greater, these values in the K_o -extension test changed little. Thus, A_f values in K_o -extension are higher than those observed in K_o -compression tests for the full range of overconsolidation ratio adopted. Similarly, KOUTSOFTAS (1981) also observed a rapid decrease in the value of A_f for K_o -overconsolidated samples as the overconsolidation ratio is increased. However, these values remained positive even for overconsolidation ratios up to 10. This observation agreed well with those made by NAKASE and KOBAYASHI (1971). Furthermore, KOUTSOFTAS (1981) reported that the values of A_f in extension were greater than the corresponding values from the compression tests. Similar trend was also shown by LADD et al. (1977).

A relationship for the shear strain, the OCR, and the A parameter for isotropically consolidated clay was suggested by YUDHBIR and VARADARAJAN (1974). These authors presented data from the conventional triaxial undrained compression tests on normally and overconsolidated clay sheared from isotropic stress conditions. The values of A at various levels of strains in the normally consolidated states converged to a lower strain-independent A value at an overconsolidation ratio termed as the 'critical overconsolidation ratio'. The critical overconsolidation ratio, which depends on the type of clay, separated the overconsolidation ratio into two zones; for overconsolidation ratios less than the critical value, A increases with the strain and for overconsolidation ratio greater than the critical value, A decreases with the strain. These authors emphasized the significance of the degree of overconsolidation on the stress-strain relationship.

(1) **Further Interpretations of Pore Pressures from Triaxial Tests - WROTH (1984)**
derived an expression for the pore pressure parameter A at failure (for a saturated clay with isotropic consolidation) under the framework of the Critical State Soil Mechanics as:

$$A_f = \frac{1}{M} \left\{ \left(\frac{R}{r} \right)^{-\Lambda} + \frac{M}{3} - 1 \right\} \quad \dots(2.15)$$

where, M : the slope of the Critical State Line in the (q, p) plot
 R : the overconsolidation ratio
 r : the spacing ratio ($r = 2$ for Modified Cam Clay Model)
 Λ : $(\lambda - \kappa)/\lambda$

WROTH (1984) confirmed the validity of this equation for a remoulded low plasticity clay by a comparison of the prediction from Eqn. 2.15 ($\Lambda \approx 0.8$, $r \approx 2$) and the experimental data on Weald clay as reported by BISHOP and HENKEL (1957).

MAYNE and STEWART (1988) presented the overall trend of A_f value from anisotropically and isotropically consolidated samples. These authors have shown that the A_f values of anisotropically consolidated sample tend to be asymptotic to zero at higher overconsolidation ratios, while those A_f values for isotropically consolidated clay became negative for overconsolidation ratios of 4 to 6. Using Critical State Soil Mechanics and the undrained strength ratio and K_o with the overconsolidation ratios, A_f (see MAYNE and KULHAWY, 1982; MAYNE, 1988) can be expressed as:

$$A_f = \frac{(1 - \sin \bar{\phi}) \left(OCR^{\sin \bar{\phi}} - \frac{2}{3} OCR^{\Lambda} \right) + (c/\sigma_{\max}) (OCR / \tan \bar{\phi})}{(1 - \sin \bar{\phi}) OCR^{\sin \bar{\phi}} + \frac{4}{3} \sin \bar{\phi} OCR^{\Lambda} - 1} \quad \dots(2.16)$$

where $\Lambda = (\lambda - \kappa) / \lambda$. FEDERICO (1990) showed that because of the approximations used in the derivation of Eqn. 2.16, its use only appears justifiable for a first-order estimation of A_f . This author further emphasized that the predictive accuracy in the case of normally consolidated clay was poor.

(2) **Handali's Formulation of Pore Pressures-** HANDALI (1986) found (as described in Section 2.3.3) that for normally consolidated clay sheared from isotropic conditions, a linear relationship existed between u/p_o and η , while for anisotropic pre-shear conditions, the relationships was bi-linear. The p_o value used in the ratio u/p_o for the anisotropically consolidated sample was the same as the pre-shear consolidation pressure of an isotropic sample having the same void ratio as the anisotropic sample.

HANDALI (1986) also normalized all excess pore pressures, u , measured from undrained tests of the overconsolidated samples with respect to the pre-shear consolidation pressure of normally consolidated samples instead of normalizing them with respect to their individual pre-shear consolidation stress. In other words, the points of reference for normalization of the excess pore pressure of overconsolidated samples were taken as the same as the pre-shear consolidation pressure of the normally consolidated sample with the same void ratio. In contrast with the normally consolidated specimen, the overconsolidated specimens sheared from the isotropic conditions produced a bi-linear relationship of $(u/p_o, \eta)$ with a well defined transition point. The stress ratio at the transition point increased as the overconsolidation ratio was increased. The gradient of the first linear section was found to depend on the overconsolidation ratio, i.e., it decreased with increasing overconsolidation ratio. The second linear section, however, appeared to have the same gradient as that of the normally consolidated sample. HANDALI (1986) found that the second linear sections for the overconsolidated specimens merged with that of the normally consolidated sample when the bi-linear relationship for the overconsolidated specimens were shifted as much as $\Delta p_{on}/p_o$ in the direction of u/p_o (where Δp_{on} is the difference between the pre-shear consolidation stress of the normally consolidated sample and the corresponding overconsolidated specimen). HANDALI (1986) noticed that there were some deviations from the usual first linear characteristics of the $(u/p_o, \eta)$ relationship in heavily overconsolidated samples. MONOI (1989) showed that the heavily overconsolidated samples ($OCR > 4.0$) have a bi-linear relationship between pore pressure and stress ratio. However, the transition points of these bi-linear relationships do not lie on the same curve as that of the normally consolidated sample. MONOI (1989) also concluded that the gradient of the second linear section of the $(u/p_o, \eta)$ relationship of heavily overconsolidated samples is constant, and is different from that of the normally consolidated sample.

As an extension of pore pressure-stress ratio relationship, HANDALI introduced a new way of interpreting test results using an (α, β) plot as illustrated in Figs. 2.1a and 2.1b. This plot was attempted in order to establish a simple relationship between the gradient of the first linear section of a bi-linear $(u/p_o, \eta)$ plot and the corresponding initial mean normal stress p_i . Hence the full range of an undrained stress path starting from p_i can be formulated once the slope of the first linear section of the $(u/p_o, \eta)$ plot is obtained from this (α, β) plot. Two dimensionless parameters α and β were defined as :

$$\alpha = \frac{C_i - C_e}{C_0 - C_e} \quad \dots(2.17)$$

$$\text{for } p_i > p_f \quad \beta = (p_i - p_f)/(p_0 - p_f) \quad \dots(2.18a)$$

$$\text{for } p_i < p_f \quad \beta = (p_i - p_f)/(p_f) \quad \dots(2.18b)$$

where, C_o : the slope of the (u, η) relationship for the normally consolidated samples sheared from the isotropic stress
 C_i : the slope of the (u, η) relationship of samples sheared from p_i
 C_e : the slope of the (u, η) relationship of samples sheared from p_f
 p_o : the pre-shear isotropic stress for normally consolidated samples
 p_f : the p value corresponding to peak deviator stress of normally consolidated samples sheared from isotropic stress
 p_i : the pre-shear consolidation stress sheared from other than the p_o states

It should be noted here that C_e was obtained based on the assumption that the undrained stress path of a sample sheared from a pre-shear consolidation pressure of p_f move upward in the (q, p) plot parallel to the q -axis. Therefore, the value of C_e was equal to $p_f/3$. Consequently, the linear (α, β) relationship appeared to be shifted slightly from the origin.

HANDALI (1986) demonstrated that the first linear section in the $(u/p_o, \eta)$ relationship of all data such as from the overconsolidated and the normally consolidated clays both under isotropic and anisotropic consolidations fell on a straight line passing through the origin in the (α, β) plot as shown in Fig. 2.1b. He also concluded from this relationship that at any p_i the stress paths were geometrically similar with each other and thus, the C_i/p_o and p_i relationship was unique regardless of the initial stress state and the stress history. Using the (α, β) plot for a certain clay, it was possible to generate a family of undrained stress paths of overconsolidated samples in the triaxial compression tests.

2.4.4 Strength Characteristics

The undrained strength of normally consolidated clays is known to increase with the consolidation pressure. However, the change in the undrained strength was observed to be small for lightly overconsolidated clay with an overconsolidation ratio less than 2.6 (PARRY and NADARAJAH, 1973). This was particularly true for the K_o -consolidated samples. This indicates that no significant increase in shear strength with increasing consolidation pressure can be expected in lightly overconsolidated samples until they reached the normally consolidated state. Similarly, HIGHT et al. (1987) reported that the undrained strength ratio was reduced with the increase in overconsolidation ratio, especially on lightly consolidated samples ($OCR < 2.0$), when those values were normalized with respect to the vertical preconsolidation pressure. These observations indicated that the failure points of four lightly overconsolidated samples were closely located to each other (preferably close to the Critical State) in the stress space. On

the contrary, the normalized undrained strength ratio with respect to vertical pre-shear consolidation pressure increased with increasing overconsolidation ratio (YUDHBIR and VARADARAJAN, 1974; LADD et al., 1977; KOUTSOFTAS, 1981; HIGHT et al., 1987). The increase being pronounced at the higher value of the overconsolidation ratio. This tendency is due to a significant increase in the effective stress during shear of the overconsolidated samples as reviewed earlier in Section 2.4.1.

The anisotropy of undrained strength between compression and extension was also demonstrated by several investigators. Recently, HIGHT et al. (1987) demonstrated that the undrained strength was significantly lower in triaxial extension than in triaxial compression. They observed, however, that the undrained strength ratio between extension and compression, s_{ue}/s_{uc} , increased only marginally with the increase in overconsolidation ratio, especially for the lightly overconsolidated samples. In the case of compression tests, peak strengths were mobilized at lower stress ratio, η , than the ultimate strengths. The difference between those values, however, decreased with the increase in overconsolidation ratio. Eventually the stress ratio mobilized at the ultimate state was independent of the overconsolidation ratio. Similar trend was also reported by KOUTSOFTAS (1981). The latter author found that the effective stress envelope at the maximum obliquity in triaxial compression was represented by a straight line with a small cohesion intercept, while that at the maximum shear stress appeared to be curved with a lower stress ratio. For the extension tests, a single straight line fits the test data both at the maximum obliquity and at the maximum shear stress.

The effect of soil structure on the strength characteristics was reported by CROOKS and GRAHAM (1976). They observed that the newly formed structure of soil by anisotropic consolidation in the laboratory to axial stresses greater than the apparent preconsolidation pressure did not possess the reserve resistance developed by the processes which induce overconsolidation during the geological life of the deposit. As a result, the value of the undrained strength ratio corresponding to the normally consolidated state was lower than the value measured on samples which had been reconsolidated to in-situ stresses. The ratio of these two values of $s_{uc}/\bar{\sigma}_{vo}$ can, therefore, be related to the degree of overconsolidation in the field.

(1) **Undrained Strength of Overconsolidated Clay** - LADD et al. (1977) have drawn a relationship between undrained strength ratio and overconsolidation ratio from direct simple shear tests as :

$$\frac{(s_{uc}/\bar{\sigma}_{vo})_{O.C}}{(s_{uc}/\bar{\sigma}_{vo})_{N.C}} = OCR^m \quad \dots(2.19)$$

with $m=0.8$, though a better fit was observed if m was decreased from 0.85 to 0.75 with the increasing overconsolidation ratio. This finding, which was solely based on empiricism, was confirmed by the Critical State Soil Mechanics Theory. KOUTSOFTAS (1981) confirmed this

relationship by showing that the value of m varies from 0.80 to 0.85. OHTA and NISHIHARA (1985) also postulated that Eqn. 2.19 was valid for K_o -consolidated clays. However, the value of m appeared to be about 10% larger for isotropically consolidated clays.

WROTH (1984) derived an expression of undrained strength ratio for overconsolidated samples with the aid of Critical State Soil Mechanics as :

$$\frac{(s_{uc}/\bar{\sigma}_{vo})_{O.C}}{(s_{uc}/\bar{\sigma}_{vo})_{N.C}} = R^\Lambda \quad \dots(2.20)$$

where R is an overconsolidation ratio and Λ is $(\lambda - \kappa)/\lambda$. He showed that the prediction made from Eqn. 2.20 with $\Lambda \approx 0.8$ coincided well with the experimental data. This expression is, in fact, strictly valid for isotropic pre-shear consolidation. ATKINSON and BRANSBY (1978) have derived a similar expression that includes the effects of K_o .

MAYNE (1980) determined the parameter Λ in Eqn. 2.20 from a knowledge of strength at various levels of overconsolidation ratio. He found that Λ was essentially constant with the overconsolidation ratio, and proposed an equation for Λ as :

$$\Lambda = \frac{\log(s_{uc}/\bar{\sigma}_{vo})_{O.C} - \log(s_{uc}/\bar{\sigma}_{vo})_{N.C}}{\log(OCR)} \quad \dots(2.21)$$

It has also been shown that Λ is essentially the same for isotropic and anisotropic tests (MAYNE and SWANSON, 1981; MITACHI and KITAGO, 1979). MAYNE (1980) concluded that although Eqn. 2.20 was originally developed for isotropically consolidated clay, the same approach can give estimates of undrained strength for anisotropically consolidated clay as well.

2.4.5 Shear Strain Contours

The pattern of the shear strain contours within the State Boundary Surface is reported to be governed by an initial stress history; the contours from isotropic pre-shear consolidation samples are different from those obtained from the K_o -consolidated samples. Furthermore, there are substantial evidence to the path-dependent stress-strain behaviour within the State Boundary Surface (e.g., BALASUBRAMANIAM, 1969, 1975).

(1) **Shear Strain Contours of Isotropically Overconsolidated Samples-** WROTH and LOUDON (1967) presented data from undrained triaxial compression tests on overconsolidated clays under isotropic stress conditions. They observed that the equal shear strain contours on

the wet side of the Critical State Line were all nearly parallel with the p-axis when they were superimposed in the (q, p) plot. However, on the dry side of the Critical State the contours formed a fan of straight lines which all appeared to pass through one point ($p/p_e = -0.13$, $q/p_e = 0$) instead of passing through the origin (see Fig. 2.2). Furthermore, they concluded that these contours can be considered not as one of total strain, but as contours of increments of shear strain. These authors showed the evidence of this statement by plotting the increments of shear strain as taken from a fresh datum coinciding with the zero value of q during cyclic loading and unloading tests on an initially normally consolidated sample. These contours agreed well with those obtained from initially overconsolidated samples. Thus, as long as the increments of shear strain are adopted as a significant parameter, the present state of stress and current stress increment control the behaviour of the sample and the next strain increment. Also, the spacing of the contours clearly depended on the level of the stress, as to being closer or away from the Critical State Line. This finding was subsequently used in the formulation of the Revised Theory by ROSCOE and BURLAND (1968).

A more detailed investigation of the stress-strain behaviour on Kaolin samples as tested from the isotropic stress state was reported by BALASUBRAMANIAM (1969, 1975). He showed that the strain contours were dependent on the stress paths followed by the samples for states below the State Boundary Surface. However, he observed that the pattern of the shear strain contours was similar to those obtained by WROTH and LOUDON (1967) irrespective of drainage conditions. Furthermore, he commented that the shear strain contour corresponding to 0.5% was approximately halfway between the p-axis and the Hvorslev failure envelope.

Subsequently, MITCHELL (1970) also presented a similar pattern of the shear strain contours to those suggested by WROTH and LOUDON (1967). He also stated that these strain contours from the conventional drained and undrained tests were close to each other inside the State Boundary Surface. These observations are in agreement with those made by BALASUBRAMANIAM (1969, 1975). However, the shear strain contours from the p-constant tests of MITCHELL (1970) tend to concave with respect to the p-axis. The higher strain contours are more concaved than the lower ones. Thus, the pattern of the contours on the wet side of the Critical State from the p-constant tests are different in shapes to those of WROTH and LOUDON (1967) and BALASUBRAMANIAM (1969), while those on the dry side of the Critical State tend to show similar patterns. As concluding remarks, MITCHELL (1970) attributed these difference to the anisotropy of the clay samples. PARRY and NADARAJAH (1973) also illustrated that the shear strain contours of overconsolidated clay ($(OCR)_{max} = 2.0$) under the isotropic stress appeared to be parallel to the p-axis at low strains. However, these became sub-parallel with the failure envelopes as failure was approached. The overall patterns of the shear strain contours in the lightly overconsolidated region under isotropic stress condition tend to be concave in shapes with respect to the $q = 0$ axis, and this tendency increased as failure was approached.

Surprisingly, similar patterns of shear strain contours were found in the triaxial extension tests of UDDIN (1975) for the overconsolidated samples of Bangkok clay tested under pre-consolidation pressure far greater than the in-situ values. However, in the apparent overconsolidated range where the consolidation stresses were less than the maximum past pressure, the

constant shear strain contours formed curved lines which tend to be slightly convex to the p-axis, but were somewhat parallel (see BALASUBRAMANIAM and UDDIN, 1977). At higher strains, the contours became more curved as the consolidation stresses increase.

(2) **Shear Strain Contours of K_0 -overconsolidated Samples** - PARRY and NADARAJAH (1973) illustrated that the shear strain contours of overconsolidated clay ($OCR < 2.6$) under the K_0 pre-shear conditions tend to be parallel to the K_0 -line both in compression and in extension. The constant strain contours were curved and were parallel to each other. They were spaced approximately in a logarithmic manner with increasing strains. PARRY and NADARAJAH (1973) mentioned that these trends were similar to those obtained from the tests run on K_0 -consolidated Weald clay by HENKEL and SOWA (1963).

Recently, HIGHT et al. (1987) presented three sets of shear strain contours for the K_0 -overconsolidated clays both in compression and in extension. Each clay showed similar pattern of shear strain contours to those presented by PARRY and NADARAJAH (1973). The contours were curved and parallel to the K_0 -swelling path with logarithmic spacing. Generally, the overconsolidated samples behaved relatively rigidly under distortion within the State Boundary Surface.

2.5 Yield Locus of Natural Clays

2.5.1 Evidence of Yielding on Natural Clays

The concept of yield surface, initially developed by the Cambridge Group, has been shown to apply to natural clays (MITCHELL, 1970; CROOKS and GRAHAM, 1976; TAVENAS and LEROUEIL, 1977) although the shape of the yield loci were significantly different from each other. MITCHELL (1970) demonstrated an overall picture of the yield locus in the stress space based on the results obtained from a series of triaxial tests run on undisturbed Leda clay. Subsequently, several investigators (e.g., TAVENAS and LEROUEIL, 1977; GRAHAM et al., 1983) have confirmed the existence of the yield locus for undisturbed natural clays. The pre-consolidation pressure defined during the consolidation process is an important example of the yield. The yield state at each of the different stress ratios formed a locus, the so-called 'yield locus' in the stress space which separates relatively stiff, pseudo-elastic pre-yield behaviour from the larger strains, the pore pressures and the dissipation times that accompany post-yield behaviour. The application of the concept of yielding allows a clear identification of the parameters governing the mechanical behaviour of natural clays and leads to an integrated description of all aspects of this behaviour. The shape and magnitude of the yield loci of clays depend on their composition, anisotropy and stress history (GRAHAM et al., 1988). Consequently, a comprehensive understanding of the yield characteristics of natural clay deposit is an essential factor in the engineering practice (e.g., FOLKES and CROOKS, 1985).

2.5.2 Techniques for Estimation of Yield Locus

The techniques used for evaluating yield states must be partly empirical. Their limitations, therefore, are to be thoroughly understood in order not to be led to spurious conclusions. Generally, graphical techniques are used to identify a yield point. In most cases, sudden change of stiffness in an appropriate stress-strain plot such as σ_1 vs. ϵ_1 , p' vs. ϵ_v , q vs. ϵ_s , σ_3 vs. ϵ_3 , and the energy absorption per unit volume versus the length of stress vector (GRAHAM et al., 1983). TAVENAS et al. (1979) showed for undisturbed lightly overconsolidated clay that the strain energy can be used with the advantage to define the limit state (i.e., the yield state). Triaxial stress-controlled drained tests showed that a clear discontinuity in the energy-stress relationship exists for all possible stress paths. GRAHAM et al. (1983) showed that the yield values obtained from the various graphical techniques mentioned earlier were remarkably similar. LEONARDS et al. (1981) suggested also that the volumetric and distortional yield loci are identical when the consistent concept of yielding is defined.

GRAHAM et al. (1988) postulated that the fitting of the observed stress-strain results with two straight lines in arithmetic scale was acceptable in a variety of natural clays over a measurable range of post-yield strain. At larger strains the behaviour reverts to the usual exponential plastic strain hardening behaviour. When soils undergo a large amount of plastic strain hardening, the behaviour linearizes in log-log plots (HOULSBY et al., 1982).

2.5.3 Geometric Properties of Yield Locus

The shapes of yield locus have shown to play an important role in the stress-strain theories. The yield locus adopted in the Critical State Theories is centered on the isotropic axis. However, a large number of experimental data obtained from natural clays, notably by the Canadian groups, have failed to support the yield locus based on isotropic pre-shear consolidation state. MITCHELL (1970) and WONG and MITCHELL (1975) presented data on the shape of the yield loci both in compression and in extension. They concluded that the yield loci were independent of the stress paths. These yield loci indicated an asymmetry about the isotropic axis.

Some elaborate research work confirmed that the yield locus of natural clay to be elliptical, and to be centered along the K_0 -line for the normally consolidated clay in the s' - t' stress space (MIT plot), wherein the major effective principal stress acts in the vertical direction (CROOKS and GRAHAM, 1976; TAVENAS and LEROUEIL, 1977; JAMIOLKOWSKI et al., 1985). This implies that the yield stress for isotropic condition is significantly less than the past maximum pressure. GRAHAM et al. (1988), however, showed that this symmetric nature of yield locus along the K_0 -line was not exhibited in the p' - q stress space (Cambridge plot). The symmetry can be shown to depend upon the definition of the stress parameter.

GRAHAM et al. (1983) presented data from a series of tests on undisturbed samples taken from four different depths. Each sample was consolidated to the in-situ stress, and then sheared along various stress paths. These authors found that the yield loci increased in size as the preconsolidation pressure increased and can be normalized with respect to the preconsolidation pressure to a single locus. Its shape was approximately elliptical and symmetrical about the K_0 -line. This asymmetry from the isotropic stress axis seems to be a common feature of natural clays reflecting the anisotropy of the clay induced by stress history. GRAHAM and LI (1985) showed that resedimented samples under anisotropic stress conditions displayed a yield locus similar to those of the undisturbed field samples.

The Critical State Concept assumed that the yield locus coincides with the undrained stress path when the swelling index κ is assumed to be zero. A large amount of experimental data on normally consolidated clay appeared to agree reasonably well with this approximation. BALASUBRAMANIAM and HWANG (1980) also mentioned that the volumetric yield locus was very similar to the undrained stress path on normally consolidated specimens of Weathered Bangkok clay when tested from the isotropic consolidation pressure. JAMIOLKOWSKI et al. (1985) reported that the yield envelope for resedimented Boston Blue clay can be defined from the effective stress paths of K_0 -compression and extension tests on normally consolidated clay and the large strain Mohr-Coulomb strength envelope. However, GRAHAM et al. (1988) noted that the specific volume traces during the drained state were elliptical and were closer in shape to the volumetric yield loci adopted in the simple Modified Cam Clay Theory, while the yield loci were not elliptical (i.e., the hydrostatic yield stress was not the largest value of the yield stress as shown in Fig. 2.3). These yield loci, however, appeared to be similar to the constant volume trace when they were normalized by the equivalent pressure p_e at the same specific volume on the K_0 -normal consolidation line corresponding to the value of p' , q at yield. Thus, the in-situ stress induced anisotropy can be somewhat erased in this proposed normalized plot.

Some authors investigated the effects of destructuration on the shape of the yield locus. LEROUEIL et al. (1979) concluded that the destructuration of a clay with a consolidation pressure greater than the preconsolidation pressure in the field produced reorientation of the yield locus. They demonstrated further that the yield locus for the destructured clay had the same shape as that for the intact clay. However, in the case of K_0 value in excess of 0.55, yielding occurs at stresses in excess of those observed in the intact clay. Thus, the yield locus of destructured clay swing to the right and become parallel to the q -axis in this region. The new shape was then maintained during further consolidation under higher stresses. JAMIOLKOWSKI et al. (1985) illustrated that the yield envelope of destructured clay was enclosed by that for the intact clay, i.e., the destructured clay yielded at lower stress levels. Nevertheless, it is interesting to note the conclusion drawn by GRAHAM and LI (1985) that many of the conceptual features of the Critical State Soil Mechanics apply equally to both natural and remoulded clays. The difference appears to be in the details and not in the principles.

2.5.4 Direction of Plastic Strain Increment Vectors and the Yield Locus

An important feature of continuum mechanics analyses for post-yield straining is that the direction of the plastic strain increment vectors being dependent on the absolute stress level at yielding, and not on the incremental stress change. The 'normality rule' postulates that irrespective of the stress increment vector which takes the sample beyond yield, the corresponding plastic strain increment vector should be normal to the yield surface. However, most soils appear not to conform precisely to the associated flow rule in view of the experimental data.

It is common to plot the plastic strain increment vector by aligning the volumetric and distortional component with the p' and the q -axis, respectively. GRAHAM et al. (1983) illustrated a technique for obtaining the strain increment ratio for the anisotropic clay. In order to obtain the plastic strain increment ratio, the elastic component must be subtracted from the measured total strains. On the contrary, WONG and MITCHELL (1975) was satisfied in assuming the plastic strain increment to be equal to the total strain increment without incurring serious error. If normality is observed, then the yield locus becomes a plastic potential for the soil. These authors then developed a plasticity theory describing the post-yield stress-strain behaviour of cemented clay based on an experimentally defined non-associated flow rule. GRAHAM et al. (1983) demonstrated that the plastic potential was broadly identical with the yield locus, i.e., deviation from the normality may not be large, in the region where the maximum principal stress was in the vertical direction. After close examination, however, the authors concluded that the normality rule was not strictly applicable to the Winnipeg clay.

2.6 Anisotropic Elasticity of Natural Clays

Clays are known to be non-linear materials. Many conceptual models for soil behaviour are strongly influenced by this understanding. A wide range of natural clays, mostly existing in the lightly overconsolidated state, have exhibited a substantial linear stress-strain behaviour prior to yield. It is, however, noticed that the strains are not fully recoverable, so this behaviour is usually characterized as pseudo-elastic behaviour. GRAHAM et al. (1983) reported that the pseudo-elastic bulk and shear moduli obtained from the pre-yield linear behaviour were not constant, but depended on the applied stress paths. LEROUEIL et al. (1979) have noted that the bulk modulus K and the shear modulus G are both functions of stresses.

TAVENAS and LEROUEIL (1979) postulated that the deformation behaviour of a natural overconsolidated clay cannot be expressed by a simple application of the theory of elasticity. Rather the volumetric and shear strains are functions of the orientation of the effective stress path in the stress space, and of the distance of the initial and final effective stress conditions to the limit state along this stress path.

GRAHAM and HOULSBY (1983) provided mathematical techniques for describing the pre-yield mechanical properties of clays using anisotropic elasticity. The form of anisotropy presented was a limited form of transverse isotropy. The anisotropy of soil was introduced by multiplying the stiffness coefficient, α , to the stiffness matrix for an isotropic material. Obviously α is unity for the isotropic material. For $\alpha > 1$, the material is stiffer horizontally than vertically and for $\alpha < 1$, the material is stiffer vertically than horizontally. They matched this stiffness matrix to the triaxial counterparts so that three (i.e., bulk and shear moduli, and cross modulus) anisotropic elastic parameters can be obtained based on experimental observations. These authors used the least square technique to minimize the random error of test data, and found that the anisotropic moduli resulted in considerable improvement in the prediction of strains compared with those made with the isotropic moduli.

2.7 Time-dependent Behaviour of Natural Clays

Following the identification by BUISMAN (1936) of the existence of 'secular settlements' that would increase linearly with the logarithm of time, TAYLOR (1942) developed a conceptual description of time effects on the deformation and strength behaviour of clays. This principle has been confirmed experimentally by several investigators (CRAWFORD, 1964; BJERRUM, 1967; TAVENAS and LEROUEIL, 1977).

BJERRUM (1973) had shown the effects of ageing of natural clays. One of the important sequences of this phenomenon for the aged clay is the development with time of 'bond' (TAYLOR, 1942) or a 'reserve resistance' (BJERRUM, 1967). More generally, as suggested by BURLAND (1971), the ageing would cause not only an increase in preconsolidation pressure, but also a homothetic displacement of the entire yield locus of clay. TAVENAS and LEROUEIL (1977) reported that the yield loci for St-Alban clay which is known to have developed its quasi-preconsolidation only from ageing are well centered on the K_0 line of the normally consolidated young St-Alban clay.

Some test results demonstrated that the preconsolidation pressure and undrained strength of clay varies with the strain rate or the duration of load application, i.e., the limit state has significant time dependency (RICHARDSON and WHITMAN, 1963; CRAWFORD, 1964; BJERRUM, 1967; CROOKS and GRAHAM, 1976; VAID et al., 1979; GRAHAM et al., 1983). All test results obtained from the remoulded and the naturally occurring sensitive clay showed that both preconsolidation pressure and undrained strength increase with increasing strain rate. Similarly, laboratory tests on a wide variety of lightly overconsolidated natural clays show that the yield loci are time dependent, and contract in the (q, p) stress space with increasing time to yield state (TAVENAS and LEROUEIL, 1977; TAVENAS et al., 1978; BARACOS et al., 1980). LO and MORIN (1972) also reported a similar time effect in which the displacement of the strength loci due to the change in the strain is more or less homothetic. BROWN (1969) showed, however, that the strain rate effect decreases significantly with increasing strain.

TAVENAS and LEROUEIL (1977) have proposed the YLIGHT model to describe the time dependent behaviour of natural clay, in which the soil behaviour is classified according to the history of consolidation and subsequent loading (e.g., the stress space is divided into five zones). This model accommodates the concept of Critical State Soil Mechanics and the findings of BJERRUM regarding the effects of ageing and strain rate on clay.

2.8 Concluding Remarks and Comments

The extensive coverage made in this chapter on the work of a limited number of researchers emphasizes the need for a comprehensive experimental study to be made on the behaviour of Bangkok clays in order to investigate the engineering behaviour of K_0 consolidated samples and to compare it with that from the isotropically consolidated ones. It also emphasizes the need to study the behaviour of K_0 consolidated samples under a variety of applied stress paths in order to pin down the essential behaviour under the State Boundary Surface. Perhaps, the briefest conclusion could be that drawn by GRAHAM and LI (1985) that "many of the conceptual features of the Critical State Soil Mechanics apply equally to both natural and remoulded clays. The difference appears to be in details not in the principles". Accepting this broad statement the following summary is made on the literature reviewed in this chapter.

2.8.1 Behaviour of Resedimented Specimens of Kaolin

Most of the data on the resedimented samples of Kaolin with little time effects do indicate that the behaviour of isotropic and anisotropically consolidated samples are the same for a first order of acceptance. The Critical State Soil Mechanics framework can explain most of the behaviour and the associated stress - strain theories can be expected to predict the behaviour of normally consolidated samples when they are subjected to monotonically increasing stress paths both in compression and in extension when the state paths lie on the State Boundary Surface. However, for stress paths below the State Boundary Surface, the constant q yield loci of ROSCOE and BURLAND (1968) and the shear strain contours of WROTH and LOUDON (1967) are applicable for the undrained behaviour. Additional investigation on the volumetric yielding and the flow rule is needed of all types of drained behaviour for stress states below the State Boundary Surface.

2.8.2 Behaviour of Remoulded and Natural Clays

The behaviour of remoulded and natural clays, especially the work of LADD and of Canadian researchers, does indicate that anisotropically consolidated behaviour deviates from the isotropically consolidated one, though the extent of differences depends on many factors, notably the time effects and the secondary consolidation prior to shear. As such, especially for natural clays, the Critical State Concepts and the associated ideas need systematic investigation and suitable simple modifications. Thus, there is a need to carry out a comprehensive study on

the K_0 consolidated behaviour of normally consolidated and overconsolidated Bangkok clays and attempt to accommodate such behaviour within the simple framework of the Critical State theories.

The yield loci traditionally determined by the researchers whose work is reported here is found to coincide with the volumetric yield locus of the type for which the stress states lie on the State Boundary Surface. This phenomenon is inherent in the methods adopted by almost all researchers to determine the yield points in a graphical manner which is similar to the determination of the maximum past pressure in an Oedometer test which has been practised for several decades.

Thus, the true determination of the volumetric yield loci beneath the State Boundary Surface can only be made by ascertaining the fact that plastic volumetric strain is zero or as close to zero as we can measure accurately with our testing devices. Attempts be made to determine such plastic volumetric yield loci inside the State Boundary Surface.

III REVIEW OF THE STRESS-STRAIN THEORIES AS BASED ON THE CRITICAL STATE CONCEPTS

3.1 Introduction

The Critical State Concept and the State Boundary Surface were proposed as early as 1958 by ROSCOE, SCHOFIELD and WROTH. The idea came from the constant void ratio contours of RENDULIC (1936), the critical void ratio and the liquefaction aspects of sand as proposed by CASAGRANDE (1938) and TAYLOR (1948) as well as the Hvorslev Failure Envelope.

The Cam Clay Theory accepts volumetric yielding only for stress paths for which the state paths lie on the State Boundary Surface (SBS). Such volumetric yielding is associated with a set of volumetric yield loci with stress states on the SBS. The normality rule is assumed to be obeyed by these volumetric yield loci and the energy dissipated in plastic distortion is purely governed by the Critical State parameter M . Especially in the Cam Clay Theory, no explicit energy dissipation is allowed for in the plastic volumetric strain. For states below the SBS, this theory only accepts elastic volumetric strains and is rigid in distortional strains. The elastic distortional strain within the SBS is also neglected.

These concepts, which were subsequently modified by ROSCOE and BURLAND (1968), allow energy dissipation in both plastic volumetric and distortional strains. They also allowed plastic distortional strains to take place inside the SBS by the use of a set of constant q yield loci, each set being associated with one volumetric yield locus and expanding proportionally as the volumetric yield locus expands as a result of isotropic strain hardening taking place. On the dry side of the Critical State, undrained distortional strains were allowed by the use of a radial fan of shear contours (see WROTH and LOUDON, 1967). Recently, the energy balance equation of the Modified Cam Clay Theory of BURLAND (1965) and ROSCOE and BURLAND (1968) was modified by DAFALIAS (1987) in order to describe the behaviour of normally consolidated clays under anisotropic stress conditions.

The Cam Clay Theory, the Revised Theory, and the Dafalias' Theory are all based on a set of volumetric yield loci with stress states on the SBS and have an 'associated flow rule'. PENDER (1978) allowed for both plastic volumetric and distortional strains to take place within the SBS and made use of a 'non-associated flow rule' in which the yield loci arose from a set of radial fans with constant stress ratio. Such yield loci differ from the plastic potential for which an 'associated flow rule' obeying Drucker's normality concept is applied. These theories and ideas arose from the work of those researchers at Cambridge University and they are always verified with greater details from experimental observations. This chapter will review these theories in a critical manner and also other associated theories developed for anisotropic behaviour.

It is also important to describe the philosophy behind the Incremental Stress-Strain Theory of ROSCOE and POOROOSHASB (1963) which appears to be somewhat empirical but which has considerable potential for its application to all types of stress paths within the SBS and to cyclic loading as well.

3.2 State Boundary Surface and Critical State Line

The State Boundary Surface (SBS) is defined as a unique surface as shown in Fig 3.1, which separates the states of an element of the soil from those that are not admissible. This surface is formed by two distinct surfaces, namely the Roscoe surface, on which volumetric yielding takes place, and the Hvorslev failure surface. The Roscoe surface is defined by undrained stress paths of normally consolidated clay while the Hvorslev surface is the locus of failure points for heavily overconsolidated samples. The existence of the State Boundary Surface has been verified by many investigators (PARRY, 1960; WROTH and LOUDON, 1967; BALASUBRAMANIAM, 1969; among others).

The end points of all specimens, when they were sheared to failure, lie on a unique line defined as the Critical State Line. Its projection on the (q, p) plane is a straight line which passes through the origin having a constant slope M . The Critical State Line separates the Roscoe surface which dictates the volumetric yielding from the Hvorslev failure surface. When a state of sample reaches the Critical State, it experiences unlimited distortion while the effective stress and the volume of the soil remains unchanged.

The area between the Critical State Line and the normal consolidation line in the water content-log mean normal stress plot is called 'wet of critical' while the area to the left of the Critical State Line is called 'dry of critical'. The soil when sheared in the 'wet' zone would generate a positive pore pressure response under undrained condition or decrease in volume under drained conditions. On the other hand, a soil in the 'dry' zone would show an increase in volume under drained conditions or tend to develop a negative pore pressure.

In its simplified form, the SBS is accepted to be symmetrical about the hydrostatic p -axis provided there is no substantial time effects and anisotropy either from the depositional mode or from the applied stress conditions. Much of the challenge and arguments on SBS and the Critical State Concept seem to be on these aspects, but nevertheless their effects can be incorporated in a primary SBS with appropriate deviations as per the perturbations.

3.3 Incremental Stress-Strain Theory for Normally Consolidated Clays (ROSCOE and POOROOSHASB, 1963)

ROSCOE and POOROOSHASB (1963) put forward a relationship which enabled the prediction of shear as well as volumetric strains without appealing to the concepts of the theory of plasticity. Assuming a unique State Boundary Surface in (p, q, e) space they proposed the

following form of an incremental stress-strain relationship for wet clays.

$$d\varepsilon_1 = \left(\frac{d\varepsilon_1}{d\eta} \right)_v d\eta + \left(\frac{d\varepsilon_1}{d\varepsilon_v} \right)_\eta d\varepsilon_v \quad \dots(3.1)$$

where the first term represents the variation of axial strain increment $d\varepsilon_1$ with stress ratio increment $d\eta$ in a constant volume shear while the second term corresponds to the variation of $d\varepsilon_1$ with the volumetric strain increment $d\varepsilon_v$ in a constant η stress path.

This incremental stress-strain relationship can be presented in a slightly different form as Eqn. 3.2.

$$(d\varepsilon_s)_{drained} = (d\varepsilon_s)_{undrained} + \left(\frac{d\varepsilon_s}{d\varepsilon_v} \right)_\eta d\varepsilon_v \quad \dots(3.2)$$

$$\text{where,} \quad (\varepsilon_s)_{undrained} = \int_0^\eta f_1(\eta) d\eta \quad \dots(3.3)$$

$$\left(\frac{d\varepsilon_s}{d\varepsilon_v} \right)_\eta = f_2(\eta) \quad \dots(3.4)$$

$f_1(\eta)$ is determined from the normalized nature of the undrained stress-strain behaviour. $f_2(\eta)$ can be estimated from the anisotropic consolidation tests as a function of stress ratio.

As described in the introductory note to this chapter, the above incremental relation described in Eqn. 3.1 allows for a variety of versatile tools in which it can be applied either in terms of total strains or in terms of plastic strains.

When applied in terms of total strains, the model accounts for the undrained deformation for any type of applied stress conditions in fine grained soils such as clays, when the permeability is extremely low. A time dependent flow of water which originates from the volume reduction or the volume expansion as a result of distortion will take substantial time and will always be accompanied by a magnitude of undrained strains due to the immediate deformation. When looked upon in terms of plastic strains, the equation proposes two sets of yield loci: one based on constant volume and the other based on a radial type of stress path for which the plastic strain increment ratio is only dependent on the stress ratio. It is then possible to find a set of volumetric yield loci which essentially give the plastic volumetric and distortional strains for the radial type of stress paths in the (q, p) plot lying on the SBS.

The equation can be extended for undrained and drained creep as well as for undrained and drained cyclic loading.

3.4 Cambridge Stress-Strain Theories for Wet Clays Based on the Critical State Concept

3.4.1 General

Stress-strain models to describe the soil behaviour are developed based on several assumptions and hypotheses in conjunction with well-known concepts of plasticity theory. The Cambridge Stress-Strain theories are conceptual models which are based on an energy balance equation and the normality condition of the plastic increment vector and the yield surface. These theories assume that the soil is isotropic, follow the Critical State Concept, and that there is no recoverable shear strain. The state of the sample inside the State Boundary Surface must remain on the elastic wall which is a vertical plane above an isotropic swelling line. The plastic deformation is assumed to occur only when the state of the sample changes on the State Boundary Surface. These theories appeal to only a few well-known soil parameters instead of depending on a large number of empirical constants.

3.4.2 Cam Clay Theory (ROSCOE et al., 1963)

The Cam-Clay model was developed for normally consolidated and lightly overconsolidated clay. The authors assumed that the energy dissipated at any infinitesimal increment of plastic work is only a function of the plastic shear strain. The proposed expression for energy dissipation with an assumption that the principal axes of stress and plastic strain increment coincide is,

$$dW = p d\epsilon_{vp} + q d\epsilon_{sp} \quad \dots(3.5)$$

where, dW : energy dissipated per unit volume of soil
 p, q : mean effective principal stress, deviator stress
 $d\epsilon_{vp}, d\epsilon_{sp}$: increments of plastic strains

Eqn. 3.5 can be expressed as,

$$dW = p d\epsilon_{vp} + q d\epsilon_{sp} = M p d\epsilon_{sp} \quad \dots(3.6)$$

where M is the slope of the Critical State Line in (q, p) plot. Eqn. 3.6 leads to the following flow rule,

$$\left(\frac{d\varepsilon_{vp}}{d\varepsilon_{sp}} \right) = M - \eta \quad \dots(3.7)$$

where η is the stress ratio, q/p .

The normality rule is applied such that the equation of the yield locus is,

$$q = Mp \ln \left(\frac{p_0}{p} \right) \quad \dots(3.8)$$

where p_0 is the preconsolidation stress. In this theory the shear and volumetric strain increments for states on the State Boundary Surface are given as,

$$d\varepsilon_s = \left(\frac{\lambda - k}{1 + e} \right) \left(\frac{pd\eta + Mdp}{Mp(M - \eta)} \right) \quad \dots(3.9)$$

$$d\varepsilon_v = \left(\frac{1}{1 + e} \right) \left(\frac{(\lambda - k)d\eta}{M} + \lambda \frac{dp}{p} \right) \quad \dots(3.10)$$

The State Boundary Surface can be derived as,

$$\eta = \frac{\lambda M}{(\lambda - k)} \ln \left(\frac{p_0}{p} \right) \quad \dots(3.11)$$

The volumetric yield loci as described by Eqn. 3.8 is bullet shaped at the p -axis and seems to be more applicable for volumetric yielding inside the SBS when the associated plastic volumetric strain is smaller than the value when the state paths lie on the SBS. This novel idea will be further elaborated in Chapters VI and VIII.

3.4.3 Modified Cam Clay Theory (BURLAND, 1965)

In an attempt to improve the limitations of the Cam-Clay model, BURLAND (1965) proposed a modified work equation which considers the work dissipated in plastic volume change. The energy dissipated in the Modified Cam-Clay Model is,

$$dW = p[(d\epsilon_{vp})^2 + (M d\epsilon_{sp})^2]^{1/2} \quad \dots(3.12)$$

The flow rule and yield locus are given by Eqns. 3.13 and 3.14, respectively.

$$\frac{d\epsilon_{vp}}{d\epsilon_{sp}} = \frac{M^2 - \eta^2}{2\eta} \quad \dots(3.13)$$

$$p = \frac{p_0 M^2}{M^2 + \eta^2} \quad \dots(3.14)$$

Hence, the shape of the volumetric yield locus was changed from the earlier log spiral to an elliptic form.

The incremental shear and volumetric strains are as follows :

$$d\epsilon_s = \frac{\lambda - k}{1 + e} \left(\frac{2\eta}{M^2 - \eta^2} \right) \left(\frac{2\eta d\eta}{M^2 + \eta^2} + \frac{dp}{p} \right) \quad \dots(3.15)$$

$$d\epsilon_v = \frac{1}{1 + e} \left(\frac{2\eta(\lambda - k)d\eta}{M^2 + \eta^2} + \lambda \frac{dp}{p} \right) \quad \dots(3.16)$$

The State Boundary Surface described in this theory is,

$$\frac{p}{p_0} = \left(\frac{M^2}{M^2 + \eta^2} \right)^{(1 - k/\lambda)} \quad \dots(3.17)$$

The Modified Theory of ROSCOE and BURLAND (1968) captured many of the behaviour of normally consolidated and lightly overconsolidated clays. Equation 3.13 when expressed in

terms of total strains with the use of the parameter ($\Lambda = 1 - \kappa/\lambda$) can make accurate predictions of K_o . Also the Eqn. 3.17 can predict the undrained stress paths and hence the pore pressures in normally and lightly overconsolidated clays.

The volumetric strains experienced by stress paths with states on the State Boundary Surface can be accurately determined using Eqn. 3.16, while the distortional strains as calculated from Eqn. 3.15 are perfectly correct for the radial type of stress paths for which the stress ratio remain constant.

3.4.4 Revised Theory (ROSCOE & BURLAND, 1968)

The Cam Clay and the Modified Cam Clay theories assumed that no shear distortion of any type can be associated with a stress path beneath the State Boundary Surface. Therefore, for states on the elastic wall, these models are rigid in shear behaviour permitting only recoverable volumetric strains. However, by replotting the undrained results of LOUDON (1967) for lightly overconsolidated clays in a (q , p) plot, ROSCOE and BURLAND (1968) showed that for specimens of overconsolidation ratio of 1 to 1.8, the contours of constant shear strain beneath the State Boundary Surface coincided with the contours of constant q . They further stated that for the normally and lightly overconsolidated clays the contours of constant q can be considered as a series of yield loci as shown in Fig. 3.2. These constant q yield loci extended up to the conventional volumetric yield loci used in the Modified Cam Clay Theory. The conventional yield locus was called as the volumetric yield locus, while the latter one was termed the constant q yield locus. When the stress increments are directed outside the volumetric yield locus the stress point was assumed to move with the intersection of the constant q yield locus and its corresponding volumetric yield locus. However, for stress increments directed inside the volumetric yield locus in a direction to which q is increasing, the stress point was assumed to move through a series of constant q yield locus. The contribution to the shear strain can be expressed as,

$$d\epsilon_q = \left(\frac{d\epsilon_{sp}}{d\eta} \right)_{v^p} d\eta \quad \dots(3.18)$$

The v^p in Eqn. 3.18 implies that the plastic volumetric strain is constant, because the state of the specimen is remaining on the elastic wall. Hence, the incremental plastic shear strain in the revised equation is given by,

$$d\epsilon_{sp} = \left(\frac{d\epsilon_{sp}}{d\eta} \right)_{v^p} d\eta + \left(\frac{d\epsilon_{sp}}{d\epsilon_{vp}} \right)_{\eta} d\epsilon_{vp} \quad \dots(3.19)$$

The second component in Eqn. 3.19 , due to the volumetric yield locus , is taken from the Modified Cam Clay Theory. The volumetric strains predicted by the Revised Theory are the same as those of the Modified Cam Clay Theory, since they are based on the same volumetric yield locus.

3.4.5 Summary of the Stress-Stress Theories of the Cambridge Group

BALASUBRAMANIAM (1976) presented the theories developed at Cambridge in similar mathematical forms to enable them to be compared with the experimental results. He concluded that the basic philosophy among all four theories is similar and hence they can be expressed mathematically in a similar form. He also confirmed that the additional constant q yield locus used in the Revised Theory is a necessity for the successful prediction of the shear strains as the theory is mathematically structured.

The Revised Theory of ROSCOE and BURLAND (1968) incorporating a constant q yield loci is the best theory for the prediction of distortional strains for stress paths which lie on the SBS and with monotonically increasing stress ratio. For stress states inside the SBS and for undrained conditions, the Revised Theory can also predict the distortional strains successfully on the wet side of the Critical State Line.

3.5 PENDER's Model (1977, 1978)

3.5.1 General

This model employed the Critical State Concept and a constitutive relationship for a work hardening plastic material as the general framework, and deals with two distinct behaviour of clay, namely one for an overconsolidated behaviour (PENDER, 1978) and the other for the normally consolidated behaviour (PENDER, 1977). The assumption of a unique State Boundary Surface between the overconsolidated and the normally consolidated region is not made. However, the undrained paths for a normally consolidated clay is proposed as a yield locus (N.C yield locus) separating the normally consolidated state from the overconsolidated state, although the model for the overconsolidated behaviour was assumed to include the undrained stress path for normally consolidated states. It is proposed that the N.C yield locus continually changes in shape and position in the stress space according to the stress history of the clay. The over-consolidated component is always operative while the normally consolidated component is used to account for the extra strains when the stress points pass through the normally consolidated yield loci. This was achieved by incorporating strains additional to those predicted by the original model for the overconsolidated clay. This model provides qualitative predictions of the stress-strain behaviour of clays both in the isotropic and in the anisotropic stress states.

3.5.2 Assumptions and Hypotheses

While retaining most of the assumptions made in the Critical State Theory, the following aspects deviate from those.

- i) Plastic strains occur within the State Boundary Surface. However, no unique State Boundary Surface is defined.
- ii) Two yield loci are engaged simultaneously when the stress path is directed outside the normally consolidated yield locus.

Hence, there exist three strains within the State Boundary Surface, i.e., the recoverable volumetric strain and the irrecoverable strains both volumetric and distortional.

A general form of constitutive relation for incremental plastic strain given by HILL (1950) was used;

$$d\epsilon_{ij}^p = h \frac{\partial g}{\partial \sigma_{ij}} df \quad \dots(3.20)$$

where, h : the hardening function
 g : the plastic potential
 df : the differential of the yield function f

The following hypotheses are adopted in Eqn. 3.20 to formulate the stress-strain behaviour of clays.

- (1) **OC-Yield Locus** - Within the State Boundary Surface, the constant stress ratio lines given by the function f (Eqn. 3.21) are yield loci (Fig. 3.3).

$$f = q - \eta_i p \quad \dots(3.21)$$

where η_i denotes a particular yield locus. The current yield locus is always attached to the stress point (i.e., a type of kinematic hardening).

- (2) **N.C Yield Locus** - The undrained stress path for the normally consolidated clay is postulated as the N.C yield locus.
- (3) **Undrained Stress Path** - The undrained paths in the (q, p) stress space below the State Boundary Surface are assumed to be parabolic (Fig. 3.4) and can be expressed as in Eqn. 3.22.

$$\left(\frac{\eta - \eta_0}{AM - \eta_0} \right)^2 = \frac{p_{cs}}{p} \left(\frac{1 - p_0/p}{1 - p_0/p_{cs}} \right) \quad \dots(3.22)$$

where η_0 and p_0 indicate the stress ratio and the mean effective stress ratio at the start of the undrained path, respectively. p_{cs} is the value of p at the point on the Critical State Line corresponding to the current void ratio. The parameter $A = 1$ for compression while $A = -1$ for extension. A family of undrained paths always moves toward the Critical State during loading.

- (4) **Strain Increment Ratio** - The ratios of plastic strain increments for overconsolidated and normally consolidated regions are as in Eqns. 3.23 and 3.24, respectively.

$$\frac{d\epsilon_{sp}}{d\epsilon_{vp}} = \frac{(AM - \eta_0)^2}{(AM)^2 (p_0/p_{cs} - 1) \{ (AM - \eta_0) - (\eta - \eta_0)p/p_{cs} \}} \quad \dots(3.23)$$

$$\frac{d\epsilon_{sp}(N.C)}{d\epsilon_{vp}(N.C)} = \frac{\eta}{(AM - \eta)} \quad \dots(3.24)$$

where the parameters are defined as in Eqn. 3.22. This strain increment vector implies a non-associated flow rule as shown in Fig. 3.3.

As a whole, two constitutive relationships of the form of Eqns. 3.25 and 3.26 are required for the calculation of the plastic strain increments.

$$d\epsilon_{sp} = d\epsilon_{sp}(N.C) + d\epsilon_{sp}(O.C) \quad \dots(3.25)$$

$$d\epsilon_{vp} = d\epsilon_{vp}(N.C) + d\epsilon_{vp}(O.C) \quad \dots(3.26)$$

where $d\epsilon_{sp}$, $d\epsilon_{vp}$ are plastic distortional and volumetric strain increment, respectively, $d\epsilon_{sp}(N.C)$ is zero in the overconsolidated region, and $d\epsilon_{sp}(O.C)$ is assumed to occur both in the normally consolidated and in the overconsolidated state.

3.5.3 Overconsolidated Behaviour

From the normality rule and the assumption that the total volume change is zero for the undrained condition (SCHOFIELD and WROTH, 1968) because the recoverable volumetric strain is accompanied by an equal and opposite plastic volumetric strain, the partial derivative of the plastic potential with respect to p and the hardening function h in Eqn. 3.20 are determined.

It is now possible to substitute the function df , g , and h into Eqn. 3.20, and then the plastic strain increments in the overconsolidated states are obtained as follows:

$$d\epsilon_{sp} = \frac{2k(p/p_{cs})(\eta - \eta_0)d\eta}{(AM)^2(1+e)(2p_0/p - 1)[(AM - \eta_0) - (\eta - \eta_0)p/p_{cs}]} \quad \dots(3.27)$$

$$d\epsilon_{vp} = \frac{2k(p_0/p_{cs} - 1)(p/p_{cs})(\eta - \eta_0)d\eta}{(AM - \eta_0)^2(1+e)(2p_0/p - 1)} \quad \dots(3.28)$$

3.5.4 Normally Consolidated Behaviour

As described earlier the shape of the normally consolidated yield locus depends on the stress history of clay when the stress path is directed outside the current yield locus. However, when the stress path is directed inside, the shape of the normally consolidated yield locus remains unchanged until the next one is engaged by the stress path. The concept of obtaining normally consolidated plastic component is quite similar to that of the Incremental Stress Strain Theory of ROSCOE and POOROOSHASB (1963), i.e., the volumetric strain due to a stress increment ($d\eta$, dp) is the same as that due to an undrained increment followed by an increment at constant stress ratio. Based on the assumption that λ is constant for any stress ratio η in the $e - \ln p$ plot, the total plastic volumetric strain increment is derived as :

$$(d\epsilon_{vp})_{total} = \frac{(\lambda - k)dp}{p(1+e)} + \frac{2\lambda p(p_0/p_{cs} - 1)(\eta - \eta_0)d\eta}{p_{cs}(1+e)(AM - \eta_0)^2(2p_0/p - 1)} \quad \dots(3.29)$$

Hence, the normally consolidated plastic volumetric strain component $d\epsilon_{vp}(N.C)$, can be obtained by substituting Eqn. 3.28 (O.C component) and Eqn. 3.29 into Eqn. 3.26. Having determined $d\epsilon_{vp}(N.C)$, it is then possible to use Eqn. 3.24 to determine the N.C plastic shear strain component.

3.5.5 Summary of PENDER's Model.

Whereas the Cambridge theories are concerned with behaviour for stress states on the State Boundary Surface, Pender's Model is concerned not only with the behaviour for stress paths beneath the State Boundary Surface but also with the behaviour for the normally consolidated states. This model's great benefit is that it requires only four soil parameters which are obtainable from common laboratory tests. This model predicts fairly well the strength in the normally consolidated state, and hence, the undrained stress path as well because of the nature of the assumption of undrained stress paths. However, for the heavily overconsolidated state, the undrained stress paths are not supported by the real behaviour. In spite of the drawbacks inherent in this model, it still provides the qualitative prediction of stress strain behaviour of clays under the various initial stress conditions such as their behaviour both in compression and in extension under the isotropic and anisotropic stress states. This model can also be extended to include the prediction of cyclic behaviour of soils.

3.6 DAFALIAS' Model (1987)

This model can be considered as an extended version of the classical Critical State Theory from an isotropic case to an anisotropic one. To include the effects of anisotropy induced by one dimensional stress states or other factors, DAFALIAS proposed a work equation including one additional term in that adopted by the Modified Cam Clay Theory of ROSCOE and BURLAND (1968) as follows :

$$dW = p [(d\epsilon_{vp})^2 + (Md\epsilon_{sp})^2 + 2\alpha d\epsilon_{vp}d\epsilon_{sp}]^{1/2} \quad \dots(3.30)$$

where α is the triaxial non-dimensional anisotropic variable accounting for the effect of internal residual stresses. For $\alpha = 0$ (isotropy exists), Eqn. 3.30 yields the identical equation (Eqn. 3.12) of the energy dissipation adopted in the Modified Cam Clay Theory. The flow rule from the Eqn. 3.30 is expressed as :

$$\frac{d\epsilon_{vp}}{d\epsilon_{sp}} = \frac{\eta^2 - M^2}{2\alpha - 2\eta} \quad \dots(3.31)$$

Hence, α is a function of η , M , and the direction of the plastic strain increment. If normality is assumed, then α is related to the shape of the yield locus. In particular under K_o loading, α should satisfy the following condition.

$$\alpha = \frac{\eta_k^2 + 3(1 - k/\lambda)\eta_k - M^2}{3(1 - k/\lambda)} \quad \dots(3.32)$$

where, η_k : stress ratio, q/p , at K_0 stress state.

Assuming an associated flow rule and α is only a function of the memory of the initial condition, the energy balance Eqn. 3.30 reduces to the form of the yield locus as :

$$\frac{p}{p_0} = \frac{M^2 + \eta_0^2 - 2\alpha\eta_0}{M^2 + \eta^2 - 2\alpha\eta} \quad \dots(3.33)$$

where p_0 and η_0 are initial values, and $M = M_c$ for η and η_0 greater than α and $M = M_e$ for η and η_0 less than α . The graphical representation of the yield locus is shown in Fig. 3.5.

By assuming that α is remaining constant during the subsequent loading, the State Boundary Surface is given as :

$$\frac{p}{p_0} = \left(\frac{M^2 + \eta_0^2 - 2\alpha\eta_0}{M^2 + \eta^2 - 2\alpha\eta} \right)^{(1 - k/\lambda)} \quad \dots(3.34)$$

THEVANAYAGAM and PRAPAHARAN (1989) presented a different form of the State Boundary Surface, but it is basically the same as Eqn. 3.33, which takes into account different initial states and different stress paths. They normalized the test data with respect to the equivalent pressure, p_e , and the equivalent specific volume v_λ as ATKINSON et al. (1987) did in their presentation.

Furthermore, DAFALIAS postulated the generalized form of yield surface in the multiaxial stress space as :

$$p^2 = pp_0 - \frac{3}{2M^2} [(S_{ij} - p\alpha_{ij})(S_{ij} - p\alpha_{ij}) + (p_0 - p)p\alpha_{ij}\alpha_{ij}] \quad \dots(3.35)$$

where, S_{ij} : deviatoric stress tensor
 α_{ij} : dimensionless deviatoric tensor

3.6.1 Summary of DAFALIAS' Model

This model deals with the behaviour of normally consolidated clay under anisotropic stress conditions. The yield surface proposed in this model consists of a rotated and distorted ellipse. The degree of rotation and distortion are determined by the value of α .

A necessary condition of the work equation suggested is that:

$$2\alpha = 2\eta + (\eta^2 - M^2) \frac{d\epsilon_{sp}}{d\epsilon_{vp}} \quad \dots(3.36)$$

If normality is assumed, α is given by :

$$\alpha = f(M, p, q, \beta) \quad \dots(3.37)$$

where β is the memory function for the initial condition.

Thus, any assumption on the algebraic form of α value has a direct impact on the shape of the yield surface. For instance, $\alpha = 0$ (Modified Cam Clay Theory) is a special case of a more general form of α . Especially p_0 in Eqn. 3.33 (yield surface) is not the intersection of the yield surface with the p-axis (see Fig. 3.4).

DAFALIAS did not extend this model to any type of incremental form of stress-strain behaviour as we usually expect in the stress-strain theories. These will be discussed in subsequent chapter.

3.7 Some Formulation of Anisotropic Behaviour of Clays

STIPHO (1982) suggested a State Boundary Surface for the anisotropic stress history (Fig. 3.6). This State Boundary Surface will be rotated along the e axis in the (p,q,e) space with a degree dependent on the anisotropic stress history and the anisotropic hardening. Furthermore, this State Boundary Surface is not a unique one, and will not be symmetrical about the p-axis. Thus, anisotropic consolidation lines do not necessarily lie on the State Boundary Surface for isotropic stress states as suggested by ROSCOE et al. (1958). However, the yield locus for any point in the consolidation process must lie on this proposed State Boundary Surface. His proposed yield function for the normally consolidated stress history is as follows :

$$\frac{p}{p_0} = \frac{-(q^2 + q_0^2 - 2qq_0)}{p_0(p_0 - p)M^2} \quad \dots(3.38)$$

where, p_o : initial mean normal stress
 q_o : initial deviator stress
 M : stress ratio, q/p , at the Critical State

Two hardening parameters were employed, i.e., the parameter q_o will control the translation of the surface, while the parameter p_o will take care of the expansion of the surface during plastic deformation as :

$$dp_o = \frac{p_o(1 + e_o)}{(\lambda - k)} d\epsilon_{vp} \quad \dots(3.39)$$

$$dq_o = \frac{q_o(1 + e_o)}{(\lambda - k)} d\epsilon_{sp} \quad \dots(3.40)$$

ATKINSON et al. (1987) proposed a State Boundary Surface for one-dimensionally normally consolidated clays based on the experimental data on reconstituted Speswhite Kaolin. These authors normalized all the test data with respect to the equivalent pressure, p_e , and the equivalent specific volume, v_λ , in order to take account of the different initial states and the different stress paths. The boundary surface which is normalized by v_λ for one-dimensionally normally consolidated stress history is given as :

$$\eta - \eta_o = (\pm M - \eta_o) \left[2 \text{Exp} \left(\frac{\Gamma - v_\lambda}{\lambda - k} \right) \right]^{1/2} \quad \dots(3.41)$$

where, η_o : stress ratio during one-dimensional consolidation
 Γ : specific volume intercept of the Critical State
line plotted as v against $\ln p'$ at $p' = 1.0$
 v_λ : equivalent specific volume :
 $v_\lambda = v + \lambda \ln p' (v = \text{specific volume})$
 M : stress ratio, q/p , at Critical State

The State Boundary Surface was simply obtained by replacing η with $(\eta - \eta_o)$ and M with $(M - \eta_o)$ as the procedures adopted by the Modified Cam Clay Theory, when $\eta_o = 0$.

3.8 Concluding Remarks and Comments

The energy balance equation proposed by DAFALIAS (1987) gives the most general expression for the volumetric yield loci which lie on the State Boundary Surface. The Cam Clay Theory is the special version perhaps when the volumetric yielding is small, as it happens inside the State Boundary Surface. Therefore, the Cam Clay type of volumetric yield loci seem more reasonable to apply when the volumetric yield is small.

The volumetric yield loci, as obtained by ROSCOE and BURLAND (1968), capture most of the behaviour of normally consolidated clays as sheared from the isotropic stress state. With the suitable selection of α , possibly the Dafalias' Model (1987) can apply for the anisotropic behaviour of clays for stress states on the State Boundary Surface. A similar statement can be made for anisotropic behaviour as presented by the work of STIPO (1982) and ATKINSON et al. (1987). Even if the models of STIPO (1982) and ATKINSON et al. (1987) are accepted for the anisotropic behaviour of the normally consolidated clays with stress states on the State Boundary Surface, it seems a set of yield loci of the form proposed by ROSCOE and BURLAND (1968) as constant q yield loci (or its modified version) would be needed to account for the undrained strains which are inevitable in low permeable soils such as clays when various types of applied stress paths are imposed during virgin loading.

Pender's Model (PENDER, 1977, 1978) based on experimentally observed undrained stress paths as parabolic idealization and the Critical State value of p (p_{cs}) when combined with an empirical flow rule more of the type adopted for the Cam Clay Theory seems rather more complicated in its formulation. However, this model (as it is perhaps based on experimental observations, possibly on Kaolin for stress state below the State Boundary Surface, see WROTH and LOUDON, 1967 and BALASUBRAMANIAM, 1969) seems to capture the bulk of the clay behaviour exhibited when stress paths lie below the State Boundary Surface.

These works indicate a need for the stress zone below the SBS to be investigated more closely for the existence of sub-sets of volumetric yield loci which can cause compressive volumetric strain on the wet side of the Critical State and dilatant volumetric strain on the dry side of the Critical State. It would then be necessary to seek appropriate flow rules in the stress regions where such sub-sets of volumetric yield loci exist. This is the major aim of the Author's experimental programme in Chapter IV and the subsequent analysis in Chapters V, VI, VII and VIII.

IV EXPERIMENTAL INVESTIGATIONS

4.1 Introduction

The behaviour of normally and lightly overconsolidated clays was studied through a comprehensive series of triaxial tests. The testing program included fourteen test series: four in undrained conditions and ten in drained conditions. The undrained test series consisted of three (CIU, CK_0U , CAU) in compression and one (CK_0UE) in extension. The drained tests included CID, CK_0D and CAD in compression together with constant p tests in compression and extension, constant q tests with p increasing and decreasing, conventional extension tests, unloading compression tests and loading extension tests. All test series were conducted on samples with OCR values of 1.00, 1.24, 1.50, 1.78, 2.15 and 2.75. Section 4.5.2 describes the testing program in detail.

This chapter contains the relevant details of the experimental investigations carried out in the study. The sampling procedures and the test apparatus used are described first. The detailed calibration process of the instruments and gauges and the testing programme are given in the subsequent sections. Finally, the testing procedures and the errors and corrections applied are presented.

4.2 Sampling

The clay samples used in this study were undisturbed soft Bangkok clay taken from a site within the Asian Institute of Technology campus. Samples were collected using 7.5 cm diameter, 90 cm long thin-walled piston samplers from a depth of 3 to 4 meters. All sampling tubes were immediately sealed at both ends with paraffin wax to prevent the loss of moisture. These tubes were then transported to the laboratory and stored in a constant humidity chamber for later extrusion.

4.3 Description of Apparatus

A detailed study on the strength and deformation characteristics of lightly overconsolidated clay was carried out through the laboratory tests. The equipment used for the experiments consisted of the triaxial cells, the loading devices, and the measuring units and instruments. All tests were carried out in a temperature-controlled room to minimize the effect of temperature variation on the test results.

4.3.1 Triaxial Cells

Standard triaxial cells manufactured by Wykeham Farrance Engineering Co. which can accommodate up to 5 cm diameter samples were used. The cell consists of three main components, namely the cell base, the removable perspex cylinder, and the top head assembly. The cell base consists of the pedestal for the set-up of specimen and three water passages - two are drainage lines and the other is a cell water line. Each drainage line can be connected to the top and the bottom of the specimen, respectively. The bottom drainage line which was connected to the cell pedestal was used together with a pore pressure transducer and a burette to measure the pore pressure response during undrained loading and a volume change for drained tests. The back pressurizing for the saturation of specimen was applied through the bottom drainage line. The cell water line was used to fill the cell chamber with the deaired and distilled water, and through which pressure was applied to the soil specimen. The base connection lines are fitted with valves to close or open the connections. The top drainage connection was not used in this study.

The removable perspex cylinder encloses the pressurized water, and can withstand an allowable stress of 11 kg/cm^2 . This perspex cylinder was fastened to the cell base by three stainless steel rods and three screws. The top head assembly consists of the top plate, loading ram which was ground and honed to close sliding fit with the cell bush, and two ports for air release and oil filling.

4.3.2 Loading Device

The desired stress conditions were imposed on the specimen by the combination of self-compensating mercury columns and dead weight suspended by hangers. The self-compensating mercury columns were the primary pressure sources for the constant cell and back pressures. This mercury column system was connected to a pressure-controlled board fitted with valve blocks and a Bourden type pressure gauge which can be read with an accuracy of 0.05 kg/cm^2 . A one-ton capacity loading machine manufactured by Wykeham Farrance Engineering Co. was used for the strain-controlled tests. The deviator stress was measured through a proving ring.

With the aid of load hangers and dead weights, the specimens could be sheared along a wide range of pre-determined stress paths in p-q stress space. A specially designed pulley system was used for some particular tests such as the p-constant extension tests and the loading extension tests. The scheme of loading in the anisotropic tests is discussed in detail in Section 4.5.2.

4.3.3 Measurement of Strains and Pore Pressures

Axial displacements were measured with the use of dial gauges which can be read with an accuracy of 0.01 mm/division. These were attached to the proving ring during the strain-controlled shearing or to the loading ram for the anisotropic tests to monitor the axial deformation

of specimens. During the isotropic consolidation process, however, the axial deformations were measured using the vernier telescope having an accuracy of 0.01 mm. In drained tests and consolidation process, the volume change of sample was measured by using the burette with capacities of 5 cc to 10 cc, which were connected to the back pressure line. In the case of undrained tests, the pore pressures were measured using the pore pressure transducer and strain indicator from the bottom of the specimen.

4.4 Calibrations

A set of calibrations had to be carried out before the commencement of the triaxial tests. In this section, the calibration processes will be described.

4.4.1 Proving Rings

All proving rings were calibrated for the compression tests as well as for the extension tests by applying simply the dead weights. A lever-arm type of calibration apparatus manufactured by Seiken Inc., Tokyo, was used to obtain the calibration factor for the compression tests. The calibration factor of each proving ring was determined based on the mean curve drawn from the relationship between proving ring readings and corresponding loads applied.

4.4.2 Pressure Gages and Pore Pressure Transducers

Since several different triaxial set-ups, pressure boards, and pore pressure transducers were used simultaneously, it was important that all instruments and gages were calibrated to a standard reference. An oil-piston pressure type of calibration apparatus, manufactured by Seiken Inc., Tokyo, was used for this purpose. The maximum pressure limits of Bourden gages were about 12 kg/cm².

The pore pressure transducers of a capacity of 7.0 kg/cm² were used for the measurement of pore pressure. The calibration was done for each combination of pore pressure transducer and strain indicator. These transducers were also calibrated using the same calibration apparatus used in the calibration of Bourden gauges.

4.4.3 Frictional Resistance and Upthrust of Loading Ram

In triaxial tests, the amount of load due to ram friction must be considered when the axial force imposed to the specimen is measured outside the cell. This frictional resistance can be divided into two components, i.e., one is due to the vertical contact between the loading ram and the bush, and the other is a horizontal force caused by the poor alignment of the load transfer

system and a single failure plane of specimen inside the cell. The error can virtually be eliminated from the test results by applying corrections using the correction factor and the careful alignment of the loading machine and the triaxial cell.

The upthrust force acting on the loading ram resulting from the application of cell pressure had to be determined to apply the correct counterbalance loads for both loading and unloading stages of the stress-controlled tests. The loading ram was fixed first with the use of a clamp at approximately the same position when a sample is being tested. The dial gauge was then attached to the ram and set to zero after applying a reasonably higher cell pressure. The dead weights were imposed to the ram through a load hanger to cause a downward movement of the loading ram. The total weight to cause a movement of about 10 divisions downward in the dial gauge within one minute was considered as the weight required to counterbalance the upthrust force relevant to the cell pressure applied. The appropriate calibration factor, which the upthrust and the frictional resistance of the loading ram have taken into account, was established by repeating the above procedures to cover the range of cell pressure applied in actual tests. A total of twelve triaxial cells were calibrated and used. The frictional resistance of the loading ram was almost independent of the direction of its movement. It was slightly dependent on the rate of ram movement and the viscosity of oil used (UDDIN, 1975). The magnitude of friction acting on the loading ram, however, was found to be negligible (BUENSUCESO, 1990).

The calibration factor was not applied for the case of strain-controlled test after isotropic consolidation. The correctional effect was directly achieved by taking the initial reading of the proving ring which already included the frictional resistance. This initial value of reading was obtained by running the shearing machine with the designated strain rate without touching the sample having the drainage line closed. All initial values in this case were taken at the contact point between the ram and the top cap.

4.5 Laboratory Testing Programme

4.5.1 Triaxial Consolidation Tests

It is generally known that K_o -value increases with the increase of the overconsolidation ratio. Several investigators have reported, as reviewed in Chapter II, that the swelling stress paths deviated from the K_o -consolidation line at the very beginning of its commencement in the q - p stress space in order to maintain the zero lateral strain. It is interesting to note, however, that these curved swelling lines can be represented by the straight line within the lightly overconsolidated region (OCR value not greater than 2.5). In this study, the idealized K_o -swelling line was used for the preparation of overconsolidated specimens. It was defined in the p - q stress space as the straight line in which the stress increment ratio is 0.95 passing through the normally consolidated stress point. Eventually, all of the final consolidation stress points of overconsolidated specimens fell on this idealized straight K_o -line.

In order to justify the idealized actual K_o -swelling line, four swelling tests (as shown in Table 4.1) were carried out with the different swelling stress increment ratio, $\left| \frac{dq}{dp} \right|$, after K_o -consolidation. These values were 0.49, 0.82, 0.85, and 0.95, respectively. Two of these samples were taken along the p-constant path, from the isotropic stress conditions, up to stress ratios, η , equal to 0.25 and 0.65, respectively. These samples were then consolidated again along these constant stress ratio paths far beyond the anticipated yield stresses in order to find out the yield points. Furthermore, three of the isotropic consolidation tests were conducted to obtain a comprehensive understanding of the consolidation characteristics of the clay. The schematic diagram of consolidation procedures is shown in Fig. 4.1. The slope of the consolidation and the swelling line in the e-lnp plot were 0.357 and 0.081, respectively. These values were used for the preparation of overconsolidated clay specimens in the laboratory. The consolidation characteristics of clay will be discussed in detail in Chapter V.

TABLE 4.1 Triaxial Consolidation Test

Test Name	No. of Test	Consolidation Stress Ratio η	Swelling Stress Ratio Increment $\left \frac{dq}{dp} \right $
CA-0.49	1	0.49	0.49
CA-0.82	1	0.49	0.82
CA-0.85	1	0.49	0.85
CA-0.95	1	0.49	0.95
CI-1,2,3	3	0	0
Total No. of Test	7		

Notes : CA : Anisotropic Consolidation
CI : Isotropic Consolidation

4.5.2 Triaxial Test Series

A systematic triaxial test programme was drawn to monitor and evaluate the properties and characteristics of lightly overconsolidated natural clays. It consisted of three test series, namely, Test Series I, II and III. Test Series I and II were the anisotropic tests, while the remaining one was isotropic tests. Test Series I was again distinguished from the Test Series II by its swelling process to prepare the overconsolidated specimens. In both Series I and II, all samples

were consolidated along the K_0 stress ratio path ($\eta = 0.49$, $K_0 = 0.63$) up to the required maximum pressures. Subsequently, the samples in the Test Series I were swelled back to the idealized actual K_0 stress state relevant to their overconsolidated ratio. On the other hand, those in the Test Series II were swelled back along the original anisotropic consolidation line, and hence the values of K_0 in this test series were always constant regardless of their overconsolidation ratio. All initial stress points of each test series are illustrated in Table 4.2 and Fig. 4.2.

In Test Series I, the laboratory-prepared overconsolidated specimens were subjected to the various stress paths such as the conventional undrained and drained paths, p or q-constant paths, unloading compression paths, and loading extension paths at each overconsolidated ratio. However, only the conventional undrained and drained tests, i.e., keeping the cell pressure constant and increasing the axial stress, were conducted in case of Test Series II and III. Detailed testing schedule is tabulated in Table 4.3 and typical stress paths are shown in Fig. 4.3. The designation of tests is explained below. The second capital letter appearing in each test name (i.e., K_0 , A, I) denotes the test series I, II, and III, respectively. The arabic numbers 1 to 6 followed by alphabets in Table 4.3 denote the overconsolidation ratios 1.00, 1.24, 1.50, 1.78, 2.15, and 2.75, respectively.

Compression Conditions

- i) **CK_0U , CAU , CIU** : Conventional undrained compression tests on K_0 , anisotropically, and isotropically consolidated specimens, i.e., increasing the axial stress with keeping the constant cell pressure. (Test Series I,II & III)
- ii) **CK_0D , CAD , CID** : Conventional drained compression tests on K_0 , anisotropically, and isotropically consolidated specimens. (Test Series I,II & III)
- iii) **CK_0DU** : Unloading drained compression tests on K_0 -consolidated specimens, i.e., decreasing radial stress with keeping the axial stress constant. (Test Series I)
- iv) **CK_0PC** : p-constant drained compression tests on K_0 consolidated specimens. (Test Series I)
- v) **CK_0QL , CK_0QU** : q-constant drained loading and unloading on K_0 -consolidated specimens. (Test Series I)

Extension Conditions

- vi) **CK₀UE, CK₀DE** : Conventional undrained and drained extension tests on K₀-consolidated specimens. (Test Series I)
- vii) **CK₀LE** : Extension drained loading tests on K₀-consolidated specimens. (Test Series I)
- viii) **CK₀PE** : p-constant drained extension tests on K₀-consolidated specimens. (Test Series I)

TABLE 4.3 Test Conditions and Test Names With Test Series

TEST SERIES I				
Undrained Compression Tests	Undrained Extension Tests	Drained Compression Tests	Drained Extension Tests	Drained Ext. Loading Tests
CK₀U1	CK₀UE1	CK₀D1	CK₀DE1	-
CK₀U2	CK₀UE2	CK₀D2	CK₀DE2	-
CK₀U3	CK₀UE3	CK₀D3	CK₀DE3	-
CK₀U4	CK₀UE4	CK₀D4	CK₀DE4	CK₀LE4
CK₀U5	CK₀UE5	CK₀D5	CK₀DE5	
CK₀U6	CK₀UE6	CK₀D6	CK₀DE6	CK₀LE6
CK₀U1-2	CK₀UE1-2			
p-constant Drained Compression Tests	p-constant Drained Extension Tests	q-constant Drained Loading Tests	q-constant Drained Unloading Tests	Drained Unloading Compression Tests
CK₀PC1	CK₀PE1	-	CK₀QU1	CK₀DU1
CK₀PC2	CK₀PE2	CK₀QL2	CK₀QU2	CK₀DU2
CK₀PC3	-	CK₀QL3	CK₀QU3	CK₀DU3
CK₀PC4	CK₀PE4	-	-	-
CK₀PC5	-	CK₀QL5	CK₀QU5	CK₀DU5
CK₀PC6	CK₀PE6	-	-	-

TEST SERIES II		TEST SERIES III		REMARKS
Undrained Compression Tests	Drained Compression Tests	Undrained Compression Tests	Drained Compression Tests	
-	-	CIU1	CID1	
CAU2	CAD2	CIU2	CID2	
CAU3	CAD3	CIU3	CID3	
CAU4	CAD4	CIU4	CID4	
CAU5	CAD5	CIU5	CID5	
CAU6	CAD6	CIU6	CID6	
		*CIU7		
		CIU1-2		
		CIU1-3		

- Notes:**
- i) - : No Test is carried out.
 - ii) Numbers 1 - 6 in each test name denote OCRs of 1.0, 1.24, 1.5, 1.78, 2.15, and 2.75.
 - iii) OCR for *CIU7 is 4.25, and p' for CIU1-2 & CIU1-3 are 6.0 and 5.0 kg/cm².

The undrained behaviour of normally consolidated clays was studied by conducting one additional set of conventional undrained compression and extension tests on K_o -consolidated specimens with different initial stresses (CK_oU1-2 & CK_oUE1-2). In addition, two additional undrained compression tests on isotropically normally consolidated specimens ($CIU1-2$ & $CIU1-3$) were also performed at different initial consolidation pressures.

A total of three conventional compression tests (with the undrained and drained conditions, respectively) were conducted at each overconsolidation ratio. These samples (K_o , anisotropically, and isotropically overconsolidated samples) also have approximately the same initial water contents, but have different pre-shear stresses and stress ratios. The test procedures are discussed in detail in Section 4.6.

4.6 Triaxial Testing Procedures

To obtain reliable results, efforts and care were given to eliminate the sources of errors.

4.6.1 Preparation and Setting-up of Specimens

As the testing programme progressed, the samples were extruded from the sampling tubes one by one. Subsequently, they were cut into pieces, 12 cm long, and immediately covered with paraffin wax, then stored in the humidity controlled sample storage room. Before trimming a clay specimen, the base of triaxial cell was connected with the pressure lines and a pore pressure transducer. The entire pressure lines were always flushed with deaired and distilled water to get rid of any entrapped air bubbles. Porous stones which were deaired and cleaned by boiling in distilled water, filter papers, and a membrane were prepared for the prompt sealing of the specimen after trimming.

Each piece of clay sample was trimmed to the required nominal dimensions of 35.5 mm in diameter and 71 mm high. The initial water content of the specimen was determined from the trimmings. The dimensions and the weight of specimen were measured with a graph paper strip and the balance. Some samples had to be discarded due to the presence of a thick silty sand layer.

The trimmed specimen was mounted on the pedestal of the cell base. The saturated porous stones and filter papers were also placed at both ends of the specimen. To accelerate consolidation, soaked filter paper strips, 6 mm wide Whatman no. 54, were placed vertically around the sample with an equal spacing. Both ends of the filter paper strip were extended to the porous stones. For the extension tests, these strips were cut from alternating sides, as much as 2/3 of its width to reduce its contribution in carrying the extension load. The sample was then enclosed within two membranes which were separated by a thin coating of silicone grease sealed with two O-rings on each end. The sides of the top loading cap and the base pedestal were also coated with silicone grease in order to prevent the leakage of water through the sealing. Care was taken to keep the specimen concentric with both the pedestal and the top loading cap.

The perspex cylinder with top head assembly was then mounted and fixed to the cell base. The chamber surrounding the specimen was filled with deaired and distilled water up to about 10 mm from the top of the cell. The rest of the cell was filled with gear oil.

4.6.2 Saturation of Specimens

Even though the specimen itself was fully saturated, there was always a certain amount of air entrapped between the rubber membrane and the sample, and perhaps, in the previously saturated porous stones and soaked filter papers. A back pressure of 2.0 kg/cm^2 was applied to obtain the fully saturated specimens. The cell pressure and back pressure were gradually increased with the pressure increment of 0.10 kg/cm^2 . During the application of pressures, the cell pressure was always maintained 0.05 kg/cm^2 higher than the back pressure. When the back pressure had reached 2.0 kg/cm^2 , accordingly the cell pressure was 2.05 kg/cm^2 , the specimens were left for at least 24 hours. At the end of 24 hours saturation, the state of saturation was

checked by the pore pressure response under undrained conditions. Most of the specimens showed that it was over 98% within one minute. The axial deformations of the sample during the saturation process were hardly detected.

4.6.3 Consolidation of Specimens

After full saturation was achieved (Skempton's B-value was greater than 0.98) the consolidation phase was commenced. The value of K_o taken for the K_o -consolidation was 0.63, accordingly the stress ratio, q/p , of 0.49 was obtained. The detailed consolidation procedures, K_o and isotropic consolidation, respectively, are as follows :

(1) K_o -Consolidation - The saturated specimens had been initially subjected to an isotropic consolidation pressure of 0.2 kg/cm^2 . The samples were then taken along the conventional drained stress path with constant cell pressure to the stress ratio of 0.49 in p - q stress space. In the subsequent consolidation stage, this stress ratio was maintained constant by increasing both the cell pressure and the hanger loads simultaneously. The entire K_o -consolidation path was applied in steps to be as close to the theoretical path as possible. The deviatoric stress increment of 0.075 kg/cm^2 a day was applied up to the mean effective normal stress, p , which was equal to 1.0 kg/cm^2 . Thereafter, the daily load increment was increased to 0.225 kg/cm^2 until the mean effective stress reached the required maximum pressures. Furthermore, each daily stress increment was applied by adding three steps of sub-increments namely, 0.025 kg/cm^2 and 0.075 kg/cm^2 , respectively, with three-hour loading intervals. After the deviator stress had been increased by a total of 0.075 kg/cm^2 or 0.225 kg/cm^2 , respectively, the load was maintained overnight (at least 18 hours).

The axial deformation and the volume change of specimens were recorded at each stress increment stage. The total hanger load was readjusted to impose the correct required stress on a newly corrected area of the sample from the measurements. Any increase in cell pressure must be accompanied by a corresponding 'net increase' in hanger load to keep the stress ratio constant. The increment in cell pressure corresponding to the deviator stress increment was calculated as :

$$d\sigma_3 = \left(\frac{1}{\eta_k} - \frac{1}{3} \right) dq \quad \dots(4.1)$$

(2) Isotropic Consolidation - After the initial reading of the burette had been made, the cell pressure was raised to the desired value gradually with the back pressure line closed. The back pressure was increased as much as the increment of cell pressure with screw-controlled pressure by closing the mercury pressure valve. The consolidation was then initiated by reopening the drain valve and reducing the back pressure slowly to the original value in order to protect the specimen from the abrupt change in pressure. The back pressure line was switched

again to the mercury column, and the volume change and vertical deformation with time were recorded. For the higher consolidation pressures, the desired pressure was reached in several incremental steps described above.

4.6.4 Overconsolidated Specimens

All specimens were attempted to swell back to the same void ratio plane with the required overconsolidated ratio. The mean effective normal stress of 4.5 kg/cm^2 and 6.5 kg/cm^2 were considered as the pressure for the normally consolidated state in preparing subsequent overconsolidated specimens for the anisotropic tests and for the isotropic tests, respectively. The values K_o , and overconsolidation ratio were used to determine the maximum consolidation pressure. The overconsolidation ratio was defined by the ratio between the maximum past effective vertical pressure and the current effective overburden pressure. The values of overconsolidation ratio employed were 1.0, 1.24, 1.50, 1.78, 2.15, and 2.75. The deviator stress increment not less than -0.3 kg/cm^2 (i.e., $\Delta q < |0.3|$) was applied for 24 hour-duration during the swelling process. Particularly, the swelling stress increment ratio of 0.82 was used during the swelling process in Test Series I in order that the final stress points fell on the idealized K_o -line.

4.6.5 Shearing of Specimens

Every specimen was allowed one more day of consolidation or swelling to ensure the full dissipation of excess pore pressure within the specimen. All conventional undrained and drained triaxial tests were strain-controlled tests while the remaining were stress-controlled tests. Particularly, in the stress controlled tests, the stress increments were gradually reduced as the specimens were approaching the failure state.

For the extension tests, two special connection devices were required between the top cap, the loading ram and the proving ring, respectively. The cap in this case had a projection of threaded rod which could be screwed into an internal thread in the loading ram. This connection was made after completing the initial isotropic consolidation for the anisotropic extension tests. The dead weight suspended on the loading hanger was used as counterbalance load against upthrust during the connection. A hinge connector between the loading ram and proving ring was provided.

(1) Conventional Undrained Tests - After a complete consolidation, the drain valve was closed. Shearing was then commenced with constant cell pressure by increasing or decreasing the axial stress. Typical rate of strain chosen was 0.009 mm/min for both in compression and in extension tests. Readings of the pore pressure response, axial deformation of specimen, and axial load from the proving ring were made. During the early stage of shearing, readings were taken at very close intervals (at every 3 divisions up to 20 divisions).

(2) Conventional Drained Tests - In this test series, all samples were sheared at a strain rate of 0.0018 mm/min. The back pressure line was kept open and the cell pressure was maintained constant throughout the test. The change in volume and axial deformation were measured with a burette and dial gauge, respectively. Shearing procedures were the same as undrained tests. It took an average of about five days to complete the shearing stage.

(3) Constant Mean Normal Stress Test (p-constant Test) - The constant mean normal stress condition was achieved by increasing the axial stress and reducing the cell pressure for the compression tests and vice versa for the extension tests. The load increment was calculated as :

$$dq = -3 d\sigma_3 \quad \dots(4.2)$$

where dq is the deviator stress increment. The deviator stress increment of $+0.1 \text{ kg/cm}^2$ with 24 hours interval was taken for the compression tests. It was doubled in opposite direction (-0.2 kg/cm^2) for the extension tests. These increments were then decreased in three steps (by reducing to half of the previous increment) once the stress ratio, η , was greater than 0.75 in order that the failure points and corresponding behaviour could be precisely monitored.

In extension tests, two sets of pulley systems were employed to apply the desired axial stresses. Thirty to forty days were taken to complete the shearing stage.

(4) Unloading Compression and Loading Extension Tests - The slope of this stress path in p-q space is $-3/2$. Unloading tests were carried out by keeping the axial stress constant and reducing the radial stress (cell pressure). On the other hand, the cell pressure was increased whilst keeping the axial stress constant in order to achieve the loading extension conditions. The same deviator stress increments duration taken in the p-constant tests were applied. The load increments were also obtained from Eqn. 4.1.

(5) q-constant Tests - In this series of tests, the deviator stresses were kept constant throughout the shearing stage. The mean normal stress increments of $\pm 0.2 \text{ kg/cm}^2$ were taken for the unloading tests and for the loading tests, respectively. This load increment was also gradually decreased as the specimen was reaching the failure state in the case of q-constant unloading tests. In q-constant loading test series, all loadings were continued until sufficient number of data points were obtained. The duration of load increment was 24 hours.

4.7 End of Test Procedures

At the end of the tests, the drainage lines were closed and the cell pressure was reduced to atmospheric pressure in one step. The triaxial cell was disassembled immediately. The mode of failure and the inclination of the failure planes were noted. The specimen was then weighed and dried in the oven for 24 hours.

4.8 Processing of Test Data

The test results were processed based on the following usual assumptions that the specimen remains as right cylinder and stresses and strains are uniform throughout the specimen during the test.

4.8.1 Calculation of Stress and Strain

In triaxial stress conditions, the stress parameters p and q , which are also a function of the invariants of stress tensor, were defined as follows :

$$p = \frac{1}{3}(\bar{\sigma}_1 + 2\bar{\sigma}_3) \quad \dots(4.3)$$

$$q = \sigma_1 - \sigma_3 \quad \dots(4.4)$$

where p and q are called the mean normal stress and deviator stress, respectively.

The incremental strain parameters for the triaxial stress conditions are as follows :

$$d\varepsilon_v = d\varepsilon_1 + 2d\varepsilon_3 \quad \dots(4.5)$$

$$d\varepsilon_s = \frac{2}{3}(d\varepsilon_1 - d\varepsilon_3) \quad \dots(4.6)$$

where $d\varepsilon_v$ and $d\varepsilon_s$ are called the volumetric and shear strain increments, respectively. The parameters $d\varepsilon_v$ and $d\varepsilon_s$, when used in conjunction with stress parameters p and q , satisfy the fundamental energy equations.

Natural strain values, i.e., the axial and volumetric strains, which were used in the analysis were calculated as follows :

$$\varepsilon_1 = \ln \left(\frac{L_o}{L} \right) \quad \dots(4.7)$$

$$\varepsilon_v = \ln \left(\frac{V_o}{V} \right) \quad \dots(4.8)$$

where L_o and V_o represent the length and volume of specimen under the initial stress conditions, while L and V represent the length and volume during the test, respectively.

4.8.2 Corrections made on the Results

The following errors and corrections had to be taken into account in interpreting the triaxial test results.

(1) Friction on the Loading Ram - The ram friction was observed to be about 1% to 3% of the axial load for most of the loading range in some studies (WARLAM, 1960; BISHOP and HENKEL, 1957). Several other investigators postulated that the ram friction can be assumed negligible (UDDIN, 1975; LEE, 1986; BUENSUCESO, 1990).

The load imposed on the triaxial specimen should ideally be measured inside the triaxial cell to eliminate the interference of the loading ram friction. The measurements, however, were made with the proving ring outside the triaxial cell. An effort was made in this study to eliminate the effect of loading ram friction as described in Section 4.4.3.

(2) Correction for Cross-sectional Area Changes - Deviator stress was calculated with the assumption that the sample remained cylindrical throughout the loading process. The expression for area correction was :

$$A = A_o \left(\frac{1 - \Delta V/V_o}{1 - \Delta L/L_o} \right) \quad \dots(4.9)$$

- where, A : the average cross-sectional area of the specimen at a certain stage
 A_o : the initial cross-sectional area after consolidation
 V_o, L_o : the initial length and volume of the specimen, respectively after consolidation
 $\Delta L, \Delta V$: the change in length and volume of specimen at certain stage, respectively

(3) Effect of Membrane Strength - In any type of triaxial test, it is necessary to enclose the specimen in a rubber membrane. The following membrane correction formula (suggested by BISHOP and HENKEL, 1957) was applied on the calculated deviator stress at each strain level.

$$\sigma_{am} = \pi D M_r \epsilon_a \frac{(1 - \epsilon_a)}{A_o} \quad \dots(4.10)$$

where, σ_{am} : the axial stress taken by the membrane
 ϵ_a : axial strain
 D : the initial diameter of sample
 M_r : the compression modulus of membrane per unit width
 A_o : the initial cross-sectional area of sample

The compression modulus of the membrane was assumed to be the same as that in extension. The thickness of membrane and modulus used in this study were 0.2 mm and 0.0006 t/cm², respectively.

V UNDRAINED BEHAVIOUR OF CLAYS

5.1 Introduction

This chapter presents experimental observations from tests conducted on normally and overconsolidated clays with isotropic and anisotropic consolidation under various triaxial stress conditions. The pre-shear void ratio of all the samples is the same and is about 1.16. Index properties and consolidation characteristics of the clay used in this study are first presented, followed by strength and deformation characteristics of normally consolidated clay. The latter are presented to establish relevant reference behaviour for their counterpart, overconsolidated clays. Finally, results of tests conducted with overconsolidated samples are presented with special emphasis on the behaviour of normally consolidated and overconsolidated samples both under isotropic and anisotropic stress conditions. Important aspects of strength and deformation characteristics of K_o -consolidated clays such as the stress-strain relationship, the pore pressure development, and failure conditions are pointed out using the Critical State Concept. Other details are given in relevant sections. The chapter ends with concluding remarks on the extensive experimental investigation conducted with the undrained tests.

5.2 Index Properties of Clay

The soil profile at the site where undisturbed samples are taken is essentially the same as that described by previous AIT researchers. A typical bore hole log indicates that the top 1.5 to 2.0 m is Weathered Crust, followed by 6 m of Soft Clay, which is underlined by Stiff Clay. The thick soft clay was considered as a suitable source for the extraction of undisturbed samples to be used in the current study. The existence of a thick silty sand seam and a dark colored organic matter below a depth of 4.5 m was revealed during sampling. Between depths of 2.5 m and 4.0 m, there is a rather uniform Soft Clay with thin silt seams. Thus, the clay used in this study was retrieved from depths of between 3.0 to 4.0 m (a narrow range) and is expected to have the same initial structure, water content and Index properties. The clay used in this study was undisturbed fairly homogeneous and dark grey in color. These properties are summarized in Table 5.1.

TABLE 5.1 Index Properties

Natural Water Content (%)	78-85
Liquid Limit (%)	98
Plastic Limit (%)	37
Plasticity Index (%)	61
Liquidity Index	0.67-0.79
Average Unit Weight (t/m^3)	1.51
Specific Gravity	2.69
Clay Content (%)	70
Silt Content (%)	24
Sand Content (%)	6

5.3 Consolidation Characteristics of Clays

Isotropic and anisotropic consolidation and swelling tests were conducted to study the consolidation and swelling characteristics. A total of seven tests were carried out: four for the K_o consolidation and three for the isotropic consolidation. The stress ratio, η , in p - q stress space for the K_o consolidation is 0.49 (since K_o is taken as 0.63) as determined by previous investigators at AIT (e.g., CHANG, 1973; CHAIYADHUMA, 1974; WANG, 1975). Since the present series of consolidation tests is aimed to obtain the compression and swelling indices and the idealized K_o swelling line, a detailed study on the compressibility of the clay such as compositional effects and time effects was not made.

5.3.1 Void Ratio- Pressure Relationships

The $(e, \ln p)$ relationships of the isotropically and K_o consolidated specimens are shown in Fig. 5.1. In this figure the curve ABC corresponds to the isotropically consolidated sample. CD refers to the swelling characteristics for the same specimen. The $(e, \ln p)$ relationships for the K_o consolidated specimens CA-0.95, CA-0.85, and CA-0.49 are indicated as ABE. Up to the maximum past pressure p_c the compressibility characteristics under isotropic and K_o conditions are virtually the same and beyond the p_c value the K_o consolidated samples have an $(e, \ln p)$ relation displaced to the left from the isotropic one. For this stress range both the isotropic and K_o behaviour are nearly parallel as implied in a unique State Boundary Surface.

During K_o swelling, the swelling characteristics are virtually the same and are as indicated by the curve EF (Fig. 5.1) and this relationship is similar to the isotropic swelling curve CD. The swelling curve EF under K_o condition is also similar to the consolidation curve AB for

stresses less than the maximum past pressure. The similarity of the K_0 swelling curve EF to the isotropic swelling curve CD offers further evidence to the acceptance of the elastic wall concept used extensively in the Cambridge stress-strain theories.

An additional observation which is of interest here is that up to a stress range of p_c , the compressibility characteristics BG is considerably steeper than the compressibility under isotropic stress increase. The ratio of p_c/p_e is about 3.3 and it seems that for consolidation pressures higher than about 3.3 times the initial pre-consolidation pressure, the effects of initial shear stress due to K_0 consolidation can be erased. This value is quite close to that reported by BALASUBRAMANIAM (1969) in which the effects of 1-D consolidation during sample preparation was erased when the samples were isotropically consolidated to three times the initial 1-D stress used in the sample preparation.

The compression index, λ in the normally consolidated state at the higher stress level is 0.357 and this value together with the appropriate κ value of 0.081 was used in the preparation of overconsolidated samples. In order to avoid testing errors due to piston friction as well as membrane correction, all samples were tested at a higher pressure range. This has resulted in isotropic consolidation pressure of as much as 6.5 kg/cm^2 and such an isotropic pressure results in a pre-shear void ratio of 1.158. Under the K_0 condition this void ratio can be achieved under a smaller p value of 4.5 kg/cm^2 .

5.3.2 Swelling Characteristics

Though some aspects of the swelling characteristics were already discussed in the previous sub-section, it is important to mention that the swelling was carried out under isotropic stress reduction as well as under K_0 conditions with reduction of q and p . It is interesting to note that the swelling lines under K_0 conditions with various value of $\left| \frac{dq}{dp} \right|$ (where both q and p are reduced) tend to give the same swelling relationship in the $(e, \ln p)$ plot and this relationship is more or less parallel to the isotropic swelling line (see Fig. 5.1). It has already been stated that this observation is in agreement with the elastic wall concept where the samples experience volumetric swelling and compressibility within the State Boundary Surface being dependent on the variation of the mean normal stress. The swelling constant κ in the $(e, \ln p)$ plot is found to be 0.081 in the early stage of the stress release.

It has already been stated that the λ value for the clay is 0.357 and this would indicate that the bulk of the volumetric strain during isotropic and K_0 consolidation is irrecoverable. The plastic volumetric strain ratio Λ , defined as $\Lambda = (1 - \kappa / \lambda)$ will be 0.77. This value is close to the value of 0.75-0.85 and 0.78 as reported by LADD et al. (1977) and MAYNE (1988), respectively. In the subsequent analysis of all data, the values of λ and κ are used as 0.357 and 0.081, respectively.

5.3.3 Experimental Determination of K_0 Swelling Line

Though mention has already been made about the K_0 swelling line in Section 5.3.1 and 5.3.2, it is important to illustrate how close the specimen was to K_0 condition when the stresses were released with constant value of $\left| \frac{dq}{dp} \right|$ in establishing the K_0 swelling line in Fig. 5.1. Such an illustration is made with respect to the Area Ratio, A_r , defined as the ratio of the cross-sectional area of the sample at the end of consolidation to its subsequent value when the specimen is subjected to a stress release with constant $\left| \frac{dq}{dp} \right|$. Figure 5.2 demonstrates the value of the area ratio, A_r , with respect to the normalized mean normal stress, p/p_o . The normalized mean normal stress, p/p_o , is defined as the ratio of the current mean normal stress during swelling to the mean normal stress prior to the stress release. In Fig. 5.2, the curves AB, AC, AD, and AE refer to the area ratio for the K_0 swelling lines under each value of $\left| \frac{dq}{dp} \right|$ plotted with respect to the normalized mean normal stress, p/p_o , as defined above. It is noted that for all values of $\left| \frac{dq}{dp} \right|$, the areal variation of the samples remained within 2%. The path CA-0.95 is found to provide the closest K_0 -state wherein the maximum variation in the area ratio is only 0.5% when the mean normal stress reduced to half its maximum value. The stress path CA-0.95 (with $\left| \frac{dq}{dp} \right|$ of 0.95) is considered as the path which is closest to the K_0 swelling conditions. Thus, overconsolidated samples under K_0 conditions were prepared using the stress path CA-0.95. The OCR value of these samples ranged from 1.0 to 2.75.

5.3.4 Coefficient of Earth Pressure, K_0

The coefficient of earth pressure at rest, K_0 , as determined above under various values of OCR are plotted with respect to OCR in Fig. 5.3a. These values of K_0 correspond to $\bar{\phi}_c$ of 22° . In this plot, the K_0 values as predicted by MAYNE and KULHAWY (1982) and SCHMIDT (1966) are also presented. MAYNE and KULHAWY's (1982) expression for K_0 is

$$K_0 = (1 - \sin \bar{\phi}) \quad OCR^{\sin \bar{\phi}} \quad \dots(5.1)$$

whereas the expression given by SCHMIDT (1966) is

$$K_0 = 1 - \sin(1.2\bar{\phi}) \quad OCR^{\sin 1.2\bar{\phi}} \quad \dots(5.2)$$

Also presented in Fig. 5.3a is the prediction of K_o by BROOKER and IRELAND (1965) where K_o values are dependent on the plasticity index I_p .

In addition, Fig. 5.3a also contains the K_o values presented by HIGHT et al. (1987) for London clay, Magnus clay, and Lower Cromer Till as well as K_o values presented by KOUT-SOFTAS (1981). It is evident that the K_o values predicted by BROOKER and IRELAND (1965) are higher than the experimental values observed by the Author. The expression given by MAYNE and KULHAWY (1982) seems to make close predictions with the experimental observations on Bangkok clay, while the prediction by SCHMIDT (1966) seems close to the K_o values quoted by HIGHT et al. (1987) especially at values of OCR less than two. The normalized value of K_o defined as K_o/K_{on} , is plotted with respect to OCR in Fig. 5.3b. In this plot K_{on} refers to the value of K_o for normally consolidated samples. Even though there is some scatter in the data in Fig. 5.3b, it is evident that the ratio, K_o/K_{on} , tends to have the same variation for all clays when plotted with respect to OCR. It seems that the value of K_o for Bangkok clay for OCR values less than three appears as a lower bound of the normalized curves presented in Fig. 5.3b. Thus, the values of K_o experimentally established by the Author seem to agree well with other published data for values of OCR in the range of 1 to 3.

5.4 Undrained Behaviour of Normally Consolidated Samples

5.4.1 Introduction

The stress-strain behaviour and strength characteristics under undrained conditions are often used in the stability analysis of embankments on soft clays. Natural deposits of soft clays are mostly under K_o condition and in a lightly overconsolidated state. In this section the undrained behaviour of normally consolidated specimens sheared from isotropic and K_o conditions will be presented and discussed. First the behaviour as sheared from isotropic conditions will be presented and this will then be followed by the presentation of the results on the K_o consolidated samples. The behaviour of overconsolidated samples both under isotropic and K_o conditions will be presented in the subsequent section.

5.4.2 Undrained Behaviour under Isotropic Consolidations

Three undrained triaxial compression tests (CIU1, CIU1-2, CIU1-3) were run on normally consolidated samples from pre-shear consolidation stresses, p_o of 6.5, 6.0 and 5.0 kg/cm², respectively. These samples were sheared at a constant strain rate of 0.009 mm/min. The results of CIU1, which has a void ratio of about 1.16, will be referred to as the normally consolidated behaviour in the subsequent discussions related to the overconsolidated behaviour. The following sub-sections delineate those test results and include related discussions.

5.4.2.1 Undrained Stress Paths

The undrained stress paths for the normally consolidated samples (Fig. 5.4) demonstrate a high degree of consistency indicating the normalizable behaviour. The normalized stress paths with respect to the pre-shear consolidation stress, thus, form an approximately single curve as shown in Fig. 5.5. Smooth transitions from the hardening part to the softening part are observed. Two different failure envelopes are illustrated in Fig. 5.4. The first corresponds to the maximum deviator stress criterion ($M = 0.83$) and the second to the maximum obliquity ratio ($M = 0.88$). The relevant stress points fall on the same straight line passing through the origin. Upon reaching the maximum stress ratio, the stress paths travel along the same stress ratio line which is referred to in this study as the Critical State Line. The mean normal stress at the Critical State p_{cs} is 3.25 kg/cm^2 , while that at peak deviator stress is 3.72 kg/cm^2 , for the normally consolidated sample under the pre-shear isotropic stress conditions.

5.4.2.2 Stress-Strain Relationships

The (q, ϵ_s) relationship of the three normally consolidated specimens are shown in Fig. 5.6. These stress-strain curves show a mild peak and a slight strain softening beyond the peak. At low strain levels the (q, ϵ_s) relationship is found to be virtually the same for all the three samples. Beyond a deviator stress of about 1.5 kg/cm^2 (point A in Fig. 5.6), the (q, ϵ_s) relationship differs for all three samples and appears to be such that the deviator stress at any particular strain level is proportional to the pre-shear consolidation pressure. The initial uniqueness in the (q, ϵ_s) relationship seems to indicate that the samples are behaving as if they were lightly overconsolidated. Such an overconsolidation can only arise from the secondary consolidation effect prior to the undrained shear. It seems that in laboratory study of the undrained behaviour of Soft Bangkok clay, the pre-shear consolidation time has a pronounced effect. Such behaviour was somewhat neglected in the earlier studies conducted at AIT on Soft Bangkok clay. Figure 5.7 illustrates the normalized behaviour in the $(q/p_o, \epsilon_s)$ plot. A unique normalized behaviour is evident.

5.4.2.3 Excess Pore Pressure-Strain Relationships

Figure 5.8 illustrates the $(u/p_o, \epsilon_s)$ relationship for the three specimens. A unique relationship between the normalized excess pore pressure and the shear strain is evident.

In the literature review of this dissertation, the Author presented in detail the work of HANDALI (1986) and BALASUBRAMANIAM et al. (1989) on the pore pressure-stress ratio relationship for normally and lightly overconsolidated clays. Figure 5.9 illustrates the $(u/p_o, \eta)$ relationship for all three normally consolidated specimens. A unique relationship between u/p_o and η is evident in this figure. According to HANDALI (1986) the $(u/p_o, \eta)$

relationship for the normally consolidated clay is linear for all stress levels even up to failure. A similar trend is also noted in Fig. 5.9, however a detailed examination of the relationship reveals that the $(u/p_o, \eta)$ variation is bi-linear. The slope of the $(u/p_o, \eta)$ relationship in Fig. 5.9 up to an η value of 0.12 (i.e., point A in Fig. 5.9) has a slope of 0.52. For values of η greater than 0.12, the $(u/p_o, \eta)$ relationship is again linear; however, now the slope is 0.75.

Two aspects of the $(u/p_o, \eta)$ relationship are worthy of discussion. The first one refers to the bi-linear nature observed by the Author in contrast to the linear variation presented by HANDALI (1986). The initial shallow slope of 0.52 in the $(u/p_o, \eta)$ plot can be attributed to the light degree of overconsolidation resulting from the pre-shear secondary consolidation. It is surprising to note that the $(u/p_o, \eta)$ relationship as predicted by the Modified Cam Clay Theory of ROSCOE and BURLAND (1968) also shows an initial shallow slope at low stress ratio followed by a steeper slope. In any case the $(u/p_o, \eta)$ relationship in Fig. 5.9 can be approximated by a single straight line with a slope of 0.73 without any major deviation.

The second aspect to be discussed here is that HANDALI (1986) obtained a C value (where $u/p_o = C\eta$) which is about 0.56 as compared to the Author's value of 0.73. HANDALI (1986) investigated the $(u/p_o, \eta)$ relationship of many clays including even Bangkok clay as tested under different strain rates. From all the available data on Bangkok clay HANDALI (1986) found that the mean value of C is 0.56 with a standard deviation of about ± 0.08 . It should also be noted that HANDALI (1986) worked at low stress levels with samples of higher void ratio ($e=2.25$) as compared to the Author's tests at a reduced void ratio of about 1.16. Notwithstanding such differences, it is important to mention that a linear relationship exists between the u/p_o and the stress ratio η which reveals the pore pressure parameter C as a strain independent parameter to be used in the formulation of the undrained stress path.

5.4.2.4 Strength Characteristics

In Section 5.4.2.1 and Fig. 5.4, the peak deviator stress envelope in (q, p) plot was noticed to be different from the maximum stress ratio line which corresponds to the Critical State. Thus, the $\bar{\phi}$ value at peak deviator stress is 21° and is slightly lower than the $\bar{\phi}$ value at the Critical State of about 23° . The parameters $s_{uc}/\bar{\sigma}_{vo}$ where s_{uc} is the undrained strength and $\bar{\sigma}_{vo}$ is the pre-shear consolidation stress for the three samples are 0.236, 0.229, and 0.239 for pre-shear consolidation stresses of 6.5, 6.0, and 5.0 kg/cm², respectively. On the other hand, the $s_{uc}/\bar{\sigma}_{vo}$ value corresponding to the Critical State is 0.215 and is slightly lower. These values may be compared with some predicted values as given in Table 5.2.

TABLE 5.2 Comparisons of Undrained Strength Ratios

Predictions and Experimental Results	Peak Strength Ratio $s_{u p}/\bar{\sigma}_{vo}$	Critical State Strength Ratio $s_{uc}/\bar{\sigma}_{vo}$
Experimental Results	0.235	0.215
PARRY, NADARAJAH (1973)	0.215	-
MAYNE (1985)	0.293	0.269
Modified Cam Clay Model (see WORTH, 1984)	0.258	0.243
SKEMPTON (1957): $I_p=61\%$	0.336	-

PARRY and NADARAJAH (1973) obtained $s_{uc}/\bar{\sigma}_{vo}$ value of 0.215 while the prediction from the Modified Cam Clay Model is 0.258. The experimentally observed values are between these two values and closer to the lower range of the values quoted by MITACHI and KITAGO (1979) which is 0.21 to 0.51.

5.4.3 Undrained Behaviour under K_0 -consolidations

The undrained behaviour from K_0 consolidation is studied both under compression and extension conditions. These tests correspond to $(p)_{K_0}$ values of 4.5 and 5.5 kg/cm². The compression tests are designated as CK₀U1 and CK₀U1-2, respectively, while the extension tests are denoted as CK₀UE1 and CK₀UE1-2. These tests were conducted at the same strain rate of 0.009 mm/min which was the same as for the samples sheared in compression from the isotropic stress state. The tests CK₀U1 and CK₀UE1 correspond to $(p)_{K_0}$ of 4.5 kg/cm² and at this stage the pre-shear void ratio of the sample was about 1.16 and this value coincides with that of sample CIU1. The presentation of the results will follow the same format as that for the isotropically consolidated samples.

5.4.3.1 Undrained Stress Paths

Figures 5.10 to 5.12 contain the undrained stress paths of the K_0 consolidated specimens. In Fig. 5.10 only the compression test results are presented. Here again, for the K_0 consolidated specimens, the peak deviator stress envelop is found to be different from the maximum stress ratio one which corresponds to the Critical State Line. The angle of friction in compression, $\bar{\phi}$ under maximum deviator stress is 21° and the $\bar{\phi}$ value at the maximum stress ratio is 23°.

In Fig. 5.11 both the compression and extension stress paths are shown. The undrained stress paths under the extension conditions are found to be quite different from those under the compression conditions. During compression, high pore pressures are developed at higher strains which made the undrained stress paths more elliptical in nature. However, the pore pressure development during the extension phase is found to be small; thus, the stress paths are less rounded and there seems to be no symmetry of the stress paths either about the K_0 -line or the p-axis. The M value in compression is 0.89 with a $\bar{\phi}$ value of 23° whereas the M value in extension is 0.93 and the $\bar{\phi}$ is 33° . A unique normalized undrained stress path is evident as shown in Fig. 5.12.

5.4.3.2 Stress-Strain Relationships

Figure 5.13 illustrates the normalized stress-strain behaviour in the $(q/p_0, \epsilon_s)$ plot both for compression and extension conditions. As stated before, p_0 refers to $(p)_{K_0}$. It is clearly seen in this figure that the stress-strain behaviour is strongly influenced by the stress system.

During triaxial compression, the peak deviator stress was achieved at a small shear strain of 3.6% and at a stress ratio lower than that at the ultimate strain ($\epsilon_s = 11.7\%$). It is interesting, however, to note that the stress-strain curves are nearly parallel to the p-axis beyond an average shear strain of 0.9%. A detailed examination of this relationship showed that the deviator stress at $\epsilon_s = 0.9\%$ and the peak deviator stress at $\epsilon_s = 3.6\%$ are 2.92 kg/cm^2 and 2.99 kg/cm^2 , respectively (for Test CK_0U1). This indicates that there is negligible gain in strength beyond a shear strain of 0.9%. The maximum obliquity ratio was obtained at a larger strain ($\epsilon_s = 11.7\%$) during the softening process. It can be concluded that the K_0 -normally consolidated samples achieve a peak deviator stress at a small strain (practically less than 1%) in triaxial compression.

On the other hand, during the extension test the deviator stress tended to increase with the strain even at strains close to failure. The samples tended to form a neck and failed at larger strains ($|\epsilon_s| = 17.5\%$). Even so, the deviator stress increased rapidly in the initial unloading stage especially in the region where $\eta > 0$, accompanied by relatively small shear strains. More than 50% of the peak deviator stress was reached within a shear strain of about 2.5%. The K_0 -normally consolidated samples are, thus, expected to experience a small shear strain during the triaxial compression and the corresponding stress reversal in the extension phase up to the isotropic stress level.

The peak q value in compression is 2.99 kg/cm^2 and the corresponding value in extension is 3.30 kg/cm^2 . Thus, the K_0 consolidated samples revealed a smaller undrained shear strength in compression than in extension.

5.4.3.3 Stress Ratio-Strain Relationships

The (η, ϵ_s) relationship for both compression and extension tests are shown in Fig. 5.14. In this figure, the corresponding relationship for the isotropically consolidated sample is also shown. The following observations can be made in this figure.

- i) Beyond a stress ratio η of 0.49 corresponding to the K_o condition, the shape of the (η, ϵ_s) relationship for the isotropically consolidated sample is roughly the same as that for the K_o consolidated samples.
- ii) The peak values of η ($= M$) for the isotropically consolidated samples and the K_o consolidated samples are nearly the same and are 0.88 and 0.89, respectively.
- iii) Even though the (q/p_o) value at the peak deviator stress in compression is substantially smaller than that in extension for the K_o consolidated sample, their M values are approximately the same. For compression conditions $M= 0.89$, and for extension conditions $M= 0.93$.
- iv) The mirror image of the curve OB in extension of the corresponding curve OA of the isotropically consolidated sample seems to be roughly the same curve O'D in extension for the K_o consolidated sample.

5.4.3.4 Excess Pore Pressures

Figure 5.15 shows the response of the normalized excess pore pressure versus shear strain for the K_o -normally consolidated samples both in triaxial compression and in extension. An examination of this figure shows two distinct responses of excess pore pressure under the different shearing stress systems. The normalizable behaviour of the excess pore pressure is obvious as reflected in the other normalized behaviour such as the undrained stress path. During compression (see Fig. 5.15), the positive excess pore pressure is continuously increasing up to the failure state. During extension, however, the negative excess pore pressure decreased rapidly up to a shear strain of about 2.5%; thereafter, it is more or less steady with the increase in shear strain. At the failure state it even tended to have a slight increase (Fig. 5.15).

As discussed in Section 5.4.2.3 normally consolidated samples under isotropic stress exhibit a linear relationship between the normalized excess pore pressure (with respect to pre-shear stress) and the stress ratio. Figure 5.16 illustrates the relationship of u/p_o with η for the compression and extension tests on K_o consolidated samples. A continuous and smooth relationship is seen for the full range of the stress ratio η spanning from $-M$ (in extension Critical State) to $+M$ (compression Critical State). However, the pore pressure parameter C as defined by HANDALI (1986), where $(u/p_o = C\eta)$, is found to be different for both the cases of compression and extension conditions. In the case of compression, the variation is bi-linear with a value of C initially of 0.48 and beyond an η of 0.66 increasing to 1.03. However, for the extension

condition the values of C are 0.4 in the initial stage and 0.06 at the second stage. Also unlike in compression, the specimens in extension show a reversal of pore pressure response corresponding to the point X (in Fig. 5.16) up to the Critical State Y.

A clarification on the use of the relationship $u/p_o = C \eta$ needs to be made here. It would have been more rigorous if HANDALI (1986) had separated the component of Δu in the above expression as contributed from the spherical pressure increase $q/3$ due to the increase in the deviator stress. It would then be truly possible to confirm the excess pore pressure development during compression and extension according to the equation $u/p_o = C \eta$ and the corresponding C parameter as defined appropriately. On the contrary, with the C parameter as defined by HANDALI (1986), the loading compression test and the unloading extension test will have positive and negative excess pore pressures arising simply from the increase and decrease in the p value under loading and unloading conditions.

It is suggested that future researchers estimate the excess pore pressure due to pure shear under constant p type of applied stress path when formulating the expression $u/p_o = C \eta$.

5.4.3.5 Strength Characteristics

The observed effective stress paths of K_o -normally consolidated samples during undrained triaxial compression and extension are presented in Figs 5.10 and 5.11. In triaxial compression a peak undrained strength is mobilized at a small shear strain ($\epsilon_s = 3.6\%$) and at a stress ratio lower than that mobilized ultimately. The strength tends to increase linearly with the magnitude of consolidation stresses. Two failure envelopes are defined, one based on the peak strength and the other on the maximum obliquity ratio. The slope of the failure envelope at peak strength is 0.81 and the corresponding value of $\bar{\phi}$ is 21° . The peak undrained strength ratios, $s_{up}/\bar{\sigma}_{vo}$, mobilized in compression are 0.251 and 0.253 for the CK_oU1 and CK_oU1-2 tests, respectively, and these average to 0.252. The effective mean normal stress at the peak strength for the CK_oU1 test (K_o -normally consolidated state) is 3.77 kg/cm^2 . On the other hand, the strength at the Critical State is slightly lower than the peak strength, and it mobilized at large shear strain. The slope of the failure envelope (referred to as the Critical State Line) is 0.89 and the corresponding $\bar{\phi}$ is 23° . The mean effective stress p_{cs} at the Critical State (for test CK_oU1) is 3.26 kg/cm^2 .

In triaxial extension, the peak strength and the maximum obliquity ratio occurs at nearly the same shear strain. The slope of the Critical State Line in extension is 0.93 and the corresponding value of $\bar{\phi}$ is 33° (Fig. 5.11). Thus, the Critical State parameter M in extension is greater than that in compression. The undrained strength ratio in extension, $s_{ue}/\bar{\sigma}_{vo}$ for the tests CK_oUE1 and CK_oUE1-2 are 0.297 and 0.286, respectively. The average value of undrained strength is 0.291. Therefore, the undrained strength ratio in extension is slightly greater than that in compression ($s_{ue}/\bar{\sigma}_{vo} = 0.252$). In other words, the undrained strength ratio in triaxial compression averages about 87% of that in extension. This result contradicts some of the data

reviewed in Section 2.3.4. However, it is quite close to the value of 0.90 which was found for the Bangkok clay by WIJEYAKULASURIYA (1986). MITACHI and KITAGO (1979) also reported that the undrained strength ratio of remoulded clay having a plasticity index of 49% in compression was about 95% of that in extension. It can be concluded, therefore, that the plasticity index plays a significant role in strength anisotropy. The lower the plasticity index the lower the strength in extension as compared with that in compression. As the plasticity index increases the strength difference between compression and extension diminishes.

5.5 Comparison of Isotropically and K_0 -normally Consolidated Samples in Triaxial Compression

5.5.1 Introduction

Even though comparisons were made earlier on the compression behaviour of isotropically and K_0 consolidated samples, a separate comprehensive description is needed in this section as often the stress-strain theories are developed based on the data from isotropically consolidated samples. Also it is common to carry out isotropically consolidated tests in practice as these tests are easy to perform than the corresponding K_0 consolidated tests.

In making the appropriate comparison here, two specimens one isotropically consolidated (CIU1) and the other K_0 consolidated (CK₀U1) with a p_0 value of 6.5 kg/cm² and $(p_0)_{K_0}$ value of 4.5 kg/cm², respectively were chosen. These samples were selected since they both have the same void ratio of about 1.16 prior to shear.

5.5.2 Undrained Stress Paths

Figure 5.17 illustrates the undrained stress paths of specimens CIU1 and CK₀U1. In this figure the dotted line AB connects the initial states of both samples and is therefore in a sense a constant void ratio contour or can even be considered as an undrained stress path with simplicity, while the curve AEF is truly the undrained stress path of the isotropically consolidated sample. The path BOF corresponds to the K_0 consolidated sample. Several points need to be clarified at this stage. One is why the point B does not lie on the undrained stress path AEF, but instead lies inside. The explanation arises from the fact that the K_0 consolidated specimen is initially sheared under a deviator stress to bring its pre-shear state to the K_0 condition. Also, substantial secondary consolidation appears to have taken place in the isotropically consolidated and even perhaps in the K_0 consolidated sample. A certain magnitude of pre-shear secondary consolidation can make the undrained stress path AEF somewhat similar to that of a lightly overconsolidated clay and evidence of this emerged earlier in discussion of the (q, ϵ_s) and $(u/p_0, \eta)$ relationships. Thus, the possibility remains that a steeper curve such as AB is more close to the undrained stress path of the normally consolidated state. In a similar manner, the K_0 consolidated specimen even shows a higher degree of overconsolidation since its stress path rises nearly vertical before

it merges with that of the isotropically consolidated specimen. It is interesting to note that the dotted curve AB in Fig. 5.17, when it is extended, tends to end up at the same point F, the Critical State of the actual samples under isotropically consolidated and K_o consolidated states eventually reached.

5.5.3 Stress-Strain Relationships

Figure 5.18 illustrates the (q, ϵ_s) relationship for the isotropically consolidated and the K_o consolidated samples. It should be noted that the datum for both q and ϵ_s for the isotropically consolidated sample is at point A in the (q, p) plot and is the same as the datum for the q values in the K_o consolidated sample as measured from the p -axis. However, the datum for the measurement of shear strain ϵ_s for the K_o consolidated sample refers to point B in the (q, p) plot and this datum is somewhat similar to the datum C for the isotropically consolidated sample when it reaches the K_o state during shear. It is, therefore, necessary to consider only the (q, ϵ_s) relationship for the isotropically consolidated specimen for values of q and ϵ_s greater than $(q)_{K_o}$ and $(\epsilon_s)_{K_o}$ when a comparison is made with the behaviour of the K_o consolidated sample. Such a shifted curve is drawn in dotted lines as C'D' in Fig. 5.18. Even for values of q greater than $(q)_{K_o}$, the isotropically consolidated sample has higher shear strain than the K_o consolidated one. Earlier it was explained that the K_o consolidated samples might have perhaps undergone substantial secondary consolidation prior to shear at its stress state B, which in a sense accounts for B is not coinciding with C along the stress path ACD.

Since the (q, p) values corresponding to B and C are different, more sensible comparison can only be made in the (η, ϵ_s) plot and this is done in the next section.

5.5.4 Stress Ratio-Strain Relationships

Figure 5.19 demonstrates the (η, ϵ_s) relationship for the isotropically consolidated sample and the K_o consolidated one. As stated before for the (q, ϵ_s) relationship, it is necessary to draw the dotted curve C'D' for the incremental (η, ϵ_s) relationship for the isotropically consolidated sample from values of η and ϵ_s beyond the values $(\eta)_{K_o}$ and $(\epsilon_s)_{K_o}$ corresponding to the K_o condition C. Such an incremental relationship C'D' in Fig. 5.19 is again found to be markedly different from the (η, ϵ_s) relationship for the K_o consolidated sample.

Even though this difference would appear rather undesirable in developing simple stress-strain theories, yet it further confirms the strong influence of time effects on the K_o consolidated sample which behaves more like a lightly overconsolidated specimen. In that sense,

the difference in ϵ_s between the curve C'D' and that of the K_0 consolidated sample appears to have built up for the initial incremental value of η from the K_0 state up to a value of about $\eta = 0.66$. Beyond this value, the two curves seem to run more or less parallel.

It is, thus, noteworthy that the Author's data reveal a strong time dependent stress-strain behaviour as opposed to that of the previous researchers who have somewhat neglected the effect of the duration of pre-shear consolidation and its dominant effect on the stress-strain behaviour of K_0 consolidated specimens which differ rather substantially from the isotropic ones.

5.5.5 Excess Pore Pressure-Strain Relationship

Figure 5.20 contains the (u, ϵ_s) relationships for the isotropically consolidated and the K_0 consolidated samples. As analyzed earlier, the dotted curve OD' for the isotropically consolidated sample which represents the (u, ϵ_s) relationship for values of u and ϵ_s beyond the K_0 stage is found to be similar to the behaviour exhibited by the K_0 consolidated sample.

5.5.6 Excess Pore Pressure-Stress Ratio Relationships

Figure 5.21 illustrates the $(u/p_0, \eta)$ relationship for the isotropically and K_0 consolidated samples. A detailed examination of this relationship is pertinent as it simplifies the strain independent nature of the definition of a pore pressure parameter C .

In Fig. 5.21, OC_1D_1 corresponds to the $(u/p_0, \eta)$ relationship for the isotropically consolidated sample. For this sample, p_0 refers to the pre-shear consolidation pressure at A in the (q, p) plot. Even though OC_1D_1 can be best fitted with a bi-linear relationship in which the initial slope C as given by $u/p_0 = C\eta$ is 0.52 and the final one is 0.75, it would be possible to approximate this relation as a linear one without any loss of accuracy. This would in a sense neglect the effect of the light overconsolidation in the specimen which gives the initial shallow slope of $C = 0.52$ up to a stress ratio $\eta = 0.12$.

The K_0 consolidated specimen gives the bi-linear relation $B_2E_2D_2$ where the slope C for the initial segment B_2E_2 is 0.37 and is even smaller than the initial value of 0.52 demonstrated by the isotropically consolidated sample. It has been mentioned repeatedly before that there is strong evidence that the K_0 consolidated sample is subjected to a higher degree of overconsolidation due to pre-shear secondary consolidation effects. The final segment E_2D_2 in Fig. 5.21 has a slope of 1.03 and differs from that of the isotropically consolidated sample which shows a C value of 0.75.

At this stage, it would be better to use the parameter p_{on} as suggested by HANDALI (1986) in the normalization of the excess pore pressure. The p_{on} value is the same as the p_0 value for

the isotropically consolidated sample. However, for the K_o consolidated sample p_o will refer to the value of $(p)_{K_o}$ at the K_o stage, while the use of p_{on} will still refer to the pre-shear consolidation pressure of the isotropically consolidated sample at the stress state A.

Figure 5.22 illustrates the $(u/p_{on}, \eta)$ relationship for the isotropically and K_o consolidated samples. The variation $OC'_1D'_1$ in Fig. 5.22 is the same as the one OC_1D_1 in Fig. 5.21. However, the relation $B'_2E'_2D'_2$ in Fig. 5.22 is different from $B_2E_2D_2$ in Fig. 5.21, since the p_{on} value used in Fig. 5.22 is 6.5 kg/cm^2 and the $(p)_{K_o}$ value used in Fig. 5.21 is 4.5 kg/cm^2 .

A simplified picture emerges in Fig. 5.22 when the final slope $E'_2D'_2$ of the K_o consolidated sample is the same as the one for the isotropically consolidated sample, i.e., $OC'_1D'_1$. In Fig. 5.22, $C''_1D''_1$ is the shifted $(u/p_{on}, \eta)$ relation $C'_1D'_1$.

Finally, it would be more appropriate to conclude this section with Fig. 5.23 which contains the data for all the four samples; two of them were sheared from the isotropic stress state and the other two from the K_o consolidation state. Irrespective of their initial pre-shear stress conditions, the $(u/p_{on}, \eta)$ relationships for both the isotropic and the K_o consolidated samples give C values of 0.75 and 0.73 which are very close to the range of stress ratio in which the apparent overconsolidation due to pre-shear stress condition is not significant.

5.6 Undrained Behaviour of Overconsolidated Samples under Isotropic Pre-Shear Conditions

5.6.1 Introduction

Almost all natural deposits of Soft Clays are in a lightly overconsolidated state. As such the stress-strain behaviour and strength characteristics of lightly overconsolidated clay become an important aspect of the behaviour of sedimentary soils which are found abundantly in Southeast Asia and other countries. In the previous section, the behaviour of normally consolidated clay under isotropic and K_o pre-shear conditions was examined in detail. In this section, the behaviour of lightly overconsolidated clay under pre-shear isotropic conditions will be examined. This will then be followed by a study of the behaviour of lightly overconsolidated clay as sheared from K_o conditions.

A total of six overconsolidated samples, with approximately the same initial water content, were sheared from different pre-shear stresses. The overconsolidation ratios employed were 1.24, 1.50, 1.78, 2.15, 2.75, and 4.25. Each sample was initially subjected to a different pre-shear consolidation stress corresponding to the overconsolidation ratio. The strain rate used for shearing is the same as that for the normally consolidated specimens (0.009 mm/min). All samples have the same pre-shear void ratio, e_o of 1.16.

5.6.2 Undrained Stress Paths

Figure 5.24 contains the undrained stress paths of the overconsolidated samples sheared from the isotropic stress states. These undrained stress paths are typical of those presented by earlier researchers for Bangkok clay as well as for other clays (see WROTH and LOUDON, 1967). The undrained stress paths of the samples CIU4, CIU5, CIU6, and CIU7 all have stress paths which are sub-parallel to the q -axis. Such a behaviour strongly supports the elastic wall concept of the Cambridge stress-strain theories. The samples CIU2 and CIU3 had stress paths initially sub-parallel to the q -axis with constant p , but then started to curve in a manner which indicates volumetric yielding. A consistent picture of the volumetric yielding emerges both for the wet and dry side of the Critical State. On the wet side, the deviator stress at which volumetric yielding commenced is found to increase with the increase in OCR. Thus, for the sample CIU5 which has an OCR of 2.15, the stress path is nearly sub-parallel to the q -axis indicating that the sample did not have any volumetric yielding even when it reached the Critical State at L. On the dry side of the Critical State, samples CIU6 and CIU7 tend to yield with dilation at values of q close to the Critical State.

The lightly overconsolidated samples on the wet side of the Critical State tend to have their end points clustered around the Critical State point L. While the samples on the dry side (CIU6 and CIU7) approached the Hvorslev strength envelope and then tend to seek the Critical State either moving on the Hvorslev envelope or failing with strain softening. The Hvorslev strength parameters $\bar{\phi}_e$ and \bar{c}_e are 19° and 0.5 kg/cm^2 , respectively. At the Critical State, $q/p_e = 0.44$ and $p/p_e = 0.50$.

The Author's results may now be compared with those of WROTH and LOUDON (1967). The OCR values used by WROTH and LOUDON are 1.0, 1.2, 1.5, 2.2, 2.5, 4.0, and 4.6. These values are close to many of the samples tested by the Author which had OCR values of 1.0, 1.24, 1.5, 1.78, 2.15, 2.75, 4.25. It should be noted that WROTH and LOUDON (1967) presented data from resedimented samples of Kaolin, while the Author's data are based on undisturbed samples of Bangkok clay as tested in the higher range of pre-shear consolidation pressure which ranges from 2.15 to 6.5 kg/cm^2 .

Figure 5.25 presents the Author's undrained stress paths together with the undrained stress paths of WROTH and LOUDON (1967). A better comparison of the two sets of data can be made in the $(q/p_e, p/p_e)$ plot as shown in Fig. 5.26. The remarkable similarity and coincidence of the two sets of undrained stress paths clearly confirm the consistency and the accuracy of both sets of test data. Such a consistency in the behaviour can be expected to some extent as the mineral composition of Bangkok clay contains a high proportion of Kaolinite and Illite. The $q/p_e, p/p_e$ values at the Critical State as observed by the Author are close to the values of WROTH and LOUDON (1967) which are $q/p_e = 0.52$ and $p/p_e = 0.47$. The p/p_e value observed by HANDALI (1986) is also 0.57 and is close to the value quoted here. It should be remembered that HANDALI (1986) worked at a substantially low stress level very close to in-situ stresses.

5.6.3 Stress-Strain Relationship

Figure 5.27 presents the (q, ϵ_s) relationship for all the overconsolidated specimens. The unique (q, ϵ_s) relationship for all samples on the wet side of the Critical State with OCR value of less than 2.15, is an excellent confirmation of the constant q -yield loci of ROSCOE and BURLAND (1968).

5.6.4 Pore Pressure-Strain Relationships

Figure 5.28 illustrates the (u, ϵ_s) relationship for all the overconsolidated samples sheared from the isotropic stress state. The consistency and trend in the continuous development of smaller pore pressures with increasing OCR at any strain level gives added credibility to the accuracy of the data.

5.6.5 Normalized Pore Pressure-Stress Ratio Relationships

In the section on the undrained behaviour of normally consolidated samples both from isotropic and K_o pre-shear states, substantial emphasis was made on the $(u/p_o, \eta)$ relationship. Figure 5.29 contains the $(u/p_o, \eta)$ relationship for all the overconsolidated samples. In this figure p_o refers to the actual pre-shear consolidation pressure. The table contained in Fig. 5.29 indicates the stress ratio, η_t , at which the two linear sections of the $(u/p_o, \eta)$ relationship intersect.

For the first linear section,

$$u/p_o = C_1 \eta \text{ and}$$

For the second linear section,

$$u/p_o = C_2 \eta$$

The values of C_1 and C_2 are also tabulated with respect to OCR. C_1 is found to decrease in a consistent manner with the OCR values. Similarly, η_t is found to increase consistently with the OCR values. In a sense the value of (q, p) corresponding to each η_t will refer to the volumetric yield point in the (q, p) plot for the specimens sheared on the wet side of the Critical State. It is interesting to note that the normally consolidated samples with OCR= 1.0, also have an η_t value of 0.12 and faithfully support the comment made earlier on the light overconsolidation experienced by the specimen from the pre-shear secondary consolidation effects.

For the specimens on the wet side of the Critical State, the parameters C_1 , C_2 , and η_i are sufficient to describe the undrained stress paths for OCR values in the range of 1.0 to 2.15. Such simple expressions for the undrained stress paths are useful for practical purposes as well as for incorporation in the development of an appropriate stress-strain theory for lightly overconsolidated clay rather more simplified than the one proposed by PENDER (1977, 1978).

Figure 5.30 illustrates the $(u/p_o, \eta)$ relationship as plotted by the Author from the data of WROTH and LOUDON (1967). There is a remarkable coincidence in the pattern of behaviour illustrated in Fig. 5.30 of the data from WROTH and LOUDON (1967) when compared with the Author's data in Fig. 5.29.

It should be emphasized that the behaviour of the overconsolidated clays on the wet and dry side of the Critical State Line show distinctly different types of characteristics when reviewed in terms of the pore pressure development. Thus, the demarcation value of the OCR between the wet and the dry side need to be investigated more precisely and perhaps when this OCR value is approached, η_i nears M the limit value of η and C_1 reaches an asymptotic lower limit for this OCR for the full range of η varying from 0 to M . Thus, it is evident that in Fig. 5.29 the $(u/p_o, \eta)$ relationship for specimens CIU6 and CIU7 are to be considered separately from all other specimens with OCR values lower than or equal to about 2.15. A similar comment would apply to the data of WROTH and LOUDON (1967), presented in Fig. 5.30, where the tests with OCR values of 2.5, 4.0, and 4.6 are to be considered separately from the other tests which are on samples on the wet side of the Critical State.

A brief comment needs to be made on the use of the parameter p_{on} by HANDALI (1986) in interpreting the data of lightly overconsolidated clay in the $(u/p_o, \eta)$ plot. HANDALI (1986) recommended the use of the maximum past pressure p_e (denoted as p_{on}) for the normalization of the excess pore pressure in overconsolidated samples. Such a plot of $(u/p_{on}, \eta)$ is shown in Figs. 5.31 and 5.32 for the Author's data and the data of WROTH and LOUDON (1967), respectively. Both figures show continuous reduction in C_1 and C_2 values with increase in OCR.

Figures 5.33a and 5.33b illustrate the variation η_i and C_1 with OCR, where the η_i and C_1 values are obtained from the $(u/p_o, \eta)$ plot. The presentation of the data in this plot gives a better understanding of the volumetric yielding inside the State Boundary Surface. It appears that as the OCR value increases, the stress ratio at which volumetric yielding takes place denoted as η_i also increases (see Fig. 5.33a). There is some logic in looking for an OCR eventually on the boundary between the wet and dry side at which η_i will become a maximum and perhaps coincide with M . The results of the Author and WROTH and LOUDON (1967) seem to indicate this trend, yet a detailed investigation is needed especially in the transition region of the OCR when η_i decrease (possibly from M).

Figure 5.33b also shows that the slope C_1 reduces with OCR from the value 0.73 to an asymptotic lower limit. It seems that this range of C_1 value corresponds to the positive pore pressure development. The Author has no data on the dry side that would enable precise statements to be made about the $(u/p_o, \eta)$ relationship when the samples tend to dilate.

Figures 5.34a and 5.34b, although containing some data on the dry side of the Critical State, show a trend in which η_r reduces and reaches a limit value with higher OCR, while C_1 approaches a constant lower value. But, these statements are to be taken with caution because of insufficient test data.

Figure 5.35a and 5.35b present the η_r and C_1 values with respect to HANDALI's (1986) use of the $(u/p_{on}, \eta)$ relationship to determine η_r and C_1 . The trend in η_r is the same as that in Fig. 5.34a in the Author's approach. However, C_1 seems to decrease continuously in HANDALI's plot and can even be stretched to a zero value for an appropriate OCR. This treatment could be more appealing as one would expect the pore pressure development to be lesser and lesser as the OCR increases. As such, there must be an OCR value for which C_1 must tend to zero. This would then help to visualize that for heavily overconsolidated clay the C_1 value would be negative indicating dilatancy rather than volumetric compression. These aspects are important for further exploration; the Author's data at the current stage are not sufficient to make further progress in these interpretations.

5.6.6 Pore Pressure Parameter A_f

Figure 5.36 shows the variation of the value of A_f , the pore pressure parameter A at failure, with the overconsolidation ratio. The value of A_f decreases with the increase in the overconsolidation ratio. The observed values of A_f for the lightly overconsolidated sample ($OCR < 4.0$) remained positive. The predicted values of A_f as made from the Modified Cam Clay Model (ROSCOE and BURLAND, 1968; WROTH, 1984) agree well with the experimental observations, for OCR values on the wet side of the Critical State.

5.6.7 Volumetric Yielding Inside the State Boundary Surface

ROSCOE and BURLAND (1968) provided a novel technique which accommodates distortional yielding inside the State Boundary Surface with the use of a set of constant q -yield loci. Evidence has also been reported in the literature on volumetric yielding especially on the wet side of the Critical State for stress state close to the undrained stress path of the State Boundary Surface and within the surface itself. In an earlier section, extensive comment and interpretations were made to estimate the stress ratio, η , at which the $(u/p_o, \eta)$ relationships revealed volumetric yielding. Such stress states are located in the (q, p) plot within the undrained stress path in Fig. 5.37. The locus of the volumetric yield points lies within the undrained stress path. Also presented in Fig. 5.37 is the volumetric yield locus as predicted by the Modified

Cam Clay Theory of ROSCOE and BURLAND (1968). A remarkable agreement is noted both in the ROSCOE and BURLAND prediction and the volumetric yield locus estimated from the test data based on the $(u/p_o, \eta)$ relationship. It would have been more rewarding if data are available to extend the volumetric yield locus to the dry side where dilatancy takes place. However, such systematic data are not yet available on Bangkok clay.

5.6.8 Shear Strength of Overconsolidated Samples

The peak deviator stress points (open circles) of the overconsolidated samples are also shown in Fig. 5.37. The failure points of the overconsolidated samples are clustered around the Critical State stress point of the normally consolidated sample. Consequently, the peak deviator stress for lightly overconsolidated samples (with OCR less than 2.15) having the same initial water content is found to be approximately the same as the normally consolidated sample. For increasing overconsolidation the peak deviator stress point is found to lie on the Hvorslev surface.

It is common to express the undrained strength as a ratio of the vertical consolidation pressure. Thus for the overconsolidated samples $(s_{up}/\bar{\sigma}_{vo})_{OC}$ is calculated wherein $\bar{\sigma}_{vo}$ refers to the pre-shear consolidation pressures and in the Author's test programme $\bar{\sigma}_{vo}$ decreases with increase in OCR. For the normally consolidated clay, the corresponding ratio is $(s_{up}/\bar{\sigma}_{vo})_{NC}$ where $\bar{\sigma}_{vo}$ refers again to the pre-shear vertical consolidation pressures. In the Author's test programme, the pre-shear void ratio of all samples was held constant, thus, the p_{max} values are also increasing with increase in OCR.

The strength ratio $(s_{up}/\bar{\sigma}_{vo})_{OC} / (s_{up}/\bar{\sigma}_{vo})_{NC}$ is plotted with respect to OCR in Fig. 5.38. It should be noted that the $\bar{\sigma}_{vo}$ value for the NC-sample is different from the pre-shear consolidation values of the overconsolidated samples. For isotropically consolidated samples $(s_{up}/\bar{\sigma}_{vo})_{OC} / (s_{up}/\bar{\sigma}_{vo})_{NC}$ is the same as $(s_{up}/p_o)_{OC} / (s_{up}/p_o)_{NC}$. In Fig. 5.38, such a strength ratio is found to increase with the OCR values. Shown in the same figure are the predictions by WROTH (1984) based on the Modified Cam Clay Model of ROSCOE and BURLAND (1968). The predicted values of the strength ratio for values of Λ of 0.77 and 0.7 seem to lie in a narrow band and contain the experimental observations. $\Lambda = (1 - \kappa/\lambda)$ is considered as a basic soil parameter which involves the compressibility and the swell coefficients.

5.6.9 Void Ratio-Stress Relationship at the Critical State and Failure

Figure 5.39a illustrates the isotropic consolidation line AB in the $(e, \ln p)$ plot for the stress range in which the tests were conducted. In this figure, the dotted lines indicate the history of the CIU samples, how they have swollen to the pre-shear consolidation stress from the isotropic

consolidation line. The line CD corresponds to the q_{\max} condition and is drawn with the same slope λ ($=0.357$) as the isotropic consolidation line AB. The q_{\max} points of all the samples both normally consolidated and overconsolidated are found to cluster around the failure line CD as defined by the q_{\max} condition. Figure 5.39b is a similar plot where the line C'D' corresponds to the maximum stress ratio (η_{\max}) condition and is more appropriate to be taken as the Critical State Line. The points clustering around the line C'D' now correspond to the end points of the test under the maximum stress ratio condition. In Fig. 5.39c it can be seen that the Critical State Line (CSL) C'D' is to the left of the q_{\max} line CD as shown in Figs. 5.39a and 5.39b, respectively.

5.6.10 Shear Strain Contours

The constant shear strain contours are superimposed on the undrained stress paths in Fig. 5.40. These contours are similar to those presented by WROTH and LOUDON (1967), BALASUBRAMANIAM (1969, 1975) among others. The contours support the idea of the constant q -yield loci on the wet side of the Critical State as proposed by ROSCOE and BURLAND and on the dry side forms a set of lines which converge to a negative value of $p_0 = -2.4$ kg/cm² on the p -axis.

Even though such a pattern of behaviour has been reported many times before, a fundamental analysis of these contours has not yet been advanced since the contribution of ROSCOE and BURLAND (1968). A simplified revision of these contours can be shown as in Fig 5.41. The undrained stress path AB of the normally consolidated clay (a version of the volumetric yield locus in ROSCOE and BURLAND, 1968, when $\kappa = 0$) intersects the Critical State Line at B. Such stress states at the Critical State do not exhibit a cohesion component, but indicate the behaviour as a frictional material with its failure envelope coinciding with the Critical State Line OBE. BG corresponds to the limit value of p for which overconsolidated samples with pre-shear consolidation pressures in the range G to A exhibit the constant shear strain contours constituting the constant q -yield loci within the State Boundary Surface. However, for values of pre-shear consolidation pressure less than that of point G, the constant shear strain contours are inclined such that they all converge to a point D, which is, in fact, determined by the Hvorslev true cohesion \bar{c}_e for overconsolidated samples and changes with the water content. Such an idealization would then offer a simple means by which the radial fan of the shear strain contours on the dry side of the Critical State can be generated once the position of the constant q -yield loci on the wet side of the Critical State is known and the Hvorslev strength envelop BC is fixed. Figure 5.42 illustrates the (η, ϵ_s) relationship of the Author's data on the wet side and those of WROTH and LOUDON (1967). In spite of the fact that the mineralogical composition of the two clays are different (i.e., one Kaolin and the other Bangkok clay with Kaolinite, Illite, and Montmorillonite in equal proportion), the (η, ϵ_s) relation which dictates the contribution from the constant q -yield loci within the State Boundary Surface is the same and offers further confirmation of the fundamental importance of such a set of yield loci.

5.7 Undrained Behaviour of Overconsolidated Samples under K_0 Pre-Shear Conditions

5.7.1 Introduction

The experimental investigation on the undrained behaviour of overconsolidated samples in the lightly overconsolidated state forms an important part of this research, since such behaviour is closer to reality than the behaviour investigated from isotropic pre-shear conditions. Also, such experimental observations on Bangkok clays have not been available nor indeed are they common for other clay deposits.

Two series of tests were carried out under K_0 type of conditions. In one series referred to as CK_0U tests, the samples are prepared in such a way that their pre-shear stress states lie on a line AB as shown in Fig. 5.43. In Sections 5.3.2 and 5.3.3, a detailed description was given as to how the idealized K_0 -line AB is established as shown in Fig. 5.43 such that the samples with stress states A, A_1 , A_2 A_5 are prepared under K_0 conditions with different OCR but with the same void ratio or water content. Unlike the normally consolidated sample with its stress state at A, all the overconsolidated samples with their stress states A_1 , A_2 A_5 were prepared such that they were initially consolidated along the path OA (on the extended segment) up to stress points a_1 , a_2 a_5 and were subsequently swollen back along each of the path a_1A_1 , a_2A_2 a_5A_5 so that there is virtually no change in the area of cross section of the samples, and when the stress states, A_1 , A_2 A_5 are reached, they all have approximately the same void ratio. This particular method adopted in reaching the pre-shear stress states yields a difference in the definition of the OCR values. The OCR values were established under two different assumptions. In one case the OCR is defined as (p_{max}/p_o) , that is, in Fig. 5.43 the OCR values for the sample A_3 and A_5 are (p_{a3}/p_{A3}) and (p_{a5}/p_{A5}) , respectively. For the other case comparisons were made to estimate OCR values based only on the vertical stresses. That is, when the sample is at A_3 , its OCR value is $(\bar{\sigma}_{va1}/\bar{\sigma}_{vA1})$ where $\bar{\sigma}_{va1}$ and $\bar{\sigma}_{vA1}$ corresponded to the axial stress for the stress states a_1 and A_1 , respectively.

For the given samples with initial stress states A_1 , A_2 A_5 (see Fig. 5.43), the OCR values based on (p_{max}/p_o) are 1.00, 1.20, 1.40, 1.60, 1.85, and 2.20 (see Table 4.2). However, when the OCR values are based on vertical stresses as $(\bar{\sigma}_{vm}/\bar{\sigma}_{vo})$, the corresponding values are 1.00, 1.24, 1.50, 1.78, 2.15, and 2.75. Thus, some differences are to be noted especially when the OCR values increase. Figure 5.44 contains both types of OCR value for the three series of tests. For Test Series I, which were prepared along an idealized K_0 -line AB (in Fig. 5.43), the curve OA (in Fig. 5.44) represents the correlation between the two types of OCR values. However, the line OB inclined at 45° indicates equal values for both types of OCR for the samples which were consolidated and swollen along the radial path OAa_5 and a_5AO (see Fig. 5.43). As already described the second series of tests referred to as CAU tests were conducted on samples which were consolidated along the radial path OA to appropriate stress level and then swollen back to its current stress along the same trace.

An important aspect of these tests is that they were all carried out in such a manner that the pre-shear void ratio of the samples are the same at about 1.16. Thus, this is the first time such a comprehensive series of tests were conducted in a manner similar to the Hvorslev type of research where the components of the strength and the stress-strain behaviour were matched under constant water content or void ratio. For the Test Series I (i.e., CK_0U tests) both compression and extension tests were conducted from the idealized K_0 -line AB. However, due to the time limitations only compression tests were conducted in the second series (i.e., CAU tests). The overconsolidation ratios as defined with respect to vertical stresses were 1.24, 1.50, 1.78, 2.15, and 2.75, respectively. A total of 15 tests were conducted; ten of these in compression, five each in CK_0U and CAU tests. The other five were extension tests from CK_0U conditions. Samples were sheared under the conventional type of triaxial loading in compression and unloading in extension. Thus, the compression tests were conducted with constant lateral stress and the axial stress increasing and the extension tests were of the unloading type with constant lateral stress and the axial stress reducing. A strain rate of 0.009 mm/min was used in all the tests

5.7.2 Undrained Stress Paths

Figure 5.45 illustrates the effective stress paths in compression and in extension as sheared from the idealized K_0 conditions (with pre-shear consolidation state along AB). The undrained stress path of the normally consolidated sample on the compression side is well rounded above the point A, while under extension conditions the undrained stress path is nearly sub-parallel to the q-axis. Thus, the curve CAD now constitutes a cross section of the State Boundary Surface which is asymmetrical about the K_0 consolidation line OA, the idealized K_0 line AB and the isotropic axis OE. Even for the normally consolidated sample under compression conditions, the undrained stress path arose nearly sub-parallel to the q-axis up to G (which is a sort of volumetric yield point and will be discussed later). Thus, the path EAG (where EA is the path of the extension test and AG is the initial part of the compression test) appears to be more like that of a lightly overconsolidated sample. Similarly, for all the overconsolidated samples the initial segment of the undrained path in extension A_1E_1 , A_2E_2 A_5E_5 are all sub-parallel to the q-axis and remain so on the compression side for values of q higher than those corresponding to the K_0 line OA and even up to points such as G_1 , G_2 G_5 which are close to the Critical State Line. On the extension side volumetric yield seems to take place at an early stage as depicted by the points H_1 , H_2 H_5 . The volumetric yielding on the extension side is less pronounced than those on the compression side.

It is interesting to note that towards the end of shearing all end points tend to cluster around the Critical State point C in compression and point D in extension. Also, now the slope of the Critical State Line in compression and extension are nearly the same; line OC with slope 0.89 and line OD with slope 0.93 (see Fig. 5.45).

The OCR values of these K_o consolidated samples ranged from 1.00 to 2.75. Also in earlier section, an alternative way of determining the OCR based on p values was described. It would be worthwhile to determine the p_e values corresponding to points A, a_1 , a_2 ,.... a_5 in Fig. 5.45 as $(p_e)_A$, $(p_e)_{a_1}$,.... $(p_e)_{a_5}$ in Fig. 5.46. Then with respect to isotropic stresses the OCR values can be computed from the p_e values and the p values at the states E, E_1 , E_2 ,.... E_5 in Fig. 5.46. The OCR values so calculated are shown in a table in Fig. 5.47 as 1.27, 1.44, 1.68, 1.91, 2.26, and 2.68. Table 5.3 compares the values of OCR calculated by all the three methods.

Table 5.3 OCR Values from Different Definitions

Test Names	OCR Values		
	$\bar{\sigma}_{vm}/\bar{\sigma}_{vo}$	p_{max}/p_o	$(p_e)_{max}/(p_e)_o$
CK _o U1	1.00	1.00	1.27
CK _o U2	1.24	1.20	1.44
CK _o U3	1.50	1.40	1.68
CK _o U4	1.78	1.60	1.91
CK _o U5	2.15	1.85	2.26
CK _o U6	2.75	2.20	2.68

Indeed the Critical State Concept ideas need to be applied with the correct stress history effects on the samples with their pre-shear stress states at A, A_1 , A_2 ,.... A_5 . These samples have been initially taken along the stress path OA (see Fig. 5.47) which corresponds to a stress ratio of η_k . Further they will also remember how they were taken to the stress ratio η_k and from which level of isotropic stress state. Thus, when the samples are sheared from the states A, A_1 , A_2 ,.... A_5 , in a sense they will tend to remember their initial stress ratio η_k as well as the initial undrained or drained shear process which took them to such a stress ratio level. Therefore, in this sense, a strict comparison of the compression and extension behaviour of these specimens can only be made for compression stress ratio η higher than η_k and for the extension case when the stress ratio $|\eta|$ exceeds $|\eta_k|$.

Thus, an asymmetry in the shape of the curve CGAED in Fig. 5.45 (and in Fig. 5.47) is logically expected and some researchers tend to confuse this behaviour as a contradiction of the State Boundary Concept advocated in the Critical State Soil Mechanics. In Fig. 5.47 when the symmetrical stress path E_oD is completed as a mirror image of the curve CGE_o (the undrained stress paths of an ideal normally consolidated clay sheared from isotropic pre-shear conditions) then $CGE_oG'D$ corresponds to the true section of the State Boundary Surface and thus the behaviour exhibited by the path GAED corresponds to an apparent overconsolidation due to secondary consolidation time effects as well as pre-shear stress effects.

Figure 5.48 shows the undrained stress paths of the CAU tests specimens. The stress paths followed by the CAU test specimens are similar to those followed by the CK_0U test specimens.

5.7.3 Stress-Strain Relationships

In the earlier section on isotropically consolidated samples, the constant q -yield loci was established and the contribution from such yield loci can be compared with the incremental (q, ϵ_s) relationship under CK_0U and CAU conditions. Further, the importance of pre-shear stress history and time effects are also emphasized in the analysis of the undrained stress paths.

Figure 5.49 illustrates how the shear strain in CK_0U and CAU tests can be estimated from the constant q -yield loci established for isotropically consolidated samples. In this figure the volumetric yield loci for two specimens sheared from K_0 stress states A_1 and A_2 are drawn through their p_{max} points a_1 and a_2 as a_1E_{a1} and a_2E_{a2} . Figure 5.50a illustrates in a clear manner the estimation of the shear strains in the CK_0U tests from the constant q -yield loci of the CIU tests. In this figure, the volumetric yield loci Ca_2E_{a2} is sketched and for any stress increment Δq for the CK_0U test and in the figure the specimen A_2 , the initial value of q for stress state A_2 is q_{A2} . The stress increment Δq moves the specimen to L along the undrained stress path LC . The q_{A2} value on the undrained stress path $E_{a2}a_2C$ corresponds to point P . Similarly corresponding to the stress $(q_{A2} + \Delta q)$, the point on the volumetric yield loci $E_{a2}a_2C$ is N . Then the incremental shear strain for the specimen A_2 , when it reaches the stress state L , is obtained from the shift in the constant q -yield loci between the point P and N on the curve $E_{a2}a_2C$ for a stress ratio increment $\Delta \eta$.

The procedure illustrated in Fig. 5.50a is for an overconsolidated undrained stress path A_2LC on the wet side of the Critical State Line. For the dry side of the Critical State Line, a similar approach can be adopted but with modifications for the contribution of the shear strain contours. As an example for the specimen with pre-shear stress state A_3 on the dry side (see Fig. 5.50b), the radial fans of constant shear strain contours with origin O' (on the extended p -axis in the negative direction) is used. If the point S corresponds to a constant q line drawn through A_3 to intersect the line CG in S , the point Q represents the stress state on the undrained stress path A_3QC after an undrained stress increment Δq . The point R is obtained in a manner similar to S on the line CG . The incremental shear strain for the stress increment Δq is now obtained as the shear strain increment bounded by the two lines $O'R$ and $O'S$ for a stress increment ratio $\Delta \eta'$ as illustrated in Fig. 5.50b.

A comparison of the (q, ϵ_s) relationship of the CK_0U specimen with OCR values of 1.24, 1.50, and 1.78 are presented in Fig. 5.51. In this figure the curves $A_1A_1'A_1''$, $A_2A_2'A_2''$, and $A_3A_3'A_3''$ correspond to the actual (q, ϵ_s) relationship for the CK_0U tests designated CK_0U2 , CK_0U3 , and CK_0U4 , respectively. Also, the (q, ϵ_s) relationships established from the constant

q-yield loci as obtained from the CIU tests are shown as $A_1B_1B_1'$, $A_2B_2B_2'$, and $A_3B_3B_3'$. It is noted that the (q, ϵ_s) relationship established for the CK_oU tests from the isotropic consolidation tests reveals higher ϵ_s values than the actual values in the CK_oU tests.

An attempt was then made to allow for the stress history effect in considering the (q, ϵ_s) relationship beyond the initial q value corresponding to the pre-shear consolidation states a_1, a_2, \dots, a_5 in Fig. 5.43. Such an incremental relationship is shown in Fig. 5.51 by the dotted curve. Here again the incremental stress-strain relationship for the CK_oU specimen and the value obtained from the CIU tests are different.

Figure 5.52 makes a comparison between the CK_oU consolidated samples and the CIU samples in the (q, ϵ_s) plot as sheared from the dry side of the Critical State. In this plot, the curves $A_4B_4B_4'$ and $A_5B_5B_5'$ correspond to the isotropically consolidated samples and the curves $A_4A_4'A_4''$ and $A_5A_5'A_5''$ correspond to the K_o consolidated samples. The dotted curve in Fig 5.52a corresponds to the incremental deviator stress - incremental shear strain relationship of the isotropically consolidated sample for stress levels beyond the initial q_{\max} value experienced during sample preparation. The use of the constant shear strain contours from the isotropically consolidated samples sheared under undrained condition to obtain the shear strain in CK_oU type of behaviour would thus need additional investigation.

Figure 5.53 illustrates the actual (q, ϵ_s) relationship for all the CK_oU specimens. For OCR values less than 1.78, the (q, ϵ_s) relationship is apparently the same. Such a behaviour is similar to the isotropically consolidated samples (CIU tests) as well. Figure 5.54 illustrates the same relationship when the incremental (q, ϵ_s) relationship is considered for stress state above the η_k line, i.e., for these curves the q and ϵ_s values are based on their datum as A_1, A_2', \dots, A_5' . Finally, in Fig. 5.55 such an incremental relationship is presented only for values of q higher than the $(q_o)_{\max}$ values during sample preparation (see inset in Fig. 5.55).

Figure 5.56 illustrates the (q, ϵ_s) relationship for the CAU tests. The specimens with OCR value 1.00 and 1.24 reveal a unique relationship which is different from the other four specimens. The extension tests data in Fig. 5.57 reveal a unique relationship between (q, ϵ_s) relationship for all the specimens with a narrow band of scatter.

5.7.4 Excess Pore Pressure Characteristics

Figure 5.58 illustrates the (u, ϵ_s) relationship for the CK_oU samples. For the samples with OCR values of 1.00, 1.24, and 1.50, the (u, ϵ_s) relationship is approximately the same up to a shear strain ϵ_s of 1%, beyond this strain level the pore pressures are found to be large when the OCR value is less. However, when the OCR values are 1.78, 2.15, and 2.75, higher pore

pressures are developed initially at low strain up to ϵ_s of about 1%, and then the (u, ϵ_s) relationship seem to rise at a lower rate. This initial rise in pore pressure makes interpretation somewhat difficult. At larger strains beyond 1.5%, there is a clear trend that the excess pore pressure developed reduces with the increase in the OCR of the samples.

Figure 5.59 illustrates similar (u, ϵ_s) relationship for the CAU samples. Here again at low strain level of less than 1%, all samples were initially found to have similar excess pore pressure development, however, beyond a strain of about 0.5%, the increase in u with ϵ_s is different for all five samples. For OCR values of 1.00 and 1.24, the excess pore pressures are found to be substantially higher than when the OCR values are 1.50, 1.78, 2.15, and 2.75. In all the latter samples, there seems to be some dilatant effect when the (u, ϵ_s) relationship shows mild peaks and then a reduction in u values and in samples CAU3 and CAU4, the excess pore pressure after reaching a peak reduces and then increases again. Figure 5.60, on the contrary, shows a steady reduction in u with strain for all the samples sheared in extension under unloading conditions. Except for samples CK₀UE3 and CK₀UE5, for all other samples the reduction in excess pore pressure consistently increases with the OCR values.

The A values at failure A_f , for all the specimens, are plotted with respect to OCR in Fig. 5.61. The CAU series seem to show a well defined reduction in A_f value with OCR as shown by the curve ABC. The CK₀U series seem to show lesser reduction as indicated by the curve ADE. Also, the isotropically consolidated samples showed the least reduction (see curve AFE). The trend established by the extension tests, i.e., samples in CK₀UE series, are quite different and is denoted as GH. The prediction made by WROTH (1984) seems to be close to the behaviour of isotropically consolidated samples, while the prediction of MAYNE and STEWART (1988) is somewhat closer to the CK₀U series of samples. It is not surprising that the CK₀UE tests showed a different trend from the others as this series was under unloading conditions while all the other series were under loading conditions.

5.7.5 Excess Pore Pressure-Stress Ratio Relationships

Figure 5.62 illustrates the $(u/p_o, \eta)$ relationship for the CK₀U series of samples. The points A, A₁, A₂,.... A₅ correspond to the initial state in the (q, p) plot (see Fig. 5.45). The points A₁', A₂'.... A₅' correspond to the states when the samples reached the η_k line during the undrained compression conditions. For samples with OCR values of 1.00, 1.24, and 1.50 (on the wet side) a clear bi-linear trend is evident as with initial segments AB, A₁B₁, and A₂B₂. The final segments are BC, B₁C₁, and B₂C₂, respectively. However, when the OCR values ranged from 1.78 to 2.75, the behaviour is somewhat different. As such these two ranges of OCR values, one consisting of tests CK₀U1, CK₀U2, and CK₀U3 on the wet side of the Critical State, are presented in a separated plot in Figs. 5.63 and 5.64. These bi-linear relations showed transition stress ratio η_t at values of 0.66, 0.76, and 0.86 when the OCR values were 1.00, 1.24, and 1.50, respectively.

It is interesting to note that the final segment of all these bi-linear relations are of similar slope, while the initial segments give slopes which are dependent on the OCR values. At stress conditions very close to the end state, deviations are noted for sample CK₀U3 from the linear segment.

Figure 5.64 shows the $(u/p_o, \eta)$ relationship for samples with OCR values of 1.78, 2.15, and 2.75. Here again the $(u/p_o, \eta)$ relationships can be approximated as bi-linear relations except at stress ratio close to the peak value. For such samples, the initial segments A₃B₃, A₄B₄, and A₅B₅ are found to be parallel with one another. Similarly, the second segments B₃C₃, B₄C₄, and B₅C₅ are also nearly parallel. Unlike the samples with OCR values of 1.00, 1.24, and 1.50 in Fig. 5.63, the bi-linear relations in Fig. 5.64 depict the slope C prior to η_i values higher than the corresponding slope for the second segment in the higher range of η greater than η_i . No clear trend is visible when the samples approach their peak stress ratio conditions close to the Hvorslev failure envelope.

Figure 5.65 contains the $(u/p_o, \eta)$ relationship for the CAU tests series of specimens. The samples CAU1 and CAU2 with OCR values of 1.00 and 1.24 show similar trend of bi-linear relation for most of the range of η . The initial segments AB and AB₁ differ slightly in slope but the final segments BC and B₁C₁ are parallel. However, towards the peak conditions the slopes of CD and C₁D₁ are different from BC and B₁C₁, respectively. The samples with OCR values of 1.50, 1.78, 2.25, and 2.75 show a different trend. For stress ratio values up to $\eta = 0.8$, the $(u/p_o, \eta)$ relationship for these samples is linear and reaches a limit boundary AE which can even be extended to AF ($\eta = 0.88$). However, for values of η in the range 0.88 to 1.0, the $(u/p_o, \eta)$ relationship shows substantial reduction when the samples approached the Hvorslev failure envelope and tends to reach the Critical State.

Figure 5.66 show the $(u/p_o, \eta)$ relationship under extension conditions in the CK₀UE series of tests. These relationships are different from those exhibited under compression conditions.

5.7.6 Yield Envelope, Critical State and Hvorslev Envelope

Interesting points emerge in relation to the yield envelope, the Critical State and the Hvorslev strength envelope. Figure 5.67 shows the CIU undrained stress path for normally consolidated sample. In this figure, the CK₀U path in compression and extension are also shown for normally consolidated samples. Apparently, the CK₀U and CK₀UE tests show apparent overconsolidation. The Hvorslev envelope BC as obtained from the overconsolidated samples in CAU and CK₀U tests are also drawn. In Fig. 5.68 the volumetric yield points as obtained from the $(u/p_o, \eta)$ relationship are plotted and these points tend to cluster around the Critical State Line OB. Thus, it is interesting to note that as all samples in the lightly overconsolidated states move close to the Critical State, extensive yielding takes place and this yielding tends to

obstruct the samples reaching the Hvorslev failure envelope BC. Thus, the samples which are in the lightly overconsolidated state close to BB_0 and on the dry side tend to yield substantially when they reach the Critical State Line before reaching the Hvorslev failure envelope.

5.7.7 Undrained Strength Characteristics

Figures 5.69 and 5.70 contain the undrained strength of the normally consolidated and overconsolidated samples as plotted with respect to the OCR. In Fig. 5.69, the undrained strength ratios are presented. The prediction by WROTH (1984) seems to match the values from all compression tests up to OCR value of 2.20. However, for the extension tests, the WROTH's predictions are on the lower side.

In Fig. 5.70, the strength ratio $(s_{up} / \bar{\sigma}_{vo})_{OC} / (s_{up} / \bar{\sigma}_{vo})_{NC}$ is plotted. In this plot, WROTH's prediction agrees well with the measured values up to an OCR of about 2.5. Finally, Figs. 5.71a and 5.71b illustrate the $(e_f, \ln p)$ relationship as well as the $(e_{K_0}, \ln p_{K_0})$ relationship for the samples sheared to failure under the CK_0U conditions. Also shown in these figures are the stress paths during K_0 swelling and their initial states prior to CK_0U shear. The projection of the CSL (i.e., $(\bar{\sigma}_1/\bar{\sigma}_3)_{max}$ condition) in Fig. 5.71b more or less coincides with the similar projection of the CIU tests presented in Fig. 5.39b.

5.7.8 Stress Ratio-Shear Strain Relationships

Figures 5.72 to 5.74 contain the (η, ϵ_s) relationship for the CK_0U , CAU, and CK_0UE tests series, respectively. In the CK_0U and CAU series (Figs. 5.72 and 5.73) for OCR values higher than 1.78 and up to 2.75, the (η, ϵ_s) relationship seems unique. This is somewhat similar to the conclusions reached by earlier researchers. A similar trend is also seen in the extension tests (Fig. 5.74).

5.8 Summary of Undrained Behaviour

The experimental observations, interpretations and discussions on the undrained behaviour of normally consolidated and overconsolidated clays as tested from isotropic and K_0 conditions both in compression and extension are presented in detail. Important aspects of these behaviour are now summarized in this section together with the consolidation characteristic of clays. The undrained behaviour of the normally consolidated samples will be first summarized and this will then be followed by the summary of the overconsolidated behaviour. The pre-shear void ratio of all the samples are the same in the order of 1.16.

5.8.1 Consolidation and Swelling Characteristics of Clays

The compressibility characteristics under isotropic and K_o conditions are virtually the same up to the maximum past pressure p_c . Beyond the p_c value, the K_o consolidated samples have an $(e, \ln p)$ relation displaced to the left from the isotropic one, and eventually the isotropic and K_o consolidation lines are parallel to one another as implied in a unique State Boundary Surface (SBS).

The swelling lines are approximately parallel in compression corresponding to p value less than p_c value of 0.58 kg/cm^2 , and the swelling indices κ are the same regardless of the swelling lines, i.e., isotropic or K_o -swelling lines. This observation confirms the elastic wall concept where the samples experience volumetric swelling and compressibility within the SBS being dependent on the change in the mean normal stress. The compression index λ and the swelling index κ obtained are 0.357 and 0.081, respectively.

The K_o stress state for the lightly overconsolidated clays ($\text{OCR} < 3$) can be achieved with an acceptable degrees of accuracy by swelling the samples along the idealized K_o -line having constant $\left| \frac{dq}{dp} \right|$ value of 0.95. The relationship between K_o and OCR obtained from swelling using the idealized K_o -line is found to agree well with the existing data and the predictions.

5.8.2 Undrained Behaviour of Normally Consolidated Samples

5.8.2.1 Undrained Stress Paths

(i) **Isotropically Consolidated Samples in Compression-** The shapes of undrained stress paths are found to be elliptical in nature. Smooth transitions from the hardening part to the softening part are observed. The Critical State parameter M corresponding to the maximum deviator stress and the maximum stress ratio Criteria are 0.83 and 0.88 respectively. Upon reaching the maximum stress ratio, the stress path travel along the same stress ratio line. A unique normalized $(q/p_o, p/p_o)$ relationship is evident.

(ii) **K_o Consolidated Samples in Compression-** The K_o consolidated specimens show a somewhat different shapes of undrained stress path as observed from the isotropically consolidated samples during compression. The initial point of K_o sample does not lie on the undrained stress path of the sample sheared from isotropic pre-shear stress condition which has the same void ratio, but instead lies inside. Its stress path rises nearly vertically in the (q, p) plot before it merges with that of the isotropically consolidated specimen. Eventually, this sample reached the same Critical State point as observed from the isotropically consolidated Samples. These trends are attributed to the significant effect of secondary consolidation during the sample preparation. Softening is also observed.

(iii) **K_0 Consolidated Samples in Extension-** The undrained stress paths are less rounded and there seems to be no symmetry between the stress paths in compression and in extension either about the K_0 -line or the p-axis. The Critical State parameter M is of the same order as for the compression case but is observed to be slightly higher in magnitude.

5.8.2.2 Stress-Strain Relationships

(i) **Isotropically Consolidated Samples in Compression-** The stress-strain curves show a mild peak and a slight strain softening beyond the peak. At low strain levels these relationships appeared to be the same irrespective of the magnitude of pre-shear consolidation stress, which indicated that the samples had been subjected to pronounced time effects resulting from secondary consolidation. The peak deviator stress is achieved at shear strains of about 10%. A unique normalized behaviour is evident.

(ii) **K_0 Consolidated Samples in Compression-** The peak deviator stresses are achieved at a small shear strain of 3.6%. However, a negligible gain in strength is observed beyond a shear strain of 0.9%. The maximum obliquity ratio was obtained at a larger strain of about 12% during the softening phase. A unique normalized behaviour is evident.

(iii) **Isotropic and K_0 Consolidated Samples in Compression-** The isotropically consolidated samples have higher shear strains than the K_0 consolidated ones even when the (q, ϵ_s) relationship for the isotropically consolidated samples beyond the K_0 state is compared to that for the K_0 consolidated specimens. This indicates that the K_0 consolidated samples have undergone substantial secondary consolidation prior to shear.

(iv) **K_0 Consolidated Samples in Extension-** The deviator stress tend to increase with the strain even at strains close to failure ($|\epsilon_s| = 17.5\%$). The deviator stress increases rapidly in the initial unloading stage accompanied by relatively small shear strains. More than 50% of the peak deviator stress is reached within a shear strain of about 2.5%.

(v) **K_0 Consolidated Samples in Compression and in Extension-** The stress - strain behaviour is strongly influenced by the stress system. The K_0 normally consolidated samples, however, are expected to experience a smaller shear strain during the triaxial compression and the corresponding stress reversal in extension phase up to the isotropic stress level. A unique normalized behaviour of K_0 consolidated specimen both in compression and in extension is apparent.

5.8.2.3 Stress Ratio-Strain Relationships

(i) **Isotropic and K_0 Consolidated Samples in Compression-** The (η, ϵ_s) relationship for the isotropically consolidated sample from η and ϵ_s beyond the values $(\eta)_{K_0}$ and

$(\epsilon_s)_{K_0}$ corresponding to the K_0 condition is found to be markedly different from the (η, ϵ_s) relationship for the K_0 consolidated sample. The difference in ϵ_s between the two relationships appeared to have been built up for the initial incremental value of η from K_0 state up to a value of η of about 0.66. Thus the time effect is revealed to be more prominent for the K_0 consolidated samples. The peak values of η ($= M$) for the isotropically and K_0 consolidated samples in compression are nearly the same and are 0.88 and 0.89, respectively. For the K_0 consolidated samples, the M values are approximately the same for compression conditions ($M= 0.89$) and for extension conditions ($M= 0.93$).

5.8.2.4 Excess Pore Pressure

(i) **Isotropically Consolidated Samples in Compression-** A unique $(u/p_o, \epsilon_s)$ relationship is observed. There exists a bi-linear relationship between u/p_o and η , which show an initial shallow slope (0.52) at low stress ratio ($\eta=0.12$) followed by a steeper one (0.75). This $(u/p_o, \eta)$ relationship can be approximated by a single straight line with a slope of 0.73 without any loss of accuracy.

(ii) **K_0 Consolidated Samples in Compression-** The $(u/p_o, \eta)$ relationship for K_0 normally consolidated samples is bi-linear with a slope initially of 0.48 and beyond an η of 0.66 increasing to 1.03. However, for the extension condition these slopes are 0.4 in the initial stage and 0.06 in the second stage.

(iii) **Isotropic and K_0 Consolidated Samples in Compression-** Irrespective of their stress condition, the $(u/p_{on}, \eta)$ relationships for the isotropic and the K_0 consolidated samples give approximately the same gradient C which are very close to the range of stress ratio in which the apparent overconsolidation due to pre-shear stress condition is not significant. That is, the slope of the second segment of the K_0 consolidated sample in the $(u/p_{on}, \eta)$ plot is the same as the one for the isotropically consolidated sample. The p_{on} value is the same as the p_o value for the isotropically consolidated sample.

5.8.2.5 Strength Characteristics

(i) **Isotropically Consolidated Samples in Compression-** The $\bar{\phi}$ value at peak deviator stress is 21° and is slightly lower than the $\bar{\phi}$ value at the Critical State of 23° . The peak strength ratio $s_{up}/\bar{\sigma}_{vo}$ is observed as 0.235, while the critical strength ratio is 0.215.

(ii) **K_0 Consolidated Samples in Compression-** The $\bar{\phi}$ values at peak deviator stress and at the Critical State are 21° and 23° , respectively. The peak undrained strength ratios mobilized average to 0.252. This value is about 87% of that in extension.

(iii) **K_o Consolidated Samples in Extension-** The peak strength and the maximum obliquity ratio occur at nearly the same shear strain. The strength parameter $\bar{\phi}$ in extension is found to be 33° with the corresponding Critical State parameter M is equal to 0.93. The average value of undrained strength ratio is 0.291 and is slightly greater than that in compression (0.252).

5.8.3 Undrained Behaviour of Overconsolidated Samples under Isotropic Pre-shear Conditions

(i) **Undrained Stress Paths-** The undrained stress paths are sub-parallel to the q -axis before yielding takes place, which supports the elastic wall concepts. On the wet side, the deviator stress at which volumetric yielding commenced is found to increase with the increase in OCR. These samples tend to have their end points cluster around the Critical State point. The samples on the dry side approached the Hvorslev failure envelope and then tend to seek the Critical State.

(ii) **Stress-Strain Relationships-** The unique (q, ϵ_s) relationship for all samples on the wet side of the Critical State with OCR values of less than 2.15 confirm the constant q yield loci of ROSCOE and BURLAND (1968).

(iii) **Normalized Pore Pressure-Stress Ratio Relationships-** The overconsolidated samples show the bi-linear $(u/p_o, \eta)$ relationship. The slope of the first linear section C_1 is found to decrease consistently with the OCR values, while the slope of the second linear section C_2 remained constant. The stress ratio, η_i , at which the two linear sections of the $(u/p_o, \eta)$ relationship intersect is found to increase consistently with the OCR values. Thus, for the specimens on the wet side of the Critical State, the parameters C_1 , C_2 and η_i are sufficient to describe the undrained stress paths for OCR values in the range of 1.0 to 2.15. The values of C_1 and C_2 in the $(u/p_{on}, \eta)$ plot continually decreased with increase in OCR. There is a demarcation value of the OCR between the wet and the dry side. Perhaps when this OCR value is approached, η_i is close to M the limit value of η and C_1 reaches an asymptotic lower limit for this OCR for the full range of η varying from 0 to M .

(iv) **Pore pressure Parameter A_f -** The value of A_f decreases with the increase in the OCR. The observed values of A_f for the lightly overconsolidated samples ($OCR < 4.0$) remained positive, and these values agree well with the predictions from the Modified Theory.

(v) **Volumetric Yielding on the SBS-** The volumetric yield points obtained from the $(u/p_o, \eta)$ relationship for the overconsolidated samples lie within the undrained stress path in the (q, p) plot. The locus of the volumetric yield points agree remarkably well with the volumetric yield locus of the Modified Cam Clay Theory.

(vi) **Undrained Strength of Overconsolidated Samples-** The peak deviator stress for lightly overconsolidated samples (with OCR less than 2.25) having the same initial water content is found to be approximately the same as the normally consolidated samples. The strength ratio $(s_{up}/\bar{\sigma}_{vo})_{OC}/(s_{up}/\bar{\sigma}_{vo})_{NC}$ is found to increase with the OCR values. $\bar{\sigma}_{vo}$ refers to the pre-shear vertical pressure. This experimental observation agrees well with the prediction from the Modified Theory with the value of Λ of 0.77.

(vii) **(e , lnp) Relationship at the Critical State and at Failure-** The Critical State Line corresponding to the maximum stress ratio condition is displaced to the left of that defined with the q_{max} condition in the (q , p) plot.

(viii) **Shear Strain Contours-** The constant shear strain contours within the SBS are similar to those presented by WROTH and LOUDON (1967) and BALASUBRAMANIAM (1969). The contours support the idea of the constant q-yield loci on the wet side of the Critical State as proposed by ROSCOE and BURLAND (1968) and on the dry side forms a set of lines which, when extended, converge to a negative value (of $p_o = -2.4 \text{ kg/cm}^2$) on the p-axis. The (η , ϵ_s) relation which dictates the contribution from the constant q yield loci within the SBS is approximately the same as that reported by WROTH and LOUDON (1967).

5.8.4 Undrained Behaviour of Overconsolidated Samples under K_o Pre-shear Conditions

(i) **Undrained Stress Paths in Compression and in Extension Conditions-** The undrained stress paths of the overconsolidated samples are nearly sub-parallel to the q-axis and are even more so for the normally consolidated sample. At the end of shear all the end points tend to cluster around the Critical State point. The asymmetry in the shape of the undrained stress path for the K_o normally consolidated sample in compression and in extension corresponds to an apparent overconsolidation due to secondary consolidation time effects as well as the pre-shear stress effects.

(ii) **Stress-Strain Relationships-** The (q , ϵ_s) relationship established for the CK_oU tests from the constant q yield loci of the isotropic consolidation tests reveals higher ϵ_s values than the experimentally observed values. The incremental stress-strain relationship (i.e., beyond the $(q_o)_{max}$) for the CK_oU specimen and the values obtained from CIU tests are again found to be different. The (q, ϵ_s) relationship of the samples with OCR value less than 1.78 are all apparently the same. In the case of the extension tests, all the specimen show a unique (q , ϵ_s) relationship within an acceptable narrow band of scatter.

(iii) **Excess Pore Pressures-** The (u , ϵ_s) relationship for the CK_oU samples with OCR values of 1.00, 1.24 and 1.50 is approximately the same up to a shear strain of 1%, beyond this strain level the pore pressures are found to be larger when the OCR value is less. The samples

with OCR values of 2.78, 2.15 and 2.75 show higher pore pressure development up to a shear strain of about 1%, and then the pore pressure seems to rise at a lower rate. At larger strains beyond 1.5%, the excess pore pressure developed reduces with the increase in the OCR values. Generally, the excess pore pressure development is found to be higher for the samples with lower OCR than for those with higher OCR. For all samples sheared in extension (except CK₀UE3 and CK₀UE5) the reduction in pore pressure consistently increased with the OCR values.

(iv) **Excess Pore Pressure-Stress Ratio Relationships-** The $(u/p_o, \eta)$ relationship for the sample belonging to the wet zone in CK₀U series is found to be bi-linear. The slopes of the initial segment are dependent on the OCR values, while the final segment of all these bi-linear relationships are of similar slope. There exists a bi-linear $(u/p_o, \eta)$ relationship for samples on the dry zone as well. However, unlike the samples in the wet zone, for the samples in the dry zone the slope of the first segment is higher than the corresponding slope for the second segment. The initial segments are parallel to one another and the second segments are also parallel to each other. In the case of extension conditions, the relationships are different from those exhibited under compression conditions. The samples sheared from the wet zone in the CAU series show a similar bi-linear relation. However, the samples on the dry side show a linear variation of up to $\eta=0.8$; thereafter the $(u/p_o, \eta)$ relationship showed a negative gradient.

(v) **Pore Pressure Parameter A_f** - The A values at failure A_f reduced with the increase in the OCR values. The isotropically consolidated sample showed the least reduction. The trends from extension tests, however, are quite different. The prediction made by WROTH (1984) seems to be close to the isotropically consolidated sample, while the predictions of MAYNE and STEWART (1988) are somewhat closer to the CK₀U samples.

(vi) **Yield Envelope and Failure Envelope-** The failure points obtained from the over-consolidated samples lie on the Hvorslev surface. The volumetric yield points tend to cluster around the Critical State Line. This yielding tend to obstruct the samples reaching the Hvorslev envelope.

(vii) **Undrained Strength Characteristics-** The undrained strength ratio increases as the OCR value is increased. WROTH's prediction (1984) agree well with the measured value of up to an OCR of about 2.5. The projection of the CSL from K₀ undrained tests more or less coincides with the similar projection from the CIU tests.

(viii) **Stress Ratio-Strain Relationships-** The (η, ϵ_s) relationship for the CK₀U and CAU specimens for OCR values higher than 1.78 and up to 2.75 seems unique. A similar trend is also found in the extension tests.

VI DRAINED BEHAVIOUR OF CLAYS

6.1 Introduction

The drained behaviour of lightly overconsolidated Bangkok clay is studied comprehensively with ten series of tests. These tests cover the bulk of the possible applied stress paths in the (q, p) plot. Initially, the conventional CID series of tests were performed with constant cell pressure on samples having OCR values of 1.00, 1.24, 1.50, 1.78, 2.15, and 2.75. All samples have the same pre-shear void ratio. Followed by this series of tests the conventional CK_oD and CAD tests were conducted. For the K_o consolidated samples, the initial pre-shear stress states are the same as those for the undrained compression and extension tests presented in Chapter V. These K_o consolidated samples had the same OCR values of 1.00, 1.24, 1.50, 1.78, 2.15, and 2.75. This series of tests was then followed by the CAD series where the samples had their pre-shear stress states on the η_k line.

Additional drained tests were carried out from the idealized K_o condition along seven other applied stress paths. Each one of them will now be described (see Fig. 6.1). In Fig. 6.1, CK_oD tests on six OCR values were carried out with constant cell pressures. The CK_oPC tests also with six OCR values were carried out with constant p conditions. The CK_oDU tests are four in numbers with OCR values of 1.00, 1.24, 1.50, and 2.15. These tests are of the unloading type with constant axial stress and the lateral stress being reduced. Then four tests were carried out designated CK_oQU with initial OCR values of 1.00, 1.24, 1.50, and 2.15. In these tests, the p values were reduced while the q values were maintained constant. Only three tests were performed with constant q and p increasing conditions. These tests are designated as CK_oQL and correspond to initial OCR values of 1.24, 1.50, and 2.15.

On the extension side, three series of tests were also conducted. One of them corresponds to loading conditions with constant axial stress and radial stress increasing. This series is designated as CK_oLE . Concluding remarks on the drained behaviour of soft Bangkok clay as studied is summarized at the end of this chapter.

6.2 Isotropically Consolidated Drained Tests (CID Tests)

6.2.1 Effective Stress Paths

The conventional drained tests with constant cell pressure were carried out on isotropically consolidated samples with OCR values of 1.00, 1.24, 1.50, 1.78, 2.15, and 2.75. The stress paths of these samples are shown in the (q, p) plot in Fig. 6.2. The end points of these specimens are found to have increasing values of (q/p) as the OCR values are increased. All these specimens

have the same pre-shear void ratio of about 1.16. In this figure, the p_{max} corresponding to each specimen is also plotted and the volumetric yield loci as predicted by the Modified Cam Clay Theory is also sketched. These volumetric yield loci correspond to preconsolidation pressures of points A, A₁₀, A₂₀.... A₅₀. Thus, for the normally consolidated sample with initial pre-shear stress state A, the drained stress path AC is completely outside of the volumetric yield locus AB. However, for all other samples, the initial stress paths A₁B₁, A₂B₂.... A₅B₅ are all inside their corresponding volumetric yield loci through the maximum preconsolidation pressure. For all these samples, only the stress states B₁C₁, B₂C₂.... B₅C₅ are in the normally consolidated state.

6.2.2 Stress-Strain Relationships

The deviator stress-shear strain relationships for all the drained specimens are shown in Fig. 6.3. It is noted that initially the (q, ϵ_s) relationship of these specimens are roughly the same up to a deviator stress of about 3.3 kg/cm². Perhaps, this value is close to the point where the volumetric yield locus through the stress point A intercepts the Critical State Line. Beyond this value of the deviator stress, the samples are each found to have a different stress-strain curve as the samples are now all in the normally consolidated states.

Figure 6.4 shows the (ϵ_v, p) relationships for the drained test specimens. The (ϵ_v, p) relationship for each stress path shows two segments AB and BC. Initially, the increase in ϵ_v with p is small and when the stress states B₁, B₂.... B₅ are reached in Fig. 6.2, the ϵ_v values increase more markedly with p . Thus, the points B₁, B₂.... B₅ correspond to drained yield points. These yield points are marked in Fig. 6.5 in the (q, p) plot. The points A, B₁, B₂.... B₅ in Fig. 6.5, when plotted in the $(q/p_e, p/p_e)$ plot, lie on a single curve where the normalized volumetric yield locus is. This volumetric yield locus is used commonly in the Cam Clay and Modified Cam Clay Theories. However, such a normalized volumetric yield locus which is similar in shape to the curve AG (in Fig 6.5) is realistically predicted by the Modified Cam Clay Theory of ROSCOE and BURLAND (1968). It, therefore, seems interesting that the yield points obtained from the (ϵ_v, p) plot in Fig. 6.4 give an outer boundary of volumetric yield locus as traditionally used in the Cambridge stress-strain theories. Whenever the stress states lie on the State Boundary Surface (SBS), the samples are in the normally consolidated state and their plastic strain increment ratio, $\frac{d\epsilon_{vp}}{d\epsilon_{sp}}$, is dependent on the volumetric yield locus shown as AG in

Fig. 6.5. This yield locus is shifted to A'₁B₁, A'₂B₂.... A'₅B₅ when the stress states B₁, B₂.... B₅ lie on the SBS.

However, in the latter sections, it will be shown that plastic volumetric strains do take place for stress states inside the SBS and such plastic volumetric strains are also associated with a sub-set of volumetric yield loci within the major volumetric yield loci which corresponds to

the normally consolidated states on the SBS. These aspects will be discussed in detail in the subsequent sections of this chapter as well as in Chapter VIII in developing a sub-set of volumetric yield loci for stress states within the SBS.

6.2.3 Constant Shear Strain Contours

Figure 6.5 shows the constant shear strain contours inside the volumetric yield locus from the drained and undrained tests. In this figure, AG corresponds to the volumetric yield locus as obtained from Modified Cam Clay Theory. The shear strain contours from undrained and drained tests are approximately the same at low levels of shear strain. This phenomenon indicates that in the lightly overconsolidated state, the shear strain associated with the dilatant phenomenon in drained tests is small. Figure 6.6 indicates the relation of the plastic volumetric strain ϵ_{vp} with ϵ_s . The plastic volumetric strain, ϵ_{vp} , is obtained by subtracting the elastic volumetric strain, ϵ_{ve} , from the total volumetric strain ϵ_v . The elastic volumetric strain is calculated from the expression, $\epsilon_{ve} = \left(\frac{k}{1+e} \right) \frac{dp}{p}$. In Fig. 6.6, most of the plastic volumetric strain, ϵ_{vp} , takes place for the stress state outside the volumetric yield locus AG (see Fig. 6.5). In plotting Fig. 6.6, the elastic shear strain, ϵ_{se} , is taken to be zero.

In Fig. 6.7, the directions of the plastic strain increment ratio, $\frac{d\epsilon_{sp}}{d\epsilon_{vp}}$, are plotted both inside the volumetric yield locus as obtained from the Modified Cam Clay Theory and outside as well. It should be noted that the ratios $\frac{d\epsilon_{sp}}{d\epsilon_{vp}}$ indicated in this plot are obtained from the CID tests on normally and overconsolidated specimens. For stress states which lie on the SBS, ROSCOE and BURLAND (1968) indicated in their Revised Theory that the use of two sets of yield loci: one is constant q yield loci and the other is the volumetric yield loci as shown in Fig. 6.7. Thus, the directions $\frac{d\epsilon_{sp}}{d\epsilon_{vp}}$ shown in Fig. 6.7 also contain the $d\epsilon_{sp}$ contribution from the constant q yield loci for stress states on the SBS. Thus, the values $\frac{d\epsilon_{sp}}{d\epsilon_{vp}}$ shown are higher than the values $\left(\frac{d\epsilon_{sp}}{d\epsilon_{vp}} \right)_\eta$ as obtained from the anisotropic consolidation type of tests for stress states on the SBS.

Similarly, inside the SBS if a sub-set of volumetric yield loci exist especially for stress states close to the SBS then the $\frac{d\epsilon_{sp}}{d\epsilon_{vp}}$ shown in Fig. 6.7 for stress states within the SBS will also include the $d\epsilon_{sp}$ as contributed from the constant q yield loci when volumetric yielding takes place. This phenomenon will become clearer from the discussions in a latter section.

6.2.4 Normalized (q/p_e , p/p_e) Plot

Figure 6.8 shows the (q/p_e , p/p_e) plot of all the overconsolidated samples sheared under CID test conditions. In this figure, the yield locus as obtained from the (ϵ_v , p) plot is also shown. It seems that the normally consolidated sample with OCR of 1.00 also shows an apparent yield point A due to pre-shear secondary consolidation. Beyond A, the (q/p_e , p/p_e) path of this sample is similar to that for the normally consolidated one. In Fig. 6.8, the q_{max} points and the end of test points are also shown. The end points are found to lie on a falling stress path and tend to cluster around the Critical State point.

6.2.5 Deviator Stress - Volumetric Strain Relationships

Figure 6.9 shows the (q , ϵ_v) relationship for all CID test specimens. This figure seems to indicate that there is an outer boundary OABC from which the (q , ϵ_v) relationship deviates as the specimens approach the SBS. As such, the normally consolidated sample CID1 deviates from this outer boundary OABC from the origin of the plot. Such deviation, however, seems to begin at higher value of deviator stress as the OCR value is increased. This is quite expected since a considerable portion of the stress path of specimen CID6 with the highest OCR value of 2.75 lie within the SBS as compared to the specimen CID2 which is a lightly overconsolidated sample with an OCR value of 1.24.

6.2.6 Stress Ratio-Strain Relationships

Figure 6.10 illustrates the (η , ϵ_s) relationship for all CID test specimens. Here again at any particular stress ratio, the normally consolidated sample has the highest shear strain and the shear strain decreases in magnitude as the OCR values increase. Figure 6.11 shows the (η , ϵ_v) relationship, where for a first order of approximation an outer boundary such as OABC exist for the higher OCR from which the (η , ϵ_v) relationship deviates as the OCR values increase. Thus, at any particular stress ratio the ϵ_v values increase as the OCR values are reduced. An important interpretation of the (η , ϵ_{vp}) relationship will be made in the next section.

6.2.7 Plastic Volumetric Strains Within and Outside the State Boundary Surface (SBS)

The elastic volumetric strain is calculated for the increments of p as :

$$d\epsilon_{ve} = \left(\frac{\kappa}{1+e} \right) \frac{dp}{p}$$

Such elastic volumetric strains are subtracted from the total volumetric strain ϵ_v to obtain the plastic component ϵ_{vp} . Figure 6.12 illustrates the (η, ϵ_{vp}) relation for all the CID test specimens. The arrows drawn horizontally indicate the locations of the stress ratio at which the stress paths reach the volumetric yield loci on the SBS as discussed in the earlier section and in Fig. 6.4. Two important observations are to be stressed at this stage.

i) The (η, ϵ_{vp}) relation indicates that for a substantial part of the initial stress ratio from the zero value, the ϵ_{vp} is zero. This would indicate that within the SBS and close to the isotropic axis there exist a region where the specimens under CID type of loading experience negligibly small plastic volumetric strain. The Author took great care in individually plotting the (η, ϵ_{vp}) relation for every specimen and obtain Fig. 6.13 which indicates that the stress ratio beyond which ϵ_{vp} is positive and greater than zero. Such stress states corresponding to zero plastic volumetric strain are shown as ADE in Fig. 6.14. Thus, for the stress domain below the curve ADE and the p-axis there exists a truly elastic nucleus with respect to volumetric strain. However, within the nucleus still plastic distortional strain can take place as postulated by the constant q yield loci of ROSCOE and BURLAND (1968).

ii) The second interesting experimental observation is that the stress ratio marked with the horizontal arrows in Fig. 6.13 constitutes a curve OA which corresponds to the traditional volumetric yield loci which lie on the State Boundary Surface (SBS). The curve shown as OA in Fig. 6.13 corresponds to the volumetric yield points as obtained in Fig. 6.4 on the (ϵ_v, p) relation and maps as the volumetric yield locus ABC shown in Fig. 6.14 which corresponds to the stress state on the SBS. In establishing the curve ABC and ADE in Fig. 6.14 data from CID and CK_oD tests are used. The interpretation of the data for CK_oD tests will be made in the next section. Also the precise location of the point E in the curve ADE need to be discussed after the interpretation of the tests below the SBS on the dry side of the Critical State Line.

6.3 Conventional Drained Tests on K_o Consolidated Samples (CK_oD Tests)

6.3.1 Effective Stress Paths

Figure 6.15 shows the stress paths from the idealized K_o condition of the normally consolidated and overconsolidated specimens. In this figure, the volumetric yield loci (lying on the SBS) through points A, a_1, a_2, \dots, a_5 are also sketched as E_AAM , $E_{a_1a_1}M_1, \dots, E_{a_5a_5}M_5$. Thus, the drained paths AD, A_1D_1, \dots, A_5D_5 intersect their corresponding volumetric yield loci at A, F_1, \dots, F_5 . For the specimen sheared from the stress state A, the full drained path AD corresponds to the normally consolidated state. However, for all other specimens, the stress states lie below

the SBS for paths A_1F_1 , A_2F_2 ,.... A_5F_5 and become normally consolidated for stress states on F_1D_1 , F_2D_2 ,.... F_5D_5 . Thus, the specimens sheared from the stress states A_2 , A_3 ,.... A_5 have almost all their states below the State Boundary Surface.

In Fig. 6.16, the undrained stress paths of the K_o consolidated specimens (in compression and in extension) are also indicated as AM and AE

6.3.2 Stress-Strain Relationships

Figure 6.17 illustrates the (q, ϵ_s) relationship for these CK_oD specimens. These relationships for all samples except for the sample CK_oD6 with OCR of 2.75 are roughly the same up to a shear strain of about 2%, thereafter the (q, ϵ_s) relationships are markedly different. Figure 6.18 shows the (ϵ_v, p) relationships for these samples. These relationships are again found to be in two distinct parts: one part corresponds to the state inside the State Boundary Surface, and the second part corresponds to the stress state on the State Boundary Surface. The arrows indicate the stress state when the stress paths reach the State Boundary Surface. These points, thus, represent the volumetric yield points for stress states on the State Boundary Surface.

6.3.3 Volumetric Strain-Shear Strain Relationships

The (ϵ_v, ϵ_s) relationship for the K_o consolidated specimens are separated into two groups. One group consists of samples on the wet side with initial OCR values of 1.00, 1.24, and 1.50 and the other corresponds to OCR values of 1.78, 2.15, and 2.75.

Figure 6.19a contains the (ϵ_v, ϵ_s) and $(\epsilon_{vp}, \epsilon_{sp})$ relationships for the samples on the wet side. The plastic strains are obtained on the assumption that the plastic volumetric strain is the difference between the total volumetric strain and the elastic volumetric strain. The elastic volumetric strain is calculated using the swelling constant κ . The elastic shear strain is assumed to be zero. From Fig. 6.19a, it is clear that the $(\epsilon_{vp}, \epsilon_{sp})$ relationships for the three specimens are somewhat different.

Figure 6.19b contains the (ϵ_v, ϵ_s) and $(\epsilon_{vp}, \epsilon_{sp})$ relationships for the specimens with OCR values of 1.78, 2.15, and 2.75. In this plot, the $(\epsilon_{vp}, \epsilon_{sp})$ relationships for all the three specimens are nearly the same. Thus, in this range of OCR values, the $\frac{d\epsilon_{vp}}{d\epsilon_{sp}}$ values seem to depend only on the stress ratio, η . These observations on the ratio, $\frac{d\epsilon_{vp}}{d\epsilon_{sp}}$, can be useful in the successful formulation

of the plastic potential. Figure 6.19c contains only the $(\epsilon_{vp}, \epsilon_{sp})$ relationships for all the samples and this plot will be used in a latter section to draw the directions of the plastic strain increment ratios.

6.3.4 Stress Ratio-Shear Strain Relationships

Figure 6.20 illustrates the (η, ϵ_s) relationship for all the K_o consolidated specimens. It is seen that for specimens CK_oD5 and CK_oD6, the (η, ϵ_s) relationships are the same and this observation indicates that on the dry side of the Critical State, the (η, ϵ_s) relationship is unique and is less dependent on the dilatancy component $\frac{d\epsilon_v}{d\epsilon_s}$. Also, at low levels of deviator stress, all specimens have their stress states below the State Boundary Surface and the shear strains are small as revealed by the (η, ϵ_s) relationship. At the higher levels of η , the (η, ϵ_s) relationships are different since the specimens are now in the normally consolidated state and are on the State Boundary Surface.

Figure 6.21 shows the $(q/p_e, p/p_e)$ relations of all the specimens sheared from the K_o state. In this plot, the yield points as obtained from Fig. 6.18 are also shown. The yield points are now found to be close to the q value at the Critical State. In this figure, the q_{\max} and $(\bar{\sigma}_1/\bar{\sigma}_3)_{\max}$ points are also shown. They all tend to cluster around the Critical State. The end points of the specimens also seek the Critical State.

6.3.5 Volumetric Strains

Figure 6.22 illustrates the (η, ϵ_v) relationship. Here again an outer boundary OABC is seen as the curve which gives the minimum volumetric strain. For the samples with OCR values of 1.00, 1.24, 1.50, and 1.78, the (η, ϵ_v) relationships deviate from the outer boundary when the stress states reach the State Boundary Surface (SBS) and this seem to happen with increasing stress ratio. The samples with OCR values of 2.15 and 2.75 tend to have a higher volumetric strain than the others at lower stress ratios.

Figure 6.23 illustrates the (q, ϵ_v) relationship. Most samples are found to show some strain softening after the peak deviator stress. Plastic volumetric strains are obtained from the total strains by the reduction of the elastic volumetric strain as calculated using the swelling coefficient κ . Figures 6.24 to 6.26 demonstrate the (η, ϵ_{vp}) , (q, ϵ_{vp}) , (p, ϵ_{vp}) relationships. The stress ratio and deviator stress plots are used to obtain the volumetric yield points inside the SBS. A typical point is marked by an arrow in Figs. 6.24 and 6.25. The Author took great care in making individual plots to determine each of this volumetric yield point.

The yield points so determined are presented in Fig. 6.14 to determine the zero volumetric yield locus inside the SBS. A discussion on the use of this volumetric yield locus is already made in an earlier section on CID tests and will also be described in detail in Chapter VIII.

6.4 Conventional Drained Tests on Anisotropically Consolidated Samples (CAD Tests)

6.4.1 Effective Stress Paths

The stress paths of the CAD specimens are shown in Fig. 6.27. In this plot, the initial states of the anisotropically consolidated samples are shown as $A, A_1', A_2', \dots, A_5'$. The idealized K_0 line is AB. The volumetric yield loci on the State Boundary Surface (SBS) through A, b_1, b_2, \dots, b_5 are also drawn as $E_AAM, E_{b_1b_1}M_1, \dots, E_{b_5b_5}M_5$. These volumetric yield loci correspond to the maximum stress points A, b_1, b_2, \dots, b_5 of the samples achieved during sample preparation before swelling to the current stress states $A, A_1', A_2', \dots, A_5'$.

6.4.2 Stress-Strain Relationships

The (q, ϵ_s) relationships of the CAD specimens are shown in Fig. 6.28 and are found to be distinctly different for all the specimens.

6.4.3 Mean Normal Stress-Volumetric Strain Relationships

The (ϵ_v, p) relationships of the CAD specimens are shown in Fig. 6.29. The (ϵ_v, p) relationship is separated into two parts: one corresponding to the stress states inside the State Boundary Surface and the other being on the State Boundary Surface. The arrows in the figure indicate the level of stress at which the samples reach the State Boundary Surface and are considered as yield points which lie on the volumetric yield loci for stress states on the SBS.

6.4.4 Volumetric Strain-Shear Strain Relationships

The (ϵ_v, ϵ_s) relationships of the specimens in CAD tests are shown in Fig. 6.30a and 6.30b. For the specimens on the wet side of the Critical State, Fig. 6.30a shows the (ϵ_v, ϵ_s) and $(\epsilon_{vp}, \epsilon_{sp})$ relationships, respectively. As observed earlier from the CK₀D specimens, the CAD specimens also reveal that the $(\epsilon_{vp}, \epsilon_{sp})$ relation is dependent on the stress ratio η and p as well. Figure 6.30b shows similar relation for the samples with OCR values of 1.78, 2.15, and 2.75. Finally, the $(\epsilon_{vp}, \epsilon_{sp})$ relationships for all the specimens are shown in Fig. 6.30c and

are found to be different for different initial pre-shear OCR values. These results would be useful at a latter section when the directions of the strain increment ratio, $\frac{d\epsilon_{vp}}{d\epsilon_p}$, are discussed for stress states inside the State Boundary Surface.

6.4.5 Stress Ratio-Shear Strain Relationships

The (η, ϵ_s) relationships for all the CAD specimens are different as one would expect them to be (see Fig. 6.31). At low levels of stress ratio, the (η, ϵ_s) relationships have an outer boundary OAB.

6.4.6 Normalized $(q/p_e, p/p_e)$ Plot

Figure 6.32 illustrates the $(q/p_e, p/p_e)$ plot followed by all the CAD specimens. Also, the volumetric yield points shown in this figure tend to lie on a constant q line close to that at the Critical State. The q_{\max} or the $(\bar{\sigma}_1/\bar{\sigma}_3)_{\max}$ points are all now found to cluster around the Critical State Line. The end points are also found to seek the Critical State. It is interesting to note that similar to the CK_oD specimens, the CAD specimens also have their q_{\max} , $(\bar{\sigma}_1/\bar{\sigma}_3)_{\max}$ and the end points all seeking the Critical State.

6.4.7 Volumetric Strains

Figure 6.33 illustrate the (q, ϵ_v) relationship for the CAD tests specimens. Similarly, the (η, ϵ_v) and (η, ϵ_{vp}) relationships are shown in Figs. 6.34a and 6.34b, respectively. In Fig. 6.34b, the arrows marked indicate the stress ratio level at which plastic volumetric strain begin to take place. Individual plots were plotted for each of this CAD test specimen to determine the stress states at which plastic volumetric strain occur within the SBS. These points are used to determine the volumetric yield loci inside the SBS in Fig. 6.14 and will be discussed in detail in Chapter VIII.

6.5 Constant p Compression Tests on K_o Consolidated Samples (CK_oPC Tests)

6.5.1 Effective Stress Paths

Figure 6.35 shows the stress paths followed by the specimens in CK_oPC tests. This novel series of tests contains all the K_o consolidated specimens sheared under constant p conditions

in compression. In this figure, the volumetric yield loci (on the SBS) through their pre-shear maximum stress states A, a_1 , a_2 , ..., a_5 are also drawn. Similar to the CK_oD and CAD test series, the stress states for specimens CK_oPC2 and CK_oPC3 lie partly below the State Boundary Surface and partly on the State Boundary Surface. Thus, the stress states for A_1C_1 and A_2C_2 are below the State Boundary Surface, while C_1B_1 and C_2B_2 are on the State Boundary Surface. For the specimens CK_oPC4, CK_oPC5 and CK_oPC6, the stress paths A_3B_3 , A_4B_4 and A_5B_5 lie almost below the State Boundary Surface.

6.5.2 Stress-Strain Relationships

Figure 6.36 illustrates the (q, ϵ_s) relationships for all the CK_oPC specimens. It appears that the (q, ϵ_s) relationships are different for all the samples. However, an interesting trend is noted in Fig. 6.37 when the incremental q and incremental shear strain relationship is plotted. In this figure, the datum for the increment of the deviator stress and the shear strain are taken to coincide with their initial pre-shear stress states A, A_1 , ..., A_5 . Now a clear trend is emerging to the effect that there is a limit boundary OABC in the (q, ϵ_s) plot which somewhat corresponds to the constant q yield loci type which governs the shear strain below the State Boundary Surface and on the wet side of the Critical State. Then, for increasing values of OCR, the $(\Delta q, \Delta \epsilon_s)$ relation tend to deviate from this limit boundary at increasing values of Δq in a systematic way.

6.5.3 Stress Ratio-Shear Strain Relationships

Figure 6.38 shows the (η, ϵ_s) relationships for all the CK_oPC specimens. For the specimens on the wet side of the Critical State, the (η, ϵ_s) relationships are all different (i.e., samples CK_oPC1, CK_oPC2 and CK_oPC3 with OCR values of 1.00, 1.24 and 1.50). This is somewhat expected and in this range the incremental deviator stress-incremental shear strain follows a limit relationship similar to the constant q yield loci in the isotropically consolidated specimens. When the OCR values are high (specimens CK_oPC4, CK_oPC5 and CK_oPC6), the (η, ϵ_s) relationships tend to be the same.

The CK_oPC tests as conducted by the Author constitute a unique series of tests within the State Boundary Surface from which the plastic volumetric strains can directly be measured and hence the plastic strain increment ratio $\frac{d\epsilon_{vp}}{d\epsilon_{sp}}$ can be easily deduced.

6.5.4 Volumetric Strain-Shear Strain Relationships

As stated earlier during the constant p tests, there will not be any elastic volumetric strain. Therefore, the $(\epsilon_{vp}, \epsilon_{sp})$ relationship will coincide with the (ϵ_v, ϵ_s) relationship if the elastic distortional strains are neglected as usually done. Thus, Fig. 6.39 illustrates the experimentally observed (ϵ_v, ϵ_s) relationship which will directly refer to $(\epsilon_{vp}, \epsilon_{sp})$ relation. It is seen that for all values of OCR the $(\epsilon_{vp}, \epsilon_{sp})$ relationships are distinctly different, though there is a tendency at higher OCR values (samples CK_oPC4 and CK_oPC5) to have roughly the same relation. The data presented in Fig. 6.39 will be used at a subsequent stage to draw the direction of the plastic strain increment ratio, $\frac{d\epsilon_{vp}}{d\epsilon_{sp}}$, in the (q, p) plot.

6.5.5 Normalized $(q/p_e, p/p_e)$ Plot

The state paths followed by the CK_oPC specimens are shown in the $(q/p_e, p/p_e)$ plot in Fig. 6.40. The state paths below the State Boundary Surface are now found to rise virtually vertical all the way up to the failure state (close to the Critical State) supporting the elastic wall concept of the Cambridge stress-strain theories. The CK_oPC2 specimen tends to have its state path rising to the State Boundary Surface. The q_{lmax} and $(\bar{\sigma}_1/\bar{\sigma}_3)_{max}$ points are also found to lie close to the Critical State Line.

6.5.6 Volumetric Strains

The volumetric strains in the CK_oPC series of tests directly correspond to the plastic volumetric strains as these tests are conducted under constant p conditions. Thus, the (q, ϵ_{vp}) and the (η, ϵ_{vp}) relations are shown in Figs. 6.41 and 6.42. The arrows in Fig. 6.41 indicate the stress level at which positive plastic volumetric strain develops. Finally, the plastic volumetric strain contours are plotted in the (q, p) plot in Fig. 6.43. Dilational plastic volumetric strains are found to take place in all the CK_oPC tests. However, the magnitude of these dilational volumetric strains are small. For example, the contour marked XYZ only represents 0.5% of plastic volumetric dilation and is almost close to the Critical State Line. When the samples reach the Hvorslev failure envelope, the dilational volumetric strain ϵ_{vp} is only -1.2%. These results will be used in Chapter VIII to plot a subset of plastic volumetric yield loci of the dilational type within the SBS.

6.6 Unloading Compression Tests (CK_oDU Tests)

6.6.1 Effective Stress Paths

This series of tests correspond to the condition that the axial stress is maintained constant and the radial stress is reduced. Such a series of test sheared from the K_o condition would correspond to the stress state adjacent to slopes on a long term basis. Figure 6.44 shows the stress paths followed by the CK_oDU specimens. Also shown in this figure are the volumetric yield loci (on the SBS) through their pre-shear maximum stress state on the η_k line. The specimen CK_oDU1 has its entire stress path on the State Boundary Surface, while all other specimens will have their stress paths inside the State Boundary Surface.

6.6.2 Stress-Strain Relationships

Figure 6.45 illustrates the (q, ϵ_s) relationship which is found to be different for all the specimens sheared from K_o condition under the CK_oDU type of drained compression unloading tests. In Fig. 6.46, an attempt is made to present the data in an incremental deviator stress-incremental shear strain plot. In this figure, the datum for the deviator stress and the shear strains are the pre-shear stress states A, A₁, A₂ and A₄ (see Fig. 6.44).

In the incremental deviator stress-shear strain plot, an outer boundary OAB seems to emerge from which the individual curve deviates with increasing value of Δq as the OCR increases. A similar trend was also observed from the CK_oPC test series as discussed earlier. This outer boundary is of a type which is similar to the constant q yield loci contribution in the incremental deviator stress plot.

6.6.3 Volumetric Strain-Shear Strain Relationships

Figures 6.46a to 6.46c illustrate the (ϵ_v, ϵ_s) , $(\epsilon_{vp}, \epsilon_{sp})$ and $(\epsilon_{ve}, \epsilon_s)$ relationships, respectively. In Fig. 6.46a both the (ϵ_v, ϵ_s) and the $(\epsilon_{vp}, \epsilon_{sp})$ relationships are shown. It appears for such drained unloading stress paths that the $(\epsilon_{vp}, \epsilon_{sp})$ relationships depend both on the stress ratio η and p . These results would be plotted as $\frac{d\epsilon_{vp}}{d\epsilon_{sp}}$ vectors in the (q, p) plot in a latter section. The $(\epsilon_{ve}, \epsilon_s)$ relationship shown in Fig. 6.46b have a clear trend and is distinctly different for each specimen. The $(\epsilon_{vp}, \epsilon_{sp})$ relationship is shown on an enlarged scale in Fig. 6.46c.

6.6.4 Stress Ratio-Shear Strain Relationships

The (η, ϵ_s) relationships for the CK_oDU specimens are shown in Fig. 6.47. At higher OCR values for specimens CK_oDU3 and CK_oDU4, the (η, ϵ_s) relationships are the same and these relationships differ from those for samples CK_oDU1 and CK_oDU2 on the wet side of the Critical State.

6.6.5 Normalized $(q/p_o, p/p_o)$ Plot

In Fig. 6.48, the state paths of the CK_oDU specimens are plotted. The q_{\max} and $(\bar{\sigma}_1/\bar{\sigma}_3)_{\max}$ points are clustered around the Critical State Line.

6.6.6 Volumetric Strains

The (η, ϵ_v) and (q, ϵ_v) relations for the CK_oDU test specimens are shown in Figs. 6.49 and 6.50. The elastic component of the volumetric strain is calculated using the swelling coefficient κ . Thus, the plastic volumetric strain is taken as the difference of the total volumetric strains and the elastic volumetric strains. These plastic volumetric strains are plotted in the (η, ϵ_{vp}) , (q, ϵ_{vp}) and (ϵ_{vp}, p) plots as shown in Figs. 6.52 to 6.53, respectively. The arrows marked in Figs. 6.52 and 6.53 correspond to the stress state at which plastic volumetric strains take place.

Finally, the plastic volumetric strain contours are plotted in Fig 6.54 in the (q, p) plot. It is interesting to note that the dilational plastic volumetric strains are experienced by specimens CK_oDU3 and CK_oDU5, while compressional volumetric strains are experienced by specimens CK_oDU1 and CK_oDU2. For the specimen CK_oDU1, the compressional volumetric strains below the SBS as much as 1%, while the specimen CK_oDU5 experienced nearly -2.25% of plastic volumetric strain when it reached the Hvorslev failure envelope. In Chapter VIII, these volumetric strain contours will be replotted within the SBS.

6.7 Constant q Unloading Tests (CK_oQU Tests)

In this series of tests, K_o consolidated samples are brought to failure by reducing the mean normal stress. Such stress paths are common in land slide problems when an increase in excess pore pressure can cause reduction in mean normal stress which reduces the strength of the natural soil in the slope thereby triggering landslides.

6.7.1 Effective Stress Paths

Figure 6.55 illustrates the stress paths of the CK_oQU tests in which the samples were subjected to reduction in mean normal stress, while the deviator stress was kept constant. The undrained stress paths of the K_o -normally consolidated state both in compression and in extension conditions are also shown in this figure. Four samples with initial pre-shear OCR values of 1.00, 1.24, 1.50, and 2.15 are taken to failure under constant q stress conditions. The failure envelope of these samples are also drawn in this plot.

6.7.2 Stress Ratio-Shear Strain Relationships

Figure 6.56 illustrates the (η, ϵ_s) relationship for the constant q unloading tests. The shear strain in the initial phase of shear is small. However, the shear strain begin to increase rapidly when the stress ratio reaches the Critical State value and tend to approach the Hvorslev failure envelope.

6.7.3 Volumetric Strains

Figure 6.57 illustrates the development of volumetric strain with the reduction in mean normal stress p . The arrows marked in this plot indicate the stress level at which volumetric yielding takes place of a type similar to the that on the wet side of the Critical State when the applied stress paths approach the SBS on the Rendulic type of surface. In this case, the stress paths approach the SBS to reach the Hvorslev failure surface.

Figure 6.58 illustrates the (ϵ_{vp}, p) relationship. For each type of test, the ϵ_{vp} values are small in compression until a substantial reduction in p takes place. When the p values reach the states C , C_1 , C_2 and C_3 , the plastic dilation takes place. For the sample CK_oQU5 , the plastic dilation is large and is about -2.2%. Figure 6.59 illustrates the (ϵ_v, ϵ_s) relationship. It is interesting to note that large plastic dilation takes place when the samples cross the Critical State Line and approach the Hvorslev failure envelope. Sample CK_oQU5 is experiencing nearly 10% volumetric strain. Figure 6.60 illustrates the $(\epsilon_{vp}, \epsilon_s)$ relationship. All three curves show initially small plastic volumetric strain and subsequently large amounts of plastic dilation.

Figure 6.61 shows the (η, ϵ_v) relationship. The (ϵ_{vp}, p) and the (ϵ_{vp}, η) relationships are shown in Figs. 6.62 and 6.63. In these figures, the arrows marked indicate the values of p and η for which plastic volumetric dilation take place.

Finally, Fig. 6.64 shows the plastic volumetric strain contours plotted in the (q, p) plot. Very small plastic volumetric strains are noted until the stress paths approach the Critical State stress values. Almost all the plastic volumetric dilation seem to occur in the stress zone between the Critical State Line and the Hvorslev failure envelope.

6.7.4 Normalized (q/p_e , p/p_e) Plot

Figure 6.65 shows how the state paths begin to rise towards the Hvorslev surface in the $(q/p_e, p/p_e)$ plot. The points marked by arrows in this plot indicate a sort of volumetric yield as the stress paths approach the SBS.

6.7.5 (e_f , $\ln p$) Plot

Figure 6.66 illustrates the initial points A, A₁, A₂, A₃ and the end points C, C₁, C₂, C₃ on the $(e_f, \ln p)$ plot. The end points are found to lie on a line with a slope of 0.08.

6.8 Conventional Drained Extension Tests (CK_oDE Tests)

The CK_oDE tests correspond to extension condition similar to the CK_oDU tests in compression. In both types of tests, the mean normal stress was reduced. Six specimens with OCR values of 1.00, 1.24, 1.50, 1.78, 2.15, and 2.75 were sheared in extension under drained conditions. Figure 6.67 illustrates the drained stress paths of each test together with the undrained stress path of the normally consolidated specimen in extension.

6.8.1 Deviator Stress-Shear Strain Relationships

Figure 6.68 shows the (q, ϵ_s) relationships in extension. The relationship is found to be approximately the same though there is a substantial difference. Figure 6.69 shows the (η, ϵ_s) relationship. They are found to be different for all six specimens, except for the cases when the OCR values are 2.15 and 2.75.

6.8.2 Volumetric Strains

Figure 6.70 shows the (ϵ_v, p) relationships. These relationships appear to be similar but are different. The arrows in this plot indicate the volumetric yield points and these are obtained at the transition point where the increase in ϵ_v with p is markedly different from the initial ones. These volumetric yield points correspond to the volumetric yield loci on the extension side when the stress paths approach the SBS. These points are marked by arrows in the (q, p) plot in Fig. 6.67. The behaviour of K_o consolidated specimens in extension can be somewhat different from the ones in compression and as such, some deviation can be expected in the SBS for the K_o consolidated extension tests as compared to the SBS from the isotropically consolidated samples in extension which is perhaps a mirror image of that in compression about the p-axis.

Figures 6.71a and 6.71b show the (ϵ_v, ϵ_s) relationships separated into two groups: one set for samples with OCR values of 1.00, 1.24 and 1.50 and other set for samples with OCR values of 1.78, 2.15 and 2.75. The dotted curves in these figures correspond to the plastic volumetric strains. Figure 6.72 shows the $(\epsilon_{vp}, \epsilon_s)$ relationship on an enlarged scale.

The (η, ϵ_v) and (q, ϵ_v) relationships are shown in Figs. 6.73 and 6.74, respectively. Finally, Figs. 6.75 and 6.76 show the (η, ϵ_{vp}) and (q, ϵ_{vp}) relationships. These figures indicate that positive plastic volumetric strains of small magnitude take place in the initial stages of shear and subsequently the samples tend to dilate. Thus, the arrows marked indicate the deviator stresses and the stress ratios when the plastic volumetric strains become negative. These plastic volumetric strains can arise from sub-sets of volumetric yield loci inside the SBS. Figure 6.77 illustrates the subsets of volumetric strain contours on the extension side within the SBS.

6.8.3 Normalized $(q/p_e, p/p_e)$ Plot

Figure 6.78 shows the state paths followed by the CK₀DE specimens in the $(q/p_e, p/p_e)$ plot. These state paths lie within the SBS when isotropically consolidated samples are sheared in extension in the normally consolidated states. It is interesting to note that even the samples in extension tend to approach the Hvorslev failure surface and then strain soften to reach the Critical State. The yield points marked in this plot correspond to the volumetric yield loci which lie on the SBS.

6.9 Constant p Extension Tests (CK₀PE Tests)

6.9.1 Effective Stress Paths

Four specimens are sheared along CK₀PE stress paths as shown in Fig. 6.79. Also shown in this figure is the undrained stress path as obtained from the K₀ conditions and the volumetric yield points when the stress paths approach the SBS on the extension side. Further discussion on the volumetric yield points will be made in a latter section.

6.9.2 Shear Strains

Figure 6.80 illustrates the (q, ϵ_s) relationship in the CK₀PE tests. The (η, ϵ_s) relationship is shown in Fig. 6.81.

6.9.3 Volumetric strains

Figures 6.82 and 6.83 illustrate the (q, ϵ_v) and (η, ϵ_v) relationships. Since these tests are performed under constant p conditions, the elastic volumetric strains are zero and hence Figs. 6.82 and 6.83 also correspond to plastic volumetric strains. The arrows marked in these figures correspond to the stress states when plastic volumetric strains take place. These stress states can help to map the sub-sets of volumetric yield loci within the SBS on the extension side. Figure 6.84 shows the sub-sets of plastic volumetric strain contours within the SBS.

6.9.4 Normalized $(q/p_e, p/p_e)$ Plot

Figure 6.85 shows the $(q/p_e, p/p_e)$ paths followed by the CK_oPE samples in extension. The end points of the specimens on the Hvorslev surface are also indicated. The yield points shown in this figure correspond to the volumetric yield locus for which the stress paths have their states on the State Boundary Surface (SBS).

6.10 Strength Envelope and Yield Locus from Drained Tests

In the earlier sections, the drained behaviour of normally and overconsolidated specimens sheared from K_o and isotropic stress conditions were discussed in detail series by series. This section presents the strength characteristics and yield locus from all K_o consolidated samples. The test results are presented in a summarized form. All samples were sheared from the same void ratio plane ($e_o \cong 1.16$) in the (q, p, e) space.

6.10.1 Strength Envelope

Figures 6.86a and 6.86b illustrate the failure points of the samples sheared with compression conditions in (q, p) plot and in $(q/p_e, p/p_e)$ plot, respectively. Undrained stress paths of normally consolidated specimens CIU1 and CK_oU1 are also shown together with the drained stress paths in Fig. 6.86a. All the samples with their stress states on the State Boundary Surface (SBS) are seeking the Critical State Line. On the other hand, samples with their stress states below the SBS failed on a Hvorslev type failure envelope. Thus, the failure points of these latter samples lie above the Critical State Line in the (q, p) plot.

Figure 6.87 shows failure points of samples sheared from K_o pre-shear stress conditions together with their applied stress paths both in compression and in extension. The curve E_oC is the undrained stress path of the normally consolidated sample having the same initial water content as the K_o consolidated samples. The curve OCN indicates the Hvorslev failure envelope and the Critical State Line on the compression side. The mirror images of these two curves about the p -axis are shown as E_oC' and $OC'N'$. The undrained stress paths of K_o normally consolidated samples both in compression (CK_oU1) and in extension (CK_oUE1) conditions are

also shown as ADE and AD'E', respectively. It is interesting to note from this figure that all the samples in extension conditions attain their failure at the curve OC'N' with little deviations. This indicates that the State Boundary Surface (SBS) is symmetric in nature about the p-axis for isotropically consolidated samples. All failure points from undrained tests are added to those from the drained tests and are plotted together in Fig. 6.88. The strength envelope OC"N" on the extension side in this figure is now drawn from the test data. These figures and data strongly support the symmetry of the SBS about the p-axis.

6.10.2 (Δe_f , p_f) Relationships

Figure 6.89 shows the overall change in void ratio, Δe_f , throughout each test, as measured from points A, A₁, A₂.... A₅ shown in Fig. 6.87. All points fall on a unique curve. This curve is very similar to the one presented by BALASUBRAMANIAM (1969) and JAMES and BALASUBRAMANIAM (1971) for samples of Kaolin sheared from isotropic pre-shear conditions. Figure 6.90 illustrates the (Δe_f , $\ln(p_f/p_e)$) relationship. The straight curve LH corresponds the Critical State Line CN in Fig. 6.87, while the curve HH' represents the Hvorslev type of curve.

6.10.3 Yielding from Drained Tests on K_0 -consolidated Samples

Volumetric yield points are normally determined from the (ϵ_v , p) relationship with a bi-linear construction. Such a construction is only an approximate technique and is somewhat similar to the Casagrande method for the determination of the maximum past pressure. Such volumetric yield points, therefore, correspond to the volumetric yield locus which lie on the Roscoe surface on the wet side of the Critical State and a similar limit state dilational yield locus on the dry side seeking the Hvorslev failure envelope.

Figure 6.91 demonstrates all volumetric yield points obtained from the various types of drained tests on K_0 and anisotropically overconsolidated samples when plotted together with the undrained stress paths of K_0 normally consolidated samples both in compression and in extension conditions. The yield points seem to lie in a zone and this zone is shown in Fig. 6.92. In the q-p space, the yield zone is somewhat elliptical in shape. The overall shape of this yield zone is quite similar to that reported by MITCHELL (1970) and WONG and MITCHELL (1975).

It should be noted here that the void ratios for all samples at the yield points are not the same, though their pre-shear void ratios were approximately the same. Thus, this volumetric yield zone is replotted in the (q/p_e , p/p_e) plot in Fig. 6.93. The yield locus shown in this figure is basically the same in shape as that shown in Fig. 6.92. The normalization somewhat reduce the scatter in the data.

Figure 6.94 illustrates a simplified elastic zone for the K_0 consolidated sample within the State Boundary Surface. This elastic zone has a distorted elliptic shape with the major axis along the idealized K_0 -line. Such a rotated elastic nucleus enclose a zone within the SBS in which the volumetric strain is elastic and the distortional strain is plastic. For the region outside this nucleus and enclosed within the SBS, subsets of volumetric yield loci could exist, which give positive plastic volumetric strains on the wet side and dilational volumetric strains on the dry side even though these volumetric strains are small in magnitude than those corresponding to yielding on the Roscoe surface.

6.10.4 Shear Strain Contours

Figure 6.95 demonstrates the shear strain contours obtained from the K_0 consolidated drained tests in compression. The shear strain contours shown in this figure are similar in shape to those from the undrained tests. The samples in the drained conditions experienced more shear strains than those in the undrained conditions, and contours are somewhat parallel to the idealized K_0 -line on the dry side of the Critical State. However, they tend to become parallel to the p-axis in the region around the Roscoe surface. The contours become closer as they approach the Critical State. It should be remembered that such drained shear strain contours, though approximate to the undrained ones near to the idealized K_0 -line, will include a substantial dilational component when the stress states approach the Hvorslev type of failure surface.

6.11 Summary of Drained Behaviour

A total of ten series of drained test were carried out. All samples had the same pre-shear void ratio as those for the undrained tests presented in the previous chapter. The initial pre-shear stress states lie inside the SBS and as such loading tests both on the compression and extension phase brought samples on the wet side of the Critical State during shear to normally consolidated states.

6.11.1 Isotropically Consolidated Drained Tests (CID Tests)

All volumetric yield points lie on a single curve when they are plotted in the $(q/p_e, p/p_e)$ plot. This normalized volumetric yield locus is realistically predicted by the Modified Theory, and it lies on the Roscoe surface of the SBS. The normally consolidated sample also show an apparent yield point due to pre-shear secondary consolidation. All the end points of the samples on the wet side are found to lie around the Critical State Line. There is an outer boundary in the (q, ϵ_v) relationship from which the samples tend to deviate as their stress state reach the Roscoe surface on the SBS. At any particular stress ratio, the normally consolidated sample has the highest shear strain and the shear strain decreases in magnitude as the OCR values increase.

The shear strain contours from drained tests are approximately the same as those from undrained tests at low levels of stress ratio (i.e., the shear strain associated with the dilatant phenomenon in drained test is small). Most of the plastic volumetric strain takes place for the stress states on the Roscoe surface of the SBS. For stress states which lie inside the SBS, there exists a nucleus within which purely elastic volumetric strain and plastic distortional strain take place. Outside of it, volumetric yielding takes place which can be compressive or dilational in nature. The plastic volumetric strain inside the SBS is an order smaller than that which takes place on the SBS.

6.11.2 Conventional Drained Tests on K_0 Consolidated Samples (CK₀D)

The (q, ϵ_s) relationships corresponding to the stress states inside the SBS are approximately the same, and these are markedly different from those on the SBS. On the dry side of the Critical State, the (η, ϵ_s) relationship is unique and is less dependent on the plastic dilatancy ratio at low values of η . All specimens having their stress state below the SBS and on the wet side of the Critical State experience small shear strains, while they give different (η, ϵ_s) relationship when the stress states lie on the SBS. The q_{\max} and $(\bar{\sigma}_1/\bar{\sigma}_3)_{\max}$ points all tend to cluster around the Critical State.

In the (η, ϵ_v) plot, there exists an outer boundary which gives the smaller volumetric strain corresponding to the stress states within the SBS. The (η, ϵ_v) relationships deviate from this outer boundary when the stress states lie on the SBS. Most samples are found to show some strain softening after peak deviator stress. The zero plastic volumetric strain locus lie inside the SBS. The $(\epsilon_{vp}, \epsilon_{sp})$ relationship for the samples on the wet zone with OCR values of 1.00, 1.24 and 1.50 are different from one another. However, this relationship for the samples on the dry zone are nearly the same. Thus, for the range of OCR of 1.78 to 2.75, the plastic dilatancy ratio seems to depend only on the stress ratio.

6.11.3 Conventional Drained Tests on Anisotropically Consolidated Samples (CAD Tests)

The (q, ϵ_s) and (η, ϵ_s) relationships are distinctly different for all the samples. However, there exist an outer boundary in the (η, ϵ_s) relationship at low levels of stress ratio when the stress states lie inside the SBS. The (ϵ_v, p) relationship is separated into two parts: one corresponding to the stress state inside the SBS and the other being on the SBS, both being separated

by the volumetric yield point. These points tend to lie on a constant q line close to the Critical State. The q_{\max} and the $(\bar{\sigma}_1/\bar{\sigma}_3)_{\max}$ points are all found to cluster around the Critical State Line. The $(\epsilon_{vp}, \epsilon_{sp})$ relation is dependent on the stress ratio η and p .

6.11.4 Constant p Compression Tests (CK_oPC Tests)

The (q, ϵ_s) relationships are different for all the samples. However, there exists a limit boundary when the incremental q and incremental shear strain relationship is plotted, which corresponds to the contribution from the constant q type of yield loci. For the specimens on the wet side of the Critical State, the (η, ϵ_s) relationships are different, while these relationships tend to be the same as the OCR values are increased. Plastic dilational volumetric strains are found to take place in all the CK_oPC samples. However, the magnitude of these strains are small, i.e., when the sample reach the Hvorslev failure envelope, the dilational volumetric strain is only 1.2%. Though there is a tendency for the samples with higher OCR values to show roughly the same $(\epsilon_{vp}, \epsilon_{sp})$ relationship, these relationships are distinctly different for all values of OCR. The state paths below the SBS are found to rise nearly vertically in the $(q/p_e, p/p_e)$ plot all the way up to the failure state. The q_{\max} and $(\bar{\sigma}_1/\bar{\sigma}_3)_{\max}$ points are also found to lie close to the Critical State Line.

6.11.5 Unloading Compression Tests (CK_oDU Tests)

The (q, ϵ_s) relationship is found to be different for all specimens. However, there exists an outer boundary from which the individual curves deviate with increasing values of Δq as the OCR increase. The outer boundary is similar to the contribution from the constant q yield loci. For the samples with the higher OCR values, the (η, ϵ_s) relationships are the same and these relationships differ from those for samples on the wet side of the Critical State. The q_{\max} and $(\bar{\sigma}_1/\bar{\sigma}_3)_{\max}$ points cluster around the Critical State point. Dilational plastic volumetric strains are experienced by the samples CK_oDU3 and CK_oDU5, while compressive plastic volumetric strains are experienced by the samples CK_oDU1 and CK_oDU2. The compressive volumetric strains below the SBS is as much as 1%, while the specimen CK_oDU experienced nearly 2.25% of dilational plastic volumetric strain when it reached the Hvorslev envelope. The $(\epsilon_{vp}, \epsilon_{sp})$ relationships are found to depend both on the stress ratio η and p .

6.11.6 Constant q Unloading Tests (CK_oQU Tests)

The shear strain in the initial phase of stress ratio is small. However, the shear strain begins to increase rapidly when the stress ratio reaches the Critical State value and tend to seek

the Hvorslev failure envelope. Yield points tend to cluster around the Critical State Line, and all failure points lie on the Hvorslev failure envelope. The plastic volumetric strains are also small in compression until substantial reduction in p takes place. However, comparatively large plastic dilation takes place when the samples approach the Hvorslev failure envelope.

6.11.7 Conventional Drained Extension Tests ((CK₀DE Tests)

All state paths followed by the CK₀DE specimens lie within the SBS. These samples approach the Hvorslev failure surface and then strain soften to reach the Critical State. The (q, ϵ_v) relationship is found to be approximately same, while the (η, ϵ_v) relationships are found to be different for all specimens, except for the cases when the OCR values are 2.15 and 2.75. Positive plastic volumetric strains of small magnitude takes place in the initial stages of shear and subsequently the samples tend to dilate when the samples approach the Hvorslev failure envelope.

6.11.8 Constant p Extension Tests (CK₀PE Tests)

From these tests data, subsets of volumetric yield loci are plotted inside the SBS. Though no experimental data is available at lower values of mean normal stress p (close to the origin) in the (q, p) plot, the trend indicates that the shape of volumetric yield loci on the dry side of the Critical State seems similar to that on the dry side in compression.

6.11.9 Strength Envelope and Yield Locus from Drained Tests

All the samples with their stress states on the SBS reached the Critical State Line. On the other hand, samples which their stress states below the SBS failed on the Hvorslev failure envelope. Thus, the failure points of these sample lie above the Critical State Line. The relationship between the change in void ratio, Δe_f , and the value of p at failure, p_f , from all the drained specimens forms a unique curve. Both the Critical state Line and the Hvorslev failure envelope are symmetrical about the p -axis. The elastic volumetric zone for K₀ consolidated samples has a distorted elliptic shape with the major axis along the idealized K₀-line. The shear strain contours inside the SBS are sub-parallel to the idealized K₀-line on the dry side of the Critical State and tend to become parallel to the p -axis on the wet side.

VII CRITICAL STATE MODELS AND THEIR COMPARISONS WITH THE EXPERIMENTAL OBSERVATIONS

7.1 Introduction

A critical review of the stress-strain theories based on the Critical State Concepts was made in Chapter III. The Critical State Concepts and the associated stress-strain theories were developed based on experimental and analytical research undertaken from 1950 to 1970. The original ideas on the existence of the State Boundary Surface (and the associated Critical State Line and the Hvorslev Failure Envelope) began with the ingenious work of RENDULIC (1936) on the constant void ratio contours and the counterpart contribution of HVORSLEV (1937) on the shear strength of clays. The critical void ratio of sand was also observed by CASAGRANDE (1938) and TAYLOR (1948). Substantial use of the data from remoulded specimens of London clay and Weald clay was also made in properly formulating the ideas on the State Boundary Surface (SBS) and the Critical State Line (CSL). These data are from tests conducted on samples with isotropic pre-shear consolidation pressures.

Much of the work associated with the development of an incremental stress-strain theory for normally consolidated clay (see ROSCOE and POOROOSHASB, 1963), the Cam Clay Theory, and their modifications (see ROSCOE, SCHOFIELD and THURAIRAJAH, 1963; SCHOFIELD and WROTH, 1968; ROSCOE and BURLAND, 1968) considered the existence of the SBS with the CSL as the backbone and it relies heavily on the elasto-plastic concepts in the theory of plasticity with an 'associated flow rule'. These theories captured the bulk of the behaviour of normally and overconsolidated clays as sheared from the isotropic pre-shear stress states with various degrees of accuracy. The authors used the observations from resedimented samples of Kaolin extensively (see THURAIRAJAH, 1961; BURLAND, 1968; BALASUBRAMANIAM, 1969) and the basic concepts are essentially verified for the behaviour in the normally consolidated state from isotropic pre-shear consolidation conditions. A comprehensive series of studies carried out at the Asian Institute of Technology in the mid seventies fully demonstrated the appropriateness of the Revised Theory of ROSCOE and BURLAND (1968) for the successful prediction of the stress-strain behaviour of normally consolidated clays as sheared from isotropic pre-shear consolidation conditions.

The Author's research is, therefore, primarily aimed in making an experimental study and in evaluating the theoretical predictions for specimens sheared from K_0 conditions both for normally and overconsolidated states of Bangkok clay. Thus the Author's work specifically aims to

- (i) experimentally study the behaviour of Bangkok clay in the overconsolidated state (i.e., within the SBS) and compare this behaviour with the predictions from the existing stress-strain theories.

(ii) experimentally study the behaviour of Bangkok clay in the normally consolidated state but sheared from K_0 pre-shear consolidation conditions.

In doing so, it is pertinent to summarize the contributions related to the prediction of stress paths, pore pressures and strains both in undrained and drained tests for stress states below the SBS. Much of the contribution related to such behaviour originated with the constant shear strain contours of WROTH and LOUDON (1967) as combined with the Cam Clay Theory and its modifications. In these theories, it is accepted that only plastic distortional strains take place inside the SBS, while the volumetric strain is elastic. BALASUBRAMANIAM (1969) demonstrated that both plastic and distortional strains do take place inside the State Boundary Surface (SBS) with a smaller magnitude as compared to those when the stress states lie on the SBS. The importance of an understanding of the dilatancy of the specimens both on the wet and dry side of the Critical State in successfully formulating the stress-strain behaviour below the SBS was also emphasized. PENDER (1978) extended the Cam Clay Theory based on the Critical State Concepts to predict the volumetric and distortional strains both below the SBS and on the SBS as sheared from isotropic and K_0 pre-shear consolidation conditions. Thus, the Author's experimental observations will be compared extensively with Pender's Model (PENDER, 1978) for the prediction of strains and pore pressures.

In making such comparisons with the theories, the K_0 consolidated behaviour will also be studied in relation to the anisotropic stress-strain models of PENDER (1977, 1978), ATKINSON et al. (1987) and DAFALIAS (1987), which all belong to the same family of Critical State Theories with varying degrees of modification. The Author also proposes a conceptual modification of Pender's Model for the undrained behaviour of lightly overconsolidated clays.

The organization of this chapter is such that the undrained behaviour for normally and overconsolidated stress states are presented first from both the isotropic and K_0 pre-shear consolidation conditions. This is then followed by the drained behaviour, and the Author's modifications to Pender's Model. Concluding remarks are included at the end of this chapter on the salient aspects of the predictions from the various theories in relation to the experimental observations.

7.2 Comparison of Undrained Behaviour of Normally Consolidated Clays Sheared from Isotropic Pre-shear Stress Conditions

Two sets of soil parameters are used in the comparisons of the samples sheared from isotropic pre-shear conditions: one from the peak deviator stress condition and the other from the Critical State condition as defined with the maximum obliquity criterion.

7.2.1 Effective Stress Paths in Compression

Figure 7.1 illustrates the state paths of the normally consolidated samples sheared from the pre-shear isotropic states together with those predicted by the Modified Cam Clay Model

and Pender's Model, respectively. This figure shows that both models predict successfully the state path when the parameters are selected from the peak deviator stress conditions ($M = 0.83$). A close examination reveals that the Modified Cam Clay provides a better prediction than Pender's Model. This trend is more clearly seen in Fig. 7.2. It is observed that the Critical State is achieved just after the peak deviator stress condition, and, thus, the slope of the Critical State Line in the (q , p) plot was 0.88. The effects of the parameter M on the Modified Cam Clay Theory are not significant since the difference between the two M values is small. However, it is interesting to point out here that the value of p_{cs} for the Critical State is comparatively less than that for the peak deviator stress condition. Therefore, the predictions made by Pender's Model with the parameter p_{cs} from the Critical State deviates from the experimental data. More care is needed for Pender's Model than the Modified Cam Clay Theory in selecting the parameters especially for the clays exhibiting a strong softening. The Modified Cam Clay Theory provides realistic undrained stress paths corresponding to the peak deviator stress conditions (see Fig. 7.2).

7.2.2 Stress-Strain Relationships

The deviator stress-strain relationships for the normally consolidated samples in the undrained compression conditions are presented in Figs. 7.3 and 7.4. The shear strain contributions from the constant- q yield loci for the Revised Theory are obtained from the experimental data (Fig. 5.42). These two figures show that the model parameter corresponding to the peak deviator stress condition give more realistic predictions (see Fig. 7.4). The Pender's Model underpredicts the strength, while the Modified Cam Clay Theory overpredicts the strength. The stress-strain relationships by the Revised Theory with the parameter corresponding to the peak deviator stress conditions agree well with the experimental data (Fig. 7.4).

7.2.3 Stress Ratio-Shear Strain Relationships

The relationship between the stress ratio and the shear strain is shown in Figs. 7.5 and 7.6. The Modified Cam Clay Theory underpredicts the shear strain as expected, while Pender's Model overpredicts the shear strain. The Revised Theory predicts the correct stress-strain relationship, when the parameters are selected from the Critical State criterion (Fig. 7.5). When the parameters are based on the peak deviator stress condition as adopted in the model calculations, all models tend to overpredict the shear strain especially when the strain exceeds 6%.

7.2.4 Excess Pore Pressures

Figures 7.7 and 7.8 demonstrate the relationship between the u/p_0 and the stress ratio. These figures confirm how successfully the Modified Cam Clay Theory predicts the undrained stress path for the triaxial compression condition. Model predictions also demonstrate a bi-linear relationship between the u/p_0 and the stress ratio, even for the normally consolidated state.

However, linear approximation with a single slope is still admissible with slight deviations in the early loading stage, which reflects the effect of the secondary consolidation during the consolidation phase of the sample preparation.

7.3 Comparison of Undrained Behaviour of Normally Consolidated Clays under K_0 Pre-shear Stress Conditions

In this section, the models used for comparisons are Pender's Model, Dafalias' Model, and the extended form of the Modified Cam Clay Theory of ATKINSON et al. (1987). These models are reviewed in Chapter III. The incremental forms of the stress-strain behaviour for Dafalias' Model are derived for the complete comparisons in Section 7.3.1. The Eqn. 3.41 proposed by ATKINSON et al. (1987) is also transformed to accommodate the same parameters for the comparisons. An incremental form of the stress-strain relationship for this approach is also derived in Section 7.3.2.

7.3.1 Incremental Form of Stress-Strain Relationships (Dafalias' Model, 1987)

As mentioned in Section 3.6.1, DAFALIAS (1987) did not extend his model to any type of incremental form for the stress-strain behaviour as we usually expect in the development of stress-strain theories. The incremental forms of the stress-strain relationship for Dafalias' Model are derived in this section by the Author for the complete comparison. The work equation for Dafalias' Model is,

$$dW = p [(d\epsilon_{vp})^2 + (Md\epsilon_{sp})^2 + 2\alpha d\epsilon_{vp} d\epsilon_{sp}]^{1/2} \quad \dots(3.30 \text{ bis})$$

From the yield locus (Eqn. 3.33) and the assumption that λ , κ are constant in the $e - \ln p$ space, the following incremental form of the stress-strain relationships are derived.

$$d\epsilon_{sp} = \frac{\lambda - k}{1 + e} \left(\frac{2(\eta - \alpha)}{M^2 - \eta^2} \right) \left(\frac{2(\eta - \alpha)d\eta}{M^2 + \eta^2 - 2\alpha\eta} + \frac{dp}{p} \right) \quad \dots(7.1)$$

$$d\epsilon_{vp} = \frac{\lambda - k}{1 + e} \left(\frac{2(\eta - \alpha)d\eta}{M^2 + \eta^2 - 2\alpha\eta} + \frac{dp}{p} \right) \quad \dots(7.2)$$

These equations are used for the calculation of the stress-strain relationships. DAFALIAS (1987) also assumed that the dimensionless parameter α is constant during undrained com-

pression. It is interesting to investigate this assumption through the monitored data. α is the function of M , η , and the plastic strain increment vector in order to satisfy the work equation (Eqn. 3.30). The equation for α is given as :

$$2\alpha = 2\eta + (\eta^2 - M^2) \frac{d\epsilon_{sp}}{d\epsilon_{vp}} \quad \dots(3.36 \text{ bis})$$

SCHOFIELD and WROTH (1968) explained that, in the case of the undrained test, the total volumetric strain is zero, because the recoverable volumetric strain is accompanied by an equal and opposite plastic volumetric strain. This assumption leads to the following plastic strain increment vector during an undrained test.

$$d\epsilon_{vp} = -d\epsilon_{ve} = \frac{-k dp}{p(1+e)} \quad \dots(7.3)$$

$$\frac{d\epsilon_{sp}}{d\epsilon_{vp}} = \frac{-p(1+e)d\epsilon_s}{k dp} \quad \dots(7.4)$$

where $d\epsilon_{sp}$ is equal to $d\epsilon_s$, since $d\epsilon_{se} = 0$. Eqn. 7.4 will be used for the calculation of the value of α for the undrained compression tests. Thus, Eqn. 3.36 can be rewritten as Eqn 7.5 for the calculation of α during undrained tests.

$$2\alpha = 2\eta + (M^2 - \eta^2)(1+e) \frac{p}{k} \frac{d\epsilon_s}{dp} \quad \dots(7.5)$$

7.3.2 Extended Form of Modified Cam Clay Theory **(ATKINSON et al., 1987)**

The extended form of the Modified Cam Clay Theory (ATKINSON et al., 1987) for the K_0 stress condition was expressed using the equivalent pressure, p_e , and the equivalent specific volume, v_λ (see Eqn. 3.41). This equation is transformed to accommodate the fundamental soil parameters for the comparison in the form of,

$$(\eta - \eta_o)^2 = (M - \eta_o)^2 \left(\frac{p_o}{p} \right)^{\frac{\lambda}{\lambda - k}} - (M - \eta_o)^2 \quad \dots(7.6)$$

The incremental form of the stress-strain relationships are similar to those for the Modified Cam Clay Theory of ROSCOE and BURLAND (1968).

$$d\epsilon_{sp} = \frac{\lambda - k}{1 + e} \left(\frac{2(\eta - \eta_o)}{(M - \eta_o)^2 - (\eta - \eta_o)^2} \right) \left(\frac{2(\eta - \eta_o)d\eta}{(M - \eta_o)^2 + (\eta - \eta_o)^2} + \frac{dp}{p} \right) \quad \dots(7.7)$$

$$d\epsilon_{vp} = \frac{\lambda - k}{1 + e} \left(\frac{2(\eta - \eta_o)d\eta}{(M - \eta_o)^2 + (\eta - \eta_o)^2} + \frac{dp}{p} \right) \quad \dots(7.8)$$

where η_o is the pre-shear stress ratio.

7.3.3 Effective Stress Paths

The undrained stress paths for the K_o -normally consolidated state from different stress-strain models are superimposed with the experimental data in Fig. 7.9. The parameters used for the model calculations are shown in the same figures. The curve ABC (dotted line, a part of the State Boundary Surface of Dafalias' Model) has been drawn in order to show the complete shape of the State Boundary Surface (SBS) of Dafalias' Model. It should be noted that Dafalias' Model assumed that the behaviour inside the SBS is elastic, and during the extension tests some portion of effective stresses lie within the SBS.

(1) **Triaxial Compression** - All model predictions deviate from the experimental observations, particularly, they fail to simulate the undrained stress path in the early stages of the loading. As stated earlier, these deviations may result since the sample exhibits the effects of secondary consolidation (gained during the consolidation phase in the sample preparation), while the models are not expected to include such time effects. Pender's Model seems to predict successfully the undrained stress path. Of course, this model is dependent on the parameter p_{cs} as seen in the case of the isotropically consolidated state. The approach reported by ATKINSON et al. might fit the behaviour when there is strong strain softening.

(2) **Triaxial Extension** - All model predictions during the extension phase above the p-axis (i.e., $0 < \eta < \eta_r$) are reasonably coincident with the experimental observations. In the pure extension stress state, when η is less than zero, all model predictions deviate from the experimentally observed stress path. Pender's Model gives the best prediction for the extension condition. As reviewed in Chapter II, the mean effective normal stress for low plasticity clay during the extension phase is drastically reduced.

It can be concluded from these comparisons that Pender's Model gives relatively good prediction of the undrained stress paths for the normally consolidated state both in the compression and in the extension conditions.

7.3.4 Stress-Strain Relationships

The stress-strain curves are shown in Figs. 7.10 to 7.11. Parameters used for Fig. 7.10 are determined from the Critical State conditions. For clarity, this figure is enlarged and separated for compression (see Fig. 7.10a) and extension (see Fig. 7.10b), respectively. These stress-strain relationships using parameters from the peak deviator stress condition are shown in Fig 7.11.

(1) **Triaxial Compression** - The prediction provided with the approach reported by ATKINSON et al. (1987) significantly underpredicts the strength as expected from an undrained stress path. Pender's Model also underpredicts the strength and overpredicts the shear strain. However, the predictions obtained from Dafalias' Model agree well with the experimental data. It seems all models fail to simulate the stress-strain relationship in the early stages of loading; probably, because the experimental observations include time effects due to secondary consolidation.

(2) **Triaxial Extension** - In the case of the extension tests, all model predictions agree well with the experimental data up to the p-axis. However, there are tendencies for Pender's Model to give larger strains, while the other two models give smaller shear strains at the same deviator stress level. Except Pender's Model, the other two models are relatively rigid in distortion for stress states less than the peak deviator stress. Upon approaching the peak deviator stress, these models show an abrupt increase in shear distortion similar to those patterns seen in the compression tests. Generally, Pender's Model, although it overpredicts the shear strains, reveals a qualitatively reasonable stress-strain relationship in the extension phase when the model parameters are determined from the peak deviator stress conditions (see Fig. 7.11).

7.3.5 Stress Ratio-Shear Strain Relationships

The stress ratio-strain relationships are illustrated in Figs. 7.12 and 7.13 for the compression and the extension conditions, respectively. It is interesting to note from Fig. 7.12 that the stress ratio-shear strain relationships predicted by the three models agree well with the experimental observations in the compression phase. This indicates that the predicted strains are uniquely dependent on the stress ratio. The model predictions deviate from the experimental observations in the extension phase. Pender's Model overpredicts, while other two models underpredict the shear strains.

7.3.6 Excess Pore Pressure

Figures 7.14 and 7.15 present the excess pore pressure-shear strain relationships. All models predict roughly the same (u, ϵ_s) relationship up to a shear strain of about 3% in the compression phase. Thereafter, they deviate from each other with increasing shear strains. All models tend to overpredict the excess pore pressures.

The patterns of model prediction in the extension phase are quite different from those in compression. Pender's Model gives a trend similar to the experimental data, although it underpredicts the negative pore pressures. This tendency is improved when the parameters are determined from the peak deviator stress condition. On the other hand, Dafalias' and Atkinson's Models predict positive pore pressures when the strain exceeds about 2%.

7.4 Variation of Parameter α in DAFALIAS' Model (1987)

DAFALIAS (1987) derived his model from a work equation (Eqn. 3.30) with an associated flow rule and the factor α accounts for the effect of internal residual stresses. The magnitude of α determines the shape of the volumetric yield locus and the undrained stress path for the K_0 -consolidated clays. The Modified Cam Clay Model can be a special case when α is equal to zero. DAFALIAS (1987) derived the State Boundary Surface (Eqn. 3.34) assuming α does not change. He also pointed out that this assumption is only an approximate one. In fact, α needs to satisfy Eqn. 3.32 for the K_0 condition. However, it is not a necessary condition that α should remain constant during the subsequent shear. Equation 7.5 gives the variation of α during an undrained test.

The α values as calculated using this equation are plotted with respect to the stress ratio in Fig. 7.16. The α values remain constant up to a stress ratio of about 0.7, thereafter, it increases rapidly as the stress ratio is increased. It is interesting to note that the value of α even for the isotropically consolidated sample (CIU1 test) is not zero whereas it should be according to the theory. The K_0 -normally consolidated samples rather give values of α close to zero up to a stress ratio η of 0.7. The variation of α with stress ratio for the K_0 -overconsolidated samples during the undrained compression tests are plotted in Fig 7.17. The samples sheared from the wet side of the Critical State show a trend which is similar to the normally consolidated samples (Fig. 7.16). It can be concluded from these figures that the value of α varies during shear.

7.5 Comparison of Undrained Behaviour of Overconsolidated Clays as Sheared from Isotropic Pre-shear Stress Conditions

Currently, the stress-strain models for the overconsolidated behaviour are quite limited when compared to the normally consolidated ones. Pender's Model (PENDER, 1978) is the

only one which deals with the behaviour of overconsolidated clays within the frame work of the Critical State Theories. Thus, Pender's Model will subsequently be used for the prediction of pore pressure and strains.

7.5.1 Effective Stress Paths

The undrained stress paths of the overconsolidated clays predicted by Pender's Model are superimposed with the experimental data in Figs. 7.18 and 7.19. The model parameters are selected from the Critical State condition (Fig. 7.18) and from the peak deviator stress condition (Fig. 7.19), respectively. These two figures indicate that Pender's Model can successfully predict the undrained stress paths for the lightly overconsolidated samples if the parameters are properly selected. The predicted undrained stress paths for the samples sheared from the wet side of the Critical State deviate from the experimental observations when the parameters are determined from the Critical State condition as shown in Fig. 7.18. However, if the model parameters are determined from the peak deviator stress condition (i.e., p_{cs}^* and M_{pi}) then the family of undrained stress paths can be successfully predicted as shown in Fig. 7.19. It can, therefore, be concluded that Pender's Model predict the undrained stress paths well for the samples which belong to the wet side of the Critical State Line.

7.5.2 Stress-Strain Relationships

Typical stress-strain curves predicted by Pender's Model are plotted together with the experimental data in Figs. 7.20 and 7.21. Figure 7.20 is related to the Critical State conditions, while Fig. 7.21 is related to the peak deviator stress conditions. Both figures indicate that Pender's Model overpredicts the shear strain, although it predicts a reasonably correct failure strength. It is noteworthy that the parameters M and p_{cs} do not affect the predicted stress-strain relationships as much as they did in the undrained stress paths. This indicates that some of the assumptions made in Pender's Model are not fully correct and possibly this could relate to the plastic strain increment vector.

7.5.3 Excess Pore Pressures

Pender's Model successfully predicts the undrained stress paths in Fig. 7.18 and 7.19. Thus, it can be expected to predict successfully the pore pressures as well. Figure 7.22 shows the pore pressure predictions with strains as based on the Critical State soil parameters are quite successful. With respect to the model parameters as determined from the peak deviator stress conditions, the predicted pore pressures are slightly less than the observed ones. Thus, Pender's Model can predict good pore pressure-strain relationships, when the model parameters are determined from the Critical State condition.

7.6 Comparison of Undrained Behaviour of Overconsolidated Samples Sheared from K_0 Pre-shear Stress Conditions

In this section, Pender's Model on K_0 overconsolidated undrained behaviour is examined both in compression and in extension.

7.6.1 Triaxial Compression

(1) **Undrained Stress Paths-** The undrained stress paths predicted by Pender's Model for the K_0 -overconsolidated samples are superimposed with the test data in Fig. 7.24. Model parameters used for the calculations are determined from the Critical State condition. Generally, the predicted undrained stress paths for the overconsolidated samples deviate from the data except for the sample sheared from the pre-shear stress close to the p_{cs} (e.g., CK₀U4). The deviations are pronounced as the overconsolidation ratio is increased. As discussed earlier, this model is quite sensitive to the value of p_{cs} . This comparison indicates that the undrained stress paths of the samples sheared from the wet side of the Critical State can be predicted using this model when the parameters are selected from the peak deviator stress condition.

(2) **Stress-Strain Relationships-** The stress-strain relationships are compared with test data in Figs. 7.25 and 7.26. Model parameters are selected from the Critical State (Fig. 7.25) and from the peak deviator stress conditions, respectively. Pender's Model overpredicts the strain at the same deviator stress level with both set of parameters. This trend becomes pronounced as the overconsolidation ratio is increased.

(3) **Stress Ratio-Strain Relationships-** Figure 7.27 demonstrates the (η, ϵ_s) relationships. The solid lines depict these relationships predicted by the Model with parameters obtained from the Critical State conditions, while the dotted lines are obtained with parameters from the peak deviator stress conditions. This figure clearly demonstrates that Pender's Model significantly overpredicts the shear strain in a shear strain-stress ratio plot.

(4) **Excess Pore Pressure-Strain Relationships-** Figures 7.28 and 7.29 show the pore pressure-shear strain relationships. The parameters are selected from the Critical State and the peak deviator stress conditions, respectively. Both figures indicate that the Model underpredicts the excess pore pressure at certain levels of shear strains. The deviations are particularly substantial for the samples sheared from the dry side of the Critical State. The comparisons shown above indicate that Pender's Model significantly overpredicts the shear strain, though it can predict the undrained stress paths for the samples belonging to the wet zone under compression conditions. This may indicate that the assumption made on the plastic strain increment ratio in the theory is not realistic.

7.6.2 Triaxial Extension

(1) **Undrained Stress Paths-** Figure 7.30 displays the undrained stress paths in the extension tests together with those in the compression tests. The parameters used in the predictions are determined from the peak deviator stress condition. The effects of the p_{cs} value are evident when this figure on the compression side is compared with Fig. 7.24. The model predictions for the extension conditions is better than those for the compression conditions, especially, for the samples sheared from the dry side of the Critical State. The parameter p_{cs} for the extension condition should be determined from the extension test instead of selecting them from the compression tests.

(2) **Stress-Strain Relationships-** The stress-strain relationships for the extension conditions are compared in Fig. 7.31. The model predicts the stress-strain relationships well.

(3) **Excess Pore Pressure-Strain Relationships-** The relationship between the excess pore pressure and the shear strains are shown in Fig. 7.32. The Model predicts successfully the excess pore pressure for the normally consolidated sample in the extension condition. However, the predictions are not good for the overconsolidated samples.

7.7 Summary of the Model Predictions for the Undrained Behaviour

7.7.1 Normally Consolidated Behaviour

(1) **Isotropic Pre-shear Stress Conditions-** The Revised Theory of ROSCOE and BURLAND (1968) is found to successfully predict the undrained stress path, the undrained shear strength, the shear strains and the excess pore pressures for the CIU type of tests. Pender's Model overpredicts the shear strains and is somewhat sensitive with the parameter p_{cs} . However, this model is found to be promising for the prediction of the undrained stress path and the undrained strength and excess pore pressure when the model parameters are selected from the peak deviator stress criterion.

(2) **K_0 Pre-shear Stress Conditions-** Pender's Model predicts reasonably well the undrained stress paths both in compression and in extension with parameters determined from the peak deviator stress criterion. However, this model overpredicts shear strain in the compression phase. The predictions from Dafalias' Model is good for the compression tests. Atkinson's Model predicts low undrained strength. All models are poor in their predictions for the extension conditions.

7.7.2 Overconsolidated Behaviour

Pender's Model generates a successful family of undrained stress paths for the overconsolidated clays on the wet side of the Critical State both for compression and for extension

conditions when the parameters are selected from the peak deviator stress conditions. However, this model overpredicts the shear strains both for the isotropically consolidated and for the K_0 consolidated samples.

7.8 Comparison of Drained Behaviour of Normally Consolidated Clays Sheared from Isotropic Pre-shear Stress Conditions

The models used in the predictions in this section are the Modified Theory and the Revised Theory of ROSCOE and BURLAND (1968) and Pender's Model (PENDER, 1977, 1978). Comparisons are only made with model predictions with parameters from the Critical State condition. These parameters are also tabulated in each figure.

7.8.1 Stress-Strain Relationships

Figures 7.33 and 7.34 illustrate the (q, ϵ_s) and (q, ϵ_v) relationships, respectively. As expected, the Modified Theory underpredicts the shear strain, while the Revised Theory provides excellent agreement with the test data. Pender's Model overpredicts shear strains.

The variation of the volumetric strain with the deviator stress is shown in Fig. 7.34. The predictions using the Modified Theory agree well with the test data, while those using Pender's Model deviate from the actual observations.

7.8.2 Stress Ratio-Strain Relationships

The variation of the shear strain and the volumetric strain with respect to the stress ratio are shown in Figs. 7.35 and 7.36, respectively. Pender's Model overpredicts both the shear strain and the volumetric strain. The Modified Theory and the Revised Theory of ROSCOE and BURLAND (1968) successfully predict the stress ratio-strain relationships.

7.8.3 Plastic Shear Strain-Plastic Volumetric Strain Relationships

Figure 7.37 contains the $(\epsilon_{vp}, \epsilon_{sp})$ relationships during the CID1 test. The entire state path of this stress path lies on the State Boundary Surface (SBS). Thus, the Modified Theory and Revised Theory assume that the strain increment ratios $\frac{d\epsilon_{vp}}{d\epsilon_{sp}}$ are uniquely dependent on the stress ratio throughout the shearing process of this sample. Here again, the Revised Theory

provides an excellent prediction. However, Pender's Model deviates to a significant extent from the measured data. This deviation is mainly attributed to the overpredicted volumetric strain. Pender's Model gives a lower dilatancy ratio $\frac{d\epsilon_{vp}}{d\epsilon_{sp}}$ than that predicted by the other models.

7.9 Comparison of Drained Behaviour of Normally Consolidated Clays Sheared from K_0 Pre-shear Stress Conditions

Drained test data from K_0 -normally consolidated samples are compared with model predictions. The models used in the comparisons are Pender's Model (PENDER, 1977, 1978), Dafalias' Model (DAFALIAS, 1987) and Atkinson's Model (ATKINSON et al., 1987). Comparisons are made only for the conventional types of loading (CK_0D1) and unloading (CK_0DE1) conditions (i.e., the radial stress is held constant while the vertical stress is increased or is decreased).

7.9.1 Triaxial Compression

(1) **Stress-Strain Relationships-** Figures 7.38 and 7.39 show the (q, ϵ_s) and (q, ϵ_v) relationships for the CK_0D1 specimen, respectively. The prediction of shear strain from all the models is good up to deviator stress of 3.2 kg/cm^2 . During further increase in deviator stress, the predictions using Pender's and Atkinson's Models deviated from the test data, while those using Dafalias' Model are surprisingly close to the experimental observations. Dafalias' Model also gives an excellent prediction of volumetric strains, while the other two models overpredict the volumetric strains.

(2) **Stress Ratio-Strain Relationships-** The variations of ϵ_s and ϵ_v with respect to stress ratio η are illustrated in Figs. 7.40 and 7.41, respectively. The predictions using Dafalias' Model again agree well with the test data in both relationships, while those from other two models deviate from the experimental observations.

(3) **Plastic Volumetric Strain-Plastic Shear Strain Relationships-** Figure 7.42 illustrates the $(\epsilon_{vp}, \epsilon_s)$ relationship for the K_0 -normally consolidated sample (CK_0D1 sample) during the conventional loading test. The prediction using Dafalias' Model agrees well with the test data. Pender's Model predicts smaller plastic volumetric strains, while Atkinson's Model predicts larger ones at the same level of shear strain.

7.9.2 Triaxial Extension

The behaviour of normally consolidated sample becomes overconsolidated immediately after applying the conventional type of unloading. Therefore, CK_0DE1 state paths no longer lie

on the State Boundary Surface (SBS). Only Pender's Model is applicable for predictions under this condition, since it deals with the overconsolidated behaviour. It would be interesting to examine the predictions from other models in this unloading type of tests.

(1) **Stress-Strain Relationships-** The comparisons of (q, ϵ_s) relationships between test data and model predictions during the conventional drained unloading test on K_0 -normally consolidated samples are shown in Fig. 7.43. Pender's model makes an excellent prediction during unloading in compression. The predictions for the stress states below the p-axis begin to deviate from the test data. The other two models give smaller strain than the test data up to the deviator stress close to failure.

(2) **Stress Ratio-Strain Relationships-** The variations of shear strains and volumetric strains with respect to stress ratio are presented in Figs. 7.44 and 7.45, respectively. Pender's Model overpredicts shear strain as discussed earlier, while the other models underpredict the shear strain. However, it is interesting to note that the (η, ϵ_v) relationship predicted by Pender's Model agrees well with the experimental observations. This seems noteworthy since this model overpredicts volumetric strain for the normally consolidated state as shown in Figs. 7.36 and 7.41. The accuracy of this model's prediction is probably dependent on the soil stress history. This aspect will further be investigated when the overconsolidated behaviour is discussed. Figure 7.45 indicates that Dafalias' and Atkinson's Models are not applicable for predictions of volumetric strain under this type of loading conditions.

7.10 Comparison of Drained Behaviour of Overconsolidated Clays Sheared from Isotropic Pre-shear Stress Conditions

Pender's Model for overconsolidated behaviour with isotropic pre-shear stress conditions is examined in this section by comparing the predictions with the experimental observations. The data from overconsolidated samples with overconsolidation ratios of 1.50 (CID3 sample) and 2.15 (CID5 sample) are used in these comparisons. The normally consolidated behaviour (CID1) which has already been compared is also shown in each figure. The model parameters used in the predictions are also tabulated in each figure.

(1) **Stress-Strain Relationships-** The (q, ϵ_s) relationships for overconsolidated samples with OCR values of 1.50 and 2.15 are compared with the predictions in Fig. 7.46. The predictions for CID1 and CID3 tests agreed well with the experimental observations up to point A, while the prediction for the CID5 sample deviates from the test data even at lower deviator stress. Generally, Pender's Model gives a larger shear strain at any particular deviator stress level. However, the model predicts the volumetric strain quite well for overconsolidated samples as seen in Fig. 7.47. It is interesting to note that Pender's Model overpredicts the volumetric strain in the case of the normally consolidated sample.

(2) **Stress Ratio-Strain Relationships-** Figures 7.48 and 7.49 illustrate the (η, ϵ_s) and the (η, ϵ_v) relationships, respectively. Pender's Model gives larger shear strains than the observed values on overconsolidated samples at the same stress level (Fig. 7.48). The model provides a reasonably good prediction for volumetric strains for overconsolidated samples as seen in Fig. 7.49.

7.11 Comparison of Drained Behaviour of Overconsolidated Clays Sheared from K_o Pre-shear Stress Conditions

The behaviour from a total of six series of drained tests on K_o overconsolidated samples are compared with the predictions using Pender's Model (PENDER, 1978). Four of the series are compression tests with different loading conditions such as CK_oD , CK_oPC , CK_oDU and CK_oQU . The remaining two test series are conventional extension unloading and constant p extension tests. Only selected test results are presented in this comparison.

7.11.1 Conventional Drained Compression Tests (CK_oD Tests)

(1) **Stress-Strain Relationships-** Figures 7.50 and 7.51 illustrate the stress-strain relationships for CK_oD tests. As discussed in the comparisons for the CID test series, Pender's Models again overpredicts shear strain (Fig. 7.50) in this case. The deviations increased with the increase in OCR values, especially for the CK_oD6 sample sheared from the dry side during the early stage of loading. In the case of the deviator stress-volumetric strain relationship demonstrated in Fig. 7.51, the prediction is improved except for the sample sheared from the dry side of the Critical State (CK_oD6).

(2) **Stress Ratio-Strain Relationships-** Figures 7.52 and 7.53 show the relationships between the stress ratio and the shear and volumetric strains, respectively. Pender's Model gives larger shear strains at the same level of stress ratio except for the CK_oD2 sample. The deviation becomes prominent as the OCR value is increased. Figure 7.53 also shows a similar trend as seen in Fig. 7.51.

7.11.2 Constant p Compression Tests (CK_oPC Tests)

(1) **Stress-Strain Relationships -** Figures 7.54 and 7.55 present the (q, ϵ_s) and the (q, ϵ_v) relationships predicted using Pender's Model together with the corresponding test data. The model predictions agree well with test data from CK_oPC1 and CK_oPC2 specimens. On the other hand, larger shear strains for the sample with higher OCR values at the same level of deviator stress are given (see CK_oPC4 and CK_oPC6 samples). Deviations especially begin to occur from a very early stage of shearing. A similar contrast for the (q, ϵ_v) relationships is also seen in Fig. 7.55. However, it is interesting to note from this figure that the prediction for

CK_oPC5 sample is successful when this is compared with the actual (q, ϵ_s) relationship. This again indicates that Pender's Model can provide good predictions of volumetric strain for overconsolidated samples.

(2) **Stress Ratio-Strain Relationships-** Figures 7.56 and 7.57 show that the predictions agreed well with the observations for the CK_oPC1 and CK_oPC2 samples both in the (η, ϵ_s) and in the (η, ϵ_v) relationships. However, the prediction is much larger for the shear strain of samples CK_oPC4 and CK_oPC6 at the same level of stress ratio, while the predictions of the (η, ϵ_v) relationships agreed well with the observations (see Fig. 7.57).

7.11.3 Unloading Compression Tests (CK_oDU Tests)

(1) **Stress-Strain Relationships-** All data obtained from this test series are compared with predictions from Pender's Model. All the stress states for these overconsolidated samples lie within the State Boundary Surface. Figures 7.58 and 7.59 illustrate the (q, ϵ_s) and the (q, ϵ_v) relationships, respectively. The predicted shear strains are slightly less for the sample sheared from the normally consolidated state (CK_oDU1). The predictions deviate substantially from the observed behaviour when the OCR values increased. As observed from the previous comparisons, Pender's Model overpredicts shear strain for the overconsolidated samples. However, the predictions for the sample with a OCR value of 1.24 agree well with the observations. Figure 7.59 provides further evidence that Pender's Model can successfully predict volumetric strains for overconsolidated specimens.

(2) **Stress Ratio-Strain Relationships-** Figures 7.60 and 7.61 illustrate the (η, ϵ_s) and the (η, ϵ_v) relationships, respectively. These figures also show that Pender's Model overpredicts shear strains, but it provides good predictions of volumetric strains for the overconsolidated samples with OCR values employed in this study.

7.11.4 Constant q Unloading Tests (CK_oQU Tests)

All the state paths of the samples belonging to this test series lie within the State Boundary Surface. Parameter M for the calculations are varied corresponding to test specimens, since all samples reached the Hvorslev failure envelope with different values of M at failure. The M values used for the calculations are 1.16, 1.18, 1.28 and 1.48 corresponding to samples CK_oQU1, CK_oQU2, CK_oQU3 and CK_oQU5, respectively.

(1) **Stress-Strain Relationships-** Figure 7.62 contains the (ϵ_v, p) relationships of the CK_oQU test series compared with the predictions. As discussed earlier, the predictions for volumetric strains agree well with the experimental observations.

(2) **Stress Ratio-Strain Relationships-** Figures 7.63 and 7.64 show the variations of the shear strains and the volumetric strains with respect to the stress ratios. All samples experience very small shear distortion up to the Critical State Line. Pender's Model seems to predict both the shear strain and the volumetric strain successfully.

7.11.5 Conventional Drained Extension Tests (CK_oDE Tests)

All the state paths of these samples lie within the State Boundary Surface.

(1) **Stress-Strain Relationships-** Figures 7.65 and 7.66 display (q, ϵ_s) and (q, ϵ_v) relationships, respectively. The shear strains predicted agree well with test data up to a deviator stress of -1.0 kg/cm^2 . Below this deviator stress level, the predicted shear strains are larger for the CK_oDE1 and CK_oDE2 samples. For the CK_oDE4 and CK_oDE5 samples, the predictions agree well with the test data. It is interesting to note that this trend is a reverse of those in compression conditions. Unlike the case of the compression tests, the predictions of the volumetric strain for the extension tests deviate as shown in Fig. 7.66. However, the predictions are acceptable for a first order approximation.

(2) **Stress Ratio - Strain Relationships -** Figures 7.67 and 7.68 show the (η, ϵ_s) and the (η, ϵ_v) relationships, respectively. The model predictions agree well with test data up to stress ratio of about -0.6 for CK_oDE4 and CK_oDE6 samples. Below this stress ratio, the model gives larger shear strain at the same level of the stress ratio. However, the predictions for CK_oDE1 and CK_oDE2 samples deviate from the test data much earlier than the other samples. Generally, Pender's Model predicts larger shear strain than the experimental results. The predicted volumetric strains are also larger at the same level of stress ratio except for the CK_oDE1 specimen (see in Fig. 7.68).

7.11.6 Constant p Extension Tests (CK_oPE Tests)

(1) **Stress-Strain Relationships-** Figures 7.69 and 7.70 demonstrate the variations of the shear strain and the volumetric strains with respect to the deviator stress. As discussed in the previous comparisons with CK_oDE tests, the predictions are better for the samples with higher OCR values. This indicates that Pender's Model overpredicts shear strain as the initial state of the sample is close to the normally consolidated state. In the case of overconsolidated samples, the predicted shear strains are larger probably after the yielding took place. The (q, ϵ_v) relation predicted using Pender's Model deviates from all the actual observations as shown in Fig. 7.70.

(2) **Stress Ratio-Strain Relationships-** Figures 7.71 and 7.72 illustrate the relationships between stress ratio and the strains. The predictions for the CK_oPE1 and CK_oPE2 samples deviate from the experimental observations, while those for CK_oPE4 and CK_oPE6 samples agree

well with the data up to a substantial magnitude of stress ratio. The model overpredicts the shear strain as the sample is drawn closer to the normally consolidated state. The (η, ϵ_v) relationships predicted using Pender's Model are not promising as seen in Fig. 7.72.

7.12 Summary of the Predictions for the Drained Behaviour

7.12.1 Normally Consolidated Behaviour

(1) **Isotropic Pre-shear Stress Conditions** - Similar to the undrained tests, the Revised Theory (ROSCOE and BURLAND, 1968) gave excellent predictions both for the (q, ϵ_s) and the (q, ϵ_v) relationships. As expected the Modified Theory slightly underpredicted the shear strains. Pender's Model overpredicted the shear strains, especially the volumetric strains.

(2) **K_0 Pre-shear Stress Conditions** - For the CK_0D type of loading, Dafalias' Model predicted the (q, ϵ_s) and (q, ϵ_v) relationship well, while Pender's Model and Atkinson's Model overpredicted the shear strains. In the case of extension tests (CK_0DE tests), Pender's Model gives an excellent prediction for the volumetric strains, while it overpredicts the shear strains. It is important to mention here that only Pender's Model among other models is truly applicable for the conventional type of drained unloading conditions since the samples become overconsolidated immediately after the commencement of unloading. In this case, the NC-component in Pender's Model is not operative. It is also interesting to note that Pender's Model predicts volumetric strain quite well for the overconsolidated stress region.

7.12.2 Overconsolidated Behaviour

Pender's Model is found to overpredict shear strain in most cases. The deviations become more and more apparent when the OCR values are increased. However, this model gives excellent predictions of the volumetric strains for the overconsolidated samples under compression types of loading. It can be concluded that Pender's Model, for the overconsolidated behaviour, overpredicts shear strain both in undrained and in drained tests.

7.13 Evaluation of PENDER's Assumption on the Plastic Strain Increment Ratio

PENDER (1978) set-up two hypotheses, in his formulations, on the ratio of the plastic strain increment within the State Boundary Surface (Hypothesis 3 and 4a in his paper): one concerns the isotropic stress history and the other the anisotropic stress history. These hypotheses do not follow the normality rule as seen in Fig. 3.3. The ratios of the plastic strain increment are always positive on the wet side of the Critical State, while those on the dry of the Critical

State are negative. These assumptions made by PENDER (1978) are studied in this section based on the experimental data, since Pender's Model overpredicts the shear strain as discussed earlier.

The plastic strain increment ratios assumed by PENDER (1978) are given by Eqns. 7.9 and 7.10 for the isotropic stress history and for the anisotropic stress history, respectively.

$$\frac{d\epsilon_{sp}}{d\epsilon_{vp}} = \frac{1}{(p_o/p_{cs} - 1) \{M - (p/p_{cs})\eta\}} \quad \dots(7.9)$$

$$\frac{d\epsilon_{sp}}{d\epsilon_{vp}} = \frac{(AM - \eta_o)^2}{(AM)^2 (p_o/p_{cs} - 1) \{(AM - \eta_o) - (\eta - \eta_o)(p/p_{cs})\}} \quad \dots(7.10)$$

where A is a parameter having a value +1 for a compressive path and -1 for the extension path. The plastic strain increment ratios calculated from Eqns. 7.9 and 7.10 are compared with the experimental observations hereafter.

(1) Variation of the Plastic Strain Increment During Drained Compression- It is interesting to examine the variation of the plastic strain increment ratio during drained shearing. The plastic strain increment ratios assumed in the formulation of Pender's Model are functions of M, p, η , p_{cs} , and p_o . It is important to remember that the values of p_o and p_{cs} should continually be updated according to the current void ratio during the drained test. That is, the undrained stress path which passes through the current stress point and the Critical State point corresponding to the current void ratio intersects the p-axis at the current p_o value. It should be pointed out, therefore, that two types of undrained stress paths, one for the region below the N.C.-yield locus and other for the region outside the N.C.-yield locus, are needed in order to calculate the value of p_o if the stress path of the isotropically overconsolidated sample is directed outside of the N.C.-yield locus. Because the shape of the undrained path depends on the stress history of the clay when the stress path is directed outside of the current yield locus, while the shape of the normally consolidated yield remains unchanged until the next one is engaged by the stress path when the stress path is directed inside. This means that the isotropically consolidated sample should use the undrained stress path for the spherical stress history not for the anisotropic stress history until it hits the current yield locus.

The plastic strain increment ratio can be calculated based on two conditions. One is the undrained condition, for which the value of p_{cs} is constant. The other is the drained condition, in which the value of p_{cs} varies with the change in void ratio. p_o varies in both conditions. Equation 7.10 is the general expression of Pender's assumption, since $\eta_o = 0$ leads from this equation to Eqn. 7.9 for the isotropic stress history. The left hand side of this equation becomes infinity when either $p_o = p_{cs}$ or $p(\eta - \eta_o) = (M - \eta_o) p_{cs}$. This might not be realistic since this

condition does not always occur at the Critical State. It was revealed in the calculation, in fact, that this phenomenon took place at the deviator stress much less than the Critical State value. It is interesting also to point out that, if a sample is sheared from the pre-shear stress less than p_{cs} and the stress path travel through the wet zone, the plastic strain increment ratio is negative even if the stress state is situated in the wet zone. This self-contradicting phenomenon in the assumption may have resulted from the stress path dependent characteristics of the plastic strain increment ratio. However, if the entire stress path lies in the dry zone or in the wet zone, this phenomenon does not take place.

Figures 7.73 to 7.80 present the variations of the plastic strain increment ratio during the drained compression on the isotropically consolidated samples and the K_0 -consolidated samples, respectively. As discussed earlier, the predicted plastic strain increment ratio reaches infinity before reaching the Critical State for the undrained conditions. Thereafter, it becomes negative, which does not agree with the test data (see Fig. 6.7). These figures show that Pender's assumption gives larger values of $\frac{d\epsilon_{sp}}{d\epsilon_{vp}}$ than those observed in the experiments. Figures 7.76 and 7.78 illustrated the effects of the location of the initial pre-shear stress as discussed earlier. The values of $\frac{d\epsilon_{sp}}{d\epsilon_{vp}}$ are positive in the wet zone, while the predictions are negative since the pre-shear stresses of these samples are less than p_{cs} and the stress paths move from the dry zone to the wet zone.

7.14 A Conceptual Modification of Pender's Model

7.14.1 For the Isotropically Consolidated Samples

Pender's Model (PENDER, 1978) overpredicted the shear strain. As discussed earlier, the plastic strain increment ratio $\frac{d\epsilon_{sp}}{d\epsilon_{vp}}$ in Pender's formulation is also larger than those observed in the experiments. Therefore, if a reasonable reduction factor is applied on the plastic strain increment ratio, the prediction might be improved. The modified version of the $\frac{d\epsilon_{sp}}{d\epsilon_{vp}}$ ratio is

$$\frac{d\epsilon_{sp}}{d\epsilon_{vp}} = \frac{1}{(OCR)(p_o/p_{cs} - 1) \{M - (p/p_{cs})\eta\}} \quad \dots(7.11)$$

The OCR is only a tentative value. The predictions in Figs. 7.79 and 7.80 are calculated using Eqn. 7.11. The stress-strain curves are slightly improved as shown in Fig. 7.78. However, the pattern of the shear strain contours does not agree with that of the test data (see Fig. 7.80).

Nevertheless, OCR can be a reduction factor to be applied in Pender's Model only for the lightly overconsolidated samples ($OCR < 3$). Of course, OCR can not be a reduction factor for the heavily overconsolidated samples, since the shear strain will be unrealistically small for the high OCR values. It can be concluded from these figures that the overprediction of the strains from Pender's Model are not purely due to the assumption of the plastic strain increment ratio. It is also partly due to the assumption on the shapes of the undrained stress paths.

7.14.2 For the K_0 -overconsolidated Samples

(1) **Undrained Stress Paths** - The experimental evidence which have so far been presented in Chapter V suggest that the behaviour of the K_0 -overconsolidated samples in the compression conditions is rigid nearly up to the failure state. A typical illustration of the rigid behaviour is the vertical rise-up of the undrained stress path for almost the full range of the deviator stress. This, further, implied that the behaviour of the overconsolidated clay can be treated as pseudo-elastic at least up to a deviator stress equal to the initial deviator stress in the normally consolidated state as imposed during the sample preparation. Consequently, Pender's hypotheses on the shapes of the undrained stress paths (parabola) is an oversimplification, specifically for those samples sheared from the dry side of the Critical State. Within this pseudo-elastic region, the undrained stress paths can be assumed as vertical in the (q, p) plot up to a deviator stress equal to the initial deviator stress in the normally consolidated state as imposed during the sample preparation. Therefore, the strain prediction will be more realistic, if Pender's Model is applied only for deviator stresses higher than the initial values imposed on the samples during the sample preparation.

Figure 7.81 illustrates the undrained stress paths as proposed above in a modified form of prediction and the actual prediction using Pender's Model. Line OB is the base line for Pender's Model, i.e., the initial stress points of the overconsolidated sample are all shifted to this horizontal line. The region between the line OA and OB is considered as a pseudo-elastic zone. It should be stated that this shifting technique cannot be applicable for the samples with the OCR values greater than 2.15, since the shifted initial stress point lies above the Critical State Line. The proposed undrained stress paths appear to be promising as indicated in Fig. 7.82. The prediction of the undrained paths are much improved.

(2) **Stress-Strain and Pore Pressure-Strain Relationships** - Stress-strain relationships from Pender's Model as used in a modified form are plotted together with the experimental data in Figs. 7.83 (wet zone) and 7.84 (dry zone), respectively. The predictions by the original Pender's Model are also shown in dotted lines. These figures demonstrate that the proposed modified approach drastically improve the predicted stress-strain relationships. The same trends are shown in Figs. 7.85 and 7.86 for the pore pressure-strain relationships.

7.15 Concluding Remarks and Comments of the Model Evaluations

The stress-strain theories based on the Critical State Concepts are examined by comparing the predictions with the experimental observations. For the K_0 consolidated samples, all model predictions deviate from the experimental observations, particularly, they fail to simulate the undrained stress path in the early stages of loading. Furthermore, all models are poor in their predictions of the K_0 extension behaviour. Brief concluding remarks for each model are made below.

7.15.1 Undrained Behaviour of Normally Consolidated Samples

(i) **Revised Theory-** This theory is found to successfully predict the undrained shear strength, the shear strain and the excess pore pressures for the CIU type of tests.

(ii) **Pender's Model-** Pender's Model overpredicts the shear strains and is sensitive with the parameter p_{cs} for the CIU type of tests. For the CK_0U test, it predicts reasonably well the undrained stress paths both in compression and in extension with parameters determined from the peak deviator stress criterion. However, it overpredicts shear strains in the compression phase, and gives poor strain predictions in extension.

(iii) **Dafalias' Model-** This model provides good stress-strain predictions for the compression tests. However, its prediction for the extension tests is poor, especially at the larger strains. The parameter α varies during undrained shearing and is not zero even for the isotropically consolidated sample whereas it should be according to the theory.

(v) **Atkinson et al.'s Model-** Atkinson's Model predicts low undrained strength in compression, and its predictions for the extension conditions are poor specifically for the larger strain range.

7.15.2 Undrained Behaviour of Overconsolidated Samples

(i) **Pender's Model-** Pender's Model generates a successful family of undrained stress paths for the overconsolidated clays on the wet side of the Critical State both for compression and for extension conditions when the parameters are selected from the peak deviator stress conditions. However, this model overpredicts the shear strains both for the isotropically consolidated and for the K_0 consolidated samples.

7.15.3 Drained Behaviour of Normally Consolidated Samples

- (i) **Revised Theory-** For the CID type of tests, the Revised Theory gives excellent predictions both for the (q, ϵ_s) and the (q, ϵ_v) relationships, while the Modified Theory slightly underpredicts the shear strains.
- (ii) **Pender's Model-** Pender's Model overpredicts the strains, especially the volumetric strains for the CID tests. It also overpredicts the shear strains for the CK_0D and CK_0DE tests. This model, however, gives good predictions of the volumetric strain both in compression and in extension.
- (iii) **Dafalias' Model-** For the CK_0D type of loading, this model predicted the (q, ϵ_s) and (q, ϵ_v) relationships well.
- (v) **Atkinson et al.'s Model-** This model overpredicts shear and volumetric strains for the CK_0D type of loading.

7.15.4 Drained Behaviour of Overconsolidated Samples

- (i) **Pender's Model-** Pender's Model is found to overpredict shear strains in most cases. The deviations become more and more apparent when the OCR values are increased. However, this model gives excellent predictions of the volumetric strains for the overconsolidated samples under compression types of loading. It can be concluded that Pender's Model, for the overconsolidated behaviour, overpredicts the shear strain both in undrained and in drained tests. This is attributed partially or fully to the incorrect assumption made on the plastic strain increment ratio in the formulation of the theory.

7.15.5 Improvement of Pender's Model

The OCR value or related parameter can be a possible reduction factor to be applied to the assumption of the plastic strain increment ratio for the lightly overconsolidated samples ($OCR < 3.0$) sheared from isotropic pre-shear stress conditions. Pender's hypotheses on the shapes of the undrained stress path for the K_0 overconsolidated sample is found to be an oversimplification. Thus, the prediction of Pender's Model for K_0 overconsolidated samples is expected to be promising when this factor is incorporated in the expression for the plastic strain increment ratio.

VIII FORMULATIONS OF STRESS-STRAIN BEHAVIOUR BELOW THE STATE BOUNDARY SURFACE

8.1 Introduction

The original Cam Clay Theory developed by ROSCOE, SCHOFIELD and THURAIR-AJAH (1963) and SCHOFIELD and WROTH (1968) is a simple one in which for stress states within the State Boundary Surface (SBS) only elastic volumetric strain is assumed to take place. Furthermore, the energy balance equation used in this theory only allowed for energy dissipation due to plastic distortion. When an 'associated flow rule' obeying Drucker's 'normality criterion' is assumed, the yield locus obtained in the Cam Clay Theory constituted a set of volumetric yield loci which displayed sharp bullet shapes at the isotropic axis. The use of such bullet shaped volumetric yield loci overpredicted the volumetric strains in all specimens tested to failure under drained conditions when the stress states lie on the SBS.

The subsequent modifications of the energy balance equation by BURLAND (1965) and ROSCOE and BURLAND (1968) which incorporated the energy dissipation both due to volumetric and distortional yielding resulted in a volumetric yield locus which is more elliptic in nature and made realistic predictions of the volumetric strains for stress states on the SBS.

Even though the elliptic type of volumetric yield locus gave better predictions of volumetric strains when the stress paths lie on the SBS, many authors have demonstrated substantial volumetric and distortional yielding inside the SBS. Thus, the Cam Clay Theory and its modification suffered from the drawback of its inadequacy in accounting for the distortional and volumetric yielding inside the SBS.

Following the classic work of WROTH and LOUDON (1967) on the establishment of the constant q shear strain contours within the SBS on the wet side of the Critical State, ROSCOE and BURLAND (1968) proposed for the first time the necessity to use two sets of yield loci: one being named the volumetric yield locus which obeys Drucker's stability criterion and the 'Associated Flow Rule', and the other being a set of constant q yield loci which are applicable for the estimation of distortional strains within the SBS. Thus, ROSCOE and BURLAND (1968) rationalized that

- (i) plastic volumetric strains are developed when the stress state lie on the SBS due to the shifting of the volumetric yield loci;
- (ii) during yielding with stress states on the SBS, distortional strains arise from two components, one associated with the plastic volumetric yielding (obeying the 'Normality Rule') and the other being contributed from the shifting of the constant q yield locus;

(iii) when the stress states lie inside the SBS, no plastic volumetric strain is accepted to take place by the Revised Theory of ROSCOE and BURLAND (1968), while plastic distortional strains are accepted as contributions from the shifting of the constant q yield locus within the SBS.

In this dissertation, the Author has attempted to investigate the plastic volumetric yielding inside the SBS and proposed subsets of volumetric yield loci which contribute positive plastic volumetric strains on the wet side of the Critical State Line and dilational volumetric strains on the dry side. In identifying such subsets of volumetric yield loci within the SBS, the Author has proposed a region or nucleus within which only elastic volumetric strains take place.

The contribution from such subsets of volumetric yield loci within the SBS is in operation with the already established constant q yield loci on the wet side and a similar set of distortional yield loci on the dry side which are radial in nature but converge to a point on the negative p -axis. Such a radial fan of distortional yield loci converging to a point on the negative p -axis can also accommodate the Hvorslev failure envelope as the outermost boundary in the (q, p) plot.

In this chapter, the Author has established such subsets of volumetric yield loci within the SBS and has also proposed an expression for the plastic strain increment ratio $\frac{d\epsilon_{vp}}{d\epsilon_{sp}}$ which is operative within such yield loci. Firstly, the subsets of volumetric yield loci will be presented. This will then be followed by the expression related to $\frac{d\epsilon_{vp}}{d\epsilon_{sp}}$ both on the wet and dry side of the Critical State Line. Then predictions are made for lightly overconsolidated samples sheared under drained and undrained conditions using the constant q yield loci and the volumetric yield loci inside the SBS as well as outside when the stress paths cross from the overconsolidated to the normally consolidated state.

8.2 Formulation of Volumetric Yield Loci Inside the SBS

8.2.1 Simplified Plastic Volumetric Strain Contours Inside the SBS

The volumetric yielding within the State Boundary Surface (SBS) was discussed in detail in Chapter VI. As shown in Fig. 6.14, the zero plastic volumetric strain points from all CID tests lie close to a Cam Clay type of yield locus. All samples are approximately rigid in plastic dilation in the region between the isotropic stress axis and the Cam Clay type of yield locus for the CID type of loading. It should be mentioned that the Author uses the terminology 'plastic dilatancy ratio' for $\frac{d\epsilon_{vp}}{d\epsilon_{sp}}$ indiscretely even though $d\epsilon_{vp} > 0$ and positive. The word dilatancy is used with an inherent meaning that there is a volume change irrespective of compressive or dilational changes in magnitude. As the stress states approached the SBS, the samples experienced larger plastic volumetric strains. On the other hand, samples on the dry side of the

Critical State experienced dilation (i.e., negative plastic volumetric strains). These experimental observations indicate that the region within the SBS can be divided into three zones with respect to plastic volumetric strains.

The plastic volumetric strains experienced by the CID specimens within the SBS and on the wet side of the Critical State are shown in Fig. 8.1a. The plastic volumetric strain contours within the SBS are then drawn in Fig. 8.1b. In this figure, the volumetric strains due to plastic dilation obtained from K_o compression tests are also shown on the dry side of the Critical State. As explained earlier, the plastic volumetric strains are obtained as the difference of the total volumetric strain and the elastic volumetric strain, the latter being dependent on the κ value. It is interesting to note that the patterns of the plastic volumetric strain contours are somewhat similar to one another about the vertical line passing through the Critical State C. However, samples are found to experience a higher degree of dilation on the dry side of the Critical State when approaching failure. These patterns of the volumetric strain contours are simplified in Fig. 8.2. Thus, the whole q - p stress space is divided into four zones: three are inside the SBS and the remaining one is the normally consolidated region. The simplified patterns of the plastic volumetric strain contours and the sub-zones are assumed to expand with the expansion of the volumetric yield locus which lies on the SBS. In Zone I, plastic volumetric strains are assumed to be zero. Plastic dilation takes place in Zone IV, while compressive volumetric strains take place in Zone II. It is important to note that the contribution from the constant q yield loci are in operation in Zones I, II and III, while for Zone IV the shear strains under constant volume conditions need to be obtained from a set of radial shear strain contours which converge to a point on the negative p -axis.

8.2.2 Stress-Strain Behaviour in Zone I to Zone IV

(i) **ZONE I** (see Fig. 8.2)

In Zone I, the volumetric strain is only elastic, so that

$$d\epsilon_{ve} = \frac{\kappa}{1+e} \frac{dp}{p} \quad \dots(8.1)$$

The plastic volumetric strain is zero, i.e., $d\epsilon_{vp} = 0$. Hence, the total volumetric strain is

$$d\epsilon_v = d\epsilon_{ve} = \frac{\kappa}{1+e} \frac{dp}{p} \quad \dots(8.2)$$

In Zone I, the plastic distortional Strains are given by the constant q yield loci as

$$d\epsilon_{sp} = \Phi^*(\eta) d\eta \quad \dots(8.3)$$

where $\Phi^*(\eta)$ indicates that the shear strains are dependent uniquely on the stress ratio as shown in Fig. 5.42. The elastic distortional strain is assumed to be zero. Thus, the total shear strain is,

$$d\epsilon_s = d\epsilon_{sp} = \Phi^*(\eta) d\eta \quad \dots(8.4)$$

(ii) **ZONE II** (see Fig. 8.2)

In Zone II, it is proposed that plastic volumetric strains take place from the shifting of a Cam Clay type of volumetric yield locus. Expressions for these plastic volumetric strains will be derived in Section 8.2.7. The elastic volumetric strain in Zone II is given by,

$$d\epsilon_{ve} = \frac{\kappa}{1+e} \frac{dp}{p} \quad \dots(8.1 \text{ bis})$$

Therefore, the total volumetric strain is,

$$d\epsilon_v = (d\epsilon_{vp})_{ISB2} + (d\epsilon_{ve}) \quad \dots(8.5)$$

where $(d\epsilon_{vp})_{ISB2}$ refers to the incremental plastic volumetric strain in Zone II within the SBS.

Also the ratio of $\left(\frac{d\epsilon_{sp}}{d\epsilon_{vp}}\right)_{ISB2}$, which is the inverse plastic dilatancy ratio for Zone II, is known.

Therefore, the associated plastic distortional strain with $(d\epsilon_{vp})_{ISB2}$ is,

$$[d\epsilon_{sp}]_2^* = \left(\frac{d\epsilon_{sp}}{d\epsilon_{vp}}\right)_{ISB2} (d\epsilon_{vp})_{ISB2} \quad \dots(8.6)$$

where subscript '2' refers to Zone II. The contribution of the distortional strain from the constant q yield loci is taken as,

$$[d\epsilon_{sp}]_2^{**} = \Phi^*(\eta) d\eta$$

Thus, the total shear strain incurred in Zone II is $d\epsilon_s = [d\epsilon_{sp}]_2^* + [d\epsilon_{sp}]_2^{**}$, and can be written as Eqn. 8.7.

$$d\epsilon_s = \left(\frac{d\epsilon_{sp}}{d\epsilon_{vp}} \right)_{ISB2} (d\epsilon_{vp})_{ISB2} + \Phi^*(\eta) d\eta \quad \dots(8.7)$$

(iii) **ZONE III** (see Fig. 8.2)

For stress states in Zone III, the volumetric and distortional strains are given by,

$$d\epsilon_{vp} = \frac{\lambda - \kappa}{1 + e} \left(\frac{dp}{p} + \frac{2\eta d\eta}{M^2 + \eta^2} \right) \quad (Modified \ Theory) \quad \dots(8.8a)$$

$$d\epsilon_{ve} = \frac{\kappa}{1 + e} \frac{dp}{p}$$

$$d\epsilon_v = d\epsilon_{vp} + d\epsilon_{ve} \quad \dots(8.8b)$$

$$\left(\frac{d\epsilon_{sp}}{d\epsilon_{vp}} \right)_{OSB3} = \frac{2\eta}{M^2 - \eta^2} \quad (Modified \ Theory) \quad \dots(8.8c)$$

$$d\epsilon_s = \left(\frac{d\epsilon_{sp}}{d\epsilon_{vp}} \right)_{OSB3} (d\epsilon_{vp})_{OSB3} + \Phi^*(\eta) d\eta \quad \dots(8.8d)$$

where $(d\epsilon_{vp})_{OSB3}$ refers to the incremental plastic volumetric strain and $\left(\frac{d\epsilon_{sp}}{d\epsilon_{vp}} \right)_{OSB3}$ refers to the inverse plastic dilatancy ratio.

(iv) **ZONE IV** (see Fig. 8.2)

In Zone IV, the plastic volumetric dilation is given by $(d\epsilon_{vp})_{ISB4}$. If the inverse plastic dilatancy ratio $\left(\frac{d\epsilon_{sp}}{d\epsilon_{vp}}\right)_{ISB4}$ is known, then the plastic shear strain can be obtained as,

$$d\epsilon_{sp} = \left(\frac{d\epsilon_{sp}}{d\epsilon_{vp}}\right)_{ISB4} (d\epsilon_{vp})_{ISB4} \quad \dots(8.9)$$

where subscript 'ISB4' indicates the stress Zone IV inside the SBS. It is also necessary to consider the distortional strain incurred from the radial fan of shear strain contours as $d\epsilon_{sp} = [\Phi^{**}(\eta)d\eta]_4$. Therefore, the total distortional shear strain is,

$$d\epsilon_s = \left(\frac{d\epsilon_{sp}}{d\epsilon_{vp}}\right)_{ISB4} (d\epsilon_{vp})_{ISB4} + [\Phi^{**}(\eta)d\eta]_4 \quad \dots(8.10)$$

It should be mentioned here that $[\Phi^{**}(\eta)]_4$ is shear strain contributions from the radial fan of shear strain contours on the dry side of the Critical State as obtained from undrained tests.

8.2.3 Plastic Strain Increment Ratio

The plastic strain increment ratio is one of the essential components in the formulation of a plastic stress-strain theory. This component also plays a significant role in the prediction of strains. The stress-strain theories based on the Critical State Concepts (developed by the Cambridge University Group) obtained this component from an energy balance equation.

The plastic strain increment ratios for stress states on the State Boundary Surface (SBS) are,

$$\frac{d\epsilon_{sp}}{d\epsilon_{vp}} = \frac{1}{\psi} = \frac{1}{M - \eta} \quad (\text{Cam Clay Theory})$$

$$\frac{d\epsilon_{sp}}{d\epsilon_{vp}} = \frac{1}{\psi} = \frac{2\eta}{M^2 - \eta^2} \quad (\text{Modified Theory})$$

$$\frac{d\epsilon_{sp}}{d\epsilon_{vp}} = \frac{1}{\psi} = \frac{2\alpha - 2\eta}{\eta^2 - M^2} \quad (\text{Dafalias' Theory})$$

These expressions are based on an energy balance equation. PENDER (1978) proposed an empirical expression for the plastic strain increment ratio for stress states both on the SBS as well as inside the SBS. Pender's general expression is given below.

$$\frac{d\epsilon_{sp}}{d\epsilon_{vp}} = \frac{(AM - \eta_o)^2}{(AM)^2 (p_o/p_{cs} - 1) \{ (AM - \eta_o) - (\eta - \eta_o)(p/p_{cs}) \}} \quad \dots(7.10 \text{ bis})$$

The Author's formulation of the plastic dilatancy ratio $\frac{d\epsilon_{vp}}{d\epsilon_{sp}}$ will be presented in the following sections.

8.2.4 Plastic Strain Increment Ratio Inside the SBS from CID Tests

The state paths for all CID tests are shown in Fig. 8.3 together with the volumetric yield locus of the Modified Cam Clay Theory and the constant stress ratio lines. The constant stress ratio lines meet the volumetric yield locus at points Y_1, Y_2, \dots, Y_7 etc.. The values of dilatancy ratio, $\frac{d\epsilon_{vp}}{d\epsilon_{sp}}$, at the same level of stress ratio (e.g., the intersection points between each state path and constant stress ratio path) are calculated from the $(\epsilon_{vp}, \epsilon_s)$ relationship of each drained test. It should be mentioned here that the undrained incremental shear strain components are deducted from the drained test values using the constant q yield loci established earlier. The constant q yield loci used for such deductions are shown in Fig. 8.4. In this figure the drained path of the specimen for which the strains are to be calculated is also shown on the wet side of the Critical State.

Figure 8.5 illustrates the variations of the plastic dilatancy ratio with the normalized mean normal stress at stress ratio levels of 0.3-0.6. The stress paths reached the volumetric yield locus on the SBS at Y_3, Y_4, Y_5 and Y_6 . This figure shows that the values of the plastic dilatancy ratio are not uniquely dependent on the stress ratio. These values decrease as the mean normal stress

decrease. It is interesting, however, to note that the plastic dilatancy ratio is uniquely dependent on the stress ratio η outside the volumetric yield locus which lies on the SBS. This gives an idea that the dilatancy ratio for the overconsolidated state can be incorporated with the value obtained from the Modified Theory for stress states on the SBS for the normally consolidated state, since most lightly overconsolidated samples become normally consolidated during the CID type of loading. In other words, the boundary values of the dilatancy ratio for the overconsolidated state will be those of the Modified Theory for the stress states on the State Boundary Surface.

The simplified $(\frac{d\epsilon_{vp}}{d\epsilon_{sp}}, p/p_e)$ relationships are presented in Fig. 8.6. The points Y_3, Y_4, Y_5 and Y_6 indicate the plastic strain increment ratio obtained from the Modified Theory (and these values correspond to stress ratios of 0.3, 0.4, 0.5 and 0.6, respectively). The horizontal lines $Y_3Y_3, Y_4Y_4, \dots, Y_6Y_6$ indicate that the $\frac{d\epsilon_{vp}}{d\epsilon_{sp}}$ values uniquely depend on the stress ratio in the Modified Theory of ROSCOE and BURLAND (1968). The variation of $\frac{d\epsilon_{vp}}{d\epsilon_{sp}}$ with respect to the stress ratio shown in Fig. 8.5 is then simplified as the linear variation from the points Y_3, Y_4, Y_5 and Y_6 , respectively. The slopes of these simplified relationships within the SBS decrease with the increase in stress ratio. The reduction in the plastic dilatancy ratio $\frac{d\epsilon_{vp}}{d\epsilon_{sp}}$ is now simplified as only dependent on the value of p/p_e for any one particular stress ratio. Figure 8.7 illustrates how the gradient \exists , the slope of the simplified $(\frac{d\epsilon_{vp}}{d\epsilon_{sp}}, p/p_e)$ relationship (i.e., $\exists = d\left(\frac{d\epsilon_{vp}}{d\epsilon_{sp}}\right) / d\left(\frac{p}{p_e}\right)$), decreases with increase in stress ratio, η . Though no experimental data are available at higher values of η close to the Critical State, the trend indicates that the gradient gradually approaches zero as the Critical State is reached.

It is also interesting to examine the stress states at which samples experience the zero plastic dilation. PENDER (1978) assumed that these states are achieved only when the states of samples lie on a straight line when p is equal to p_{cs} . The simplified $(\frac{d\epsilon_{vp}}{d\epsilon_{sp}}, p/p_e)$ relationship in this case should pass through one point where p/p_e is equal to p_{cs}/p_e . However, the experimental observations show that the value of p/p_e at zero plastic dilatancy ratio are different for each stress ratio (see Fig. 8.8). This indicates that the plastic dilation begins to take place at greater values of p than the mean normal stress at the Critical state p_{cs} in the wide range of stress ratios (0.3 to 0.6) investigated in the study.

8.2.5 Plastic Strain Increment Ratio Inside the SBS from K_0 Tests

The same procedure explained in Section 8.2.4 is applied to the K_0 drained compression and extension tests to obtain the dilatancy ratio on the constant stress ratio lines within the SBS. Figures 8.9a and 8.9b show the $(\frac{d\epsilon_{vp}}{d\epsilon_{sp}}, p/p_e)$ and the (Ξ, η) relationships from K_0 drained compression tests. Here again the plastic dilatancy ratio is maintained constant on the SBS for each value of η as per the Modified Cam Clay Theory. The points Y_5' , Y_6' , Y_8' in Fig. 8.9a indicate those values given by the Modified Theory. The test data and these simplified straight lines in Fig. 8.9a are shown in Figs. 8.10a and 8.10b. The stress paths applied are also shown in the inset in each figure. The simplification as straight lines for these relationships seems reasonable as was the case for the CID tests. The (Ξ, η) relationship for the K_0 consolidated specimens when plotted together with those from the CID test specimens demonstrates the same variation (see Fig. 8.9b).

Figure 8.11 illustrates the $(\frac{d\epsilon_{vp}}{d\epsilon_{sp}}, p/p_e)$ relationship for the extension tests. The arrows marked in this figure correspond to the values of $\frac{d\epsilon_{vp}}{d\epsilon_{sp}}$ as determined from the Modified Theory. How much these simplified straight lines deviate from the actual data is also shown in Figs. 8.12a to 8.12f. The $(\eta, p/p_e)$ variation for zero dilatancy (i.e., $\frac{d\epsilon_{vp}}{d\epsilon_{sp}} = 0$) is shown in Fig. 8.13. It is interesting to note that for all stress ratios, η , the zero plastic dilatancy ratio occurs at approximately the same value of p/p_e , and these values are quite close to the Critical State value of about 0.55.

8.2.6 Simplified (Ξ, η) Relationship within the SBS

Figure 8.14 demonstrates the variation of the simplified $(\frac{d\epsilon_{vp}}{d\epsilon_{sp}}, p/p_e)$ relationship with stress ratio from CID, K_0 -compression and K_0 -extension tests. In this figure, the curve AB is taken from the compression tests as a mirror image on the η equal to zero axis. The curve CD indicates the results from the extension tests. It is interesting to note that both curves are mirror images of one another about the η axis. This indicates that the dilatancy ratio relationship with respect to the mean normal stress is the same for both the compression and extension conditions. This trend is clearly shown when the absolute values of Ξ and η are presented in one plot.

Figure 8.15 illustrates the variation of $|\Xi|$ with respect to $|\eta|$ for all the compression and extension tests. All values lie on a unique curve with acceptable deviations. The $|\Xi|$ value approaches infinity as the stress ratio is close to zero, while it asymptotically approaches zero

as η is close to the M value. It is important to comment here that $|\Xi|$ values are not zero at the stress ratio equal to M , since overconsolidated samples reach the failure state at peak stress ratio higher than the Critical State parameter M . The arrows marked in this figure show the pattern of plastic strain increment vector at the constant stress ratio line within the SBS. The curve shown in Fig 8.15 is represented as the following equation.

$$d\left(\frac{d\epsilon_{vp}}{d\epsilon_{sp}}\right)_\eta = \left(\frac{M^2}{\eta} - \eta + \frac{3}{2}\right) d\left(\frac{p}{p_e}\right)_\eta \quad \dots(8.11)$$

Now, the magnitude of the change in plastic strain increment ratio at a particular stress ratio, $d\left(\frac{d\epsilon_{vp}}{d\epsilon_{sp}}\right)_\eta$, is expressed as a function of η and $d(p/p_e)_\eta$. The value of $d(p/p_e)_\eta$ is the difference between the current value of p/p_e and that on the State Boundary Surface at the same stress ratio η (see Fig. 8.15a). Therefore, the plastic dilatancy ratio at any stress state within the State Boundary Surface (SBS) can be calculated by adding the incremental value of $d\left(\frac{d\epsilon_{vp}}{d\epsilon_{sp}}\right)_\eta$ from

Eqn. 8.11 to the reference values on the SBS obtained from the Modified Theory. The general expression of the plastic dilatancy ratio within the State Boundary Surface in the compression zone is then expressed as :

$$\frac{d\epsilon_{vp}}{d\epsilon_{sp}} = \left(\frac{M^2 - \eta^2}{2\eta}\right) - \left(\frac{M^2}{\eta} - \eta + \frac{3}{2}\right) \left(\frac{M^2}{M^2 + \eta^2} - \frac{p}{p_e}\right) \quad \dots(8.12)$$

where, $\text{Exp}(\eta/M) \leq p_e/p \leq (M^2 + \eta^2)/M^2$

Values of $\frac{d\epsilon_{vp}}{d\epsilon_{sp}}$ are neglected inside the elastic nucleus for volumetric strains. The second

term on the right hand side of Eqn. 8.12 will be involved when the stress state reaches the Cam Clay type of yield locus inside the SBS and would vanish when the stress state reaches the SBS when the volumetric yield locus of the Modified Theory begin to operate. For the extension conditions, this term becomes negative. The plastic strain increment ratio for overconsolidated states within the SBS as derived above can be usefully employed with the subset of the volumetric yield loci inside the SBS to formulate a stress-strain theory for lightly overconsolidated clays.

8.2.7 Derivation of the Volumetric Yield Loci within the SBS

The shapes of the plastic volumetric strain contours within the SBS and on the wet zone (Zone II) are quite similar to the Cam Clay type of yield locus. This indicates that the hardening of samples in this zone can be described using the Cam Clay type of yield locus with some modifications. A simple modification is made in the original yield locus of the Cam Clay Theory as follows :

$$q = \beta^* M p \ln(p_o/p) \quad \dots(8.13)$$

$$\text{where,} \quad \beta^* = \epsilon_{vp} / C + 1$$

The parameter β^* is a variable dependent on the plastic volumetric strain ϵ_{vp} (which is in percentage) that takes place on the wet side of the Critical State within the SBS. C is a constant equal to 3.5. The yield locus of the Cam Clay Theory is, thus, slightly modified with the parameter β^* as plastic volumetric strains take place. When ϵ_{vp} is equal to zero, Eqn. 8.13 becomes identical to the volumetric yield loci of Cam Clay Theory. A family of plastic volumetric strain contours generated with Eqn. 8.13 is illustrated in Fig. 8.16. From Eqns. 8.12 and 8.13, the following incremental forms of the plastic volumetric strain and the shear strain for a stress path in Zone II can be obtained as contributed from the Cam Clay type of yield locus inside the SBS.

$$d\epsilon_{vp} = \frac{\lambda_{oc} - \kappa}{1 + e} \left(\frac{dp}{p} + \frac{d\eta}{\beta^* M} \right) \quad \dots(8.14)$$

$$d\epsilon_{sp} = \left[\frac{\lambda_{oc} - \kappa}{1 + e} \left(\frac{dp}{p} + \frac{d\eta}{\beta^* M} \right) \right] / \left[\psi - \left(2\psi + \frac{3}{2} \right) \left(\zeta - \frac{p}{p_e} \right) \right] \quad \dots(8.15)$$

$$\text{where,} \quad \beta^* = \epsilon_{vp} / C + 1$$

$$\psi = (M^2 - \eta^2) / (2\eta) \quad (\text{as in the Modified Theory})$$

$$\zeta = M^2 / (M^2 + \eta^2)$$

where λ_{oc} is a measure of the plastic void ratio reduction in the $(e, \ln p)$ plot for stress state within the SBS on the wet side of the Critical State. The constant C is equal to 3.5. Figure 8.17

illustrates the relationships among λ , λ_{oc} and κ in the $(e, \ln p)$ plot. The parameter λ_{oc} is only involved for the stress state between points A_e and B in this figure since the behaviour between the point A and the point A_e is assumed to be elastic (i.e., λ_{oc} is equal to κ). The value of κ is the same in the Zones I, II and III. The value of λ_{oc} obtained from CID tests is 0.146 for stress state in Zone II within the SBS. Thus, λ/λ_{oc} is equal to $(0.357/0.146)$ and is equal to 2.45.

8.3 Prediction of Strains using Author's Model for Lightly Overconsolidated Clays

The model developed for the lightly overconsolidated clays as described above is now examined by comparing its predictions with experimental observations in the following subsections. Undrained behaviour as well as drained behaviour are compared and relevant discussions are also made.

8.3.1 Undrained Behaviour

The pore pressure parameters C_1 and C_2 were introduced for normally and overconsolidated samples in Section 5.6.5. These parameters indicate the slopes of the first and the second linear sections of the $(u/p_o, \eta)$ relationship. The stress ratio at the intersection of these segments was defined as η_t . The pore pressure developed in these two segments is determined as :

$$\frac{u}{p_o} = C_1 \eta \quad (\eta \leq \eta_t) \quad \dots(8.16)$$

$$\frac{u}{p_o} = (C_1 - C_2) \eta_t + C_2 \eta \quad (\eta > \eta_t) \quad \dots(8.17)$$

where p_o is pre-shear mean normal stress. These Eqns. 8.16 and 8.17 are used for the generation of undrained stress paths as Eqns. 8.18 and 8.19.

$$\frac{p}{p_o} = \frac{1 - C_1 \eta}{1 - \eta/3} \quad (for \quad \eta \leq \eta_t) \quad \dots(8.18)$$

$$\frac{p}{p_o} = \frac{1 + (C_2 - C_1) \eta_i - C_2 \eta}{1 - \eta/3} \quad (\text{for } \eta \geq \eta_i) \quad \dots(8.19)$$

As discussed in Chapter V, the pore pressure parameter C_1 decreased as OCR values increased, while the corresponding η_i values increased. These relationships for CIU type of loading (see Figs. 5.44a and 5.34b) are simplified in Fig. 8.18. Thus, C_1 and η_i values are directly determined from this figure if OCR is known. The C_2 value is constant and can be determined by running an undrained test on a normally consolidated sample. Therefore, a family of undrained stress paths in the wet zone ($\text{OCR} < 2.15$) can be generated from Fig. 8.18 (related to values of C_1 and η_i), C_2 values and Eqns. 8.18 and 8.19. Typical stress-strain curve for samples with OCR values of less than 2.15 is shown in Fig. 8.19.

The undrained stress paths predicted using Fig. 8.18 and Eqns. 8.18 and 8.19 are compared with the experimental observations in Fig. 8.20. A C_2 value of 0.75 is used in the calculations. This figure indicates that the approach is quite promising as a solution for practical problems. Also, the relations expressed in Eqns. 8.18 and 8.19 can be useful components in the mathematical formulation of the undrained behaviour of lightly overconsolidated clays.

8.3.2 Drained Behaviour in the Wet Zone

A schematic diagram for the calculation of plastic strains during the CID type of loading in the wet zone is demonstrated in Fig. 8.21. Curves $E_oA_3'RM_o$ and E_oNB_3M are the yield locus of the Cam Clay and the Modified Cam Clay Theories, respectively. These two curves are the lower and the upper boundaries for volumetric yielding in Zone II. The stress Zone II is, thus, enclosed by these two curves and curve MG' . In the wet side of the Critical State and within the SBS, the plastic volumetric strain is assumed to take place only when the state paths lie in this zone. The plastic strains in this zone are calculated from Eqns. 8.18 and 8.19. On the other hand, the sample is assumed to experience only an elastic volumetric strain for the stress path A_3A_3' (Zone I). For the stress path which lies on the SBS (stress path beyond point B_3), the Revised Theory is used in the strain calculations. Constant q yield loci such as SN and TB_3 are used for the contribution of the shear strain for the stress state inside the SBS.

The stress-strain model formulated in Section 8.2 is now applied to four CID tests having OCR values of 1.24, 1.50, 1.78 and 2.15. Pender's Model is also applied for all cases. The parameter M used for both model calculations is 1.0. Figures 8.22a to 8.29b demonstrate the deviator stress-strain relationships and the stress ratio-strain relationships for all samples with corresponding OCR values. For each sample, the (q, ϵ_s) and (q, ϵ_v) relationships are first compared. Subsequently, (η, ϵ_s) and (η, ϵ_v) relationships for these samples are compared with the predictions. The points corresponding to Zone II are marked in each figure.

Predictions made by the Author's model agree well with the experimental data. Pender's Model also predicts a similar order of strains. However, Pender's Model tends to deviate from the test data as the OCR values are increased.

8.3.3 Drained Behaviour in the Dry Zone

Incremental forms of the stress-strain relationships for the dry zone are not yet complete at this moment. Thus, a tentative manner of strain calculations based on the volumetric strain contours from experimental observations is presented here. Figures 8.30 and 8.31 illustrate sets of strain contours on the dry zone for the samples sheared from the isotropic and the K_o pre-shear stress conditions, respectively. Each figure contains two subsets of strain contours: one is shear strain contours (a sets of full lines) and the other is plastic volumetric strain contours (a sets of dotted lines). Typical stress paths which are selected for the calculations are also shown in both figures.

(1) **Isotropic Pre-shear Conditions** - Stress-strain relationships for two typical stress paths: one, the constant p path (D_oD_1) and the other, the unloading compression stress path (D_oD_2) are calculated using the strain contours (see Fig. 8.30) and these are compared with those from Pender's Model. Figure 8.32a and 8.32b illustrate the observed and predicted strains for the constant p stress path. Pender's Model seems to predict larger shear strains for both paths. The comparison for the drained unloading compression tests are shown in Figs. 8.33a and 8.33b.

(2) **K_o Pre-shear Conditions** - Stress-strain relationships for three stress paths shown in Fig. 8.31 are calculated from the strain contours and Pender's Model, and then these are compared with the test data. These stress paths are unloading compression (A_4T_3), constant p (A_4T_2) and conventional drained (A_4T_1) paths, respectively. Figures 8.34a and 8.34b illustrate (q , ϵ_s) and (q , ϵ_v) relationships for A_4T_3 path. Shear strains predicted by the Author's model agree reasonably well with the test data. The Author's model successfully predicts the volumetric strain as well. Shear strain predictions by the Author's model for the path A_4T_2 are better than those for A_4T_3 (see Fig. 8.35a). However, it overpredicts volumetric strains as seen in Fig. 8.35b. For the stress path A_4T_1 as illustrated in Figs. 8.36a and 8.36b, the Author's model slightly overpredicts shear strains, while it underpredicts volumetric strains.

Generally, the Author's model on the dry side of the Critical State successfully predicts the shear strains, while the predictions of the volumetric strains deviate from the test data. However, these deviations are not significant. Therefore, the pattern of the plastic volumetric and shear strain contours are quite promising tools for the direct and easy calculation of strains. Moreover, this will now provide a strong base for the mathematical formulation of a suitable stress-strain theory on the dry side of the Critical State.

8.4 Concluding Remarks and Comments

(i) **Behaviour within the SBS-** Subsets of volumetric yield loci which contribute positive plastic volumetric strain on the wet side of the Critical State Line and dilational volumetric strain on the dry side have been proposed. In identifying such subsets of volumetric yield loci, a region within which only elastic volumetric strains take place has been proposed. Thus, the whole q-p stress space is divided into four zones: three (Zones I, II, and IV) are inside the SBS and the remaining one (Zone III) is in the normally consolidated state. In Zone I, plastic volumetric strains are assumed to be zero. Plastic dilation takes place in Zone IV, while compressive volumetric strains take place in Zone II. These sub-zones are assumed to expand with the expansion of the volumetric yield locus which lies on the SBS. The constant q yield loci are in operation in Zone I, II and III, while a fan of radial shear strain contours which converge to a point on the negative p-axis is needed for Zone IV.

(ii) **Plastic Volumetric Strain Contours within the SBS-** The plastic volumetric strain contours in Zone II are quite similar to the Cam Clay type of yield locus. The patterns of the plastic volumetric strain in Zone IV are somewhat similar to those in Zone II about the vertical line passing through the Critical State point. Samples in this zone are found to experience a higher degree of dilation when approaching failure.

(iii) **Plastic Strain Increment Ratio Inside the SBS-** The plastic strain increment ratio within the SBS is not uniquely dependent on the stress ratio η , but decrease as the mean normal stress decreases for a particular stress ratio. The plastic strain increment ratio is, however, uniquely dependent on the stress ratio for the stress states on the SBS. Therefore, the boundary values of the plastic dilatancy ratio for the overconsolidated state will be those from the Modified Theory for the stress states on the SBS.

(iv) **Reduction of $\frac{d\epsilon_{vp}}{d\epsilon_{sp}}$ with p/p_e for Constant Stress Ratio Inside the SBS-** The variation

of $\frac{d\epsilon_{vp}}{d\epsilon_{sp}}$ with respect to the stress ratio within the SBS can be simplified as a linear variation

in which the plastic dilatancy ratio is only dependent on the value of p/p_e for any one particular stress ratio. Furthermore, this trend is found to be the same for both compression and extension conditions. The slope of this simplified relationship approaches infinity as the stress ratio is close to zero, while it asymptotically approaches zero as η comes close to M. Equation 8.11 describes this relationship. Thus, the plastic dilatancy ratio at any stress ratio within the SBS can be calculated using Eqn. 8.12 as shown below.

$$\frac{d\varepsilon_{vp}}{d\varepsilon_{sp}} = \left(\frac{M^2 - \eta^2}{2\eta} \right) - \left(\frac{M^2}{\eta} - \eta + \frac{3}{2} \right) \left(\frac{M^2}{M^2 + \eta^2} - \frac{p}{p_e} \right) \dots(8.12 \text{ bis})$$

where, $\text{Exp}(\eta/M) \leq p_e/p \leq (M^2 + \eta^2)/M^2$

(v) **Volumetric Yield Loci in Zone II-** The plastic volumetric yield loci are quite similar to the Cam Clay type of yield locus on the wet side of the Critical State in Zone II, and they are nesting with the volumetric yield locus of the Modified Theory type on the SBS (see Fig. 8.2). This subset of volumetric yield loci passes through the Critical State point. This subset of yield loci is given by Eqn. 8.13.

$$q = \beta^* M p \ln(p_o/p) \dots(8.13 \text{ bis})$$

where, $\beta^* = \varepsilon_{vp} / C + 1$

(vi) **Stress-Strain Relationships for Lightly Overconsolidated Clays-** The incremental form of stress-strain relationships for lightly overconsolidated clays obtained from Eqns. 8.12 and 8.13 are given as :

$$d\varepsilon_{vp} = \frac{\lambda_{oc} - \kappa}{1 + e} \left(\frac{dp}{p} + \frac{d\eta}{\beta^* M} \right) \dots(8.14 \text{ bis})$$

$$d\varepsilon_{sp} = \left[\frac{\lambda_{oc} - \kappa}{1 + e} \left(\frac{dp}{p} + \frac{d\eta}{\beta^* M} \right) \right] / \left[\psi - \left(2\psi + \frac{3}{2} \right) \left(\zeta - \frac{p}{p_e} \right) \right] \dots(8.15 \text{ bis})$$

where, $\beta^* = \varepsilon_{vp} / C + 1$

$$\psi = (M^2 - \eta^2)/(2\eta) \quad (\text{as in the Modified Theory})$$

$$\zeta = M^2/(M^2 + \eta^2)$$

(vii) **Author's Model for Lightly Overconsolidated Clays-** The undrained stress paths of lightly overconsolidated clays ($\text{OCR} < 2.15$) can be successfully generated using the

pore pressure parameters C_1 , C_2 and η , obtained from the $(u/p_o, \eta)$ relationships. The predictions using the stress-strain model formulated in this chapter agree quite well with the experimental observations for clays on the wet side of the Critical State.

The model presented here is developed within the framework of the Critical State Soil Mechanics (SCHOFIELD and WROTH, 1968; ROSCOE and BURLAND, 1968). Two additional subsets of volumetric yield loci inside the State Boundary Surface (SBS) are proposed: one on the wet side of the Critical State and the other on the dry side to describe the plastic stress-strain behaviour of overconsolidated clays during volumetric yielding. The subset of volumetric yield loci on the wet side needs an additional constant β^* and is in operation with the constant q yield loci on the wet zone. β^* is a sort of hardening parameter which modifies the Cam Clay type yield locus slightly with plastic volumetric strain.

The model proposed by the Author uses a 'flow rule' which is valid both for the wet and dry zones inside the SBS as well as on the SBS. On the SBS, the Author's 'flow rule' merges with that from the Modified Theory of ROSCOE and BURLAND (1968). Algebraic expressions for the distortional strains associated with plastic volumetric strains on the wet side are derived in Section 8.2.7 as Eqns. 8.14 and 8.15. The actual shear strain increment is obtained from the contribution of the constant q yield loci and those given by Eqn. 8.15 as described in Section 8.2.2. The exact algebraic formulation of the volumetric yield loci on the dry side of the Critical State is not yet completed. The experimentally observed volumetric yield loci are currently used in the prediction of plastic strains associated with volumetric yielding. The plastic distortional strains obtained from these yield loci are combined with the distortional strains contributed by the radial fan of constant shear strain contours obtained from the undrained shear on the dry side of the Critical State.

The Author's Model make successful predictions of pore pressure and strains for practical purposes inside the State Boundary Surface (SBS).

IX CONCLUSIONS

The stress-strain behaviour and strength characteristics of normally and overconsolidated soft Bangkok clay are studied both under isotropic and K_o pre-shear consolidation conditions in compression and in extension. The experimental programme includes (i) triaxial consolidation and swelling tests (both isotropic and K_o consolidation and swelling) (ii) four series of undrained triaxial tests of which three are in compression and one in extension (iii) ten series of drained tests. All samples were prepared with the same pre-shear void ratio.

The undrained behaviour is presented in Chapter V, and the drained behaviour is presented in Chapter VI. Stress-strain theories based on the Critical State Concepts are reviewed in Chapter III and their predictions are compared with the experimental observations in Chapter VII. The theories used include the Cam Clay Theory and its modifications, Dafalias' Theory, Atkinson et al.'s Theory and Pender's Theory. With the exception of Pender's Theory, they are based on an 'associated flow rule' but with single and double yield loci.

Finally, subsets of volumetric yield loci are identified by the Author inside the State Boundary Surface (SBS) and a flow rule is established to cater for the stress-strain behaviour within and on the SBS. Simple expressions are derived for the volumetric and distortional strains for each zone within the SBS and on the SBS. The detailed conclusions are presented below in addition to the concluding remarks made under individual chapters.

9.1 Consolidation and Swelling Characteristics

- (1) The λ and κ values of the soft Bangkok clay in the $(e, \ln p)$ plot for the stress range covered in the testing programme are 0.357 and 0.081, respectively.
- (2) The idealized K_o -line for the overconsolidated sample is established along a stress path $(dq/dp) = 0.95$ and with both dq and dp less than zero.

9.2 Undrained Behaviour of Normally Consolidated Soft Bangkok Clays

- (1) A unique SBS is observed in the $(q/p_e, p/p_e)$ plot both for isotropically and K_o consolidated samples in compression and in extension. The initial states of the K_o consolidated samples are found to lie inside the SBS as obtained from the isotropic tests, but with progressive shear their states rise to lie on the surface of the isotropically consolidated samples. The initial states of the K_o consolidated samples are thought to have a substantial pre-shear secondary consolidation effect. The

Critical State Line for normally consolidated samples have the same slope both in compression and in extension and the Hvorslev strength envelope for the over-consolidated states also displays symmetry about the p-axis.

- (2) The peak deviator stress of isotropically consolidated samples reaches a larger shear strain of about 10%, while the K_o consolidated samples reach such a state within 4% strain. The stress-strain behaviour is influenced by the pre-shear consolidation conditions and the direction of the major principal stress whether in compression or in extension.
- (3) The excess pore pressure generation shows a bi-linear relationship in the $(u/p_o, \eta)$ plot. Such a relationship can be used to determine the undrained stress path and the excess pore pressure.
- (4) The M values corresponding to the peak deviator stress and peak stress ratio conditions are 0.83 and 0.88 in compression and the latter value increases to 0.93 in extension. The corresponding $\bar{\phi}$ values are 21° and 23° , respectively in compression and 33° in extension. The corresponding strength ratio $s_{uc}/\bar{\sigma}_{vo}$ are 0.235, 0.252 and 0.291, respectively.

9.3 Undrained Behaviour of Overconsolidated Bangkok Clays under Isotropic Pre-shear Consolidation Conditions

- (1) The state paths of the overconsolidated samples lie within the SBS and exhibit volumetric yielding at higher stress ratio levels. The initial stress paths are sub-parallel to the q-axis confirming the elastic wall concept of the Cambridge stress-strain theories.
- (2) The constant shear strain contours on the wet side of the Critical State (for OCR values less than 2.15) confirm the constant q yield loci concept. On the dry side, the constant shear strain contours form a radial fan when extended converging to a negative p_o value on the p-axis.
- (3) The overconsolidated samples also display a bi-linear $(u/p_o, \eta)$ relationship, and these relations can be used to describe successfully the undrained stress paths and the generation of excess pore pressures. The A_f values corresponding to various OCR agree well with the predictions from the Modified Theory.
- (4) The end points of the lightly overconsolidated samples seek the Critical State and tend to lie on the Hvorslev type of failure envelope. The strength ratio $(s_{up}/\bar{\sigma}_{vo})_{OC}/(s_{up}/\bar{\sigma}_{vo})_{NC}$ increases with increasing OCR values. These strength ratios are predicted consistently with the Modified Theory using Λ of 0.77.

9.4 Undrained Behaviour of Overconsolidated Bangkok Clays under K_0 Pre-shear Consolidation Conditions

- (1) The undrained stress paths are such that their state paths lie inside the SBS. The initial parts of the state paths are sub-parallel to the q-axis in the $(q/p_e, p/p_e)$ plot confirming the elastic wall concept. When volumetric yielding takes place at higher stress ratio levels, the state paths rise and lie on the SBS.
- (2) The constant shear strain contours tend to be sub-parallel to the idealized K_0 -line on the dry side and become parallel to the p-axis on the wet side.
- (3) The $(u/p_o, \eta)$ relationships are bi-linear on the wet side of the Critical State and can be used to produce the undrained stress paths and the excess pore pressure developed during shear. The A_f values are found to be different in magnitude for compression and extension tests, but can be predicted with the equation of MAYNE and STEWART (1988).
- (4) The end points of the overconsolidated samples lie on the Hvorslev strength envelope and are seeking the Critical State for lightly overconsolidated samples.

9.5 Drained Behaviour of Isotropically and K_0 Consolidated Samples

- (1) The drained stress paths of the CID specimens approach the SBS at higher stress levels and the samples reach the normally consolidated states. When the stress paths lie on the SBS, the strains are of higher magnitude due to larger plastic volumetric strains. For all the drained specimens when the stress paths cross from the overconsolidated to the normally consolidated state, the (ϵ_v, p) relation is used to determine the volumetric yield points. Such volumetric yield points constitute the volumetric yield locus on the SBS.
- (2) For all drained tests, the (q, ϵ_{vp}) or the (ϵ_{vp}, p) values are used to define the zones in which only elastic volumetric strain takes place and the zones in which plastic volumetric strains both compressive and dilational take place inside the SBS.
- (3) From the $(\epsilon_{vp}, \epsilon_{sp})$ relationships, the plastic dilatancy ratio $\frac{d\epsilon_{vp}}{d\epsilon_{sp}}$ is calculated for each stress path and this ratio is estimated such that it does not include the undrained shear strain component $d\epsilon_s$ both on the wet and dry side.

9.6 Critical State Models and Their Predictions

- (1) **Revised Theory-** This theory is found to successfully predict the undrained shear strength, the shear strains and the excess pore pressures for the CIU type of tests. For the CID type of tests, this theory gives excellent predictions both for the (q, ϵ_s) and the (q, ϵ_v) relationships, while the Modified Theory slightly underpredicts the shear strains.
- (2) **Pender's Model-** (i) N.C.-Behaviour : Pender's Model overpredicts the shear strains and is somewhat sensitive to the parameter p_{cs} for the CIU type of tests. For the CK_0U test, it predicts reasonably well the undrained stress paths both in compression and in extension with parameters determined from the peak deviator stress criterion. However, it overpredicts shear strains in compression phase, and gives poor strain predictions in extension. For the drained conditions, Pender's Model also overpredicts shear strains, especially volumetric strains for the CID tests. It also overpredicts shear strains for the CK_0D and CK_0DE tests. This model, however, gives a good prediction for the volumetric strain both in compression and in extension.

(ii) O.C.-Behaviour : Pender's Model generates a successful family of undrained stress paths for the overconsolidated clays on the wet side of the Critical State both for compression and for extension conditions when the parameters are selected from the peak deviator stress conditions. However, this model overpredicts the shear strains both for the isotropically consolidated and for the K_0 consolidated samples. This model is found to overpredict shear strains in most cases. The deviations become more and more apparent when the OCR values are increased. However, this model gives excellent predictions of volumetric strains for the overconsolidated samples under compression types of loading. Pender's Model overpredicts shear strains both in undrained and in drained tests on overconsolidated samples. This is attributed in part or fully to the incorrect assumption made on the plastic strain increment ratio in the formulation of the theory.

(iii) Suggested Improvement to Pender's Model : The OCR or a related parameter can be a possible reduction factor to be applied to the assumption of the plastic strain increment ratio in Pender's Model for the lightly overconsolidated samples ($OCR < 3.0$) sheared from isotropic pre-shear stress conditions. Pender's hypotheses on the shapes of the undrained stress paths for the K_0 overconsolidated samples is found to be an oversimplification. Thus, the prediction of Pender's Model for K_0 overconsolidated samples is expected to be promising when this factor is incorporated in the expression for the plastic strain increment ratio.

- (3) **Dafalias' Model-** This model provides good stress-strain predictions for compression tests. However, its predictions for the extension tests are poor especially at larger strains. The parameter α varies during undrained shearing and is not zero even for the isotropically consolidated sample whereas it should be according to the theory. For the CK_oD type of loading, this model predicts the (q, ϵ_s) and (q, ϵ_v) relationships well.
- (4) **Atkinson et al.'s Model-** Atkinson's Model predicts low undrained strength in compression, and its predictions for the extension conditions are poor specifically at larger strains. This model overpredicts shear and volumetric strains for the CK_oD type of tests.

9.7 Stress-Strain Behaviour within the SBS for Drained Tests

- (1) Subsets of volumetric yield loci which contribute positive plastic volumetric strain on the wet side of the Critical State Line and dilational volumetric strain on the dry side have been proposed. In identifying such subsets of volumetric yield loci, a region is also identified within the SBS of which only elastic volumetric strain takes place. Thus, the whole q - p stress space is divided into four zones: three (Zones I, II, and IV) are inside the SBS and the remaining one (Zone III) is in the normally consolidated state. In Zone I, plastic volumetric strains are assumed to be zero. Plastic dilation take place in Zone IV, while compressive volumetric strains take place in Zone II. These sub-zones are assumed to expand with the expansion of the volumetric yield locus which lie on the SBS.
- (2) The plastic volumetric strain contours in Zone II are quite similar to the Cam Clay type of yield locus. The patterns of the plastic volumetric strain in Zone IV are somewhat similar to those in Zone II about the vertical line passing through the Critical State point. However, samples in this zone are found to experience a higher degree of dilation when approaching failure.
- (3) The plastic strain increment ratio within the SBS is not uniquely dependent on the stress ratio η , but decrease as the mean normal stress decreases for a particular stress ratio. The plastic strain increment ratio is, however, uniquely dependent on the stress ratio for the stress states on the SBS. Therefore, the boundary values of the plastic dilatancy ratio for the overconsolidated state can be derived from those given by the Modified Theory for the stress states on the SBS.
- (4) The variation of $\frac{d\epsilon_{vp}}{d\epsilon_{sp}}$ with respect to the stress ratio within the SBS can be simplified as a linear variation in which the plastic dilatancy ratio is only dependent on the value of p/p_e for any one particular stress ratio. Furthermore, this trend is found

to be the same for both compression and extension conditions. The slope of this simplified relationship approaches infinity as the stress ratio is close to zero, while it asymptotically approaches zero as η approaches to M .

9.8 Proposed Model for Stress-Strain Behaviour below the SBS

- (1) The undrained stress paths of lightly overconsolidated clays ($OCR < 2.15$) can be successfully generated using the pore pressure parameters C_1 , C_2 and η , obtained from the $(u/p_o, \eta)$ relationships. The predictions using the stress-strain model formulated in this study (see Eqns. 8.18 and 8.19) agree quite well with the experimental observations for clays on the wet side of the Critical State.
- (2) The Author's model presented in this study is developed within the framework of the Critical State Soil Mechanics (SCHOFIELD and WROTH, 1968; ROSCOE and BURLAND, 1968). Two additional subsets of volumetric yield loci inside the State Boundary Surface (SBS) are proposed: one on the wet side of the Critical State and the other on the dry side to describe the plastic stress-strain behaviour of overconsolidated clays during volumetric yielding. The subset of volumetric yield loci on the wet side need an additional constant β^* and is in operation with the constant q yield loci on the wet side. β^* is a sort of hardening parameter which modifies the yield locus slightly with plastic volumetric strains.
- (3) The model proposed by the Author uses a 'flow rule' which is valid both for the wet and dry zones inside the SBS as well as on the SBS. On the SBS, the Author's 'flow rule' merges with that from the Modified Theory of ROSCOE and BURLAND (1968). Algebraic expressions for the distortional strains associated with plastic volumetric strains on the wet side are derived in Section 8.2.7 as Eqns. 8.14 and 8.15. The actual shear strain increment is obtained from the contribution of the constant q yield loci and those given by Eqn. 8.15 as described in Section 8.2.2. The exact algebraic formulation of the volumetric yield loci on the dry side of the Critical State is not yet completed. The experimentally observed volumetric yield loci are currently used in the prediction of plastic strains associated with volumetric yielding. The plastic distortional strains obtained from these yield loci are combined with the distortional strains contributed by the radial fan of constant shear strain contours obtained from the undrained shear on the dry side of the Critical State.
- (4) The Author's model makes successful predictions of pore pressures and strains for practical purposes inside the SBS.

9.9 Recommendations for Further Research

- (1) Systematic investigation of time effects during the sample preparation both for undrained and drained behaviour is needed.
- (2) The demarcation value of OCR between the wet and the dry side need to be investigated in detail. Furthermore, a detailed investigation of the (u/p_o , η) relationship on the dry side of the Critical State is needed.
- (3) It is suggested that an investigation be conducted on the $u/p_o = C \eta$ relation due to the pure shear condition (i.e., constant p type of applied stress path) in order to separate the component of Δu as contributed from the spherical pressure increase $q/3$ due to increase in deviator stress. It would then be truly possible to confirm the excess pore pressure development during compression and extension according to the equation $u/p_o = C \eta$ and the corresponding C parameter as defined appropriately.
- (4) Subsets of volumetric yield loci within the SBS on the extension side need to be established by carrying out extension loading tests.
- (5) Supplementary investigation of the plastic dilatancy ratio in Zone IV both in compression and in extension sides in the (q, p) plot will provide a comprehensive understanding of the stress-strain behaviour of the clays within the State Boundary Surface.

REFERENCES

- ABDELHAMID, M. S. & KRIZEK, R. J.** (1976), At Rest Lateral Earth Pressure of a Consolidating Clay, J. of the Geotech. Engg. Div. ASCE, Vol. 102, GT7, pp. 721-738.
- AL-HUSSAINI, M.** (1981), Comparison of Various Methods for Determining K_0 , Laboratory Shear Strength of Soils, ASTM STP 740, pp. 78-93.
- ALI, M. M.** (1981), Statistical Evaluation of Effective Strength Parameters for Soft Clay, M. Eng. Thesis, GT-80-7, AIT, Bangkok.
- ALPAN, I.** (1967), The Empirical Evaluation of the Coefficients K_0 and K_{or} , Soils and Foundations, Vol. 7, No. 1, pp. 31-40.
- ATKINSON, J. H. & BRANSBY, P. L.** (1978), The Mechanics of Soil- An Introduction to Critical State Soil Mechanics, London, McGraw-Hill.
- ATKINSON, J. H., RICHARDSON, D. & ROBINSON, P. J.** (1987), Compression and Extension of K_0 Normally Consolidated Kaolin Clay, J. Geotech. Engg. Div., ASCE, Vol. 113, No. 12, pp. 1468-1482.
- BALASUBRAMANIAM, A. S.** (1969), Some Factors Influencing the Stress-Strain Behaviour of Clays, Ph. D. Thesis, Cambridge Univ., Cambridge.
- BALASUBRAMANIAM, A. S.** (1973), Stress History Effects on Stress-Strain Behaviour of a Saturated Clay, Geotechnical Engineering, Vol. 4, pp. 91-111.
- BALASUBRAMANIAM, A. S.** (1975), Stress-Strain Behaviour of a Saturated Clay for States below the State Boundary Surface, Soils and Foundations, Vol. 15, No. 3, pp. 13-15.
- BALASUBRAMANIAM, A. S.** (1976), Stress-Strain Theories for Normally Consolidated Clay, Aust. Geomech. J., pp. 43-49.
- BALASUBRAMANIAM, A. S., HANDALI, S., PHIENTWEJA, N. & KUWANO, J.** (1989), Pore Pressure Stress Ratio Relationship for Soft Clay, Proc. 12th ICSMFE, Rio de Janeiro, Vol. 1, pp. 11-14.
- BALASUBRAMANIAM, A. S. & HWANG, Z. M.** (1980), Yielding of Weathered Bangkok Clay, Soils and Foundations, Vol. 20, No. 2, pp. 1-15.
- BALASUBRAMANIAM, A. S., LI, Y. G., WAHEED, U., HWANG, Z. M. & CHAUDRY, A. R.** (1977), Application of Critical State Theories to the Prediction of Strains in Triaxial Specimens of Soft Bangkok Clay, Specialty Session on Constitutive Equations of Soils, Proc. 9th ICSMFE, Tokyo, pp. 11-20.
- BALASUBRAMANIAM, A. S. & UDDIN, W.** (1977), Deformation Characteristics of Weathered Bangkok Clay in Triaxial Extension, Geotechnique, Vol. 27, No. 1, pp. 75-92.

- BARACOS, A., GRAHAM, J. & DOMASHUK, L. (1980), Yielding and Rupture in a Lacustrine Clay, Can. Geotech. J., Vol. 77, pp. 559-573.
- BISHOP, A. W. & HENKEL, D. J. (1957), The Measurement of Soil Properties in the Triaxial Test, London, Arnold.
- BJERRUM, L., SIMONS, N. E. & TORBLAA, I. (1958), The Effects of Time on the Shear Strength of a Soft Marine Clay, Proc. Brussels Conf. on Earth Pressure Problems, Vol. 1, pp. 148-158.
- BJERRUM, L. (1967), Engineering Geology of Norwegian Normally Consolidated Marine Clays as Related to Settlements of Buildings, Geotechnique, Vol. 17, No. 2, pp. 83-117.
- BJERRUM, L. (1973), Problems of Soil Mechanics and Construction on Soft Clay, Proc. 8th ICSMFE, Moscow, Vol. 3, pp. 111-159.
- BROOKER, E. W. & IRELAND, H. O. (1965), Earth Pressures at Rest Related to Stress History, Can. Geotech. J., Vol. 2, pp. 1-15.
- BROWN, J. D. (1969), Measurement of the Effect of Strain Rate on Undrained Shear Resistance, Int. Report, F83-4, NGI, Oslo.
- BUENSUCESO, Jr. B. R. (1990), Engineering Behaviour of Lime Treated Soft Bangkok Clay, Doctoral Dissertation, AIT, Bangkok.
- BUISMAN, A. S. (1936), Results of Long Duration Settlement Test, Proc. 1st ICSMFE, Cambridge, Vol. 1, pp. 103-107.
- BURLAND, J. B. (1965), The Yielding and Dilation of Clay, Correspondence, Geotechnique, Vol. 15, No. 2, pp. 211-214.
- BURLAND, J. B. (1971), A Method of Estimating the Pore Pressures and Displacements Beneath Embankments on Soft Natural Clay Deposits, Proc. Rescoe Memorial Symp., Cambridge, (ed. R.H.G. Parry), pp. 505-536, Henley on Thames, Faulis.
- CASAGRANDE, A. (1938), Compaction Tests and Critical Density Investigations of Cohesionless Materials for Franklin Falls Dam, U.S. Engineer Corps, (from TAYLOR, D. W., 1948).
- CHANG, M. F. (1973), A Rational Method for Determining the In-situ Coefficient of Earth Pressure at Rest, M. Eng. Thesis, No. 510, AIT, Bangkok.
- CHAIYADHUMA, W. (1974), Undrained Shear Strength Characteristics of Nong Ngoo Hao Soft Clay under K_0 -anisotropic Consolidation, M. Eng. Thesis, No. 698, AIT, Bangkok.
- CHAUDHRY, A. R. (1975), Effects of Applied Stress Path on the Stress-Strain Behaviour and Strength Characteristics of Soft Nong Ngoo Hao Clay, M. Eng. Thesis, No. 760, AIT, Bangkok.
- CLAUSEN, C. J. F. (1969), Loading Test, Mastemyr, Proc. Bolkesjø Sym. No. 42, NGI, Oslo.

- CRAWFORD, C. B.** (1964), Interpretation of the Consolidation Test, J. Soil Mech. and Found. Div., ASCE, Vol. 90, SM5, pp. 87-102.
- CROOKS, J. H. A. & GRAHAM, J.** (1976), Geotechnical Properties of the Balfast Estuarine Deposit, Geotechnique, Vol. 26, No. 2, pp. 293-315.
- DAFALIAS, Y. F.** (1987), An Anisotropic Critical State Clay Plasticity Model, Constitutive Laws for Engineering Materials Theory and Applications, Vol. 1 (C. S. Desai et al., eds.), pp. 513-522.
- DRUCKER, D. C., GIBSON, R. E. & HENKEL, D. J.** (1957), Soil Mechanics and Work-Hardening Theories of Plasticity, Trans. ASCE., Vol. 122, pp. 338-346.
- FEDERICO, A.** (1990), Discussion on 'Pore Pressure Behaviour of K_0 -consolidated Clays', J. of the Geotech. Engg. Div., ASCE, Vol. 116, No. 9, pp. 1436-1440.
- FOLKES, D. J. & CROOKS, J. H. A.** (1985), Effective Stress Paths and Yielding in Soft Clay below Embankments, Can. Geotech. J., Vol. 22, pp. 357-374.
- GRAHAM, J. & HOULSBY, G. T.** (1983), Anisotropic Elasticity of a Natural Clay, Geotechnique, Vol. 33, No. 2, pp. 165-180.
- GRAHAM, J., NOONAN, M. L. & LEW, K. V.** (1983), Yields States and Stress-Strain Relationships in a Natural Plastic Clay, Can. Geotech. J., Vol. 20, pp. 502-516.
- GRAHAM, J. & LI, E. C. C.** (1985), Comparison of Natural and Remoulded Plastic Clay, J. of the Geotech. Eng. Div., ASCE, Vol. 111, No. 7, pp. 865-881.
- GRAHAM, J., CROOKS, J. H. A. & LAU, S. L. K.** (1988), Yield Envelops: Identification and Geometric Properties, Geotechnique, Vol. 38, No. 1, Technical Note, pp. 125-134.
- HANDALI, S.** (1986), Cyclic Behaviour of Clays for Offshore Type of Loading, Doctoral Dissertation, AIT, Bangkok.
- HENKEL, D. J. & SOWA, V. A.** (1963), The Influence of Stress History on the Stress Paths Followed in Undrained Triaxial Tests, Laboratory Shear Testing of Soils, ASTM STP 361, pp. 280-291.
- HIGHT, D. W., JARDINE, R. J. & GENS, A.** (1987), The Behaviour of Soft Clays, Embankments on Soft Clays, The Public Works Research Center, pp. 33-158.
- HILL, R.** (1950), The Mathematical Theory of Plasticity, Oxford Univ. Press, London.
- HOULSBY, G. T., WROTH, C. P. & WOOD, D. M.** (1982), Predictions of the Results of Laboratory Tests on a Clay using Critical State Model, Proc. Int. Workshop Constitutive Relations of Soils, (eds. G. Gudehus, F. Darve & I. Vardoulakis), Grenoble, Rotterdam.
- HVORSLEV, M. J.** (1937), On the Physical Properties of Disturbed Cohesive Soils (from ROSCOE et al., 1958)

- JAKY, J.** (1944), The Coefficient of Earth Pressure, J. for Soc. of Hungarian Architects and Engineers, Budapest, pp. 355-358.
- JAMES, R. G. & BALASUBRAMANIAM, A. S.** (1971), A Comprehensive Experimental Study of the Strength Characteristics of Remoulded Specimens of Kaolin, Geotechnical Engineering, VOL. 2, pp. 21-33.
- JAMIOLKOWSKI, M., LADD, C. C., GERMAINE, J. T. & LANCELLOTTA, R.** (1985), New Developments in Field and Laboratory Testing and Soils, Proc. 11th ICSMFE, Vol. 1, pp. 57-153, San-Francisco.
- KOUTSOFTAS, D. C.** (1981), Undrained Shear Behaviour of a Marine Clay, Laboratory Shear Strength of Soils, ASTM STP 740, pp. 254-276.
- LADD, C. C.** (1964), Stress-Strain Behaviour of Saturated Clays and Basic Strength Principles, Research Report R74-17, MIT.
- LADD, C. C.** (1965), Stress-Strain Behaviour of Anisotropically Consolidated Clays during Undrained Shear, Proc. 6th ICSMFE, Vol. 1, pp. 282-285.
- LADD, C. C., FOOTT, R., ISHIHARA, K., SCHLOSSER, F. & POULOS, H. G.** (1977), Stress-Deformation and Strength Characteristics; State-of-the-Art Report, Proc. of 9th ICSMFE, Vol. 2, pp. 421-494, Tokyo.
- LAMBE, T. W.** (1964), Methods of Estimating Settlement, J. Soil Mech. and Found. Div., ASCE, Vol. 90, No. SM5, pp. 43-67.
- LEE, Y. H.** (1986), Strength and Deformation Characteristics of Rockfills, Doctoral Dissertation, AIT, Bangkok.
- LEONARDS, G. A., CHANG, M. F., DEWEY, R., MUNDELL, J., GONZALEZ, R. & HARRIS, A.** (1981), Discussions: Yielding of Weathered Bangkok, Clays, Soils and Foundations, Vol. 21, No. 2, pp. 129-131.
- LEROUEIL, S., TAVENAS, F., BRUCY, F., La ROCHELLE, P. & ROY, M. L.** (1979), Behaviour of Destructured Natural Clays, J. of the Geotech. Engg. Div., ASCE, Vol. 105, No. GT6, pp. 759-778.
- LO, K. Y. & MORIN, J. P.** (1972), Strength Anisotropy and Time Effects of Two Sensitive Clays, Can. Geotech. J., Vol. 9, pp. 261-277.
- LOUDON, P. A.** (1967), Some Deformation Characteristics of Kaolin, Ph.D. Thesis, Cambridge Univ., Cambridge.
- MAYNE, P. W.** (1980), Cam-Clay Predictions of Undrained Strength, J. of the Geotech. Engg. Div., ASCE, Vol. 106, No. GT11, pp. 1219-1241.
- MAYNE, P. W.** (1985), Stress Anisotropy Effects on Clay Strength, J. of the Geotech. Engg. Div., ASCE, Vol. 111, No. 3, pp. 356-365.

- MAYNE, P. W. (1988), Determining OCR in Clays from Laboratory Strength, J. of the Geotech. Engg. Div., ASCE, Vol. 114, No. 1, pp. 76-92.
- MAYNE, P. W. & KULHAWY, F. H. (1982), K_0 -OCR Relationships in Soils, J. of the Geotech. Engg. Div., ASCE, Vol. 108, GT6, pp. 851-872.
- MAYNE, P. W. & SWANSON, P. G. (1981), The Critical State Pore Pressure Parameter from Consolidated-Undrained Shear Tests, Laboratory Shear Strength of the Soil, ASTM STP 740, pp. 410-430.
- MAYNE, P. W. & STEWART, H. E. (1988), Pore Pressure Behaviour of K_0 -consolidated Clays, J. of the Geotech. Engg. Div., ASCE, Vol. 114, No. 11, pp. 1349-1346.
- MITACHI, T. & KITAGO, S. (1979), The Influence of Stress History and Stress System on the Stress-Strain-Strength Properties of Saturated Clay, Soils and Foundations, Vol. 19, No. 2, pp. 45-61.
- MITCHELL, R. J. (1970), On the Yielding and Mechanical Strength of Leda Clay, Can. Geotech. J., Vol. 7, pp. 297-312.
- MONOI, Y. (1989), Deformation Behaviour Heavily Overconsolidated Clay, M. Eng. Thesis, GT-88-5, AIT, Bangkok.
- NAKASE, A. & KAMEI, T. (1983), Undrained Shear Strength Anisotropy of Normally Consolidated Cohesive Soils, Soils and Foundations, Vol. 23, No. 1, pp. 91-101.
- NAKASE, A. & KOBAYASHI, M. (1971), Change in Undrained Shear Strength of Saturated Clay due to Rebound, Proc. 4th Asian Regional Conf., Bangkok, Vol. 1, pp. 147-150.
- OHTA, H. & NISHIHARA, A. (1985), Anisotropy of Undrained Shear Strength of Clays under Axi-Symmetric Loading Conditions, Soils and Foundations, Vol. 25, No. 2, pp. 73-86.
- PARRY, R. H. G. (1960), Triaxial Compression and Extension Tests on Remoulded Saturated Clay, Geotechnique, Vol. 10, pp. 166-180.
- PARRY, R. H. G. & NADARAJAH, V. (1973), Observations on Laboratory Prepared Lightly Overconsolidated Specimens of Kaolin, Geotechnique, Vol. 24, No. 3, PP. 345-358.
- PENDER, M. J. (1977), A Unified Model for Soil Stress- Strain Behaviour, Proc. 10th ICSMFE, Specialty Session No. 9, Constitutive Equation of Soils, Tokyo, pp. 213-222.
- PENDER, M. J. (1978), A Model for Behaviour of Overconsolidated Soil, Geotechnique, Vol. 28, No. 1, pp. 1-25.
- POULOS, H. G. & DAVIS, E. H. (1972), Laboratory Determination of In-situ Horizontal Stress in Soil Masses, Geotechnique, Vol. 22, No. 1, pp. 177-182.
- RENDULIC, L. (1936), Relation between Void Ratio and Effective Principal Stress for a Remoulded Silty Clay, Discussion, Proc. 1st ICSM, Vol. 3, pp. 48-51.

- RICHARDSON, A. M. Jr. & WHITMAN, R. V.** (1963), Effects of Strain-Rate upon Undrained Shear Resistance of a Saturated Remoulded Fat Clay, Geotechnique, Vol. 13, pp. 310-324.
- ROSCOE, K. H. & BURLAND, J. B.** (1968), On the Generalized Stress-Strain Behaviour of Wet Clay, Engineering Plasticity, Cambridge Univ. Press, Cambridge, pp. 535-609.
- ROSCOE, K. H. & POOROOSHASB, H. B.** (1963), A Theoretical and Experimental Study of Strains in Triaxial Tests on Normally Consolidated Clays, Geotechnique, Vol. 13, No.1, pp. 12-38.
- ROSCOE, K. H., SCHOFIELD, A. N. & THURAIRAJAH, A.** (1963), Yielding of Clays in States Wetter than Critical, Geotechnique, Vol. 13, No. 3, pp. 535-609.
- ROSCOE, K. H., SCHOFIELD, A. N. & WROTH, C. P.** (1958), On the Yielding of Soils. Geotechnique, Vol. 8, pp. 22-53.
- ROWE, P.** (1957), $C_c=0$ Hypothesis for Normally Loaded Clays at Equilibrium, Proc. 4th ICSMFE, London, Vol. 1, pp. 189-192.
- RUJIRAAPA, V.** (1971), Effects of Consolidation Stress Ratio on Shear Strength of a Sedimented Clay, M. Eng. Thesis, No. 405, AIT, Bangkok.
- SCHMERTMANN, J. S.** (1975), Measurement of In-situ Shear Strength: State-of-the -Art Report, Proc. ASCE Specialty on In-Situ Measurement of Soil Properties, Vol. 2, pp. 57-138, Releigh.
- SCHMIDT, B.** (1966), Discussion of Earth Pressure at Rest Related to Stress History, Can. Geotech. J., Vol. 3, No. 4, pp. 239-242.
- SCHOFIELD, A. N. & WROTH, C. P.** (1968), Critical State Soil Mechanics, McGraw-Hill, 310p.
- SIVAKUGAN, N., HOLTZ, R. D. & CHAMEAW, J. L.** (1988), CK_0 UC Shear Strength of Normally Consolidated Clays from CIUC Tests, J. of the Geotech. Engg. Div., ASCE, Vol. 114, No. 3, pp. 284-295.
- SKEMPTON, A. W.** (1957), Discussion on the Planning and Design of the New Hong Kong Airport, Proc. Instn. Civ. Engrs., Vol. 7, 306.
- STIPHO, A. S.** (1982), Extended Critical State Model for Anisotropically Consolidated Clays, Int. Symp. on Numerical Models in Geomechanics, Zurich, pp. 183-188.
- TAMPUBOLON, M.** (1981), Behaviour of Soft Bangkok Clay under Horizontal Loading, M. Eng. Thesis, GT-80-3, AIT, Bangkok.
- TAVENAS, F. & LEROUEIL, S.** (1977), Effects of Stress and Time on Yielding of Clays, Proc. 9th ICSMFE, Vol. 1, Tokyo, pp. 319-326.

- TAVENAS, F. & LEROUEIL, S.** (1979), Clay Behaviour and the Selection of Design Parameters, Proc. 7th European Conf. on Soil Mech. and Found. Engg., Brighton, London, pp. 281-291.
- TAVENAS, F., LEROUEIL, S., La ROCHELLE, P. & ROY, M.** (1978), Creep Behaviour of an Undisturbed Lightly Overconsolidated Clay, Can. Geotech. J., Vol. 15, pp. 402-423.
- TAVENAS, F., Des ROSIERS, J. P., LEROUEIL, S., La ROCHELLE, P. & ROY, M.** (1979), The Use of Strain Energy as a Yield and Creep Criterion for Lightly Overconsolidated Clays, Geotechnique, Vol. 29, No.3, pp. 285-303.
- TAYLOR, D. W.** (1942), Research on Consolidation of Clays. MIT Report, Serial 82.
- TAYLOR, D. W.** (1948), Fundamentals of Soil Mechanics, Wiley, New York
- THAVANAYAGAM, S. & PRAPAHARAN, S.** (1989), Discussion on ' Compression and Extension of K_0 -normally Consolidated Kaolin Clay', J. of the Geotech. Engg. Div., ASCE, Vol. 115, No. 8, pp. 1173-1175.
- THURAIRAJAH, A.** (1961), Some Shear Properties of Kaolin and of Sand, Ph.D Thesis, Cambridge Univ., Cambridge
- UDDIN, W.** (1975), Stress Strain Behaviour and Shear Strength Characteristics of Weathered Bangkok Clay under Extension Conditions, M. Eng. Thesis, No. 774, AIT, Bangkok.
- VAID, Y. P. & CAMPANELLA, R. G.** (1974), Triaxial and Plane Strain Behaviour of Natural Clay, Pro. J. Geotech. Engg. Div., ASCE, Vol. 100, No. GT3, pp. 207-224.
- VAID, Y. P., ROBERTSON, P. K. & CAMPANELLA, R. G.** (1979), Strain-Rate Behaviour of Saint-Jean-Vianney Clay, Can. Geotech. J., Vol. 16, pp. 34-42.
- WANG, W. T.** (1975), K_0 Determination by Hydraulic Fracturing, M. Eng. Thesis, AIT, Bangkok.
- WARLAM, A. A.** (1960), Recent Progress in Triaxial Apparatus Design, Proc. ASCE Research Conf. Shear Strength of Cohesive Soil, Boulder, pp. 859-876.
- WIJEYAKULASURIYA, C. V.** (1986), Shear Behaviour of Soft Clay with Particular Reference to Soft Bangkok Clay, M. Eng. Thesis, GT-85-33, AIT, Bangkok.
- WONG, P. K. K. & MITCHELL, R. J.** (1975), Yielding and Plastic flow of Sensitive Clay, Geotechnique, Vol. 25, No. 4, pp. 763-782.
- WROTH, C. P.** (1984), The Interpretation of In-situ Soil Test, Geotechnique, Vol. 34, No. 4, pp. 449-489.
- WROTH, C. P. & LOUDON, P. A.** (1967), The Correlation of Strains within a Family of Triaxial Tests on Overconsolidated Samples of Kaolin, Proc. of the Geotech. Conf., Oslo, Vol. 1, pp. 159-163.
- YUDHBIR & VARADARAJAN, A.** (1974), Undrained Behaviour of Overconsolidated Saturated Clays during Shear, Soils and foundations, Vol. 14, No. 4, pp. 1-12.

**Table 4.2 Stress Conditions for the Overconsolidated Samples
in the q-p Stress Space**

OCR		TEST SERIES I					
OCR ($\bar{\sigma}_{vm}/\bar{\sigma}_{vo}$)	(OCR) _p (p_{max}/p_o)	p_{max} (kg/cm ²)	q_{max} (kg/cm ²)	p_o (kg/cm ²)	q_o (kg/cm ²)	K_o	η_o
1.00	1.00	4.500	2.205	4.500	2.205	0.63	0.49
1.24	1.20	4.690	2.298	3.908	1.657	0.67	0.42
1.50	1.40	4.857	2.380	3.469	1.242	0.71	0.36
1.78	1.60	5.006	2.453	3.129	0.914	0.76	0.29
2.15	1.85	5.174	2.535	2.797	0.586	0.82	0.21
2.75	2.20	5.382	2.637	2.446	0.230	0.91	0.09

OCR		TEST SERIES II					
OCR ($\bar{\sigma}_{vm}/\bar{\sigma}_{vo}$)	(OCR) _p (p_{max}/p_o)	p_{max} (kg/cm ²)	q_{max} (kg/cm ²)	p_o (kg/cm ²)	q_o (kg/cm ²)	K_o	η_o
1.00	1.00	4.500	2.205	4.500	2.205	0.63	0.49
1.24	1.24	4.725	2.315	3.811	1.867	0.63	0.49
1.50	1.50	4.934	2.418	3.289	1.612	0.63	0.49
1.78	1.78	5.129	2.513	2.882	1.412	0.63	0.49
2.15	2.15	5.354	2.623	2.490	1.220	0.63	0.49
2.75	2.75	5.661	2.774	2.059	1.009	0.63	0.49

OCR		TEST SERIES III					
OCR ($\bar{\sigma}_{vm}/\bar{\sigma}_{vo}$)	(OCR) _p (p_{max}/p_o)	p_{max} (kg/cm ²)	q_{max} (kg/cm ²)	p_o (kg/cm ²)	q_o (kg/cm ²)	K_o	η_o
1.00	1.00	6.500	0	6.500	0	1	0
1.24	1.24	6.840	0	5.516	0	1	0
1.50	1.50	7.155	0	4.770	0	1	0
1.78	1.78	7.451	0	4.186	0	1	0
2.15	2.15	7.792	0	3.624	0	1	0
2.75	2.75	8.260	0	3.004	0	1	0

notes: OCR : the ratio of the maximum past vertical stress to the pre-shear vertical stress
 (OCR)_p : the ratio of the maximum past mean normal stress to the pre-shear mean normal stress

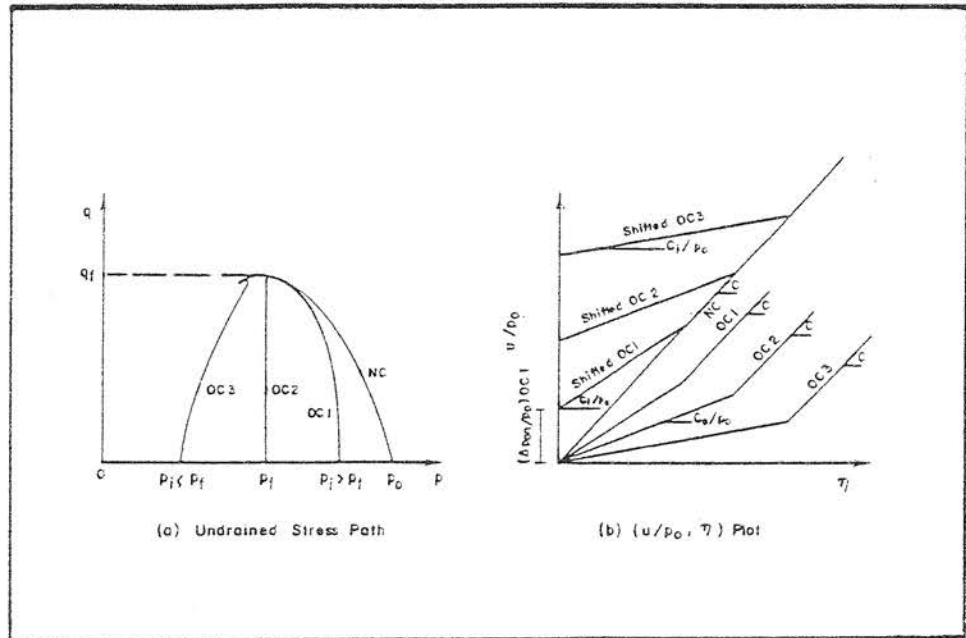


Fig. 2.1a Typical Undrained Paths and $(u/p_o, \eta)$ plot for Overconsolidated Samples (After HANDALI, 1986)

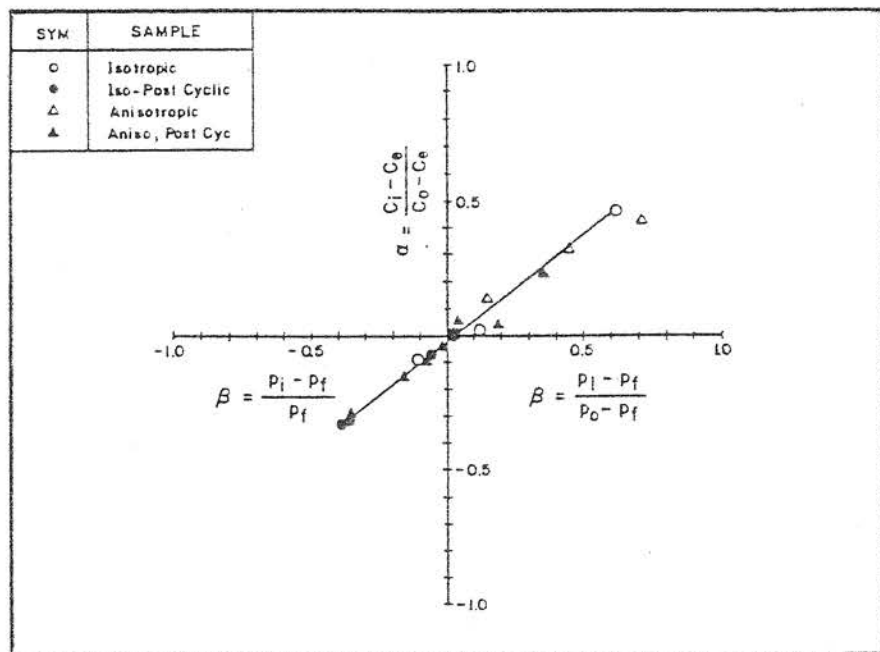


Fig. 2.1b (α, β) Plot for Isotropically Consolidated Samples and Anisotropically Consolidated Samples (After HANDALI, 1986)

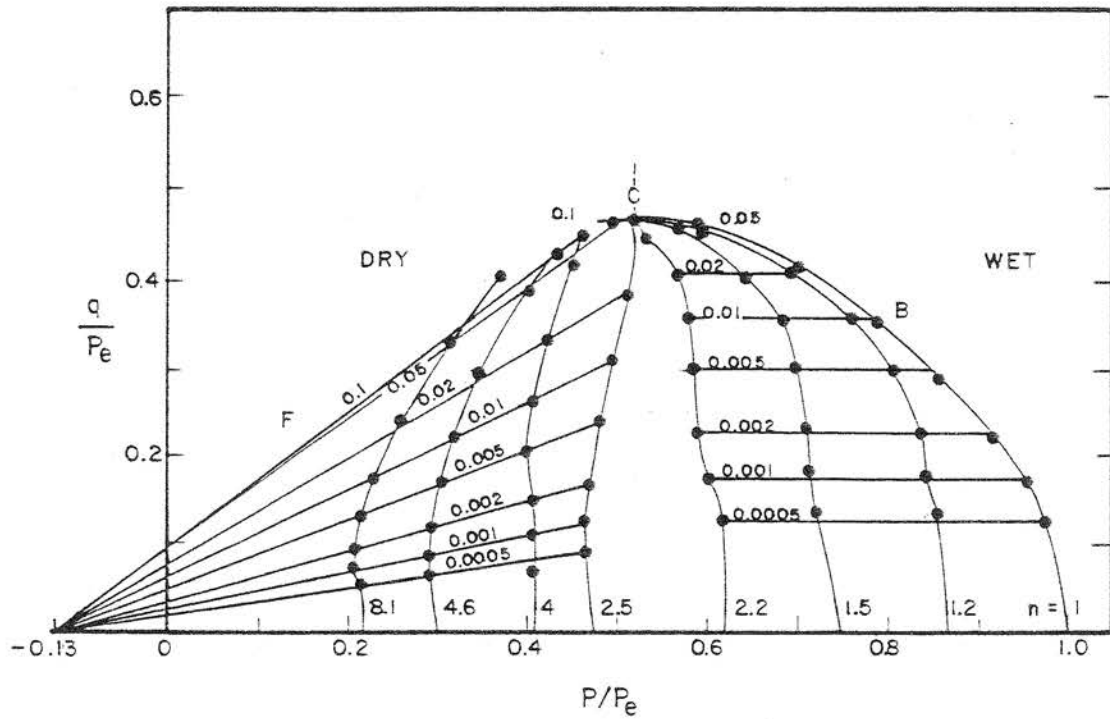


Fig. 2.2 Stress Paths and Strain Contours for Undrained Triaxial Tests on Kaolin (After WROTH and LOUDON, 1967)

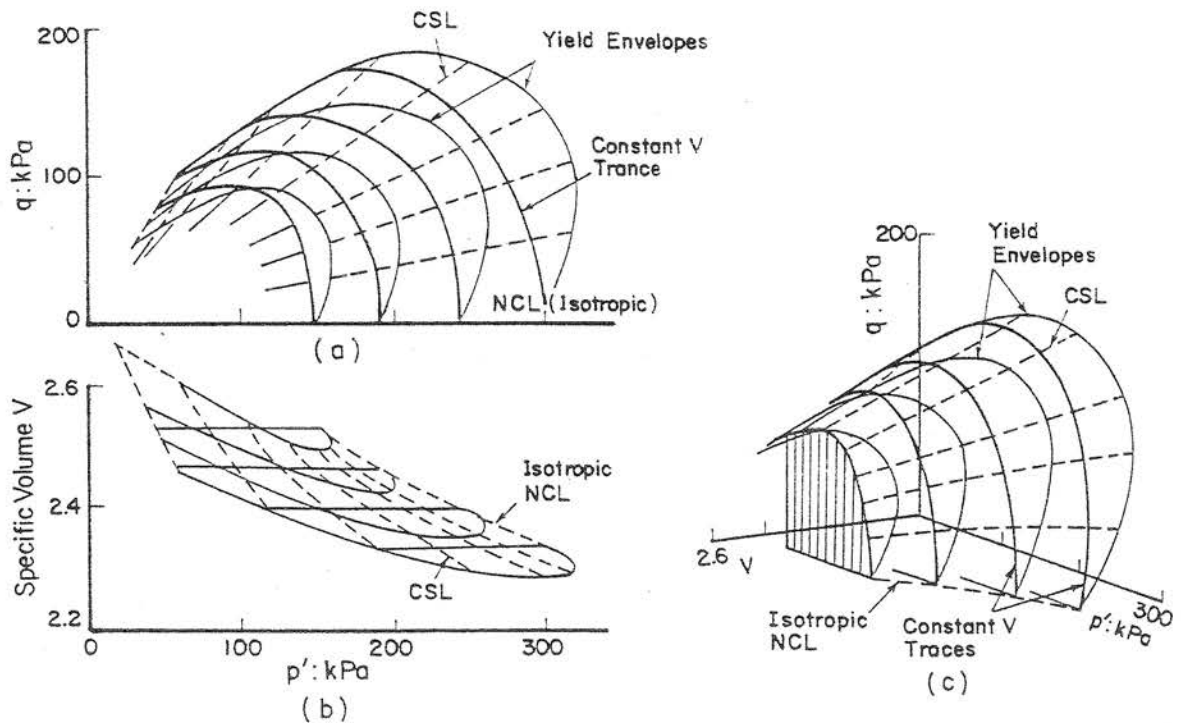


Fig. 2.3 Measured Yield Envelope for Natural Plastic Winnipeg Clay Showing Graphically Constructed V Traces and the Shape of the State Boundary Surface (After GRAHAM et al., 1988)

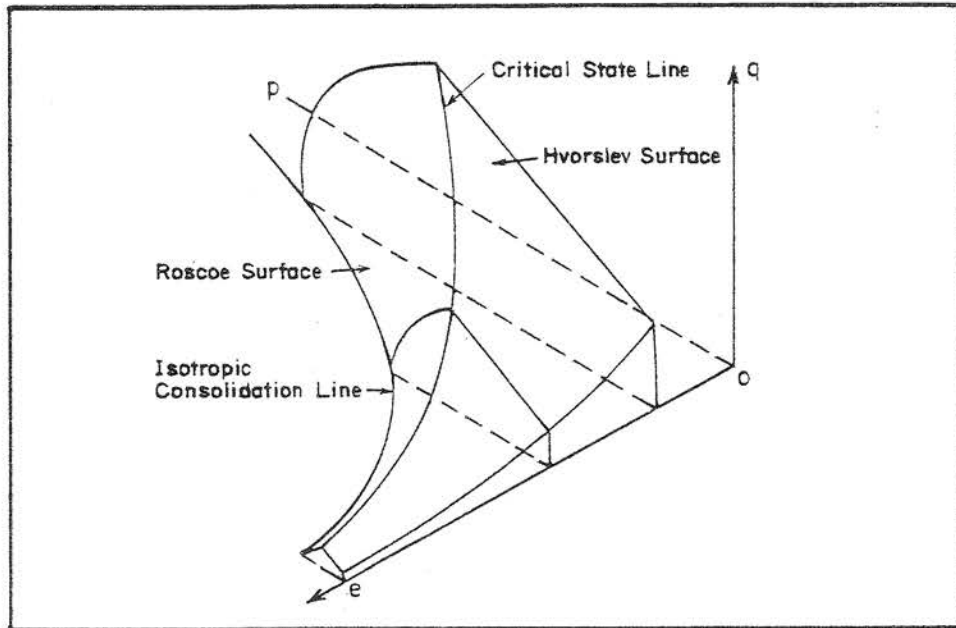


Fig. 3.1 Three Dimensional Presentation of the State Boundary Surface and the Critical State Line

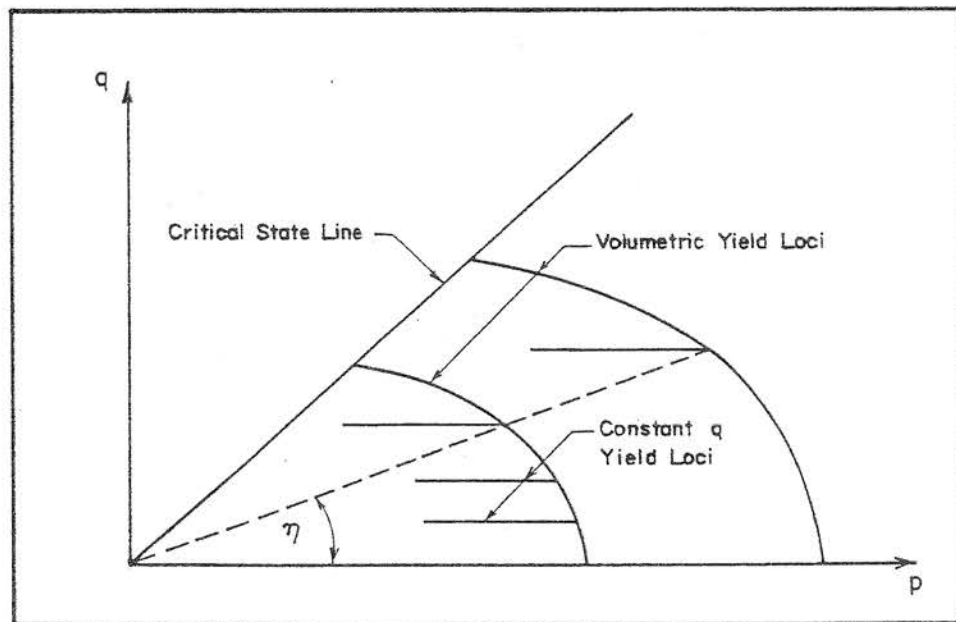


Fig. 3.2 Volumetric and Constant- q Yield Loci of ROSCOE and BURLAND (1968)

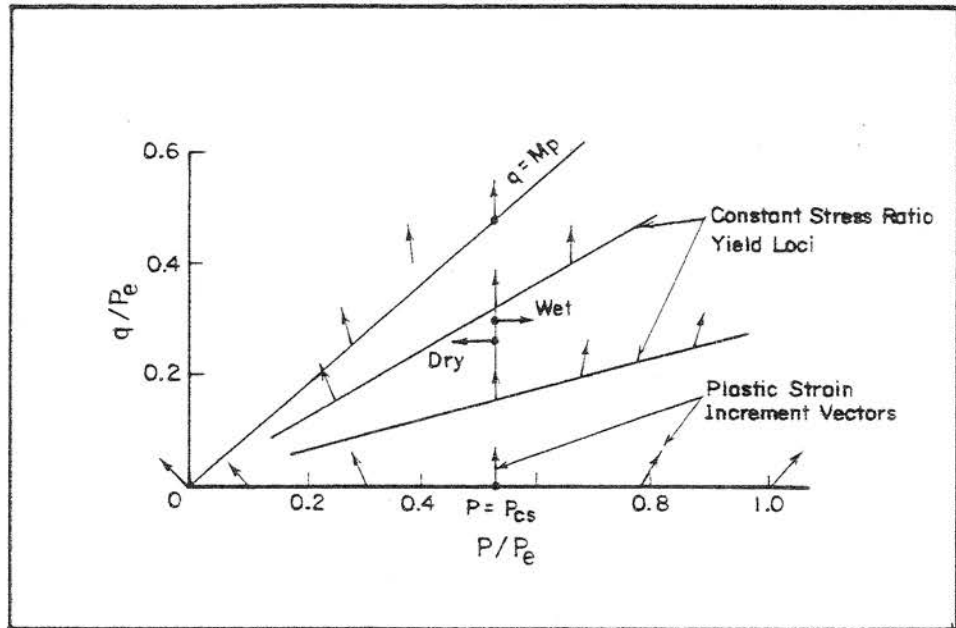


Fig. 3.3 Direction of Plastic Strain Increment Vectors
(After PENDER, 1978)

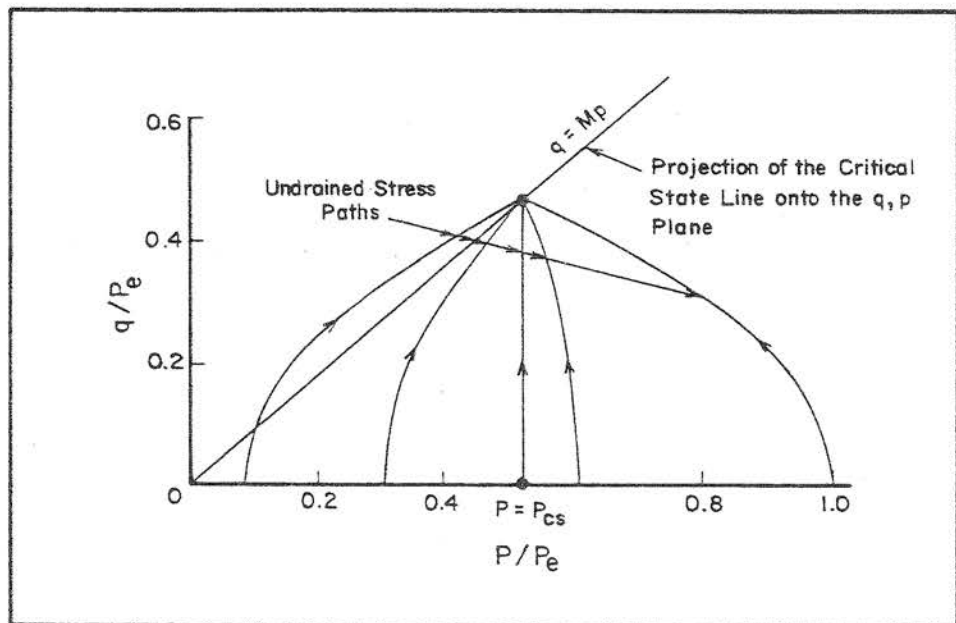


Fig. 3.4 Parabolic Undrained Stress Path for Various OCR Values
(After PENDER, 1978)

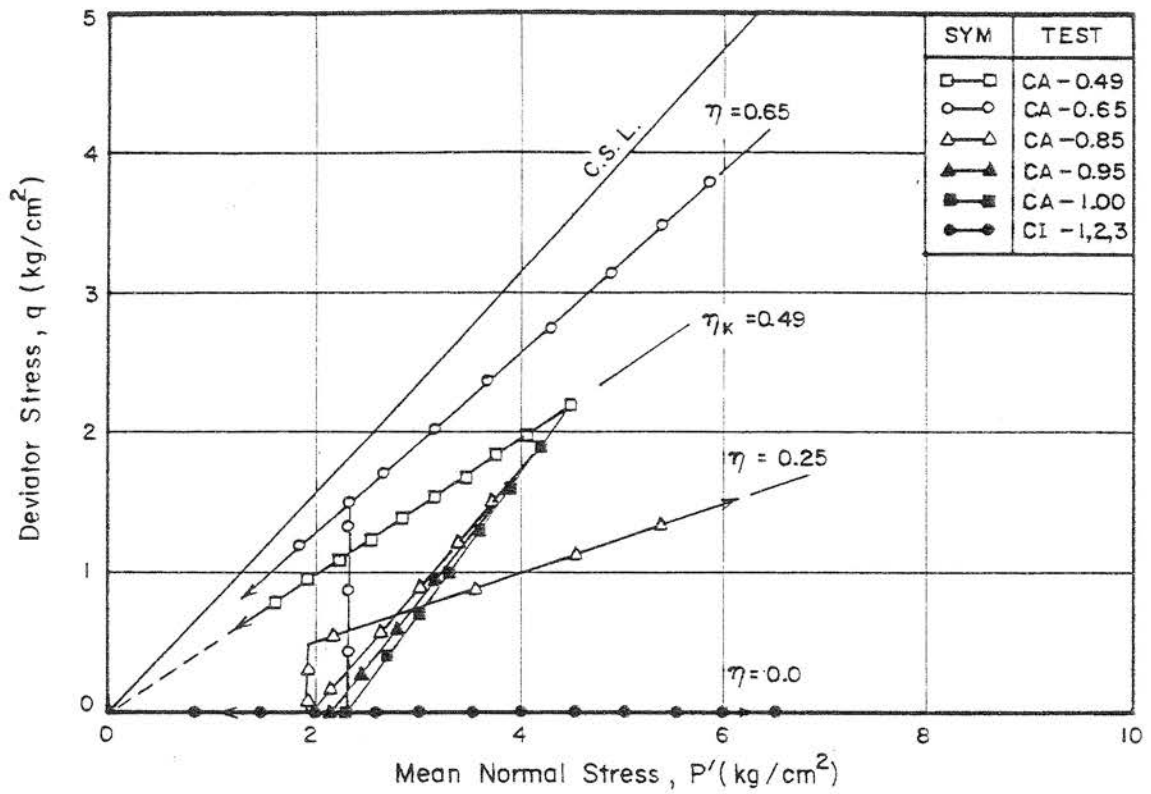


Fig. 4.1 Schematic Diagram of Consolidation Process

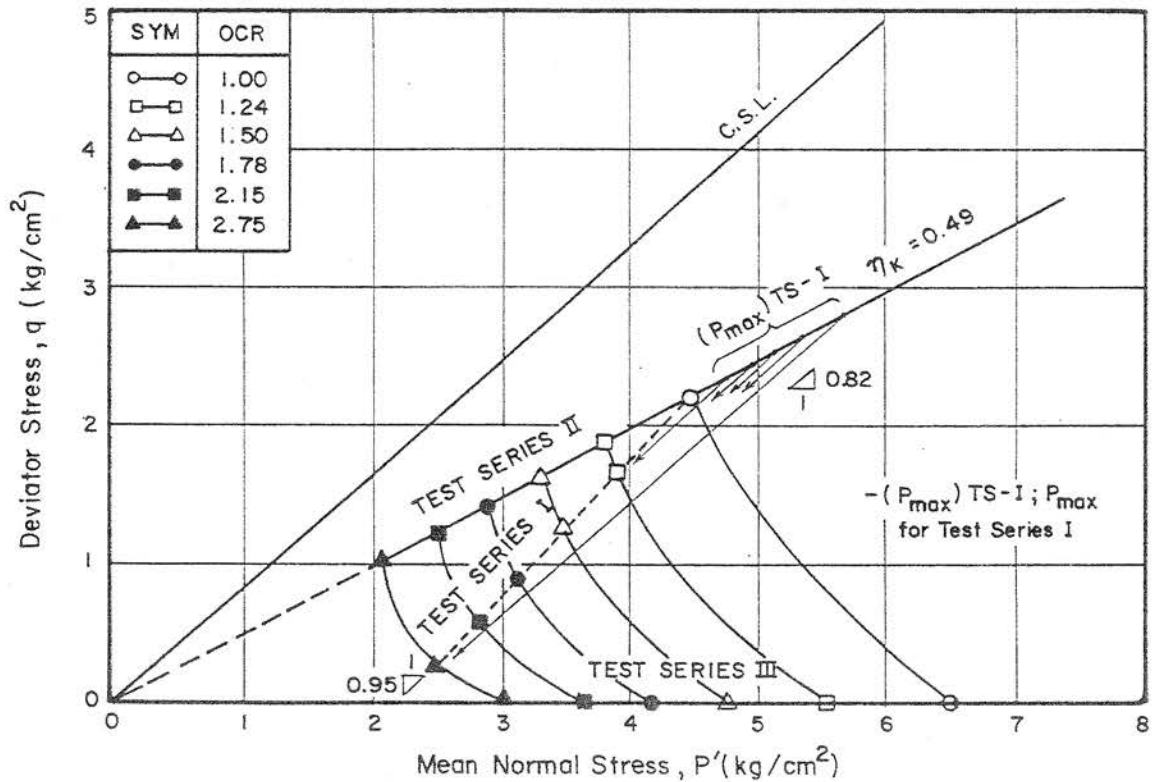


Fig. 4.2 Initial Stress Points of Test Series I, II & III

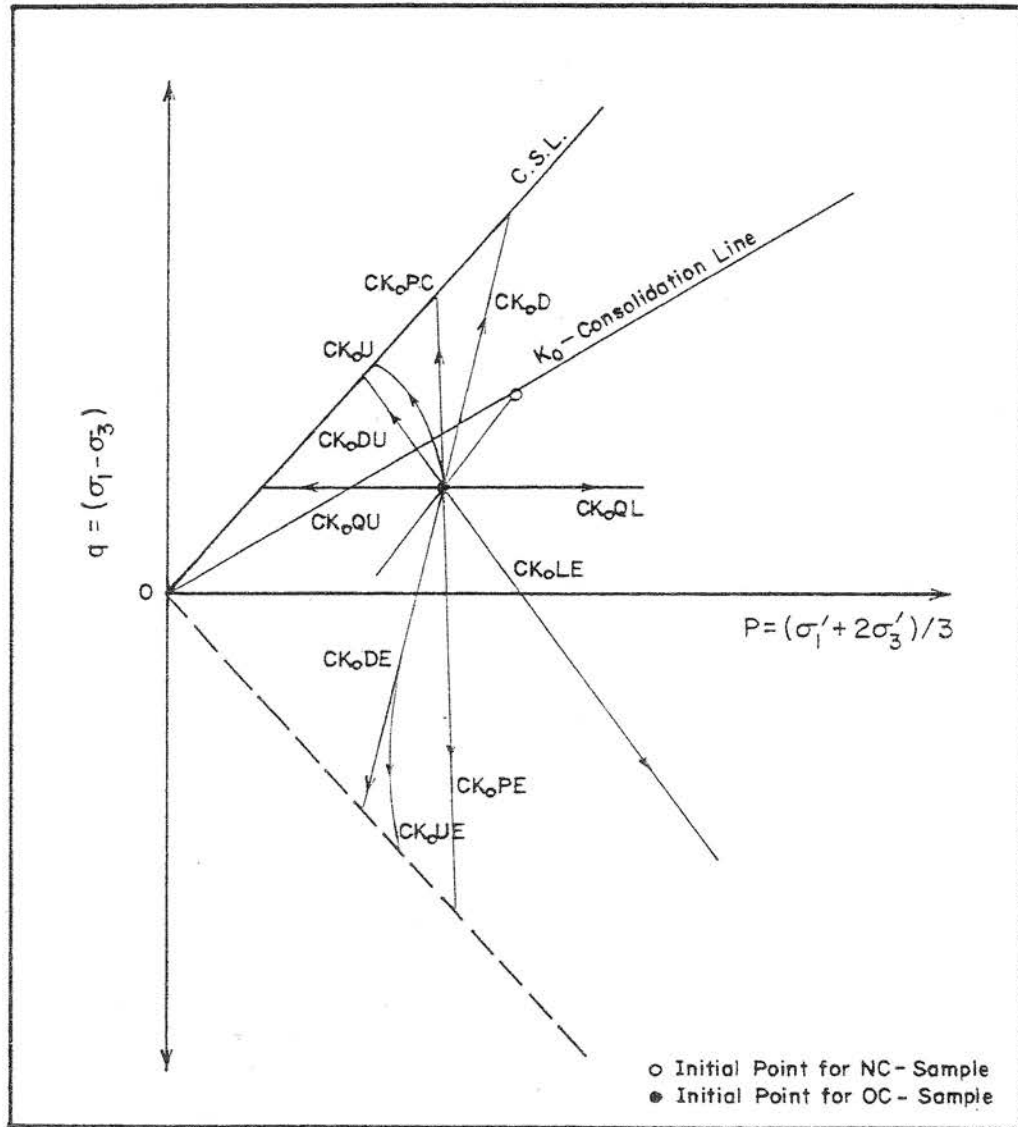


Fig. 4.3 Typical Stress Paths followed in this Investigation of the Behaviour of Lightly Overconsolidated Clay (Test Series, I)

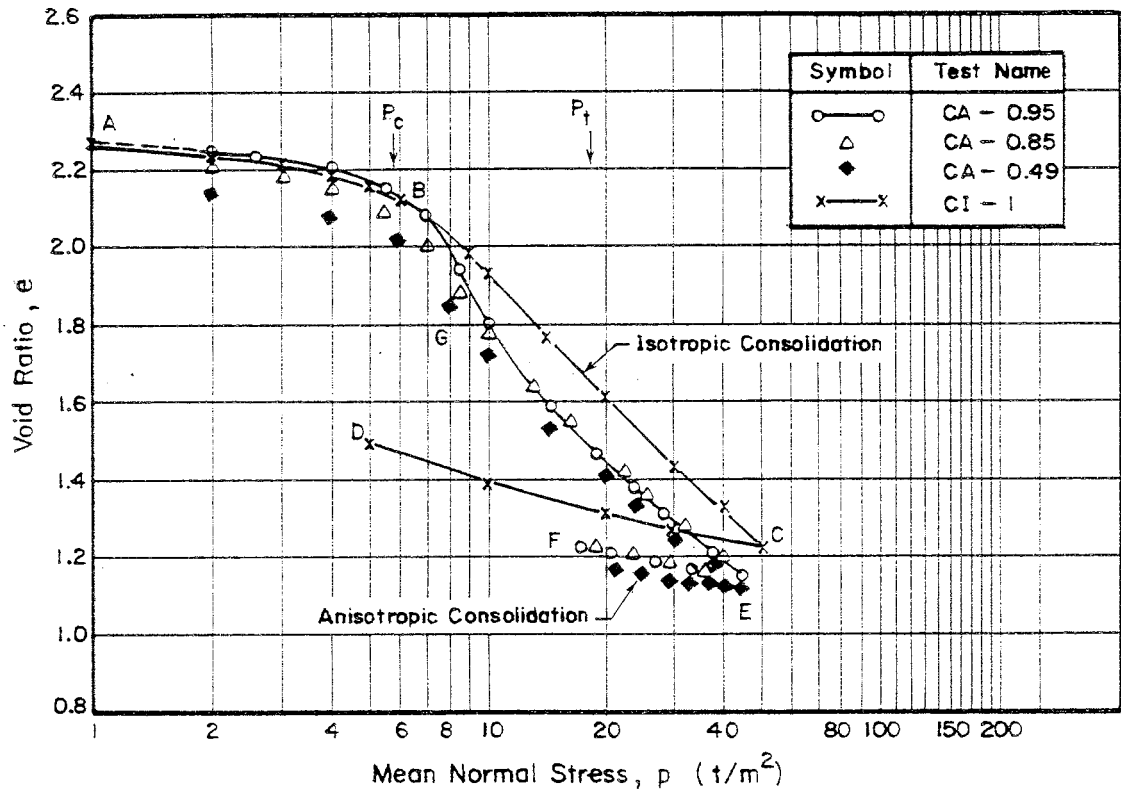


Fig. 5. 1 Typical Consolidation and Swelling Curves

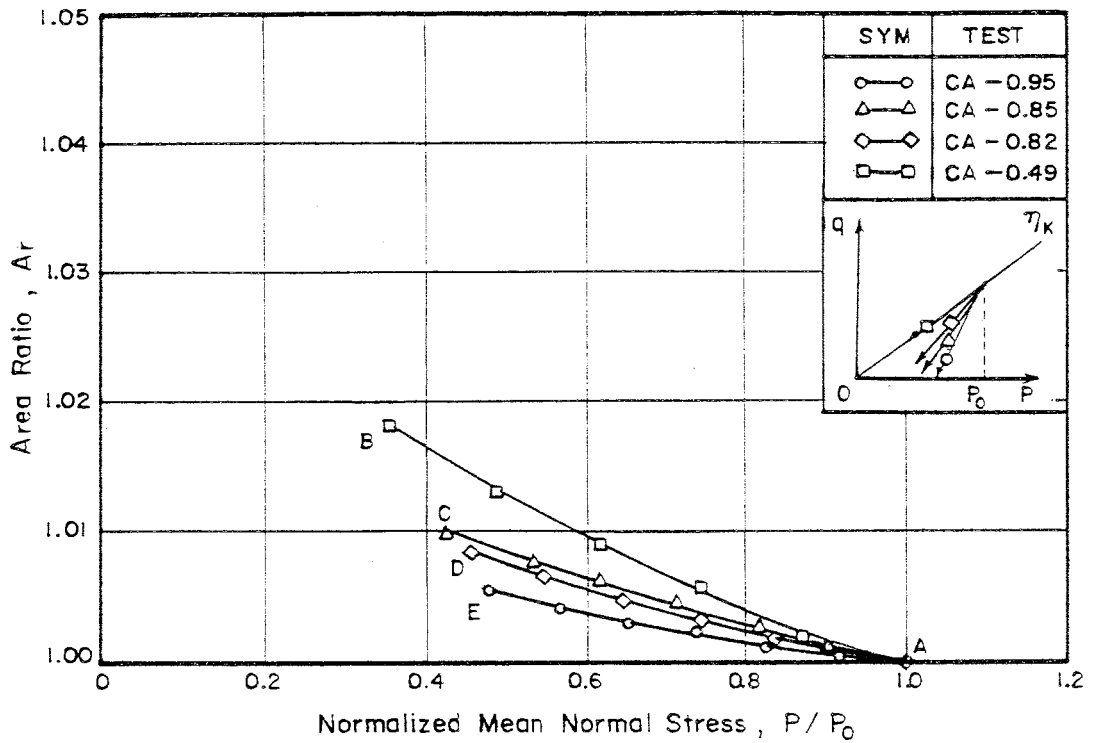


Fig. 5. 2 Variation of Cross-Sectional Area in Swelling Process

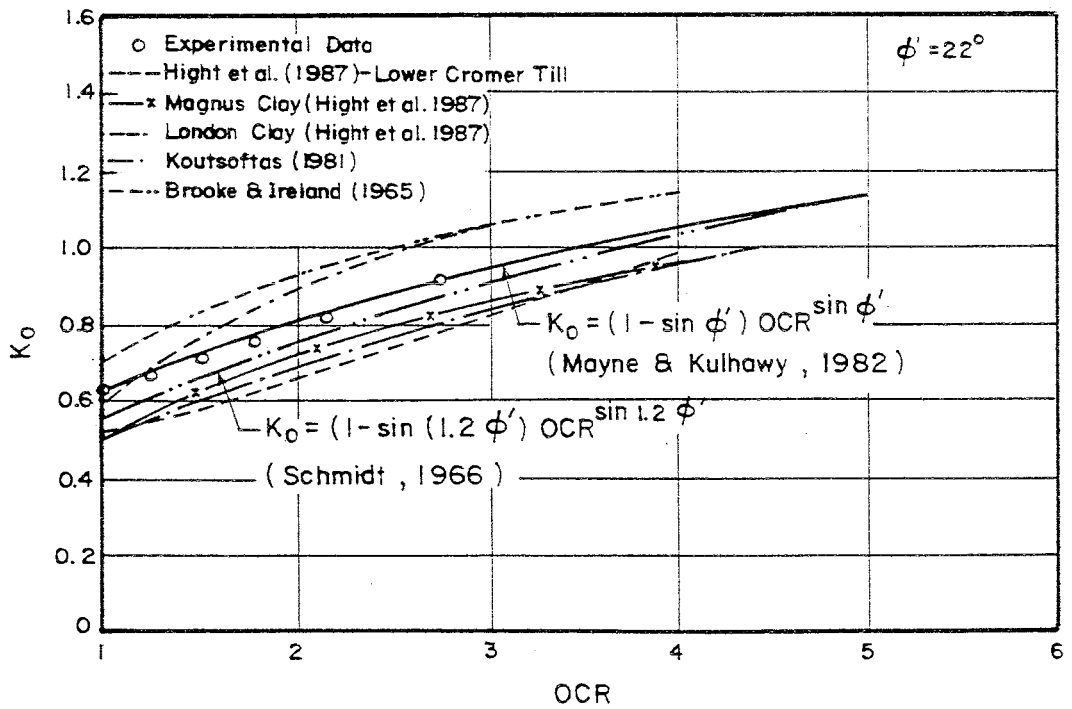


Fig. 5. 3a Relationship between K_0 and OCR

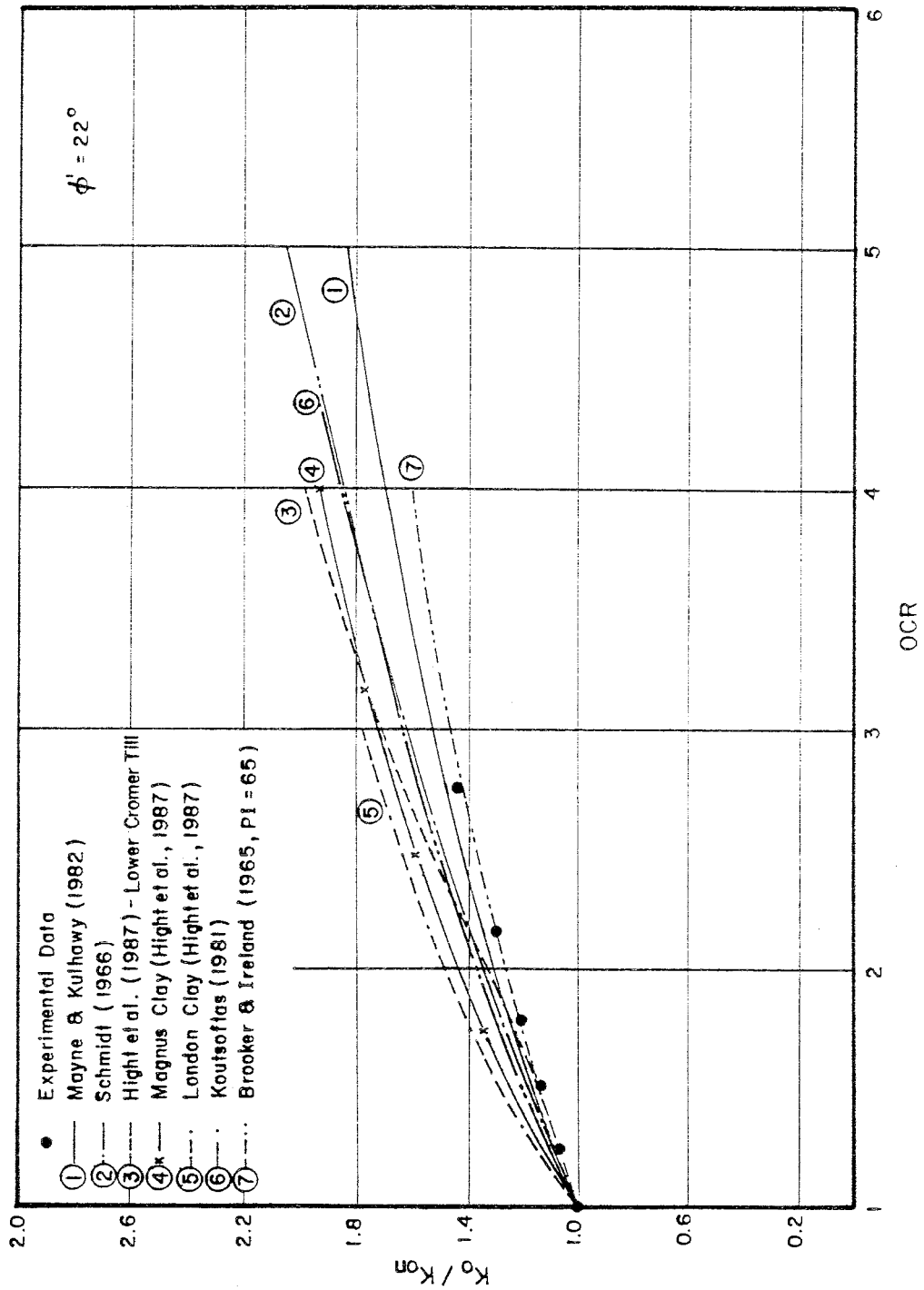


Fig. 5. 3b Relationship between Normalized K_0 and OCR

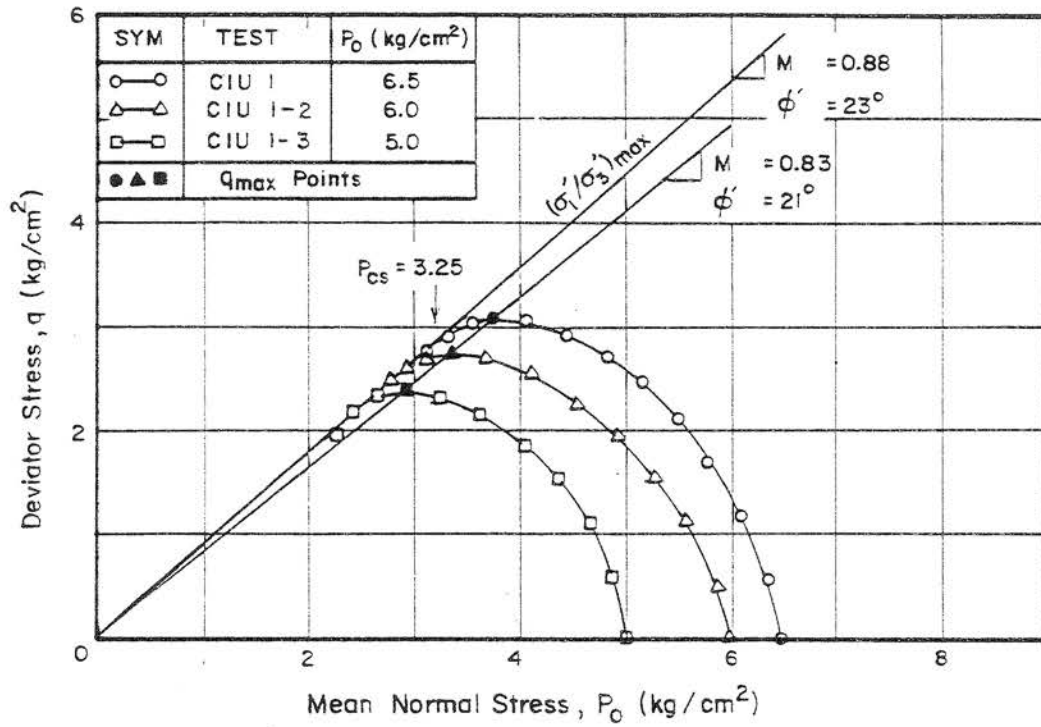


Fig. 5. 4 Undrained Stress Paths of Normally Consolidated Samples at Different Isotropic Stresses

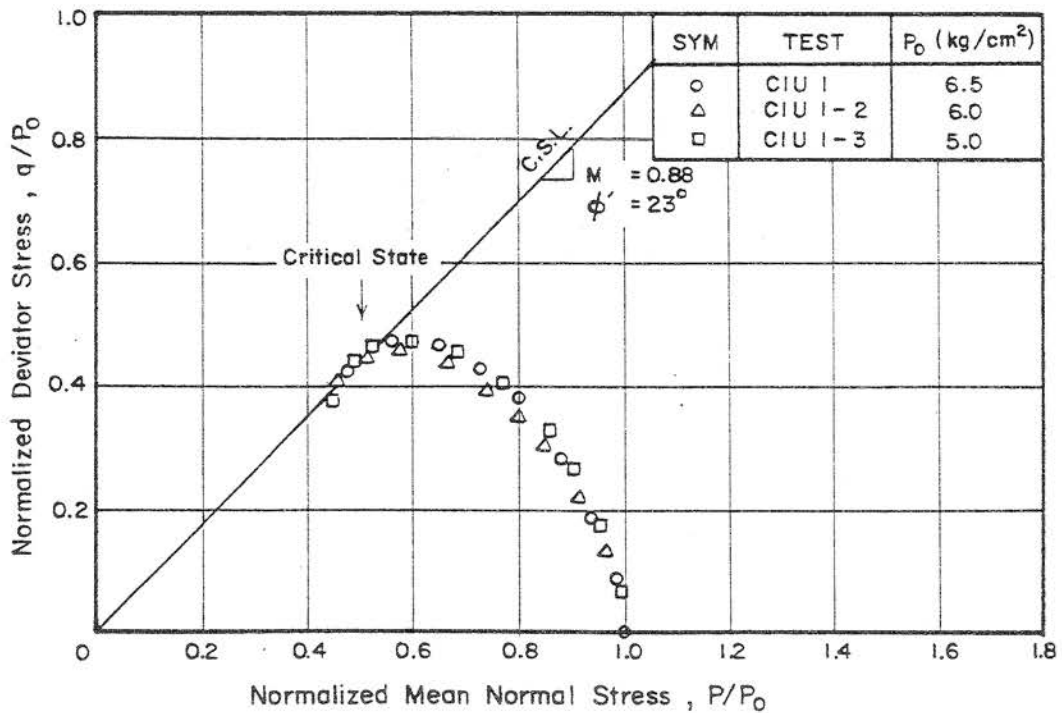


Fig. 5. 5 Normalized Undrained Stress Paths of Normally Consolidated Samples under Isotropic Stress

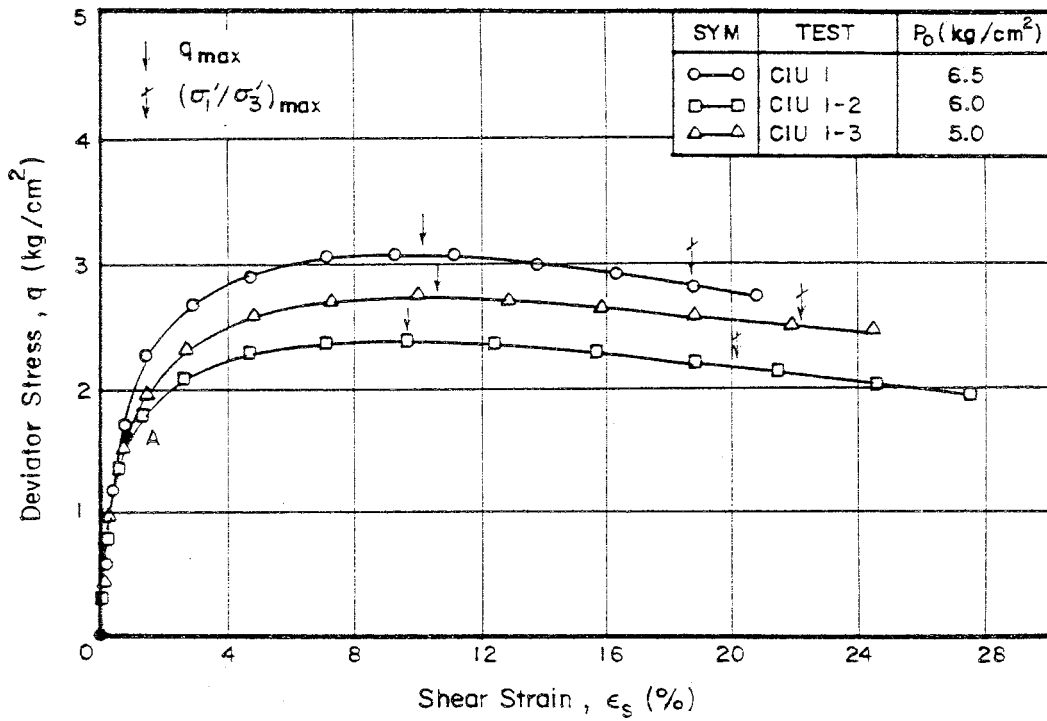


Fig. 5. 6 (q , ϵ_s) Plot for Normally Consolidated Samples under Isotropic Stress

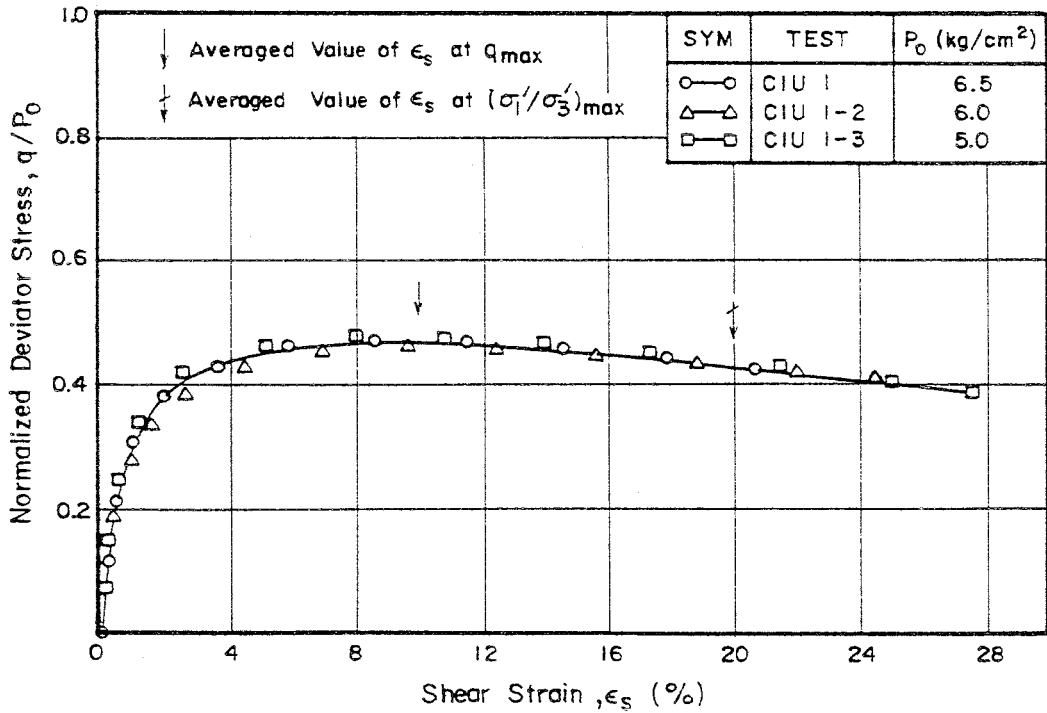


Fig. 5. 7 (q/p_0 , ϵ_s) Plot for Normally Consolidated Samples under Isotropic Stress

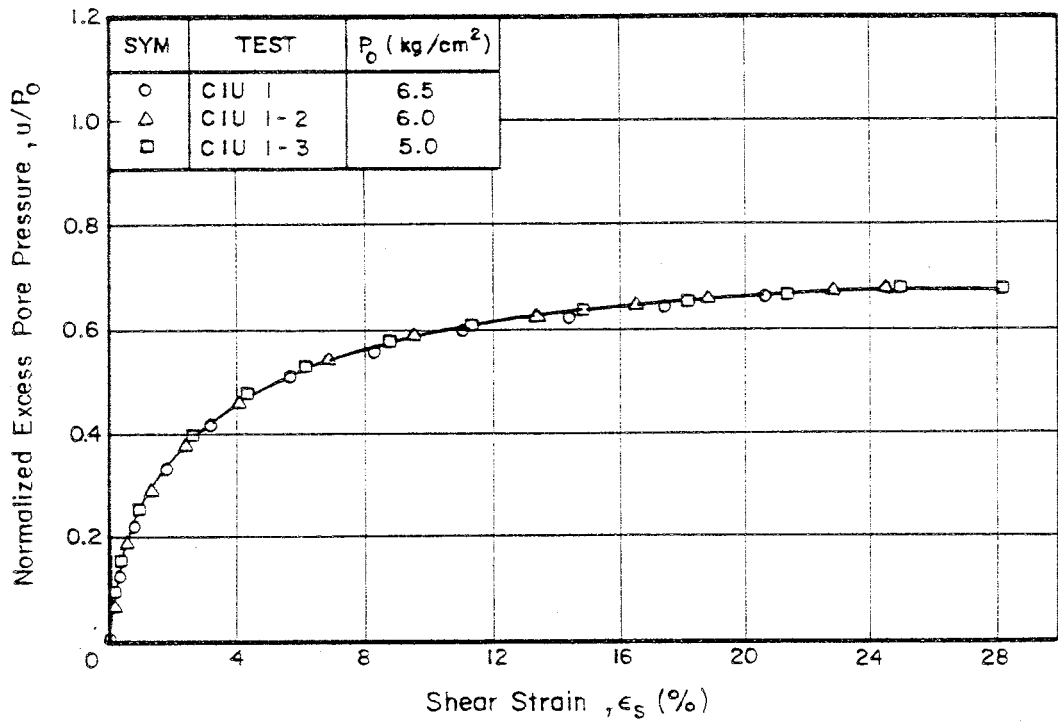


Fig. 5. 8 (u/p_0 , ϵ_s) Plot for Normally Consolidated Samples under Isotropic Stress

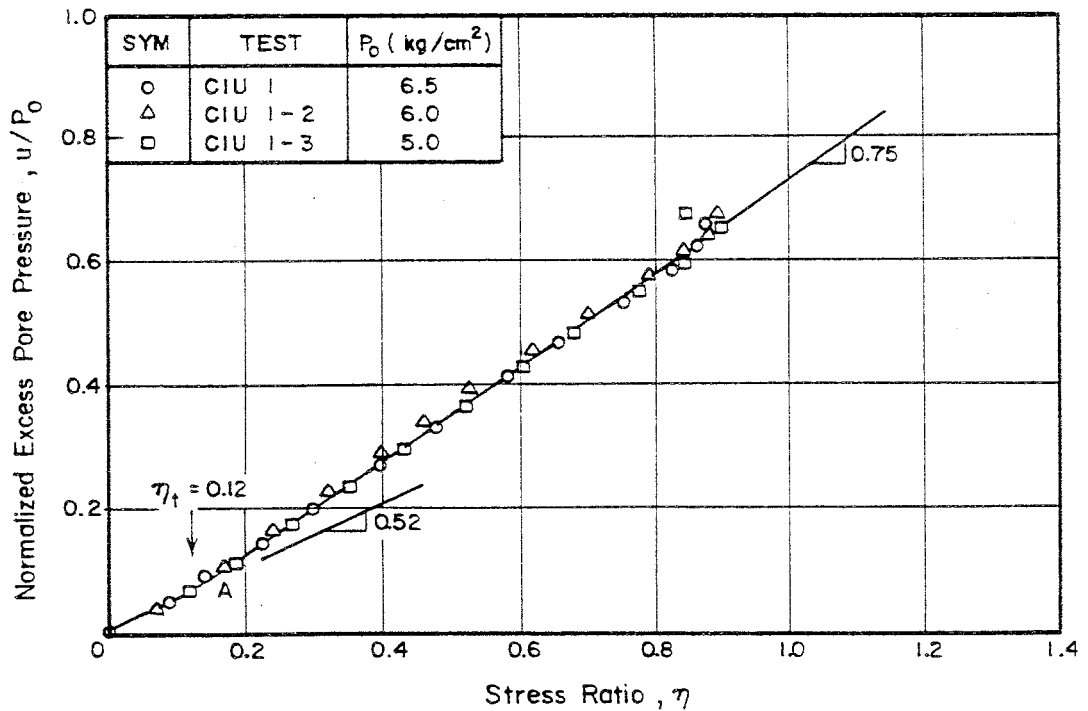


Fig. 5. 9 (u/p_0 , η) Plot for Normally Consolidated Samples under Isotropic Stress

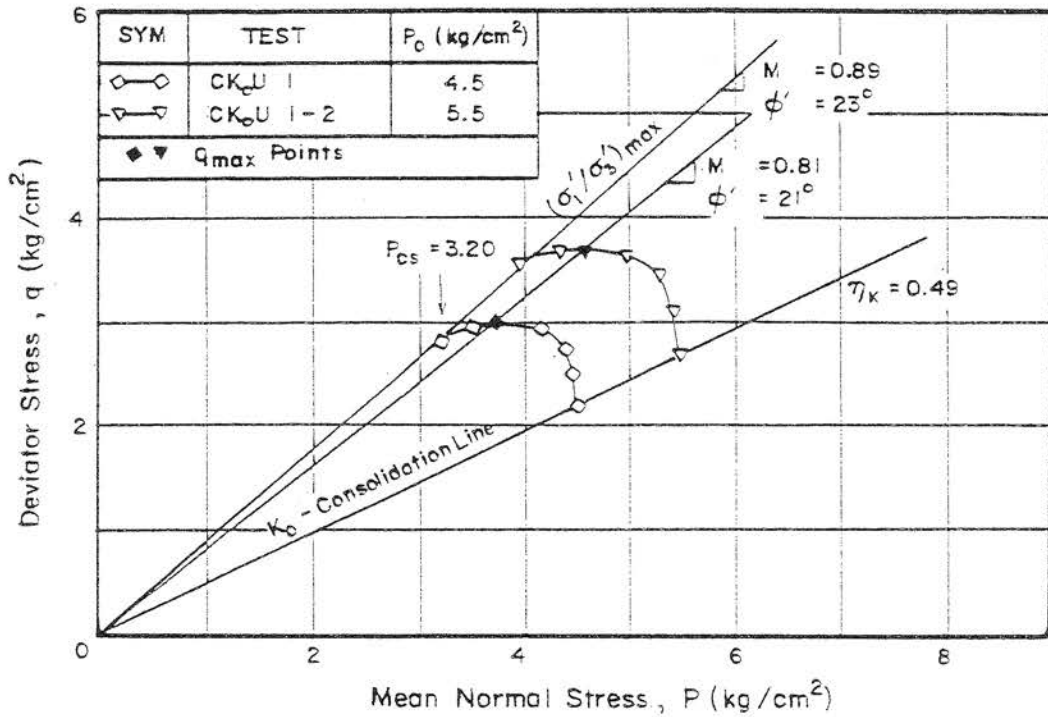


Fig. 5.10 Undrained Stress Paths of K_0 -normally Consolidated Samples in Triaxial Compression

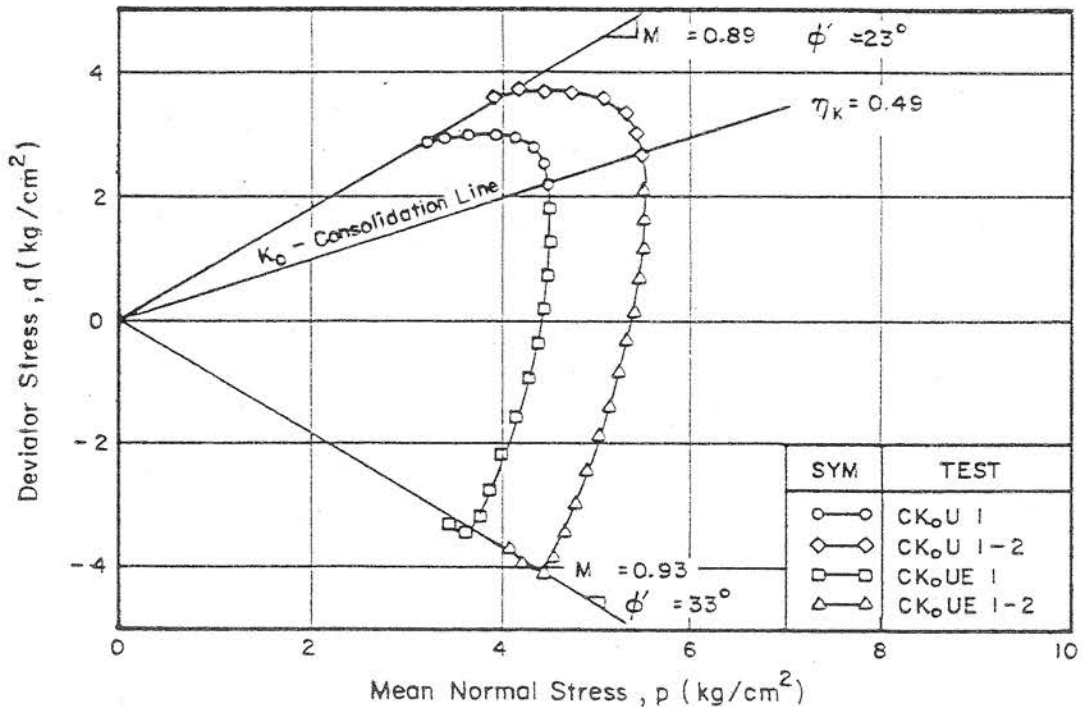


Fig. 5.11 Undrained Stress Paths of K_0 -normally Consolidated Sample both in Triaxial Compression and Extension

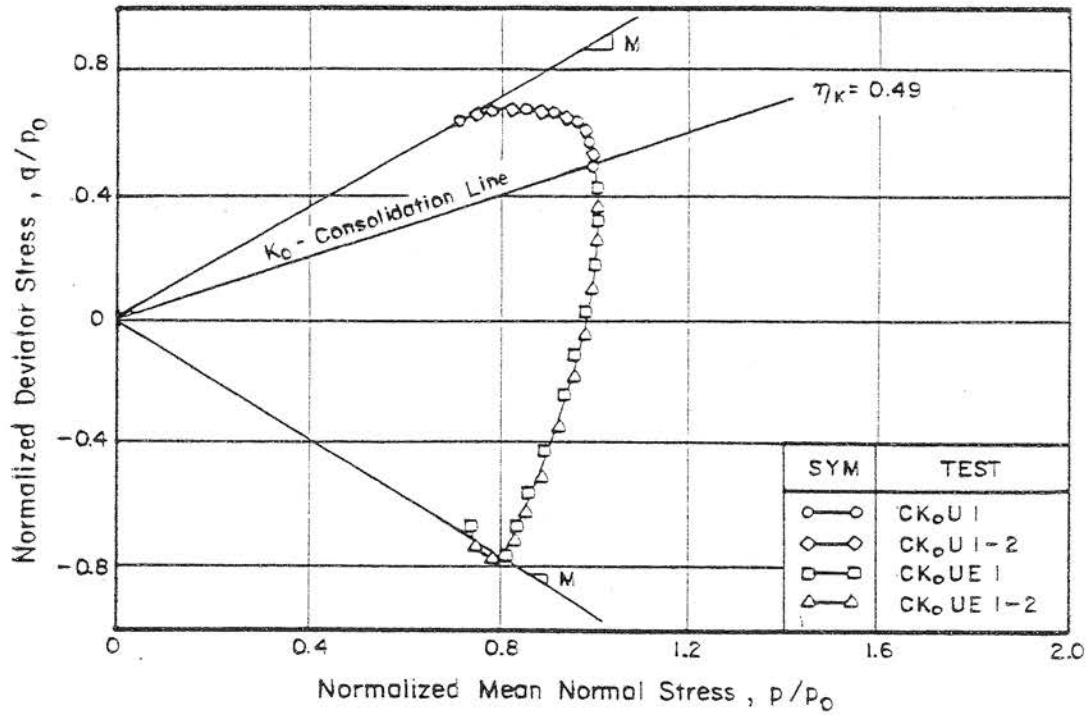


Fig. 5.12 Normalized Undrained Stress Paths of K_0 -normally Consolidated Sample both in Triaxial Compression and Extension

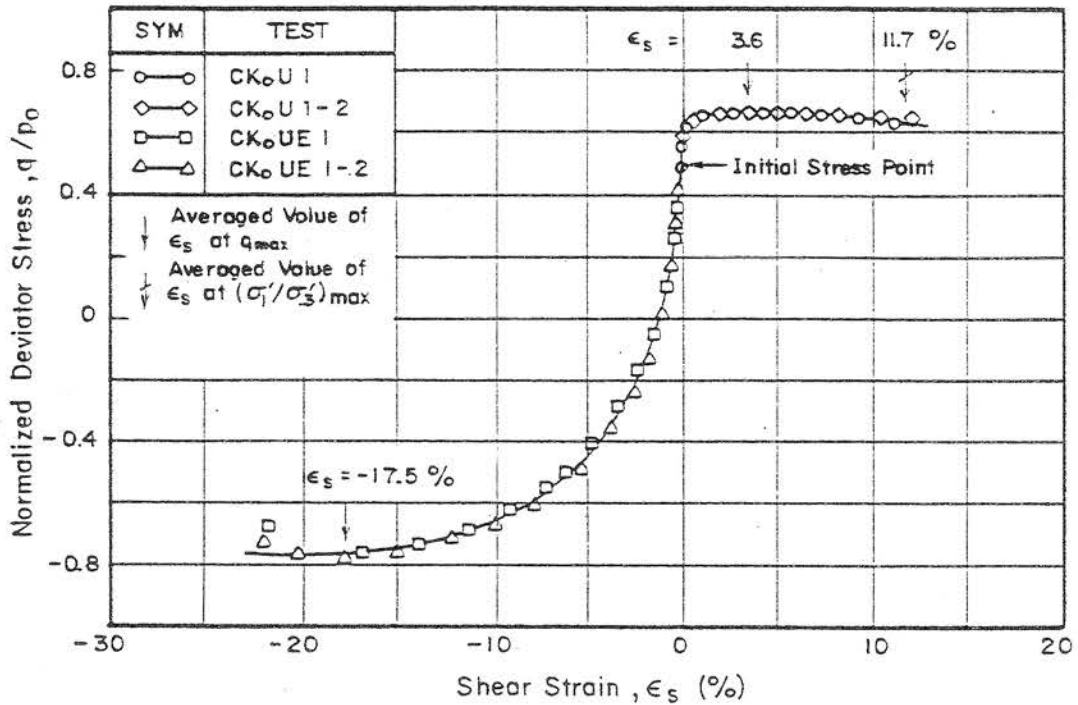


Fig. 5.13 $(q/p_0, \epsilon_s)$ Plot for K_0 -normally Consolidated Samples both in Triaxial Compression and Extension

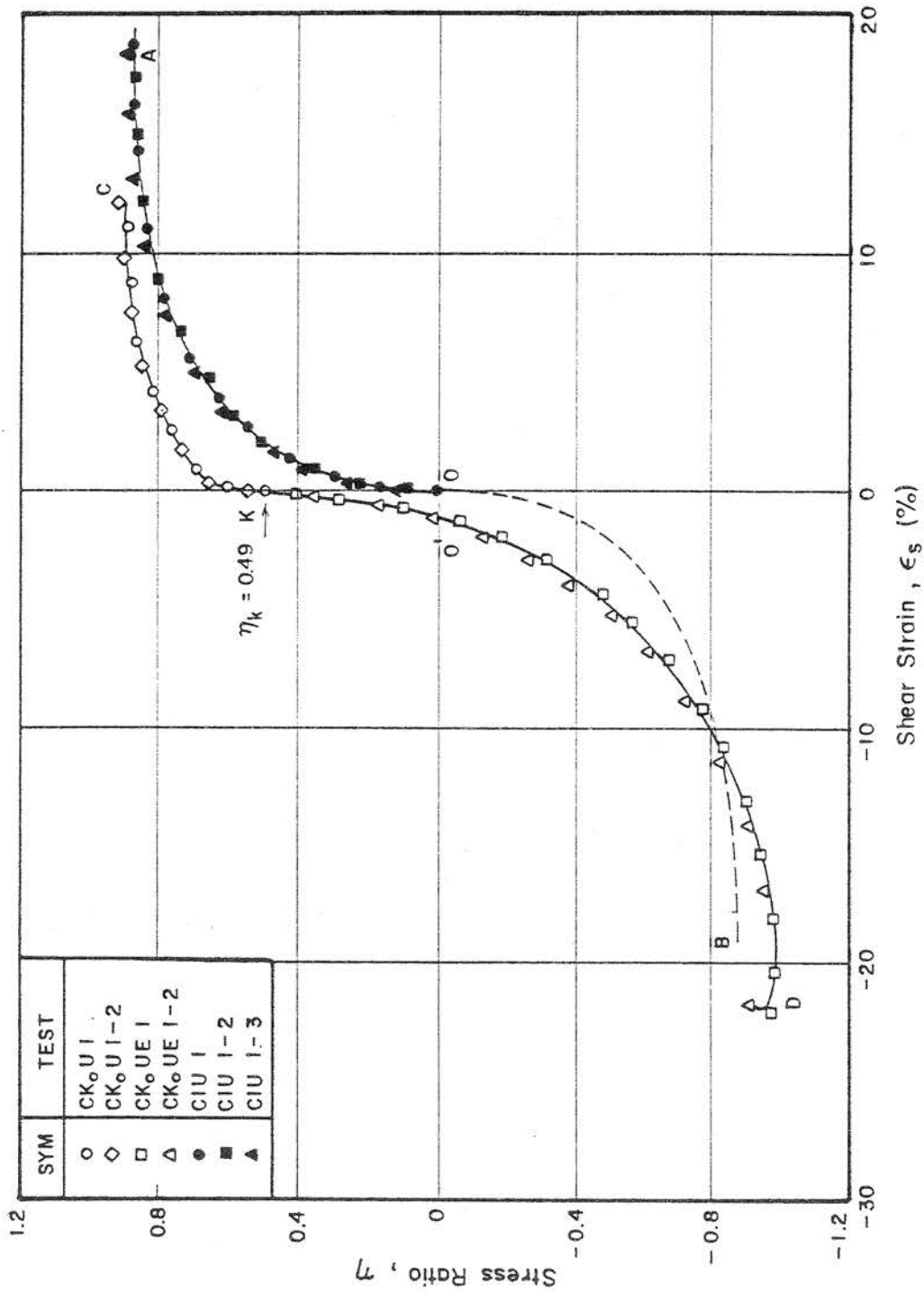


Fig. 5.14 (η , ϵ_s) Plot for Normally Consolidated Sample under K_o and Isotropic Stresses

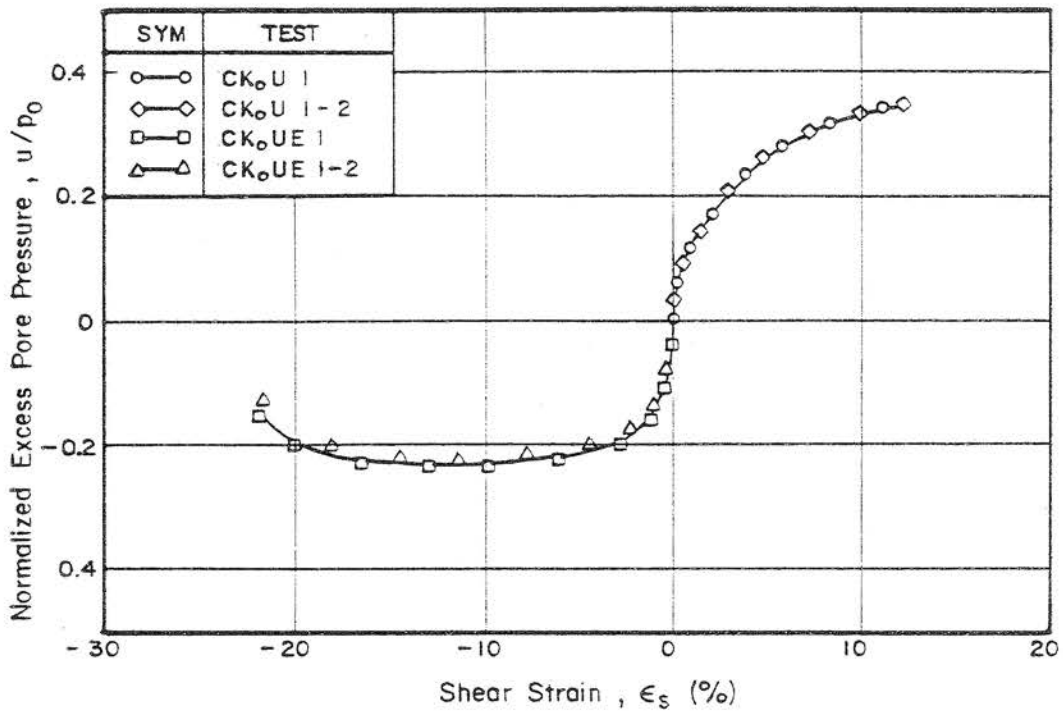


Fig. 5.15 (u/p_0 , ϵ_s) Plot for K_0 -normally Consolidated Samples both in Triaxial Compression and Extension

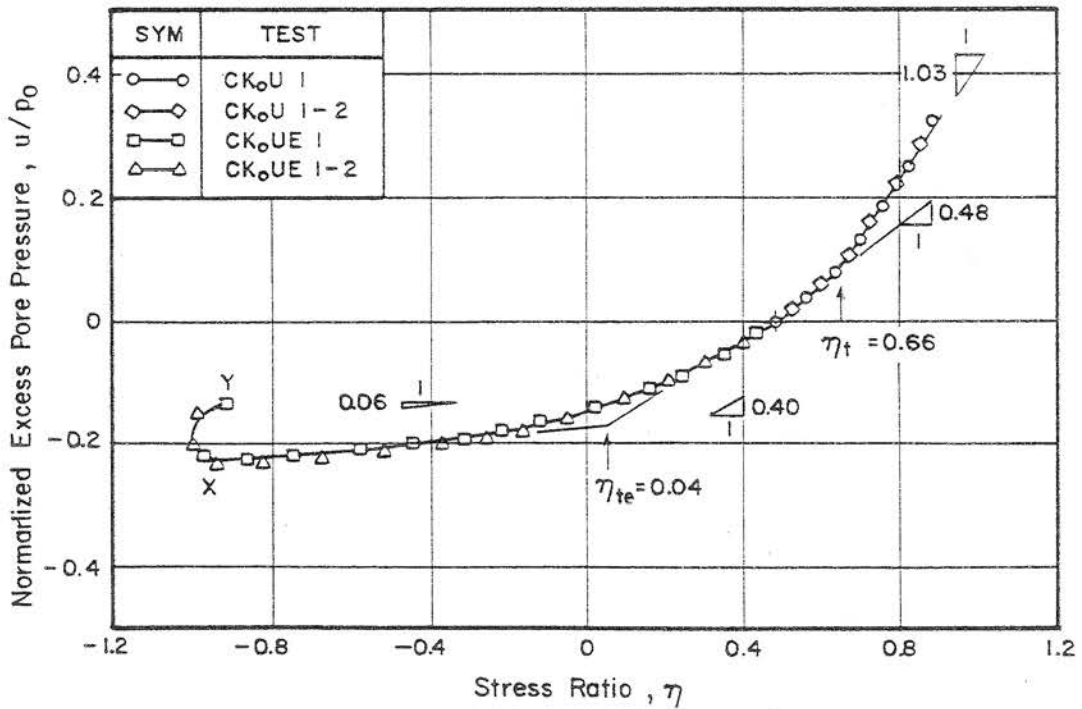


Fig. 5.16 (u/p_0 , η) Plot for K_0 -normally Consolidated Samples both in Triaxial Compression and Extension

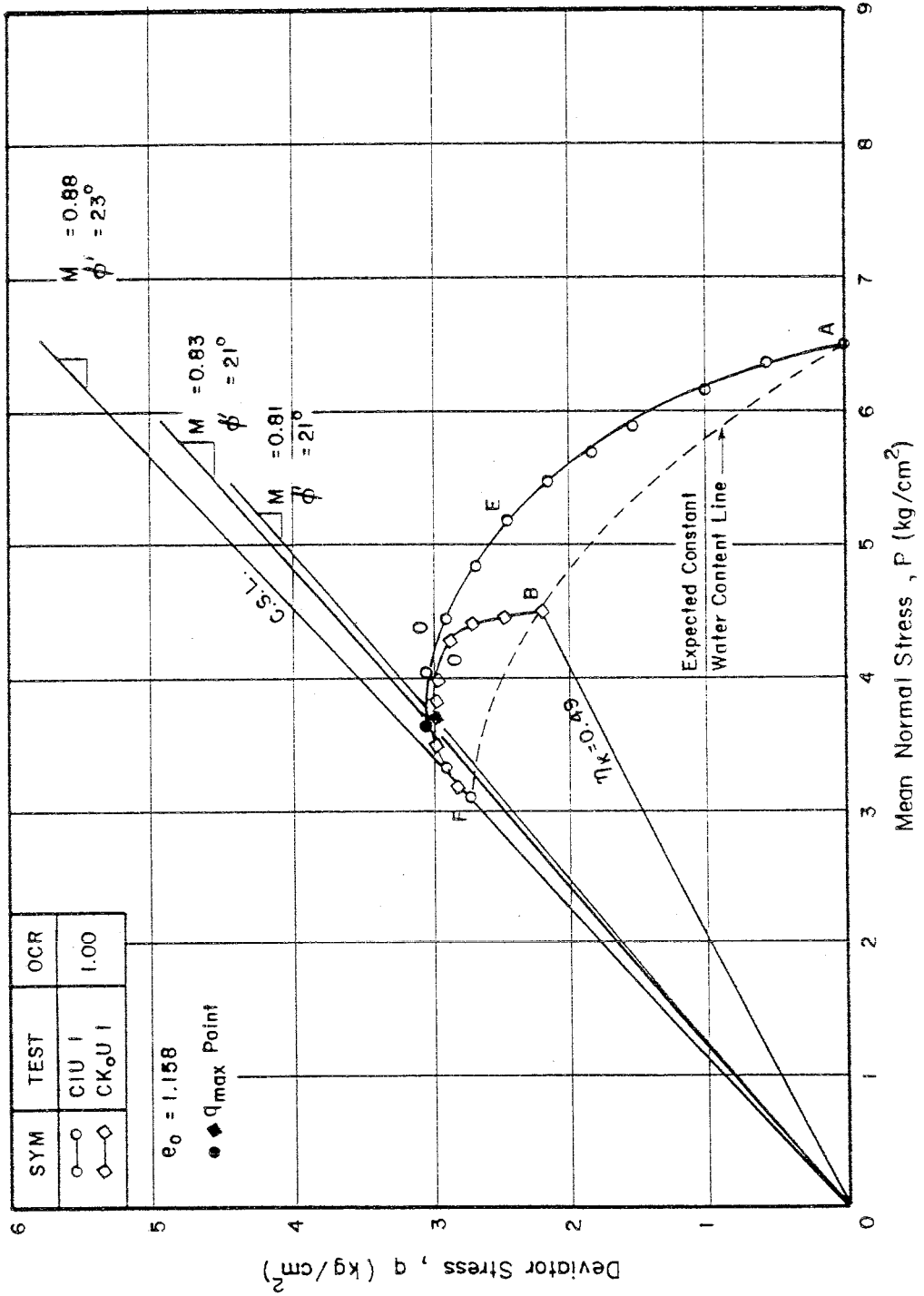


Fig. 5.17 Undrained Stress Paths of K_0 and Isotropically Consolidated Samples

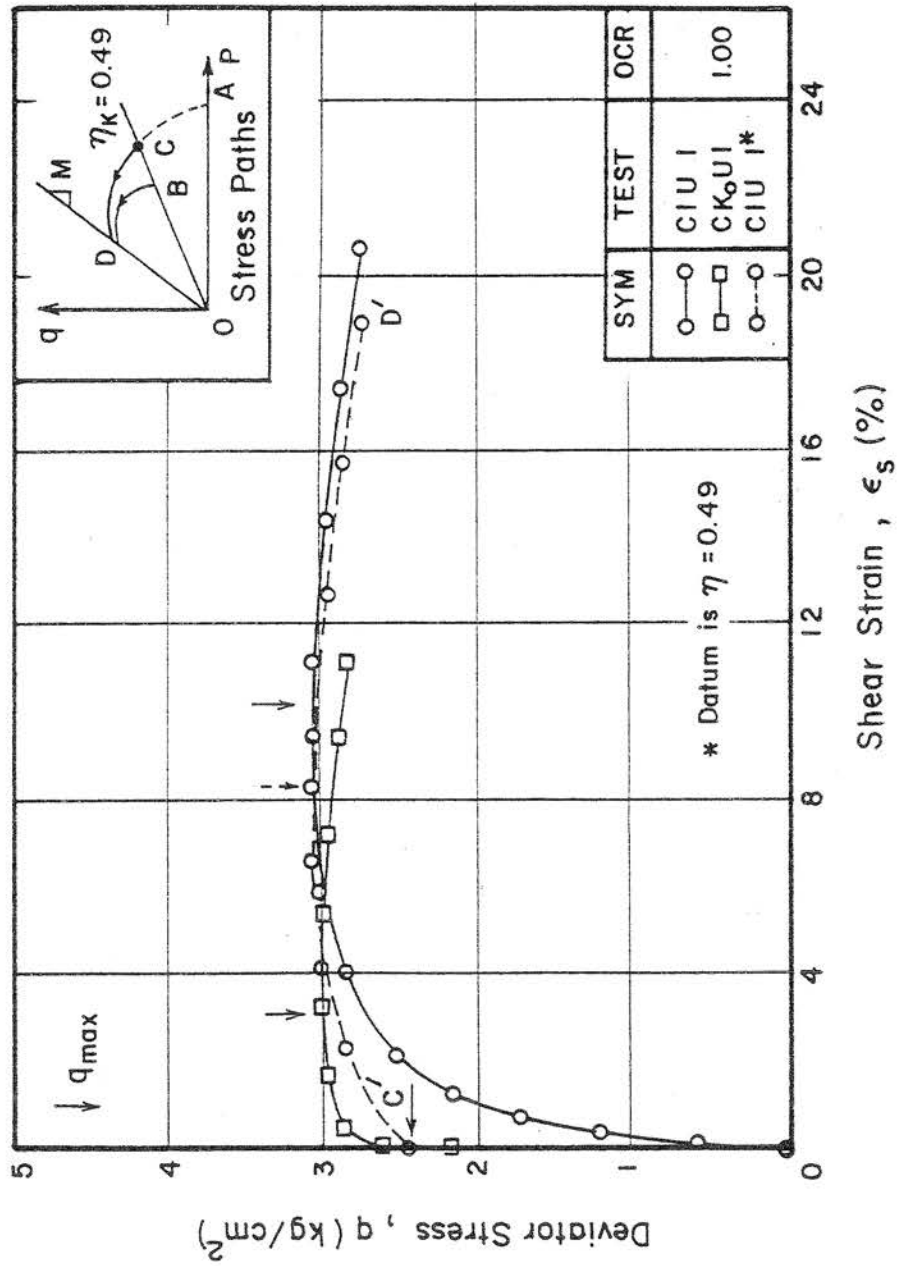


Fig. 5.18 (q , ϵ_s) Plot for K_o and Isotropically Consolidated Samples

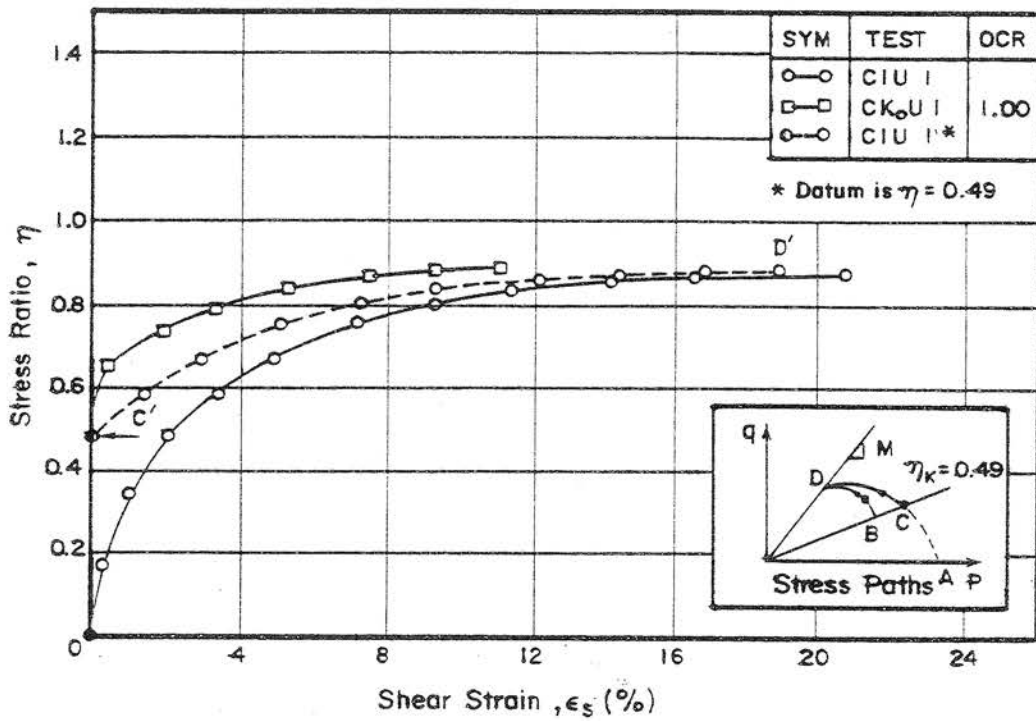


Fig. 5.19 (η, ϵ_s) Plot for K_0 and Isotropically Consolidated Samples

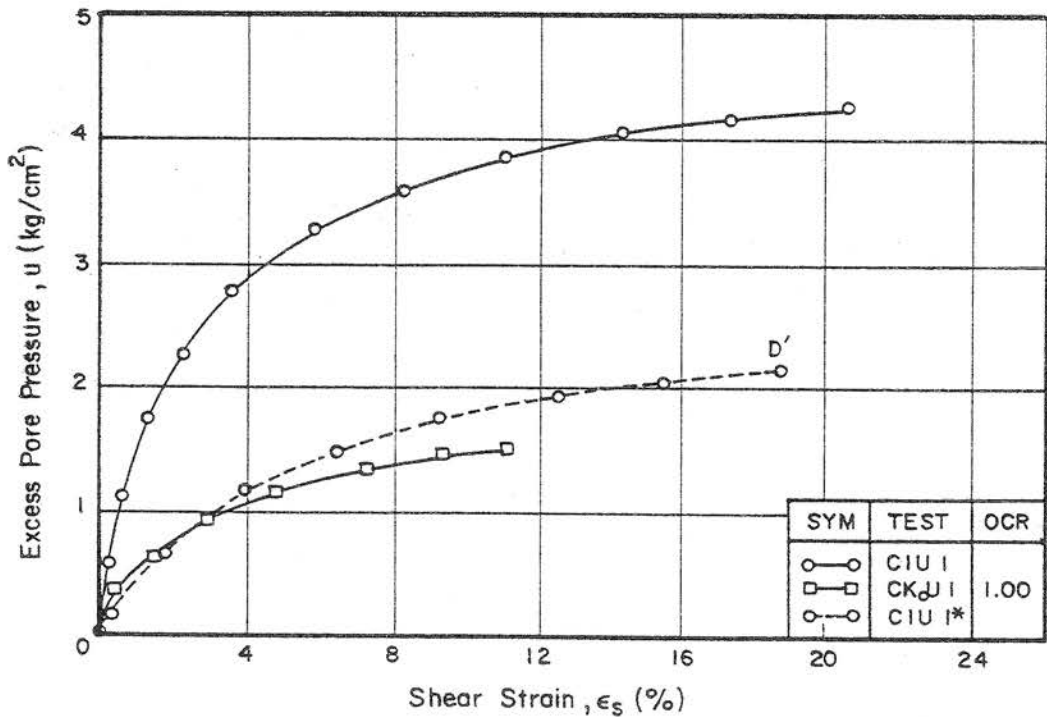


Fig. 5.20 (u, ϵ_s) Plot for K_0 and Isotropically Consolidated Samples

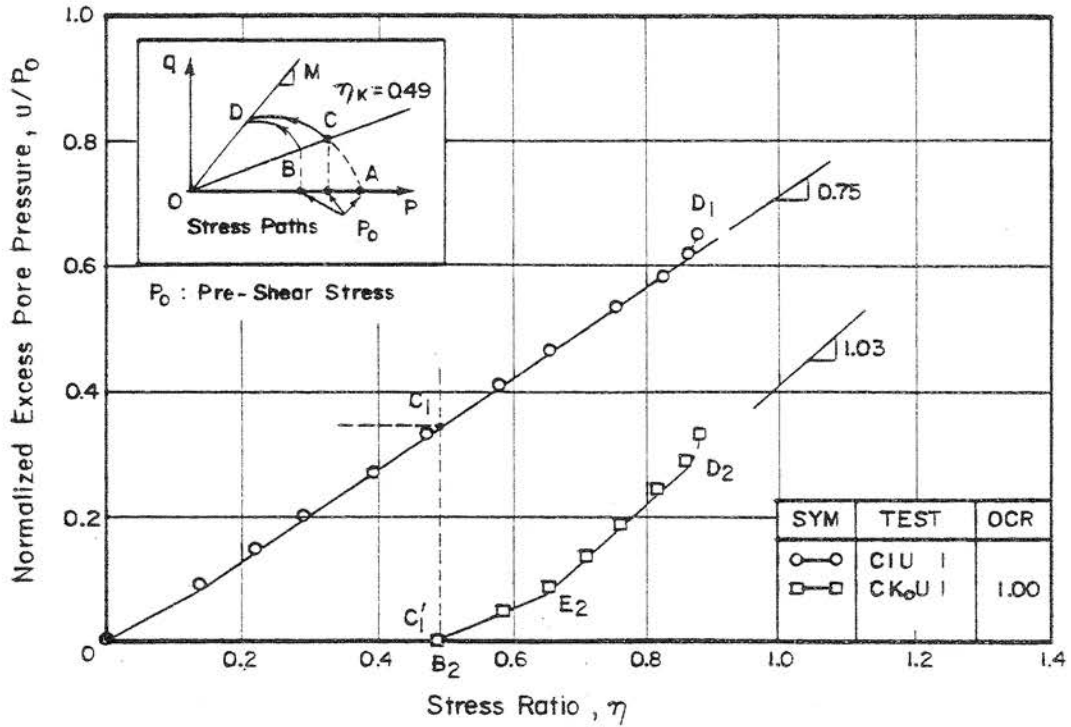


Fig. 5.21 ($u/p_0, \eta$) Plot for K_0 and Isotropically Consolidated Samples beyond K_0 State

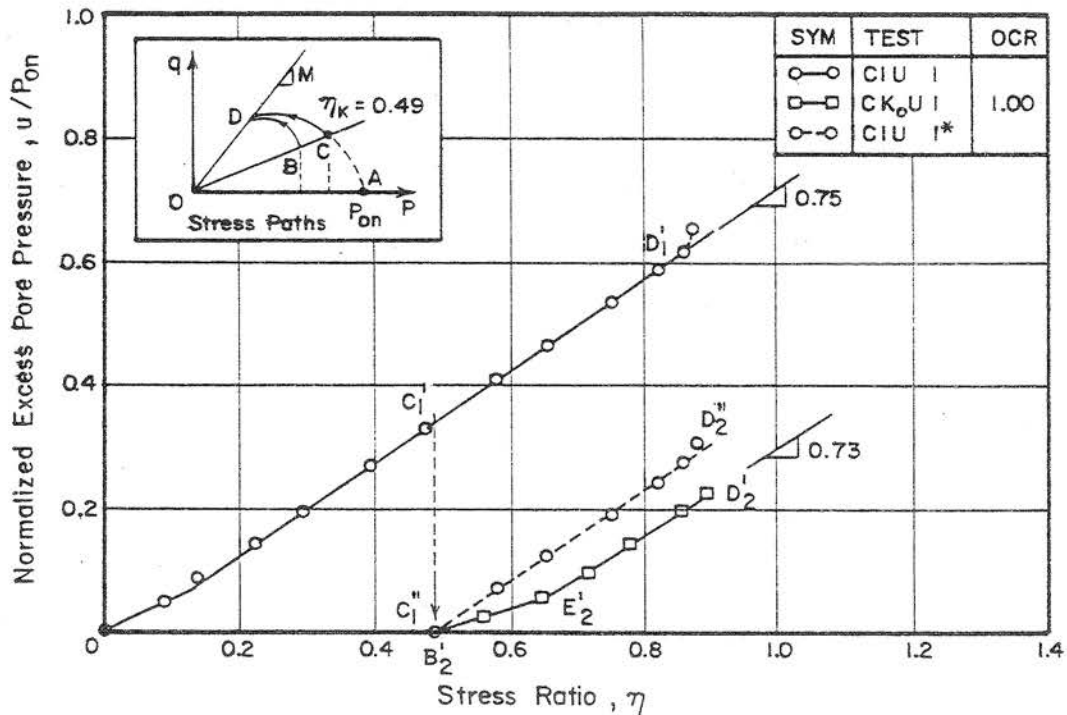


Fig. 5.22 ($u/p_{on}, \eta$) Plot for K_0 and Isotropically Consolidated Samples beyond K_0 State

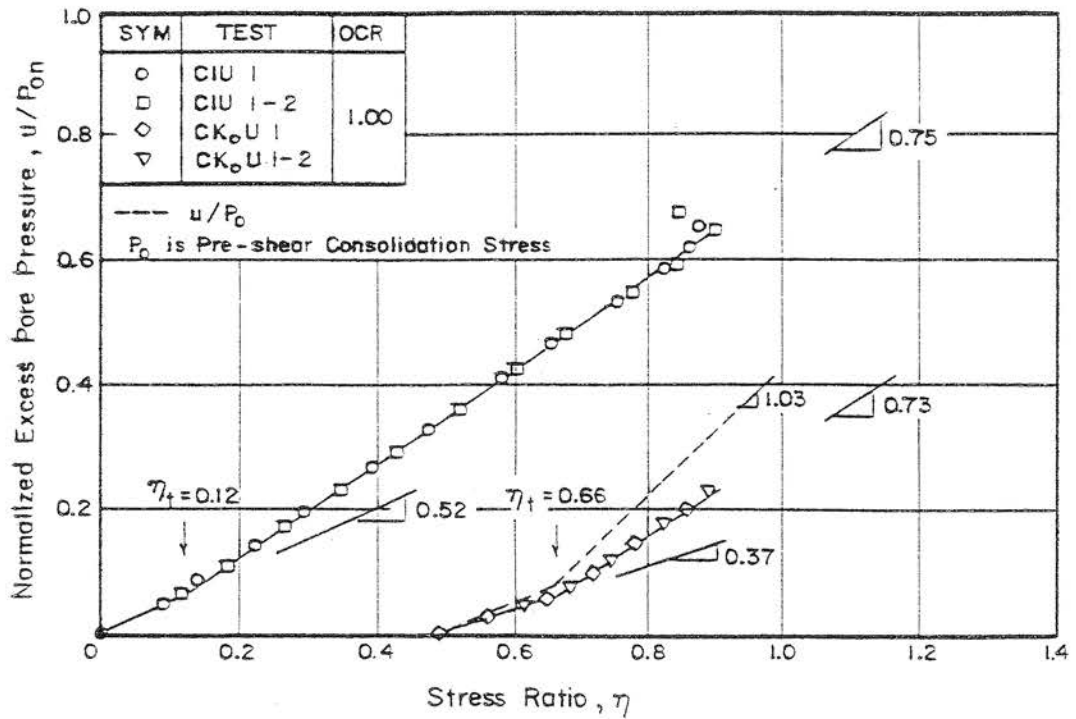


Fig. 5.23 (u/p_{0n} , η) Plot for K_0 and Isotropically Consolidated Samples

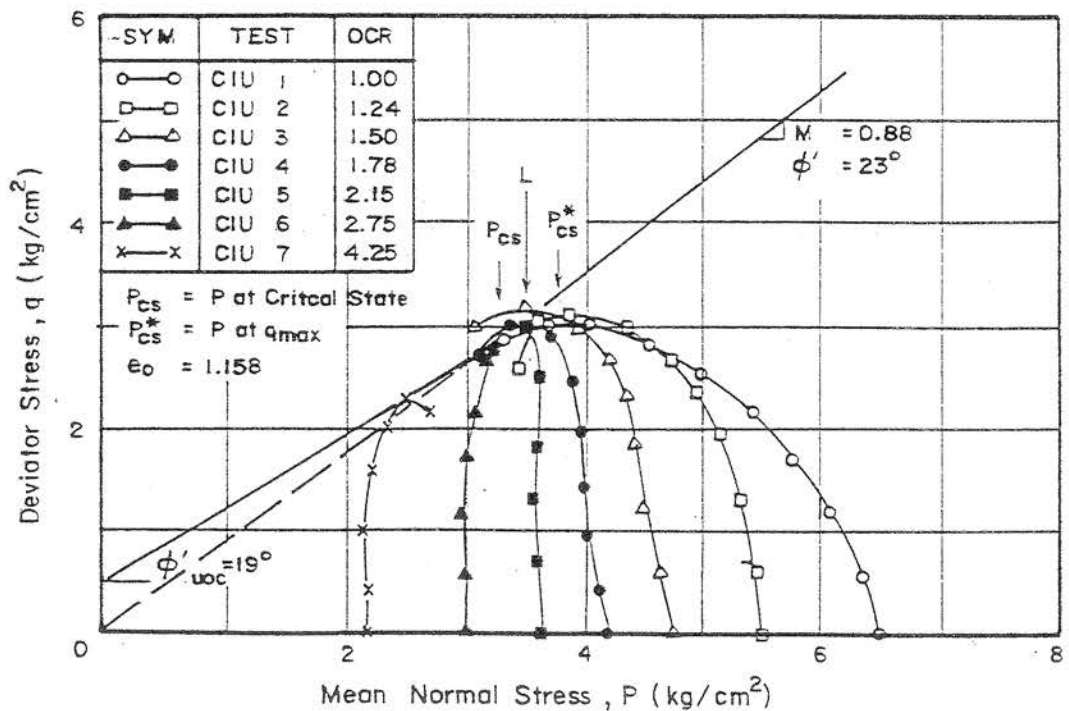


Fig. 5.24 Undrained Stress Paths of Overconsolidated Samples from CIU Tests

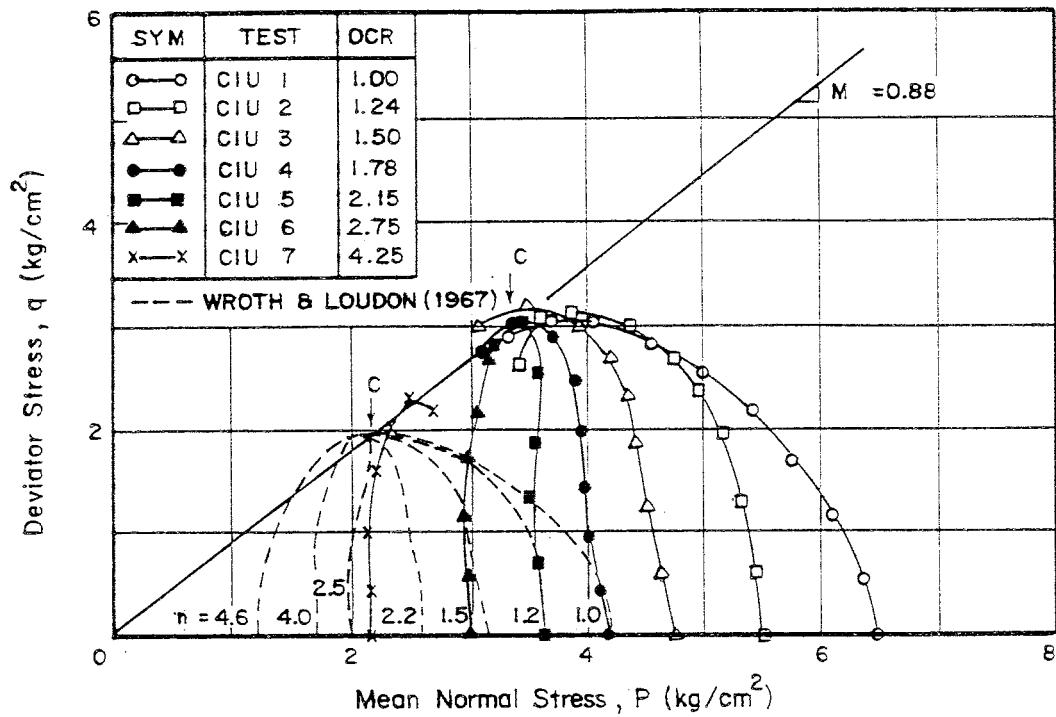


Fig. 5.25 (q, p) Plot for CIU Tests with Results Obtained by WROTH and LOUDON (1967)

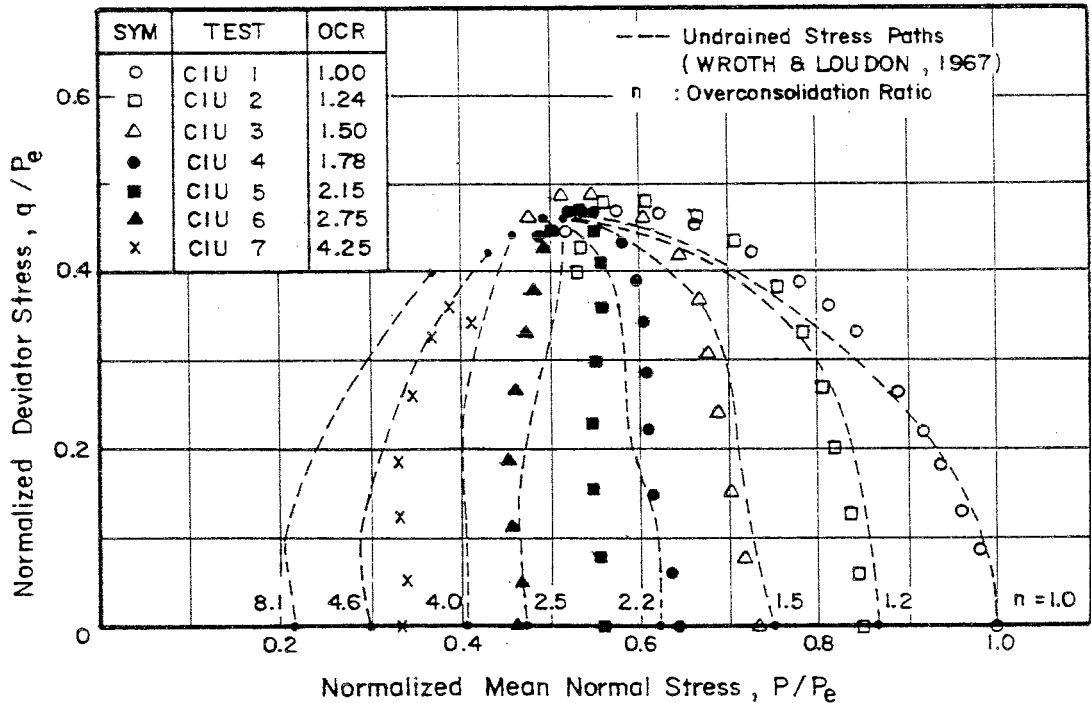


Fig. 5.26 ($p/p_e, q/p_e$) Plot for CIU Tests with Results Obtained by WROTH and LOUDON (1967)

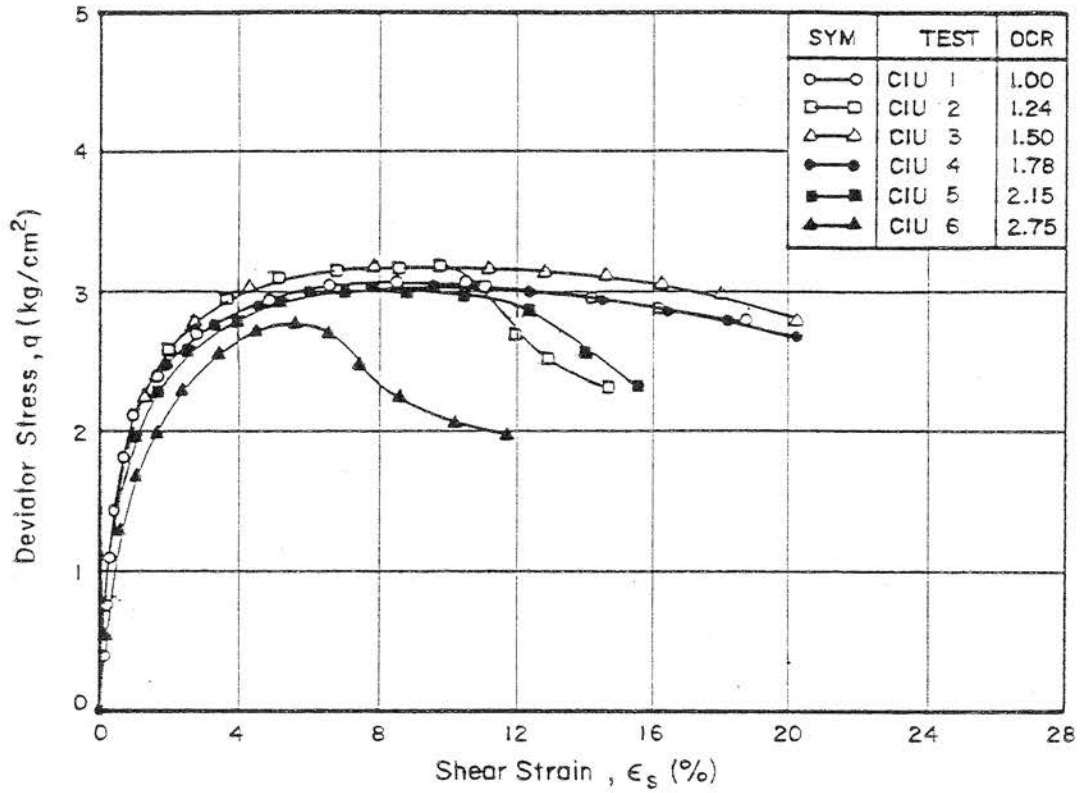


Fig. 5.27 (q, ϵ_s) Plot for Overconsolidated Samples from CIU Tests

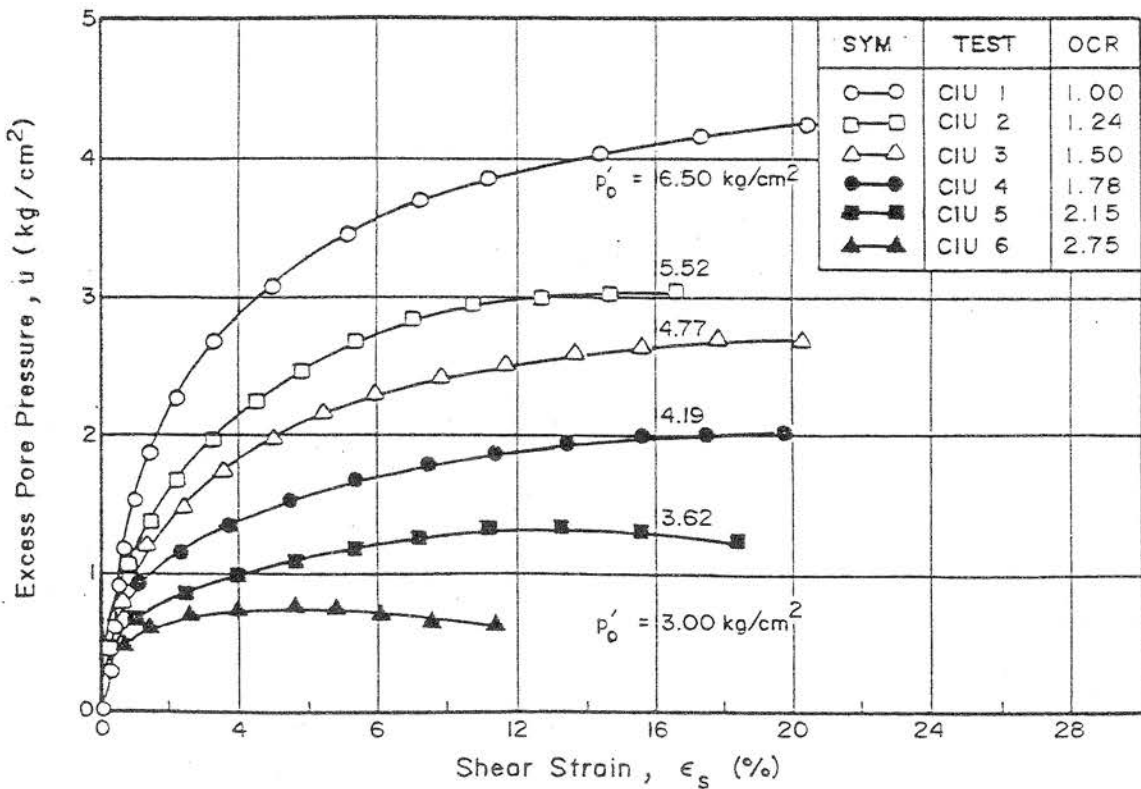


Fig. 5.28 (u, ϵ_s) Plot for Overconsolidated Samples from CIU Tests

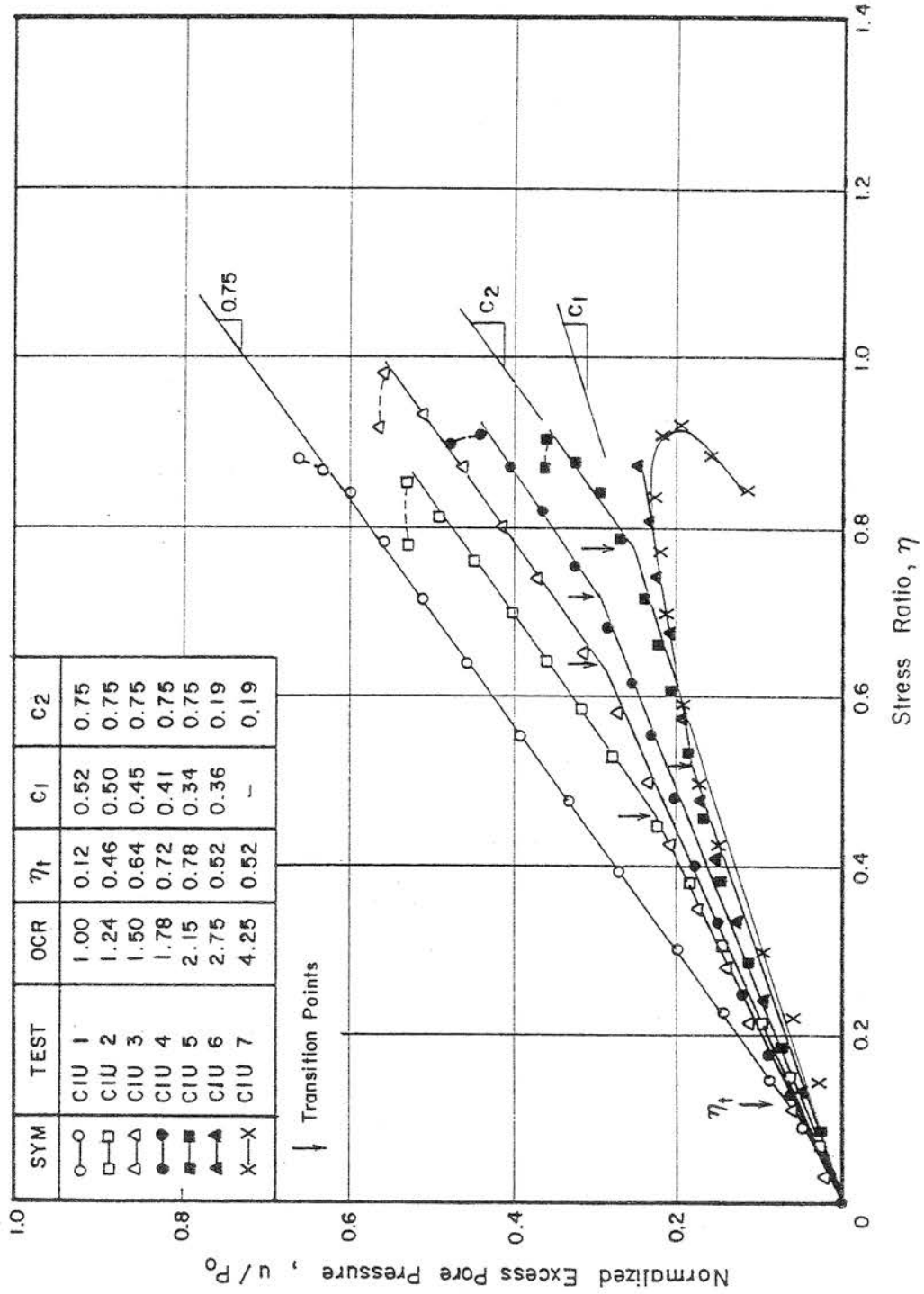


Fig. 5.29 (u/p_0 , η) Plot for Overconsolidated Samples from CIU Tests

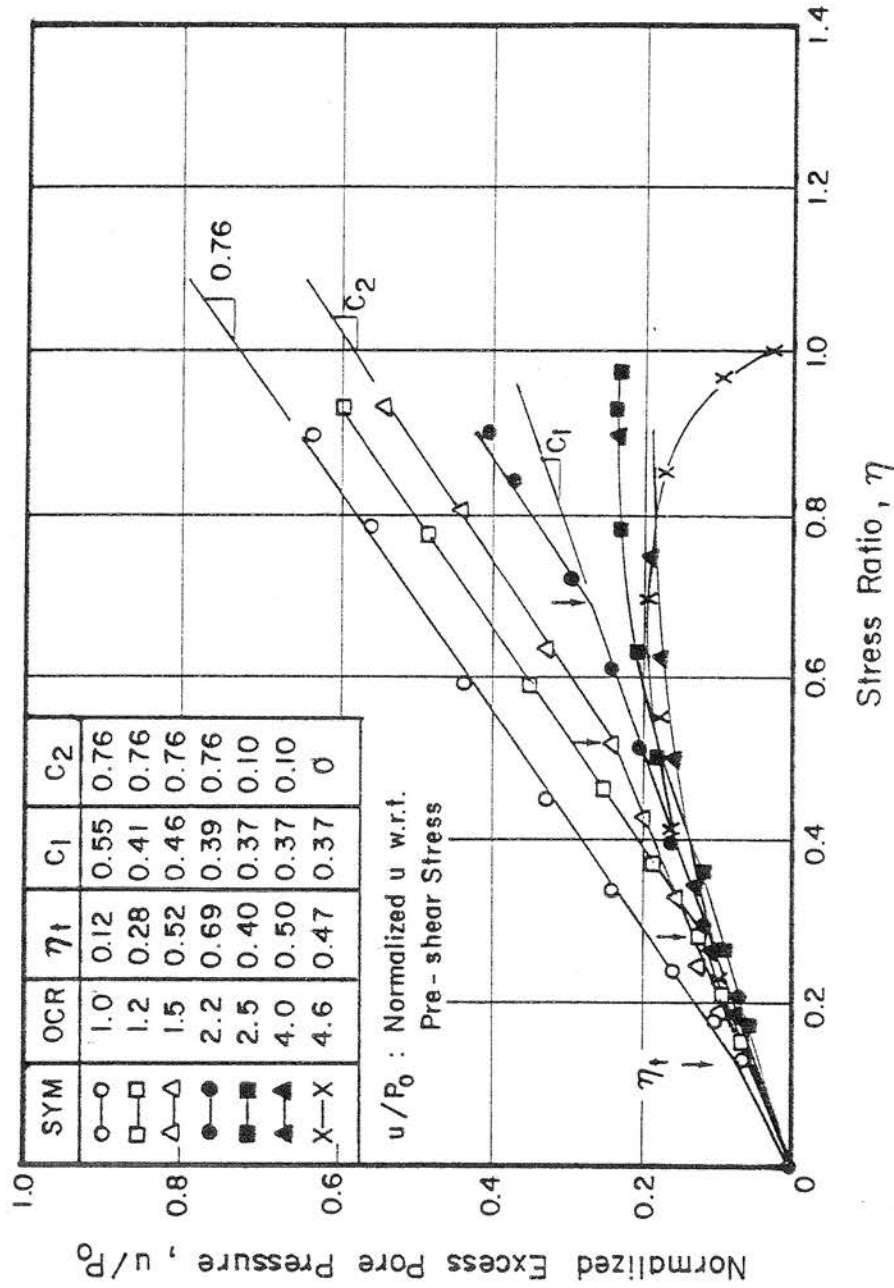


Fig. 5.30 ($u/p_0, \eta$) Plot for Overconsolidated Samples under Isotropic Stress (after WROTH and LOUDON , 1967)

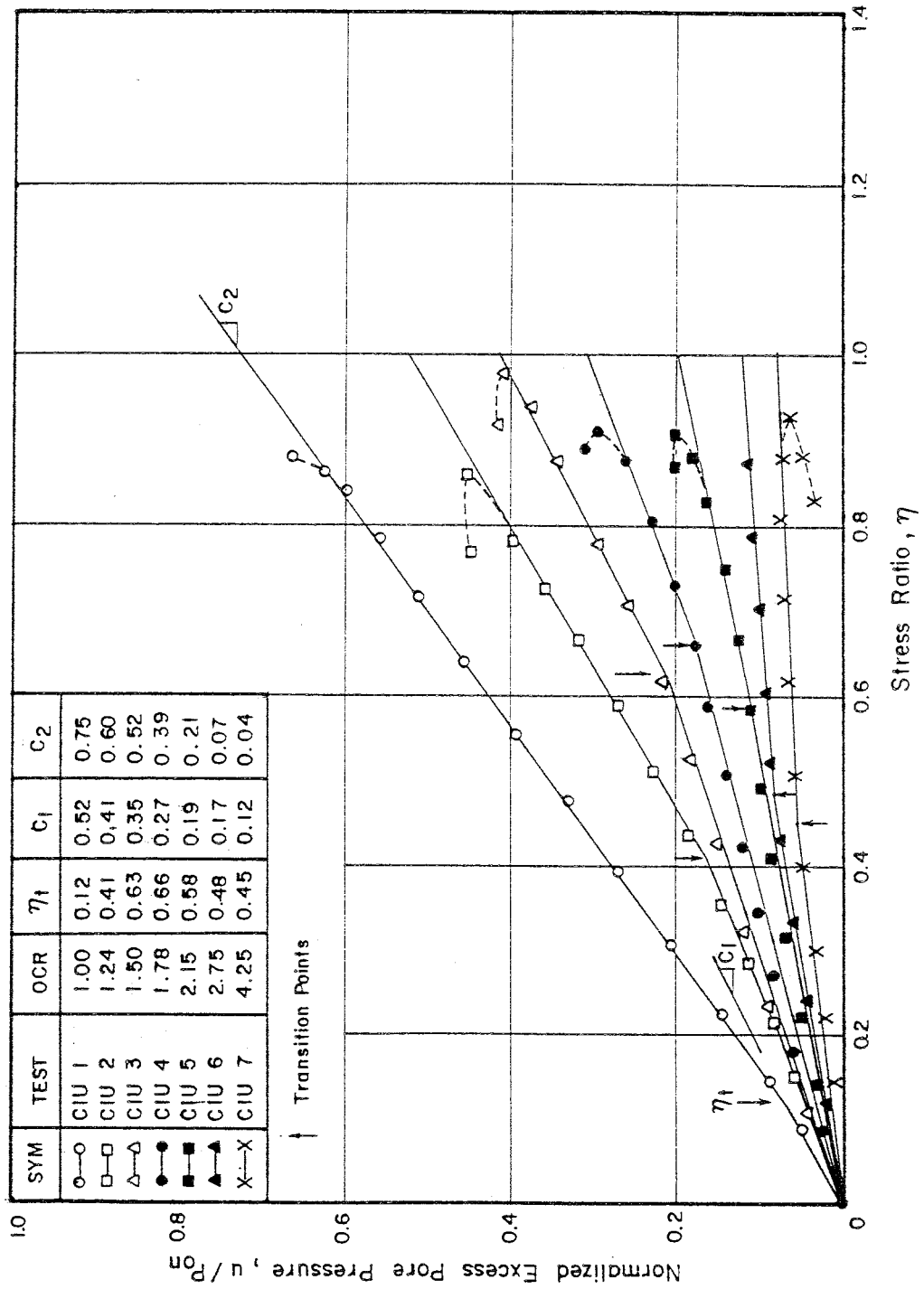


Fig. 5.31 (u/p_{on} , η) Plot for Overconsolidated Samples from CIU tests

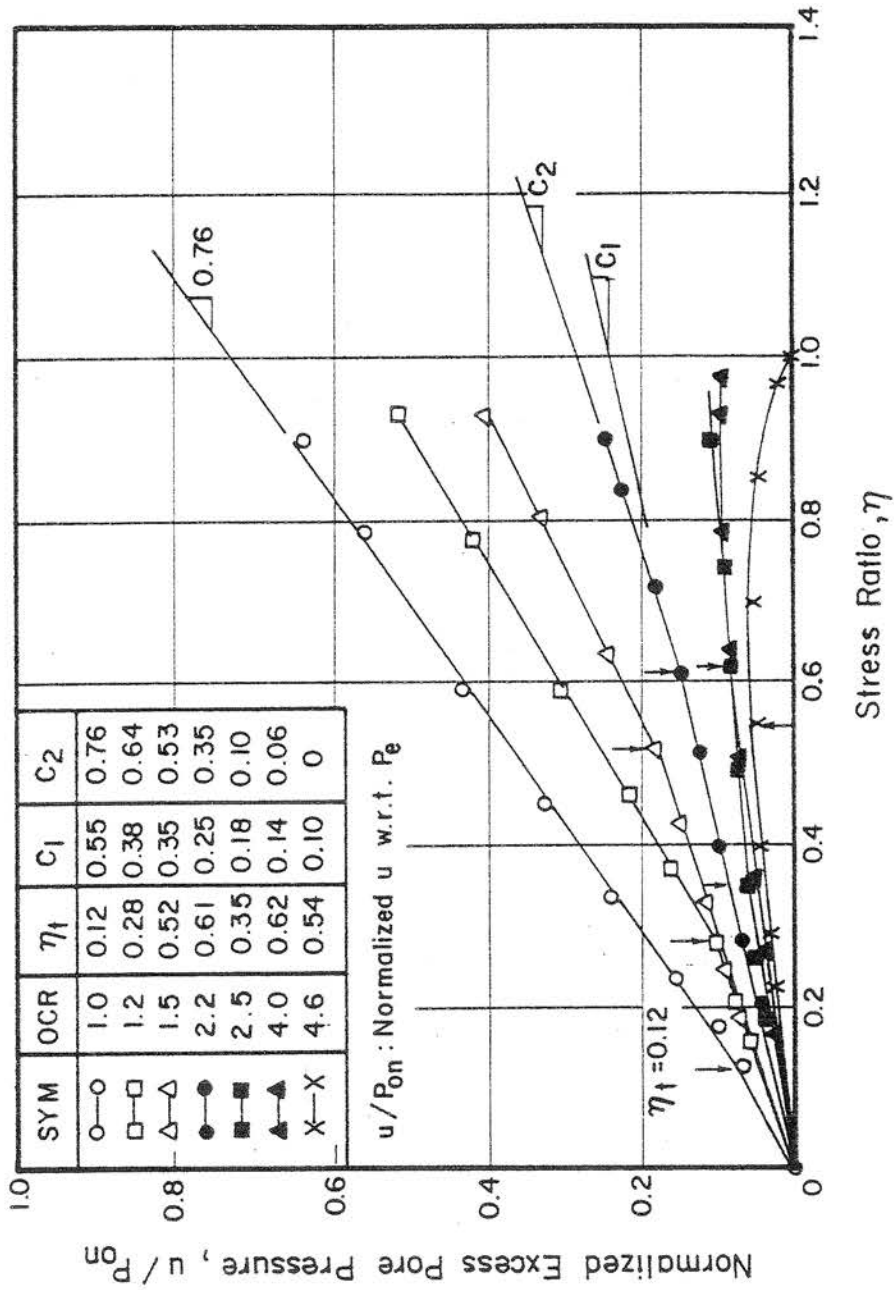


Fig. 5.32 (u/P_{on} , η) Plot for Overconsolidated Samples under Isotropic Stress (after WROTH and LOUDON , 1967)

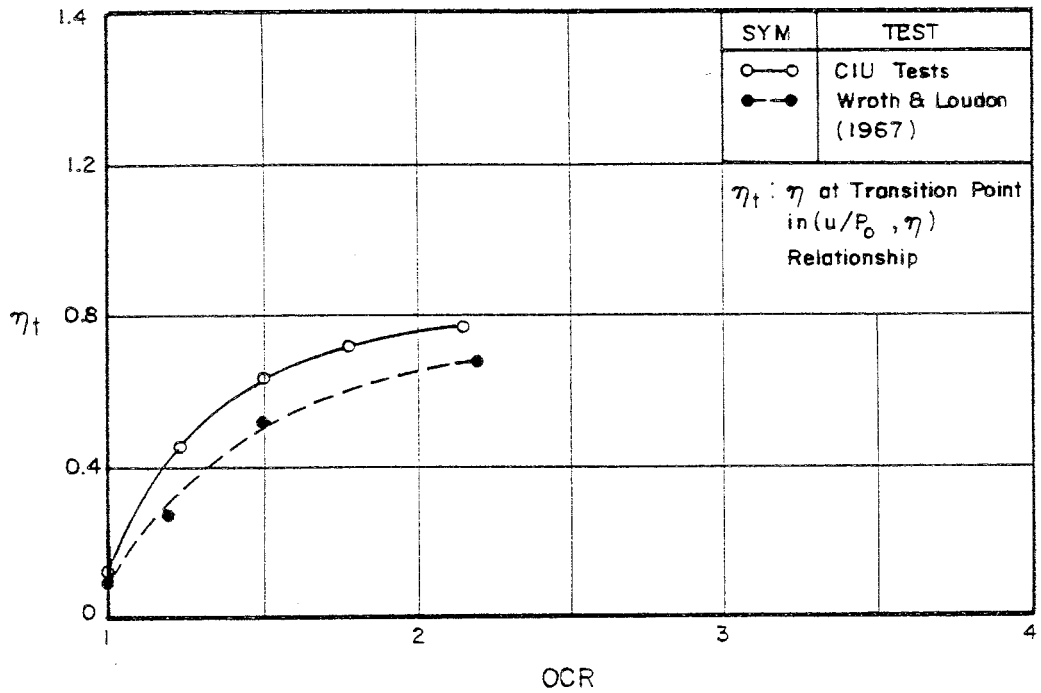


Fig. 5.33a Variation of η_t with OCR in the $(u/p_0, \eta)$ Relationship from CIU Tests (Wet Zone)

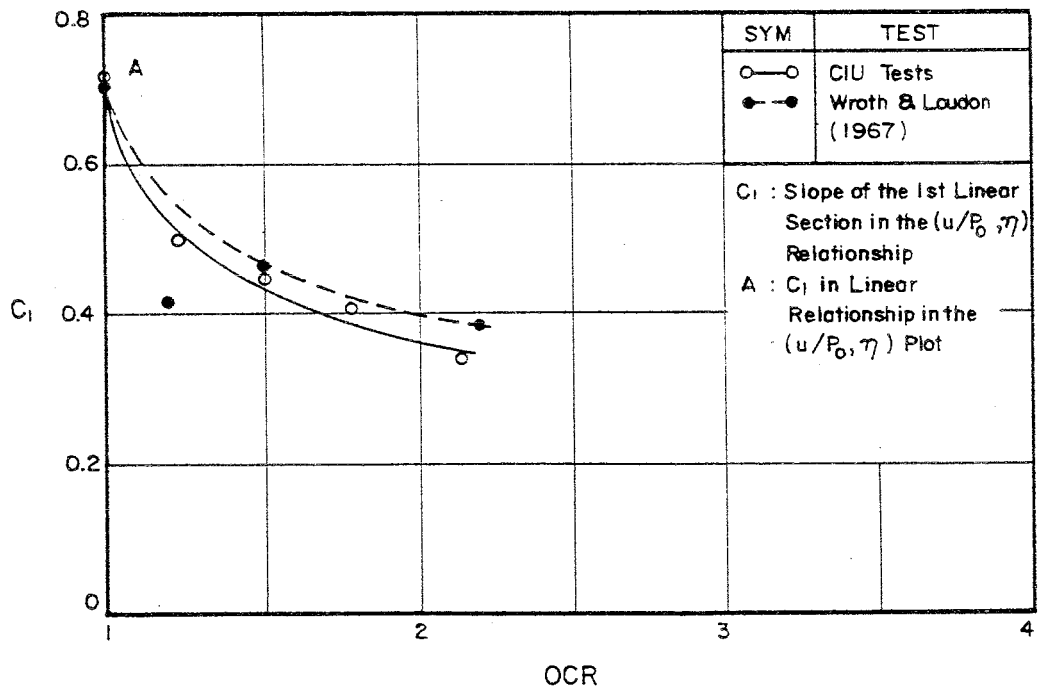


Fig 5.33b Variation of C_1 with OCR in the $(u/p_0, \eta)$ Relationship from CIU Tests (Wet Zone)

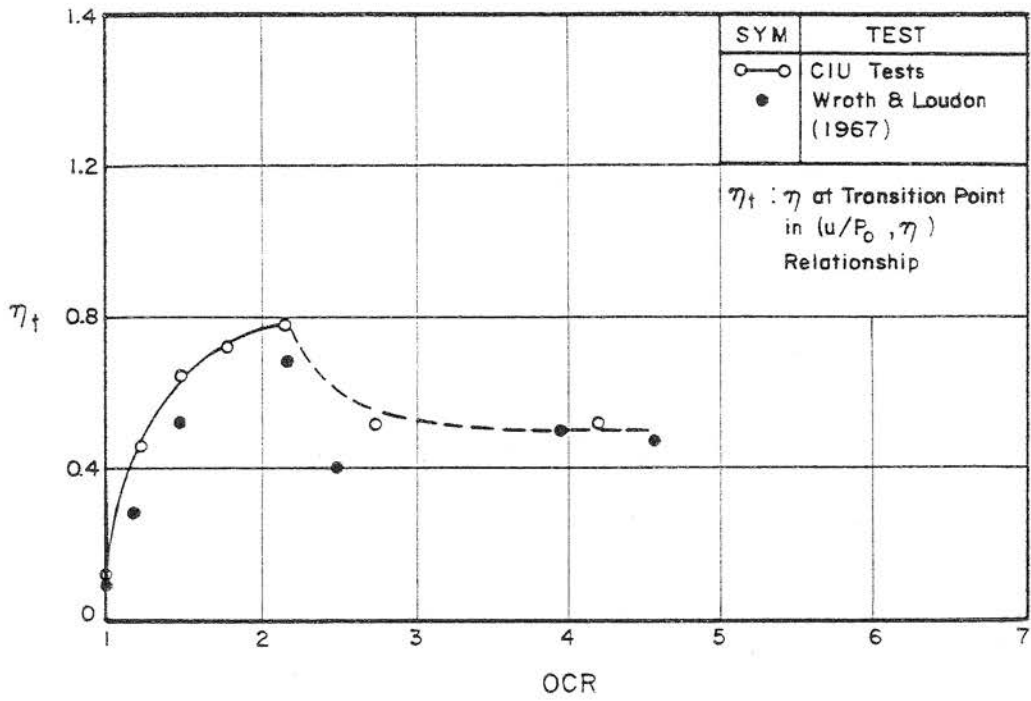


Fig. 5.34a Variation of η_t with OCR in the $(u/p_o, \eta)$ Relationship from CIU Tests

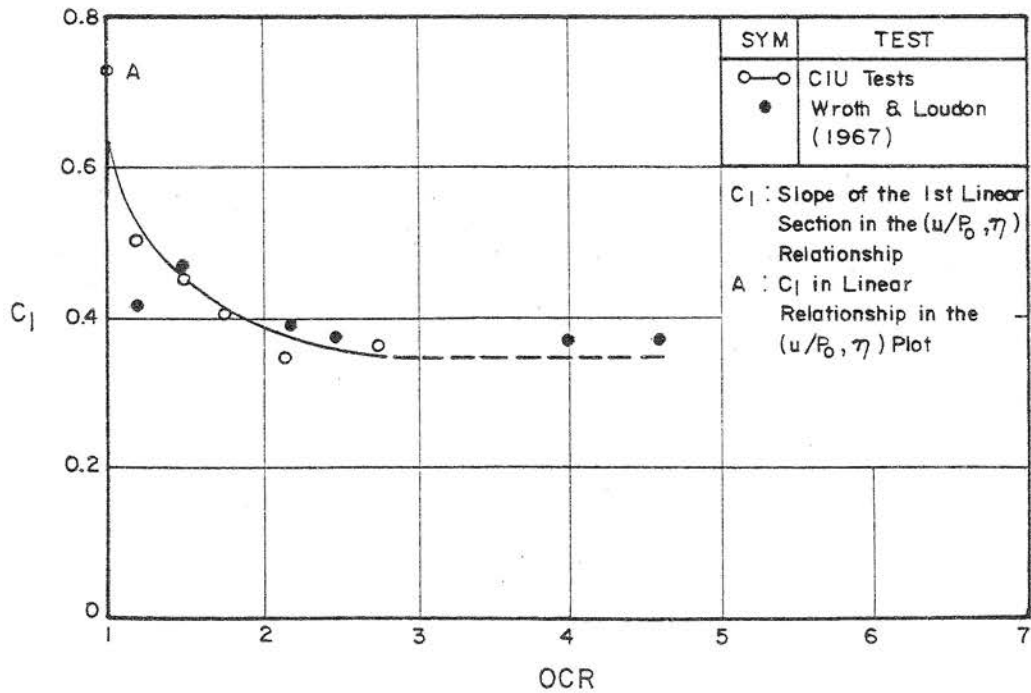


Fig. 5.34b Variation of C_1 with OCR in the $(u/p_o, \eta)$ Relationship from CIU Tests

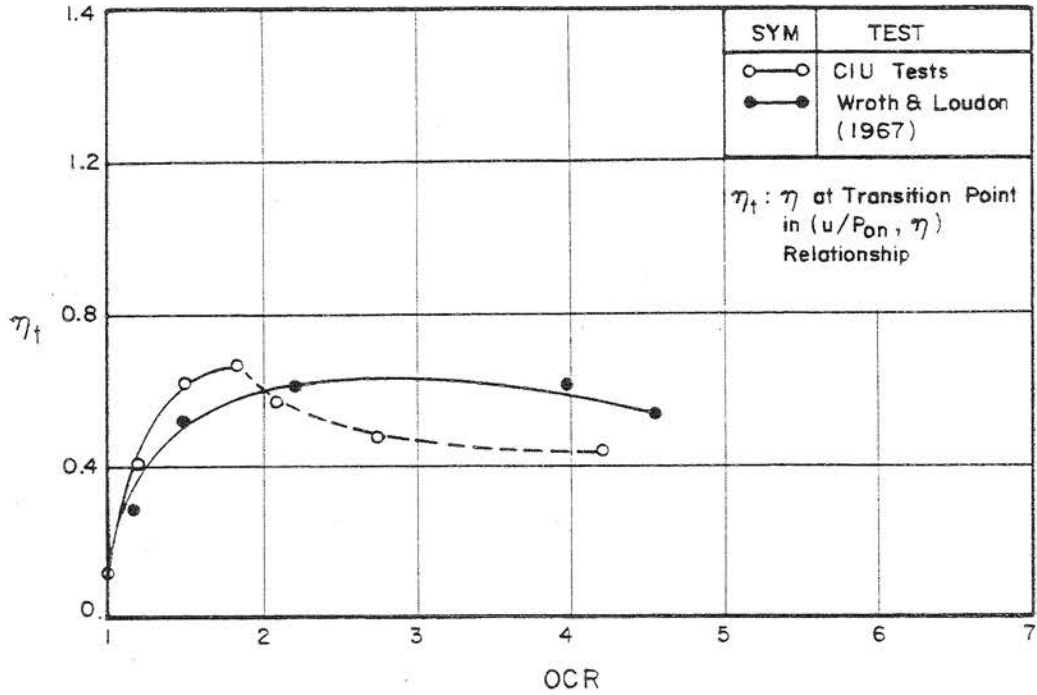


Fig. 5.35a Variation of η_t with OCR in the $(u/p_{on}, \eta)$ Relationship from CIU Tests

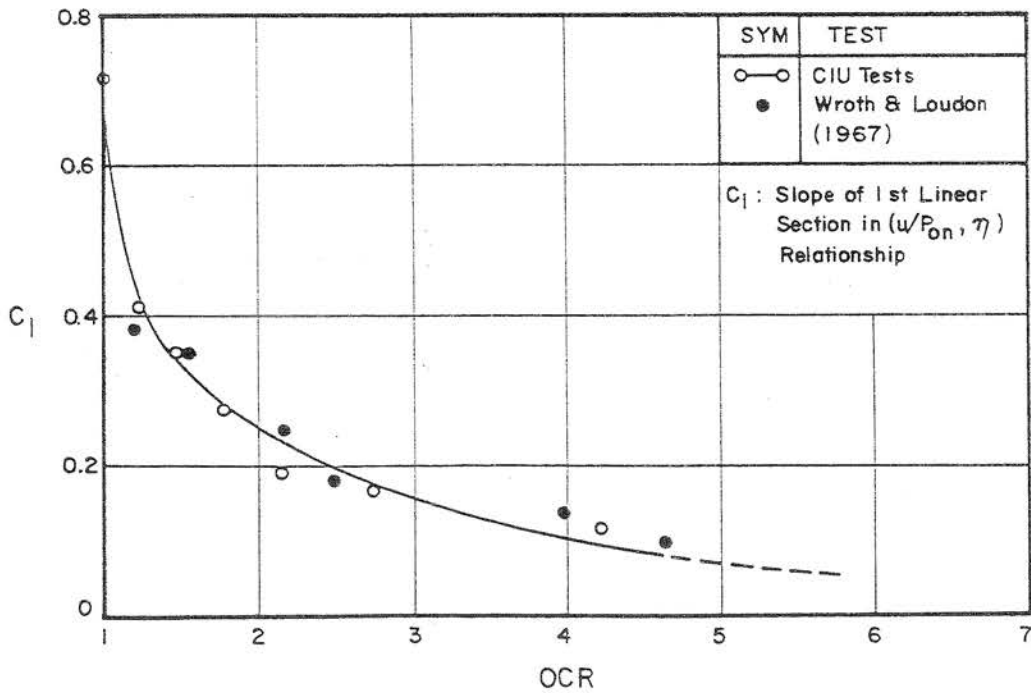


Fig. 5.35b Variation of C_1 with OCR in the $(u/p_{on}, \eta)$ Relationship from CIU Tests

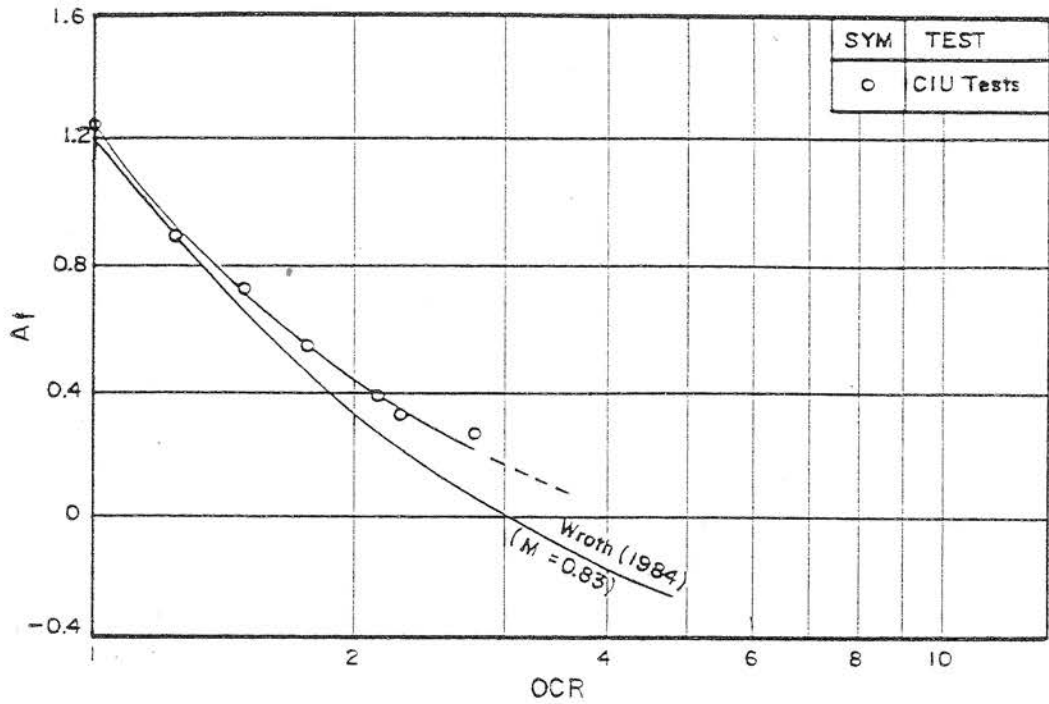


Fig. 5.36 Variation of A_f with OCR for the Overconsolidated Samples from CIU Tests

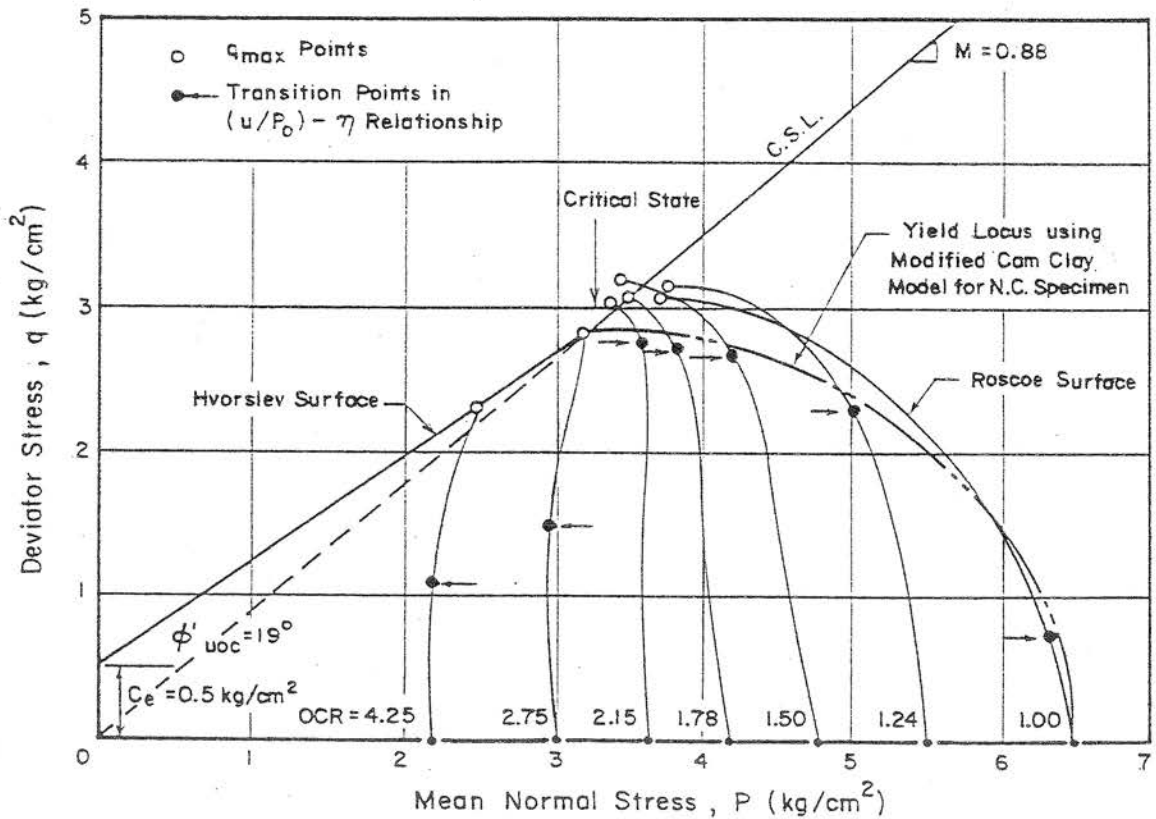


Fig. 5.37 Failure and Yield Points of the Overconsolidated Samples from CIU Tests

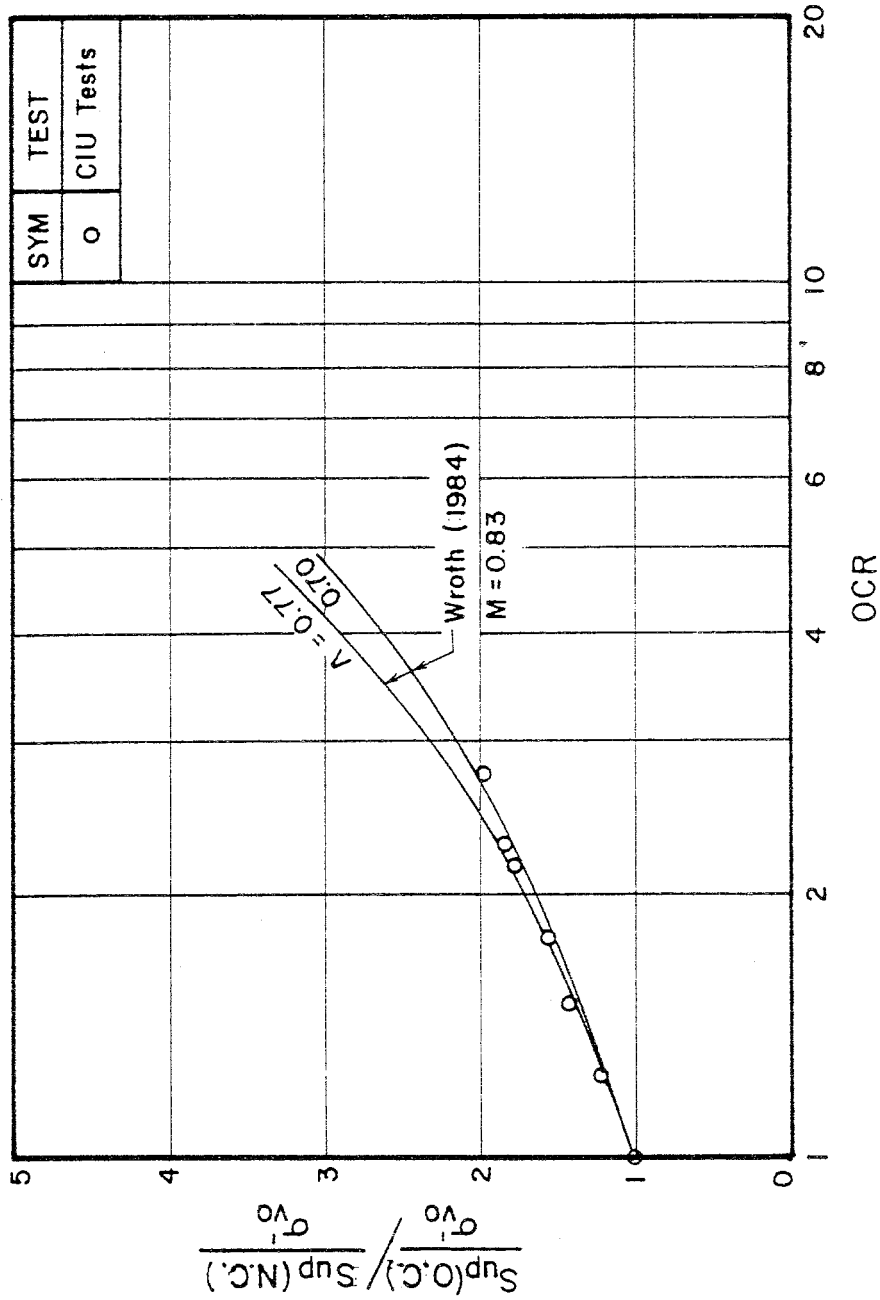


Fig. 5.38 Variation of Undrained Strength Ratio with OCR for Overconsolidated Samples from CIU Tests

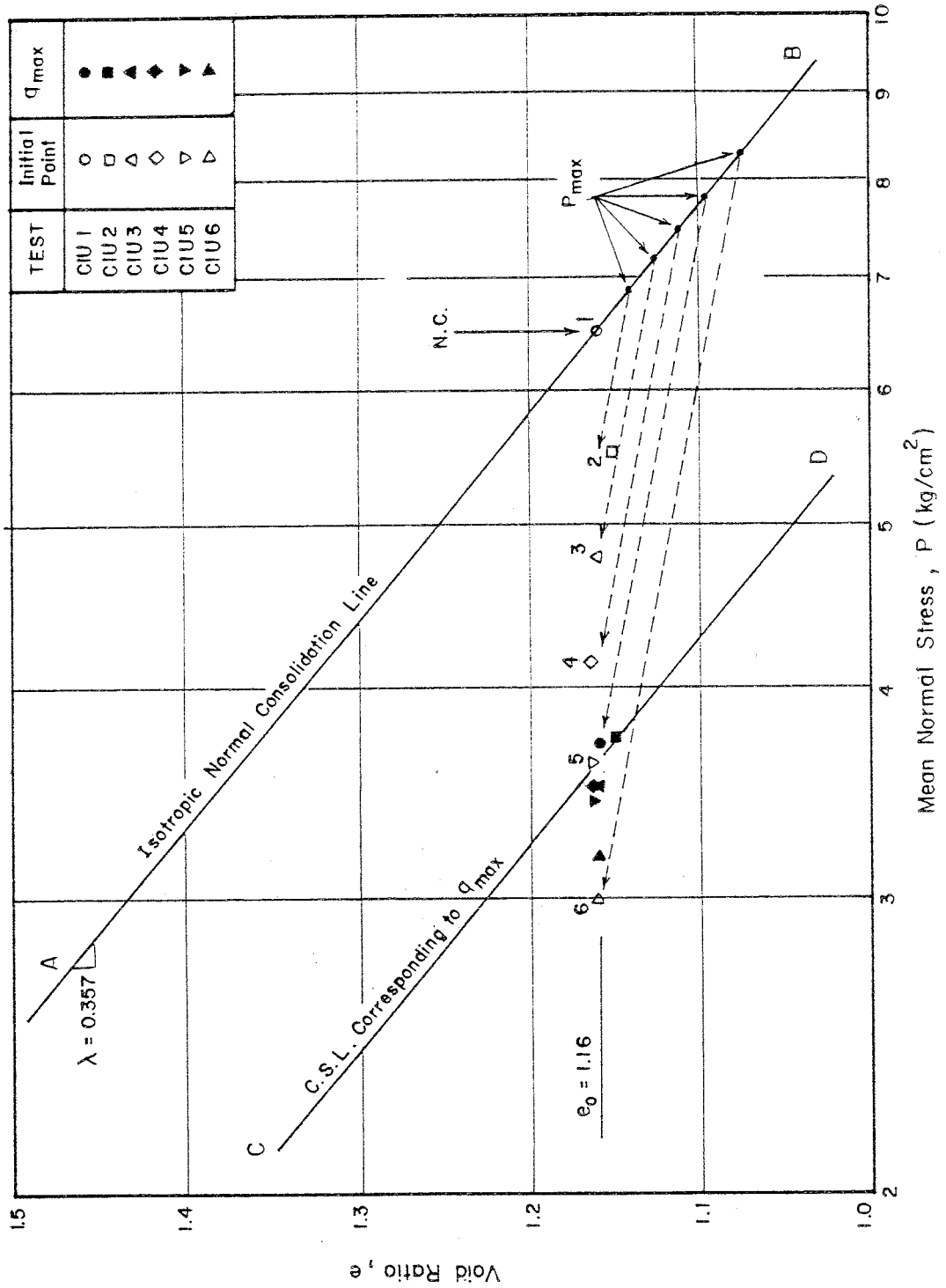


Fig. 6.39a Critical State Line Corresponding to q_{max} Conditions from CIU Tests

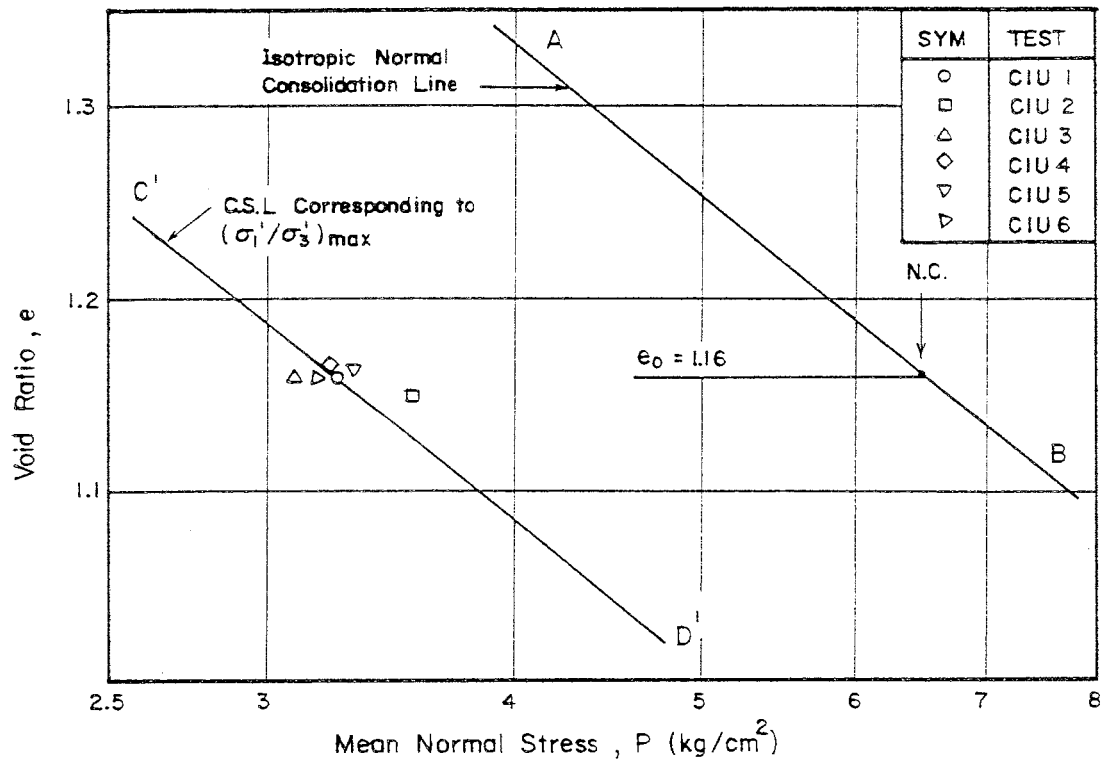


Fig. 5.39b Critical State Line Corresponding to the $(\bar{\sigma}_1'/\bar{\sigma}_3')_{\max}$ Conditions from CIU Tests

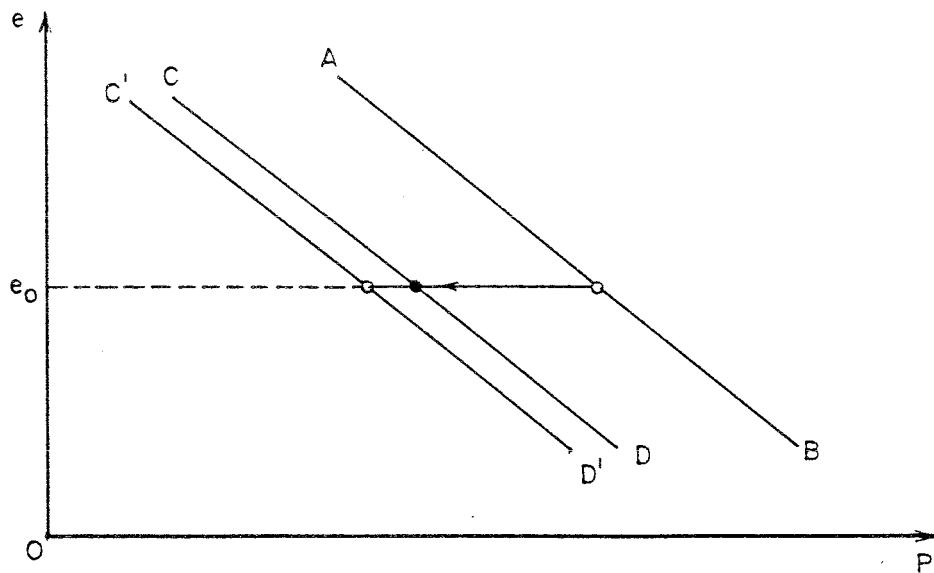


Fig. 5.39c Critical State Lines Corresponding to the Different Criteria

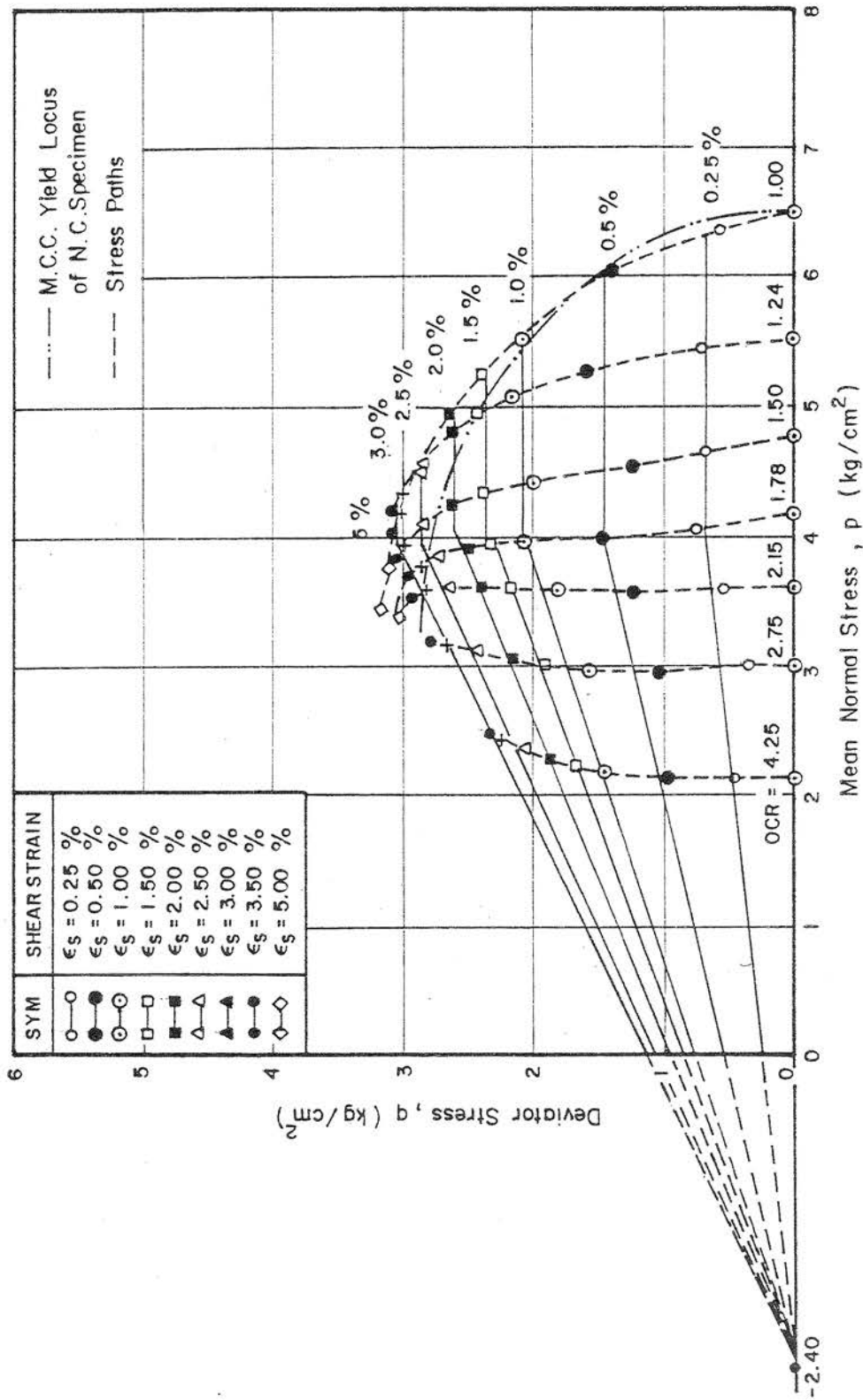


Fig. 5.40 Shear Strain Contours of Overconsolidated Samples from CIU Tests

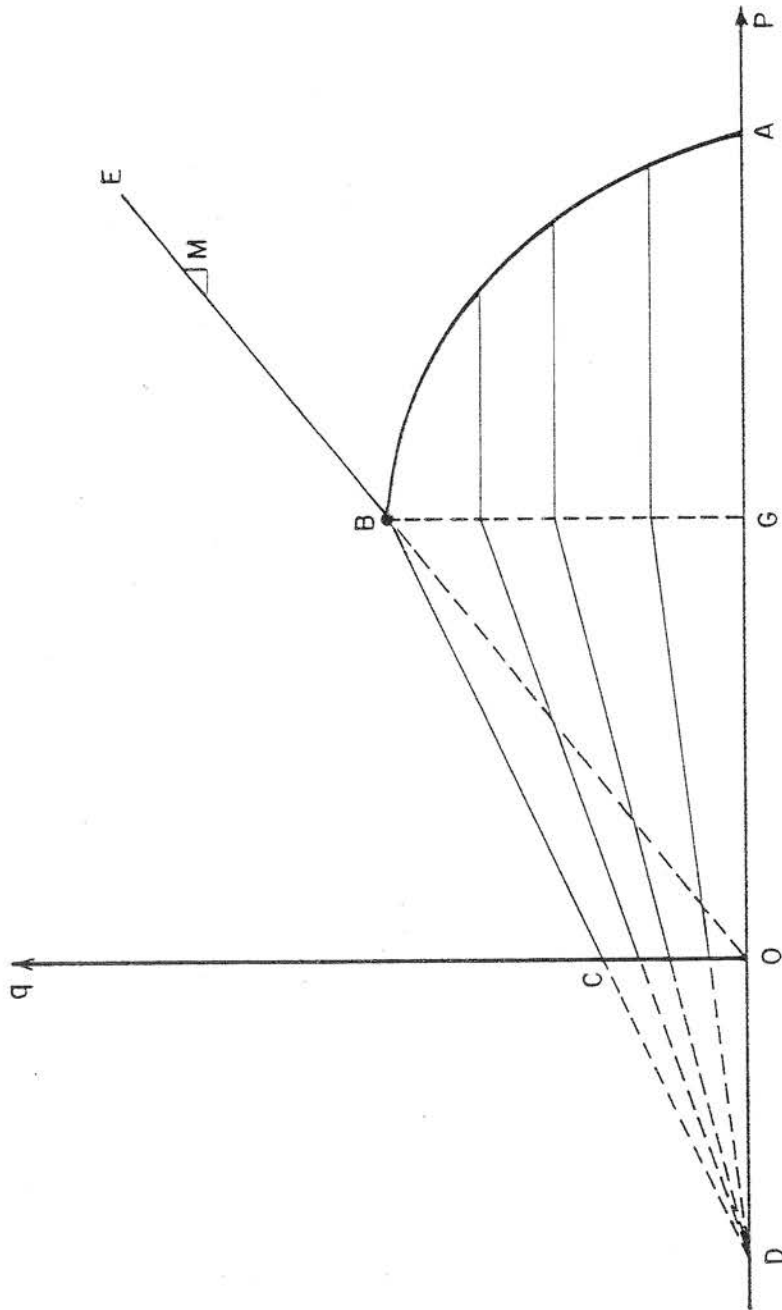


Fig. 5.41 Simplified Shear Strain Contours for Overconsolidated Samples from CIU Tests

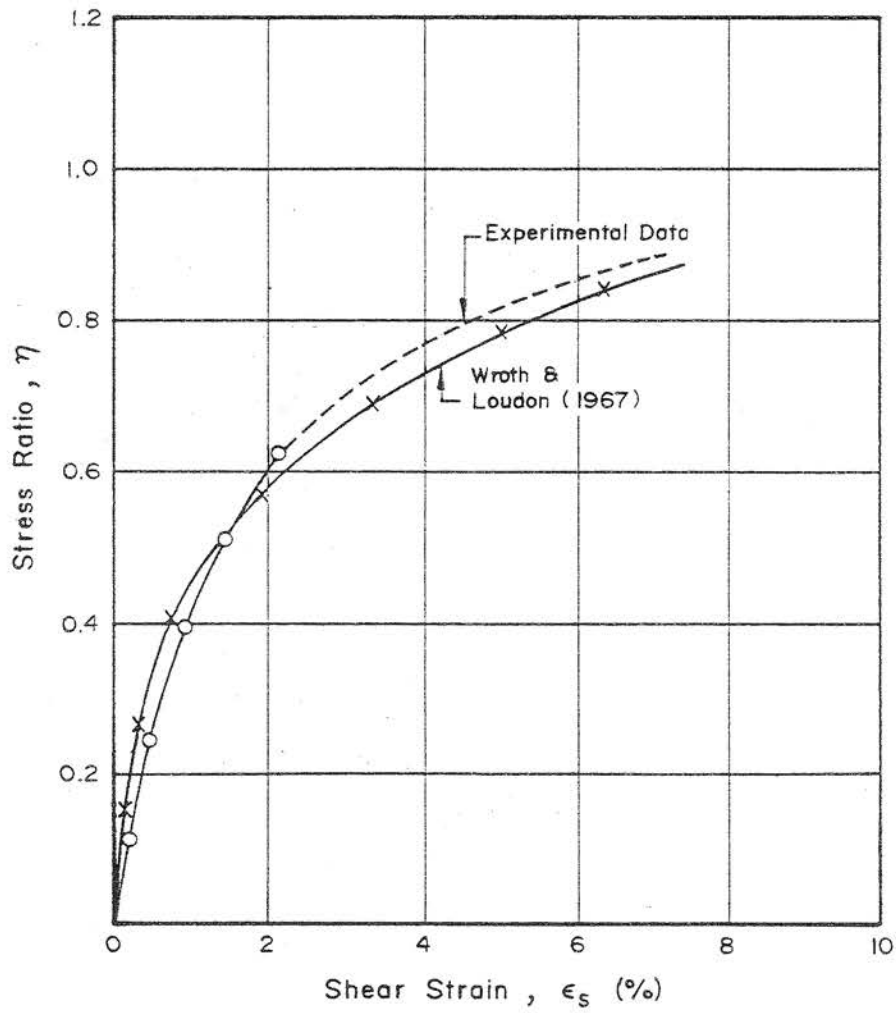


Fig. 5.42 (η , ϵ_s) Relationship for Overconsolidated Samples from Strain Contours of Fig. 5.40

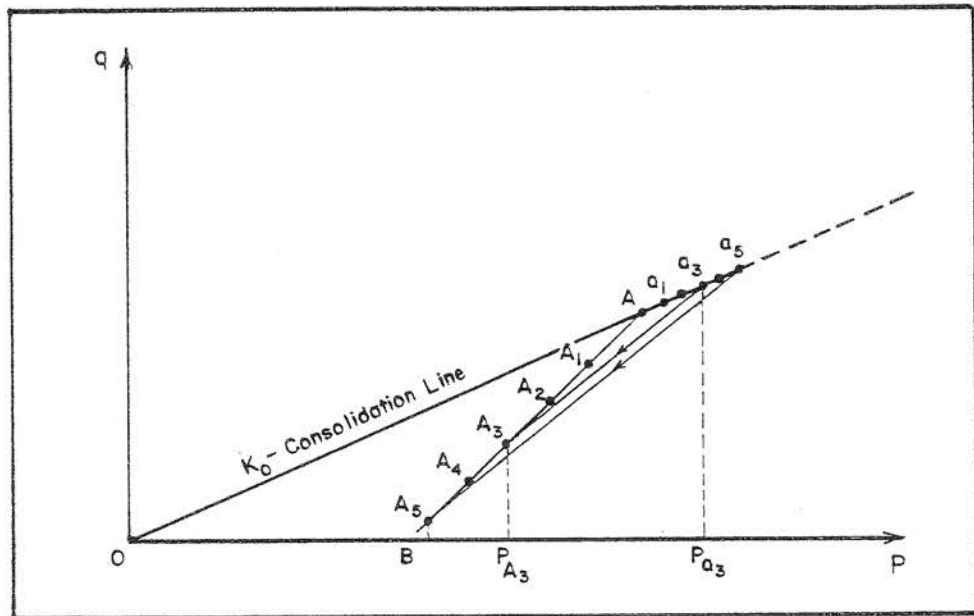


Fig. 5.43 Schematic Diagram of Sample Preparation for the Test Series I

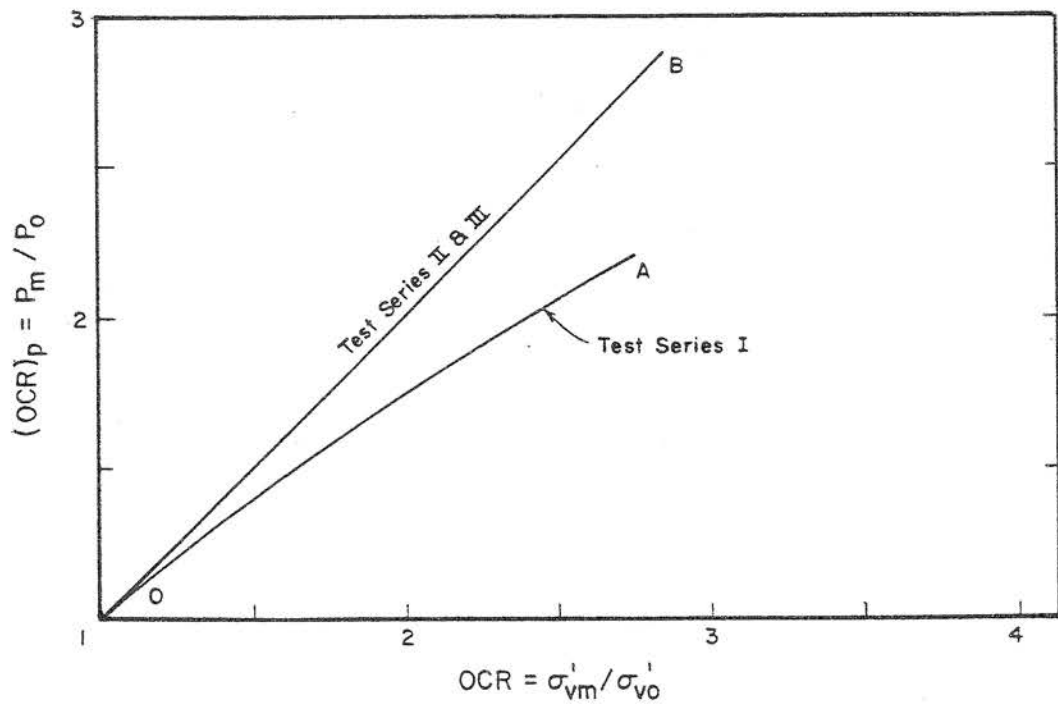


Fig. 5.44 Correlation between Two Types of OCR Values

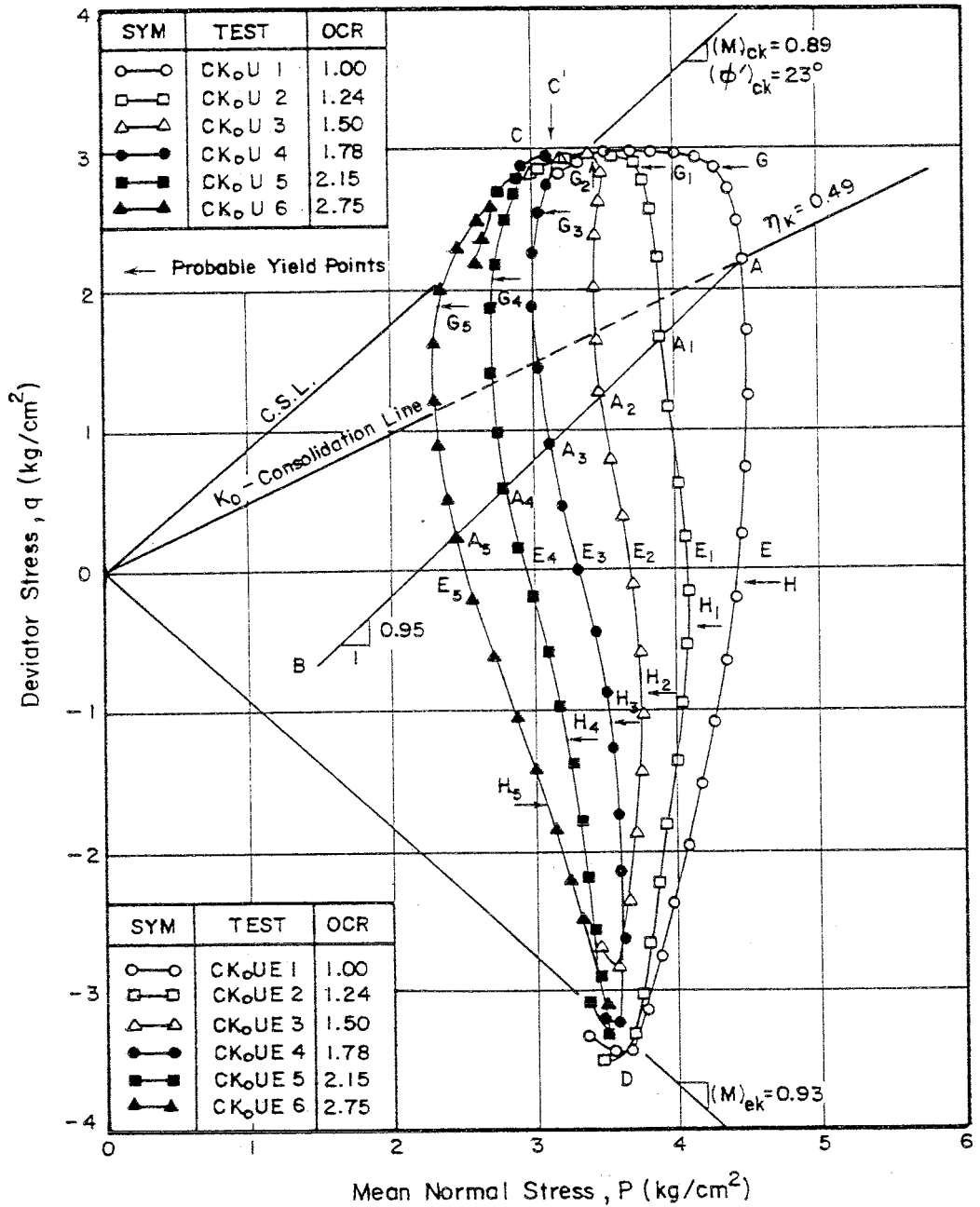


Fig. 5.45 Undrained Stress Paths for K_0 -overconsolidated Samples from CK₀U & CK₀UE Tests

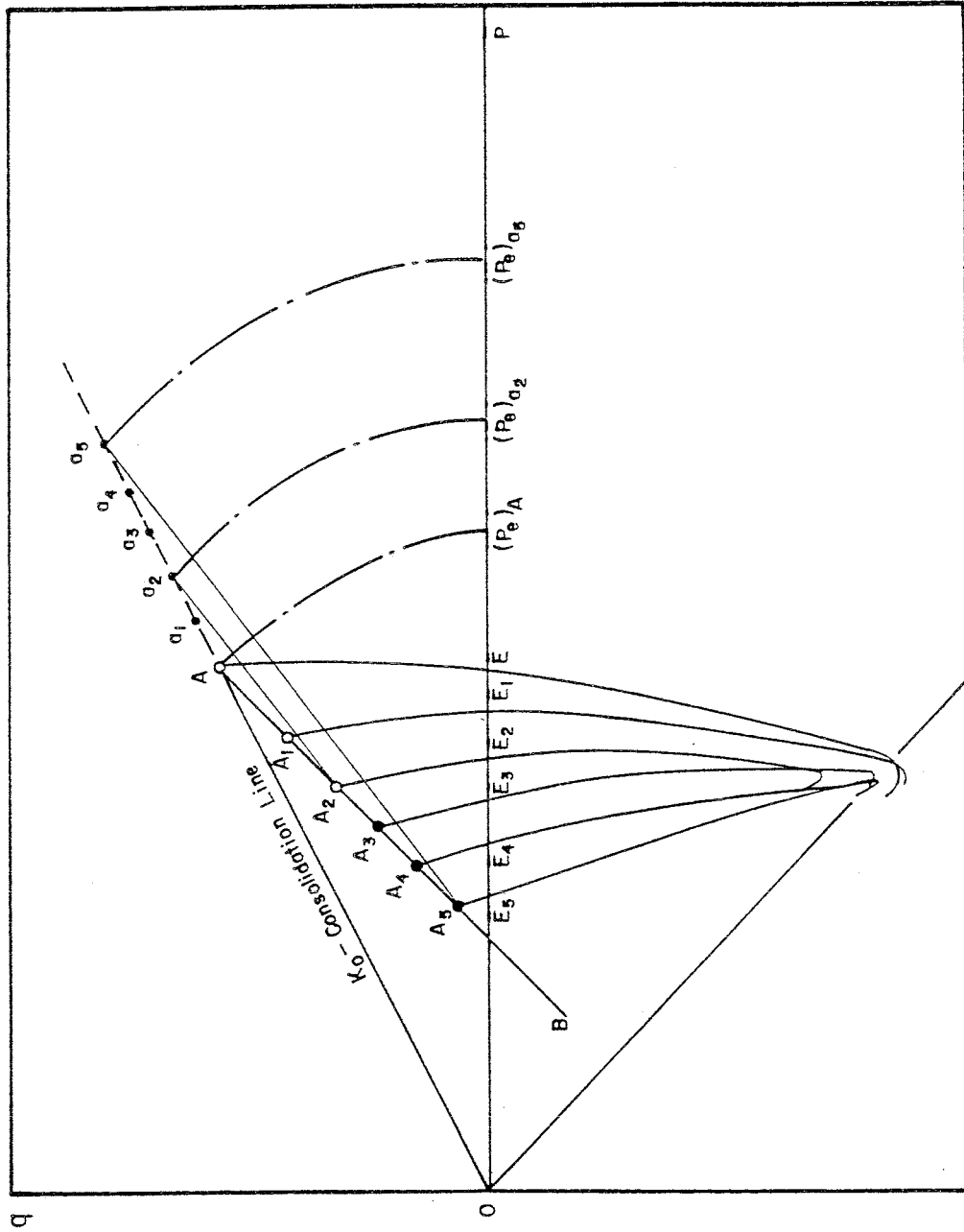


Fig. 5.46 Schematic Diagram for Determining the OCR Values for the Samples in the Test Series I based on the Isotropic Stresses

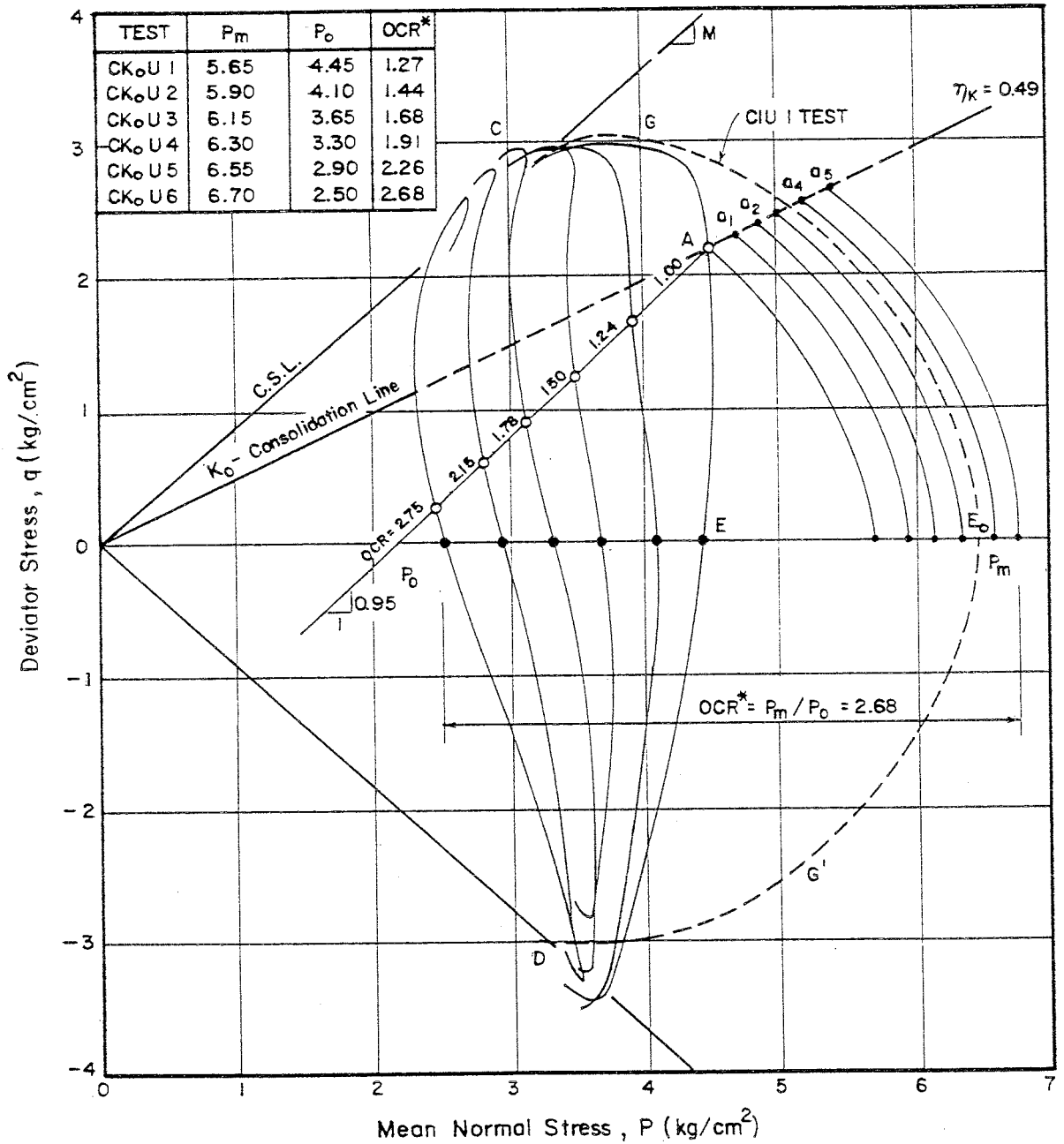


Fig. 5.47 OCR Values for the Samples in the Test Series I based on the Isotropic Stresses

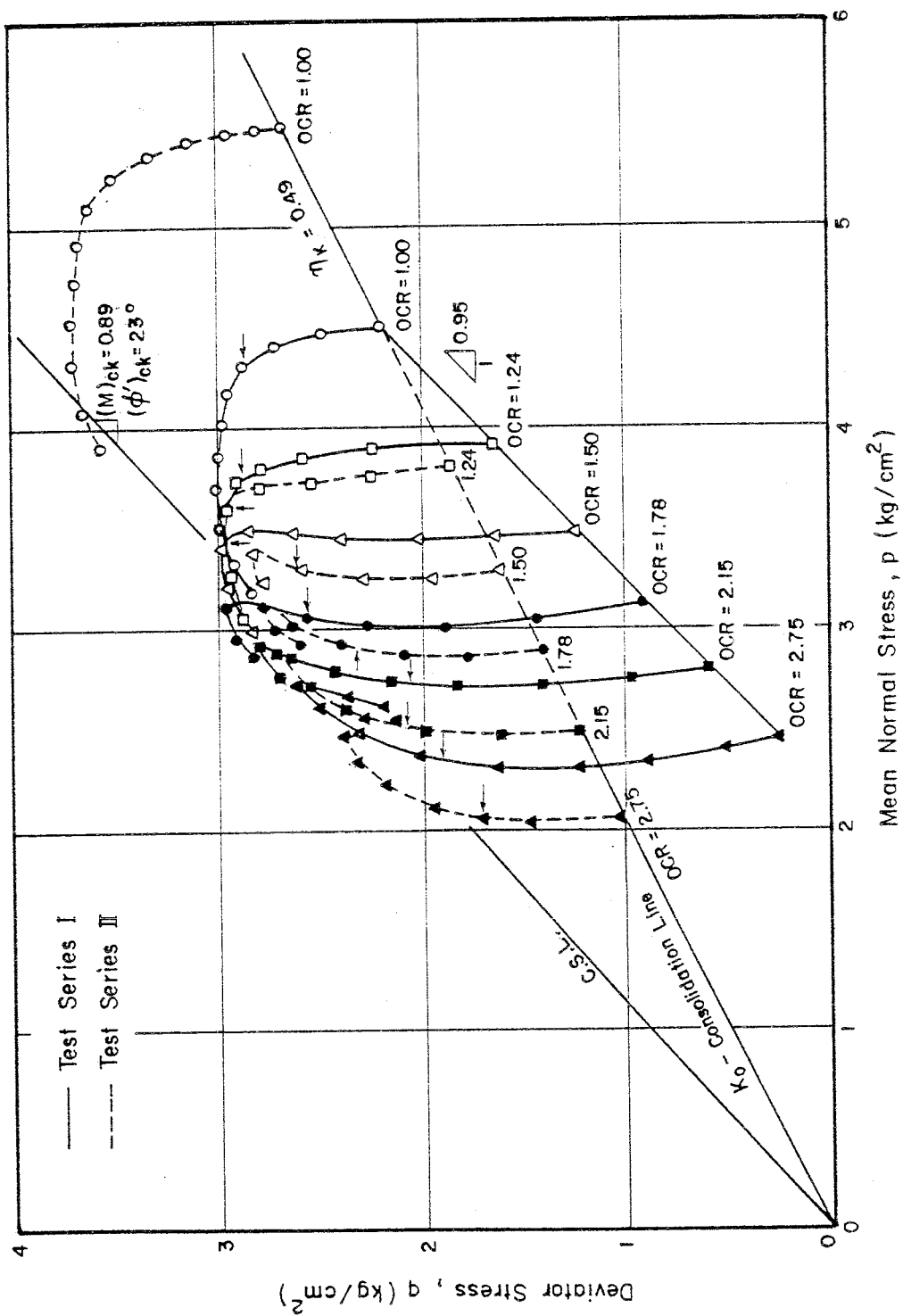


Fig. 5.48 Undrained Stress Paths for K_0 -overconsolidated Samples from CK₀U & CAU Tests

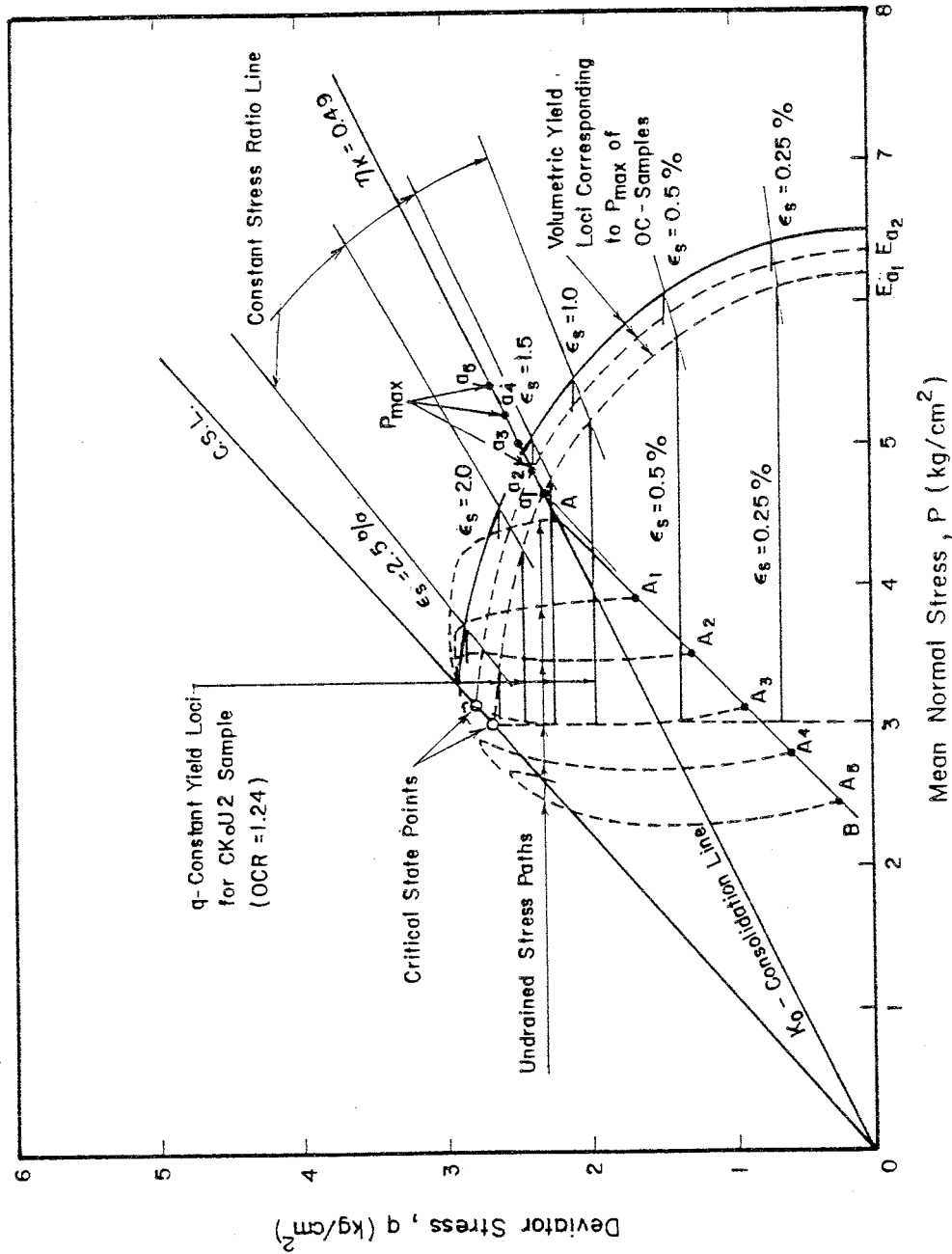


Fig. 5.49 Schematic Diagram for the Estimation of the Shear Strains of CKoU & CAU Tests from the Constant q -yield Loci of the Isotropically Consolidated Samples

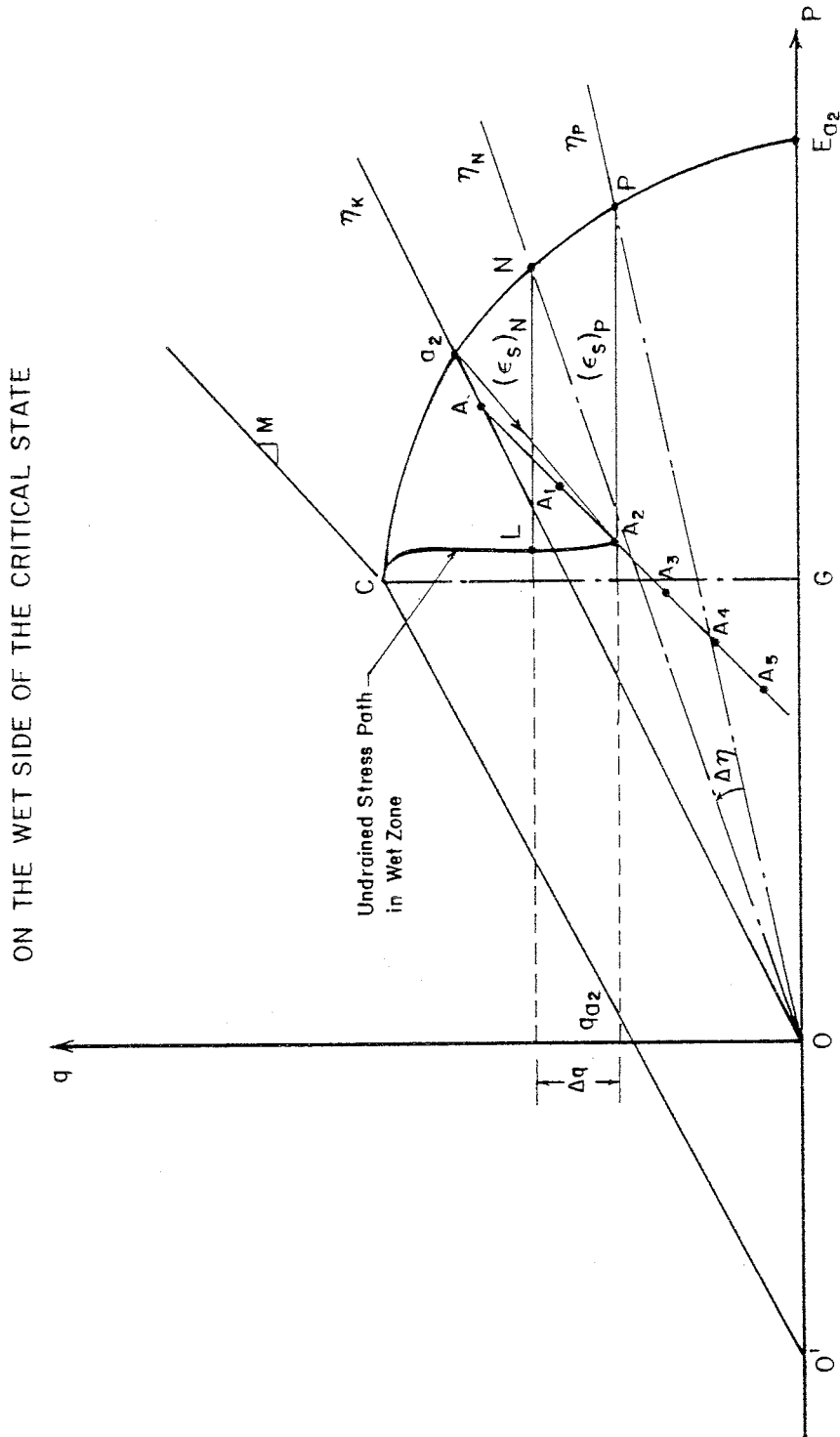


Fig. 5.50a An Illustration of the Estimation of the Shear Strains in the CKoJ Test from the Constant q -yield Loci of the CIU Tests (Wet Zone)

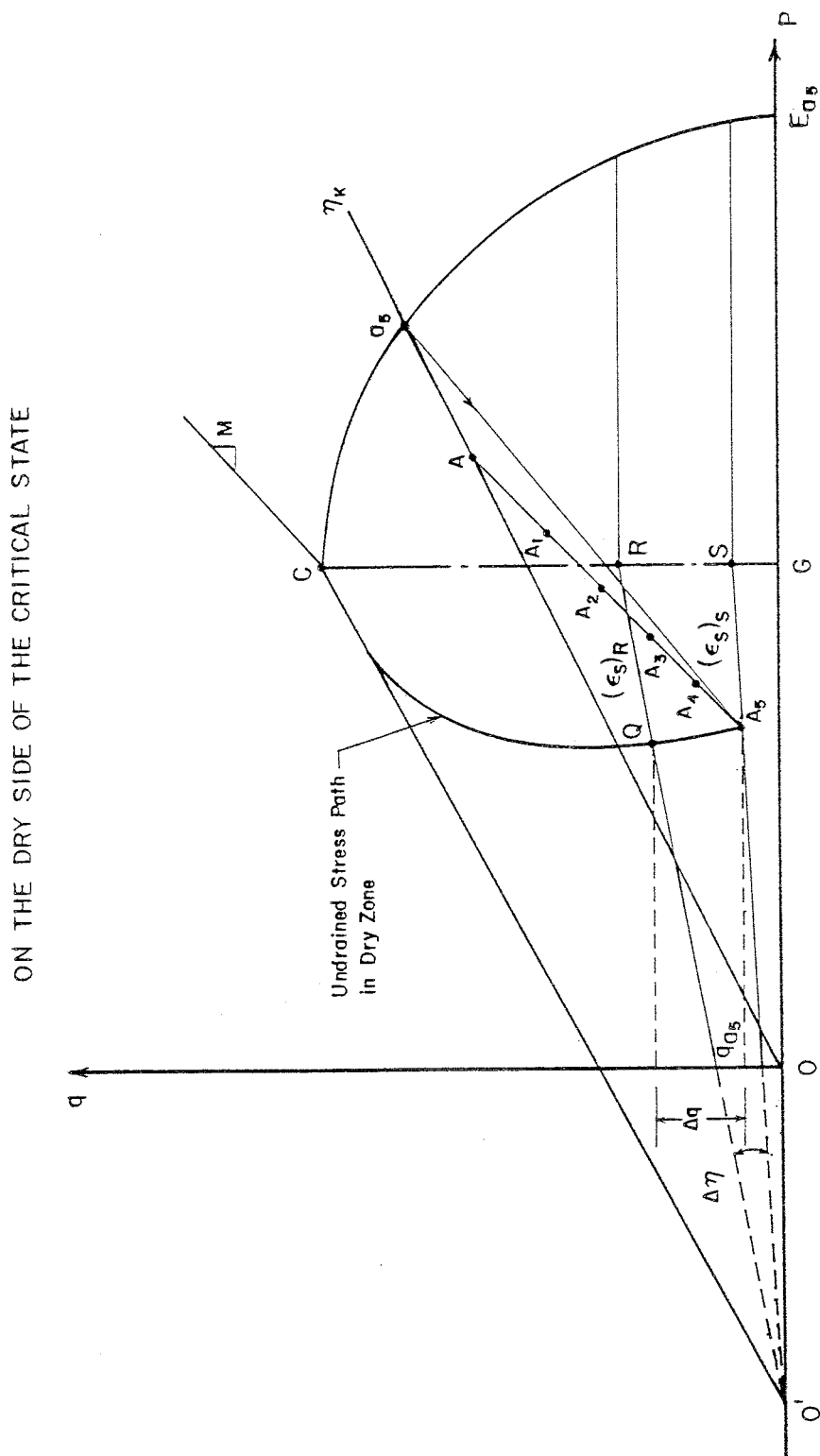


Fig. 5.50b An Illustration of the Estimation of the Shear Strains in the CK₀U Test from the Constant q -yield Loci of the CU Tests (Dry Zone)

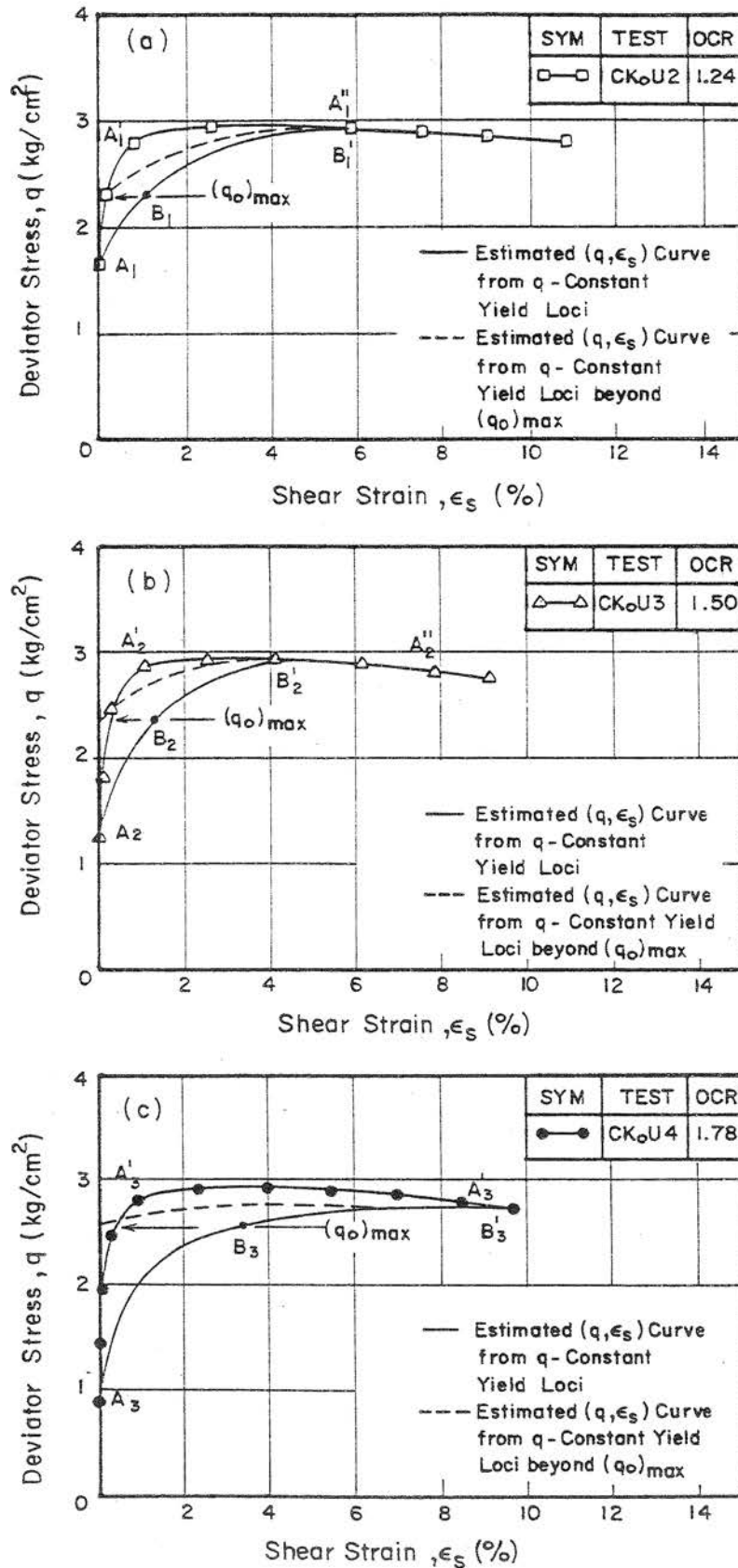


Fig. 5.51 Comparisons of (q, ϵ_s) Relationship between the CKoU Tests and the Estimated Ones from the Constant q -yield Loci of CIU Tests; (a) OCR = 1.24; (b) OCR = 1.50; (c) OCR = 1.78

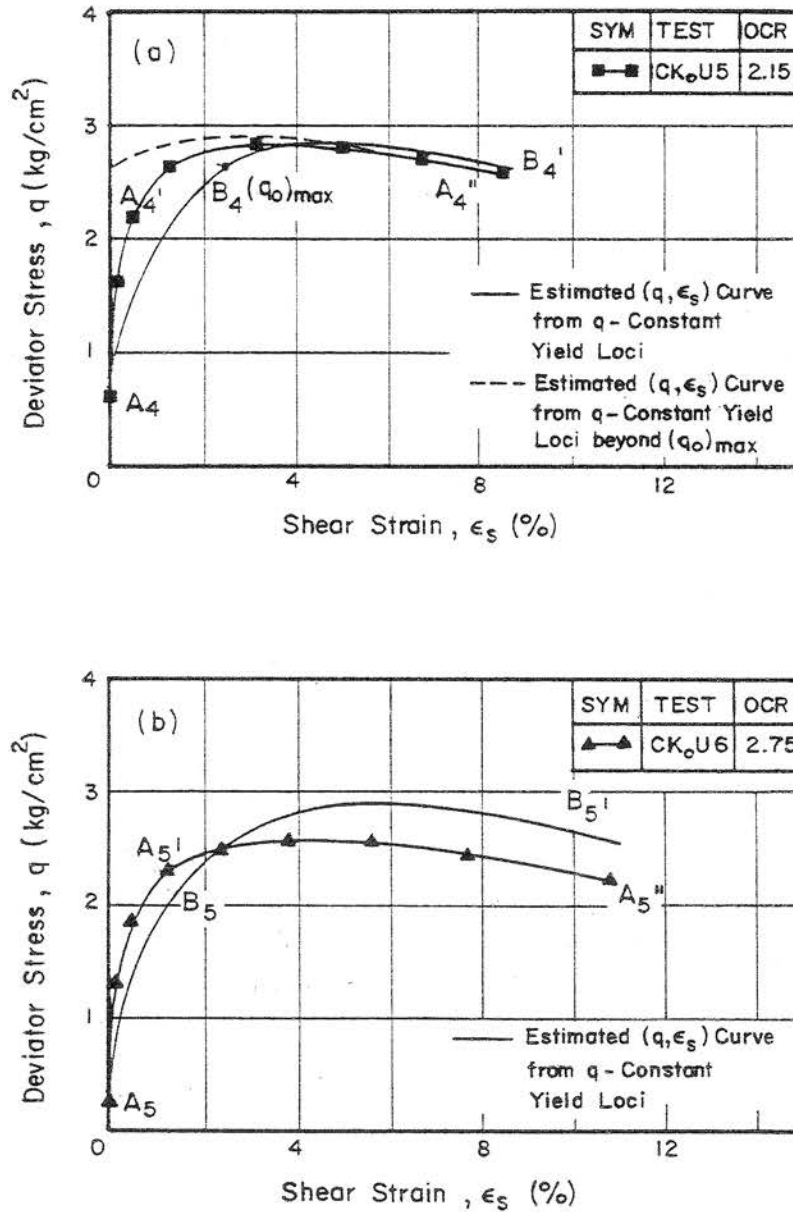


Fig. 5.52 Comparisons of (q, ϵ_s) Relationship between the CKoU Tests and the Estimated Ones from the Constant q -yield Loci of CIU Tests; (a) OCR = 2.15; (b) OCR = 2.75

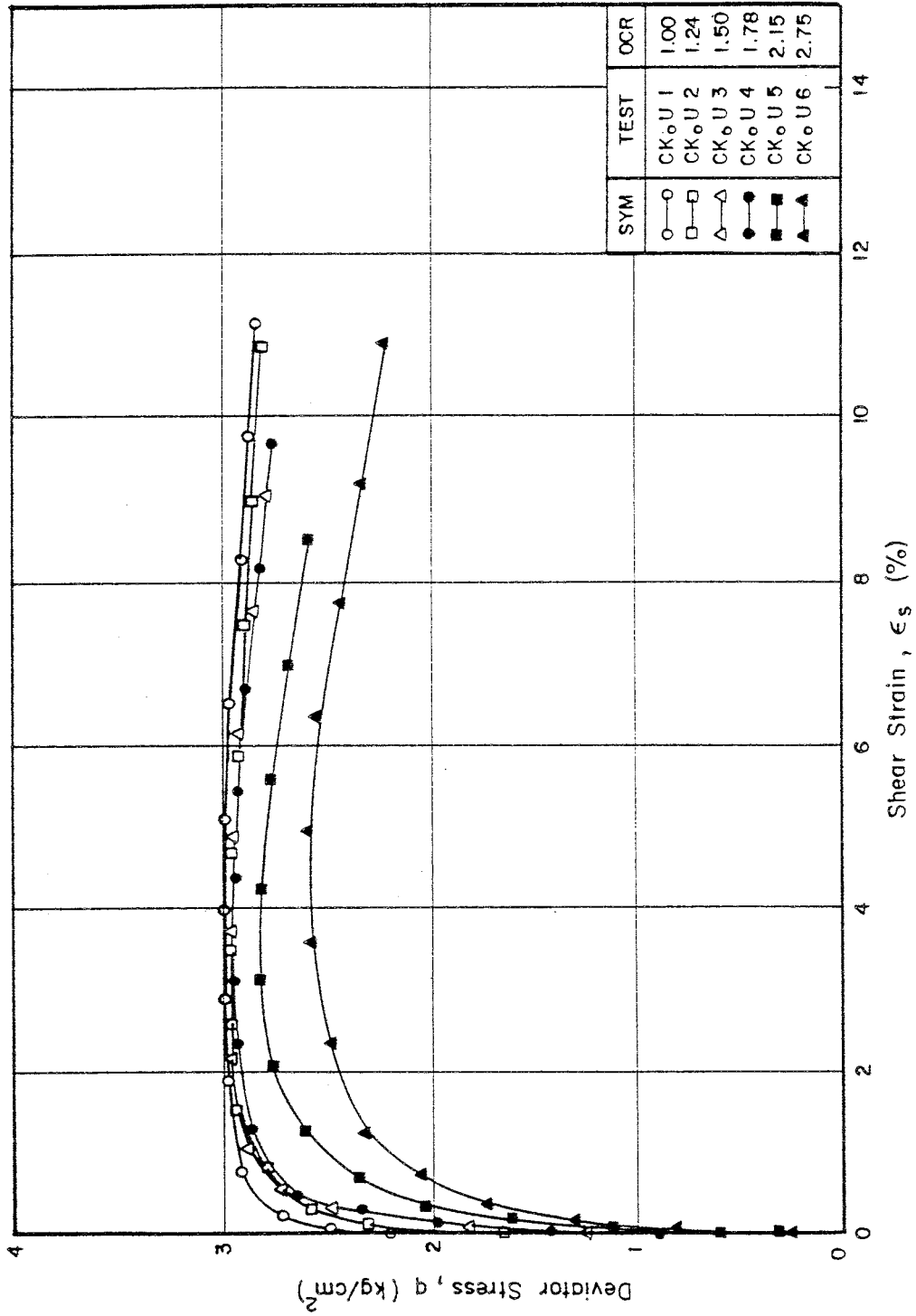


Fig. 5.53 (q , ϵ_s) Plot for K_o -overconsolidated Samples from CK_oU Tests

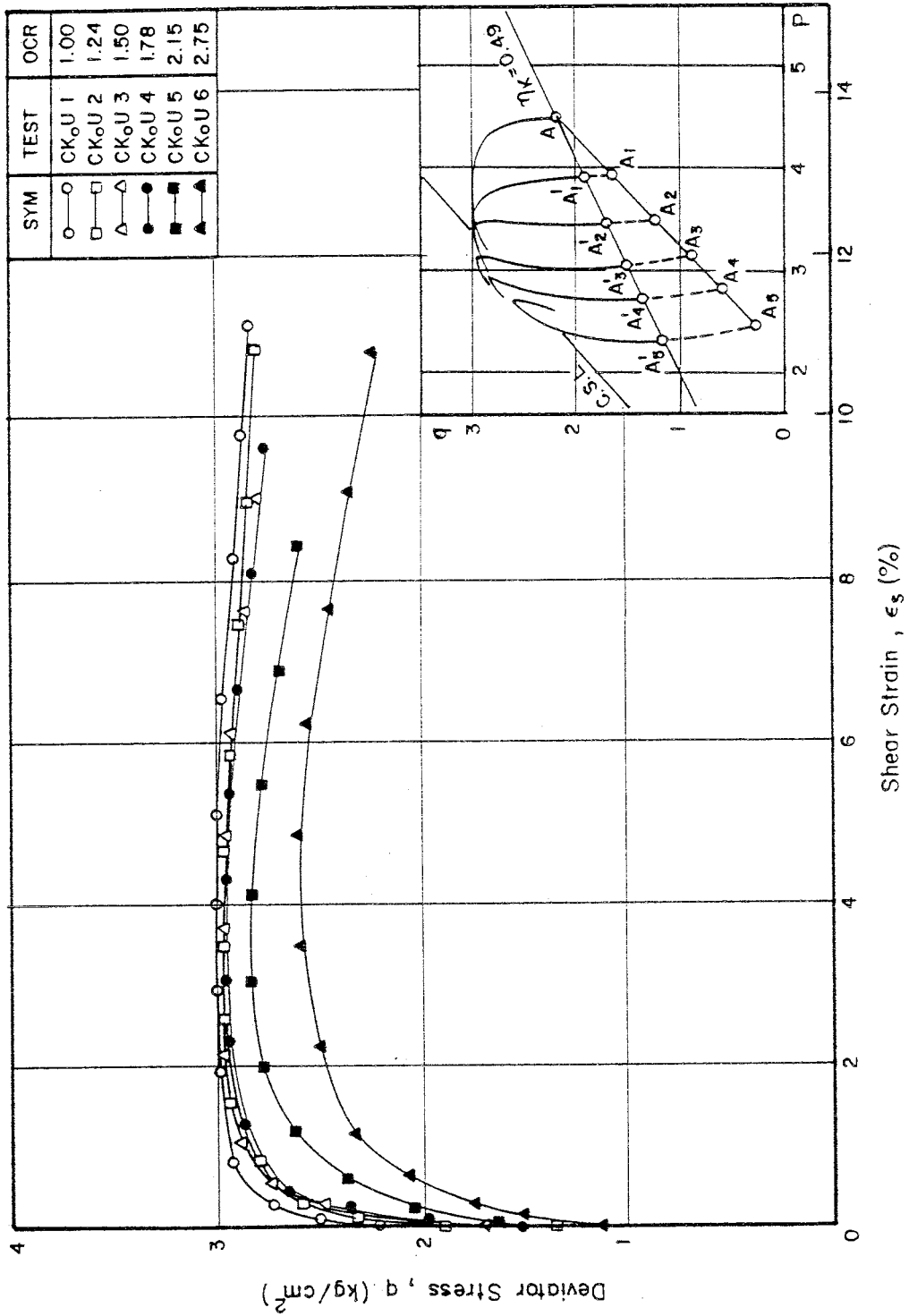


Fig. 5.54 (q, ϵ_s) Plot of K_o -overconsolidated Samples from CKoU
Tests for the Stress Ratios greater than η_k

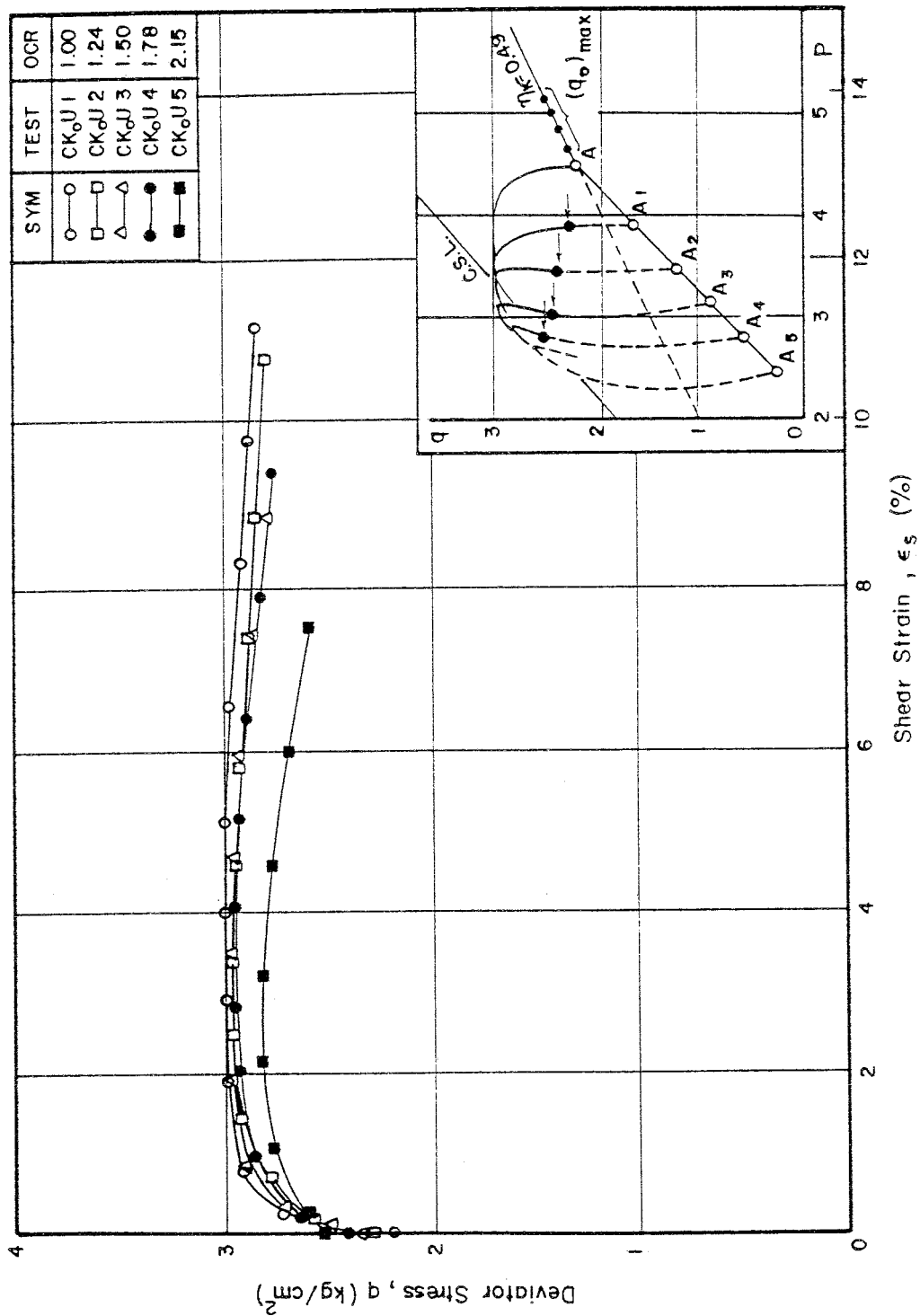


Fig. 5.55 (q , ϵ_s) Plot of K_0 -overconsolidated Samples from CK₀U Tests for the Deviator Stress greater than the Past Maximum Deviator Stress, $(q_0)_{max}$

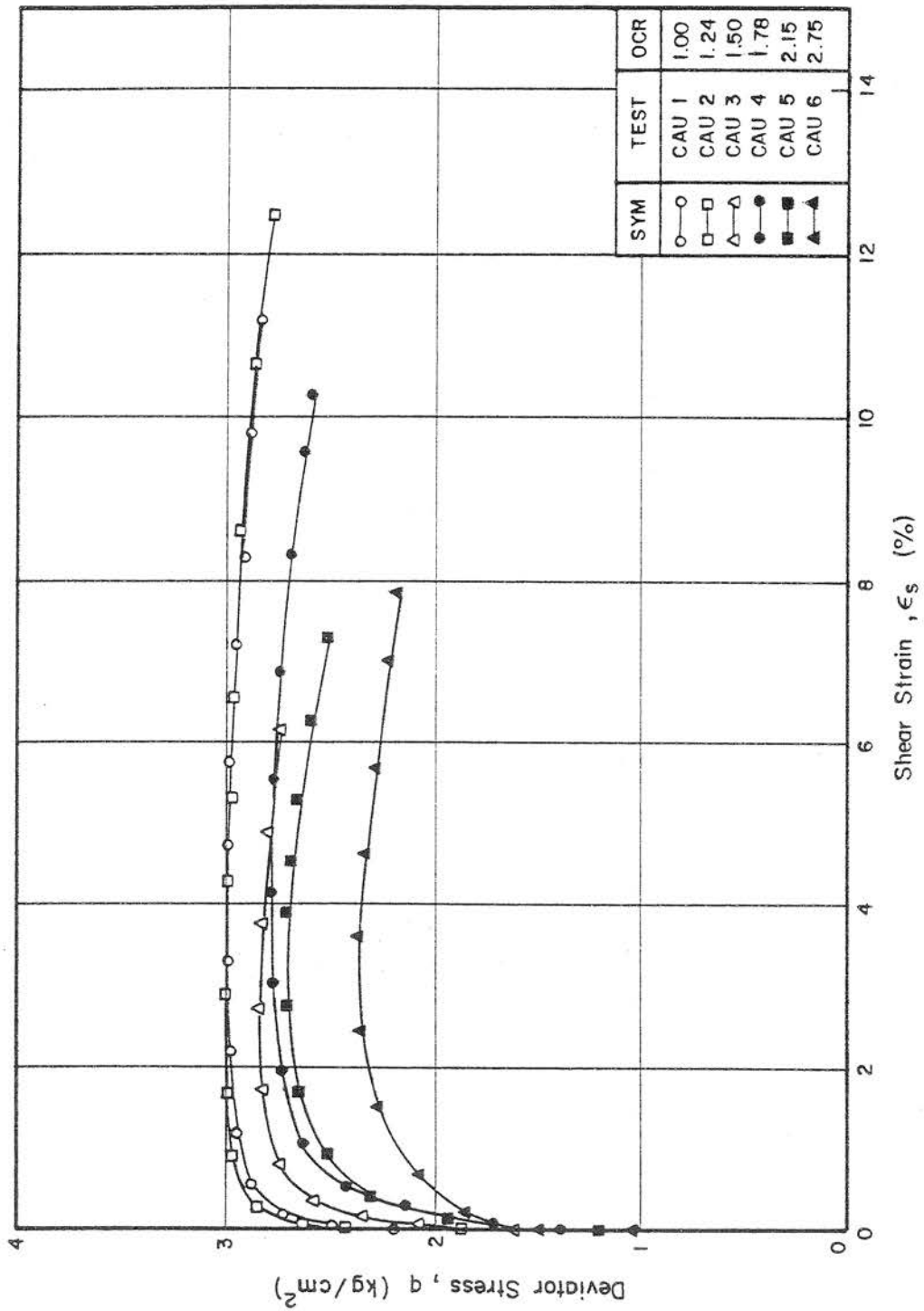


Fig- 5.56 (q, ϵ_s) Plot for Anisotropically Overconsolidated Samples from CAU Tests

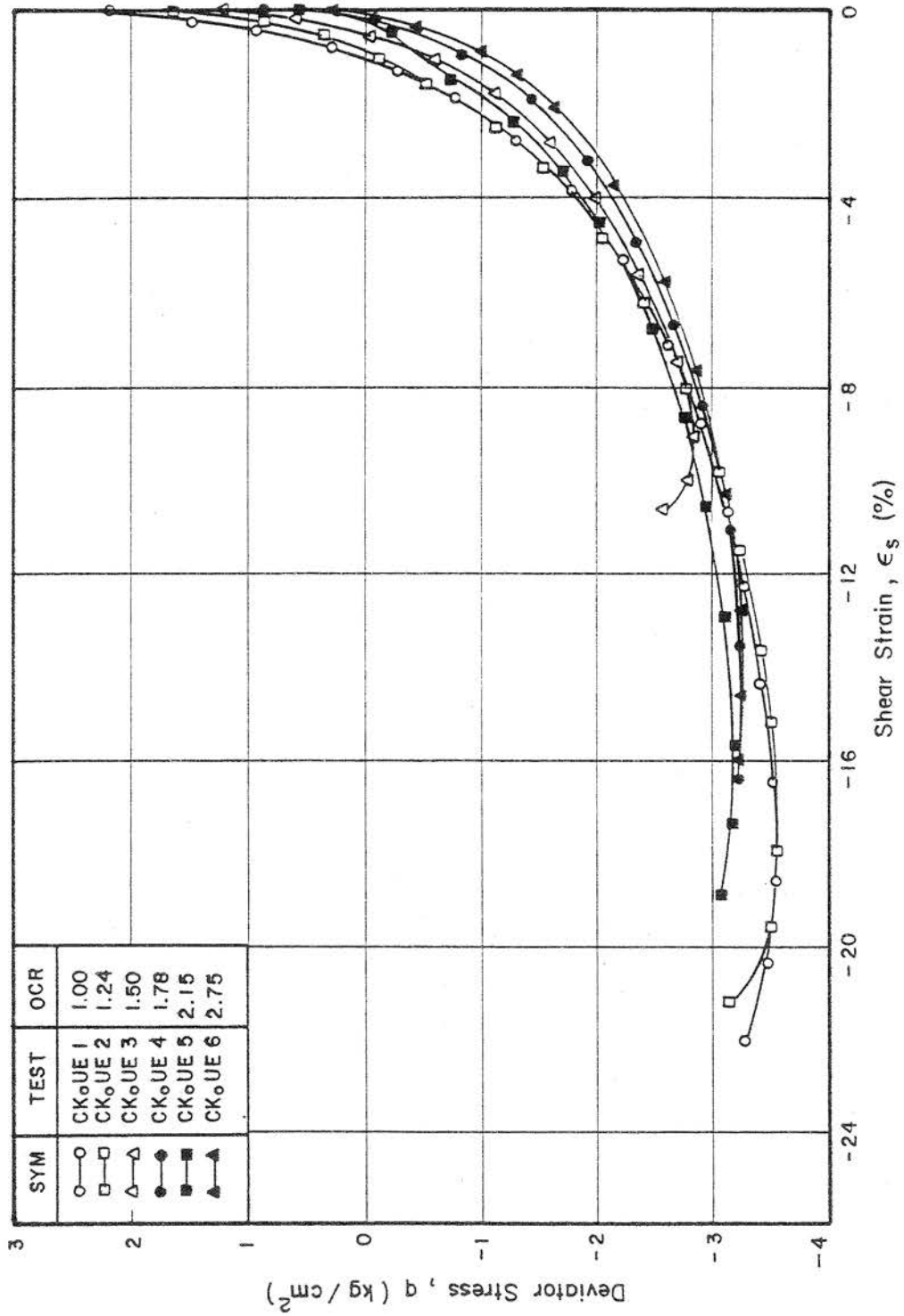


Fig. 5.57 (q , ϵ_s) Plot for K_o -overconsolidated Samples from CKoUE Tests

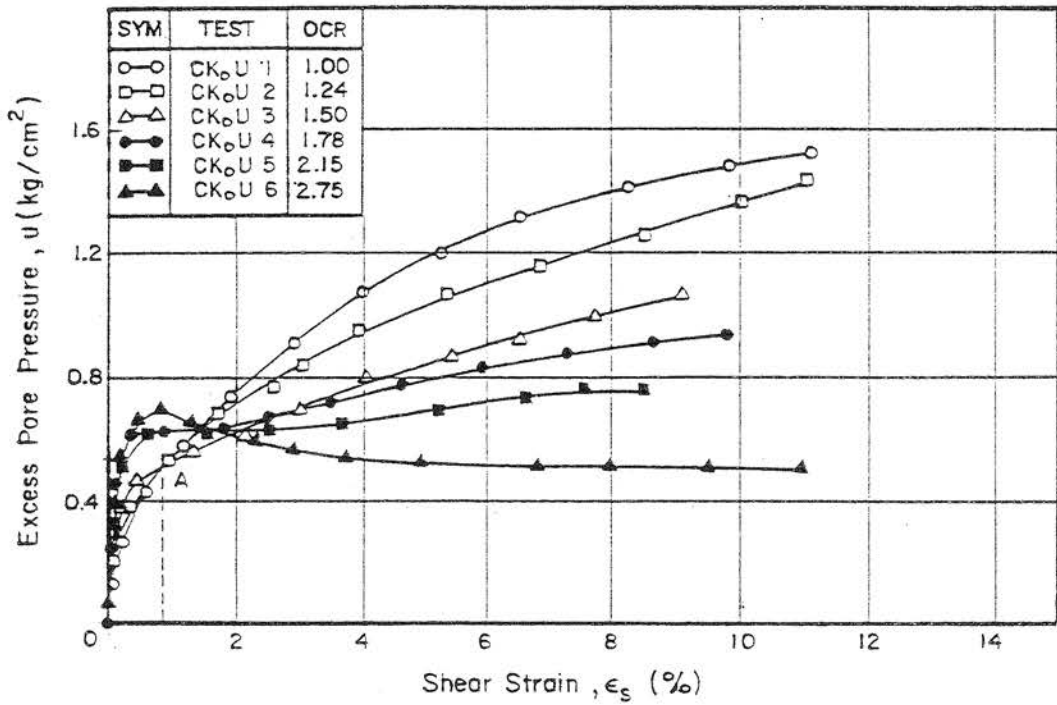


Fig. 5.58 (u , ϵ_s) Plot for K_0 -overconsolidated Samples from CK₀U Tests

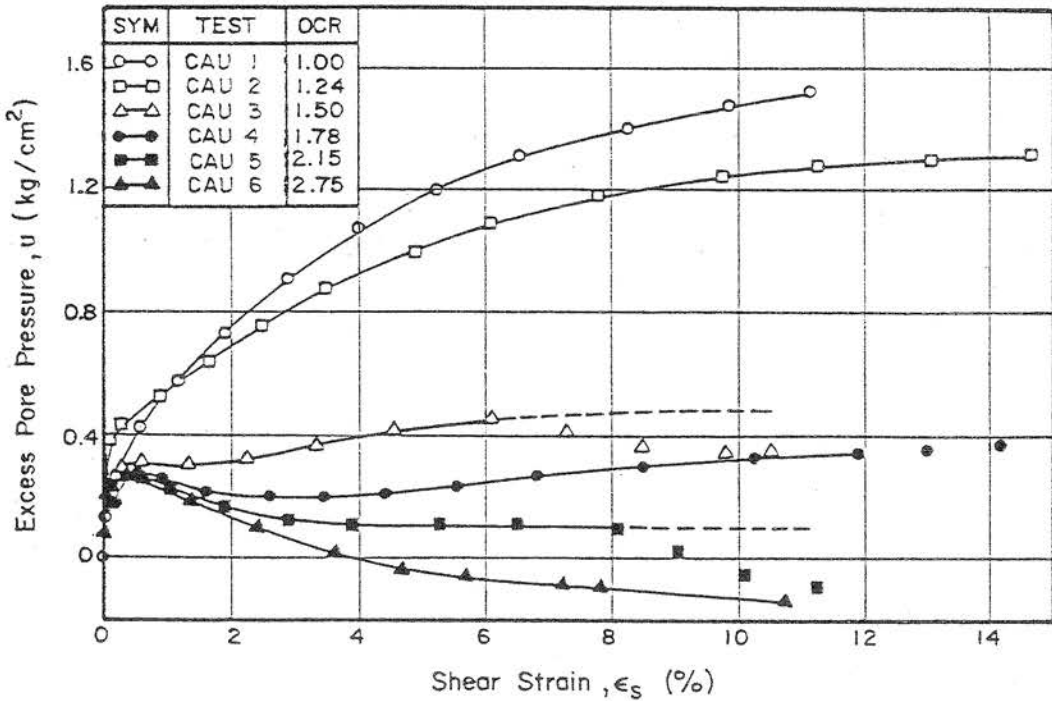


Fig. 5.59 (u , ϵ_s) Plot for Anisotropically Overconsolidated Samples from CAU Tests

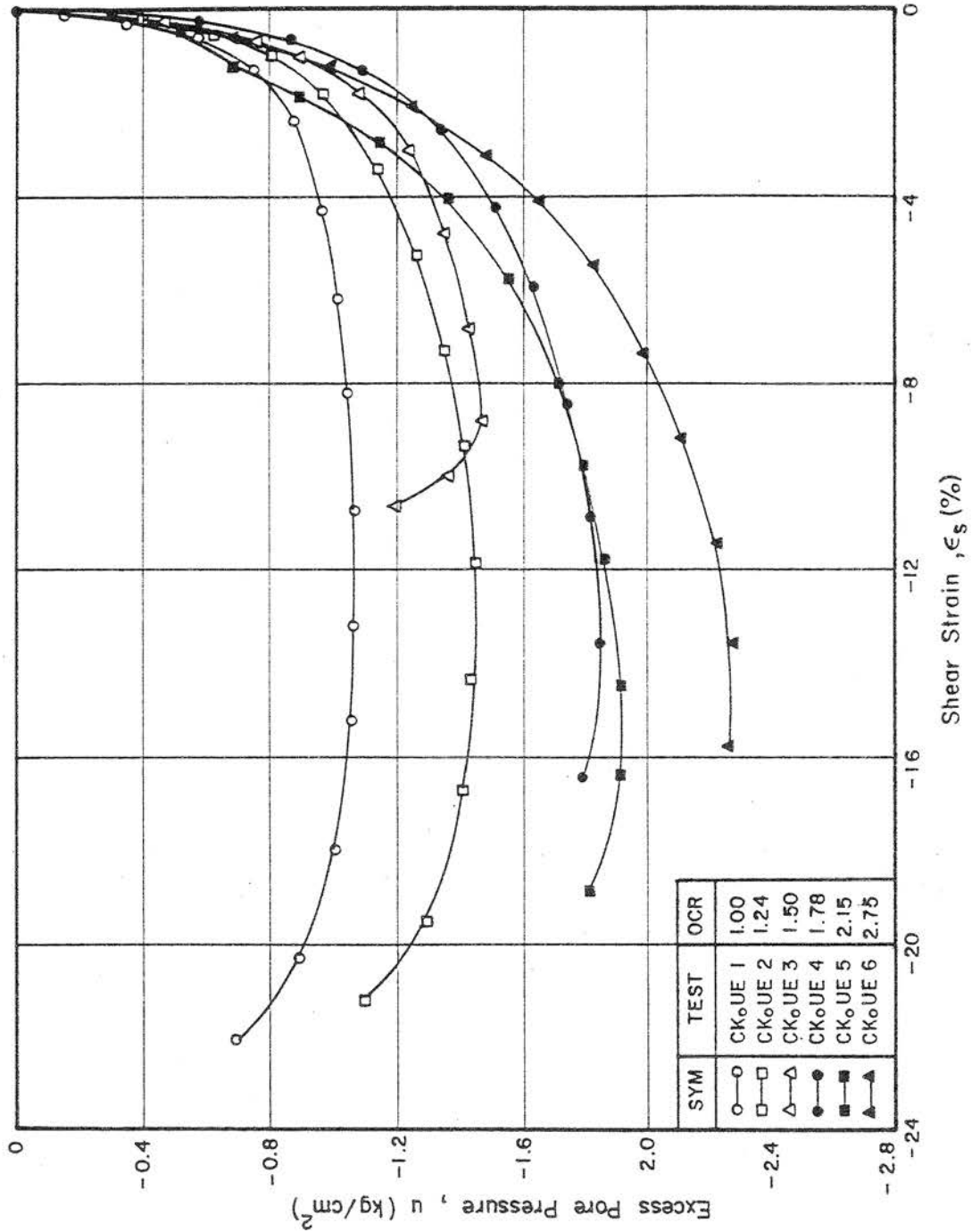


Fig. 5.60 (u , ϵ_s) Plot for K_0 -overconsolidated Samples from CK₀UE Tests

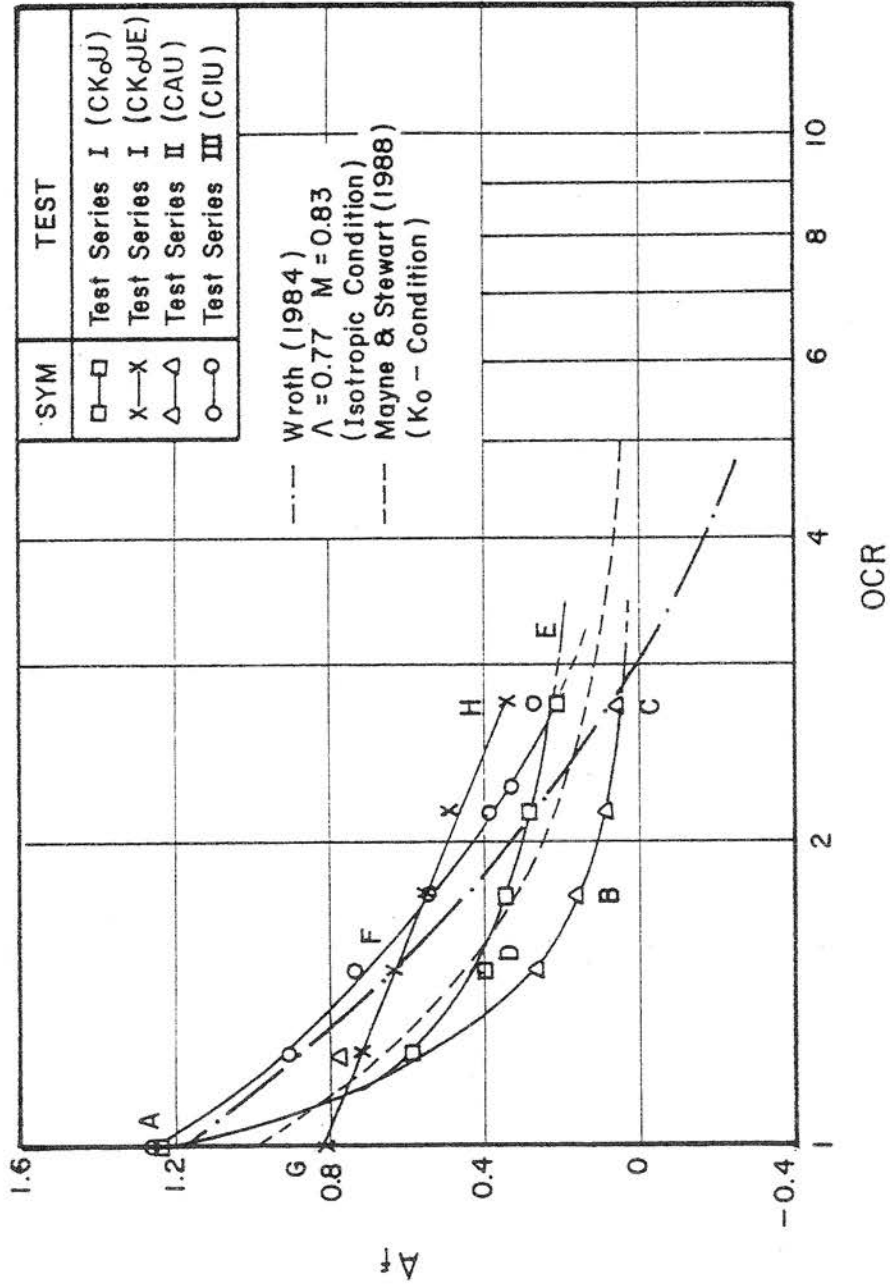


Fig. 5.61 Variation of A_f with OCR for the Overconsolidated Samples

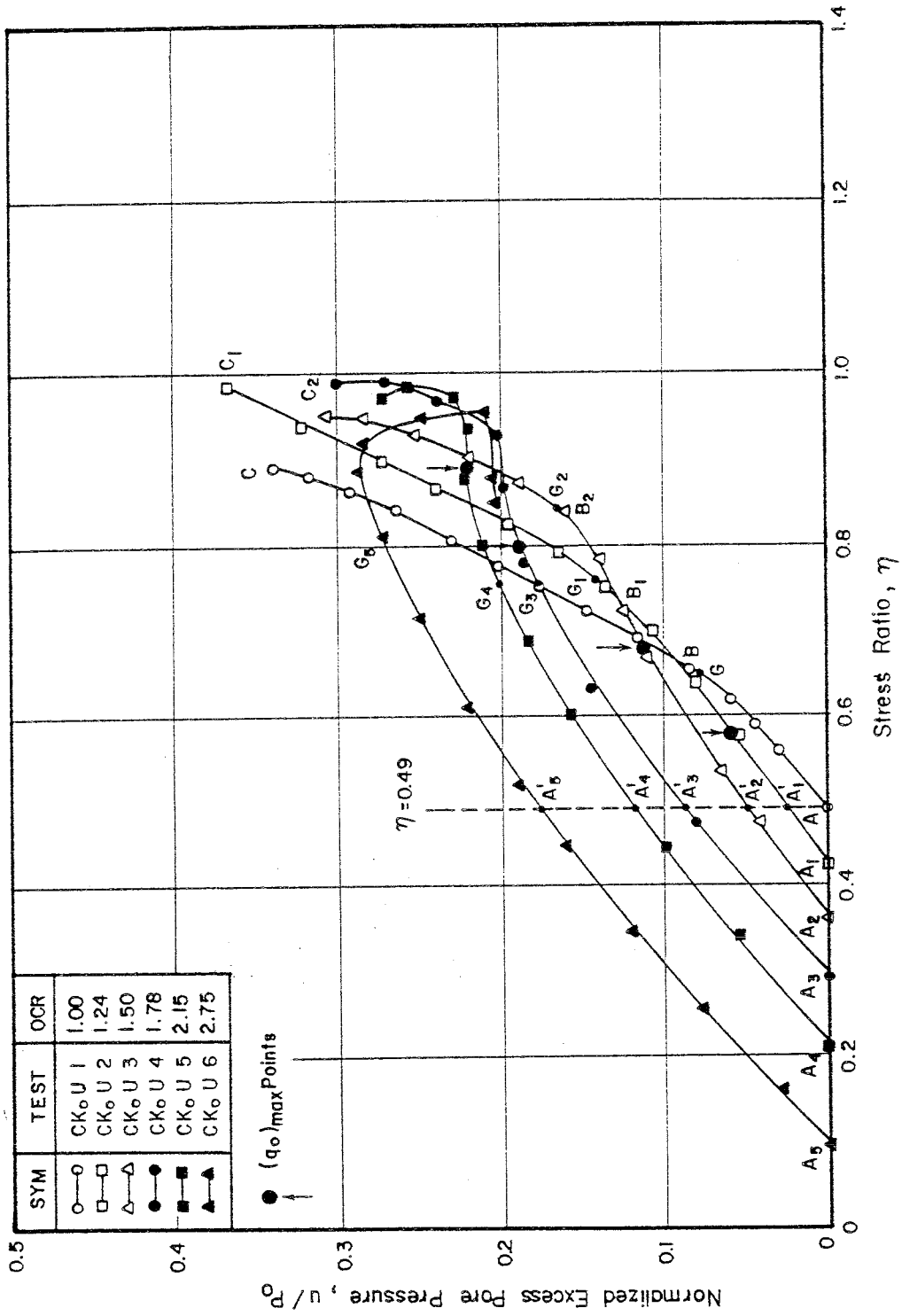


Fig. 5.62 ($u/p_0, \eta$) Plot for K_0 -overconsolidated Samples from CK₀U Tests

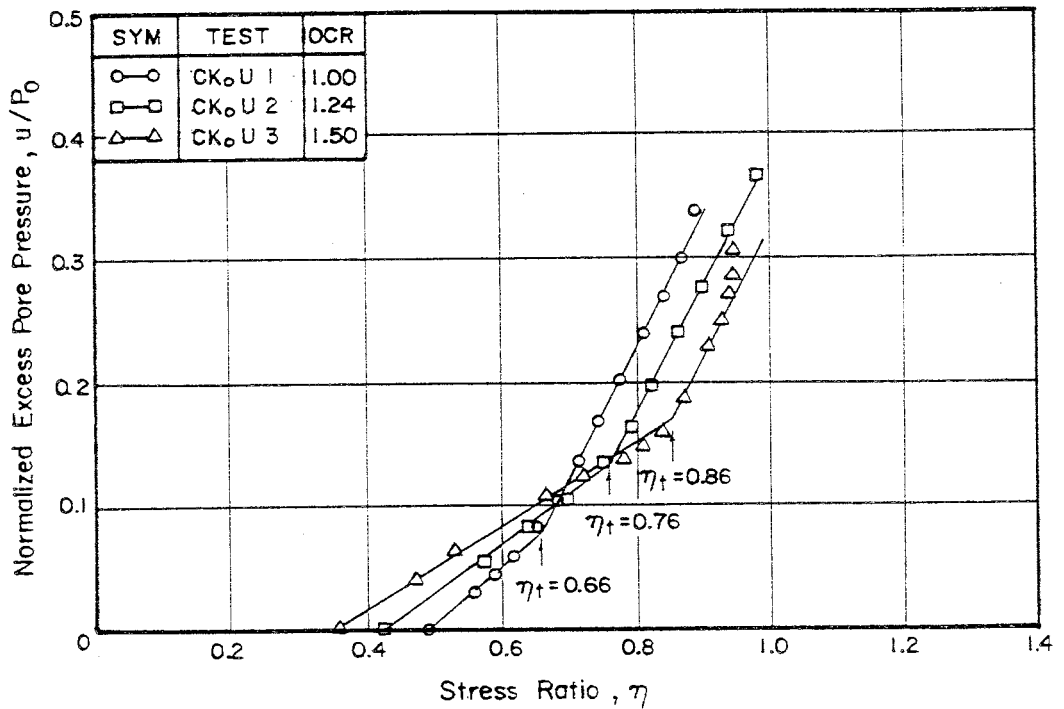


Fig. 5.63 Simplified (u/p_0 , η) Relationship for K_0 -overconsolidated Samples from CK₀U Tests (Wet Zone)

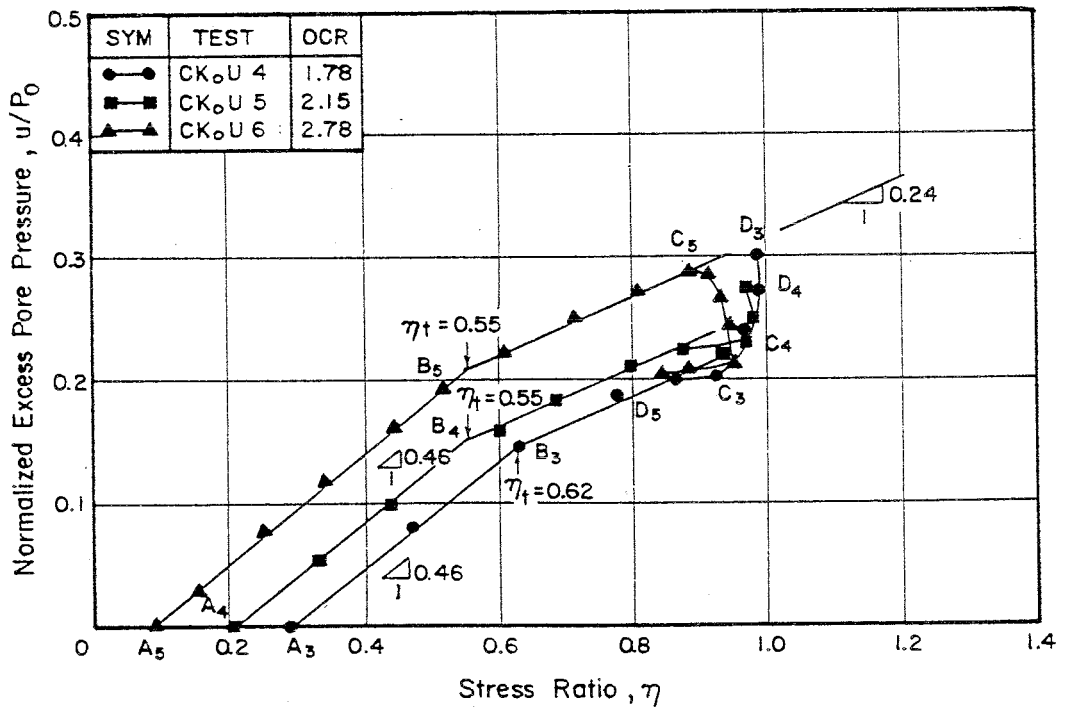


Fig. 5.64 Simplified (u/p_0 , η) Relationship for K_0 -overconsolidated Samples from CK₀U Tests (Dry Zone)

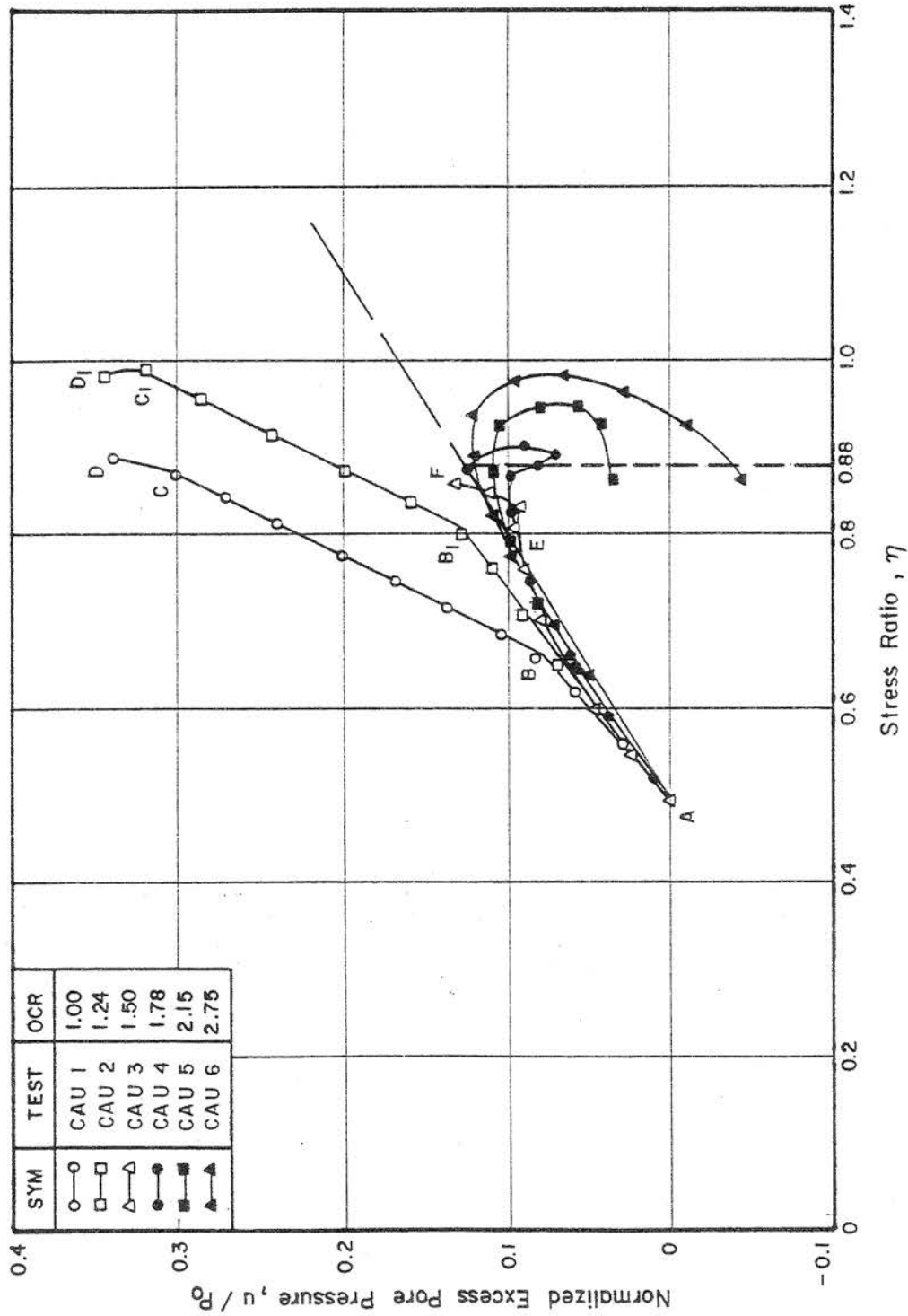


Fig. 5.65 Simplified (u/p_0 , η) Relationship for Anisotropically Consolidated Samples from CAU Tests

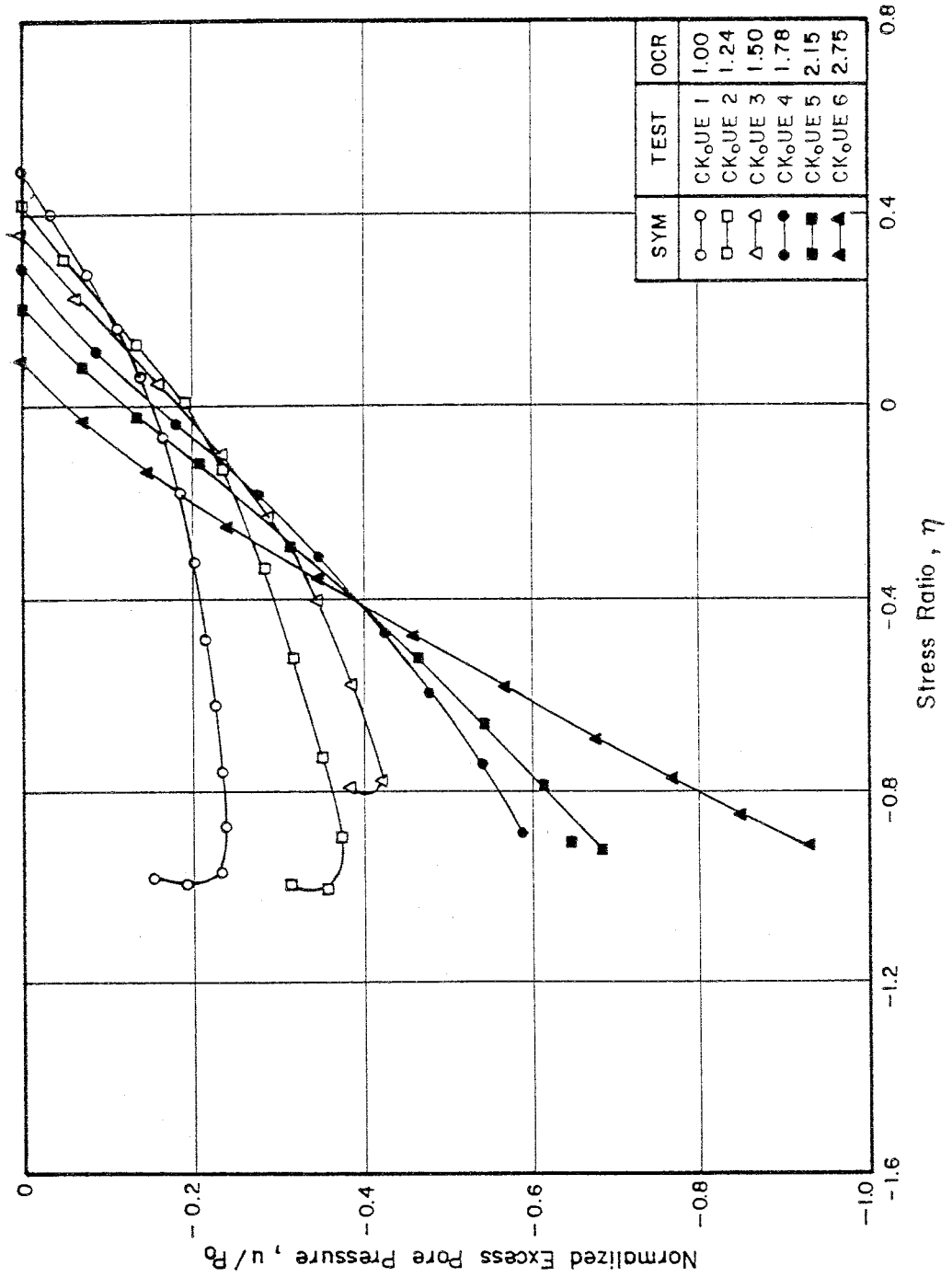


Fig. 5.66 (u/p_0 , η) Relationship for K_0 -overconsolidated Samples from CK₀UE Tests

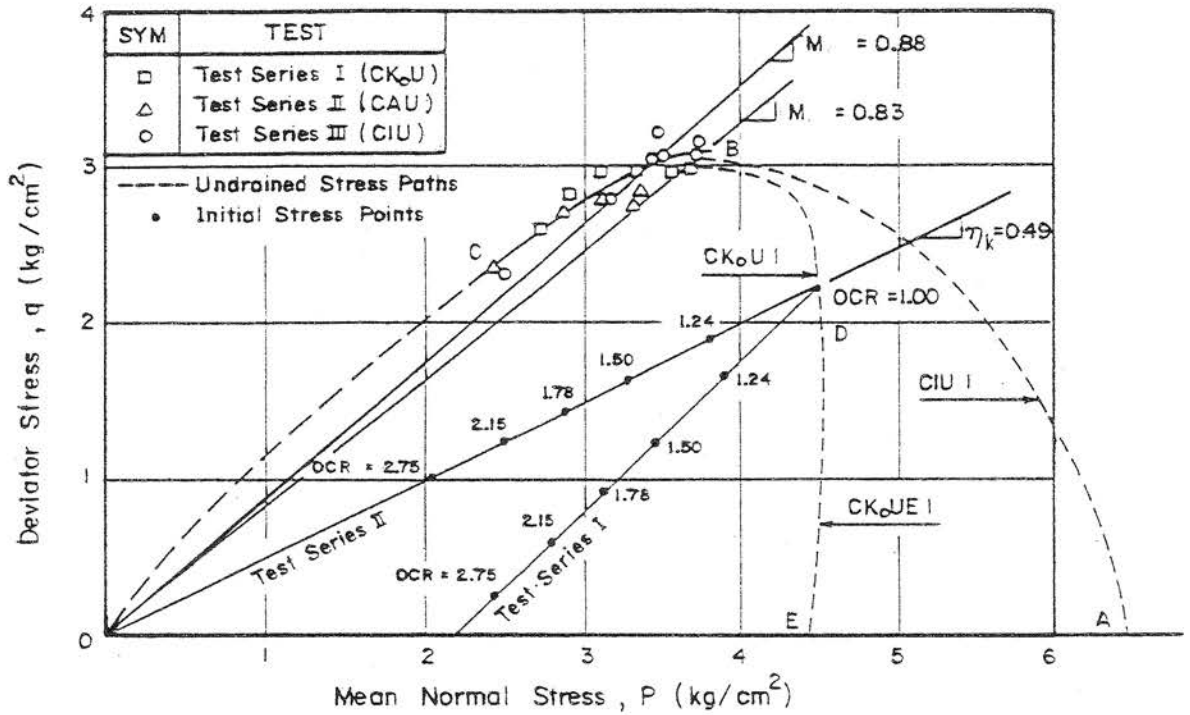


Fig. 5.67 Failure Points from the Undrained Compression Tests (Test Series I, II & III)

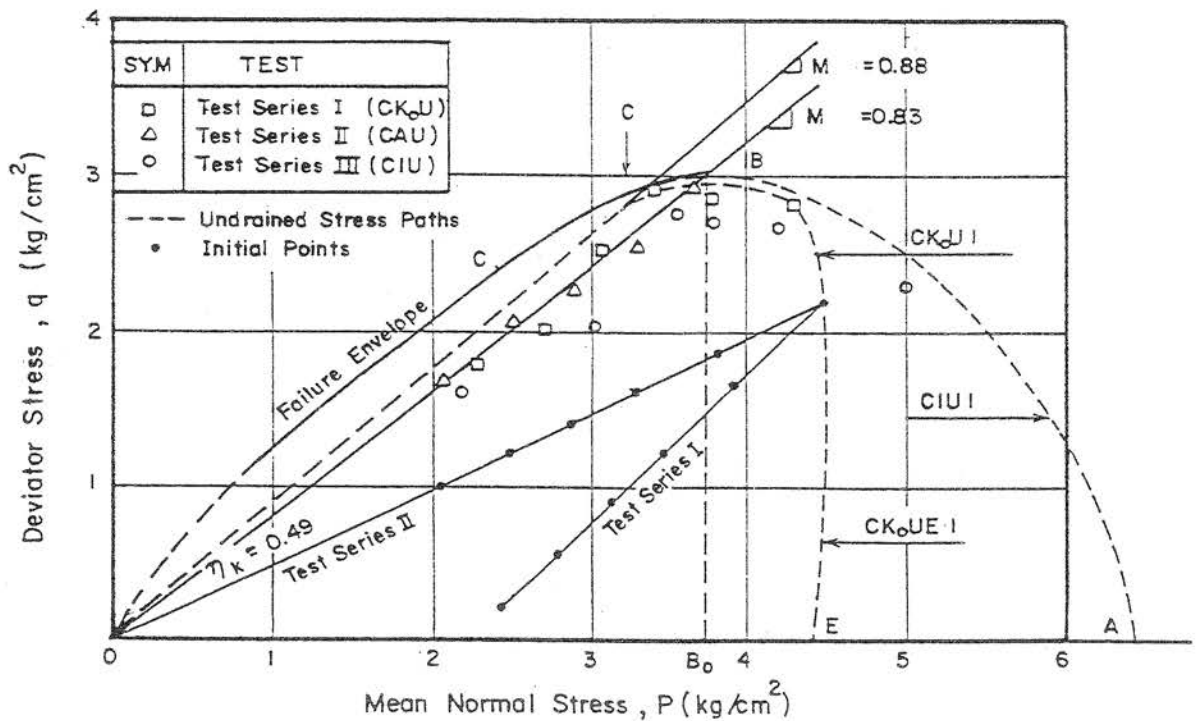


Fig. 5.68 Volumetric Yield Points from the Undrained Compression Tests (Test Series I, II & III)

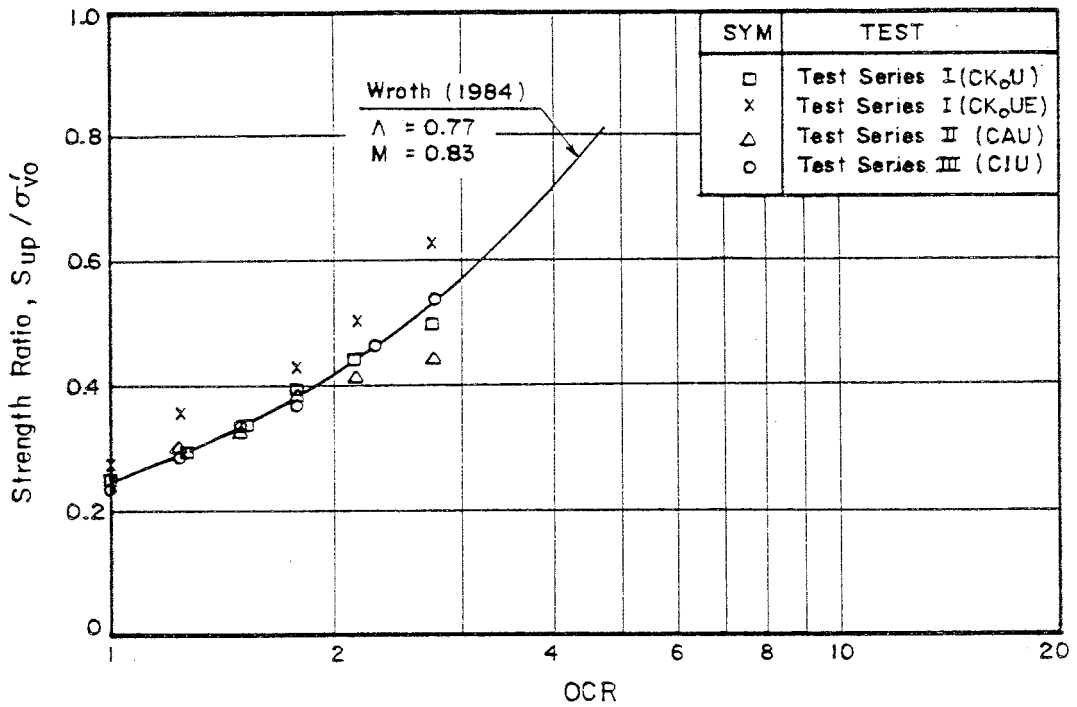


Fig. 5.69 Strength Ratios and OCR from Undrained Tests
 (Test Series I, II & III)

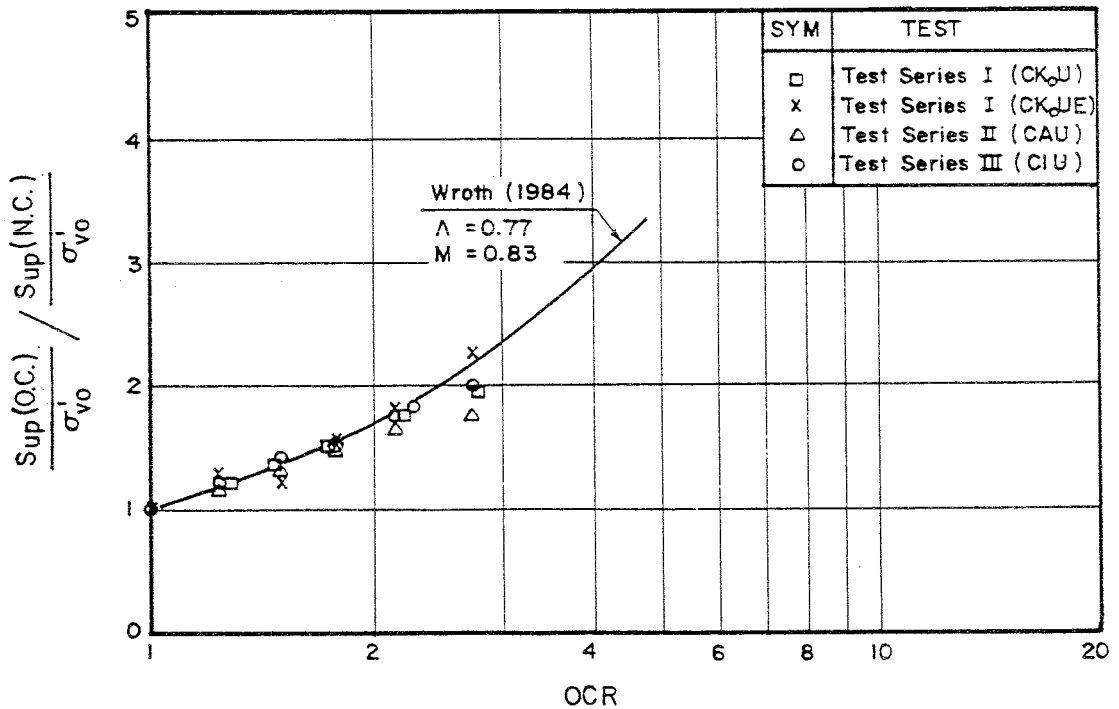


Fig. 5.70 Normalized Strength Ratios and OCR from Undrained Tests
 (Test Series I, II & III)

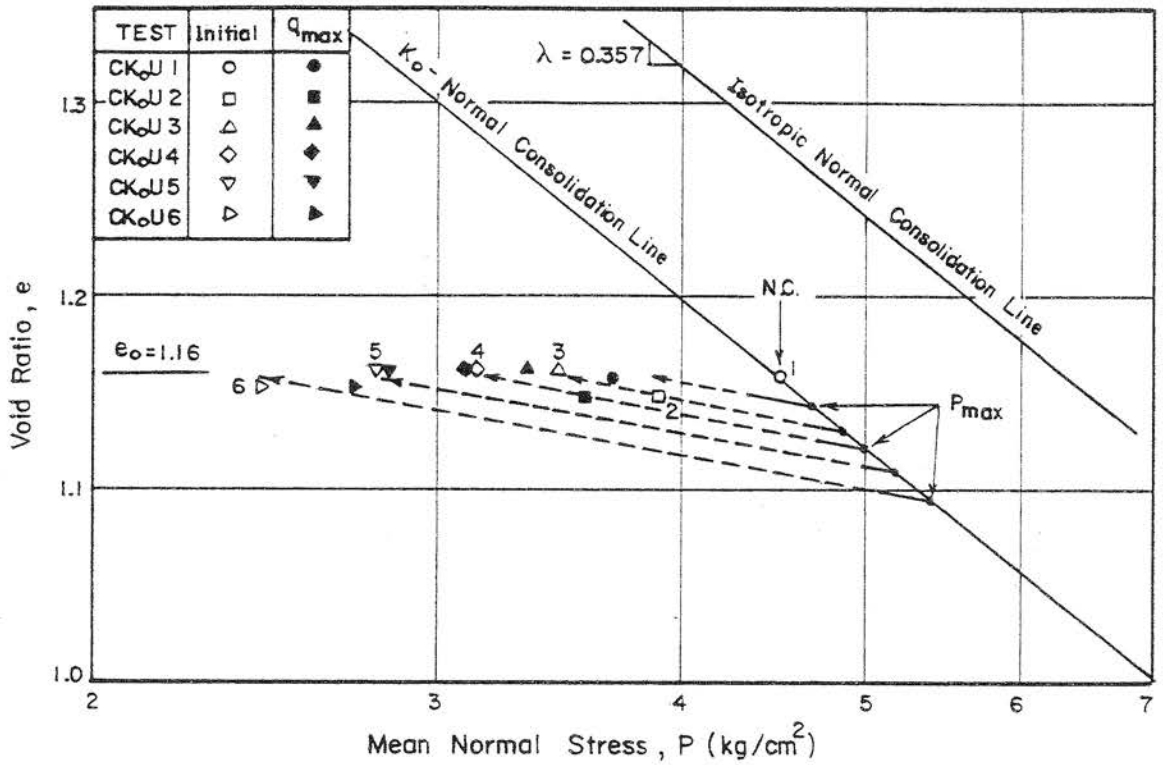


Fig. 5.71a Pre-shear Stresses and q_{max} Points with the Maximum Past Pressures for CKoU Tests

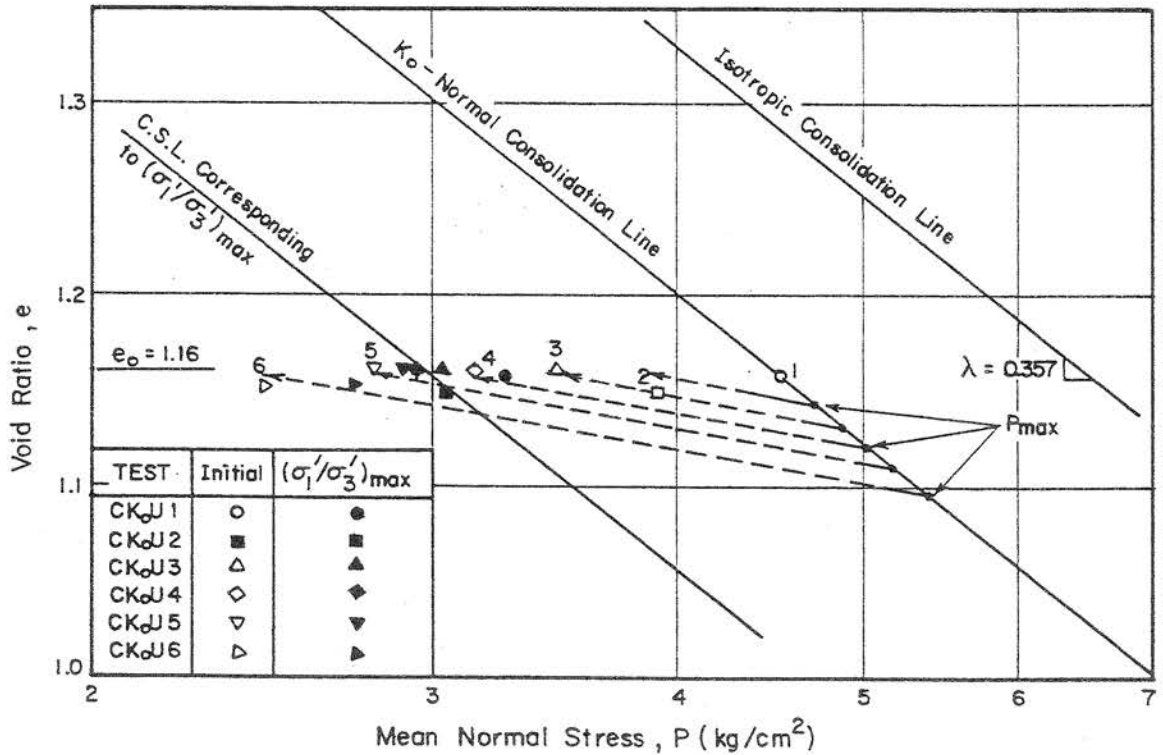


Fig. 5.71b Critical State Line Corresponding to the $(\bar{\sigma}_1'/\bar{\sigma}_3')_{max}$ Conditions from CKoU Tests

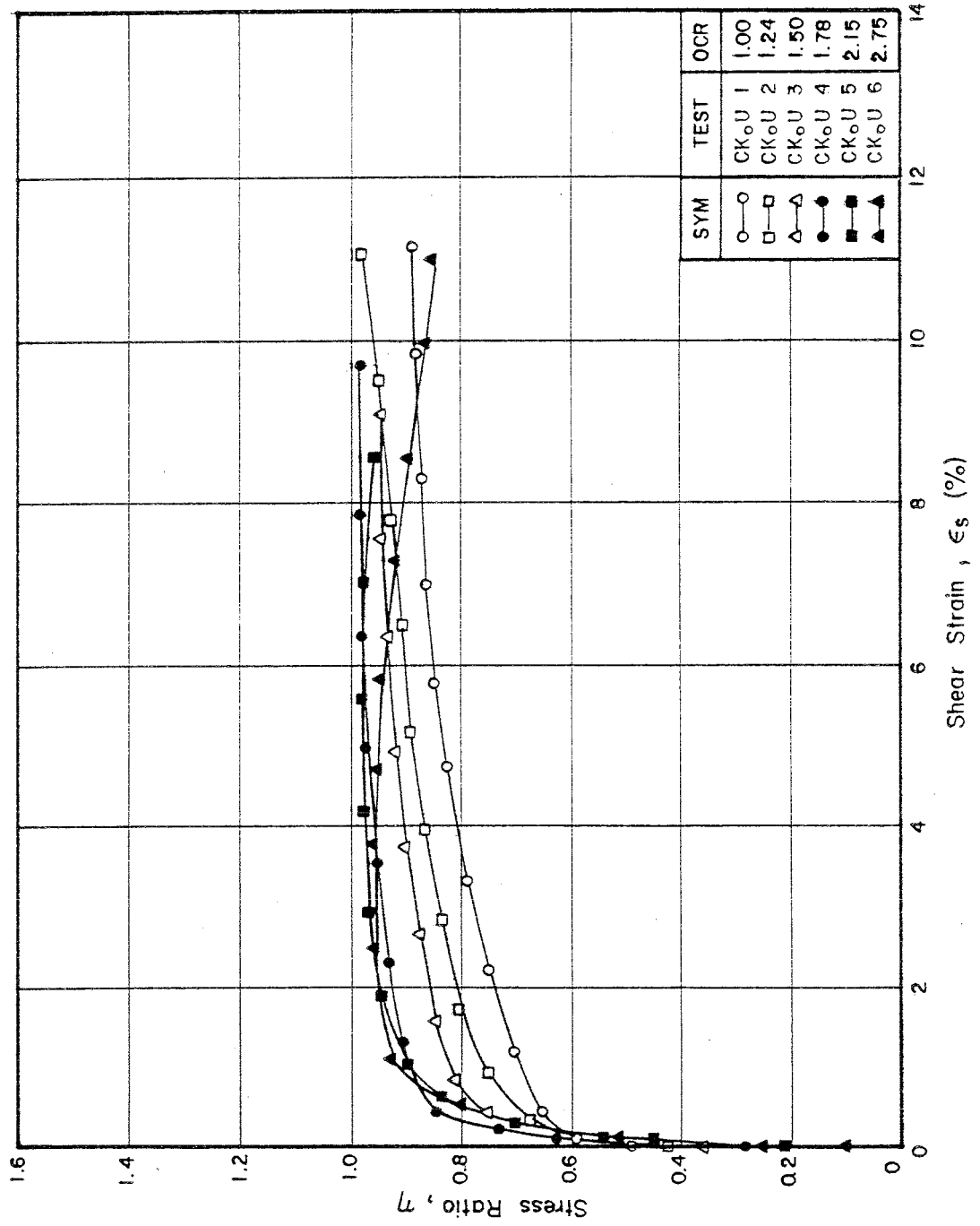


Fig. 5.72 (η , ϵ_s) Relationship for K_o -overconsolidated Samples from CK_oU Tests

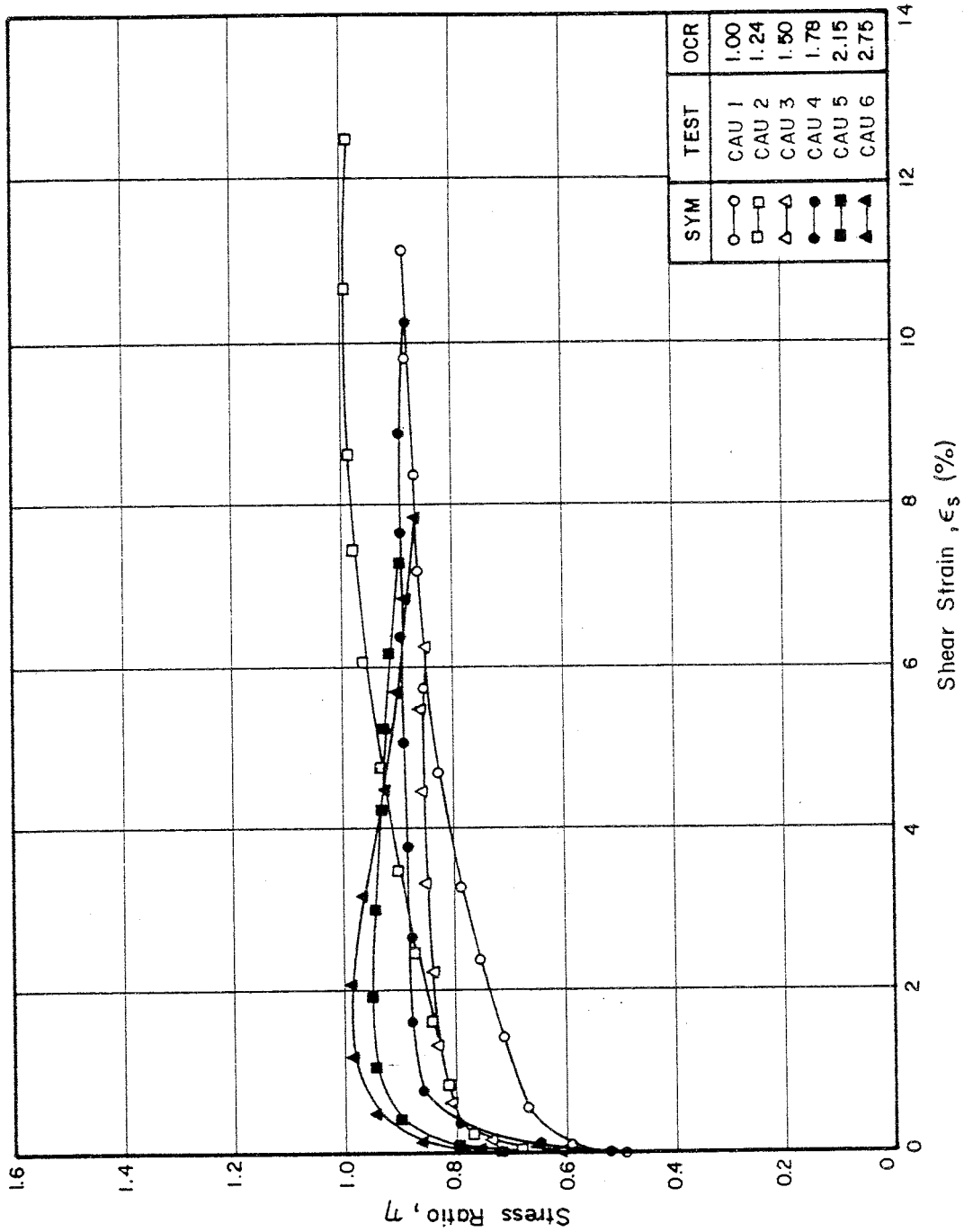


Fig. 5.73 (η , ϵ_s) Relationship for Anisotropically Overconsolidated Samples from CAU Tests

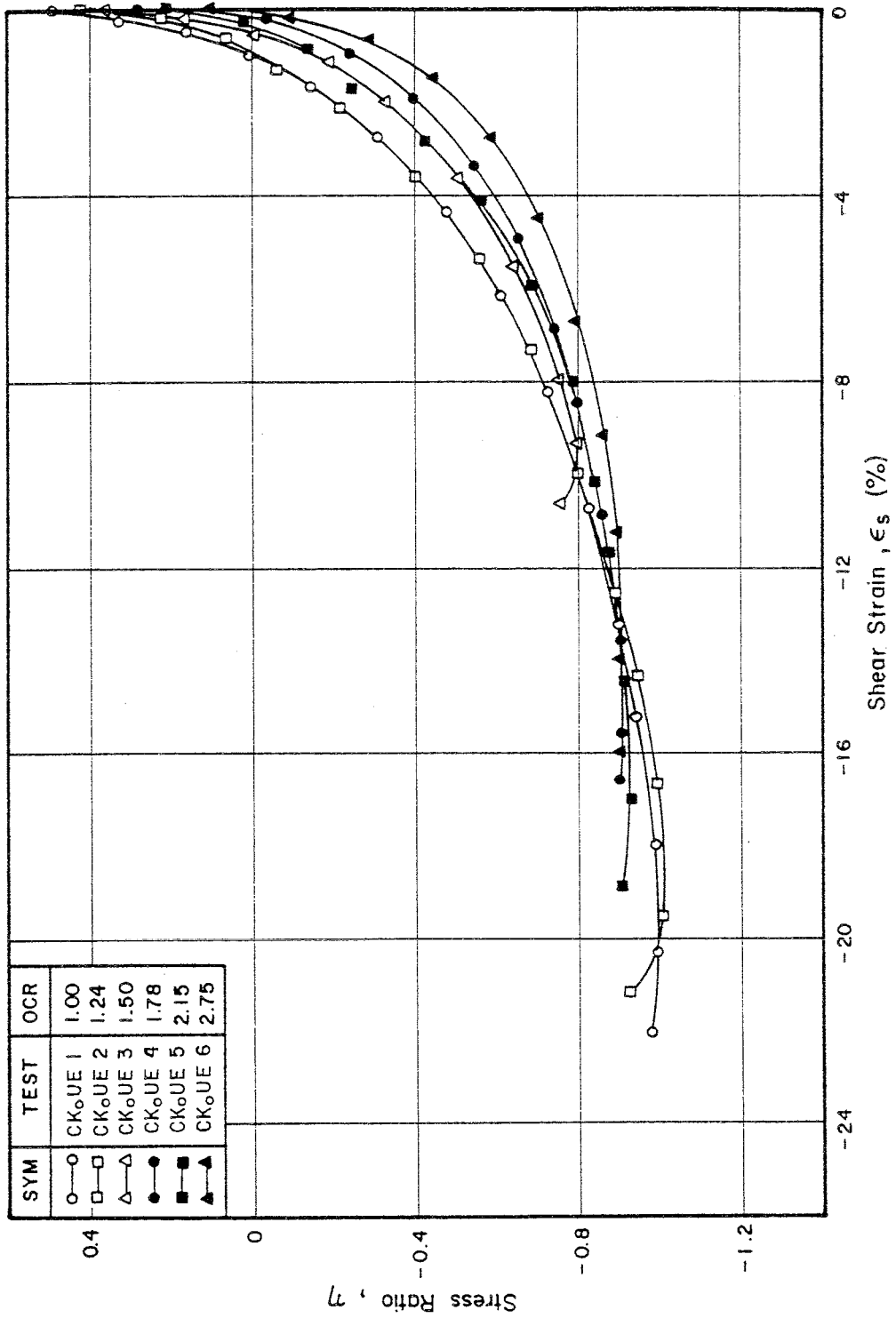


Fig. 5.74 (η , ϵ_s) Relationship for K_o -overconsolidated Samples from CK_oUE Tests

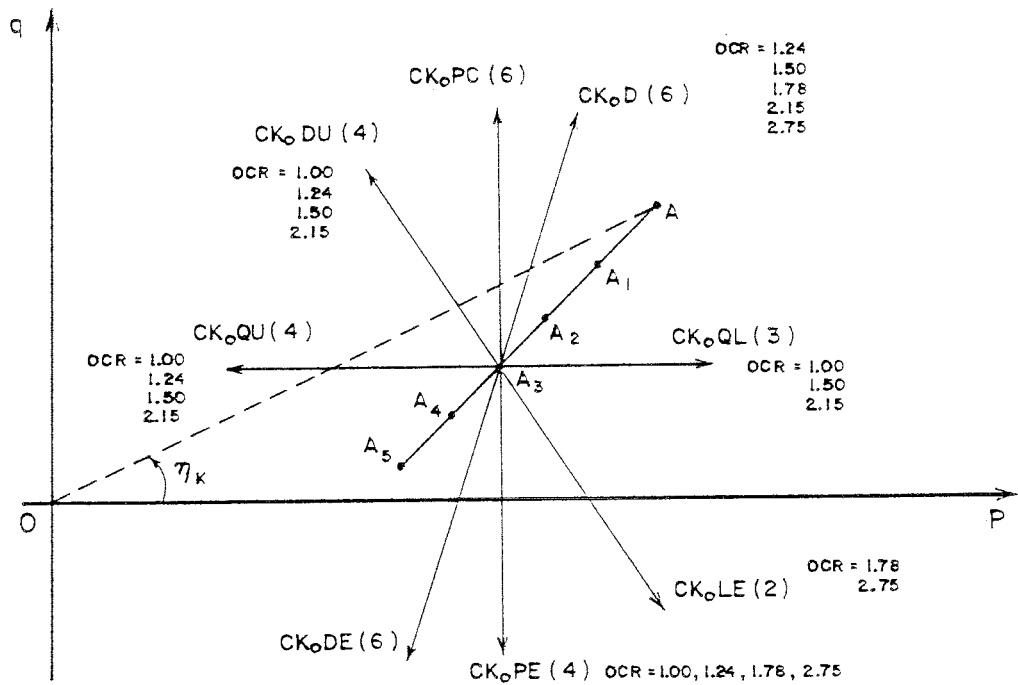


Fig. 6.1 Typical Drained Stress Paths and Test Names of K_0 Overconsolidated Samples (Test Series I)

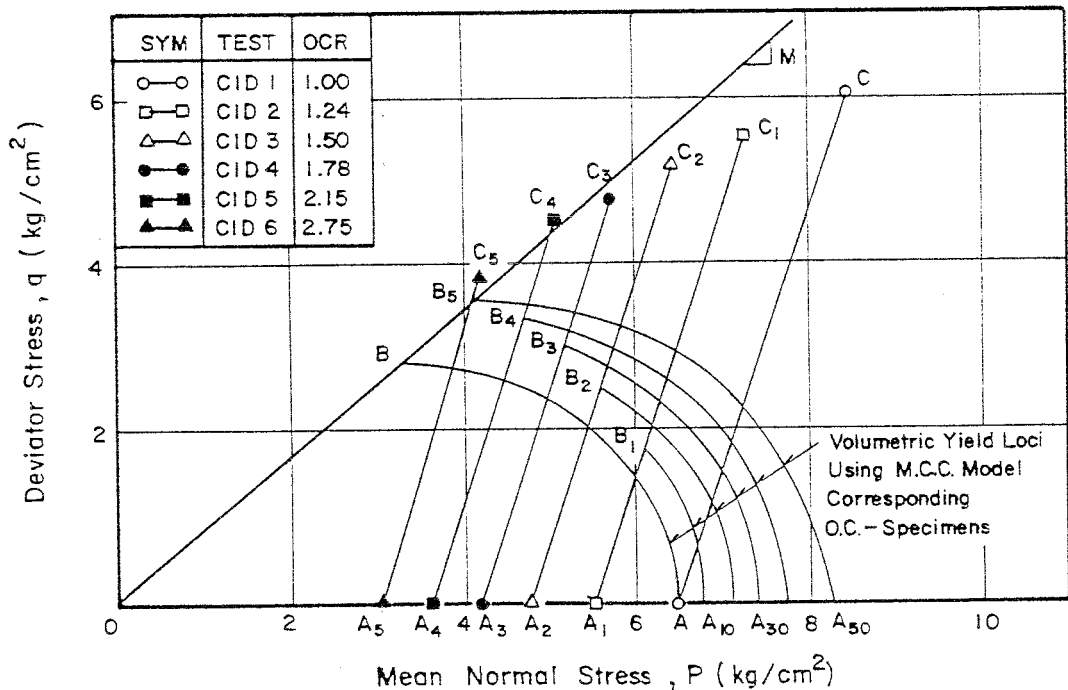


Fig. 6.2 Drained Stress Paths from CID Tests

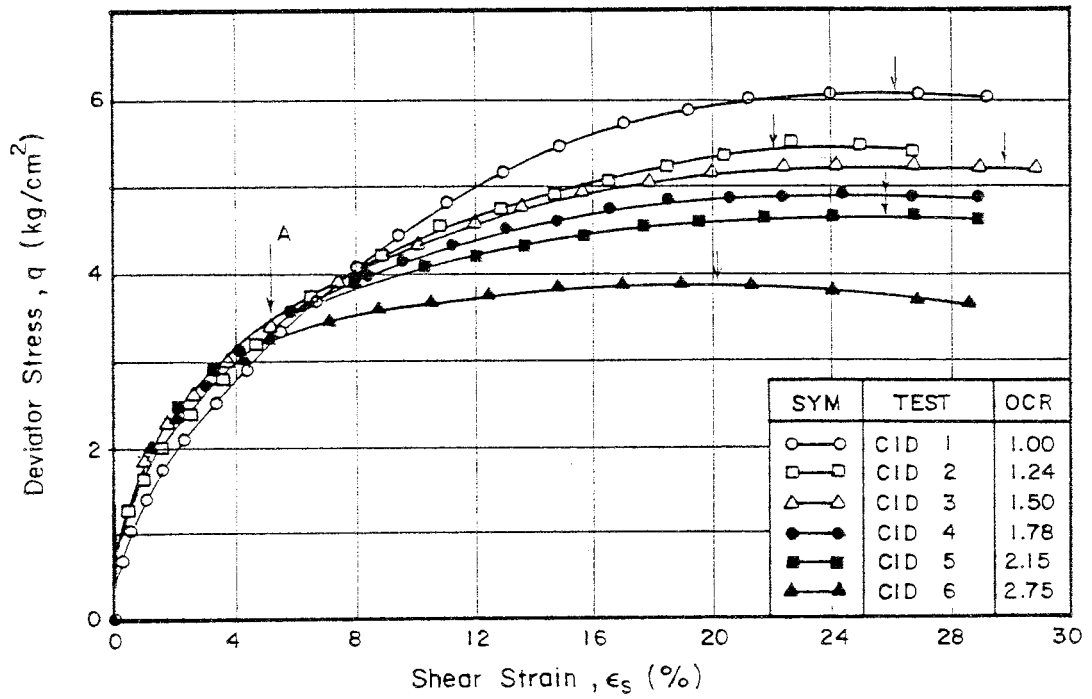


Fig. 6.3 (q , ϵ_s) Plot from CID Tests

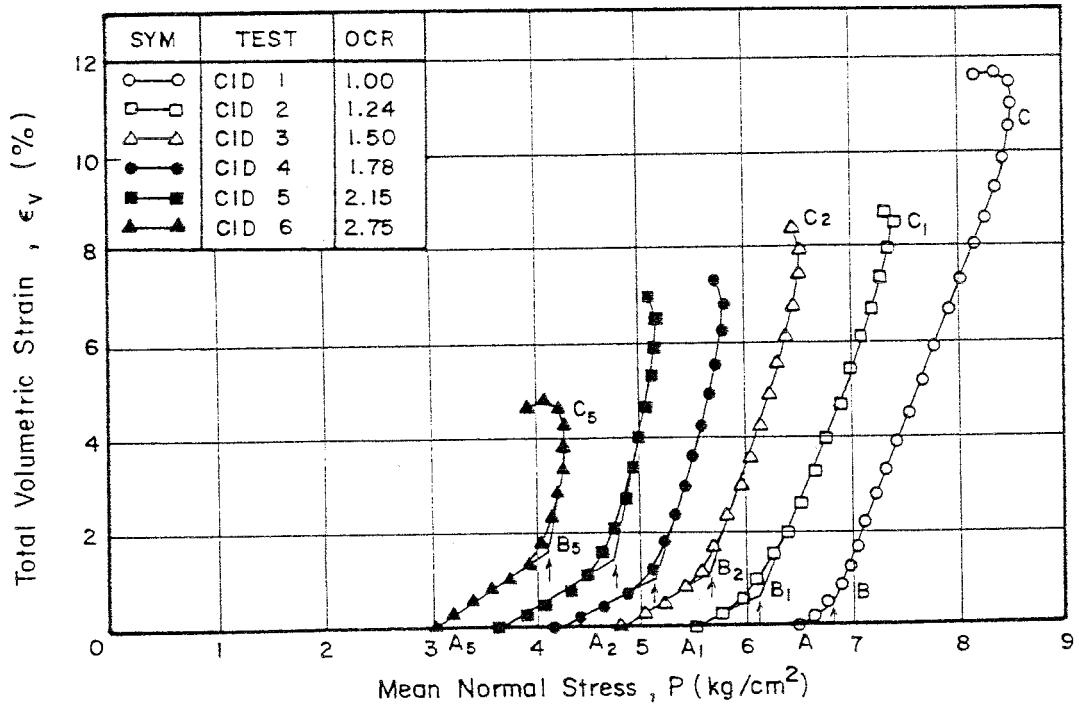


Fig. 6.4 (p , ϵ_v) Plot from CID Tests

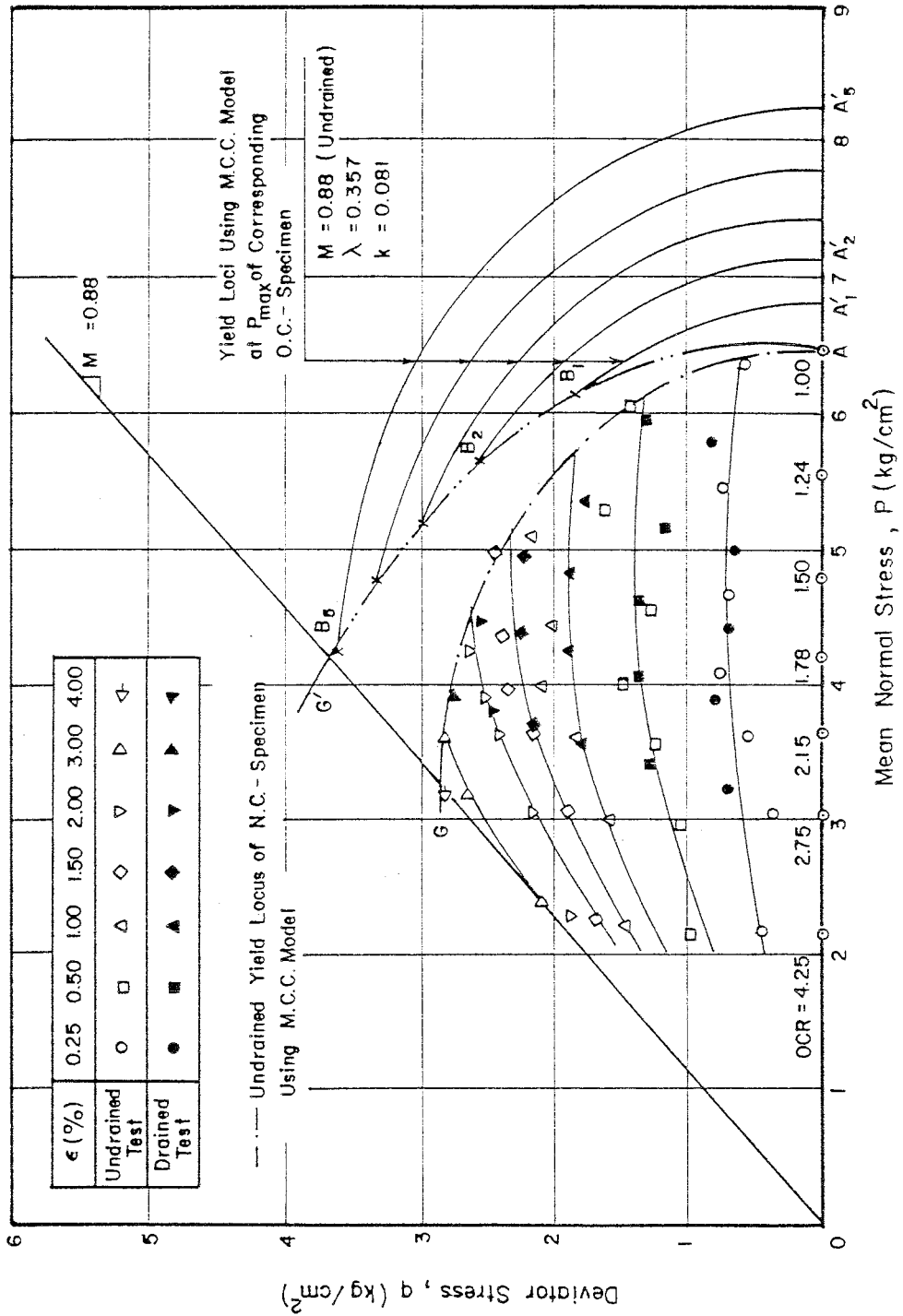


Fig. 6.5 Shear Strain Contours within the State Boundary Surface from CIU & CID Tests

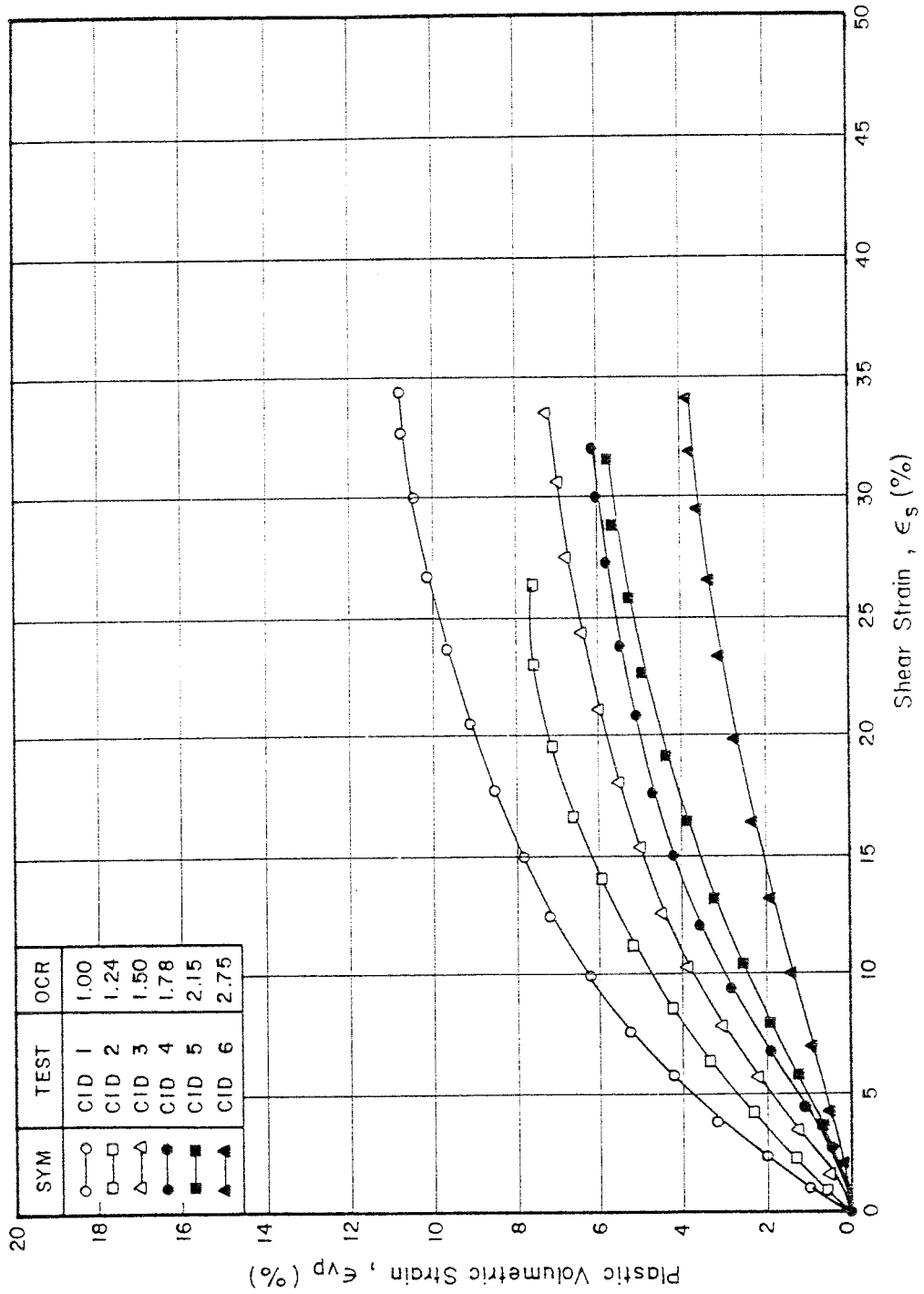


Fig. 6.6 (ϵ_{vp} , ϵ_s) Plot from CID Tests

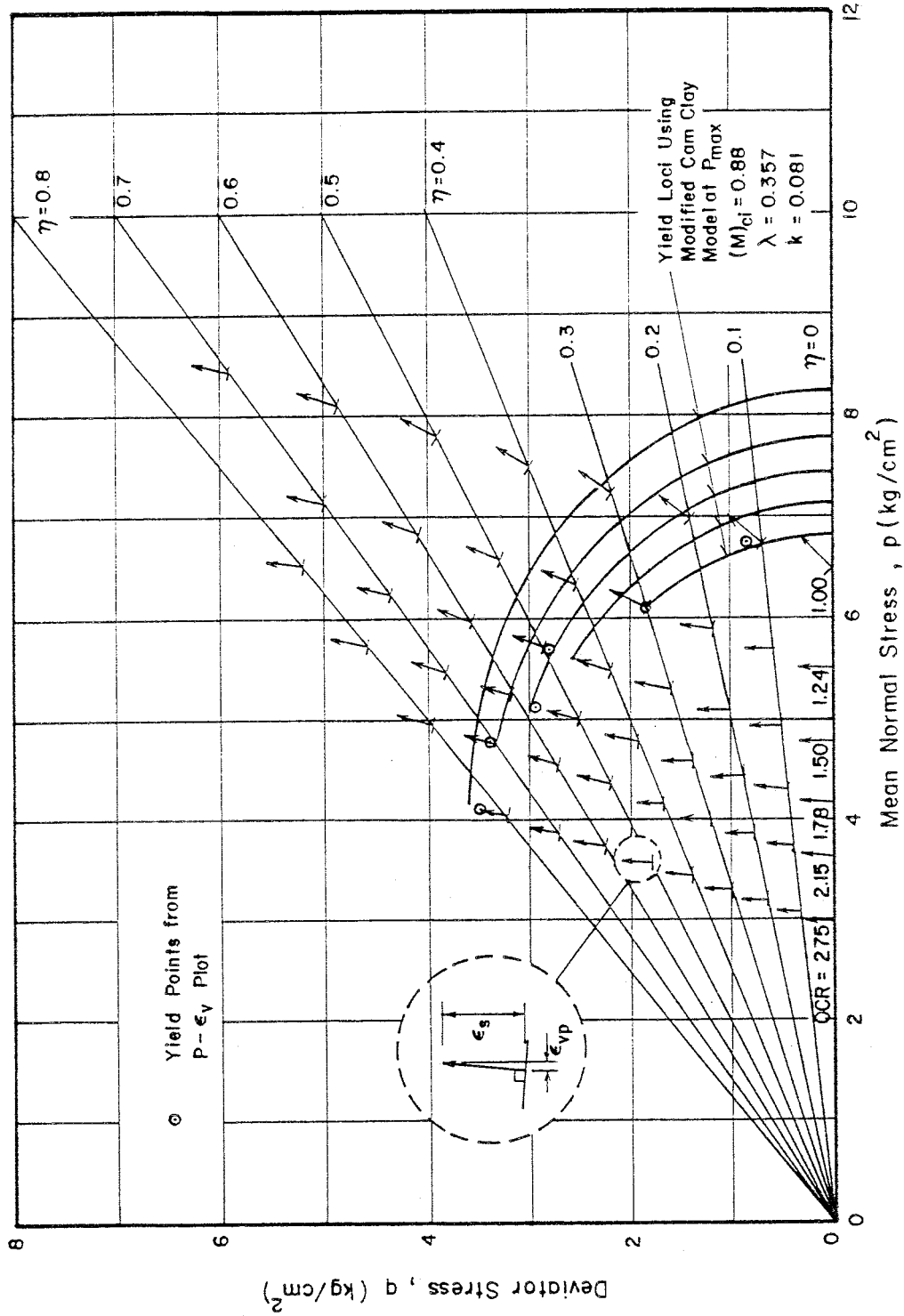


Fig. 6.7 Direction of the Plastic Strain Increment Vectors from CID Tests

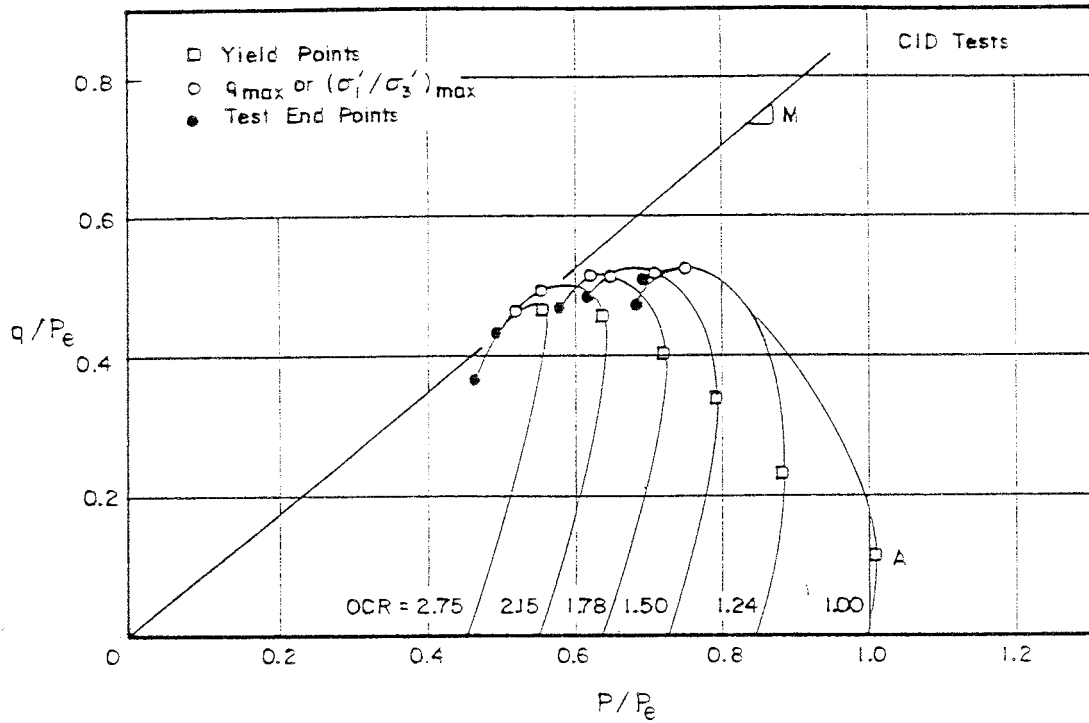


Fig. 6.8 (q/p_e , p/p_e) Plot from CID Tests

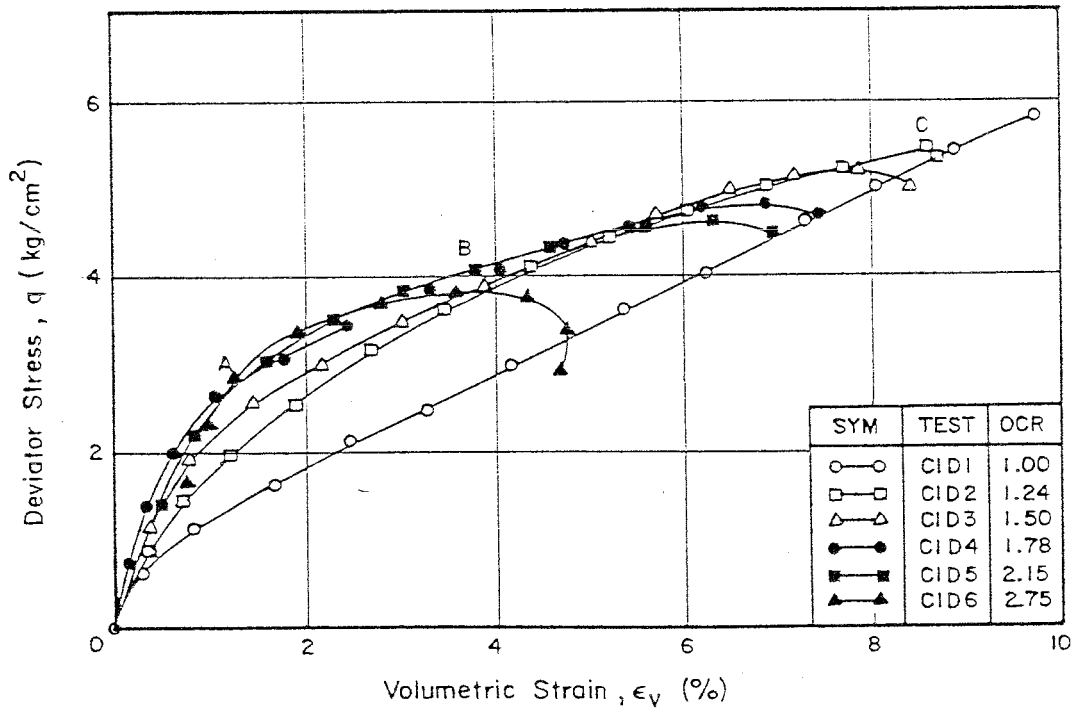


Fig. 6.9 (q , ϵ_v) Plot from CID Tests

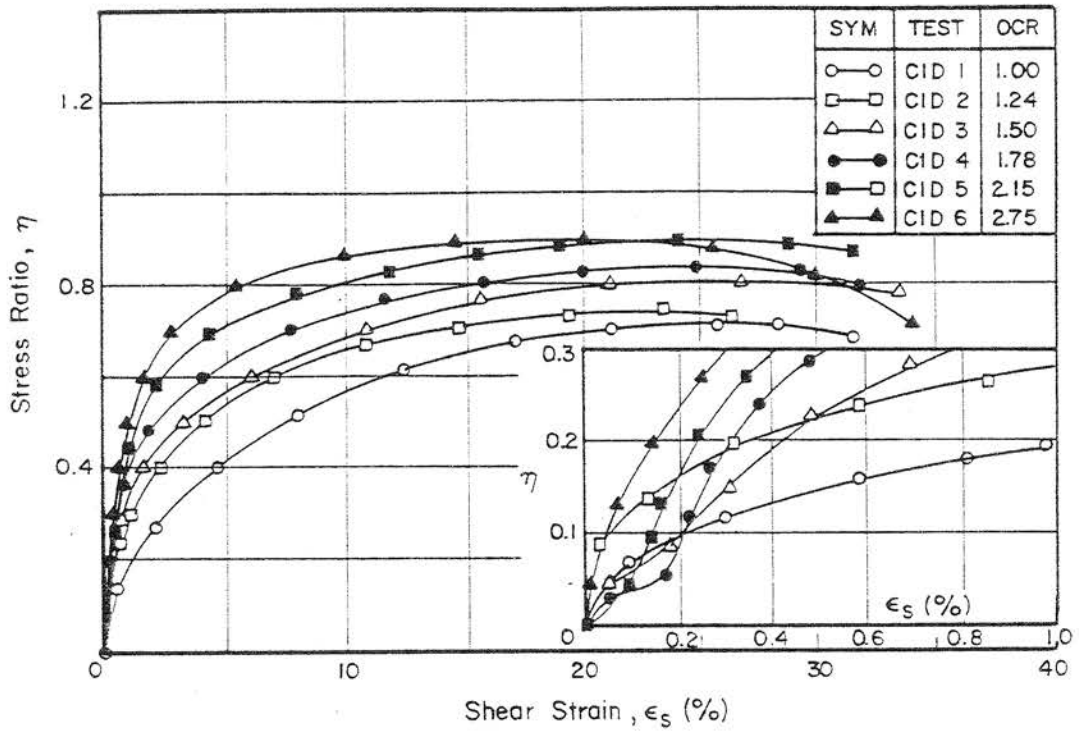


Fig. 6.10 (η , ϵ_s) Plot from CID Tests

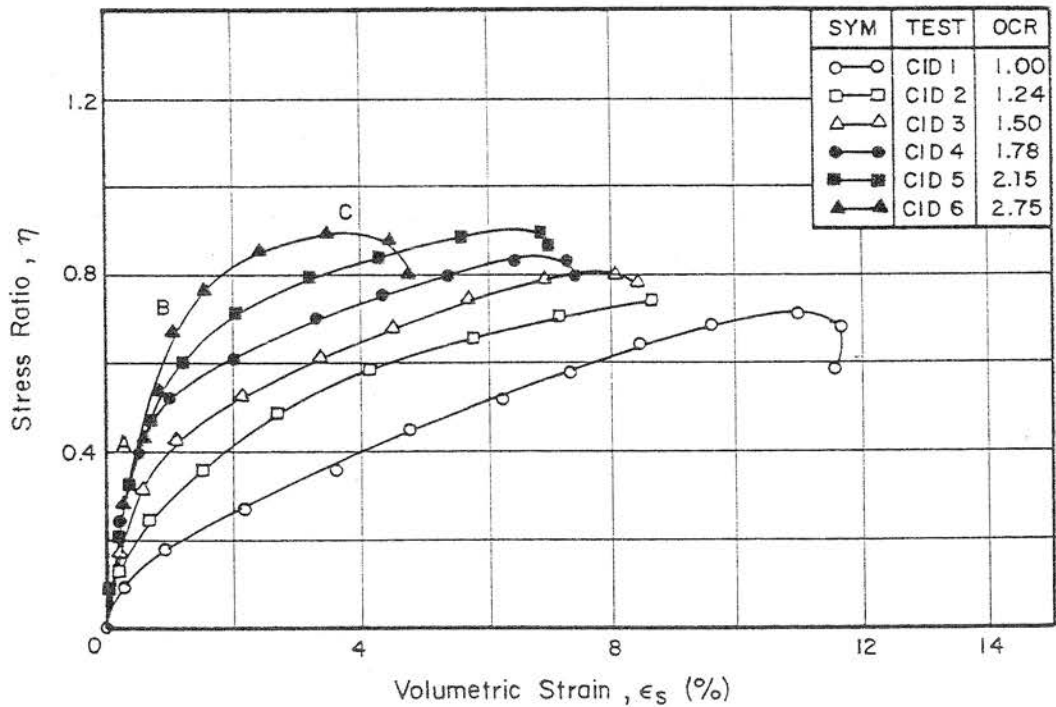


Fig. 6.11 (η , ϵ_v) Plot from CID Tests

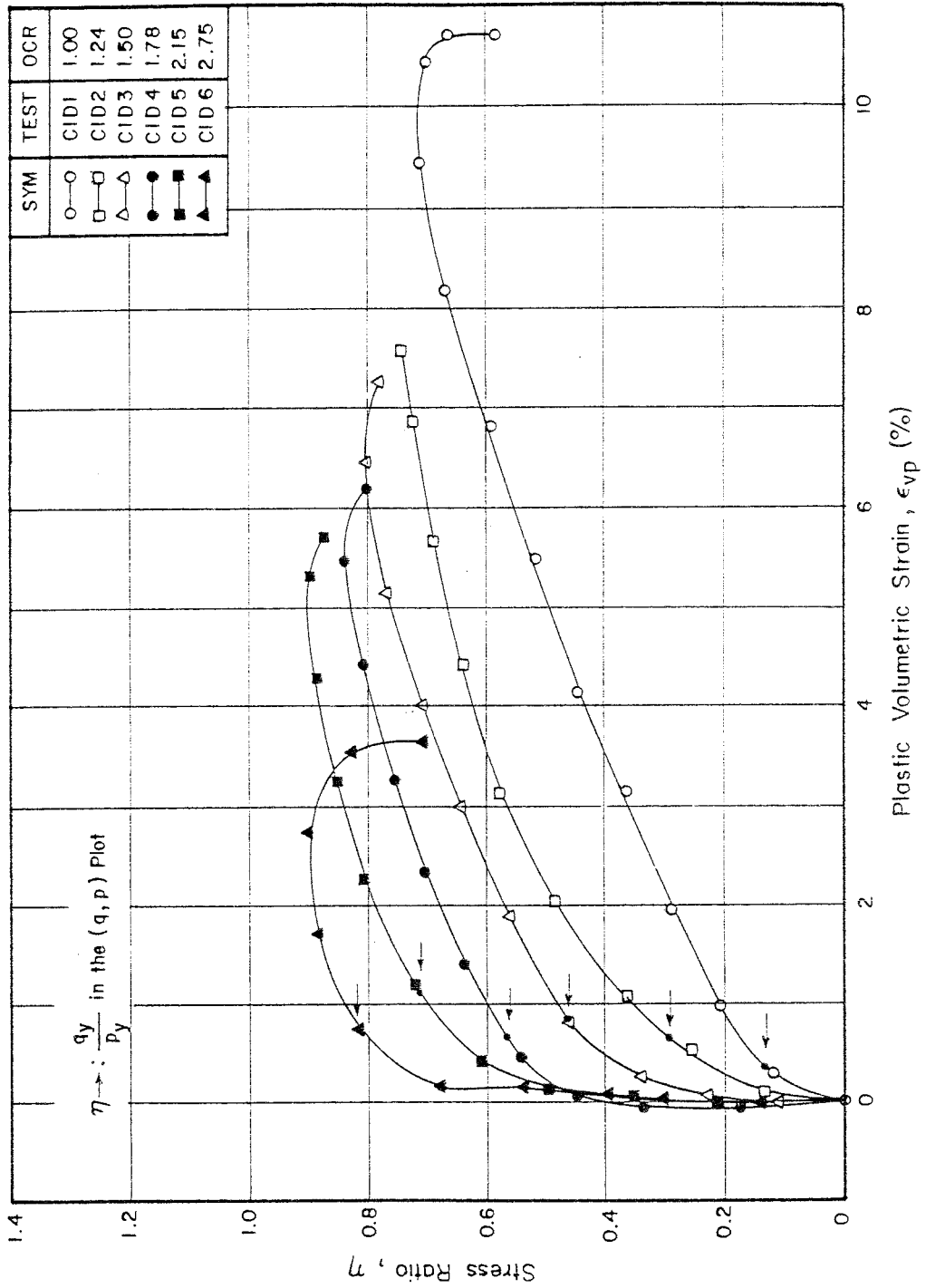


Fig. 6.12 (η , ϵ_{vp}) Plot from CID Tests

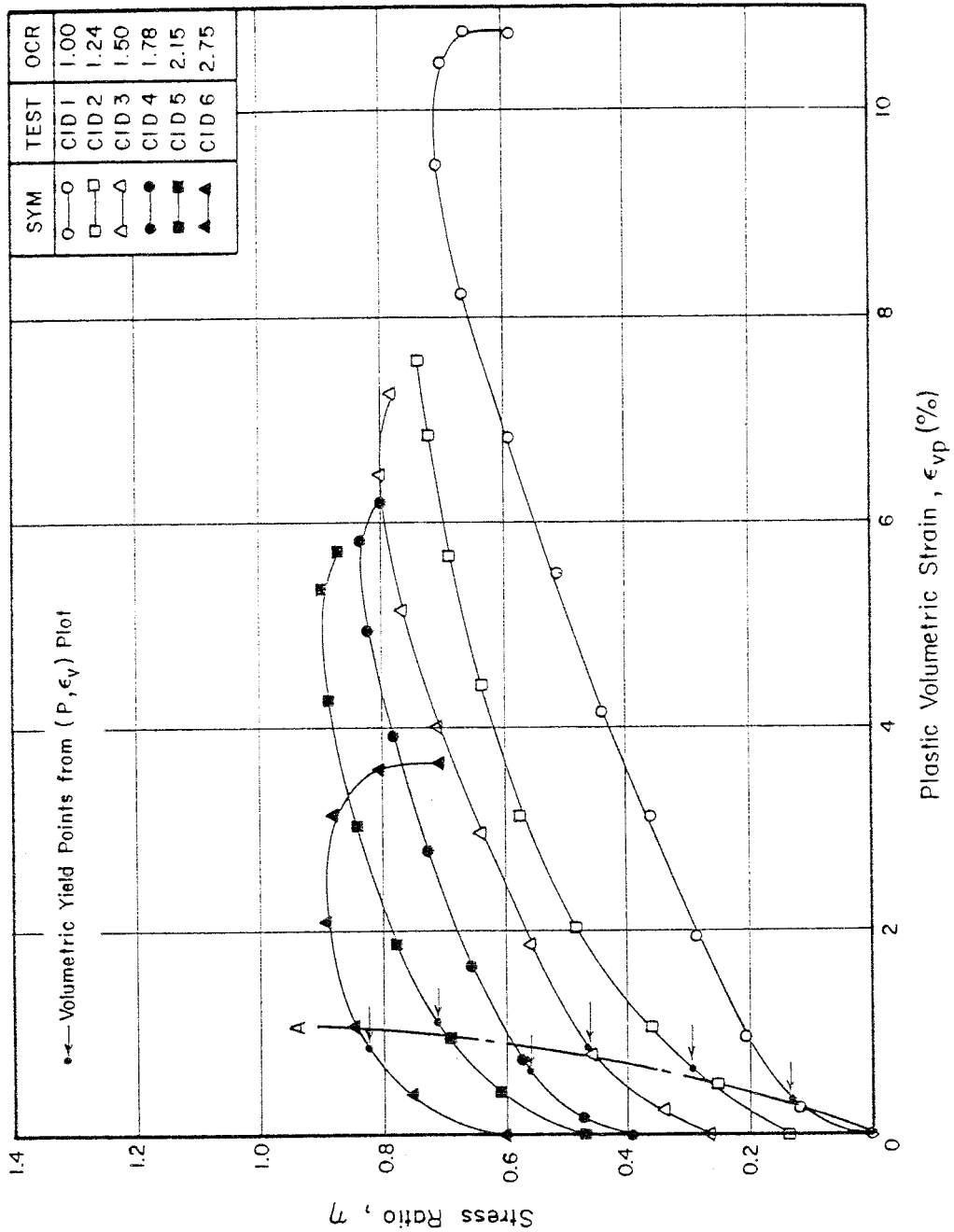


Fig. 6.13 Relationships between η and Positive Plastic Volumetric Strains from CID Tests

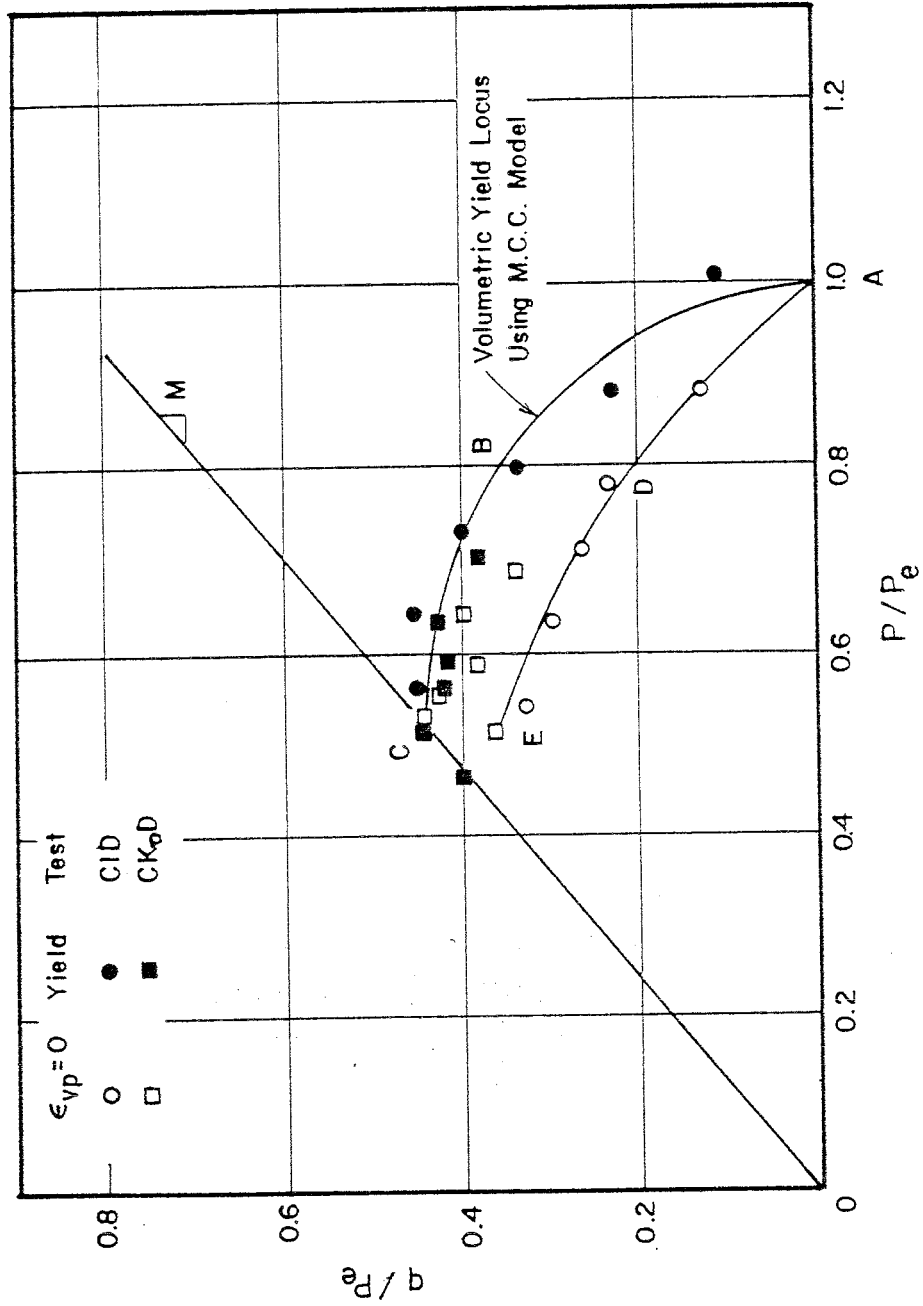


Fig. 6.14 Zero Plastic Volumetric Strain and Yield Points from CID and CKoD Tests

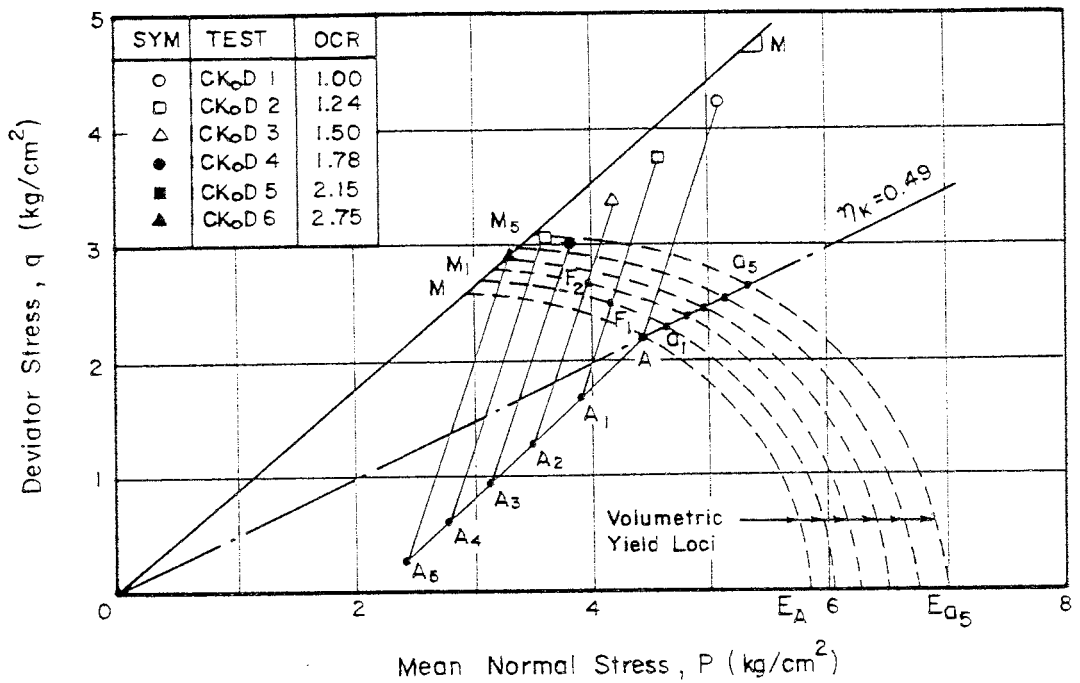


Fig. 6.15 Volumetric Yield Loci and Stress Paths for CKoD Samples

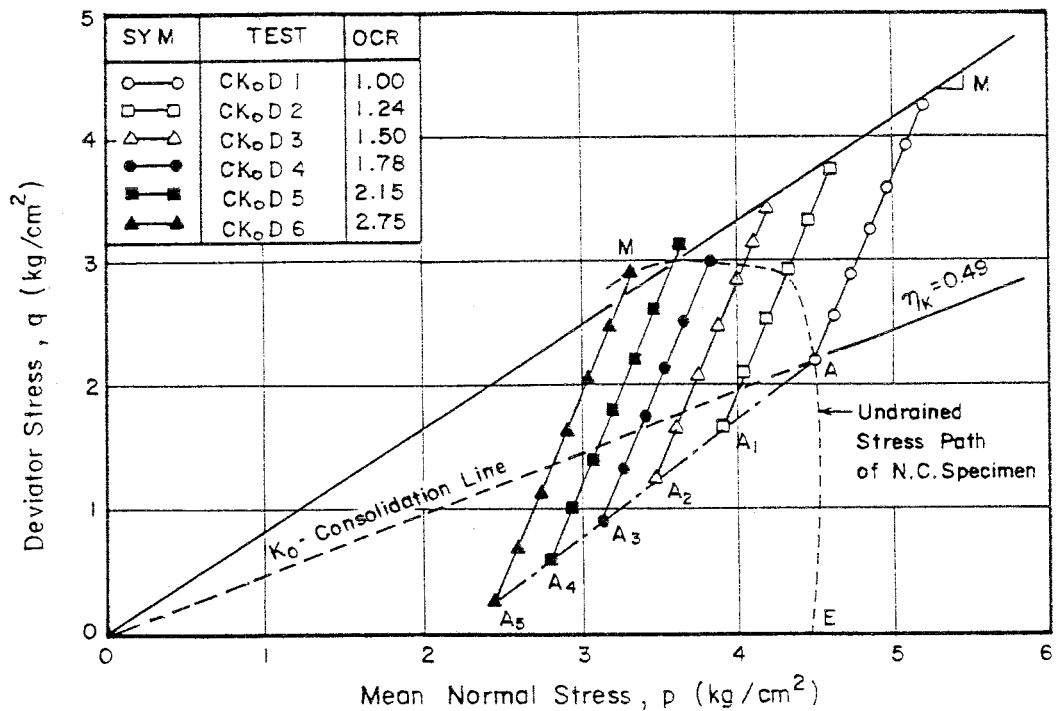


Fig. 6.16 Drained Stress Paths from CKoD Tests with Undrained Stress Paths of K_o -normally Consolidated Samples

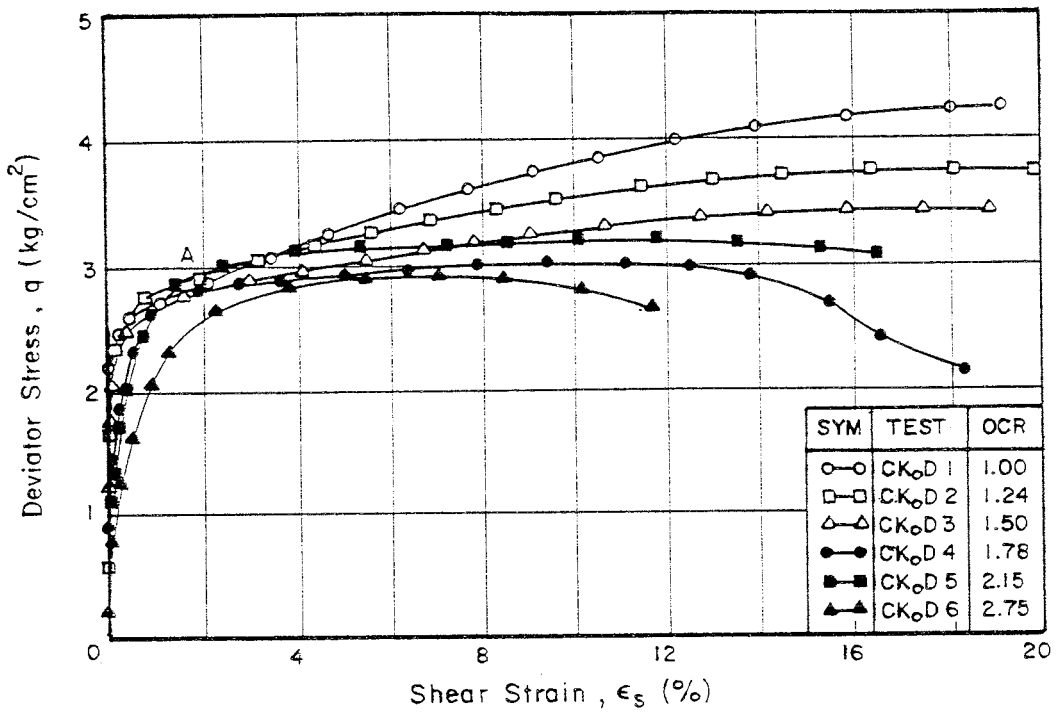


Fig. 6.17 (q , ϵ_s) Plot from CKoD Tests

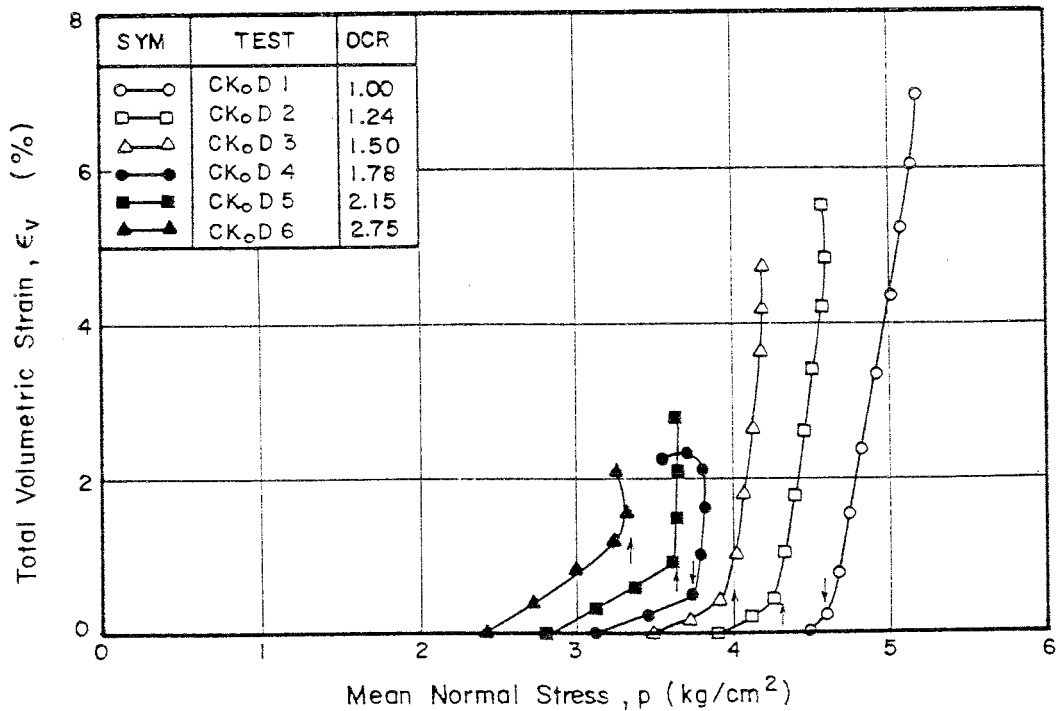


Fig. 6.18 (p , ϵ_v) Plot from CKoD Tests

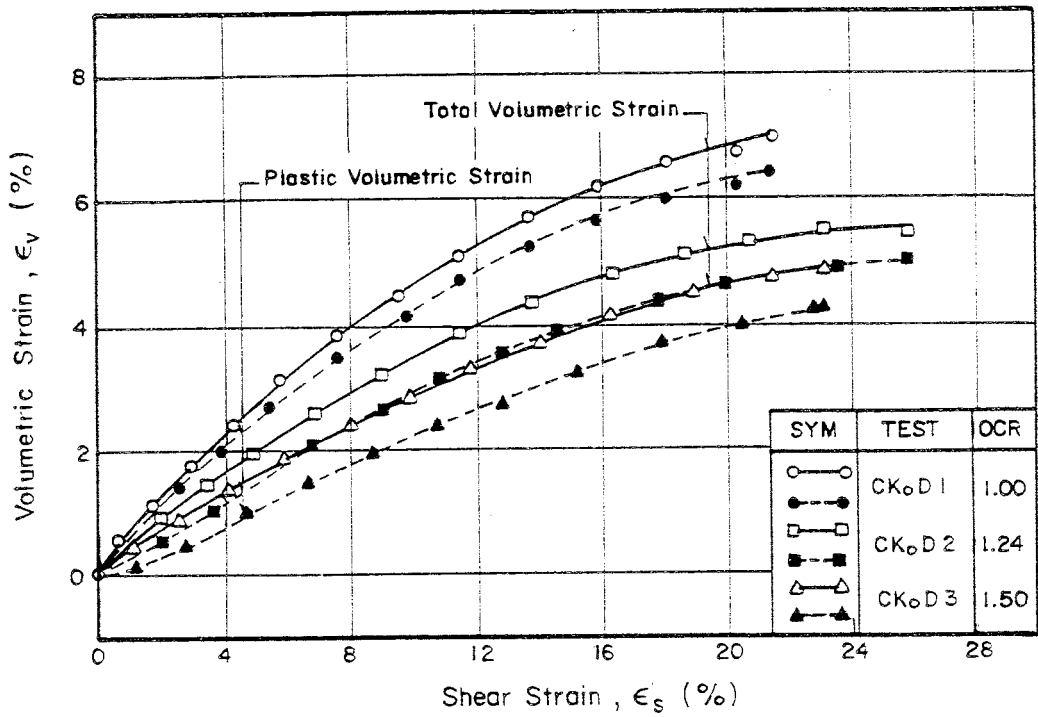


Fig. 6.19a (ϵ_v , ϵ_s) Plot from CKoD Tests (Wet Zone)

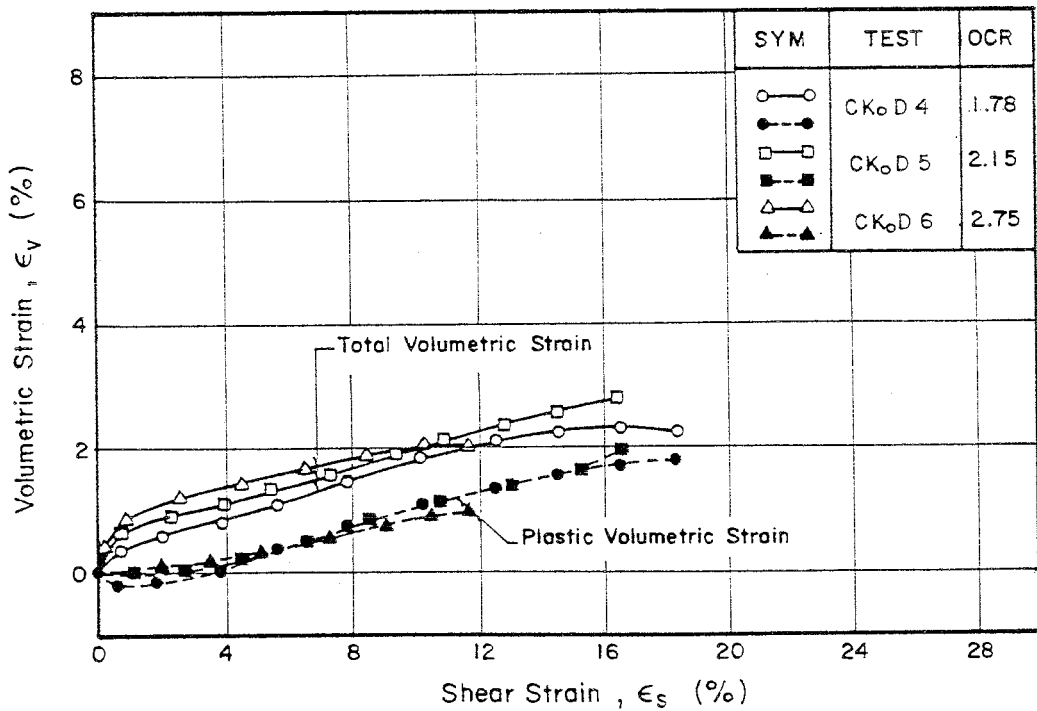


Fig. 6.19b (ϵ_v , ϵ_s) Plot from CKoD Tests (Dry Zone)

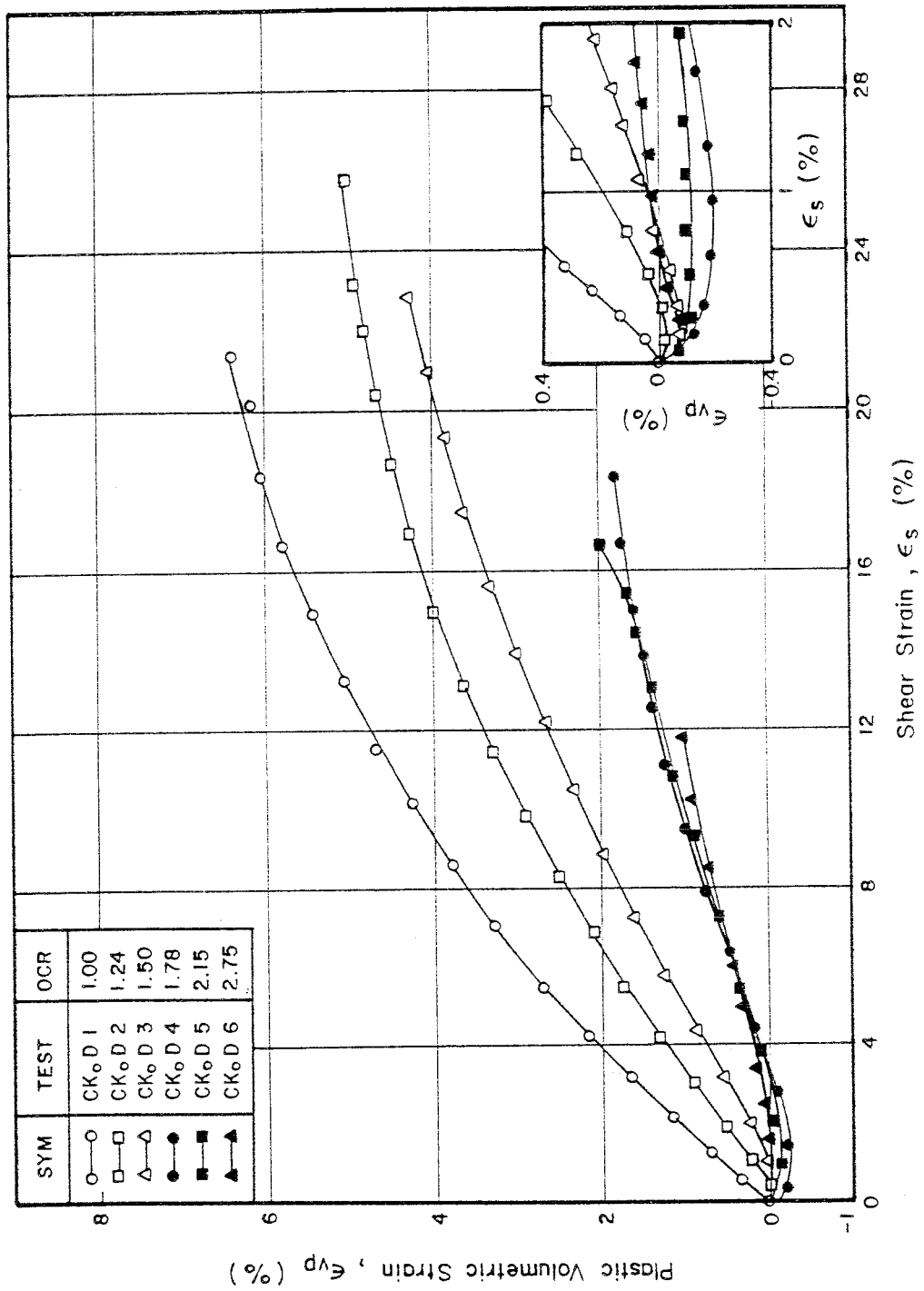


Fig. 6.19c (ϵ_{vp} , ϵ_s) Plot from CK₆D Tests

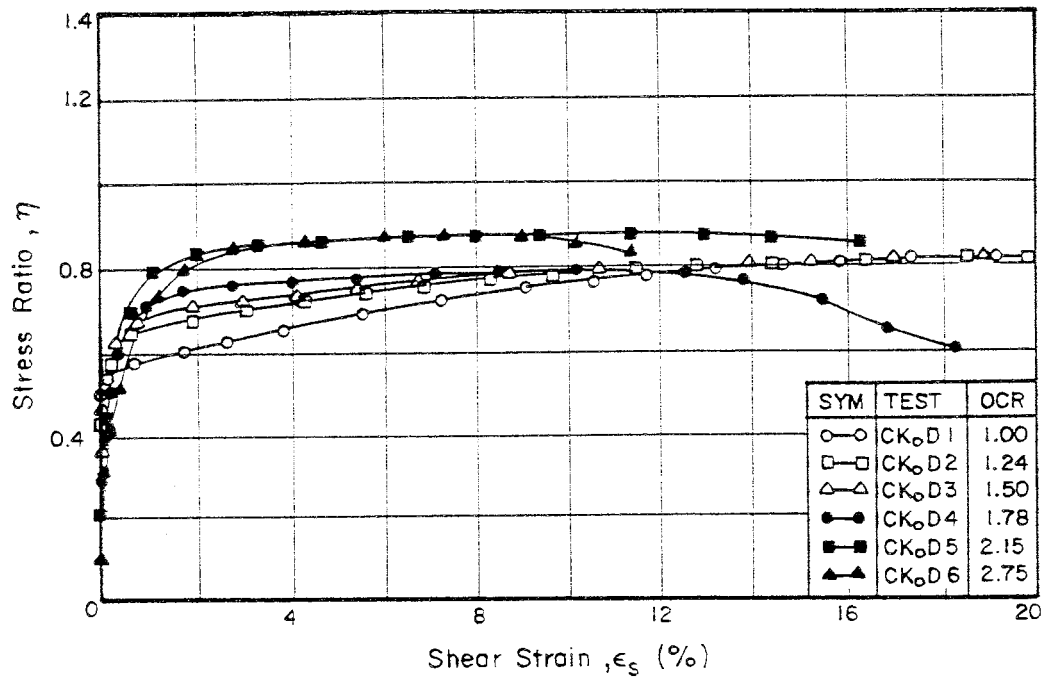


Fig. 6.20 (η , ϵ_s) Plot from CK_oD Tests

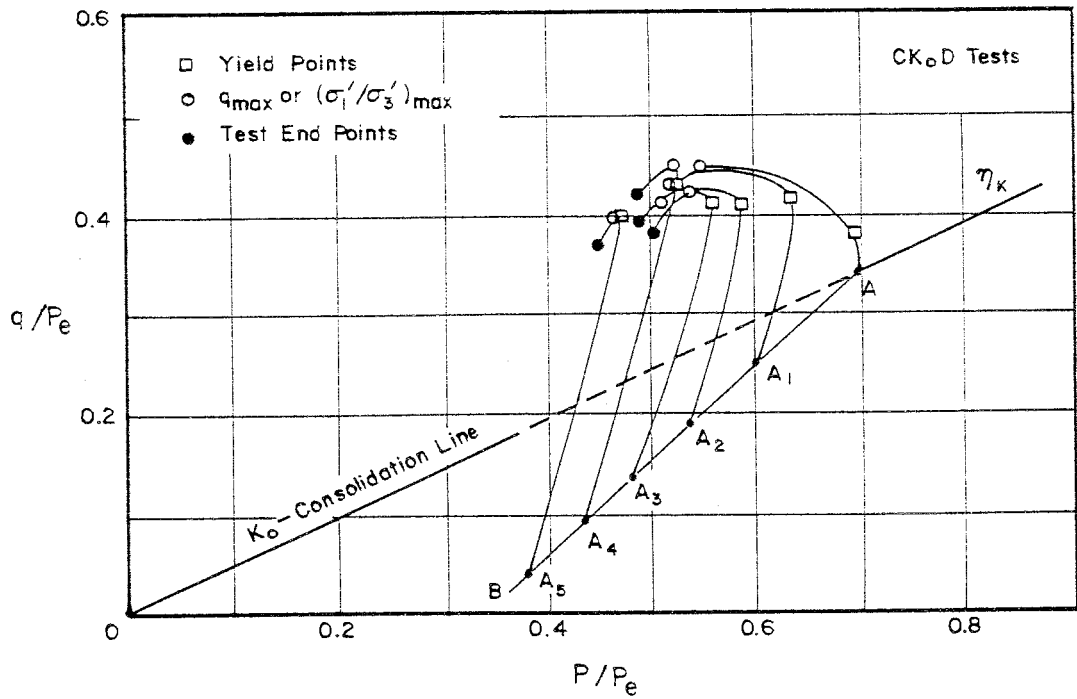


Fig. 6.21 (q/p_e , p/p_e) Plot from CK_oD Tests

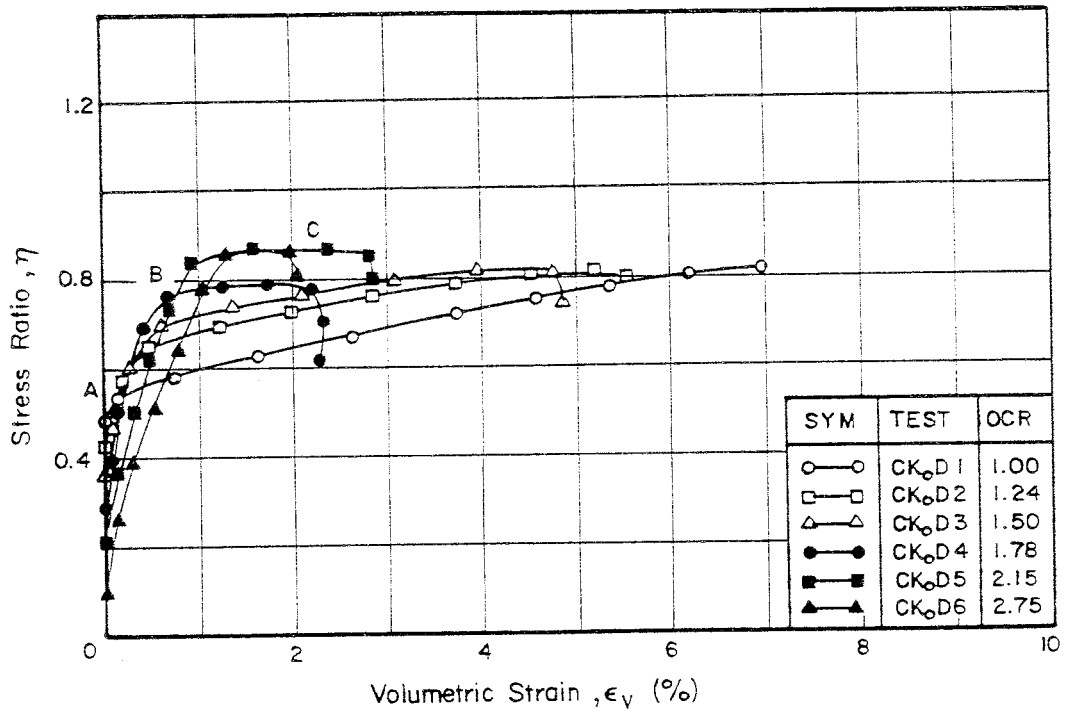


Fig. 6.22 (η , ϵ_v) Plot from CK_oD Tests

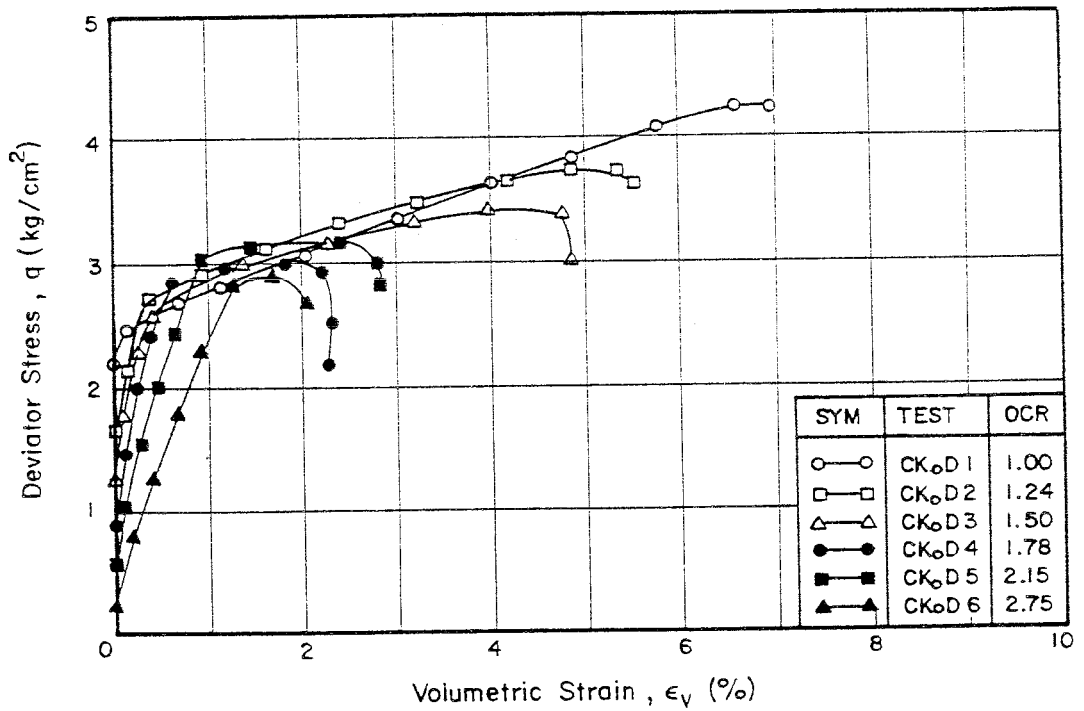


Fig. 6.23 (q , ϵ_v) Plot from CK_oD Tests

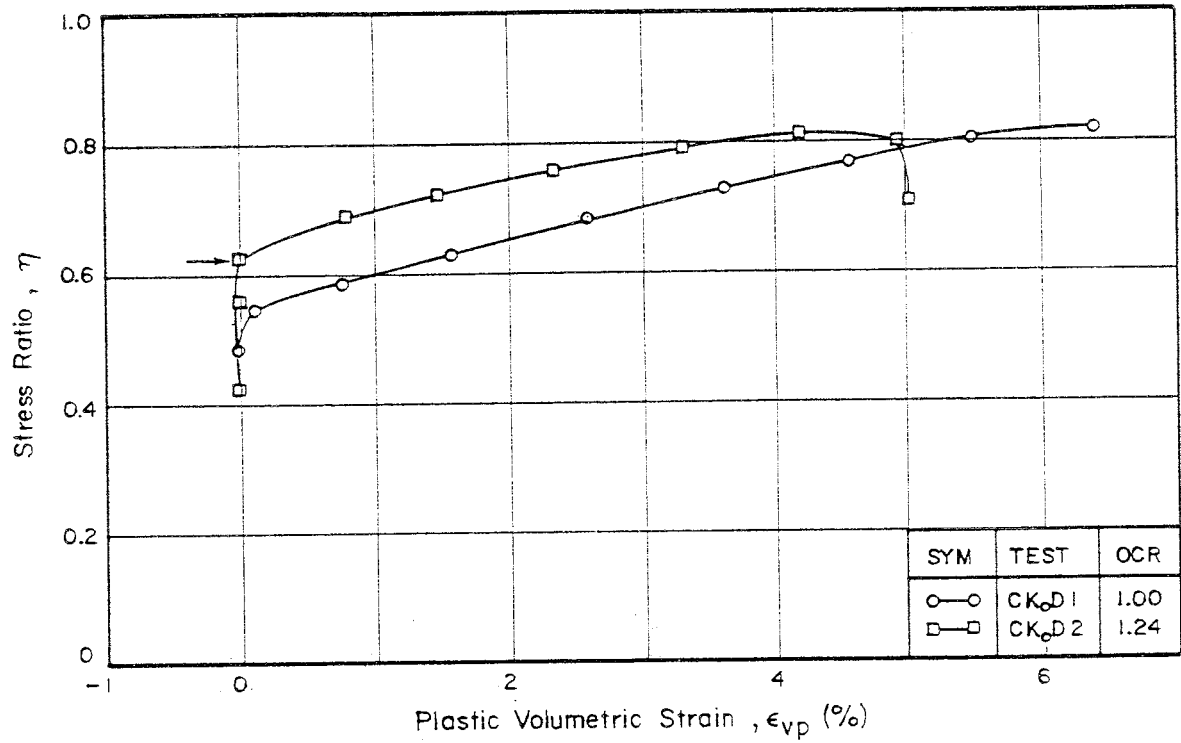


Fig. 6.24 (η , ϵ_{vp}) Plot from CKoD1 and CKoD2 Samples

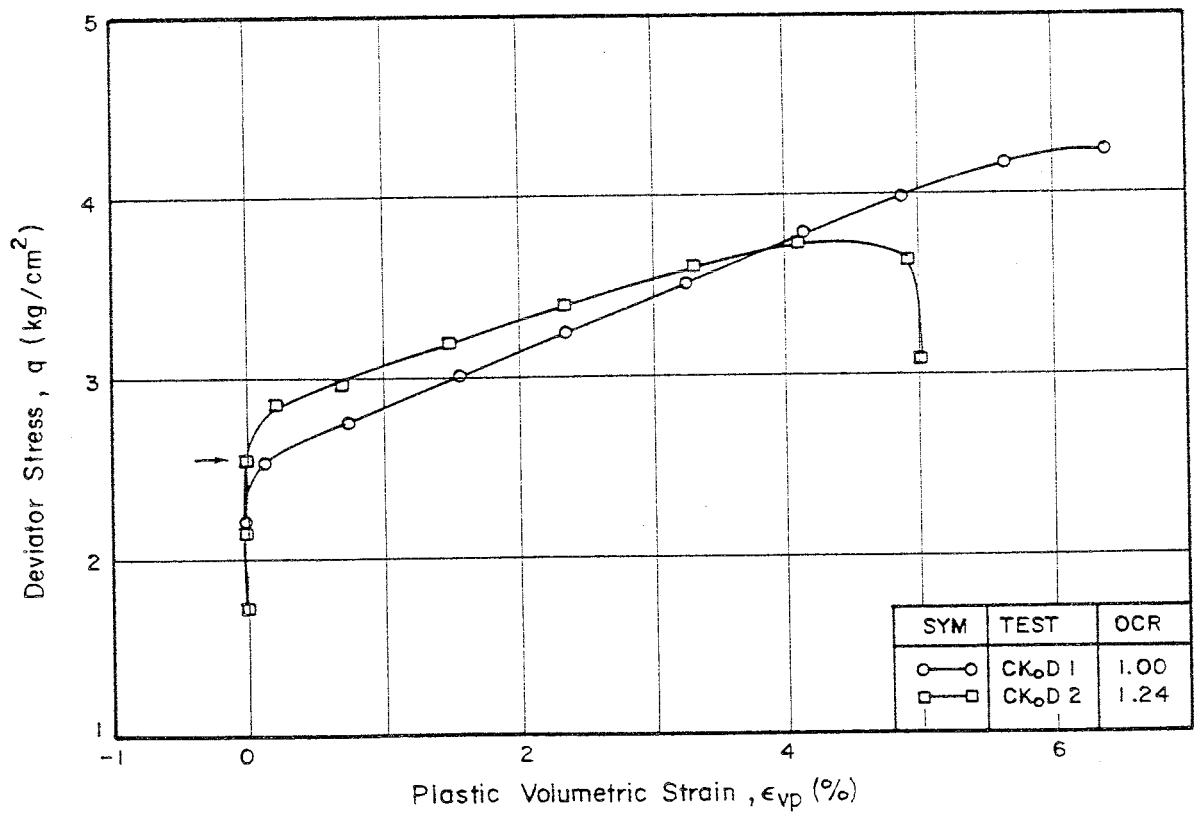


Fig. 6.25 (q , ϵ_{vp}) Plot from CKoD1 and CKoD2 Samples

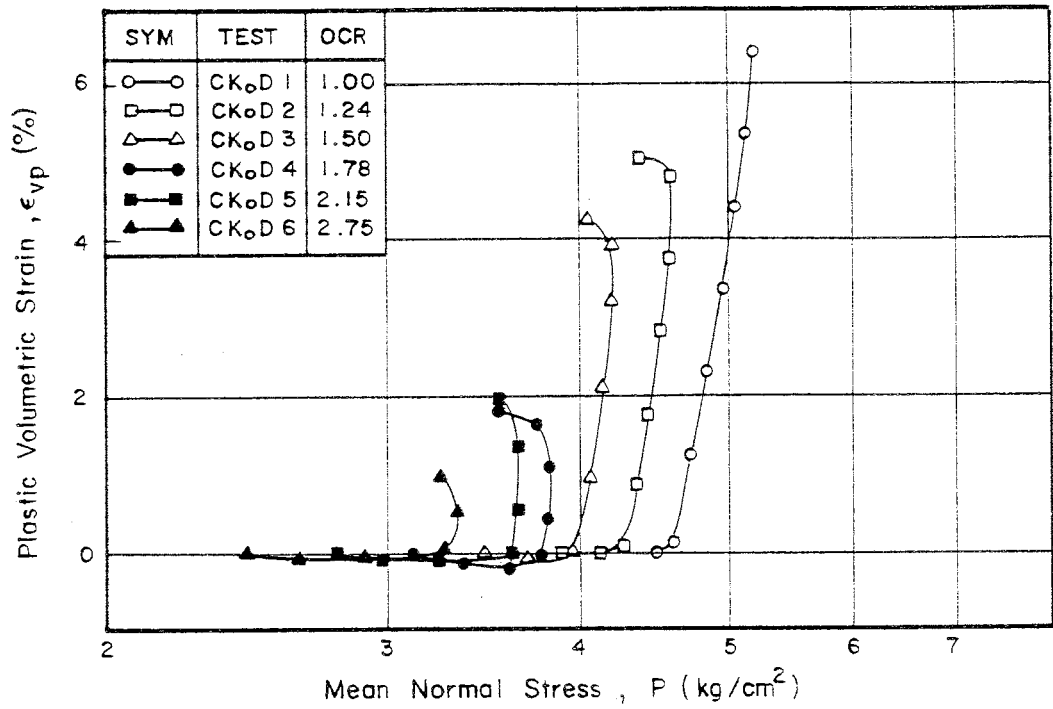


Fig. 6.26 (ϵ_{vp} , p) Plot from CK_oD Tests

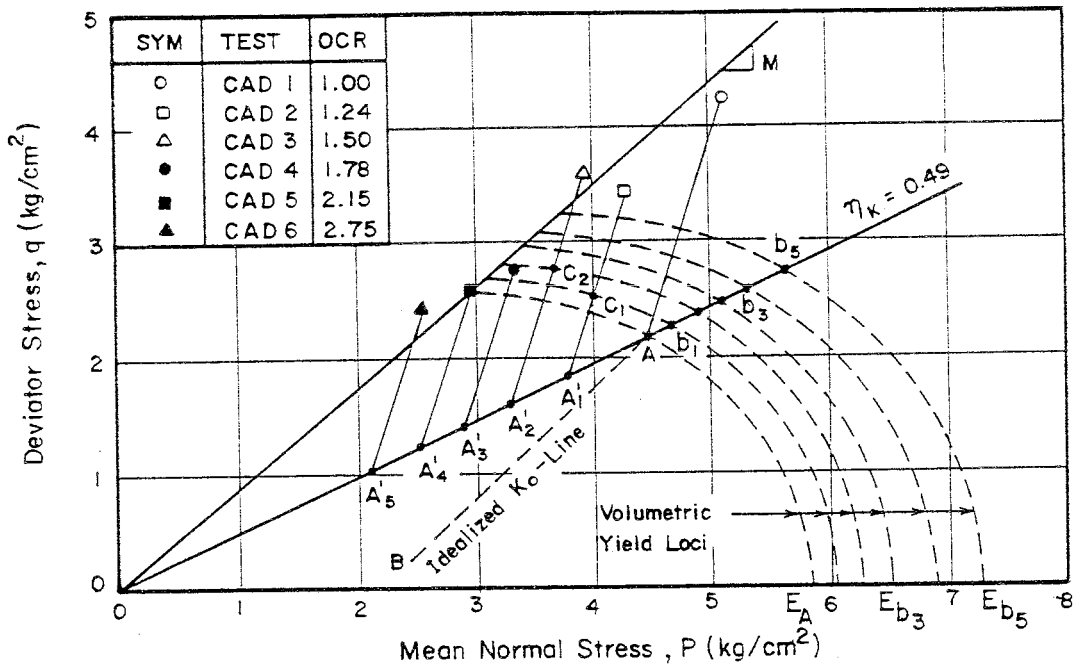


Fig. 6.27 Volumetric Yield Loci and Stress Paths for CAD Samples

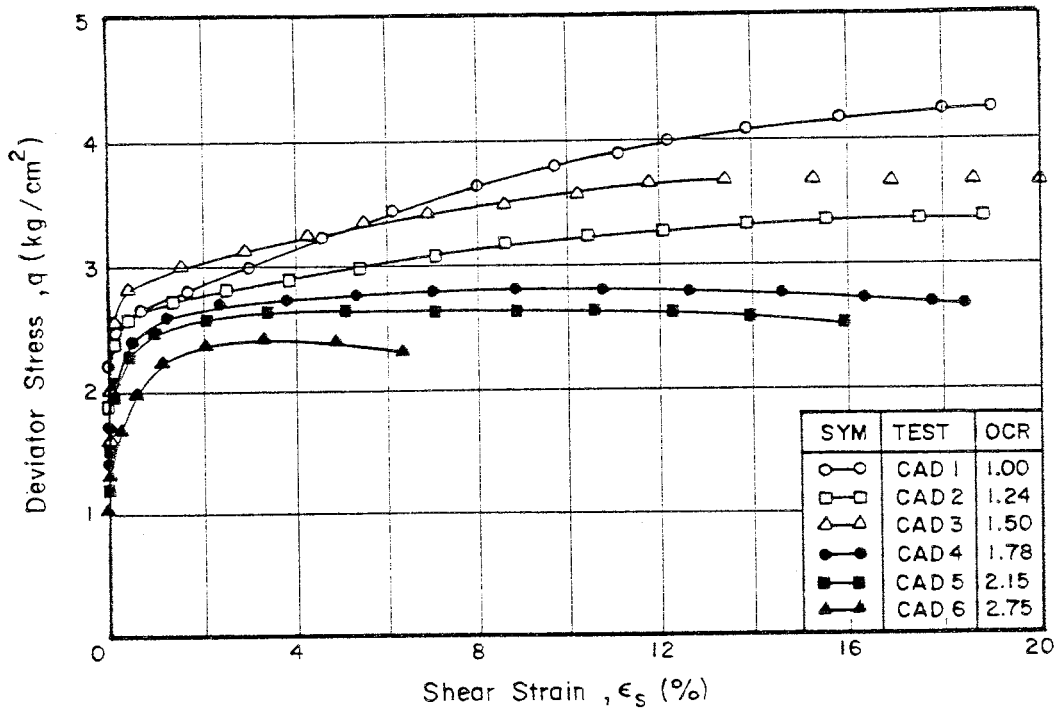


Fig. 6.28 (q , ϵ_s) Plot from CAD Tests

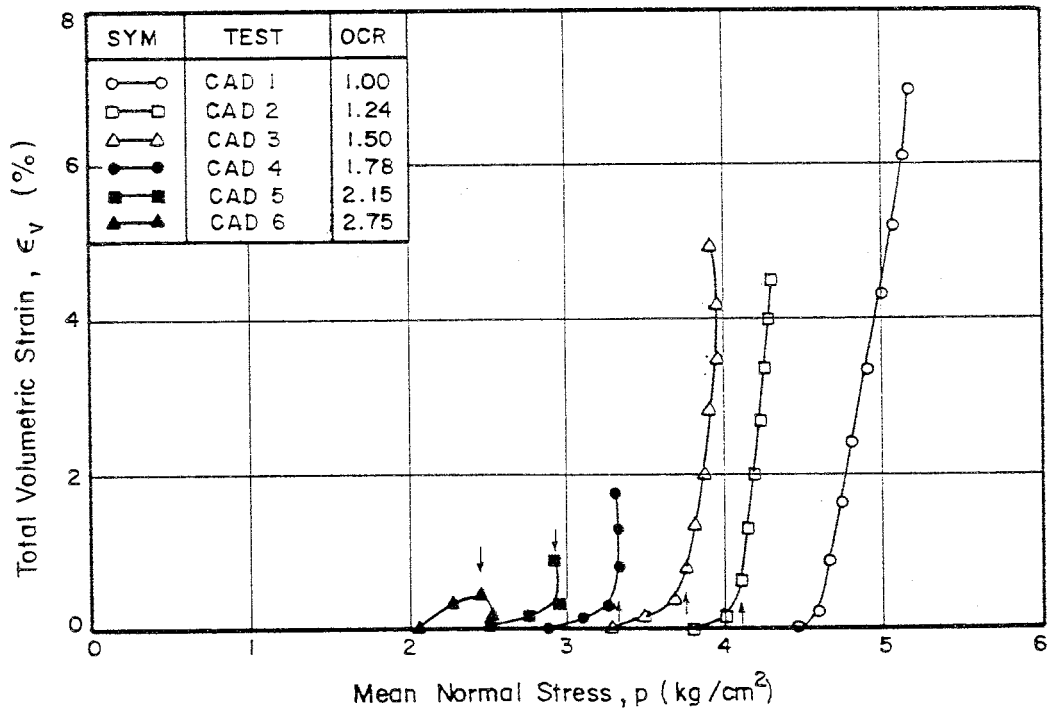


Fig. 6.29 (ϵ_v , p) Plot from CAD Tests

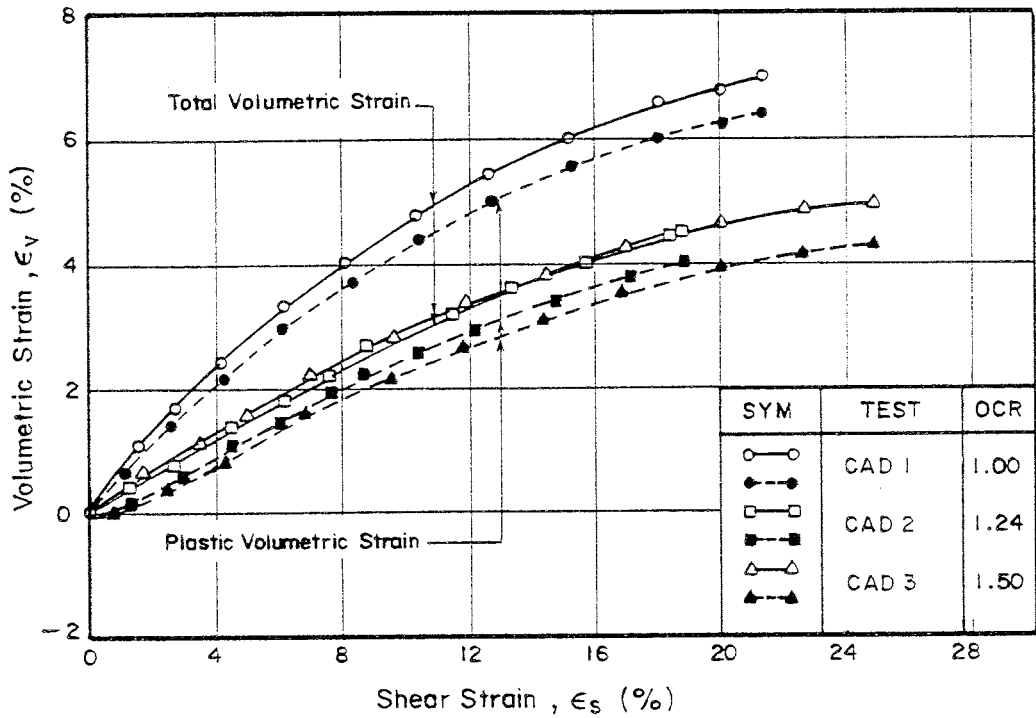


Fig. 6.30a (ϵ_v , ϵ_s) Plot from CAD Tests (Wet Zone)

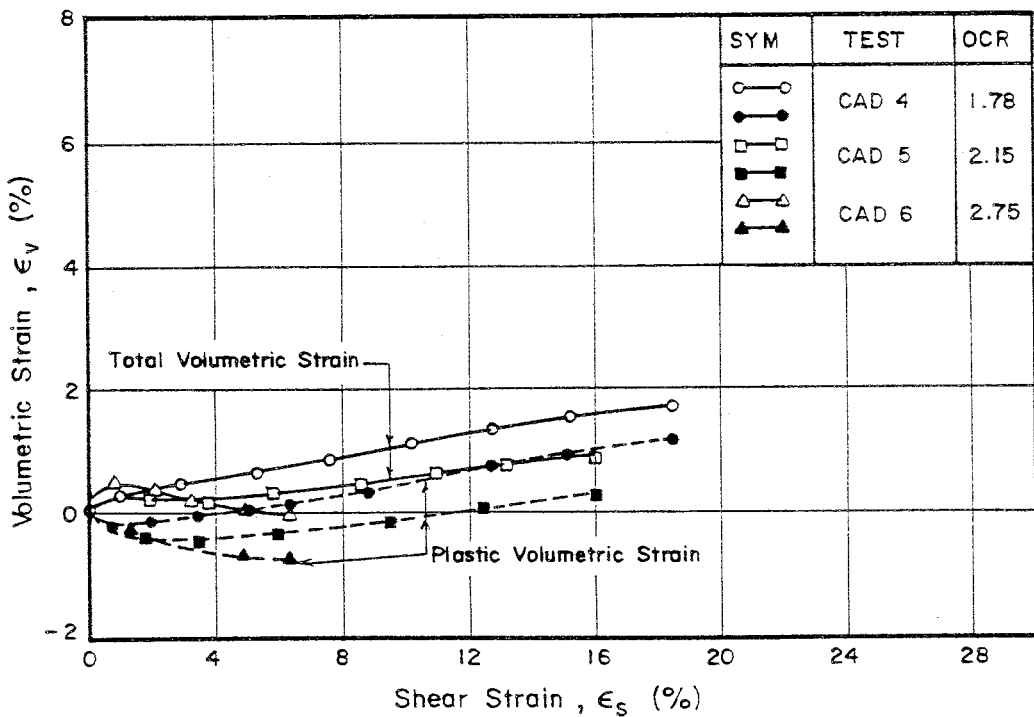


Fig. 6.30b (ϵ_v , ϵ_s) Plot from CAD Tests (Dry Zone)

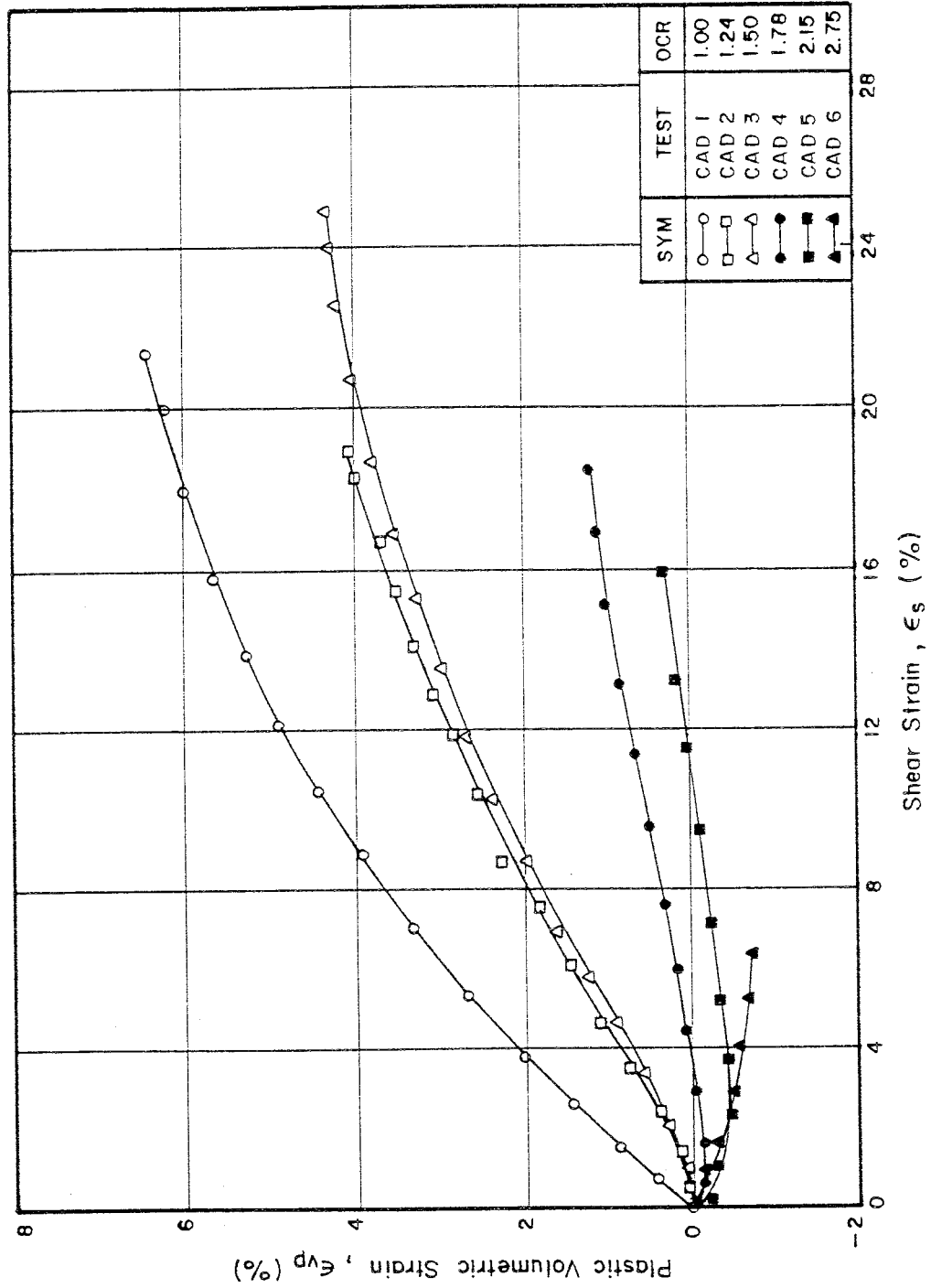


Fig. 6.30c (ϵ_{vp} , ϵ_s) Plot from CAD Tests

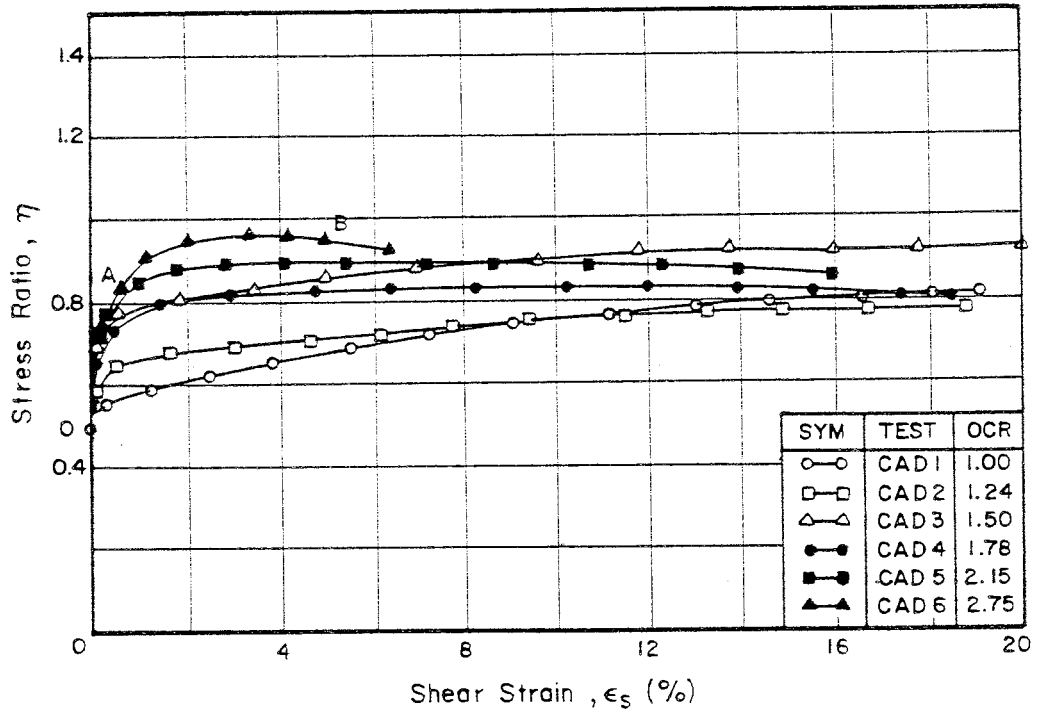


Fig. 6.31 (η, ϵ_s) Plot from CAD Tests

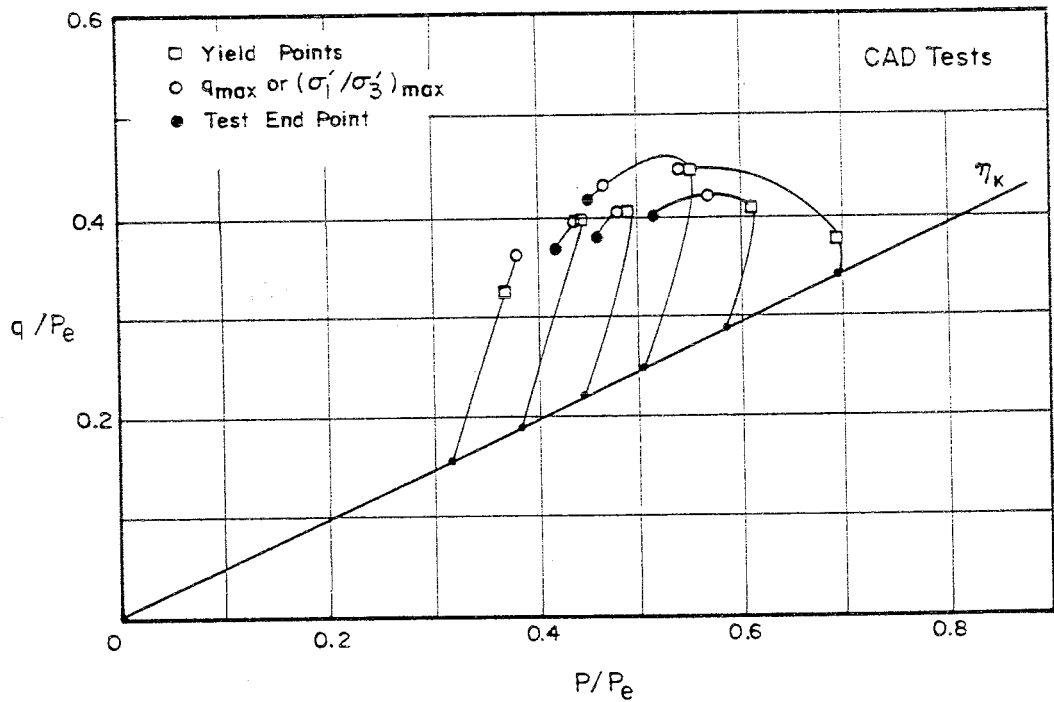


Fig. 6.32 $(q/p_e, p/p_e)$ Plot from CAD Tests

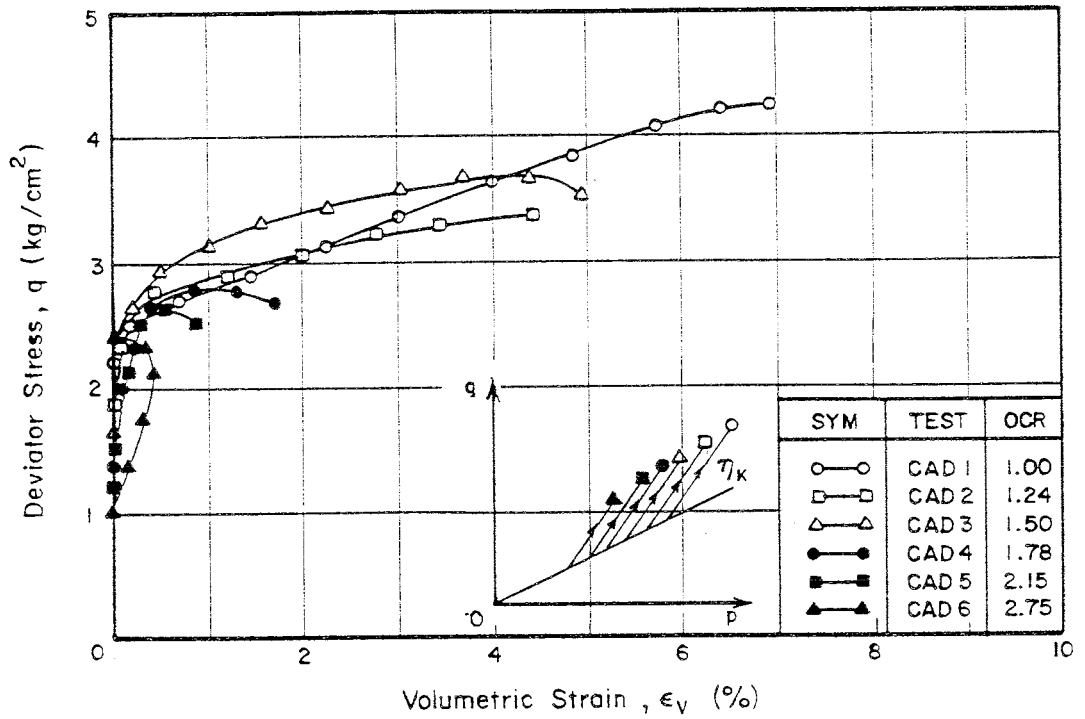


Fig. 6.33 (q , ϵ_v) Plot from CAD Tests

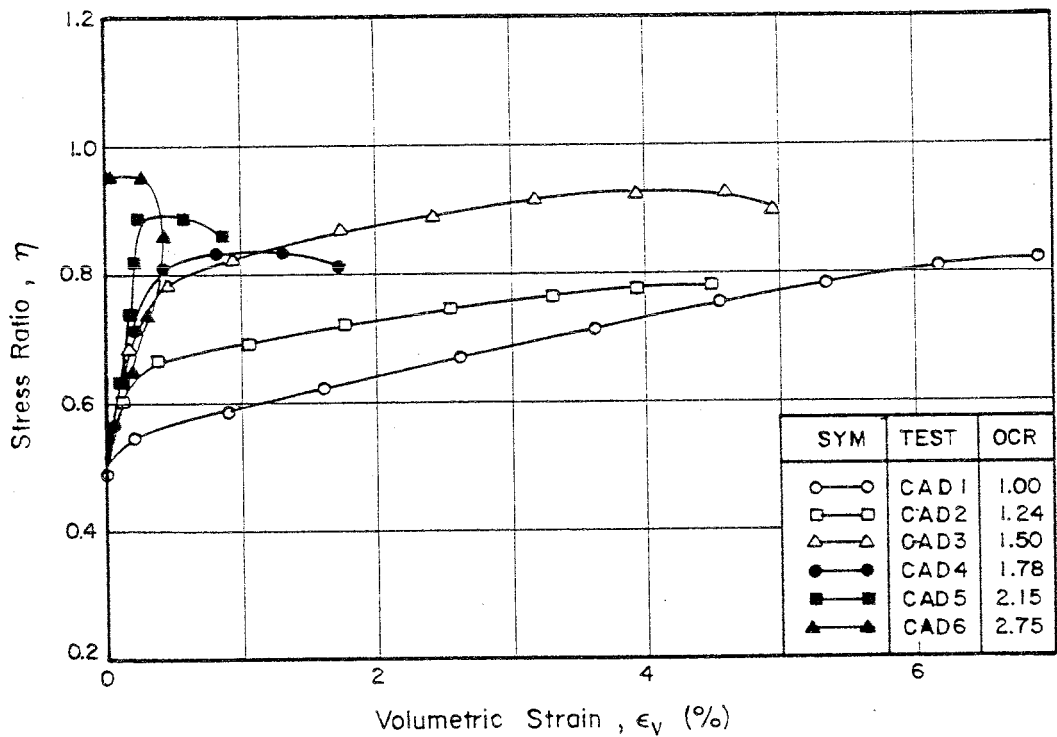


Fig. 6.34a (η , ϵ_v) Plot from CAD Tests

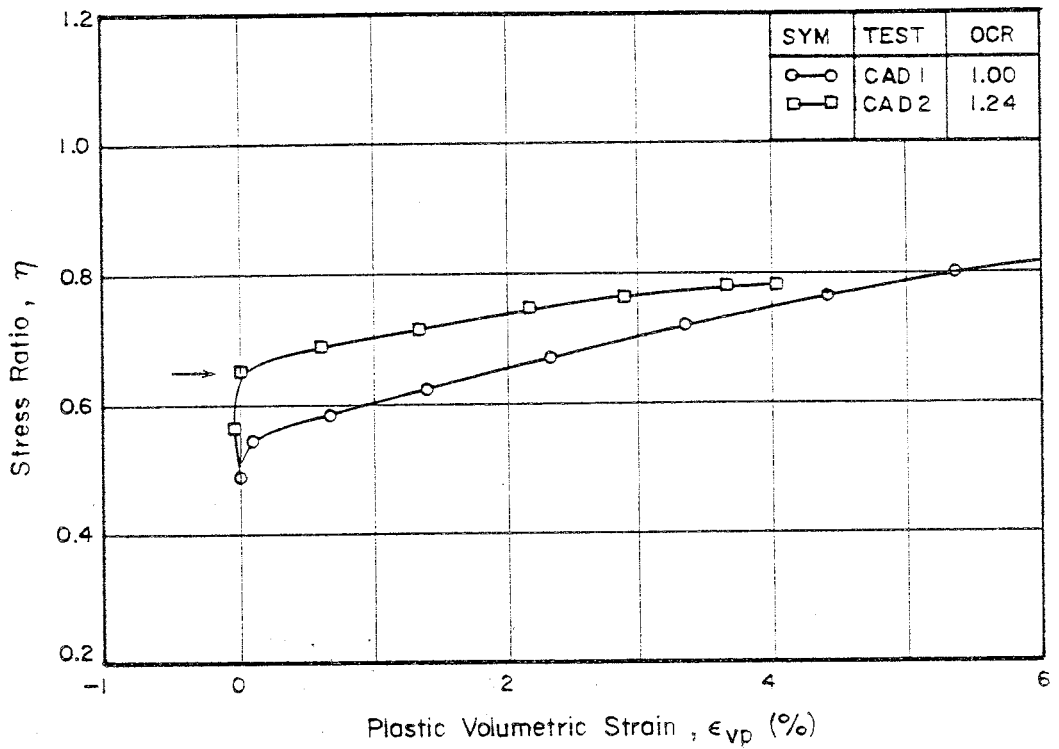


Fig. 6.34b (η , ϵ_{vp}) Plot from CAD1 and CAD2 Samples

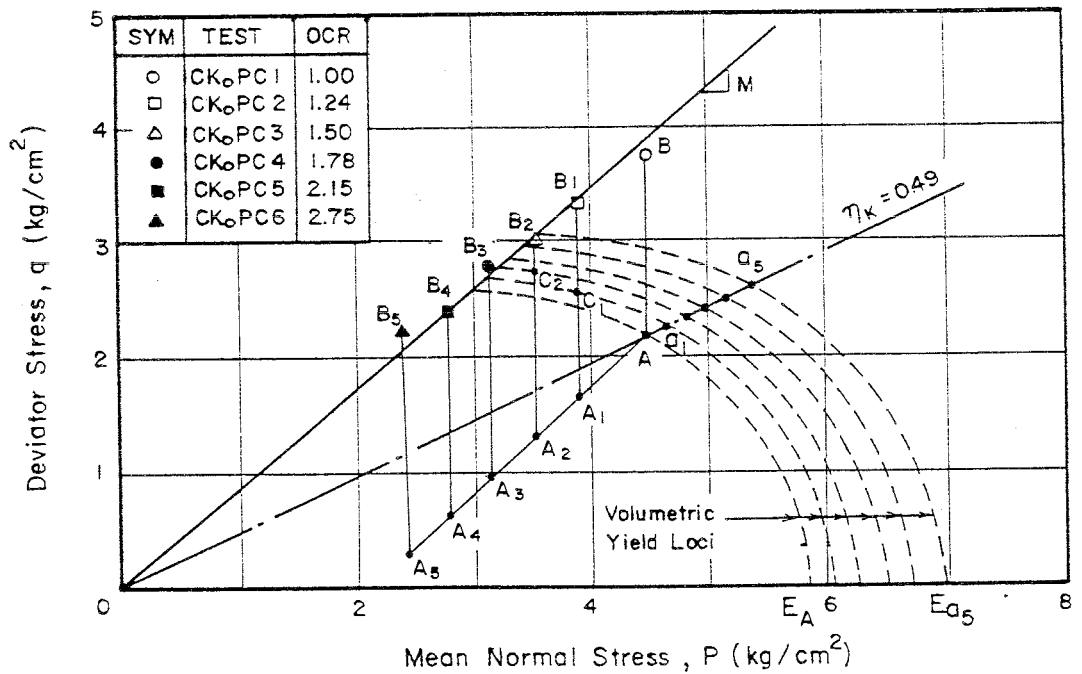


Fig. 6.35 Volumetric Yield Loci and Stress Paths for CKoPC Samples

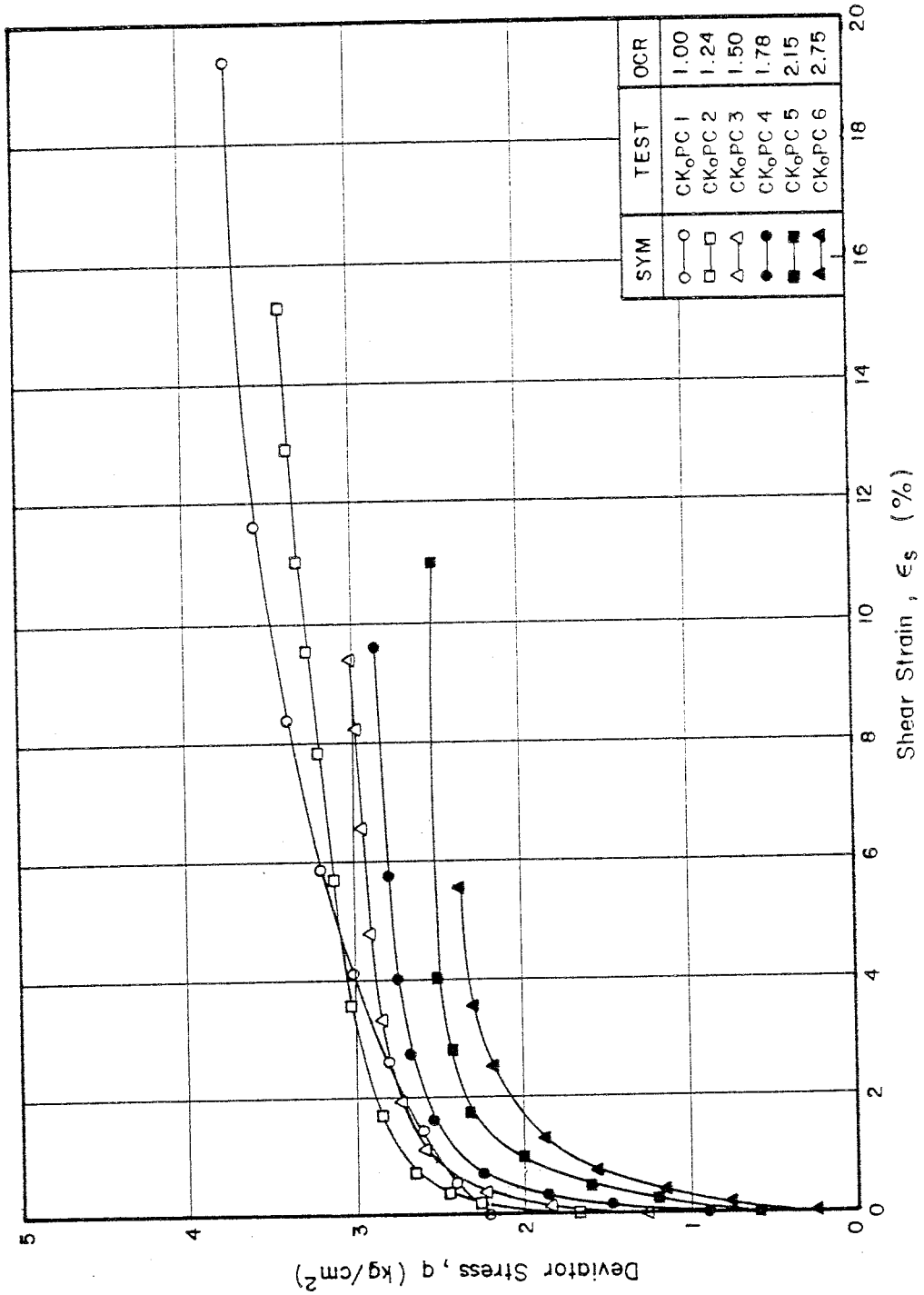


Fig. 6.36 (q , ϵ_s) Plot from CK_oPC Tests

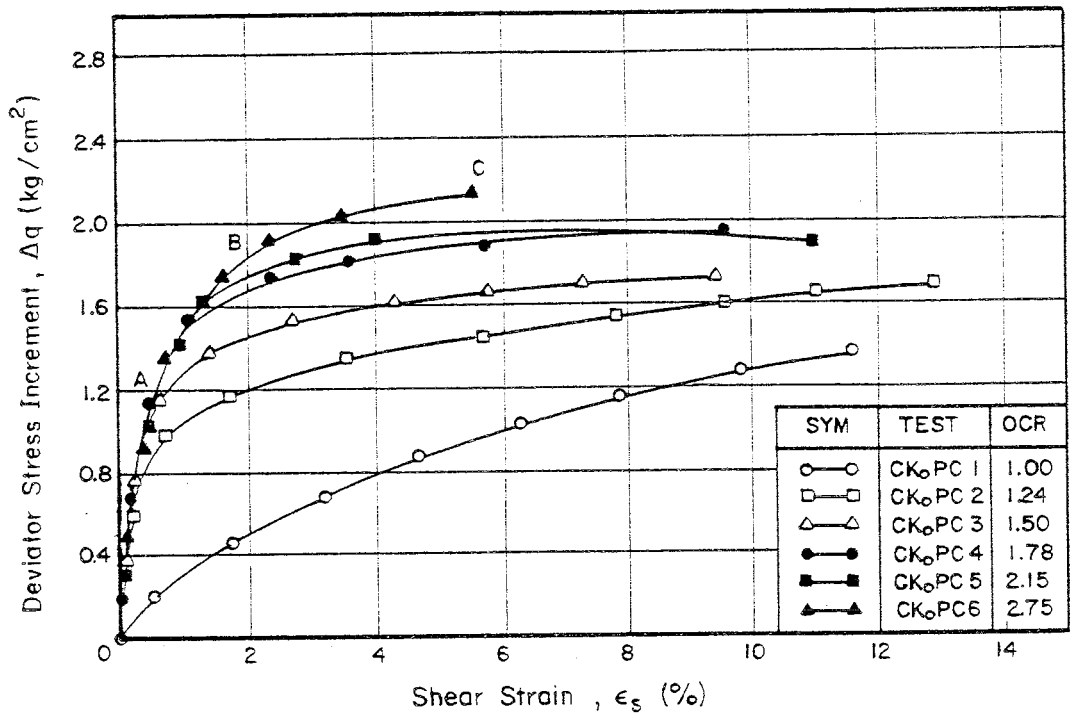


Fig. 6.37 Deviator Stress Increment and Shear Strain Relationship from CK_oPC Tests

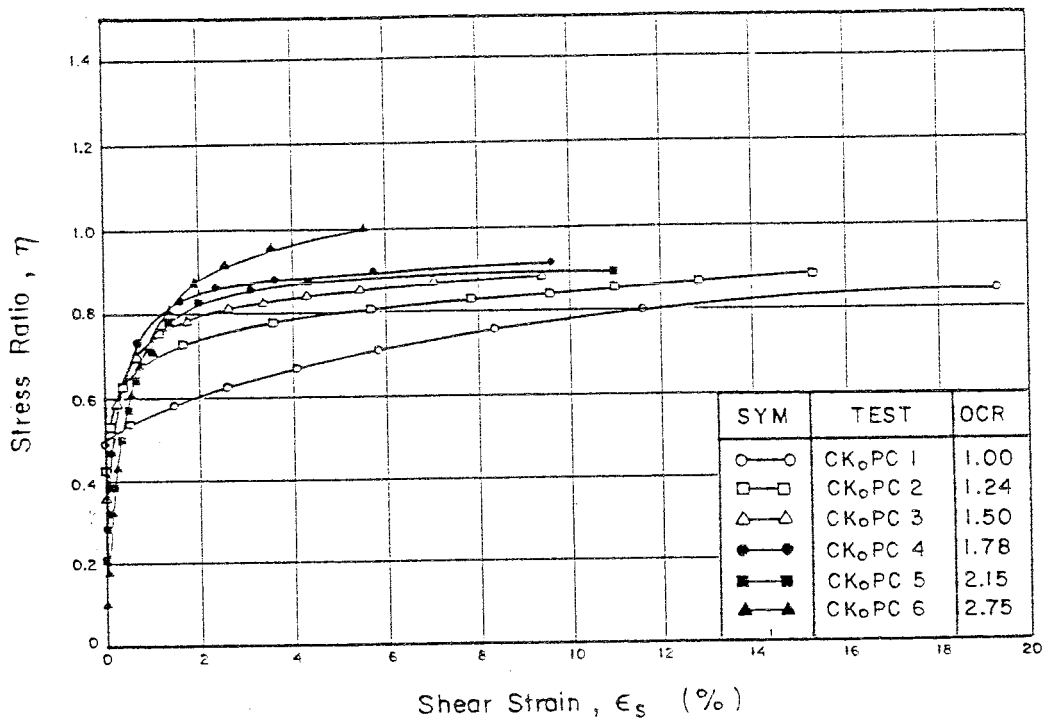


Fig. 6.38 (η , ϵ_s) Plot from CK_oPC Tests

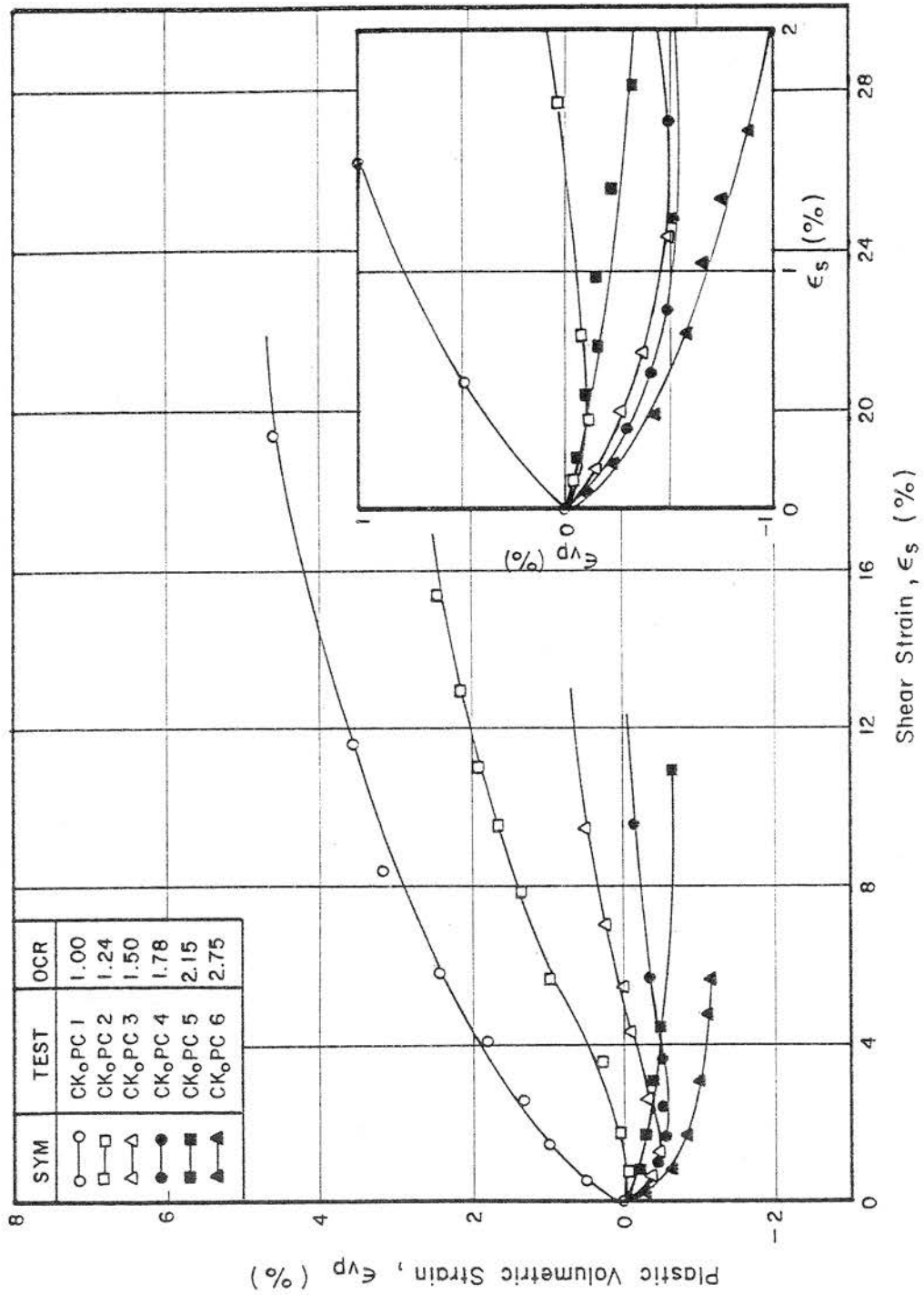


Fig. 6.39 (ϵ_{vp} , ϵ_s) Plot from CKoPC Tests

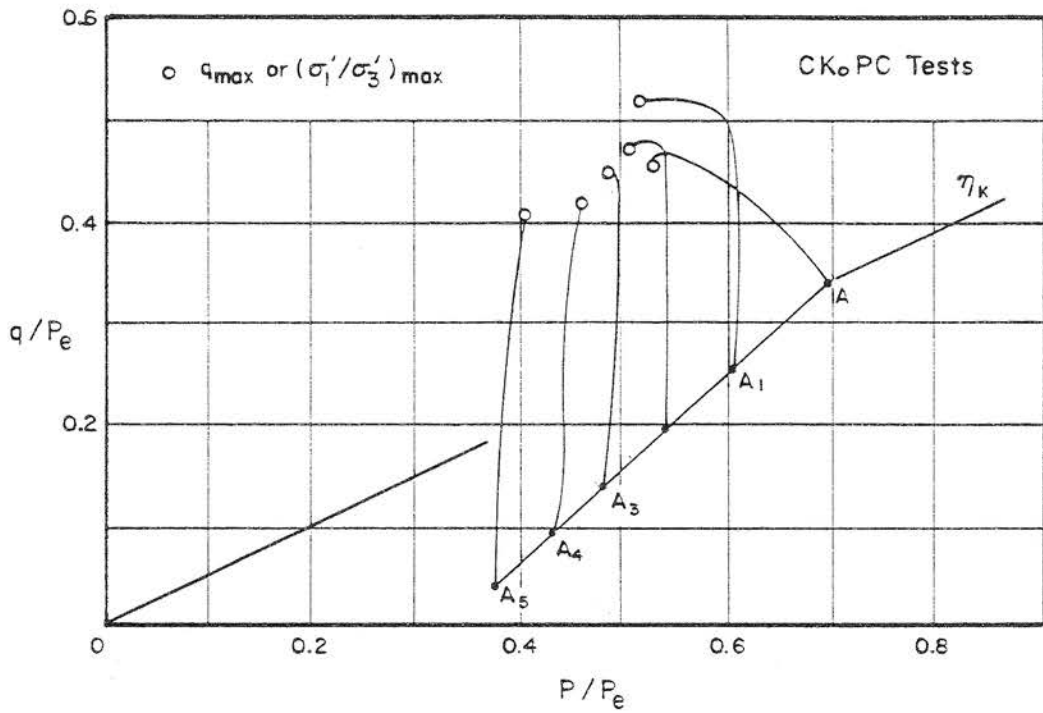


Fig. 6.40 (q/p_e , p/p_e) Plot from CKoPC Tests

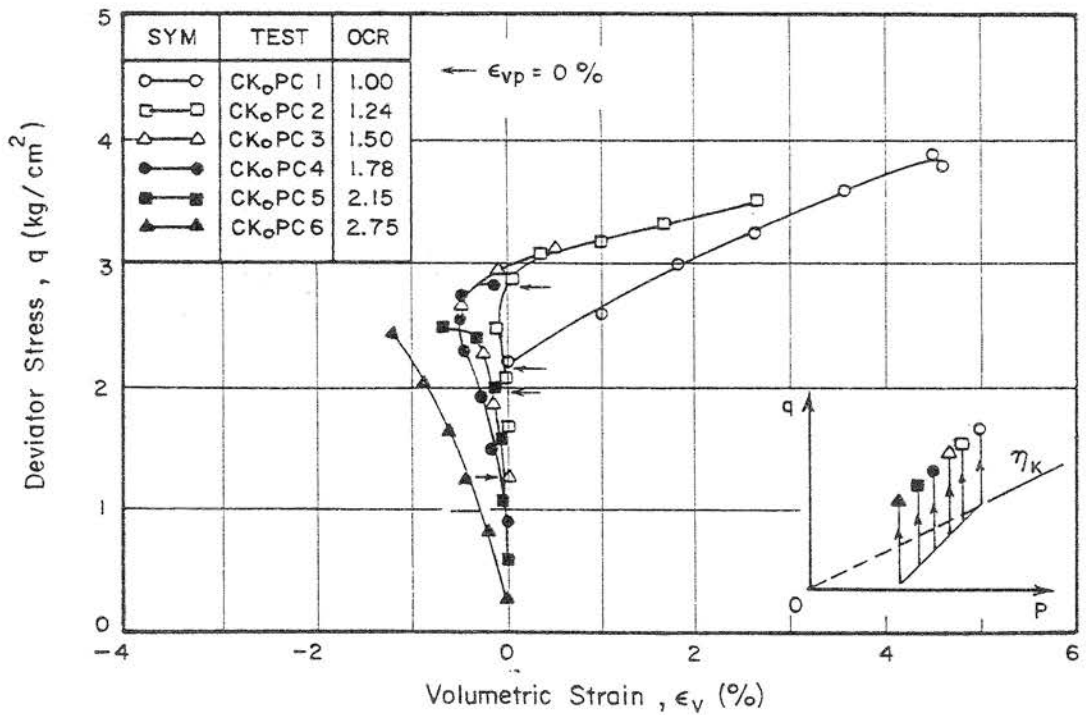


Fig. 6.41 (q , ϵ_v) Plot from CKoPC Tests

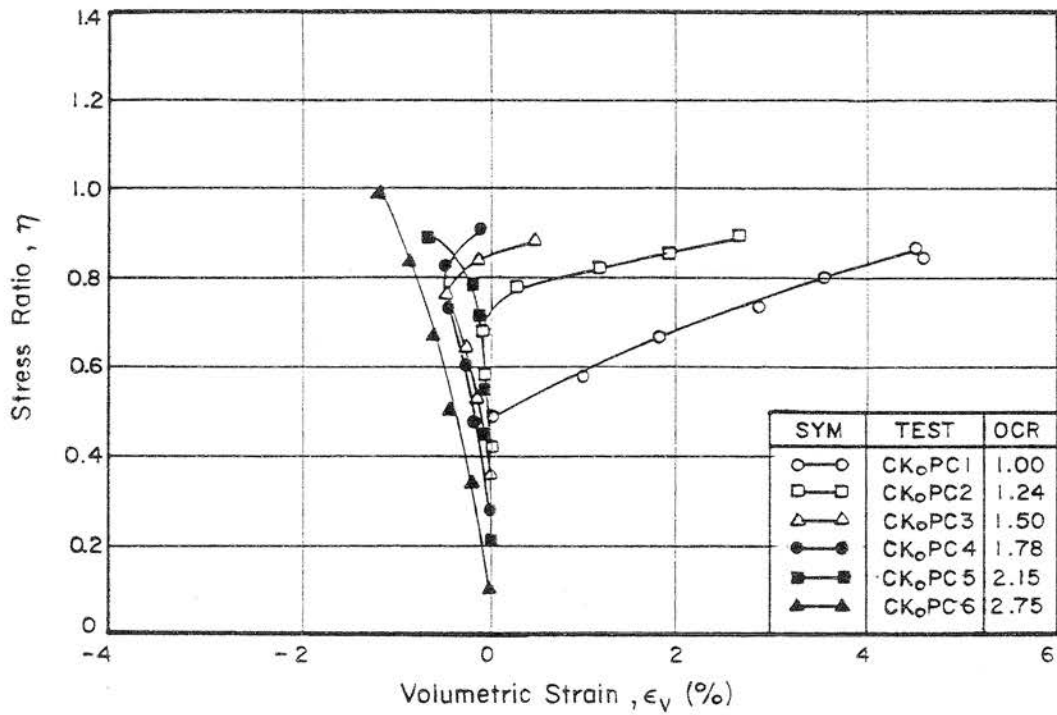


Fig. 6.42 (η , ϵ_v) Plot from CKoPC Tests

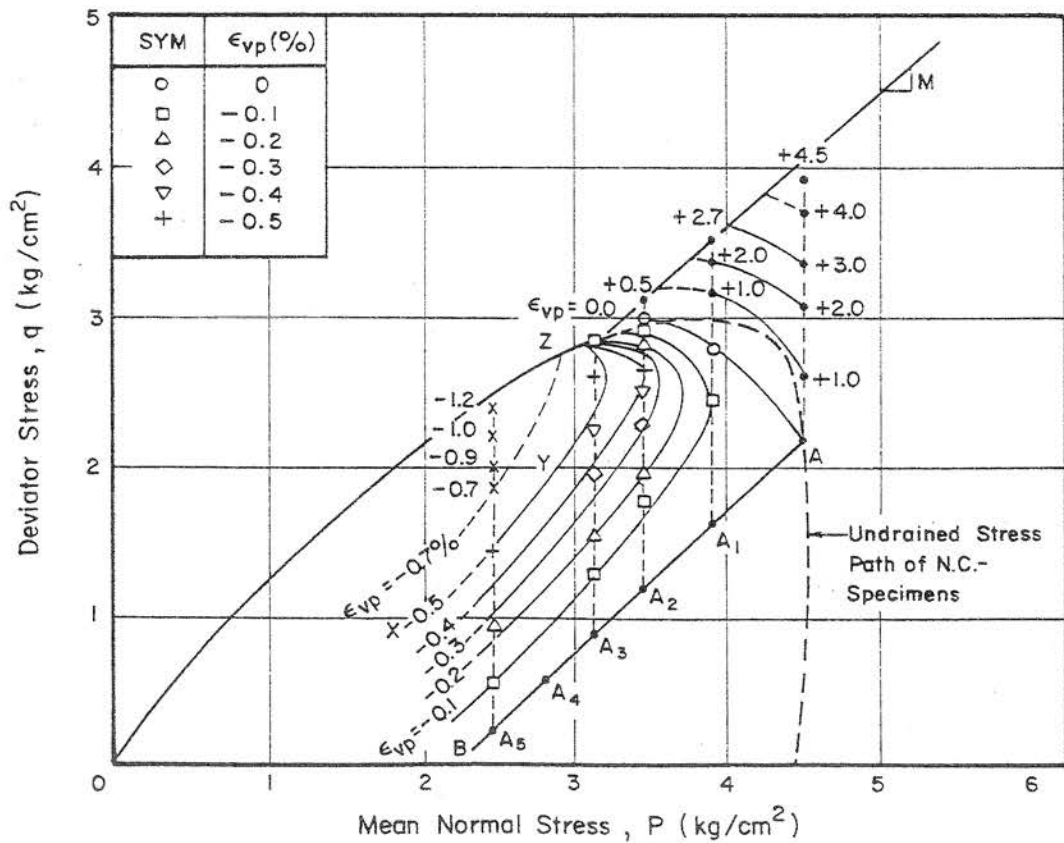


Fig. 6.43 Plastic Volumetric Strain Contours from CKoPC Tests

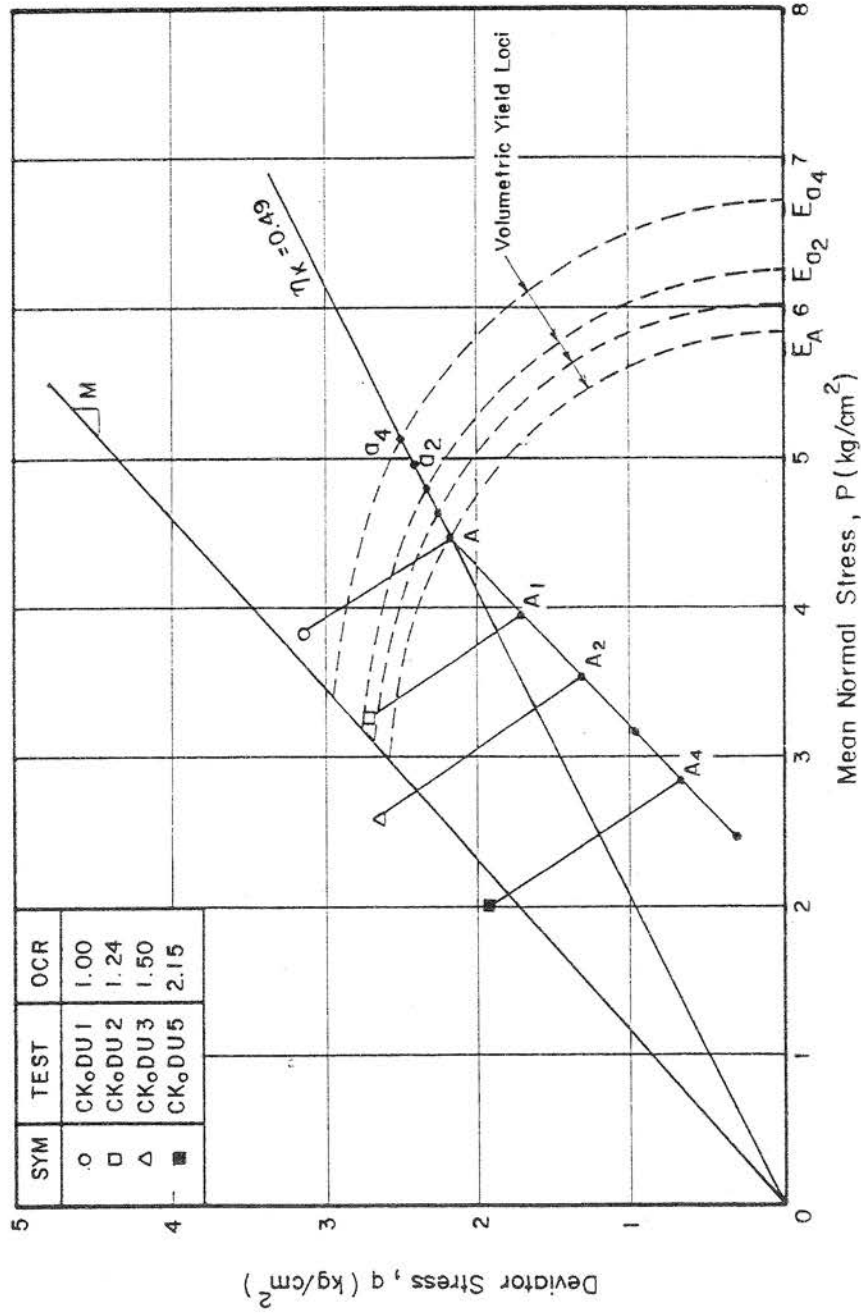


Fig. 6.44 Volumetric Yield Loci and Stress Paths for CKoDU Tests

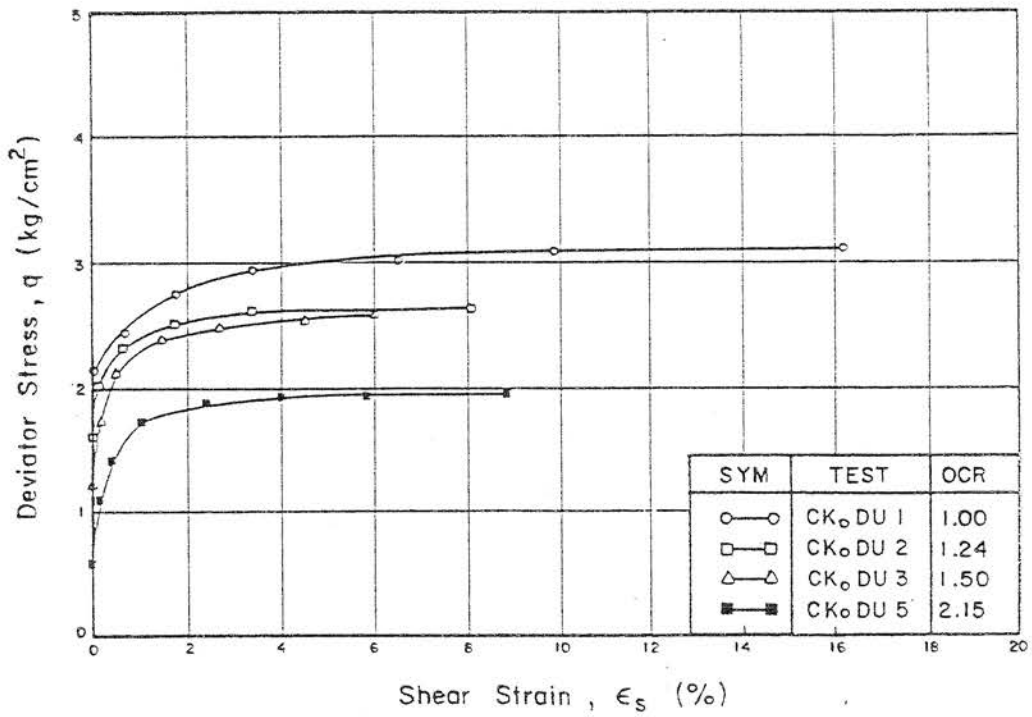


Fig. 6.45 (q , ϵ_s) Plot from CK_oDU Tests

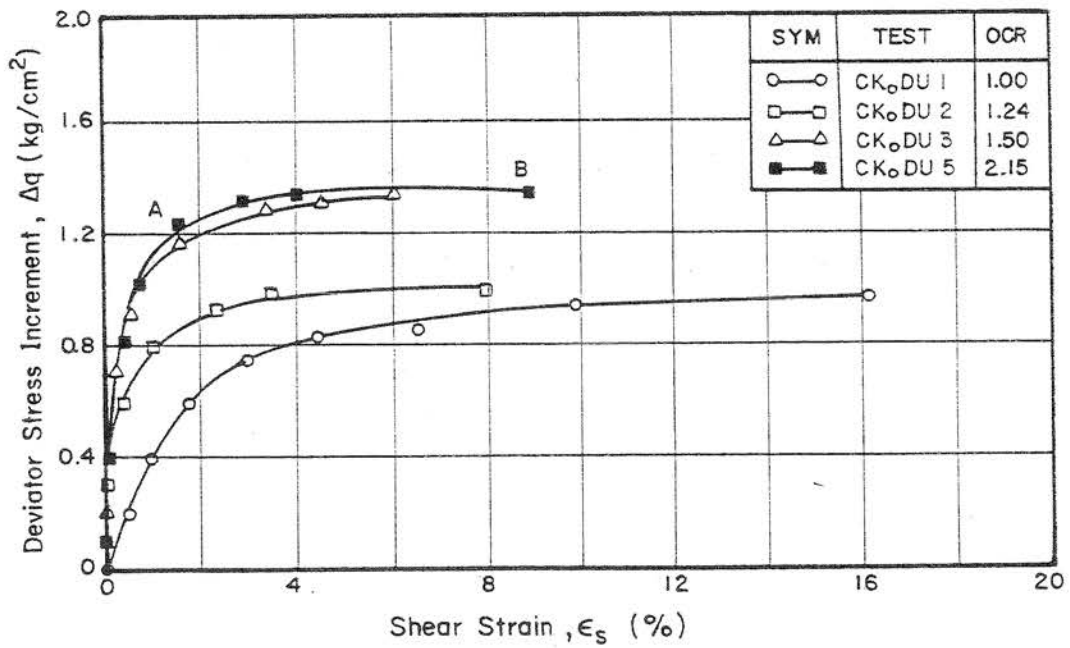


Fig. 6.46 Deviator Stress Increment and Shear Strain Relationship from CK_oDU Tests

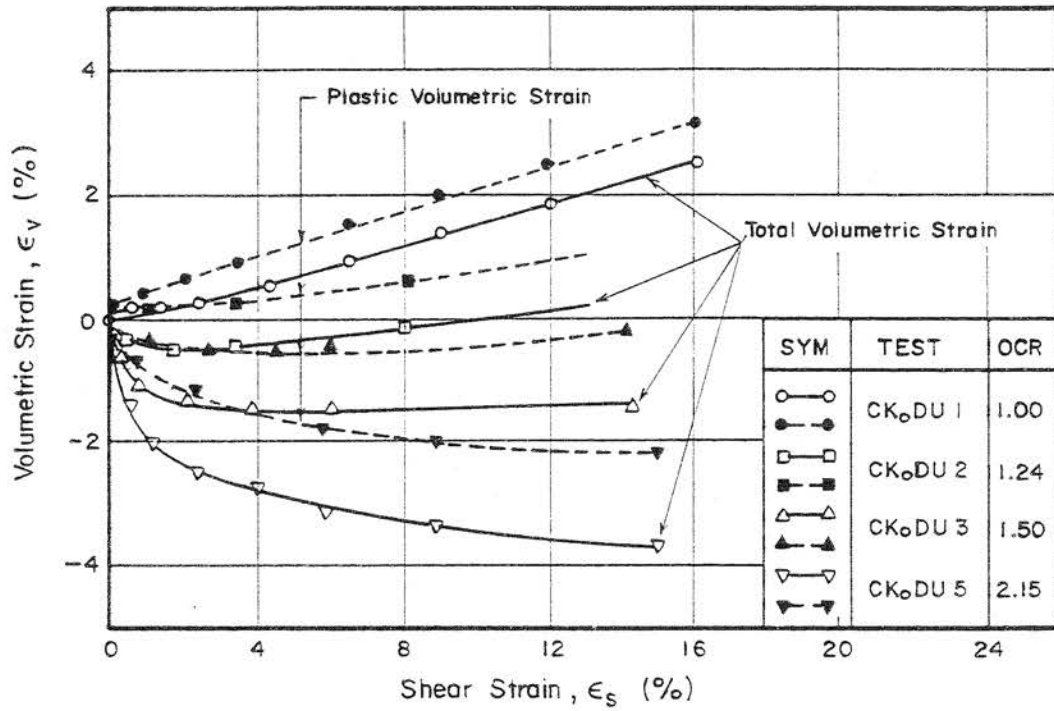


Fig. 6.46a (ϵ_v , ϵ_s) Plot from CKoDU Tests

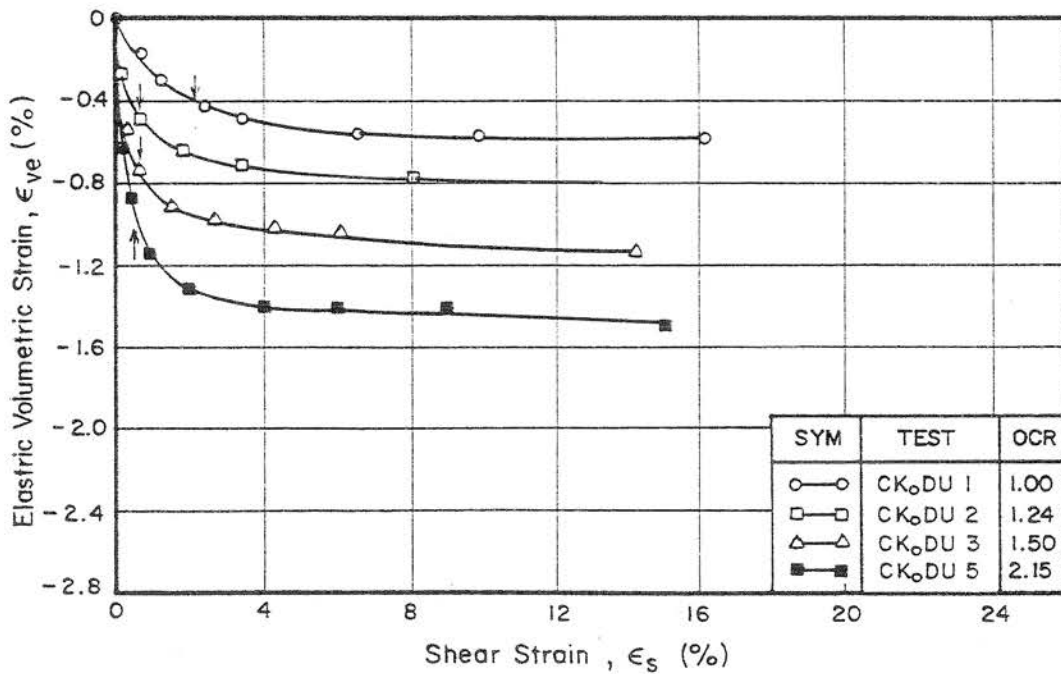


Fig. 6.46b (ϵ_{ve} , ϵ_s) Plot from CKoDU Tests

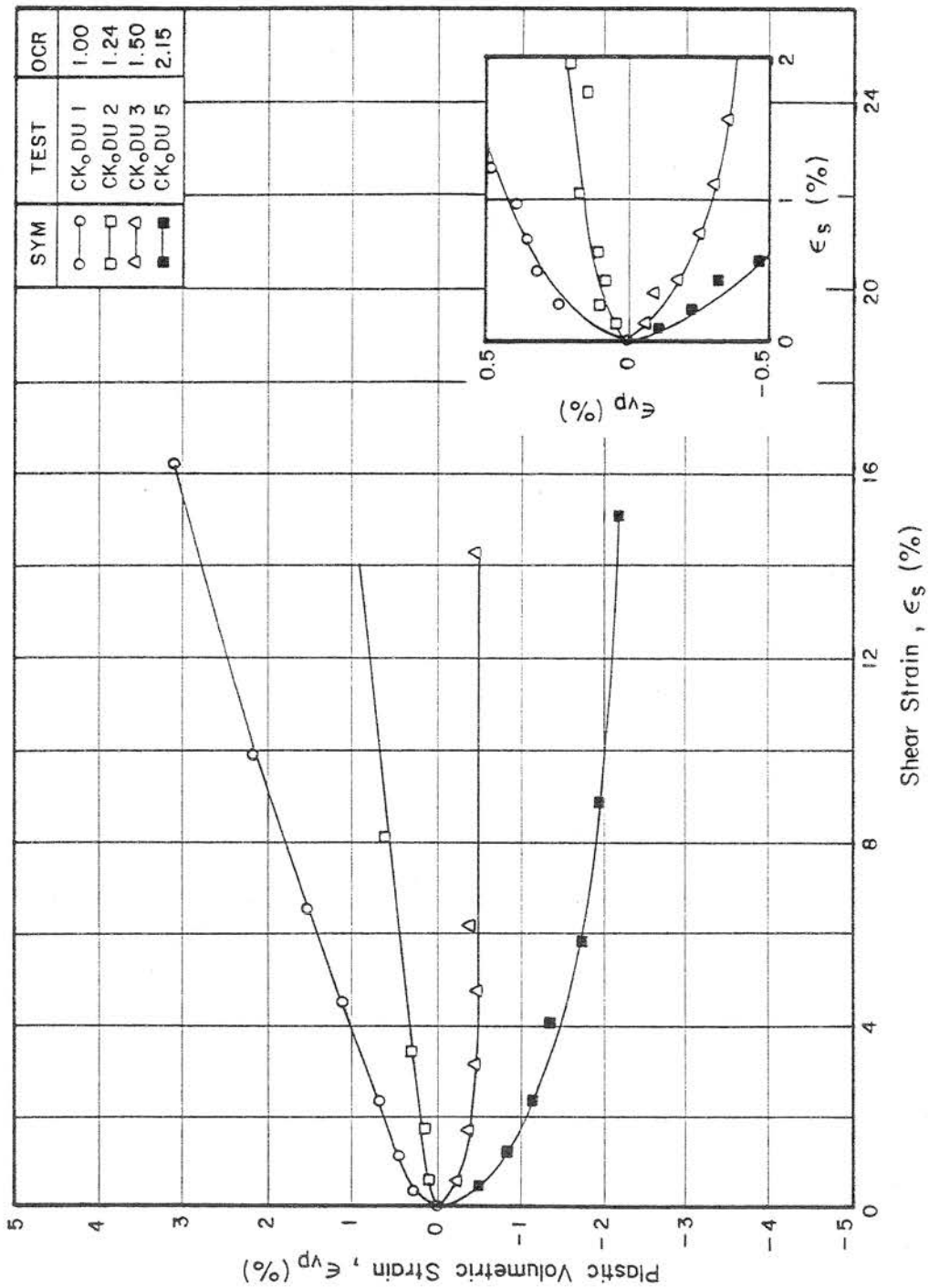


Fig. 6.46c (ϵ_{vp} , ϵ_s) Plot from CK_oDU Tests

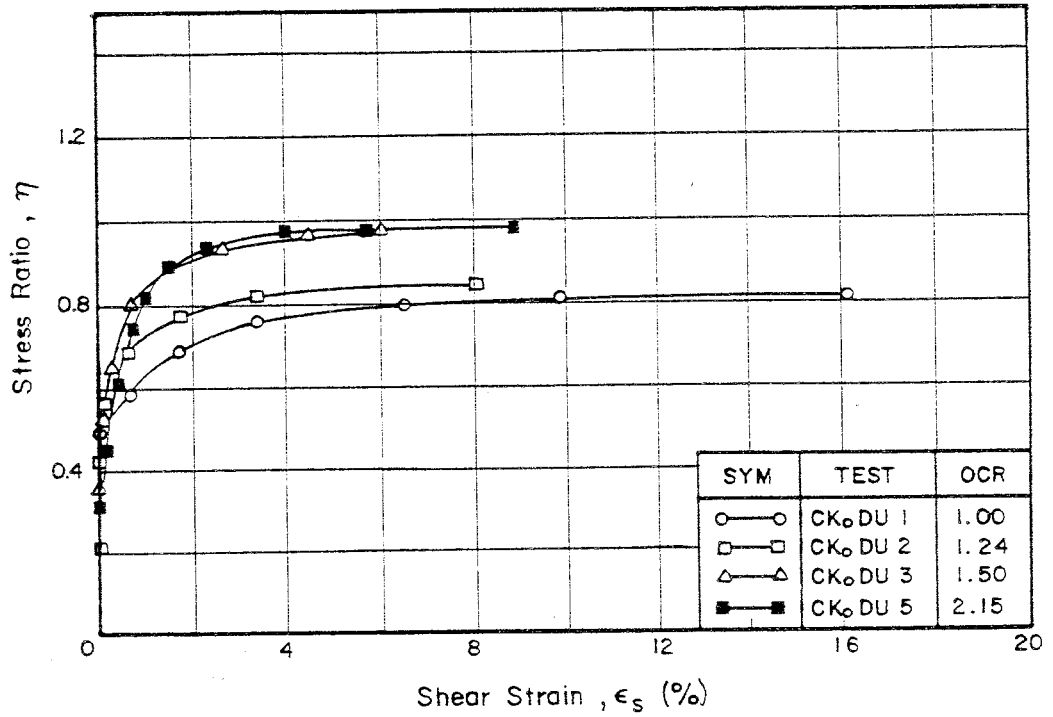


Fig. 6.47 (η , ϵ_s) Plot from CK_oDU Tests

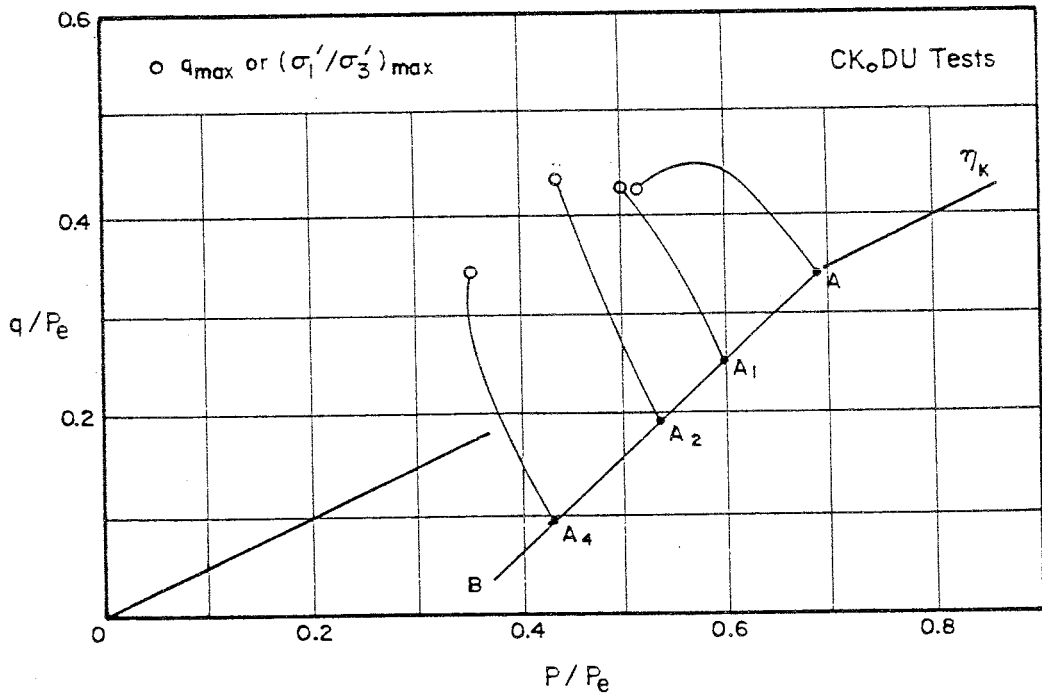


Fig. 6.48 (q/p_e , p/p_e) Plot from CK_oDU Tests

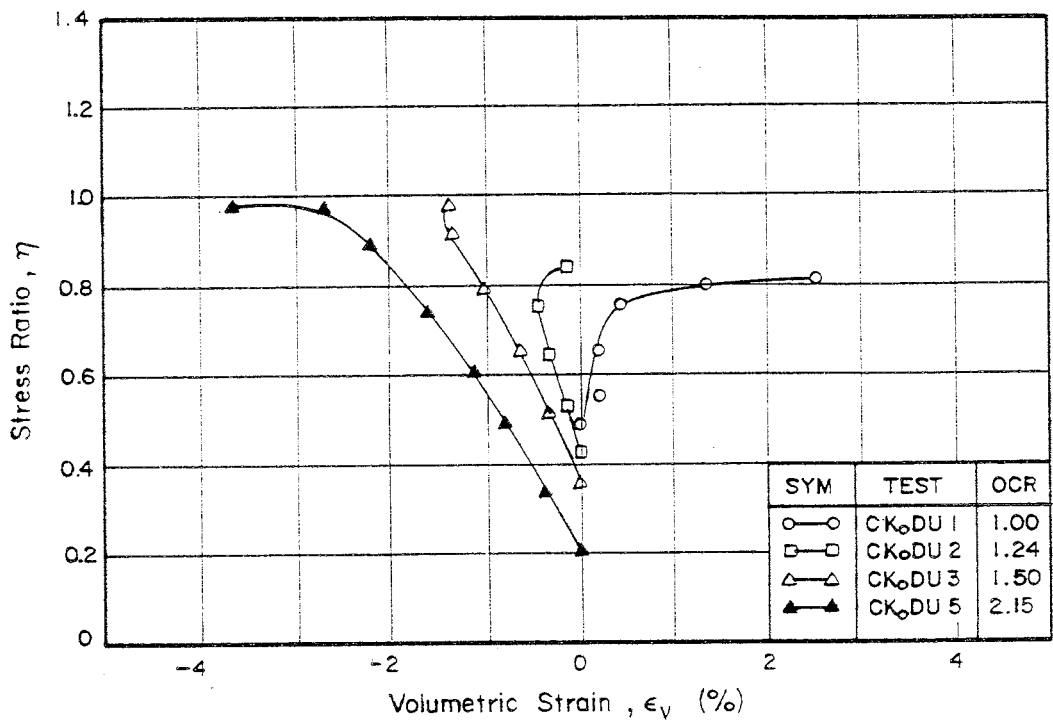


Fig. 6.49 (η , ϵ_v) Plot from CKoDU Tests

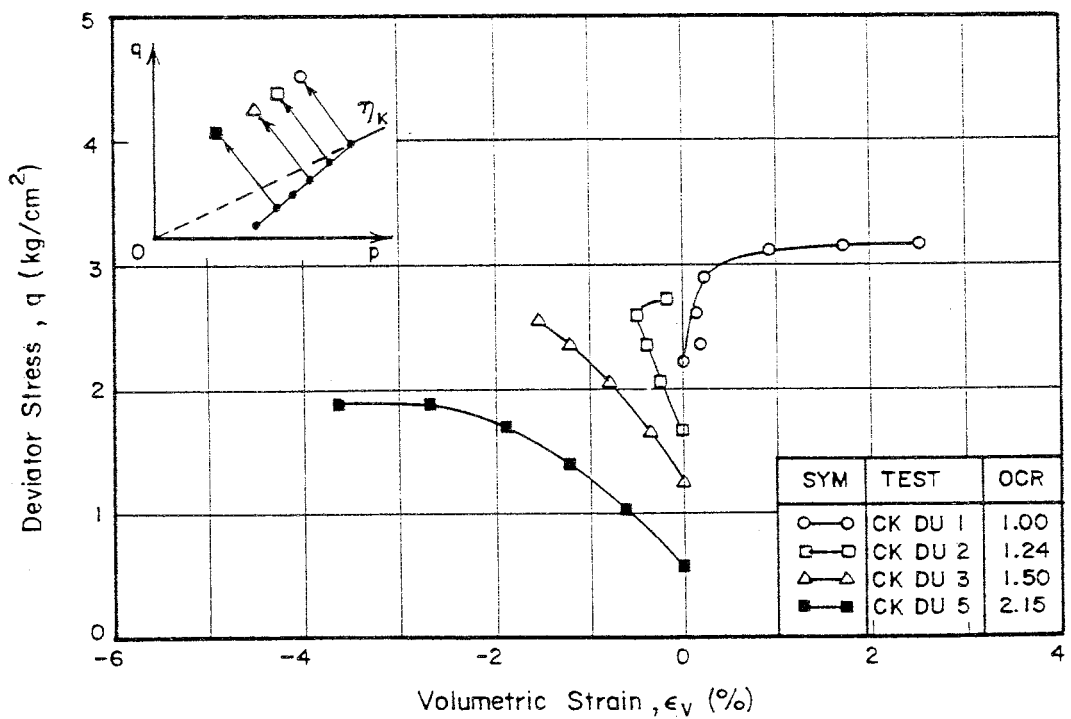


Fig. 6.50 (q , ϵ_v) Plot from CKoDU Tests

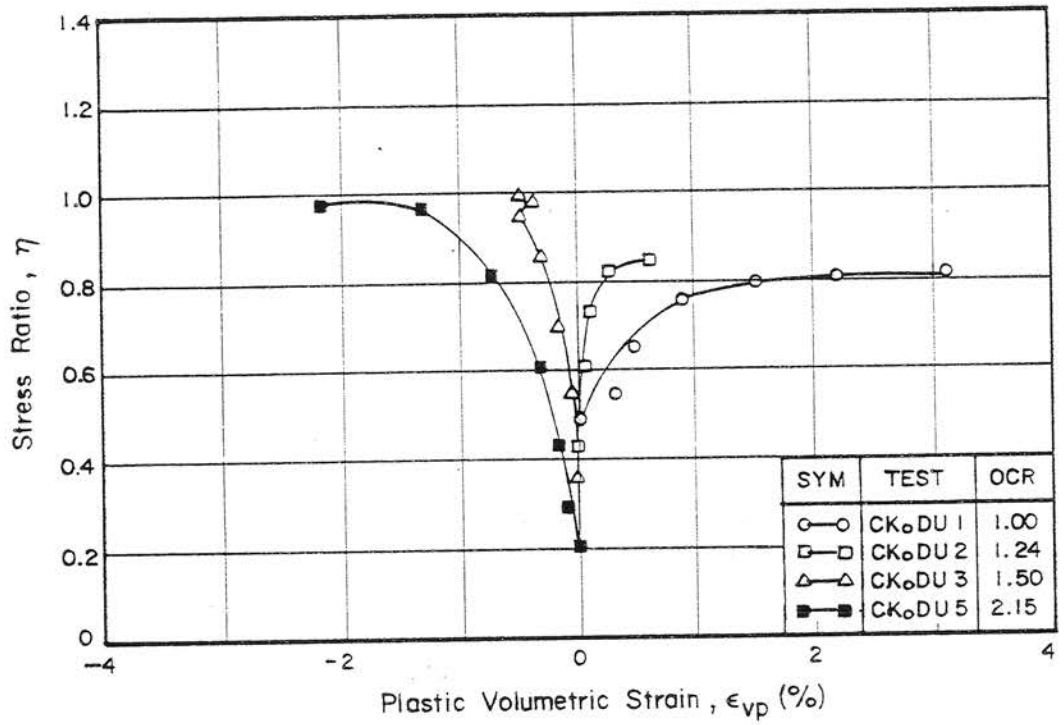


Fig. 6.51 (η , ϵ_{vp}) Plot from CKoDU Tests

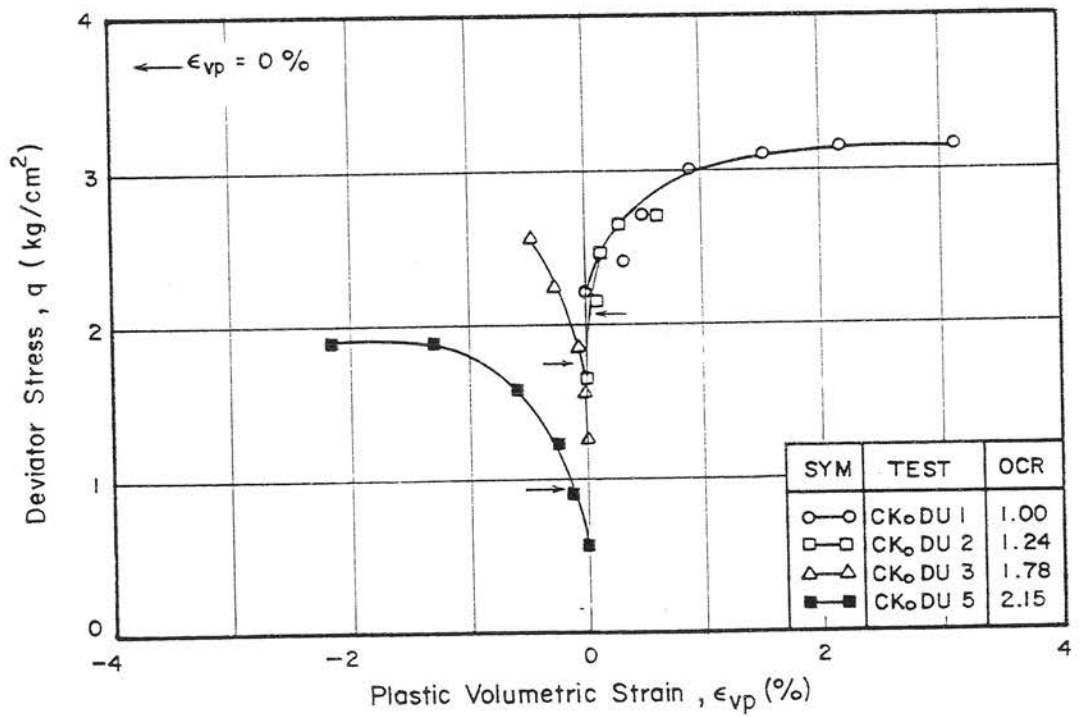


Fig. 6.52 (q , ϵ_{vp}) Plot from CKoDU Tests

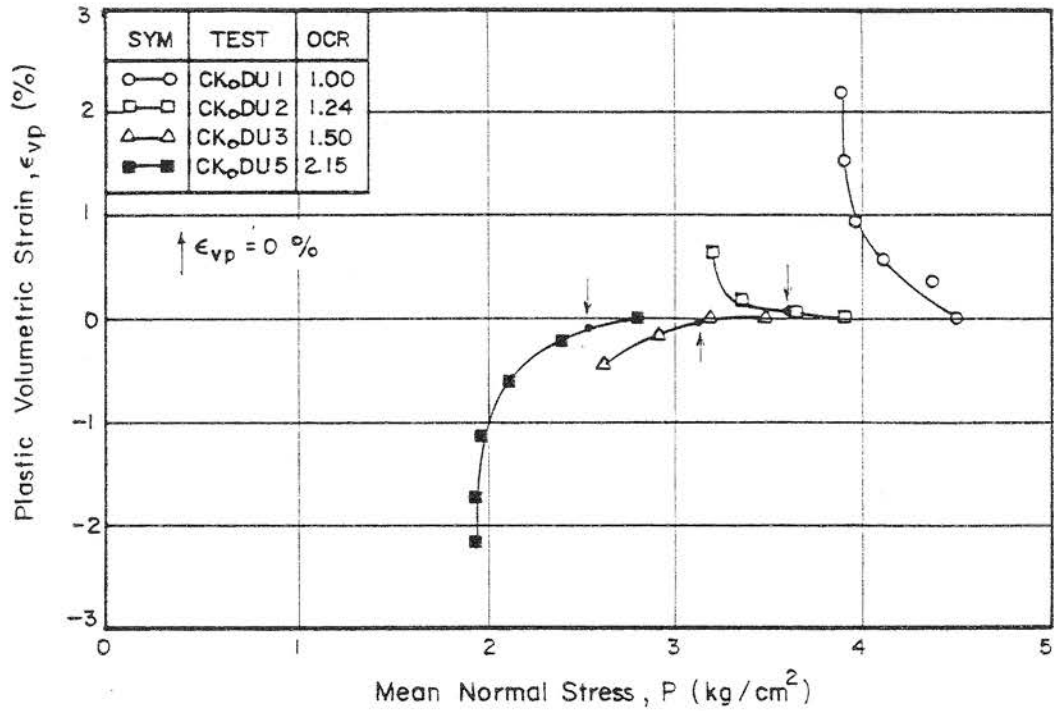


Fig. 6.53 (ϵ_{vp}, p) Plot from CKoDU Tests

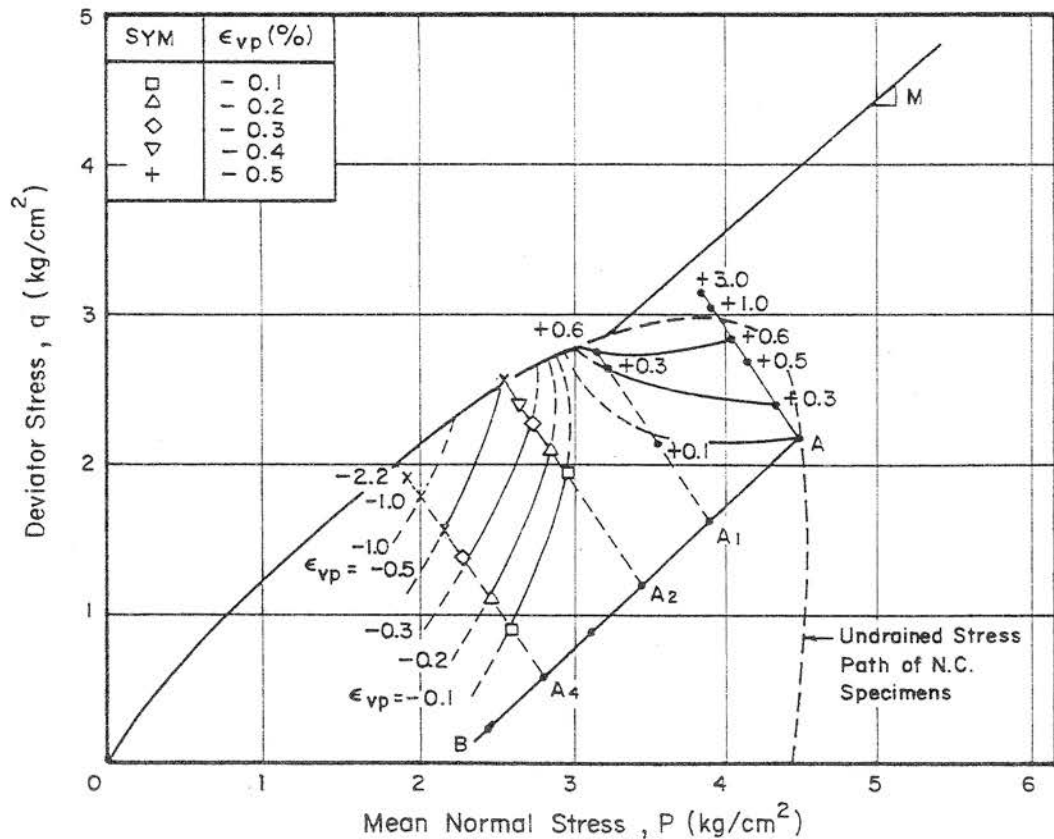


Fig. 6.54 Plastic Volumetric Strain Contours from CKoDU Tests

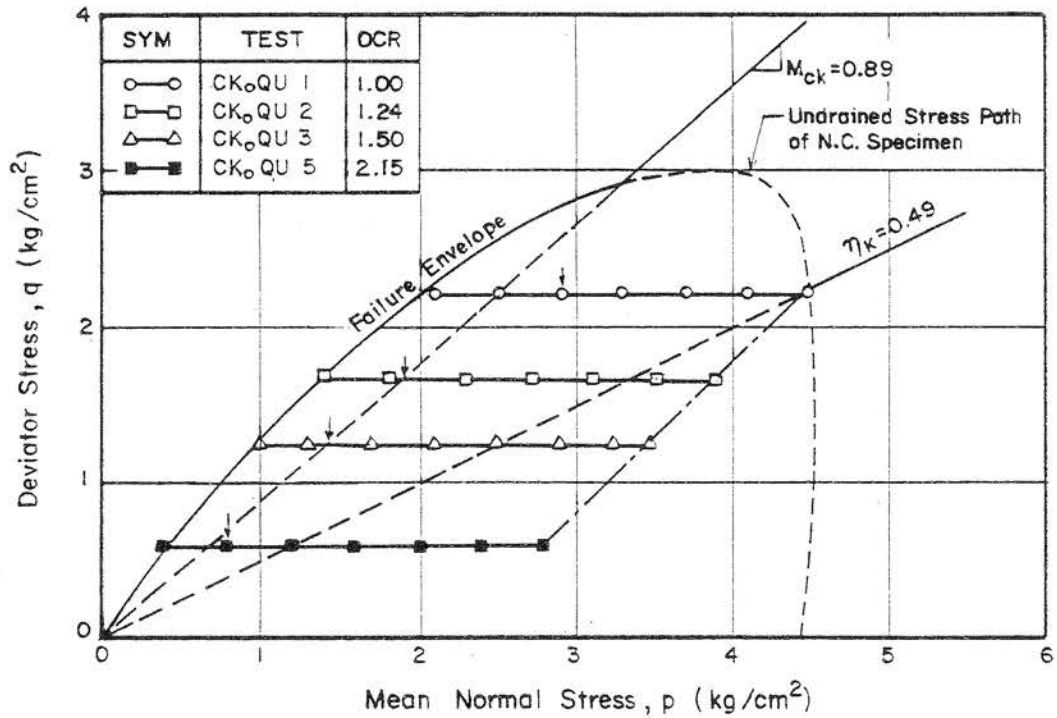


Fig. 6.55 Drained Stress Paths from CKoQU Tests

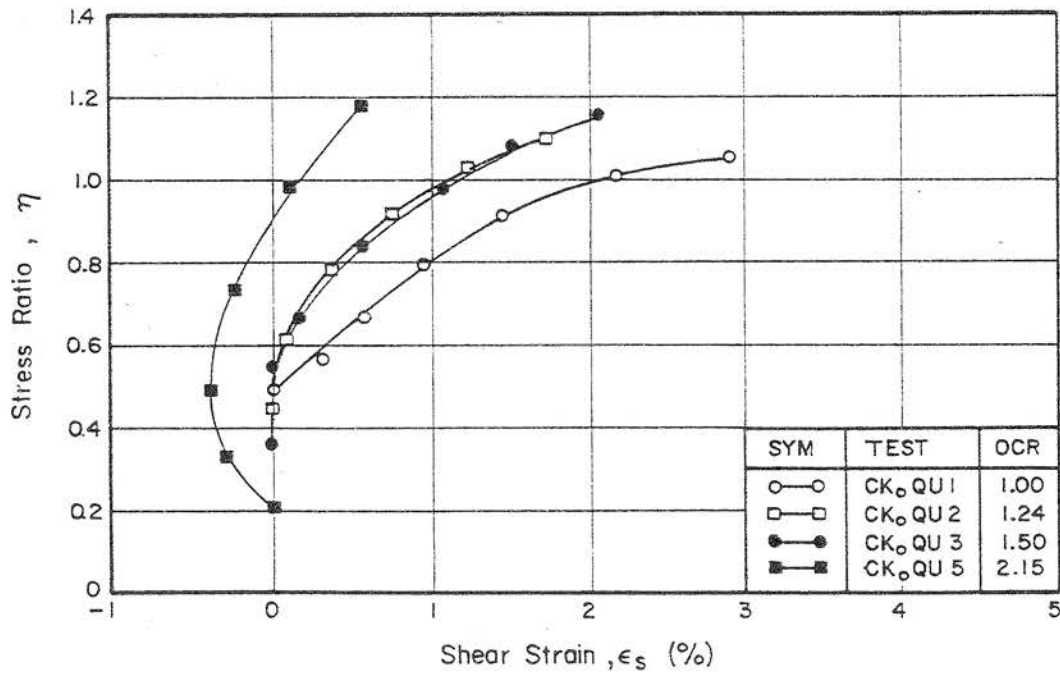


Fig. 6.56 (η, ϵ_s) Plot from CKoQU Tests

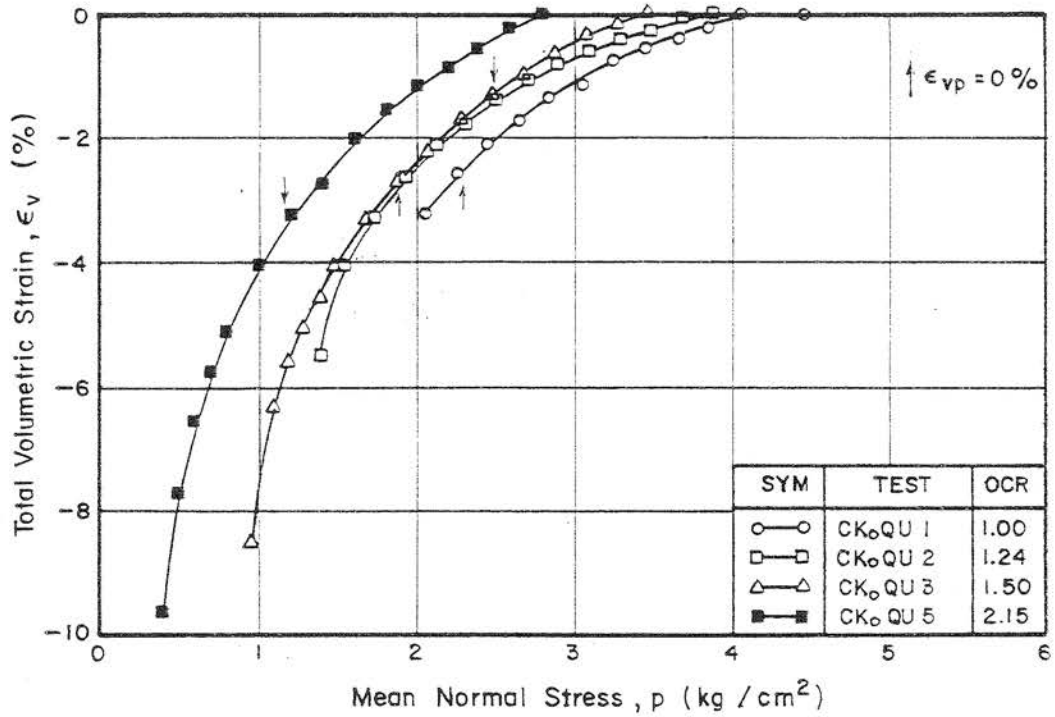


Fig. 6.57 (ϵ_v, p) Plot from CKoQU Tests

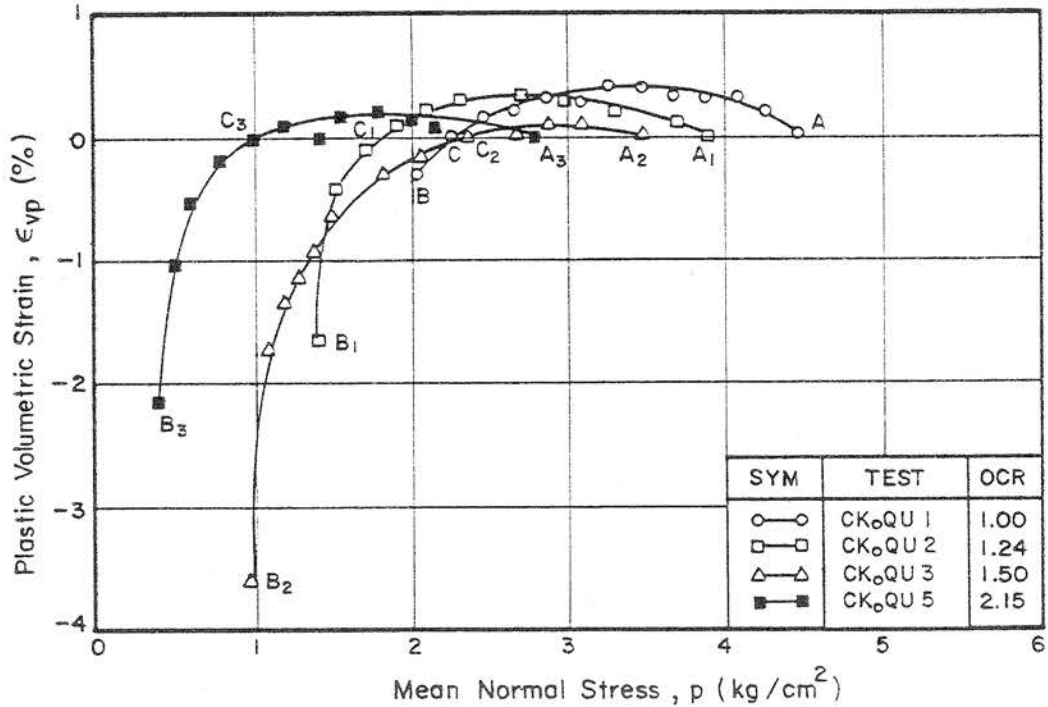


Fig. 6.58 (ϵ_{vp}, p) Plot from CKoQU Tests

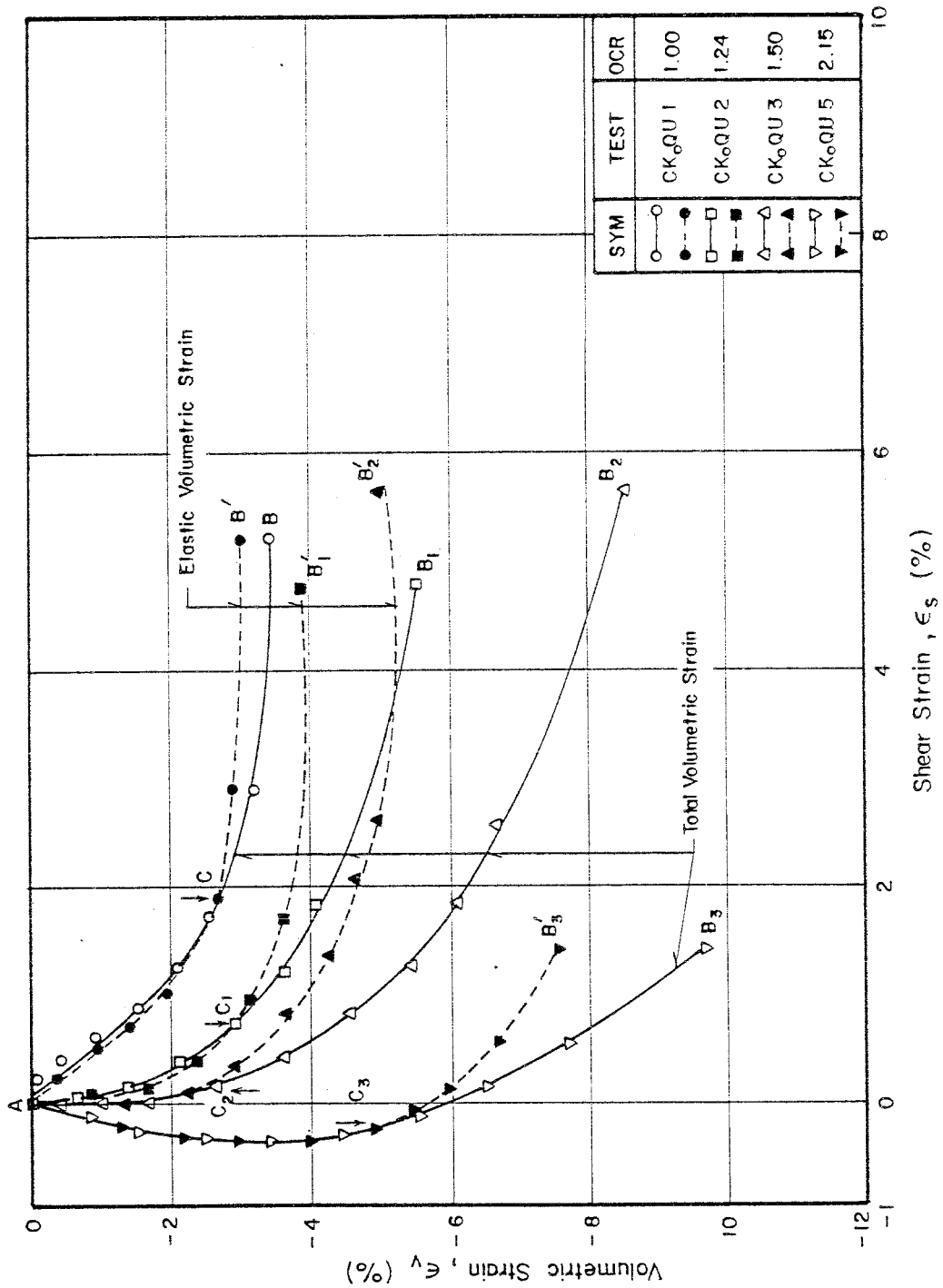


Fig. 6.59 (ϵ_v , ϵ_s) Plot from CK_oQU Tests

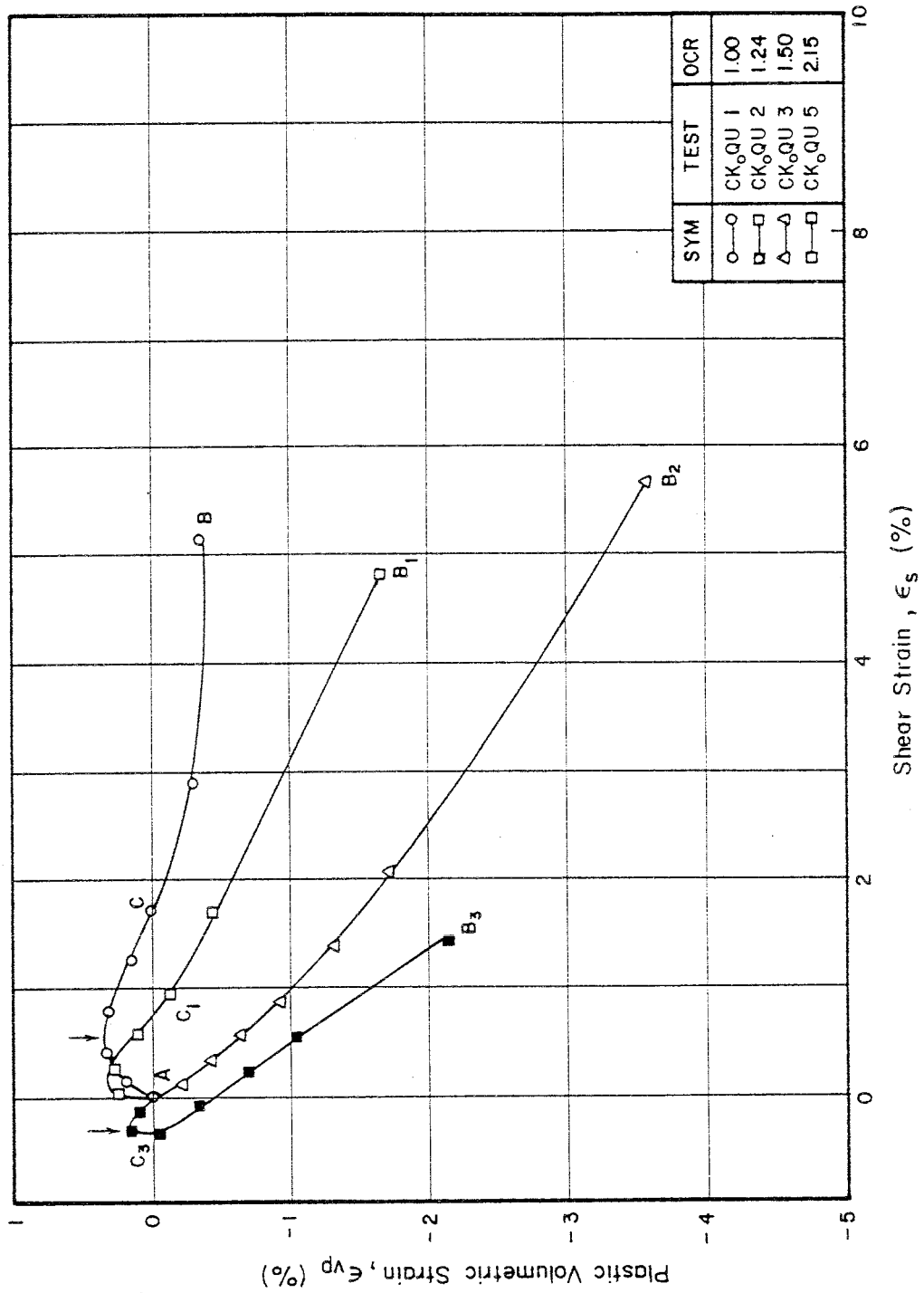


Fig. 6.60 (ϵ_{vp} , ϵ_s) Plot from CK₀QU Tests

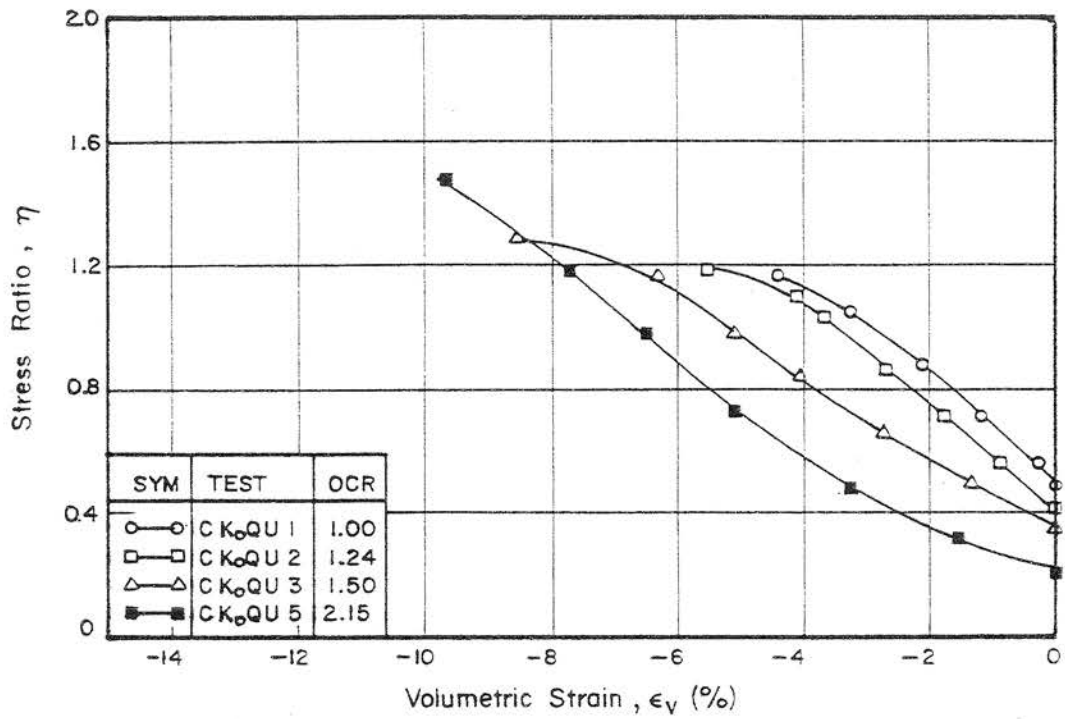


Fig. 6.61 (η , ϵ_v) Plot from CK_oQU Tests

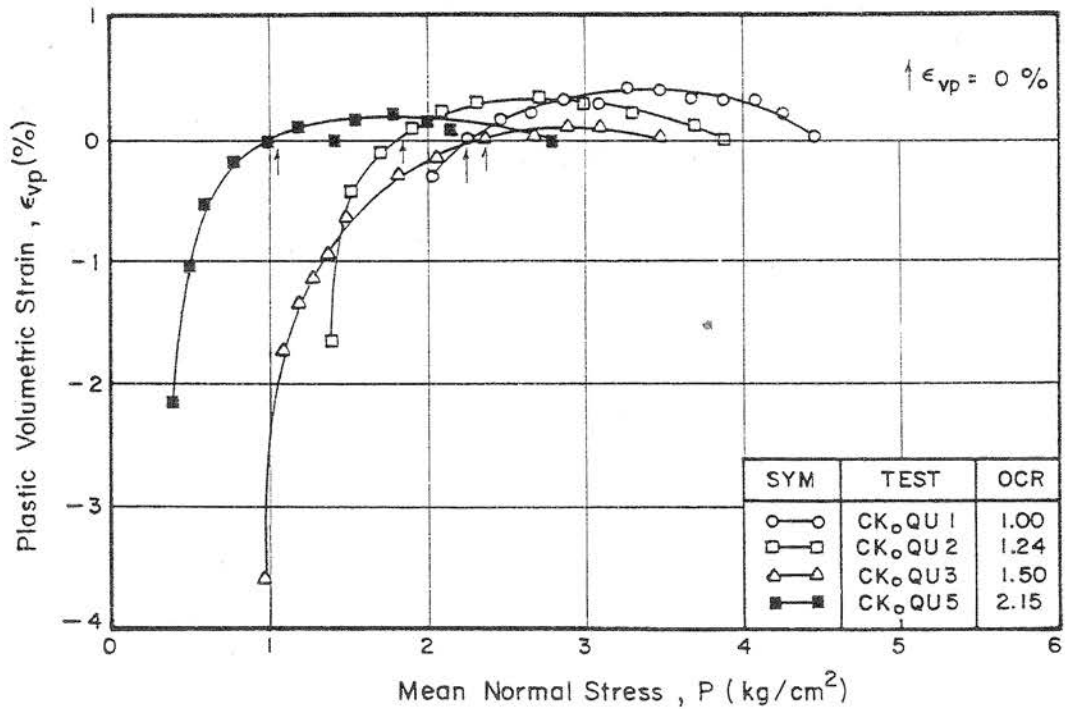


Fig. 6.62 (ϵ_{vp} , p) Plot from CK_oQU Tests

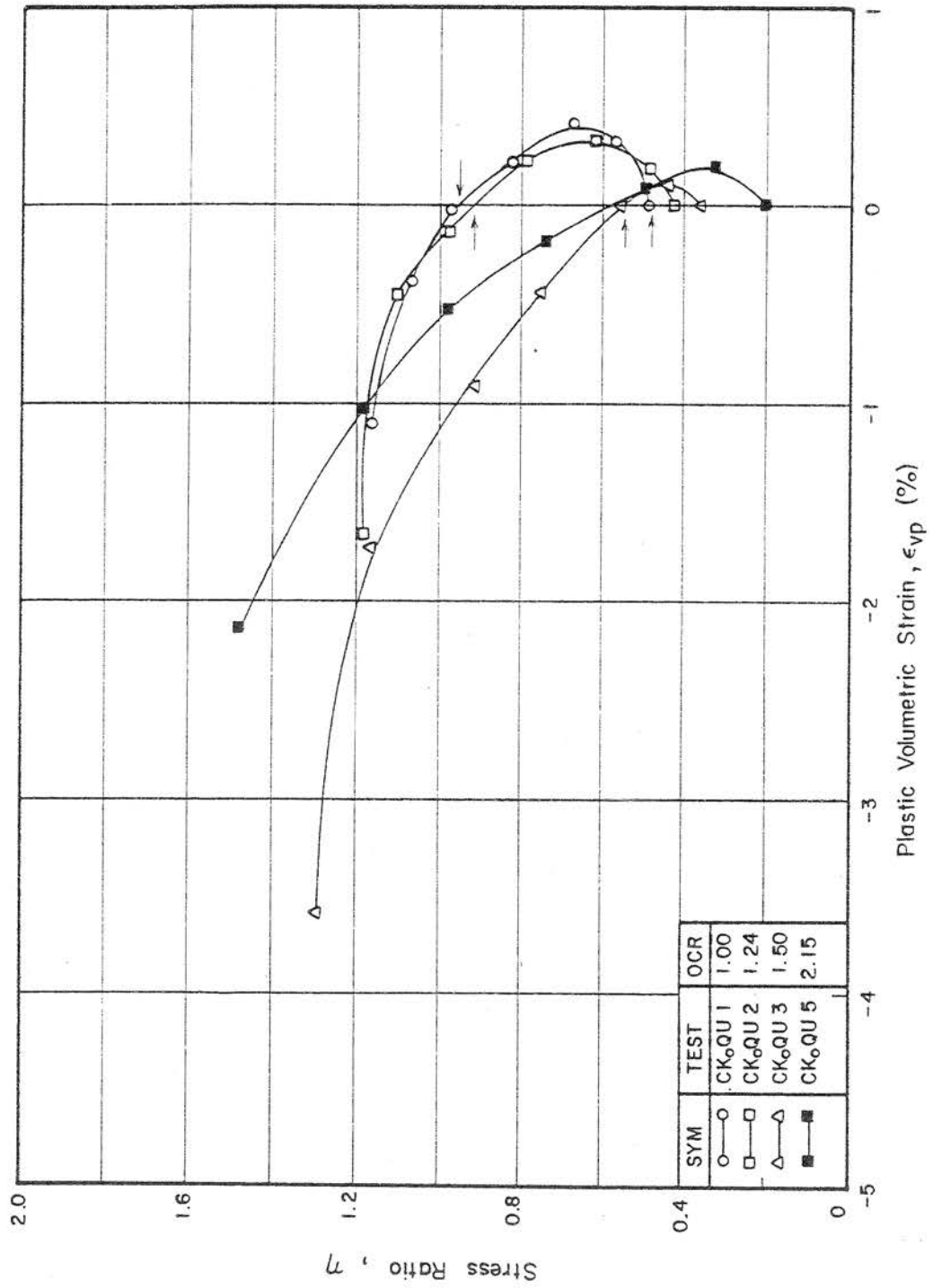


Fig. 6.63 (η , ϵ_{vp}) Plot from CKoQU Tests

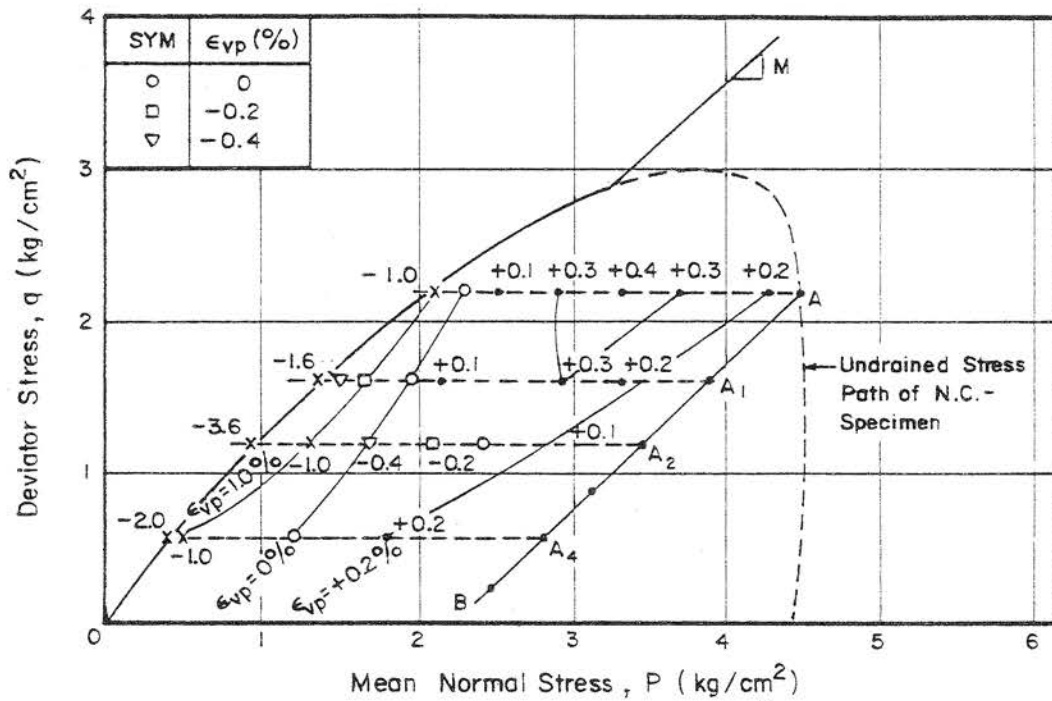


Fig. 6.64 Plastic Volumetric Strain Contours from CK₀QU Tests

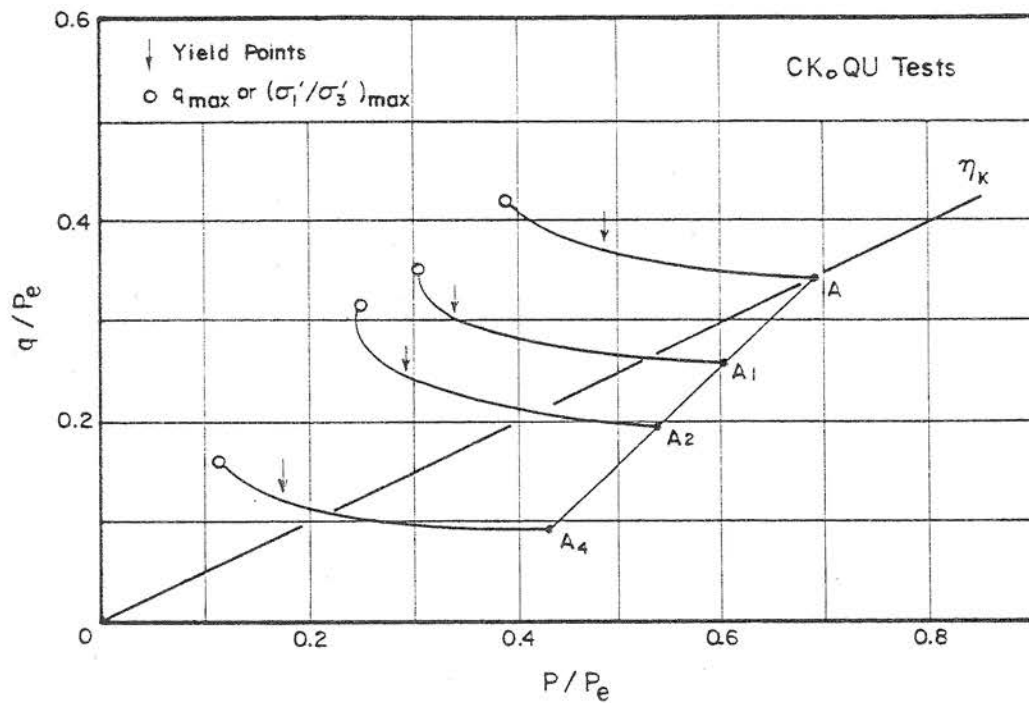


Fig. 6.65 (q/p_e , p/p_e) Plot from CK₀QU Tests

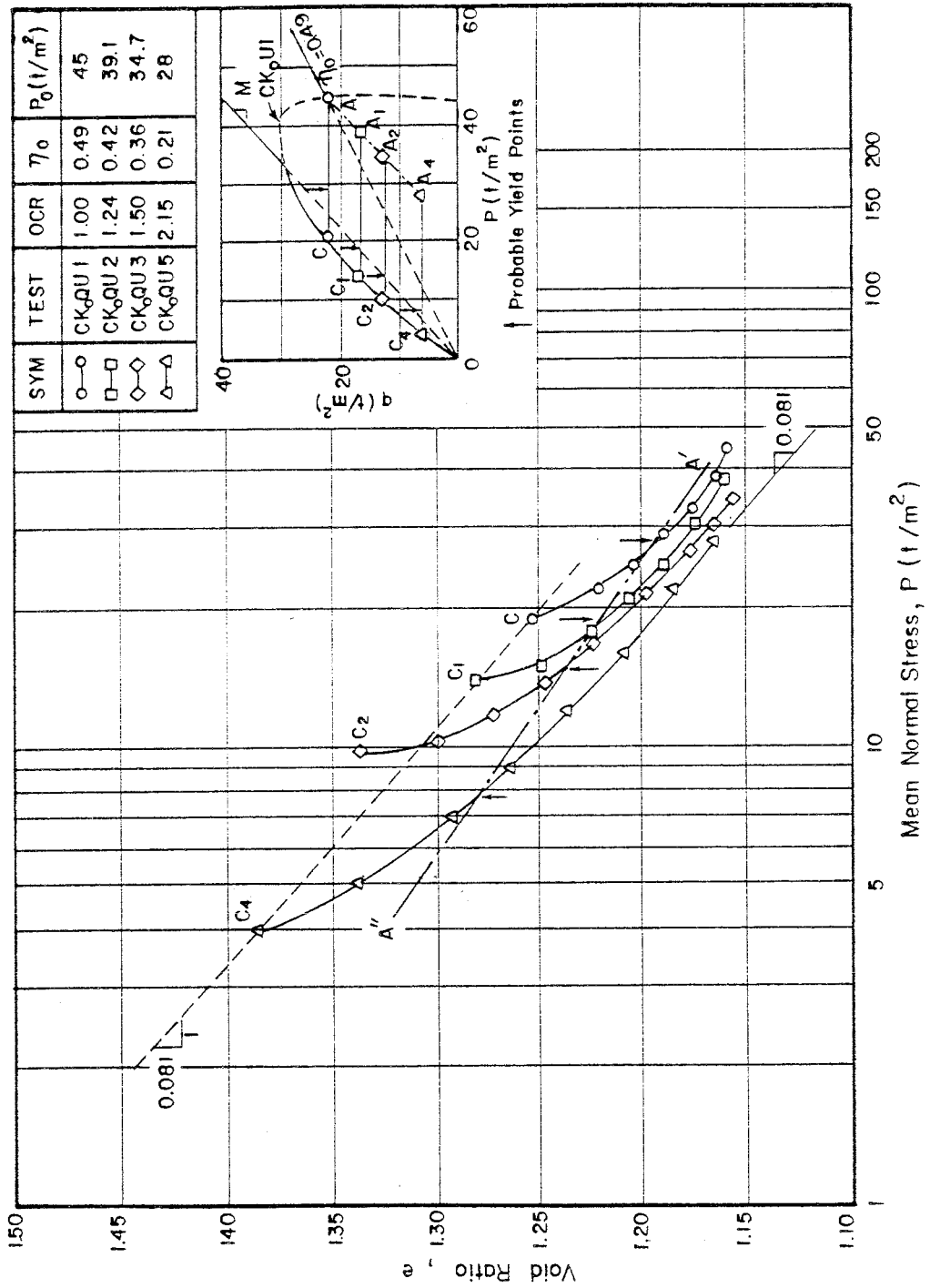


Fig. 6.66 (e , ln p) Plot from CK6QU Tests

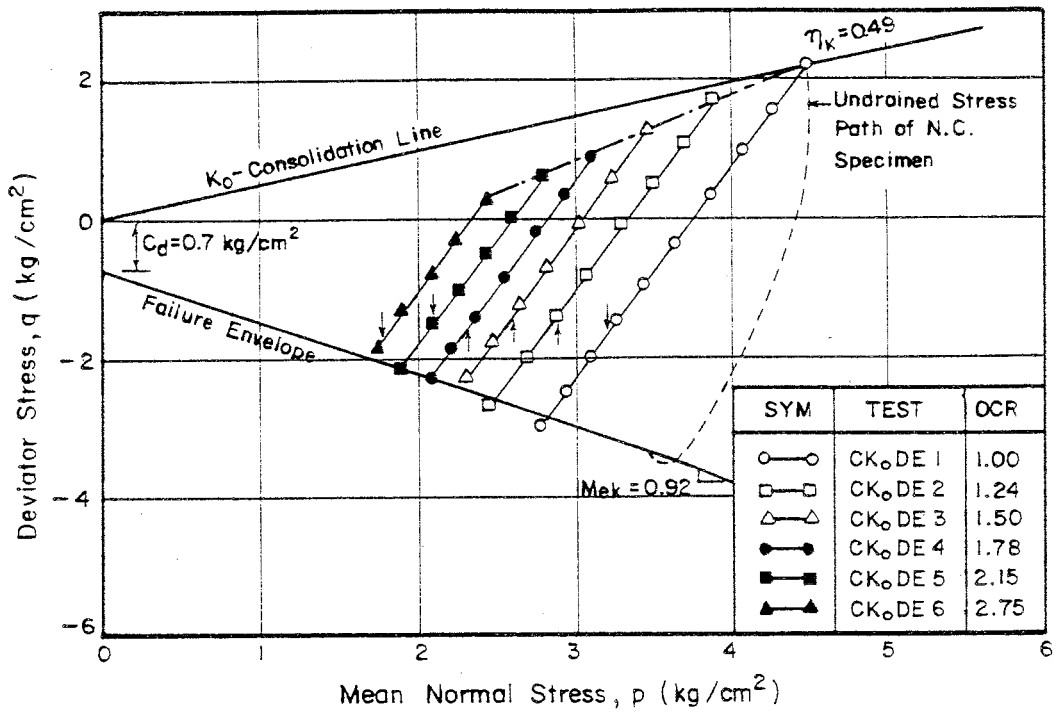


Fig. 6.67 Drained Stress Paths from CK_oDE Tests

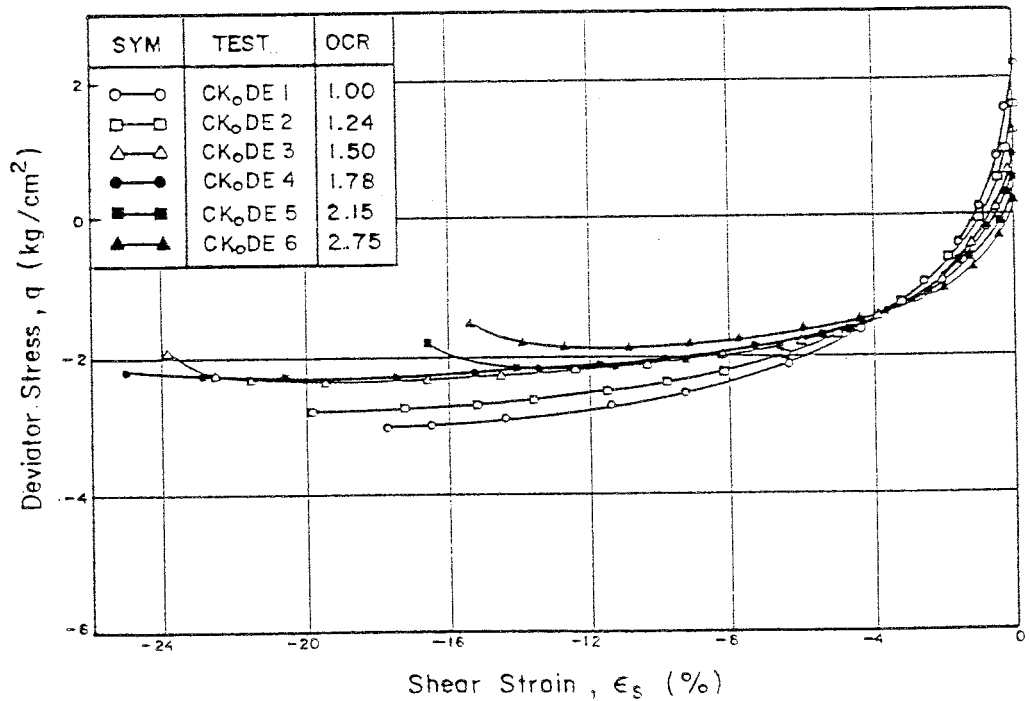


Fig. 6.68 (q , ϵ_s) Plot from CK_oDE Tests

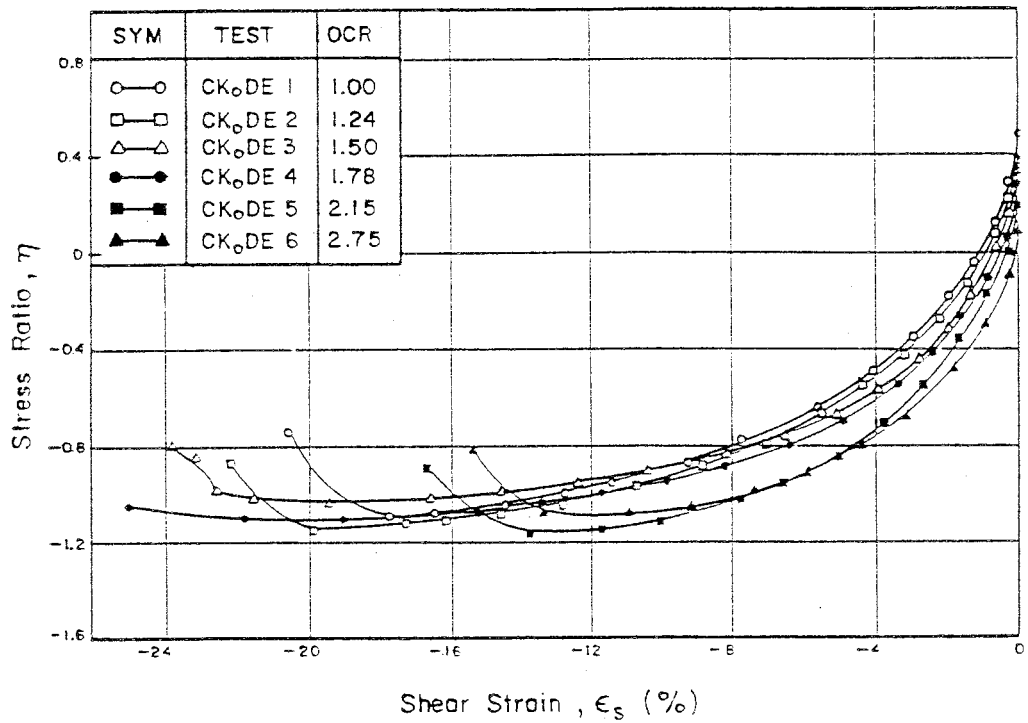


Fig. 6.69 (η , ϵ_s) Plot from CK_oDE Tests

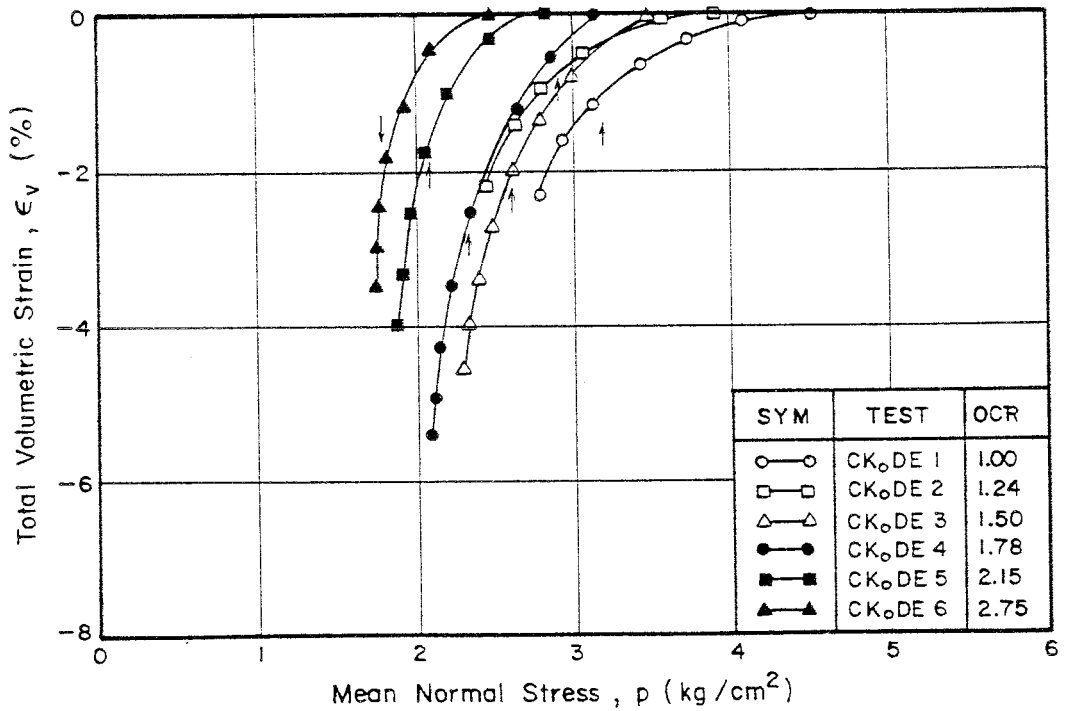


Fig. 6.70 (ϵ_v , p) Plot from CK_oDE Tests

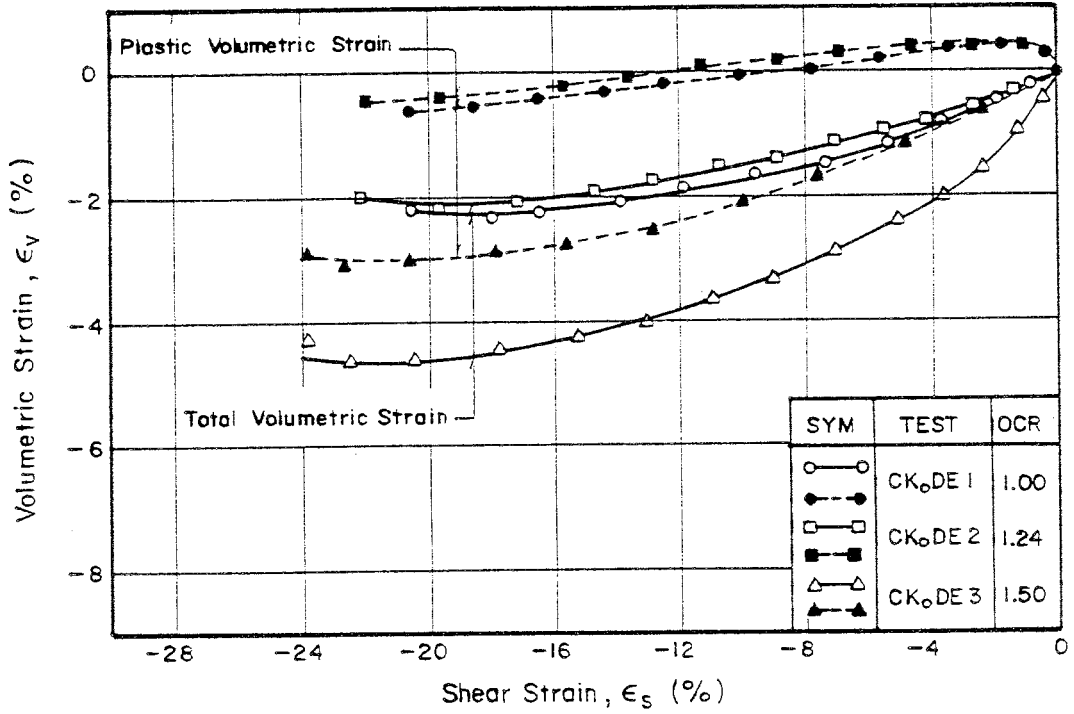


Fig. 6.71a (ϵ_v ; ϵ_s) Plot from CKoDE Tests (Wet Zone)

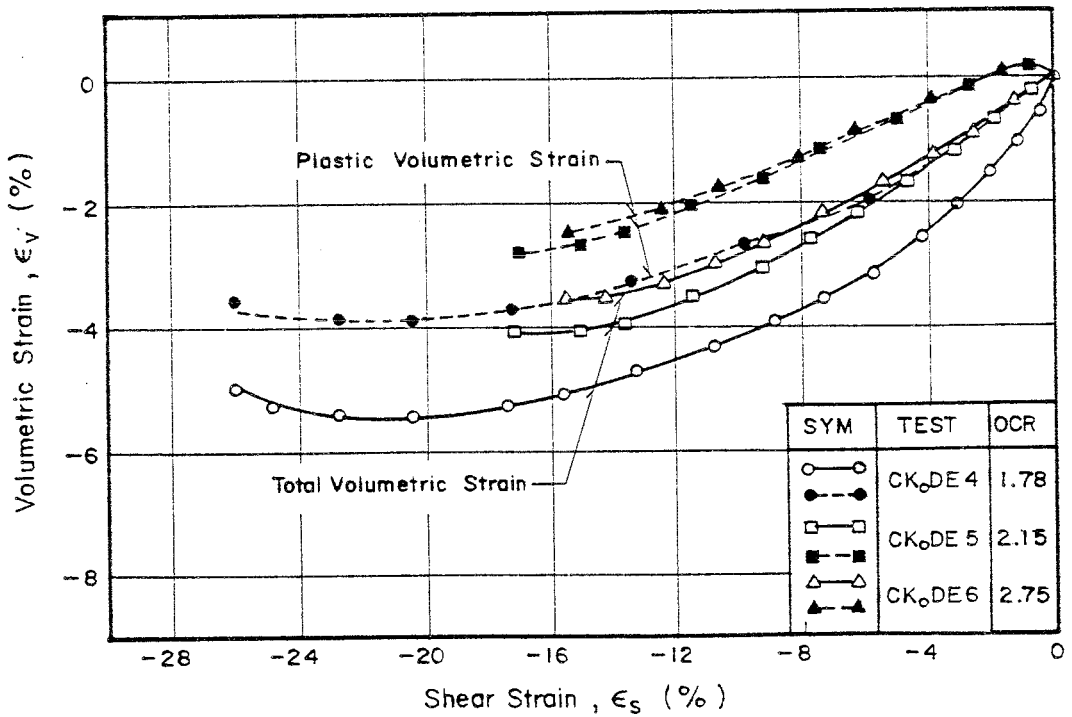


Fig. 6.71b (ϵ_v , ϵ_s) Plot from CKoDE Tests (Dry Zone)

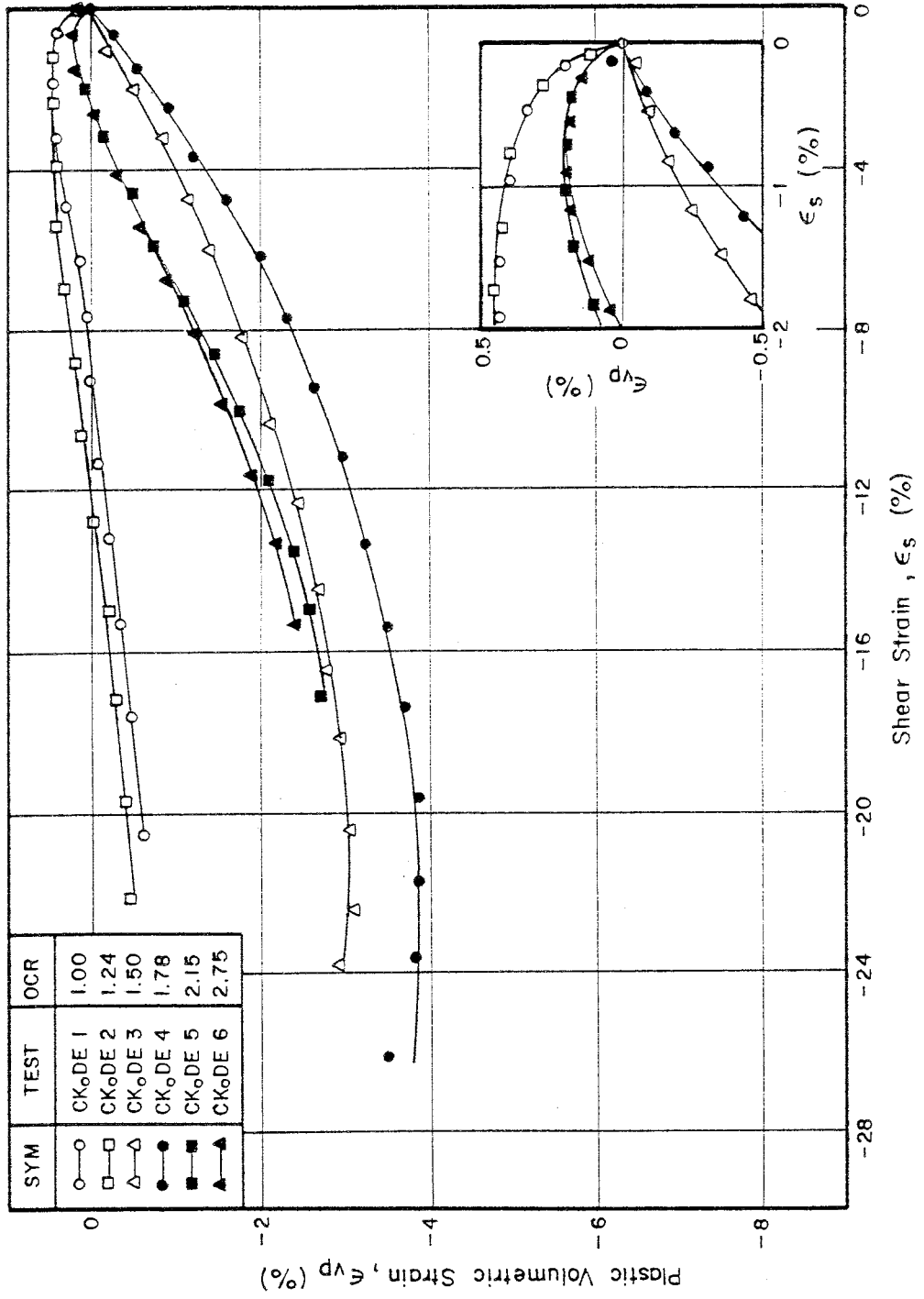


Fig. 6.72 (ϵ_{vp} , ϵ_s) Plot from CK₀DE Tests

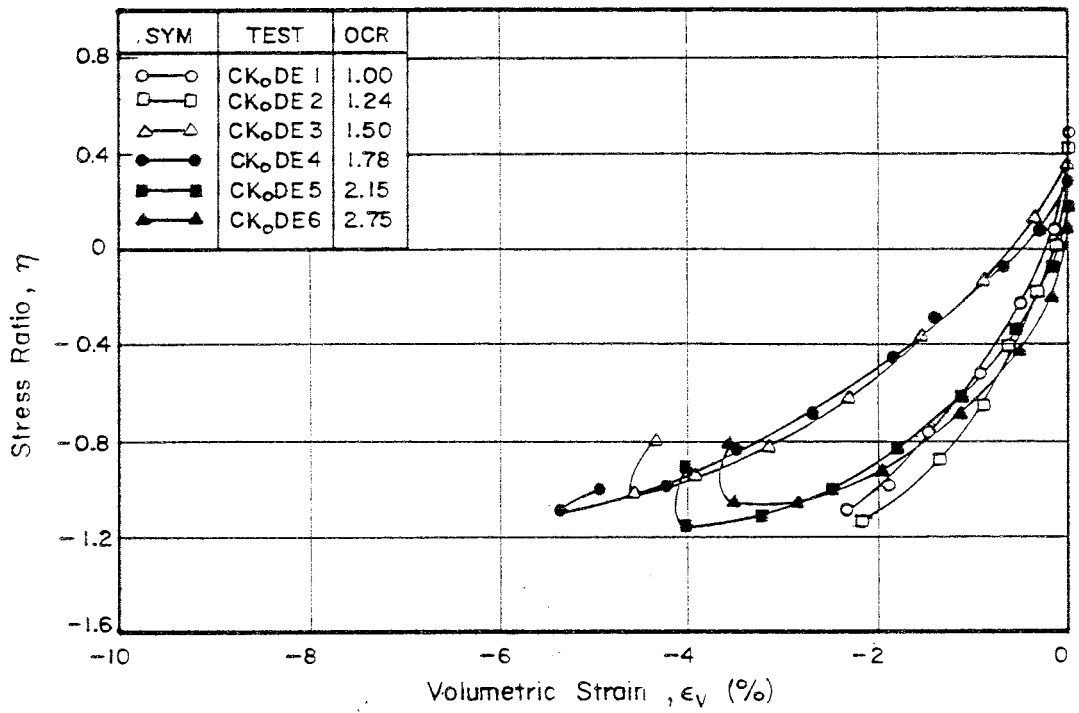


Fig. 6.73 (η , ϵ_v) Plot from CKoDE Tests

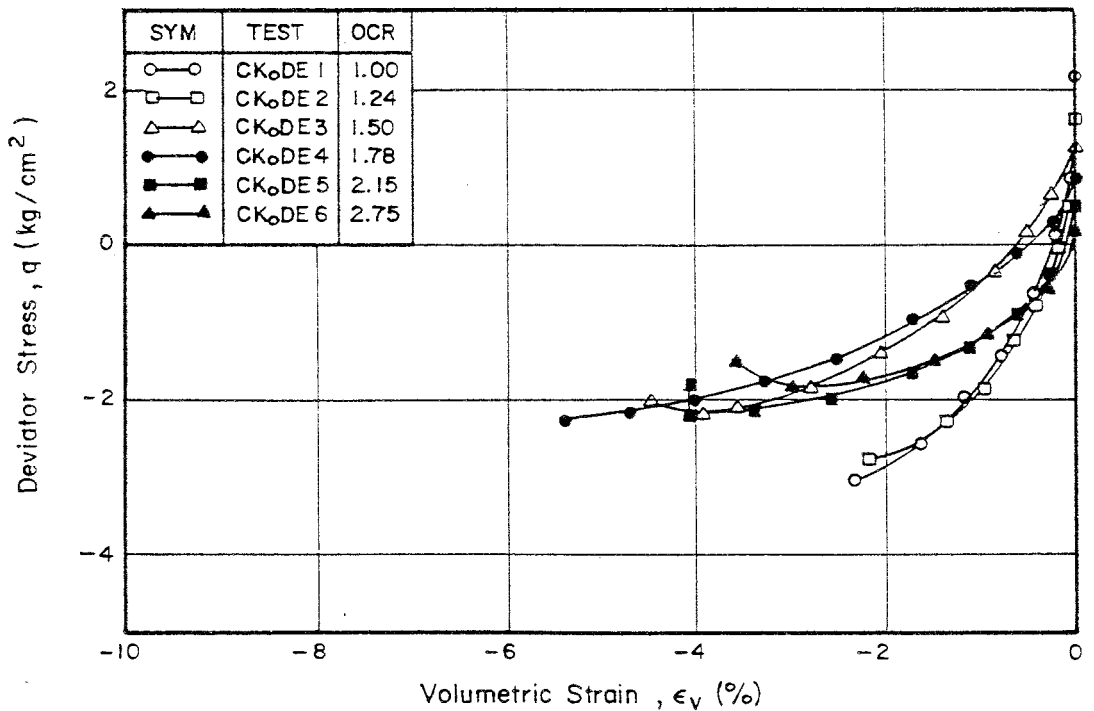


Fig. 6.74 (q , ϵ_v) Plot from CKoDE Tests

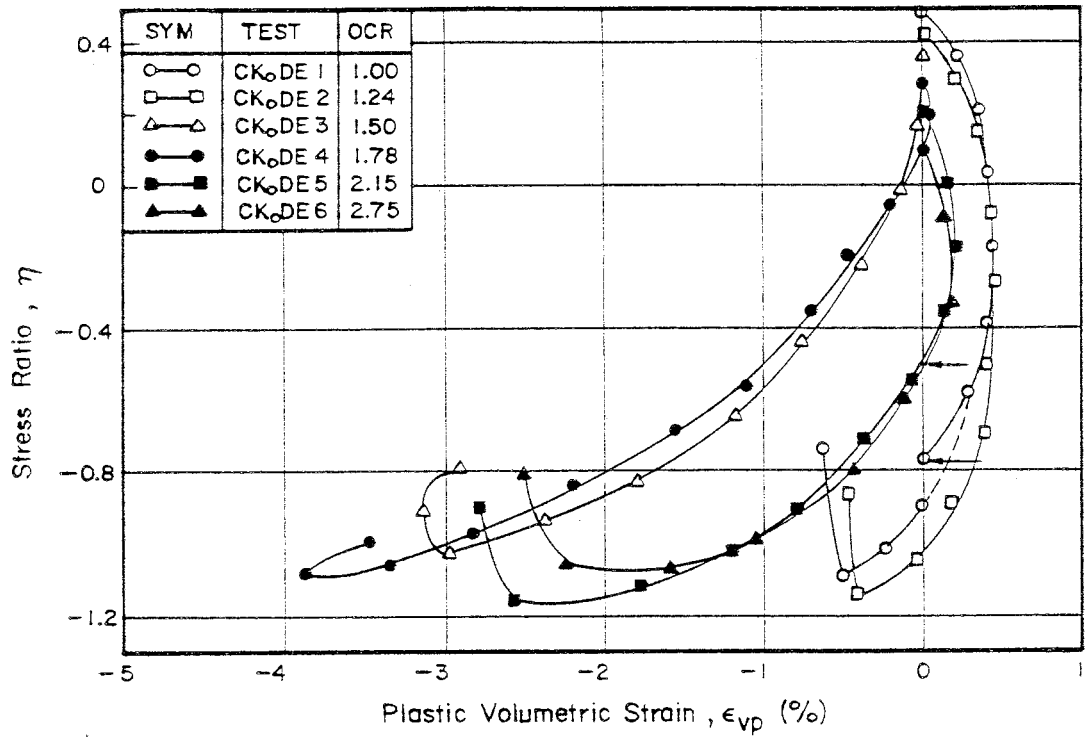


Fig. 6.75 (η , ϵ_{vp}) Plot from CKoDE Tests

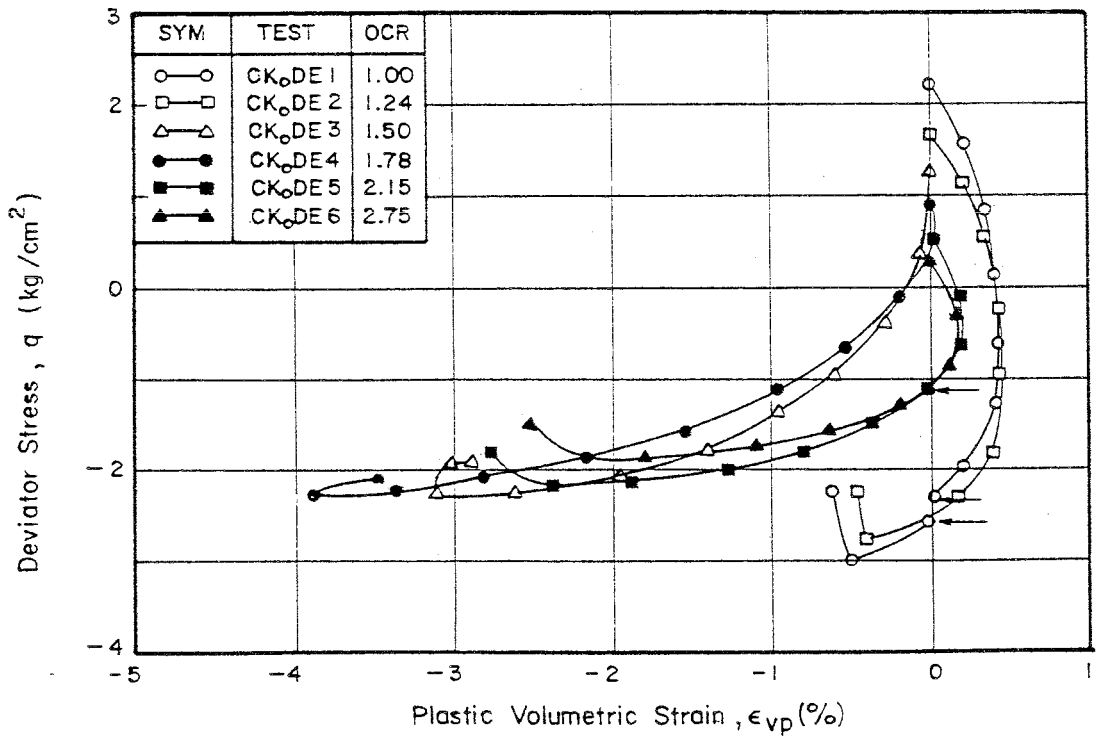


Fig. 6.76 (q , ϵ_{vp}) Plot from CKoDE Tests

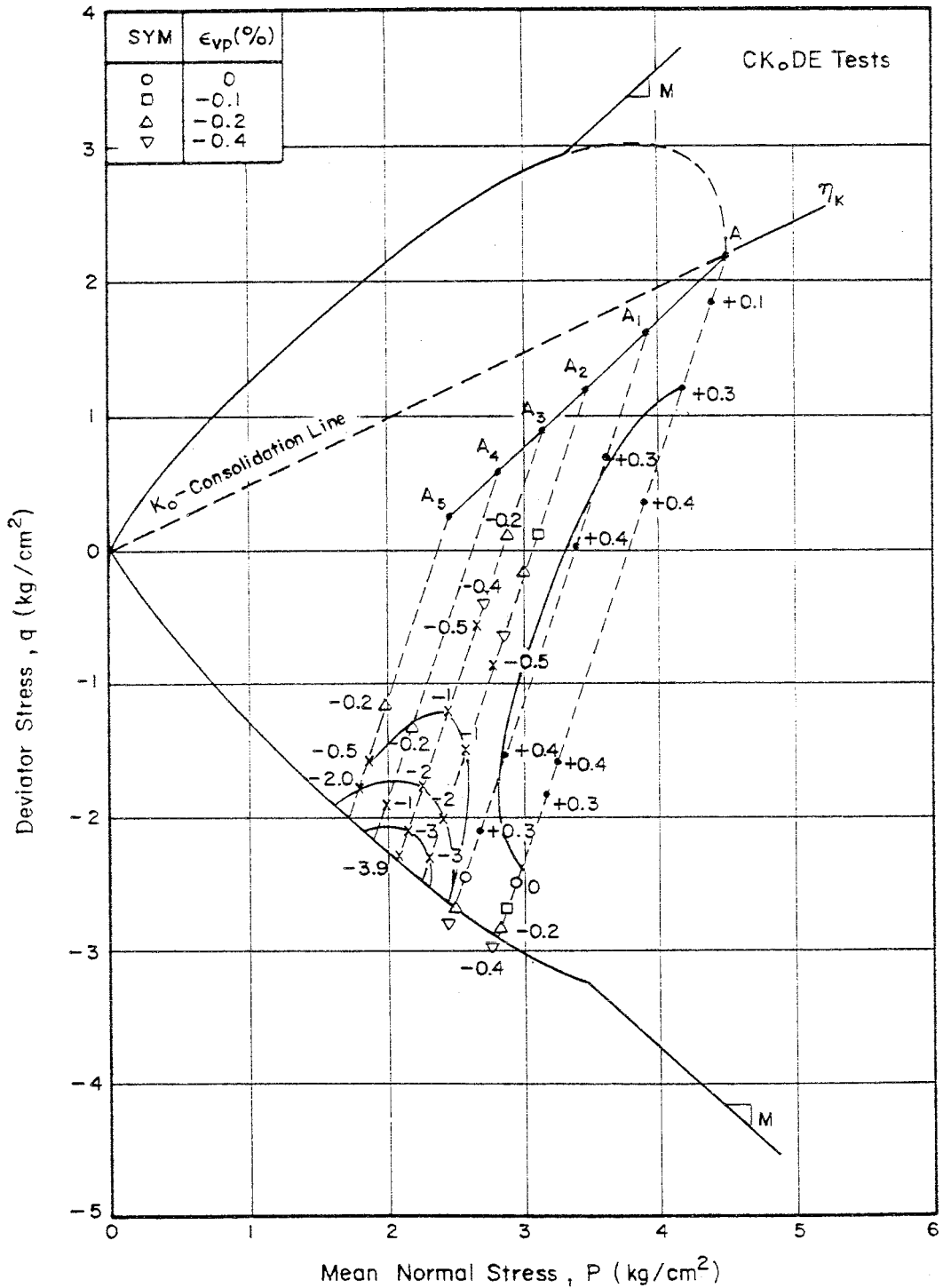


Fig. 6.77 Plastic Volumetric Strain Contours from CK_oDE Tests

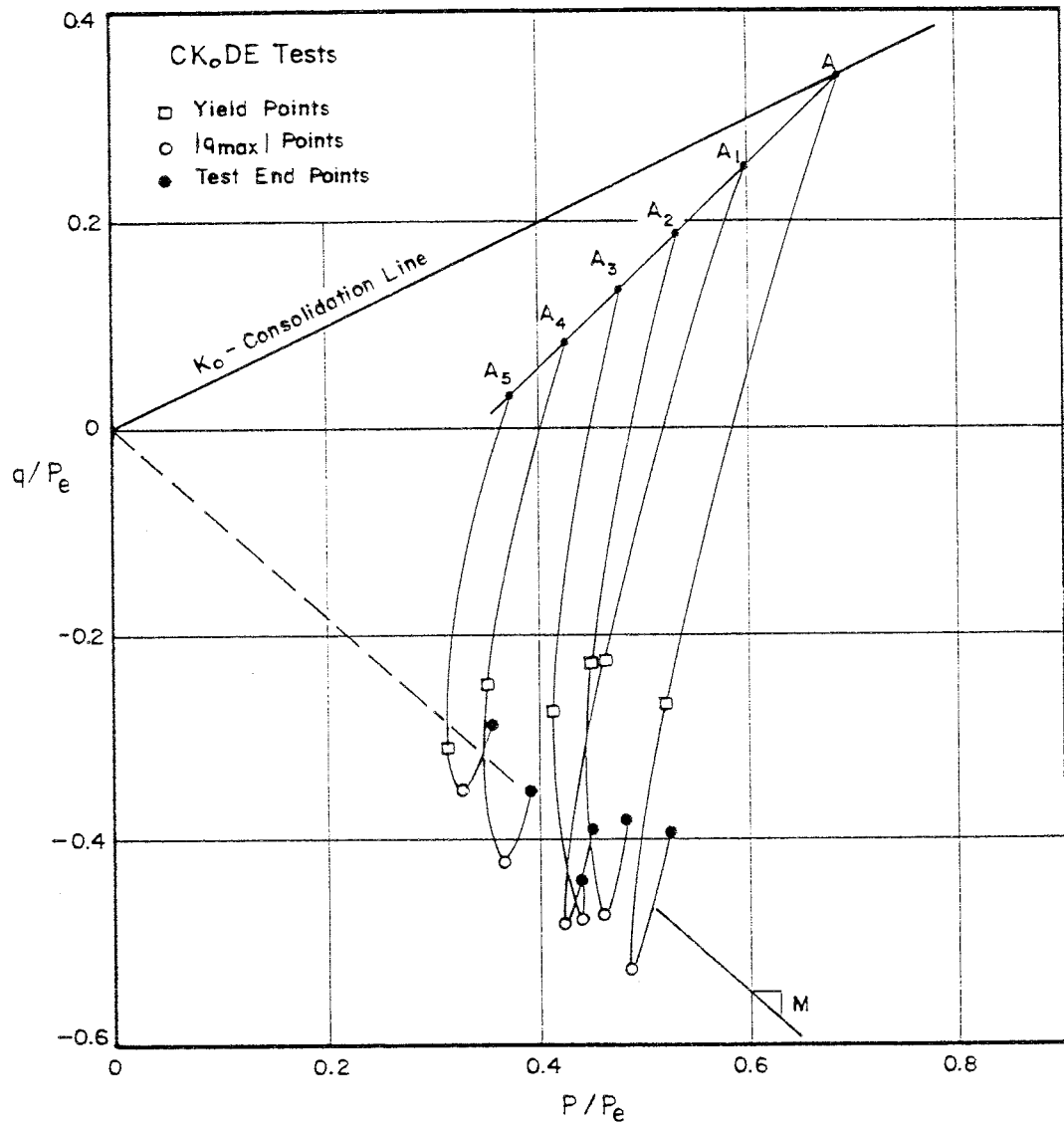


Fig. 6.78 (q/p_e , p/p_e) Plot from CKoDE Tests

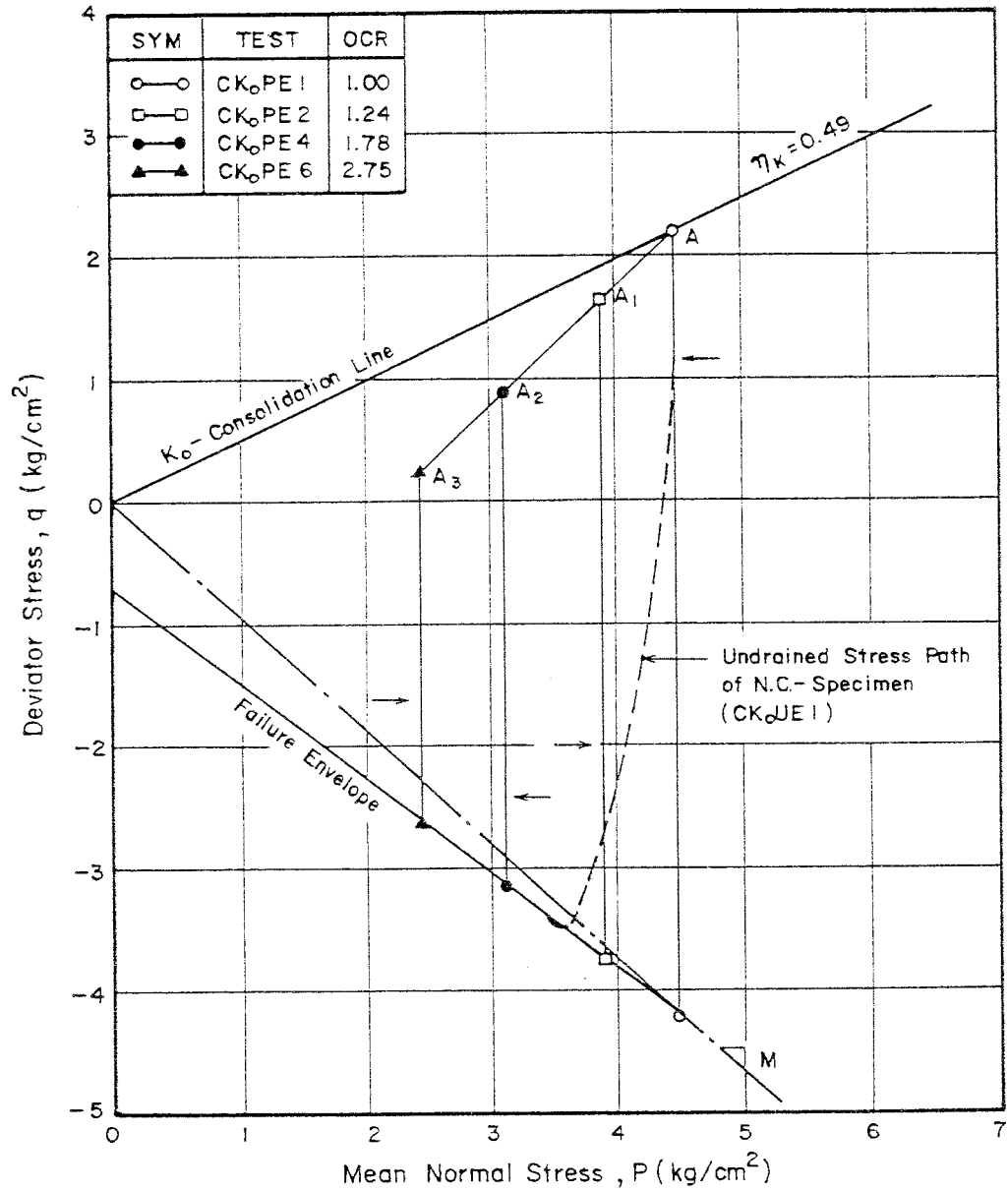


Fig. 6.79 Drained Stress Path from CK₀PE Tests

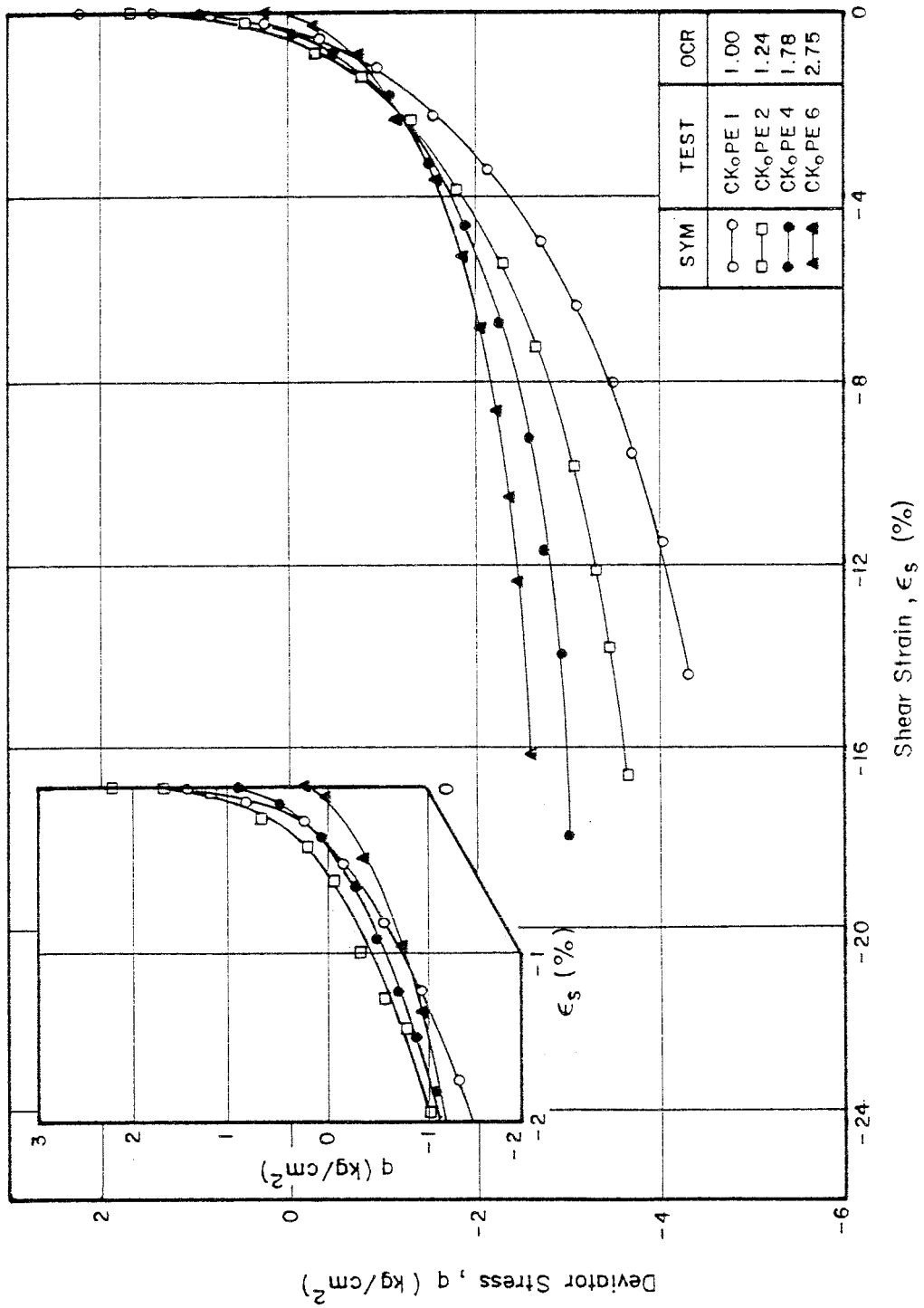


Fig. 6.80 (q , ϵ_s) Plot from CK₀PE Tests

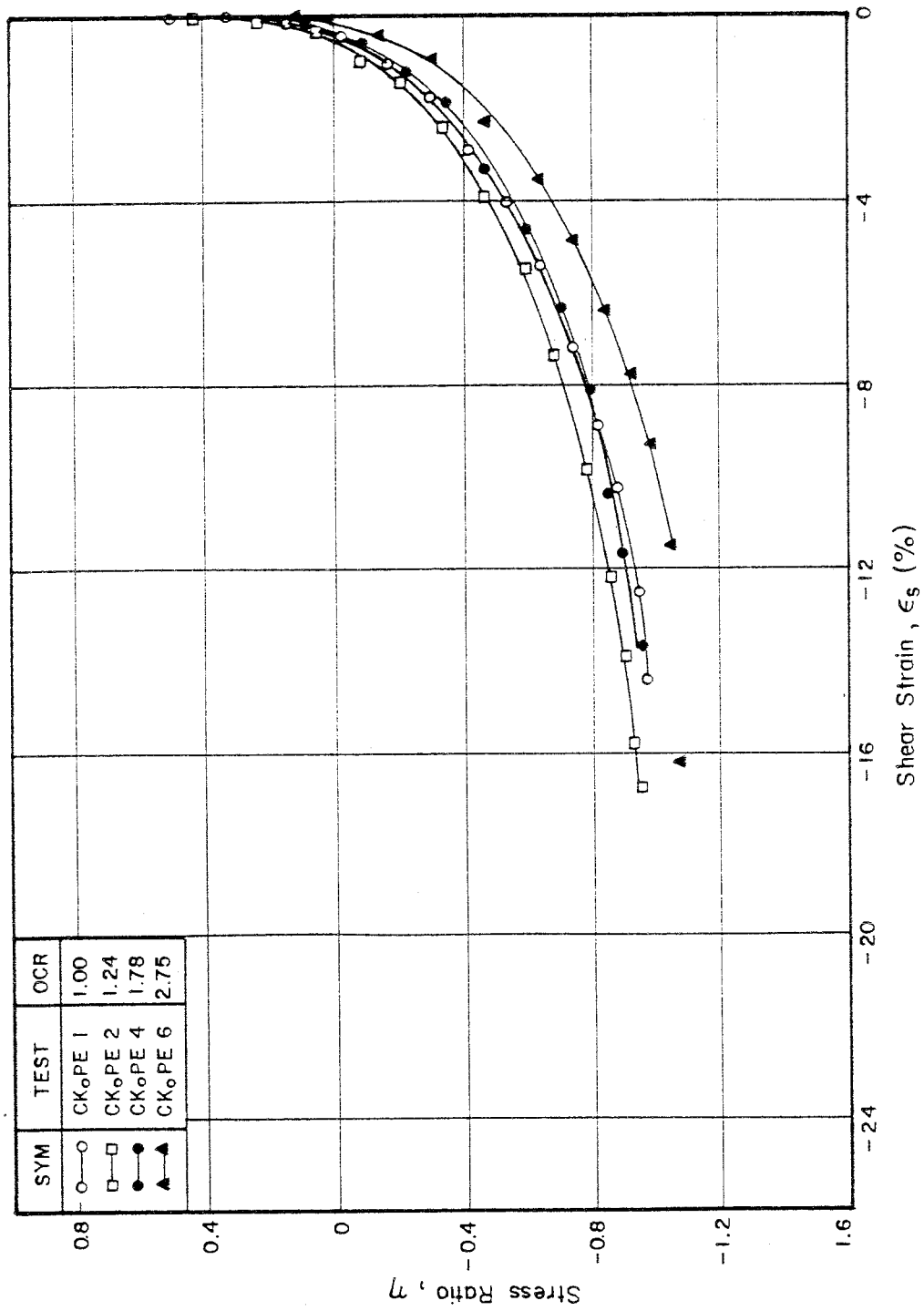


Fig. 6.81 (η , ϵ_s) Plot from CKoPE Tests

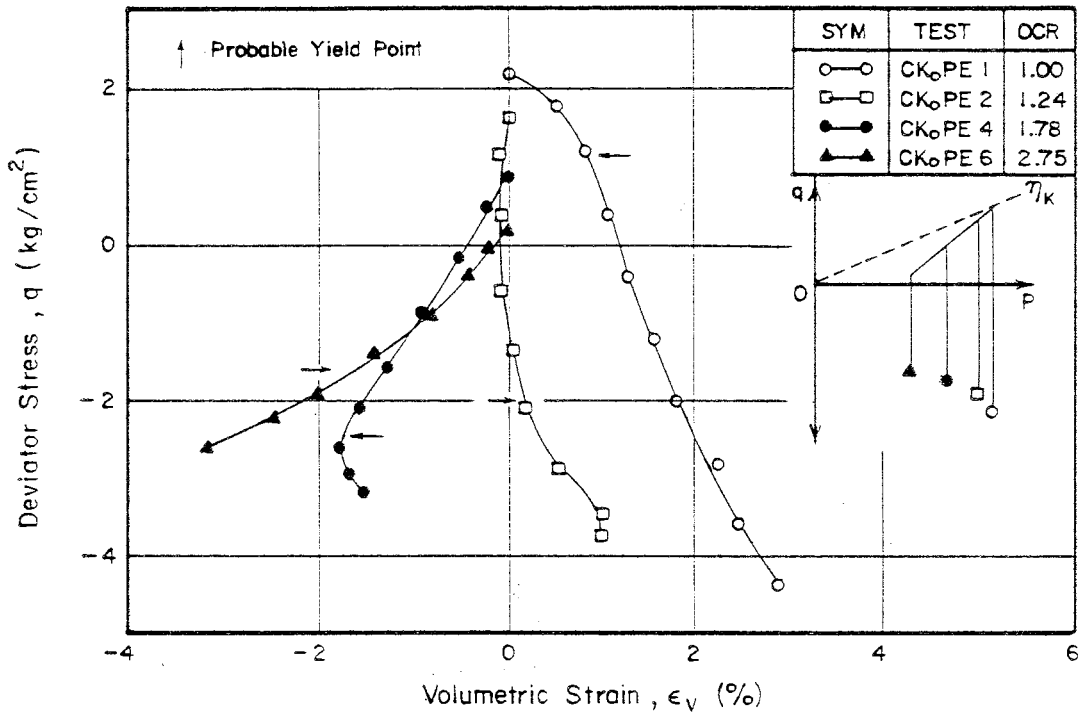


Fig. 6.82 (q , ϵ_v) Plot from CK_oPE Tests

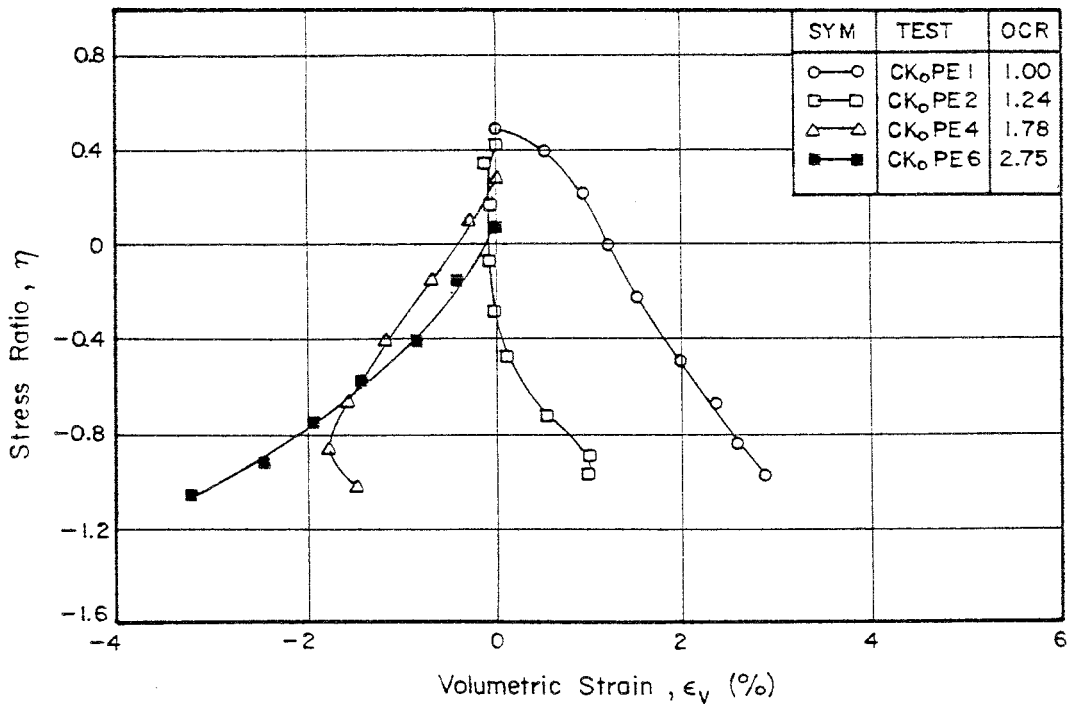


Fig. 6.83 (η , ϵ_v) Plot from CK_oPE Tests

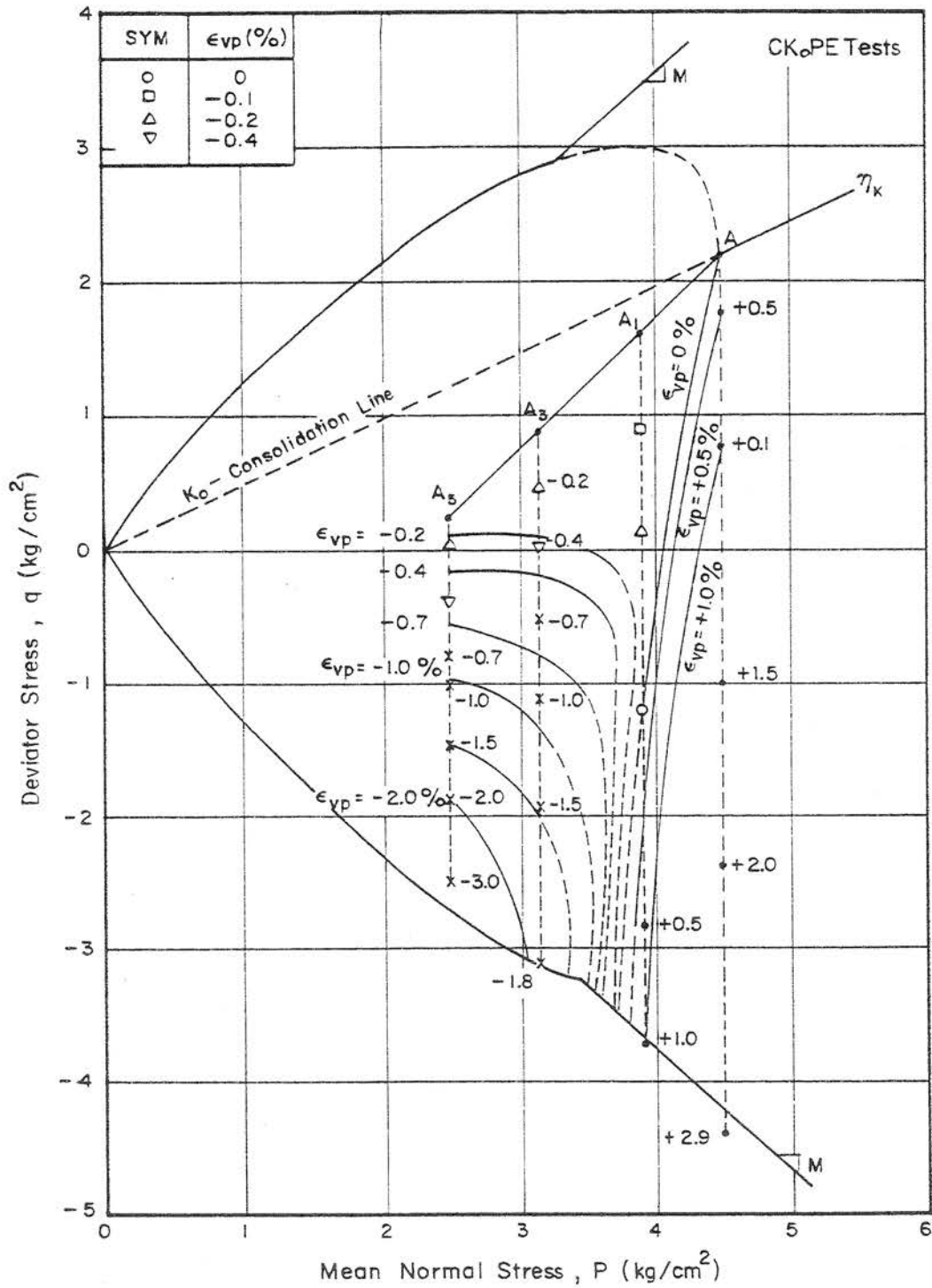


Fig. 6.84 Plastic Volumetric Strain Contours from CKoPE Tests

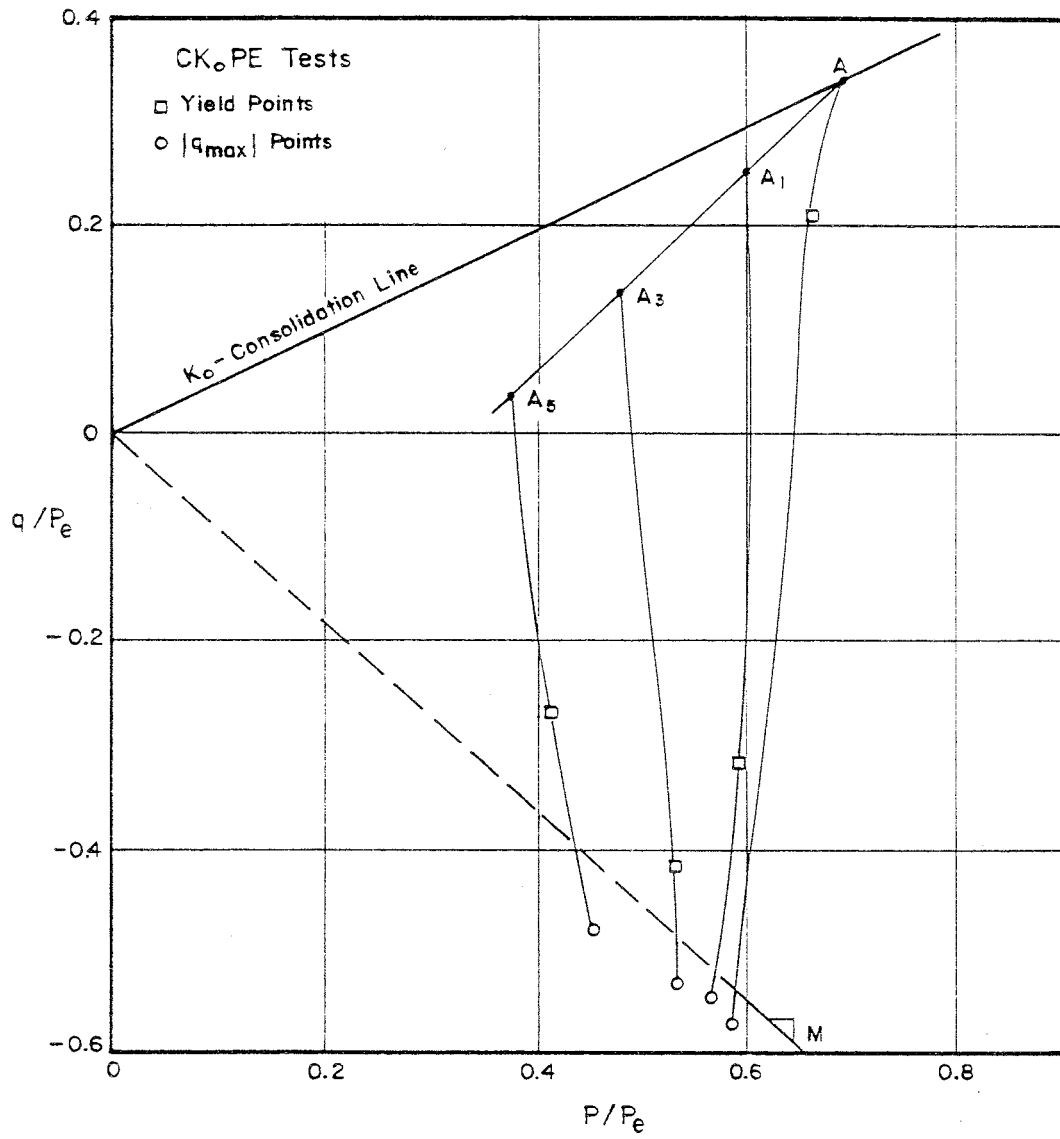


Fig. 6.85 (q/p_e , p/p_e) Plot from CKoPE Tests

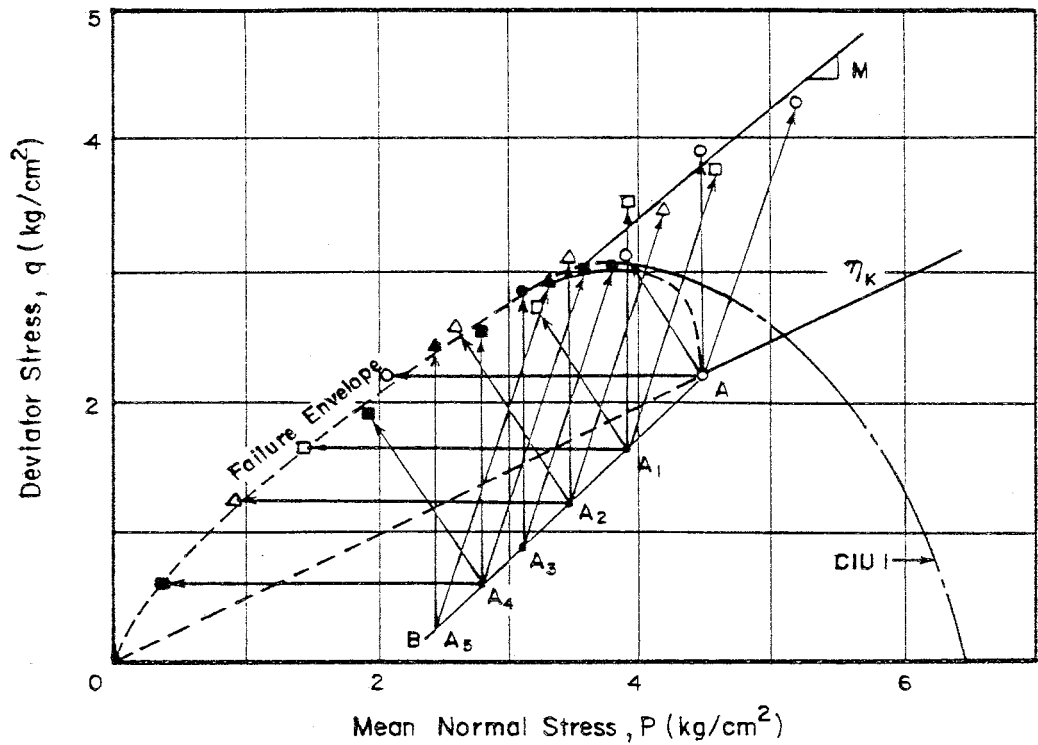


Fig. 6.86a Failure Envelope from Drained Tests on K_0 Consolidated Samples in the Compression Side

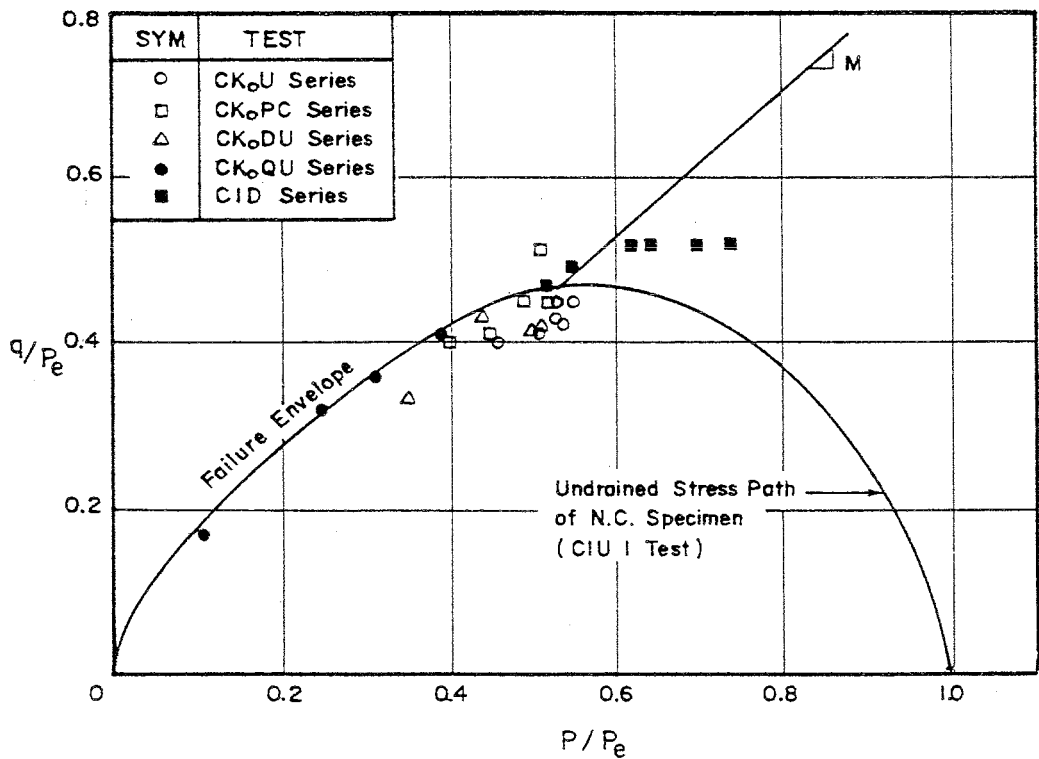


Fig. 6.86b Failure Points from Drained Tests in the $(q/p_e, p/p_e)$ Plot

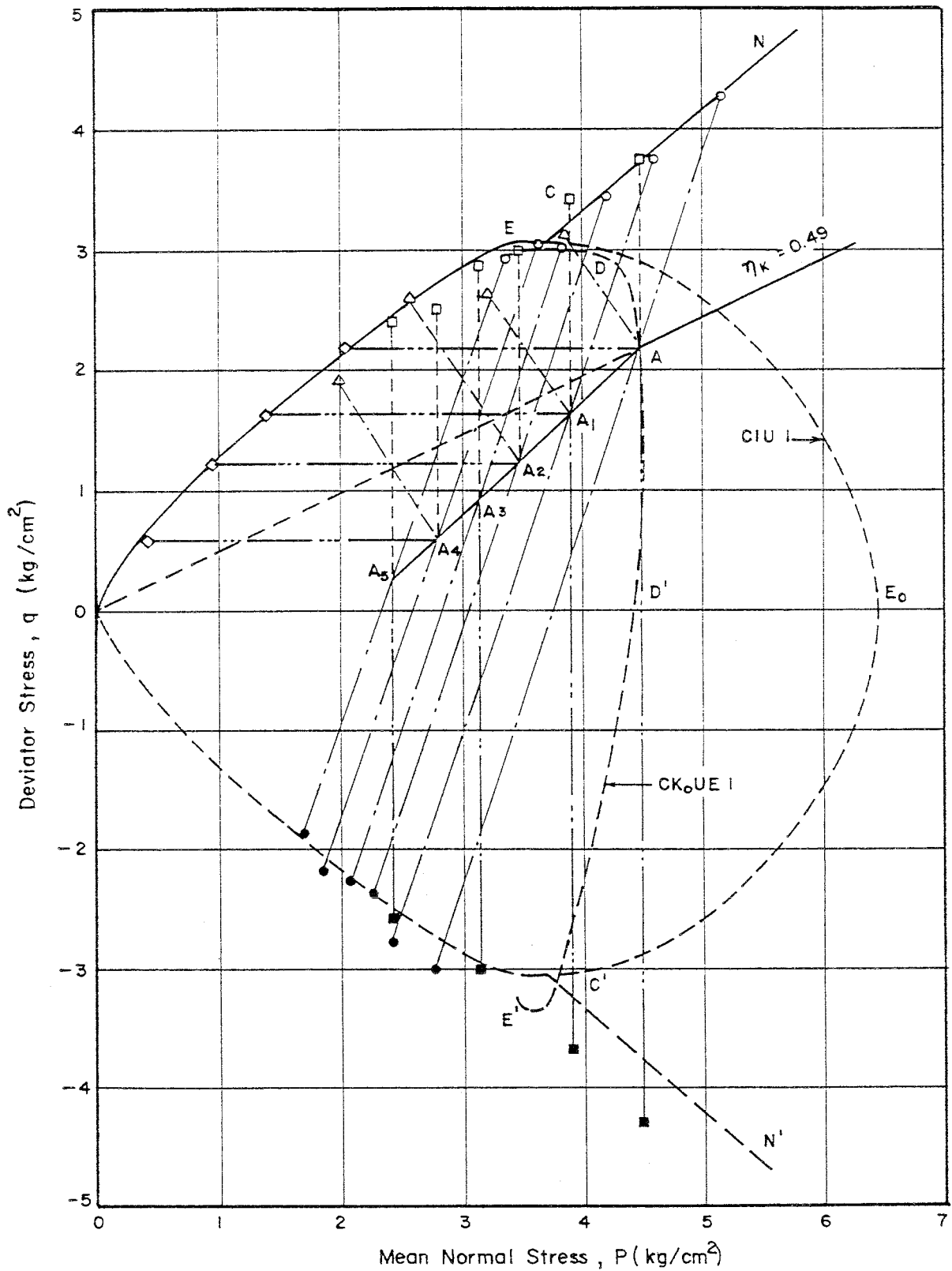


Fig. 6.87 Strength Envelope and Stress Paths in the (q, p) Plot

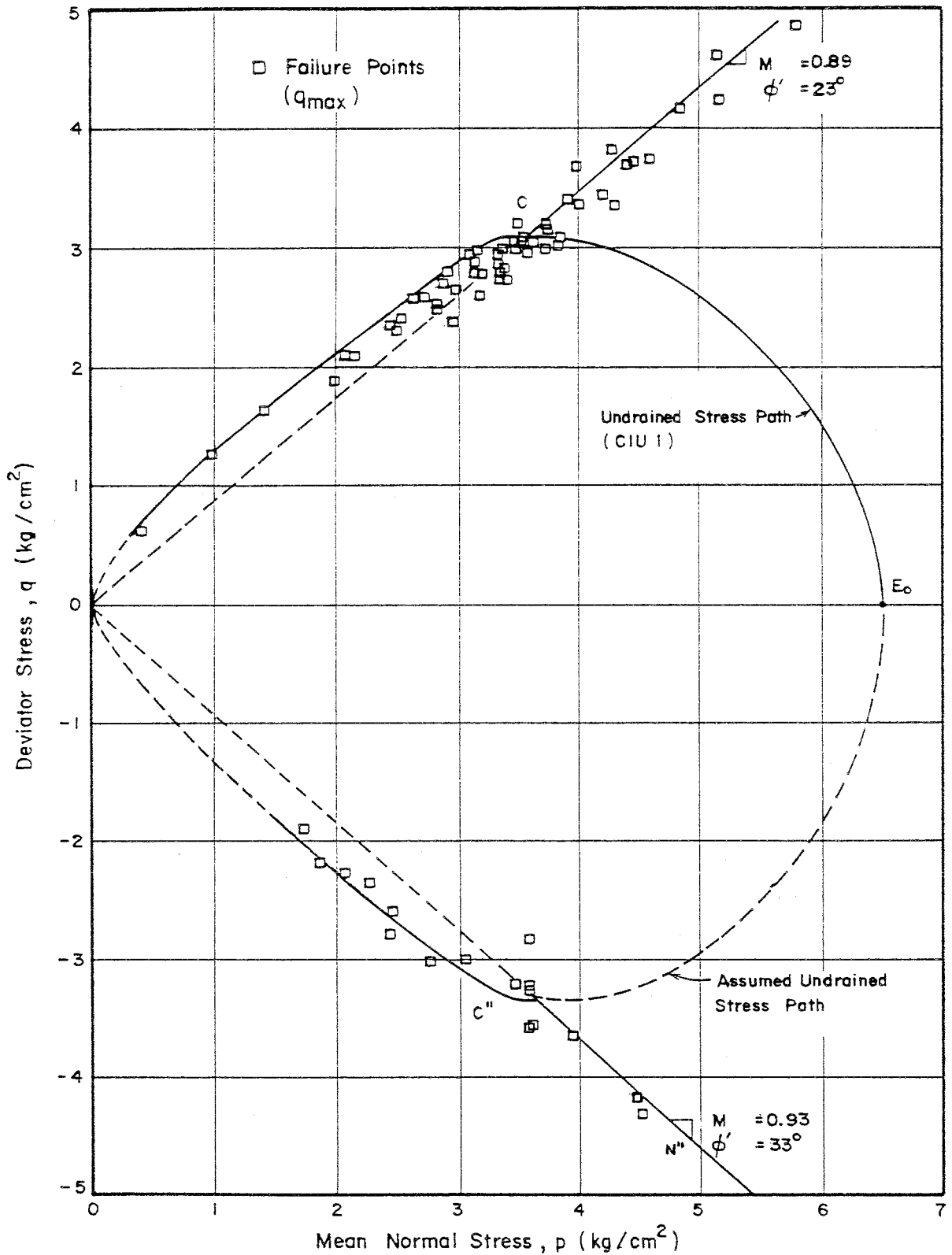


Fig. 6.88 State Boundary Surface and Failure Points from Drained and Undrained Tests (Test Series I, II & III) in the (q , p) Plot

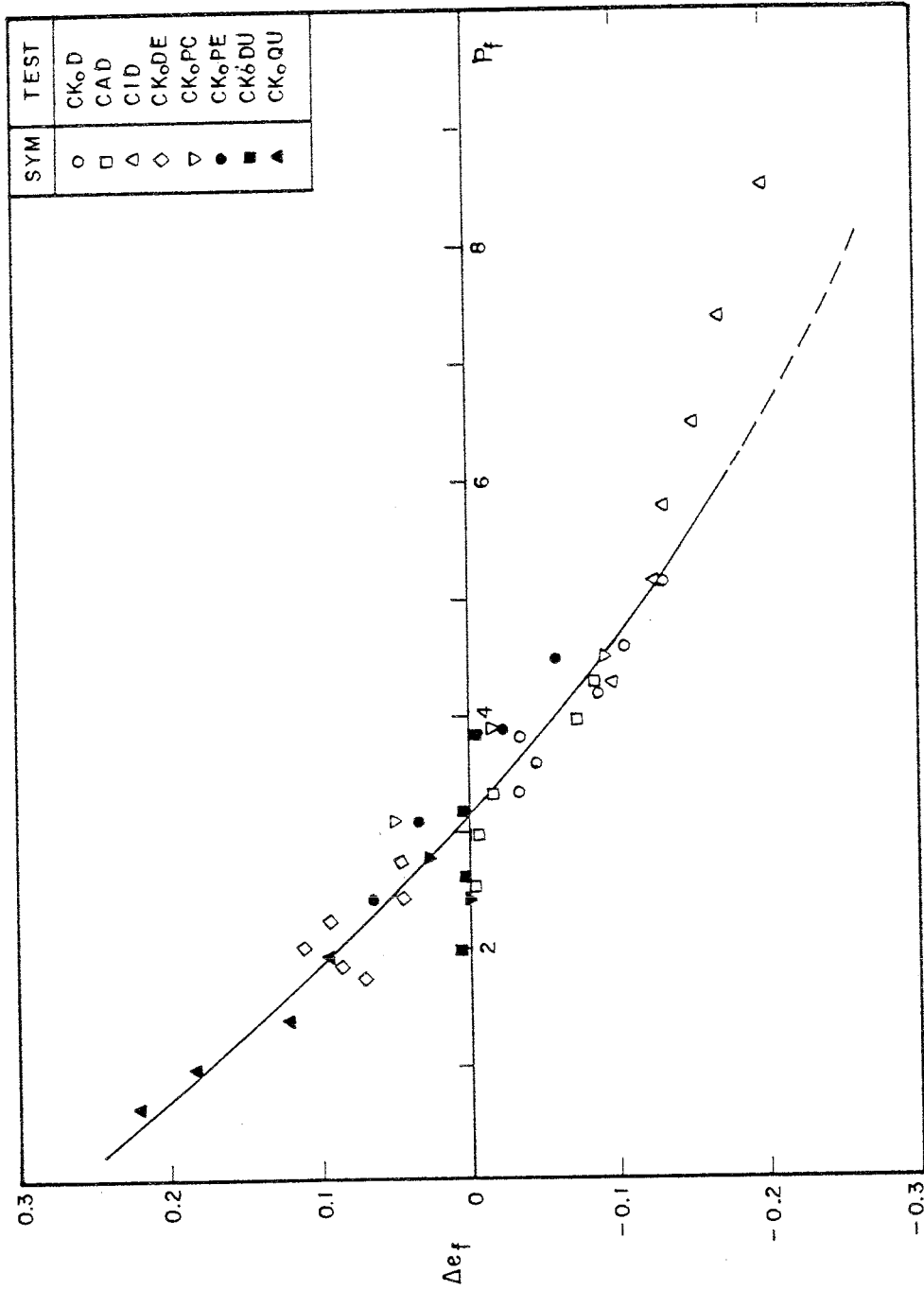


Fig. 6.89 ($\Delta \epsilon_f$, p_f) Plot from Drained Tests

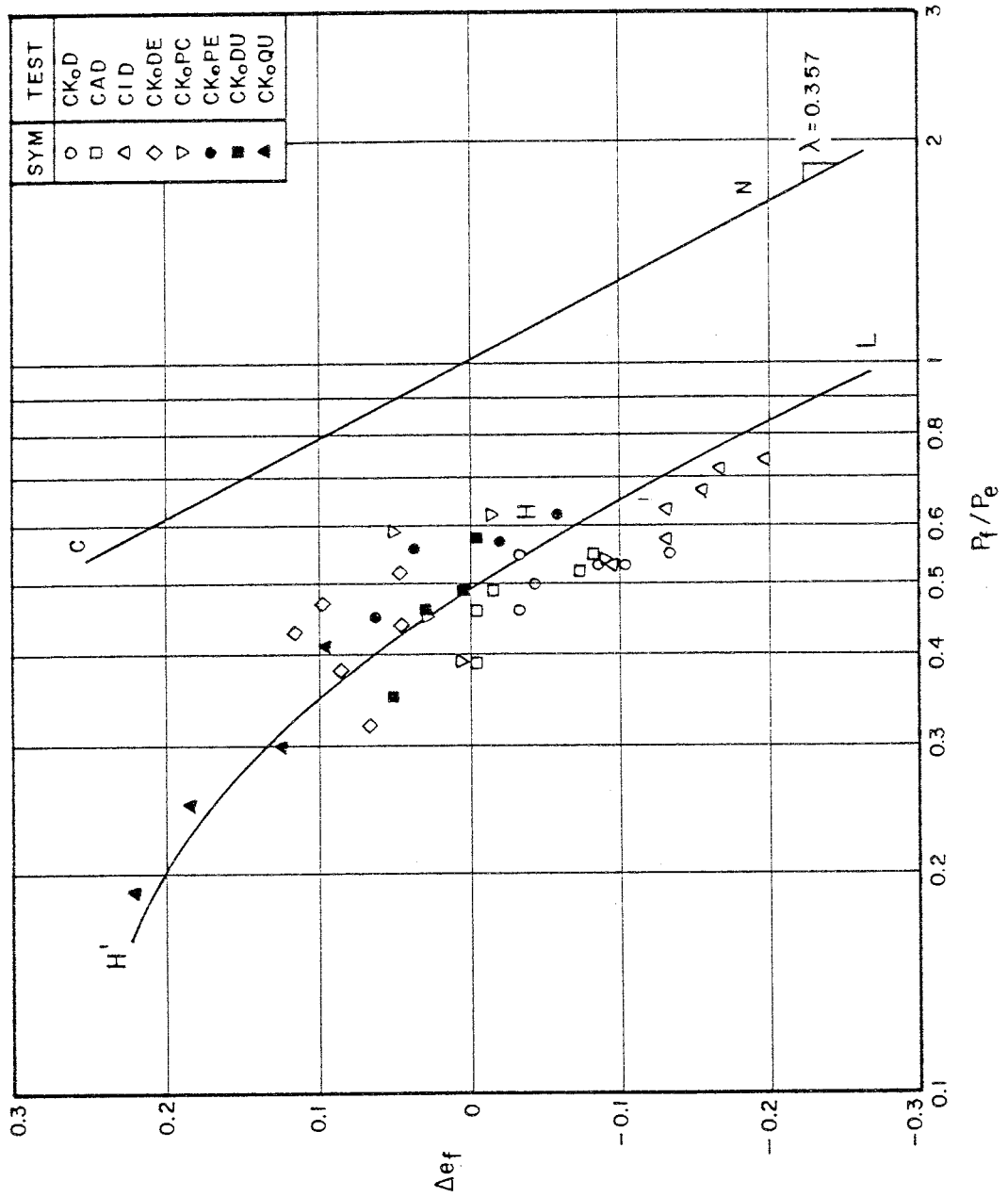


Fig. 6.90 ($\Delta e_f, \ln(p_f/p_e)$) Plot from Drained Tests

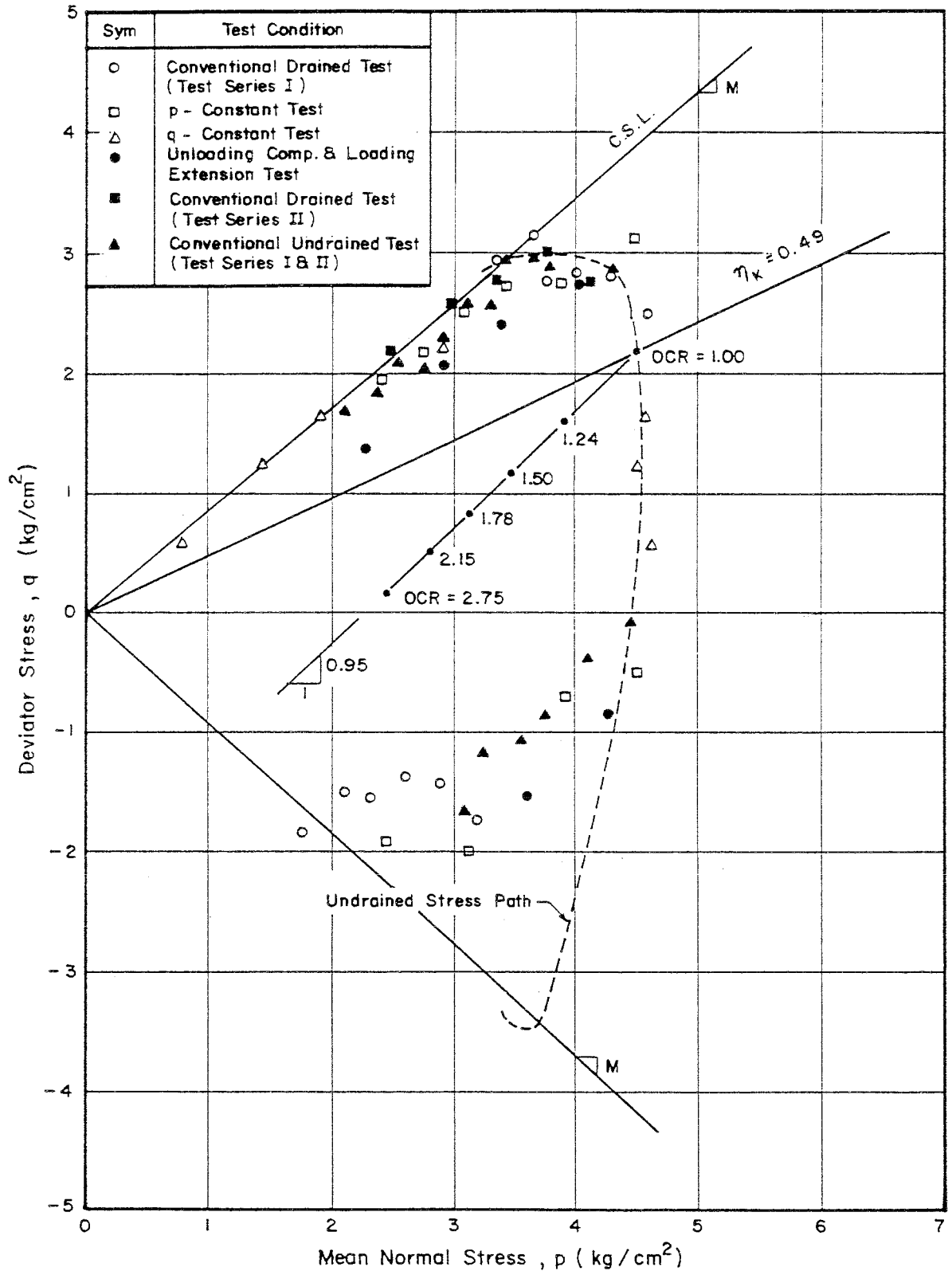


Fig. 6.91 Volumetric Yield Points from Drained and Undrained Tests on K_0 Consolidated Samples in the (q , p) Plot

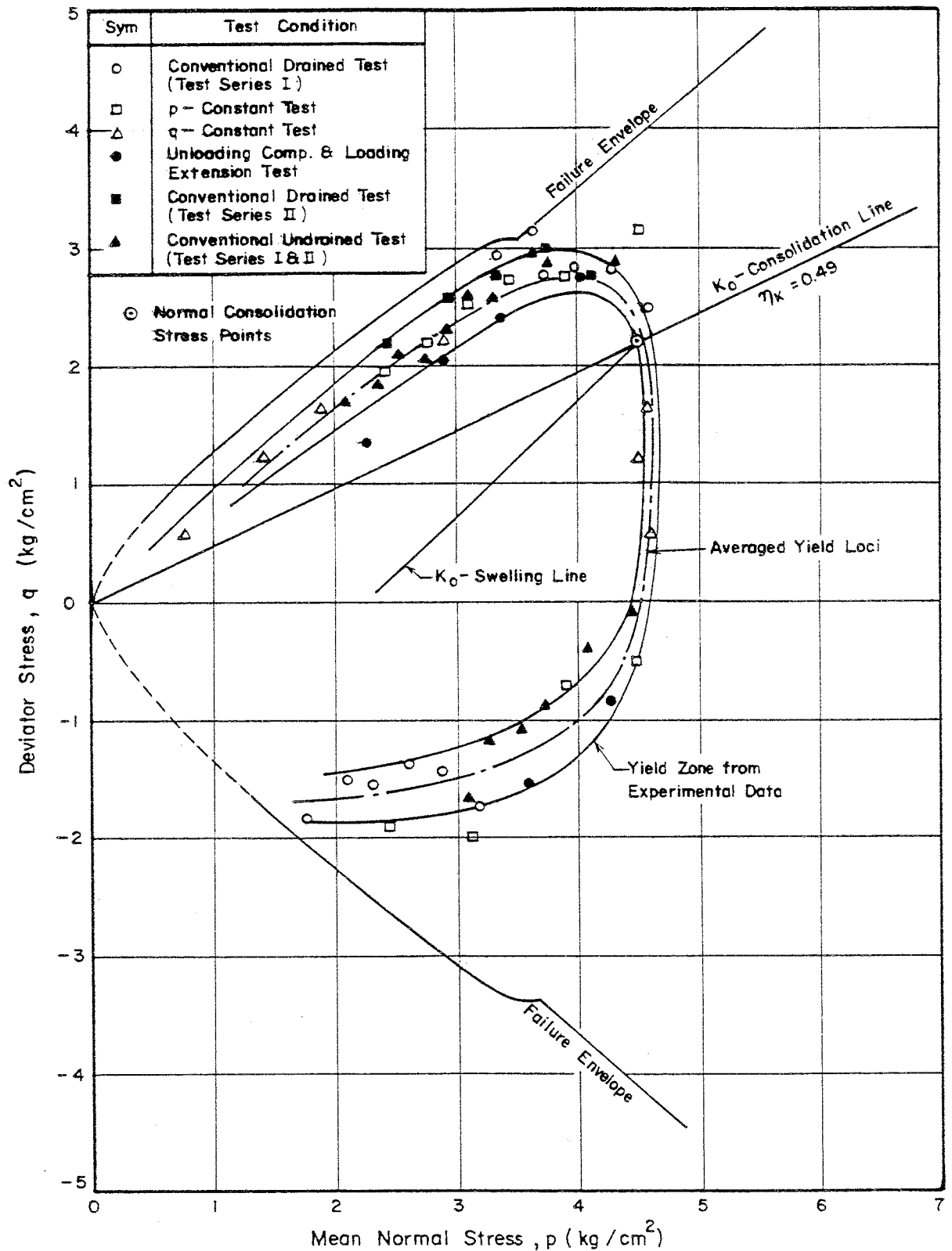


Fig. 6.92 Volumetric Yield Zone from Drained and Undrained Tests on K_0 Consolidated Samples in the (q , p) Plot

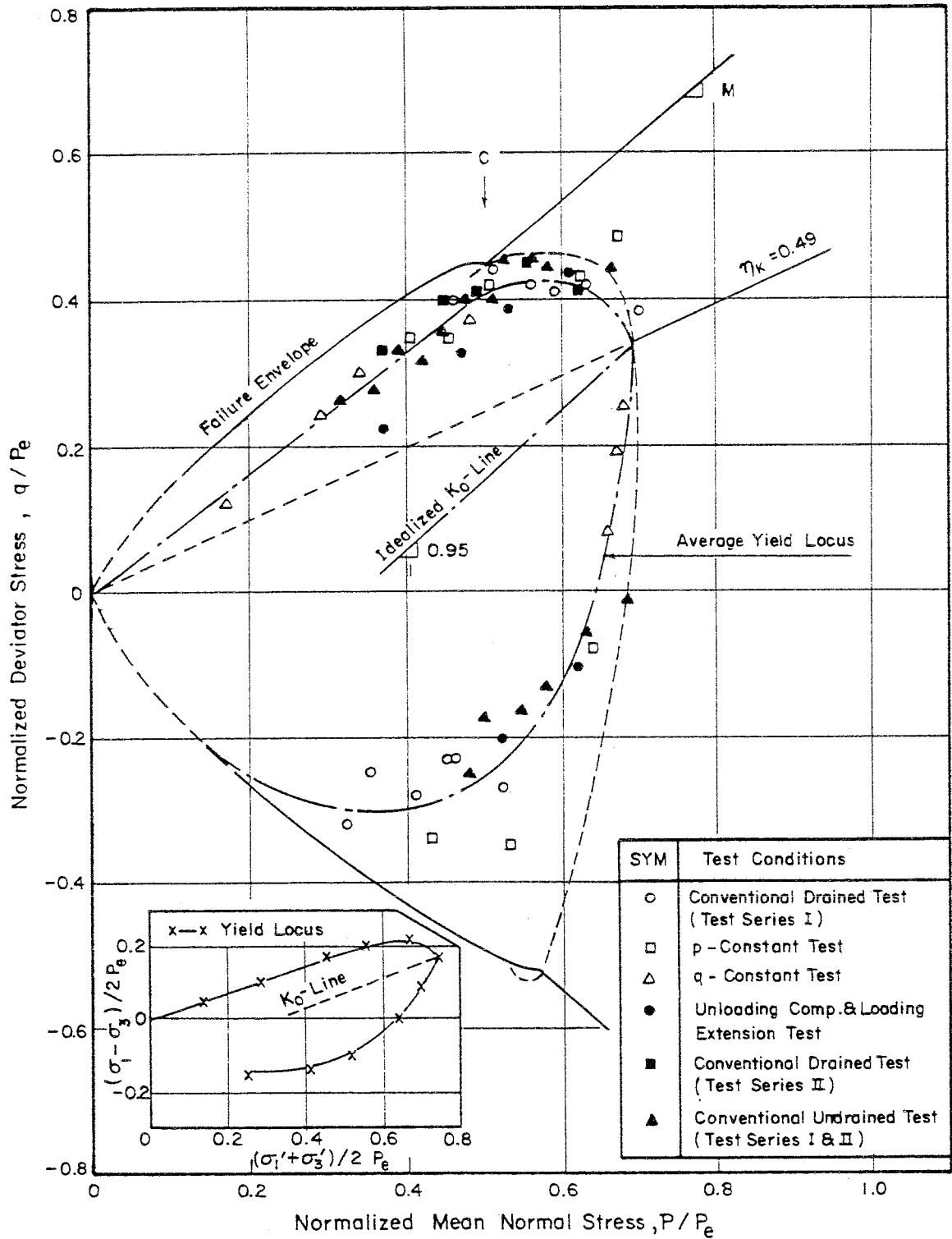


Fig. 6.93 Volumetric Yield Locus from Drained and Undrained Tests on K_0 Consolidated Samples in the $(q/p_e, p/p_e)$ Plot

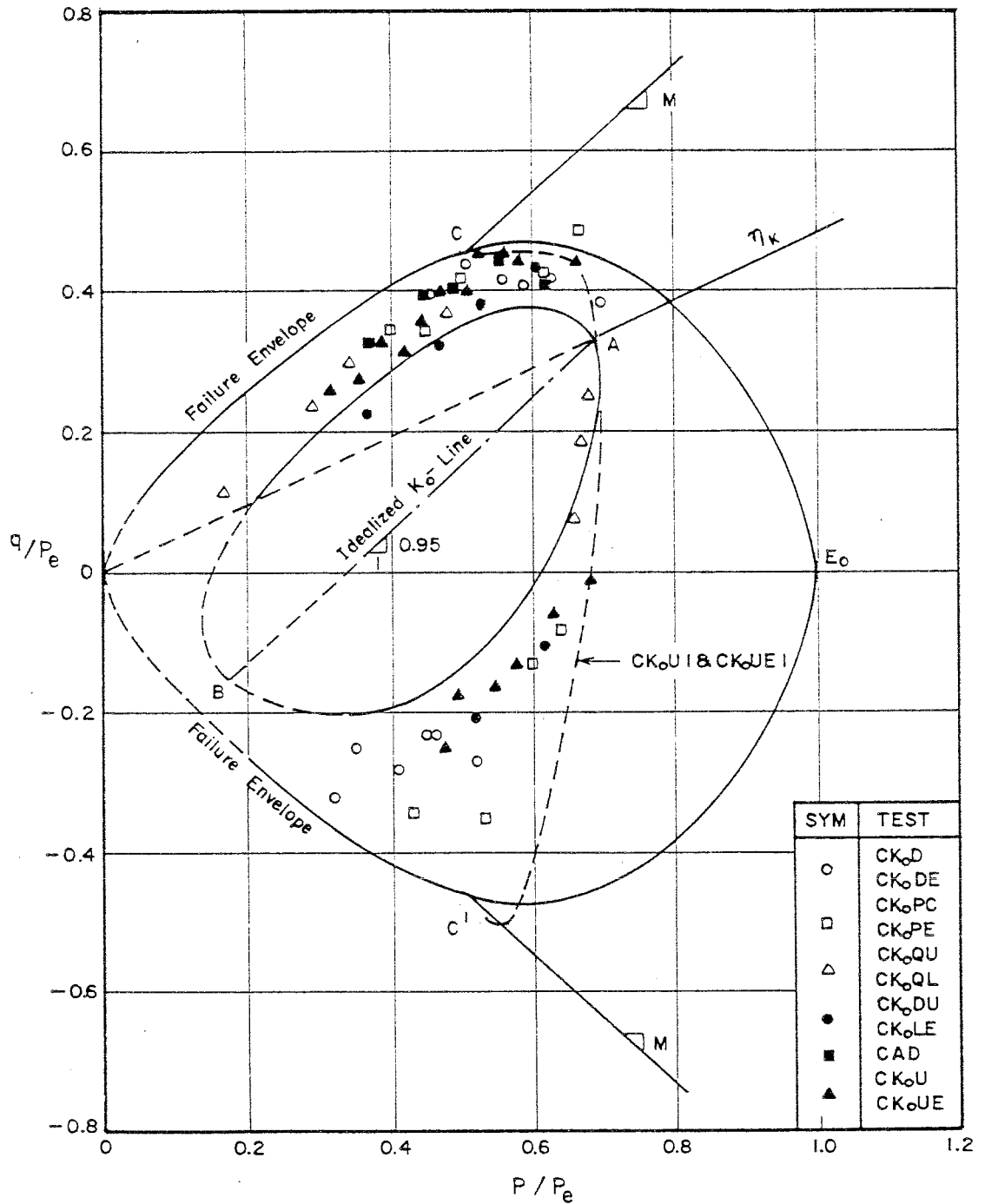


Fig. 6.94 State Boundary Surface and Elastic Zone for K_0 Consolidated Samples in the $(q/p_e, p/p_e)$ Plot

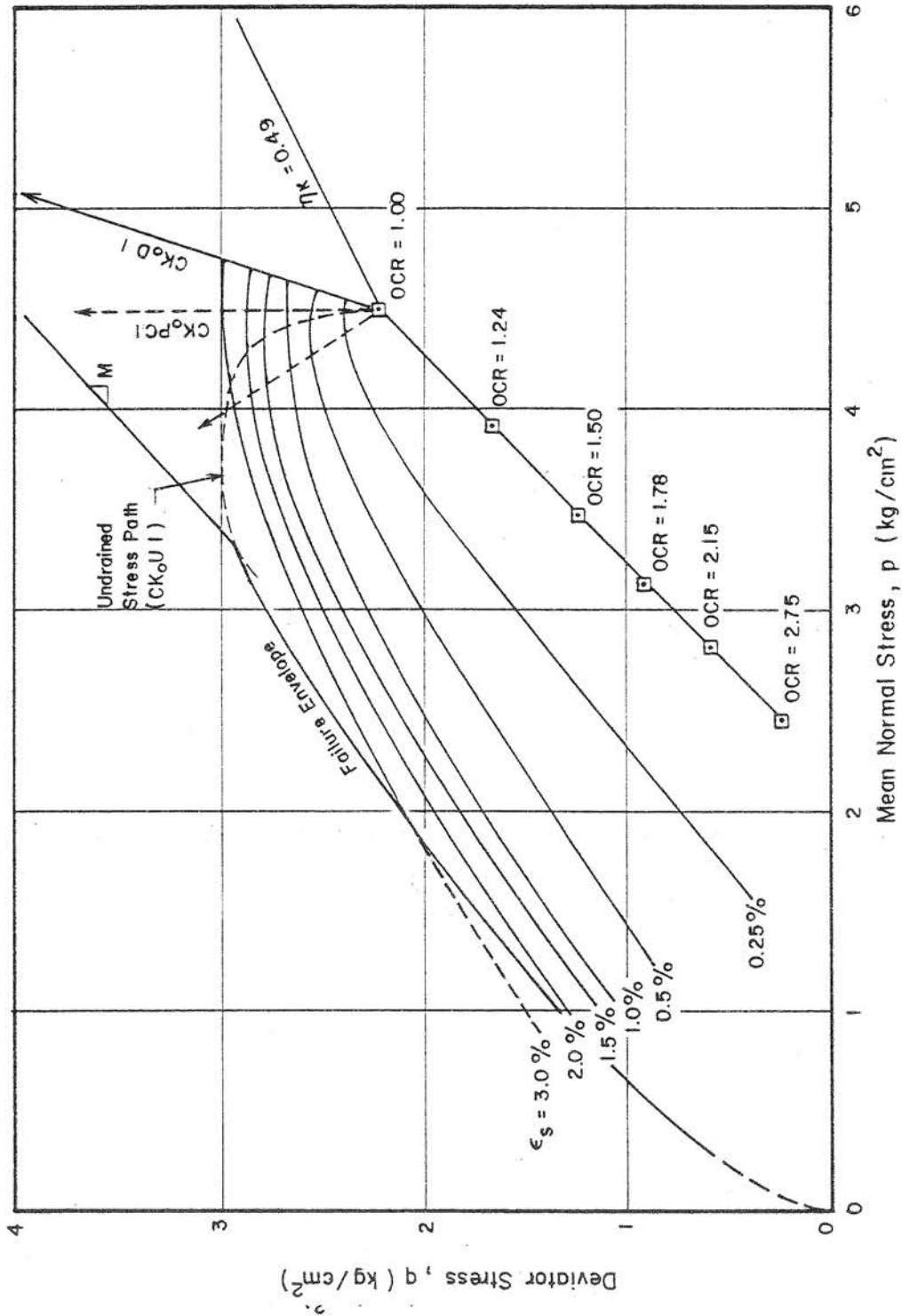


Fig. 6.95 Shear Strain Contours from Drained Tests on K_0 Consolidated Samples in the (q, p) Plot

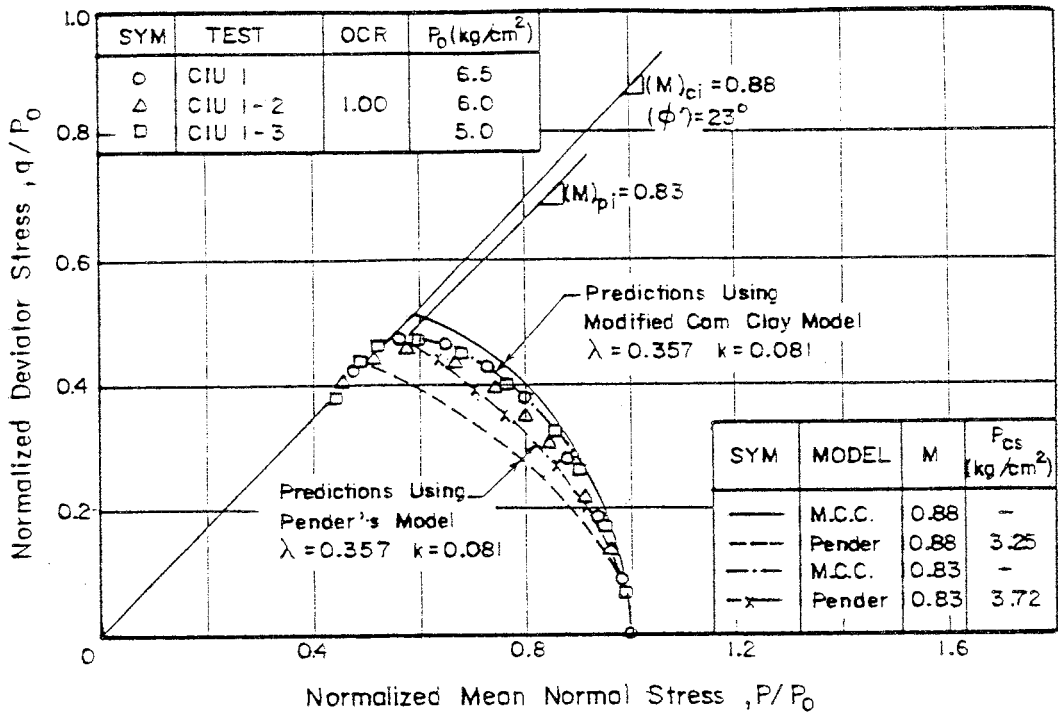


Fig. 7.1 $(q/p_0, p/p_0)$ Plot for Isotropically Normally Consolidated Samples Compared with the Model Predictions (Critical State)

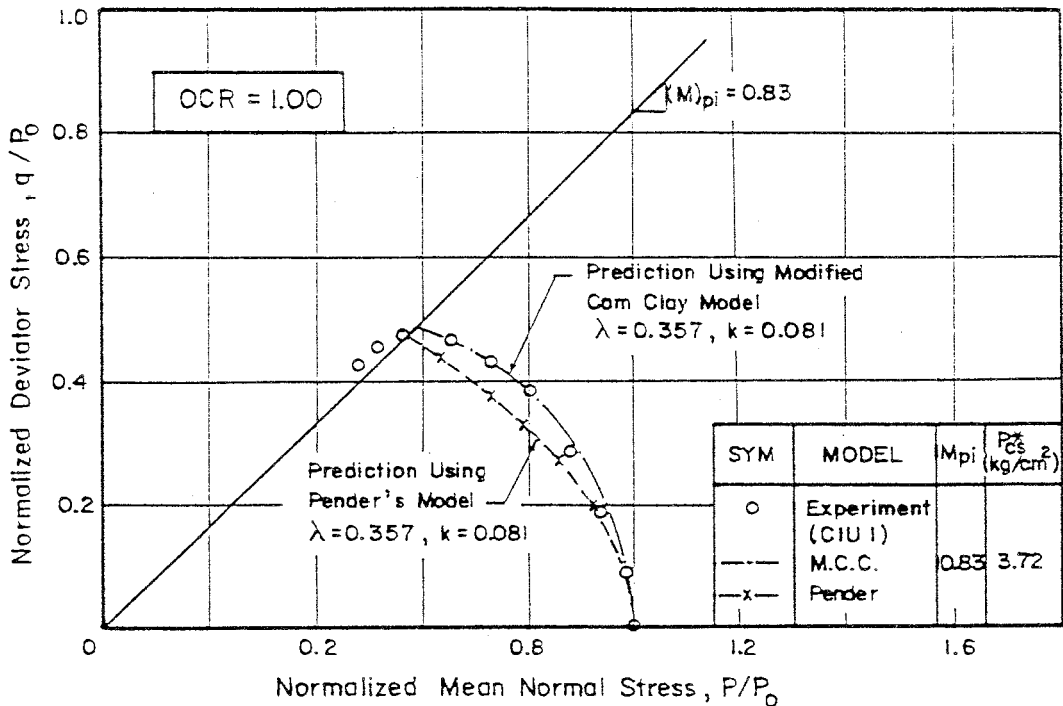


Fig. 7.2 $(q/p_0, p/p_0)$ Plot for CIU1 Sample Compared with the Model Predictions (Peak Stress State)

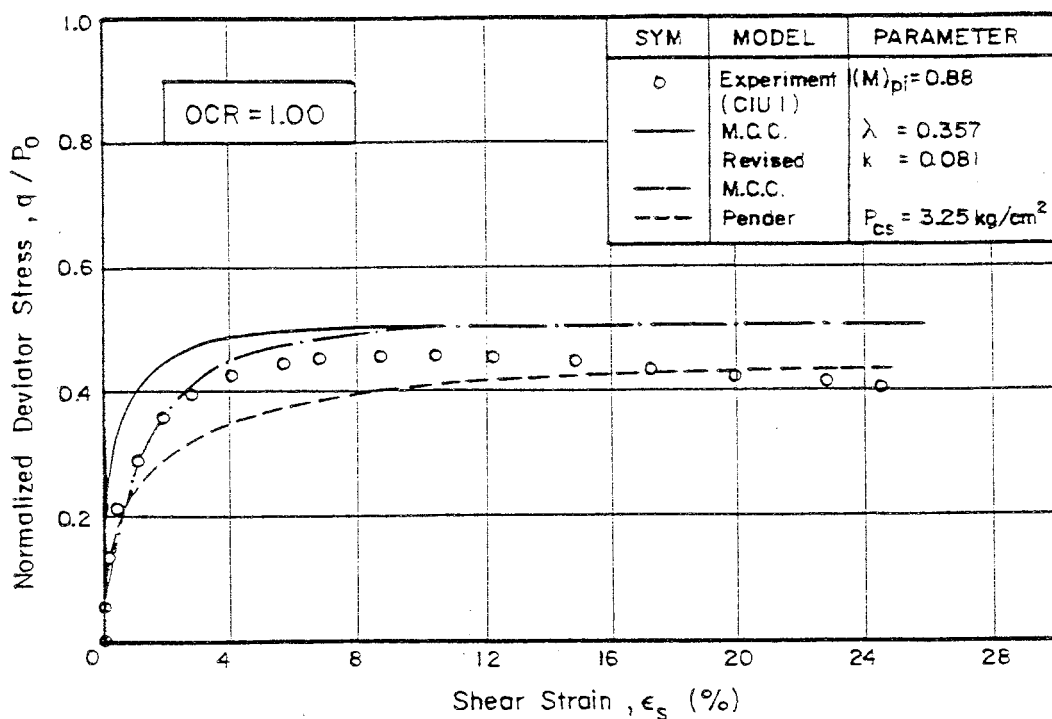


Fig. 7.3 $(q/p_0, \epsilon_s)$ Plot for CIU1 Sample Compared with the Model Predictions (Critical State)

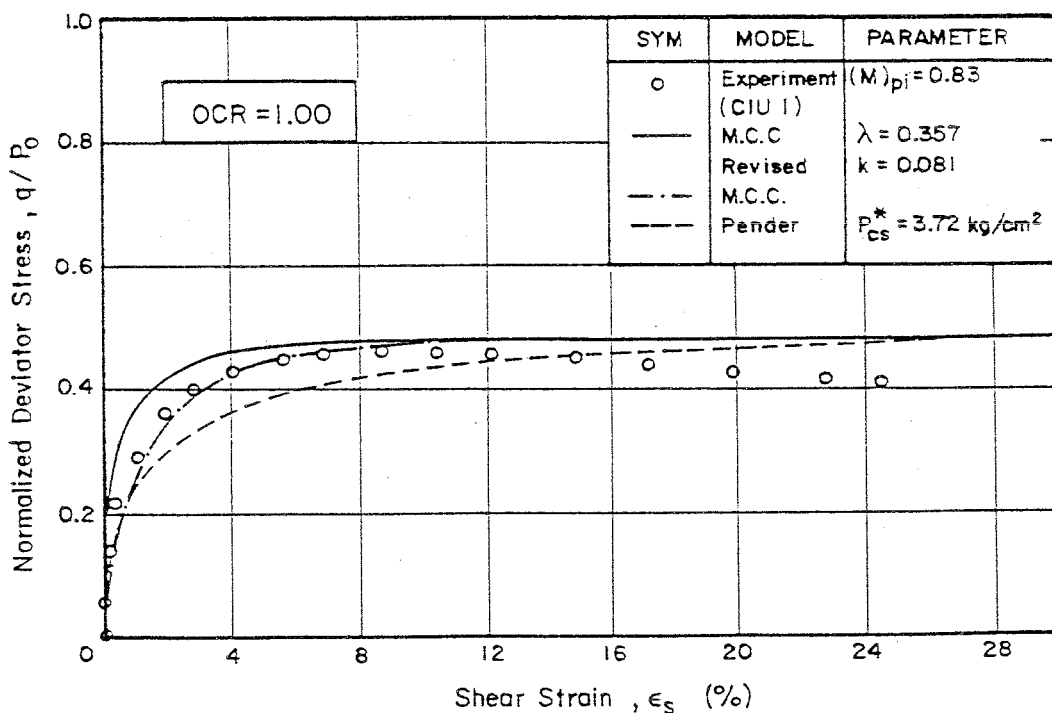


Fig. 7.4 $(q/p_0, \epsilon_s)$ Plot for CIU1 Sample Compared with the Model Predictions (Peak Stress State)

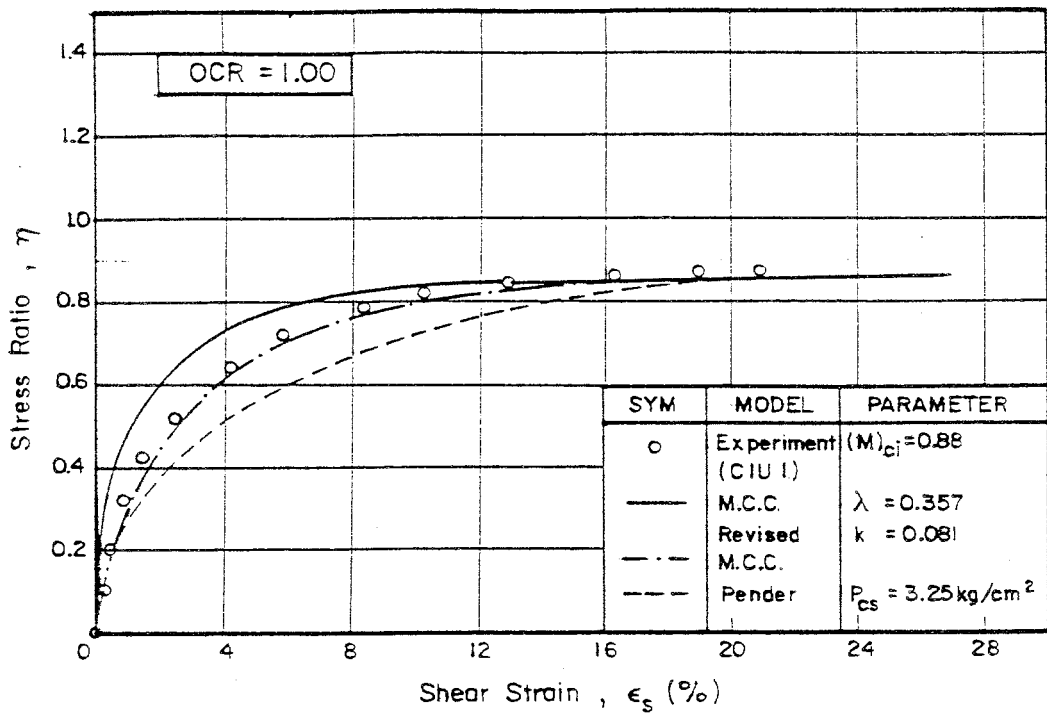


Fig. 7.5 (η, ϵ_s) Plot for CIU1 Sample Compared with the Model Predictions (Critical State)

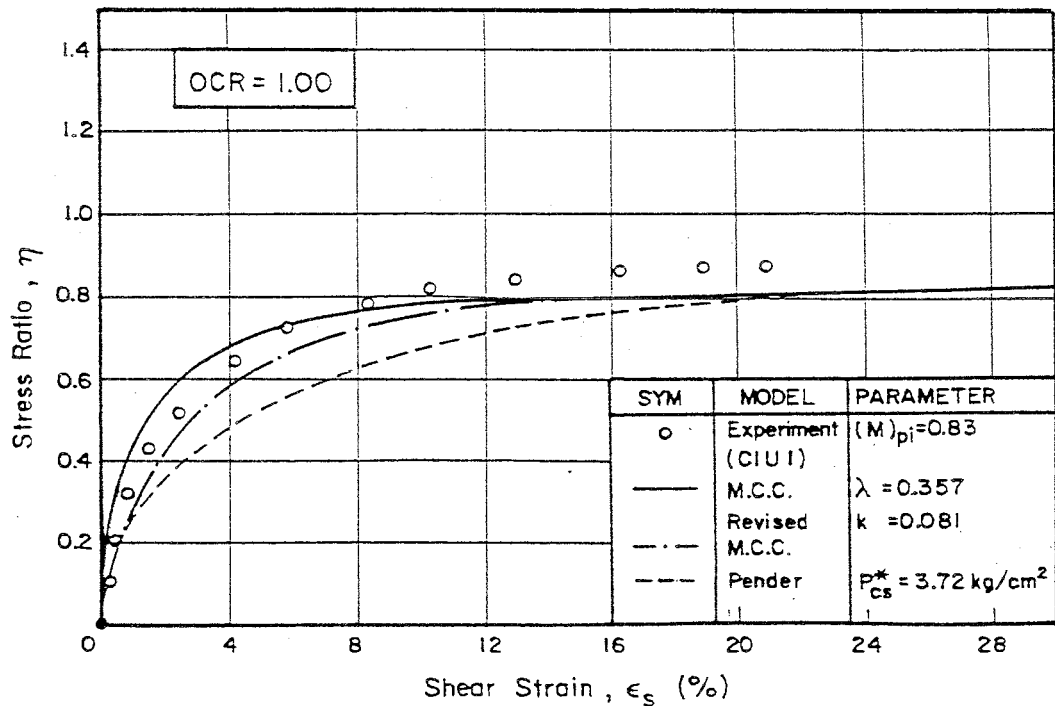


Fig. 7.6 (η, ϵ_s) Plot for CIU1 Sample Compared with the Model Predictions (Peak Stress State)

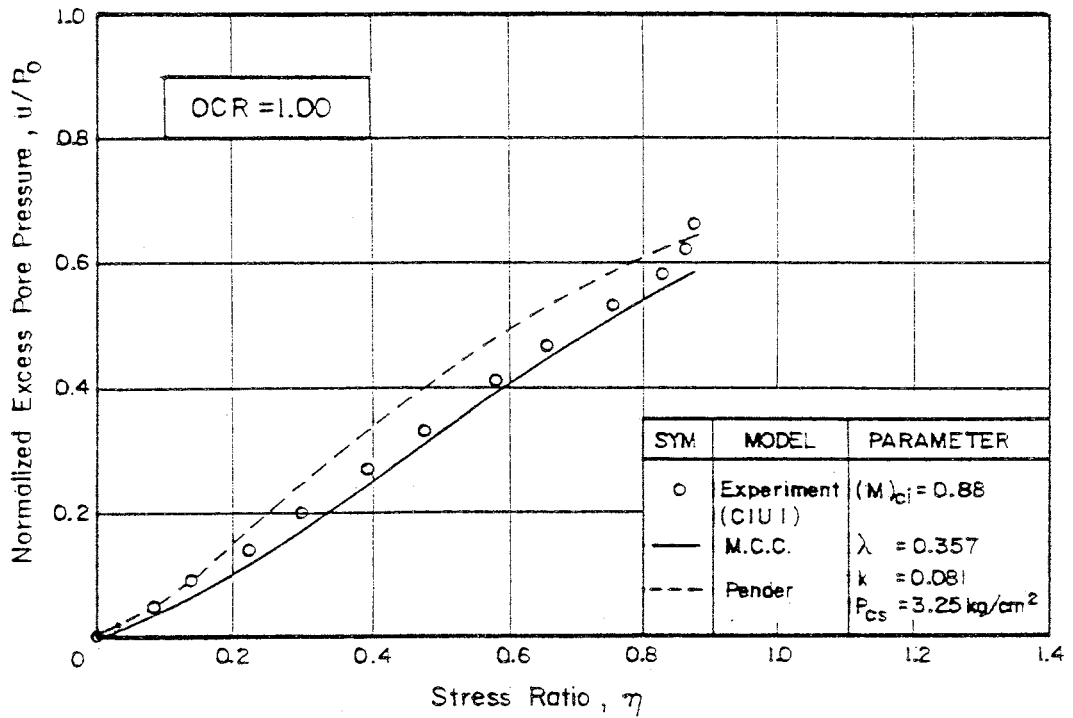


Fig. 7.7 $(u/p_0, \eta)$ Plot for CIU1 Sample Compared with the Model Predictions (Critical State)

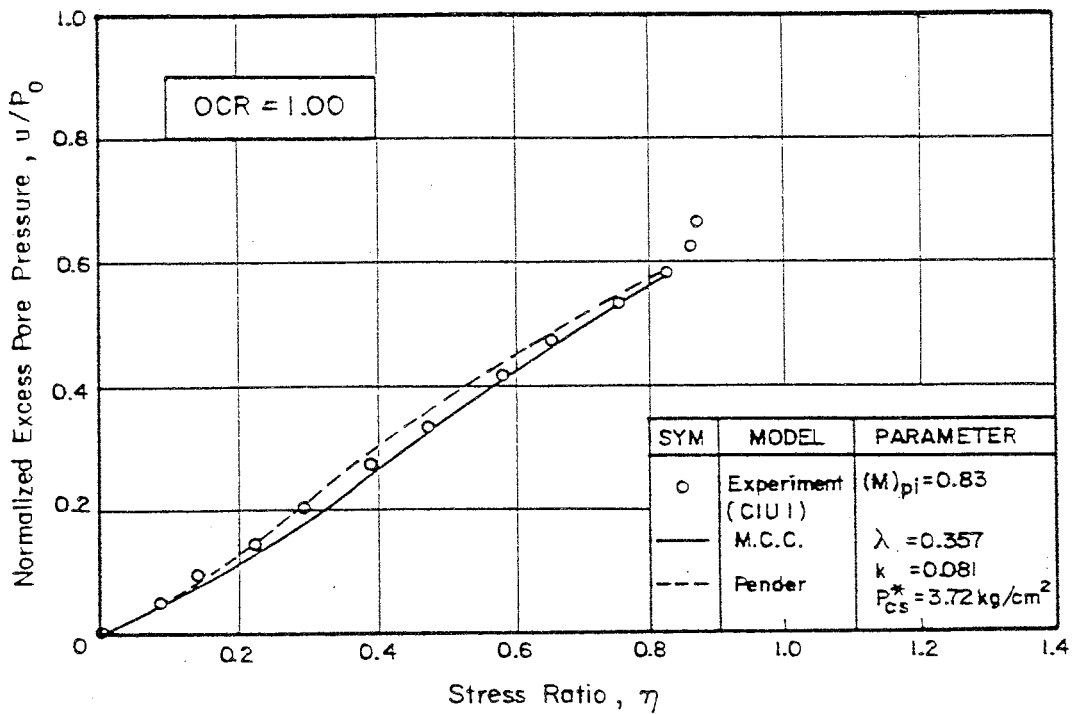


Fig. 7.8 $(u/p_0, \eta)$ Plot for CIU1 Sample (Peak Stress State)

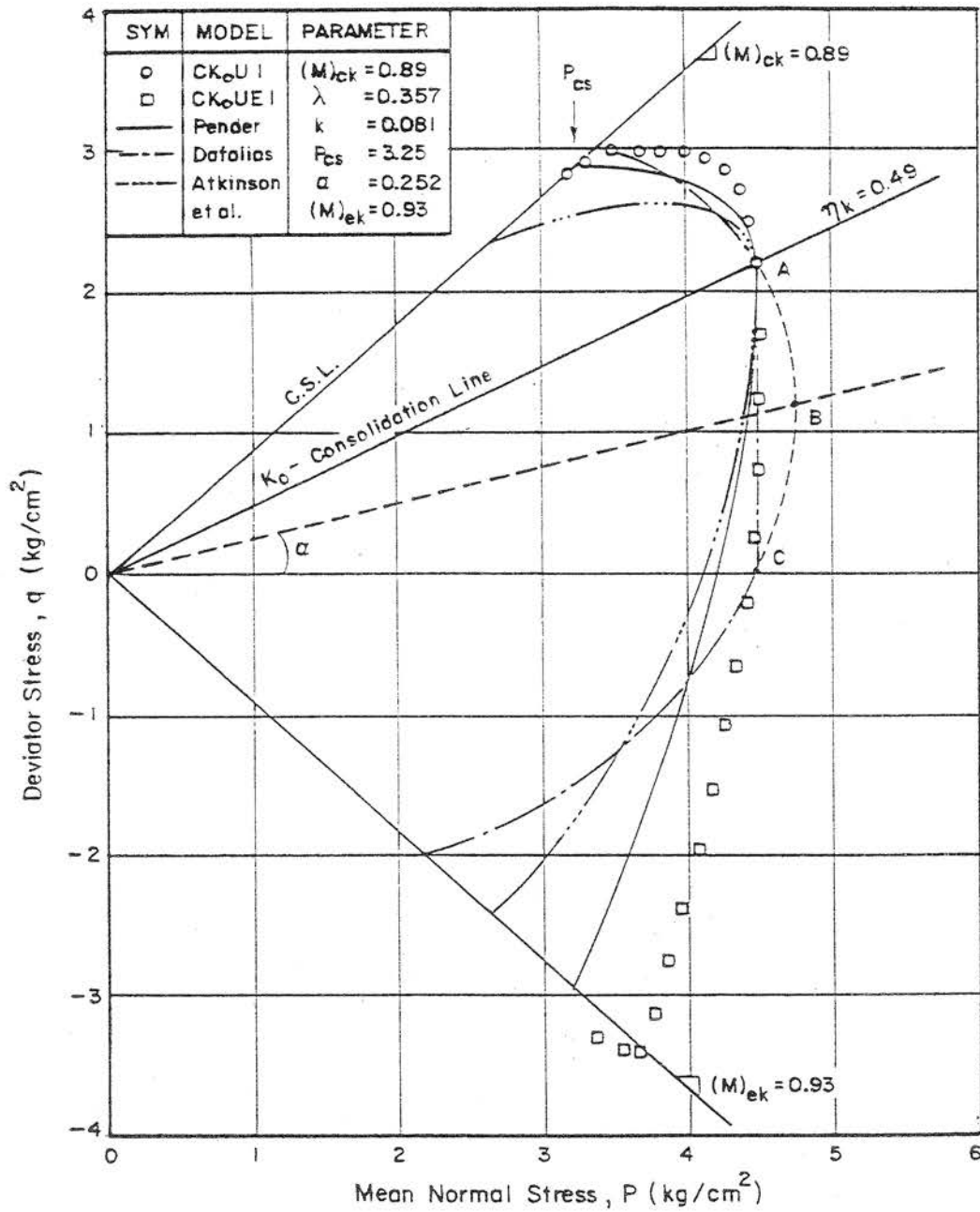


Fig. 7.9 (q, p) Plot for K_0 -normally Consolidated Samples Compared with Predictions from Pender's Model (Critical State)

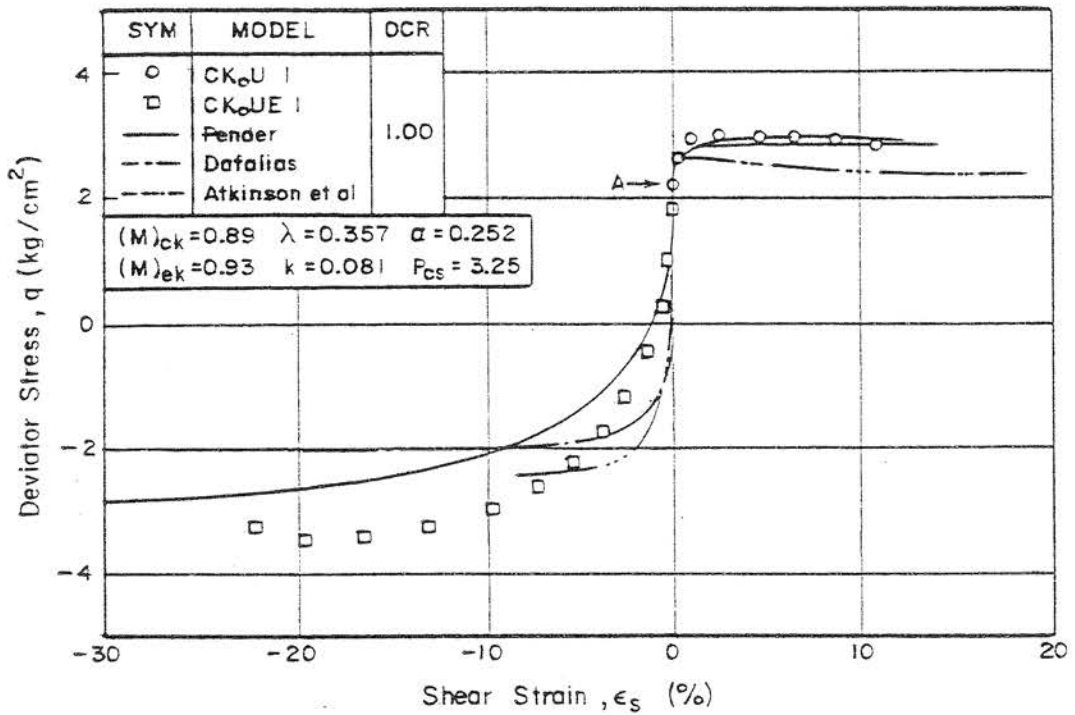


Fig. 7.10 (q, ϵ_s) Plot for K_o -normally Consolidated Samples Compared with the Model Predictions (Critical State)

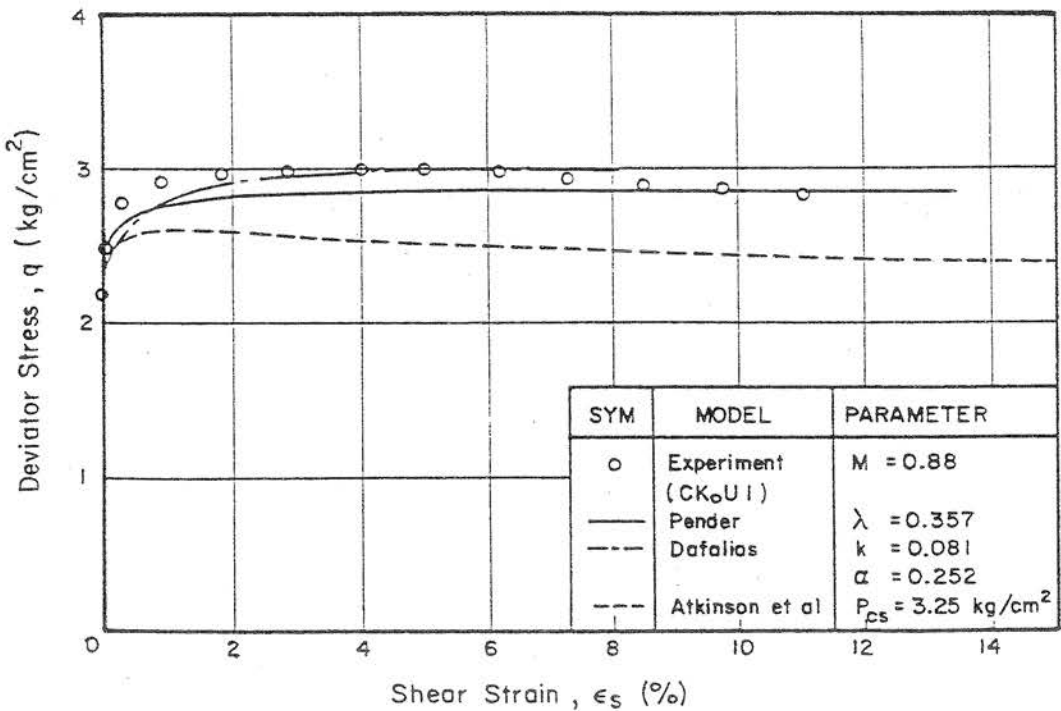


Fig. 7.10a (q, ϵ_s) Plot for CKoU1 Sample Compared with the Model Predictions in Compression Conditions

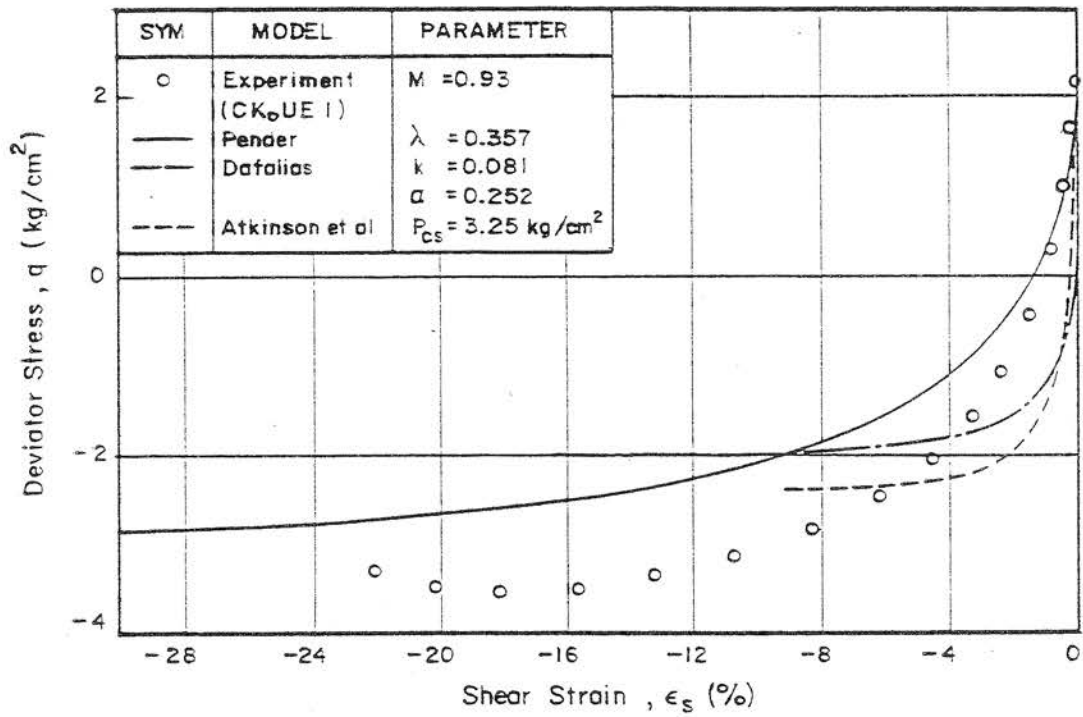


Fig. 7.10b (q, ϵ_s) Plot for CK₀UE1 Sample Compared with the Model Predictions in Compression Conditions

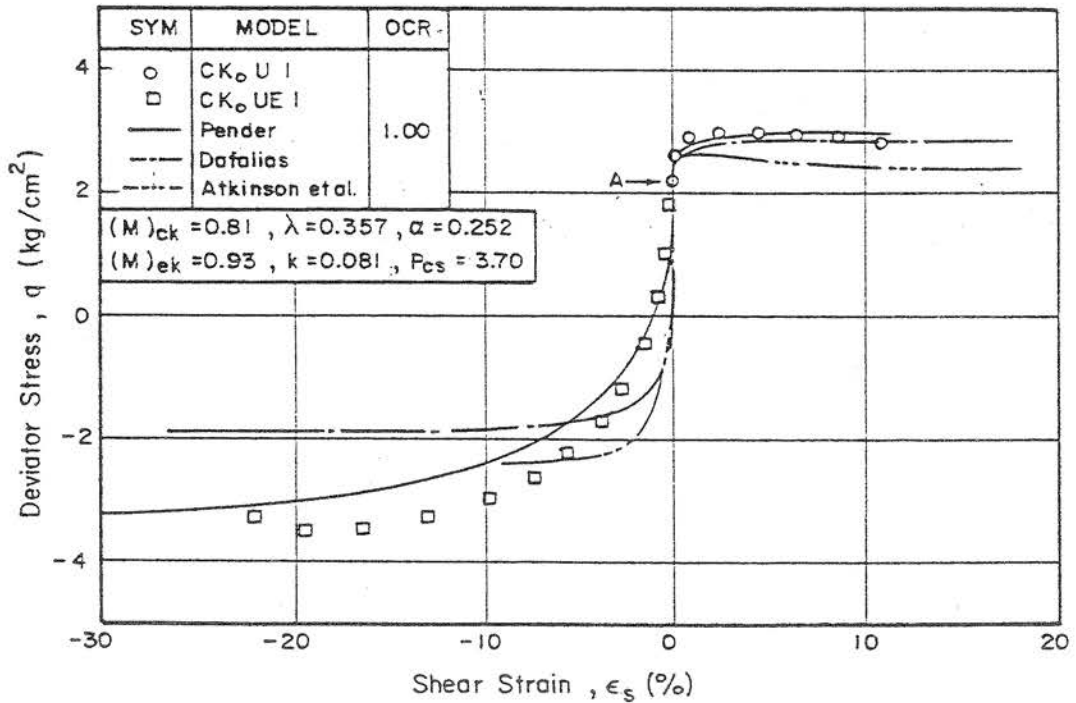


Fig. 7.11 (q, ϵ_s) Plot for K₀-normally Consolidated Samples Compared with the Model Predictions (Peak Stress State)

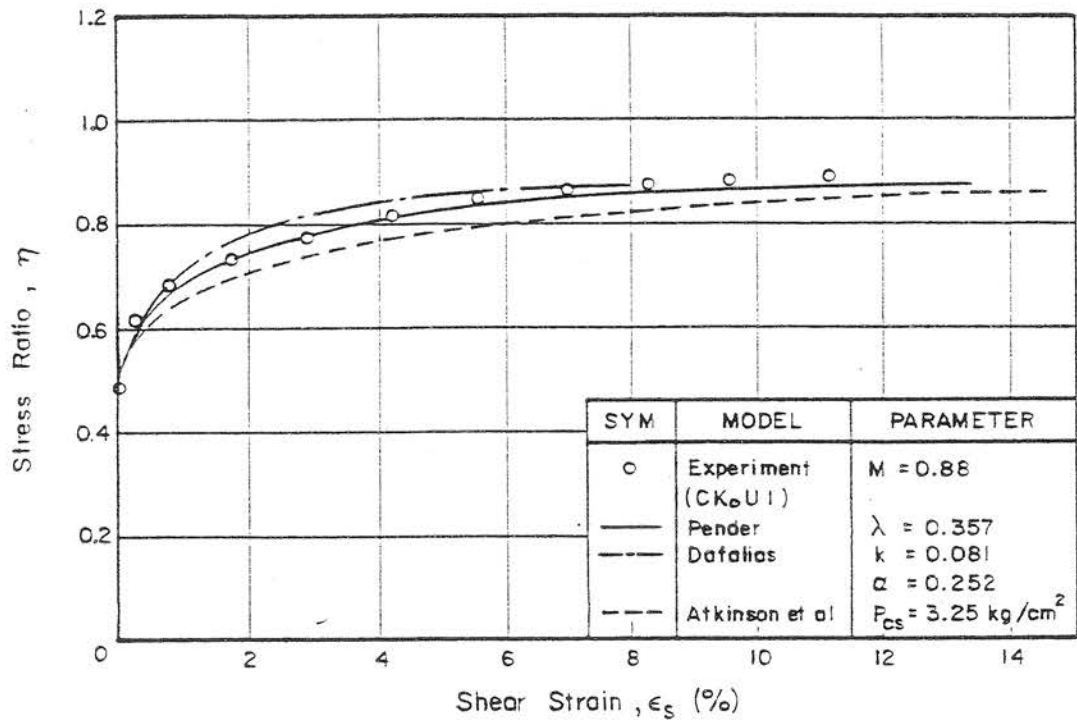


Fig. 7.12 (η , ϵ_s) Plot for CK₀U1 Sample Compared with the Model Predictions

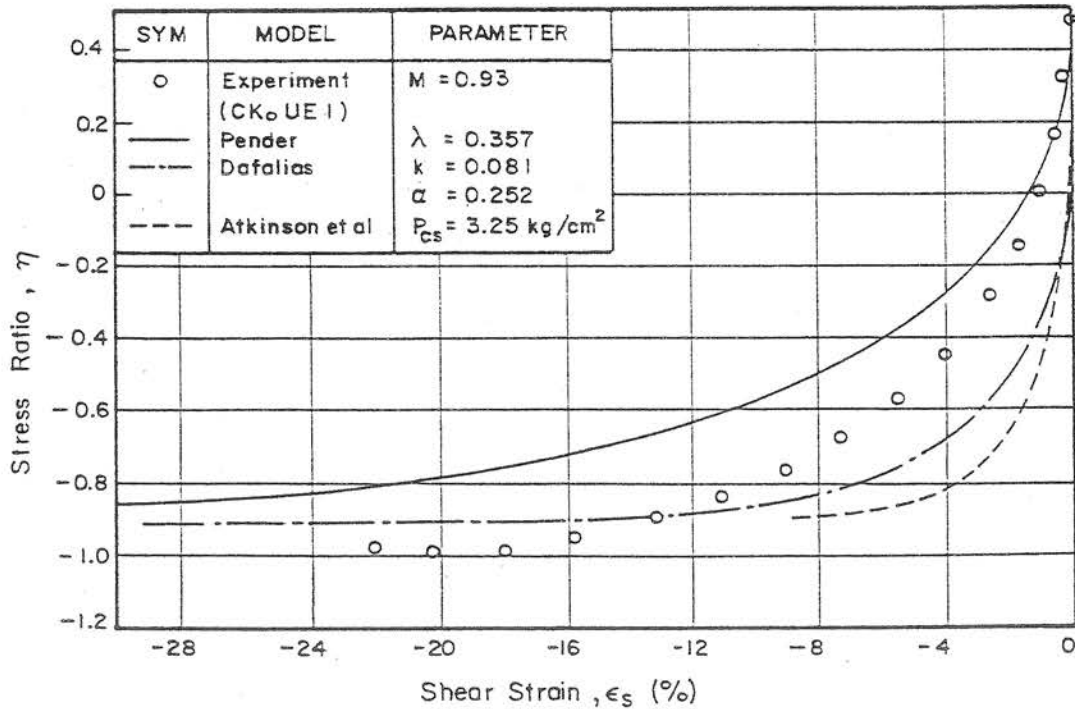


Fig. 7.13 (η , ϵ_s) Plot for CK₀UE1 Sample Compared with the Model Predictions

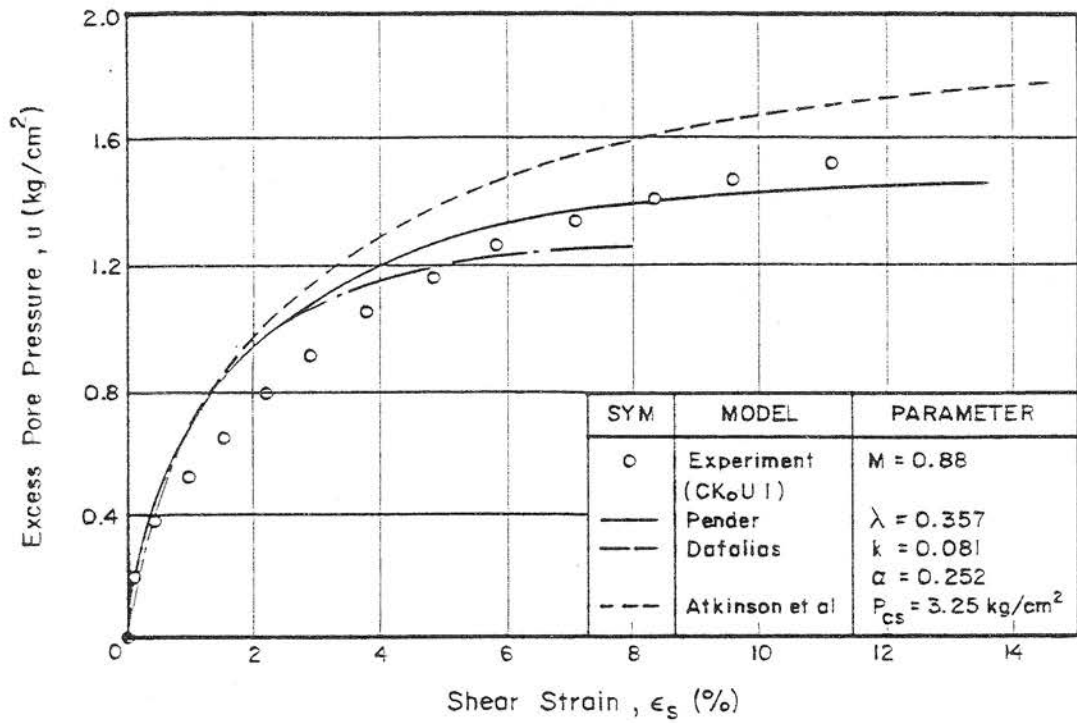


Fig. 7.14 (u, ϵ_s) Plot for CK0U1 Sample Compared with the Model Predictions

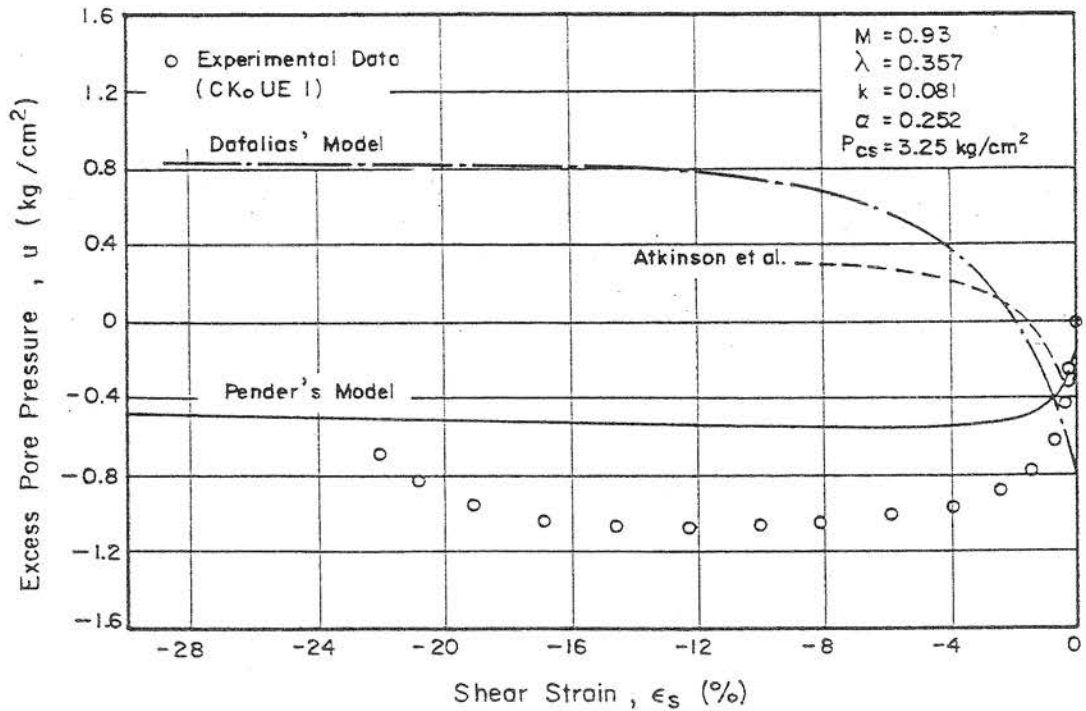


Fig. 7.15 (u, ϵ_s) Plot for CK0UE1 Sample Compared with the Model Predictions

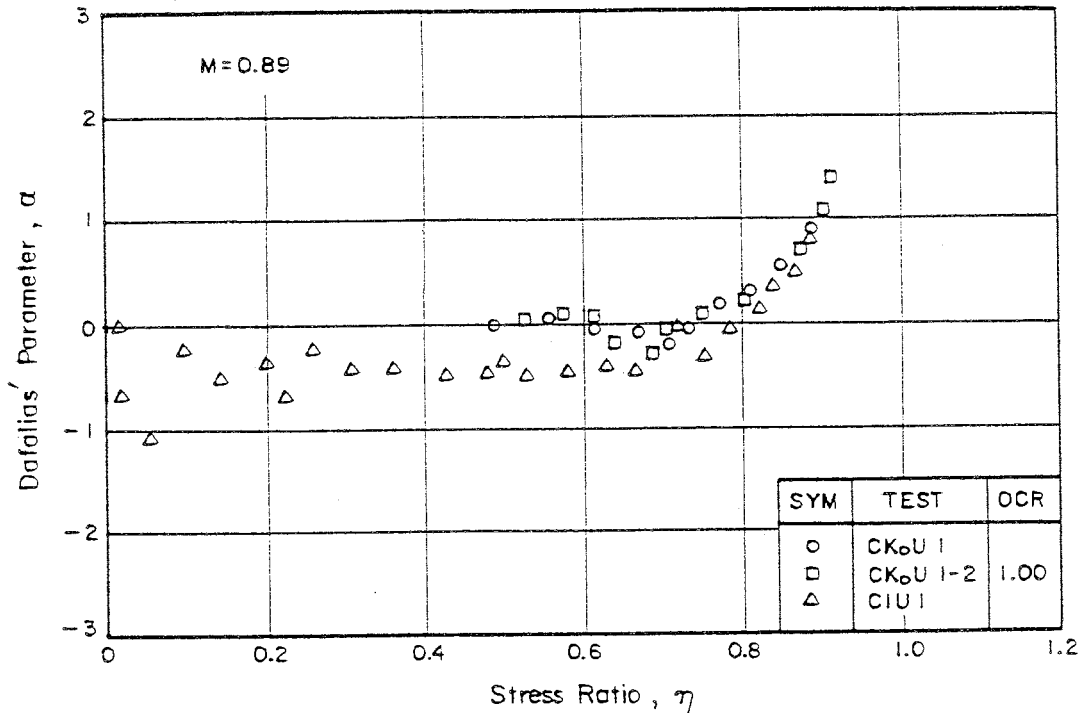


Fig. 7.16 Variations of Dafalias' α -parameter with the Stress Ratio for K_0 -normally Consolidated Samples

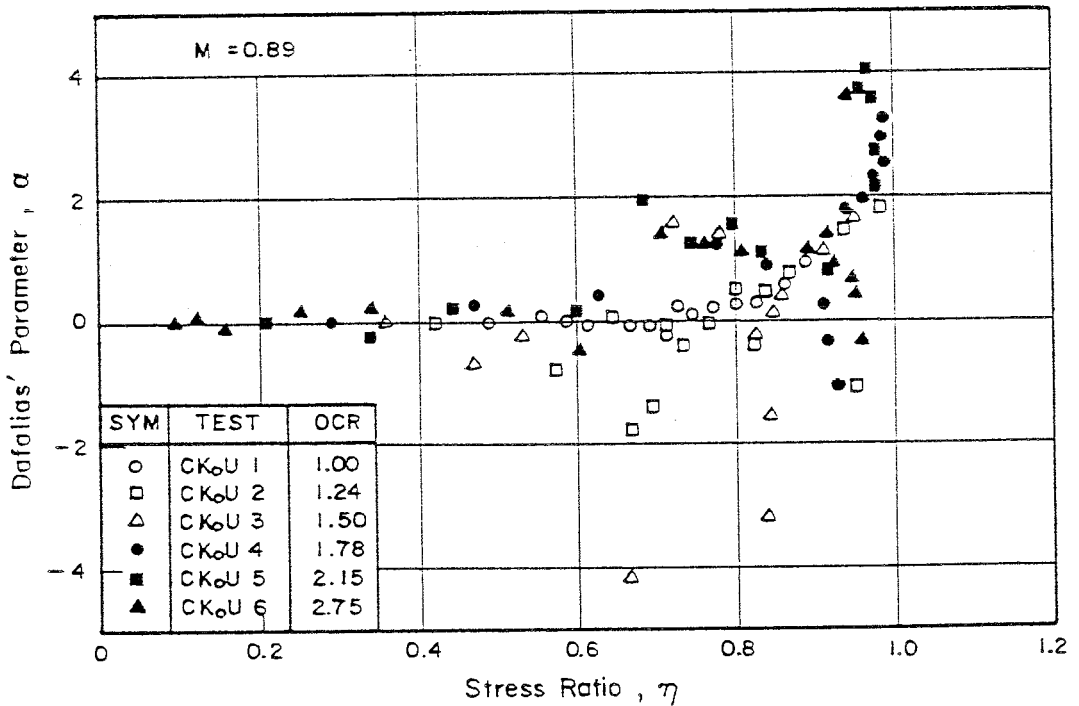


Fig. 7.17 Variations of Dafalias' α -parameter with the Stress Ratio for K_0 -overconsolidated Samples

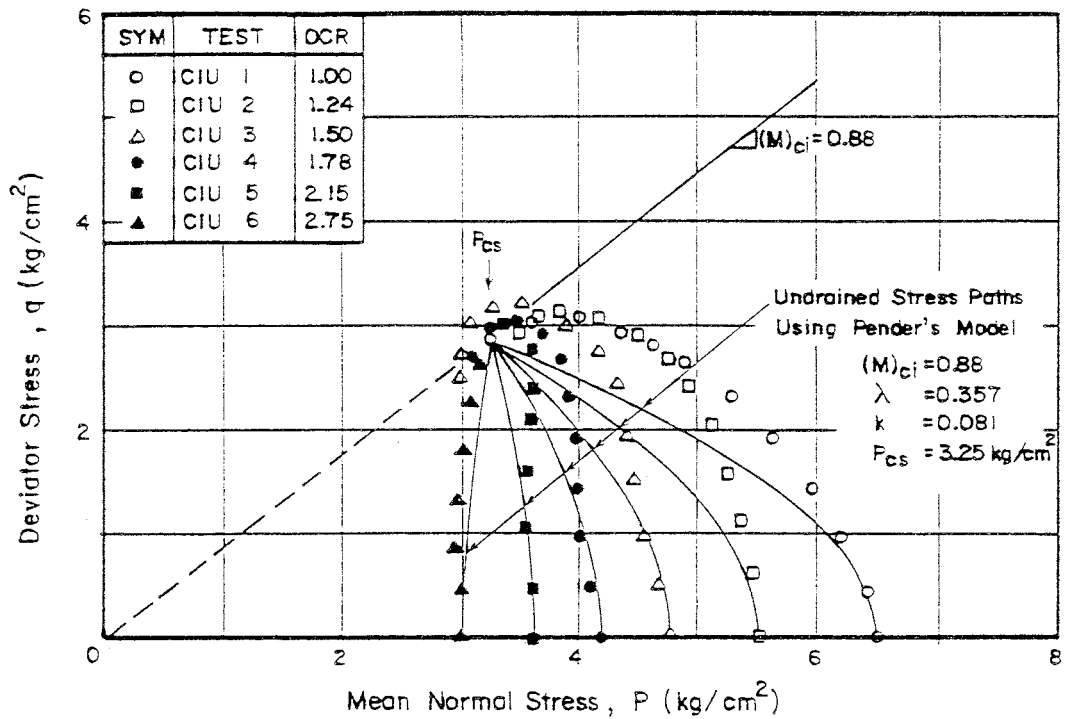


Fig. 7.18 (q, p) Plot for Isotropically Overconsolidated Samples Compared with the Predictions from Pender's Model (Critical State)

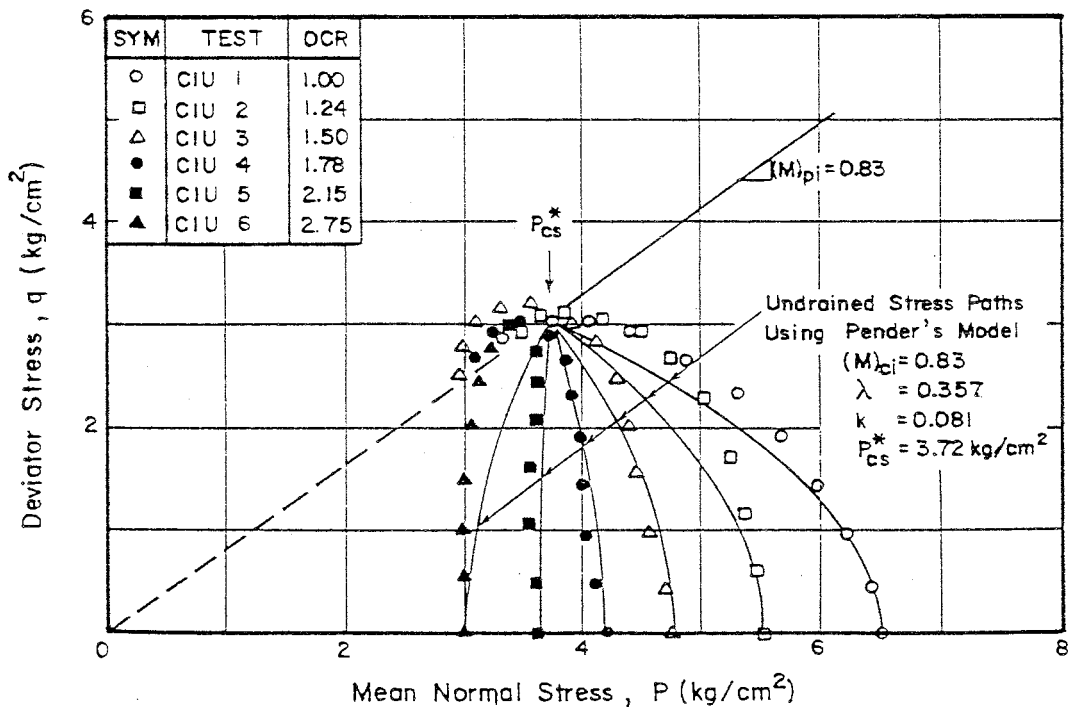


Fig. 7.19 (q, p) Plot for Isotropically Overconsolidated Samples Compared with the Predictions from Pender's Model (Peak Stress State)

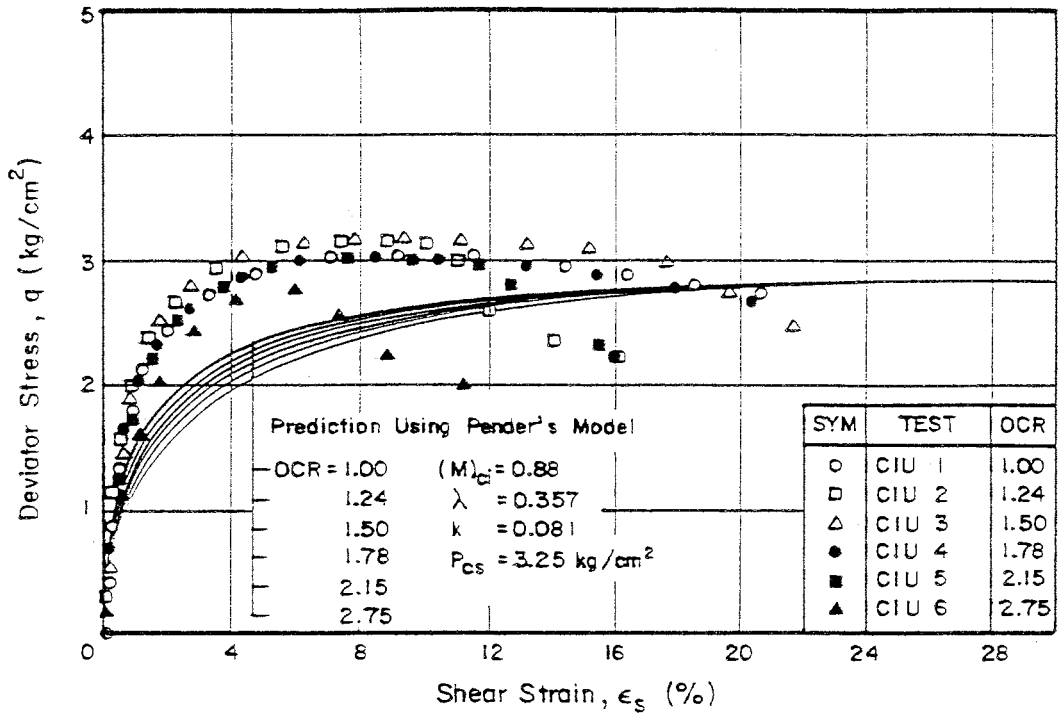


Fig. 7.20 (q , ϵ_s) Plot for Isotropically Overconsolidated Samples Compared with the Predictions from Pender's Model (Critical State)

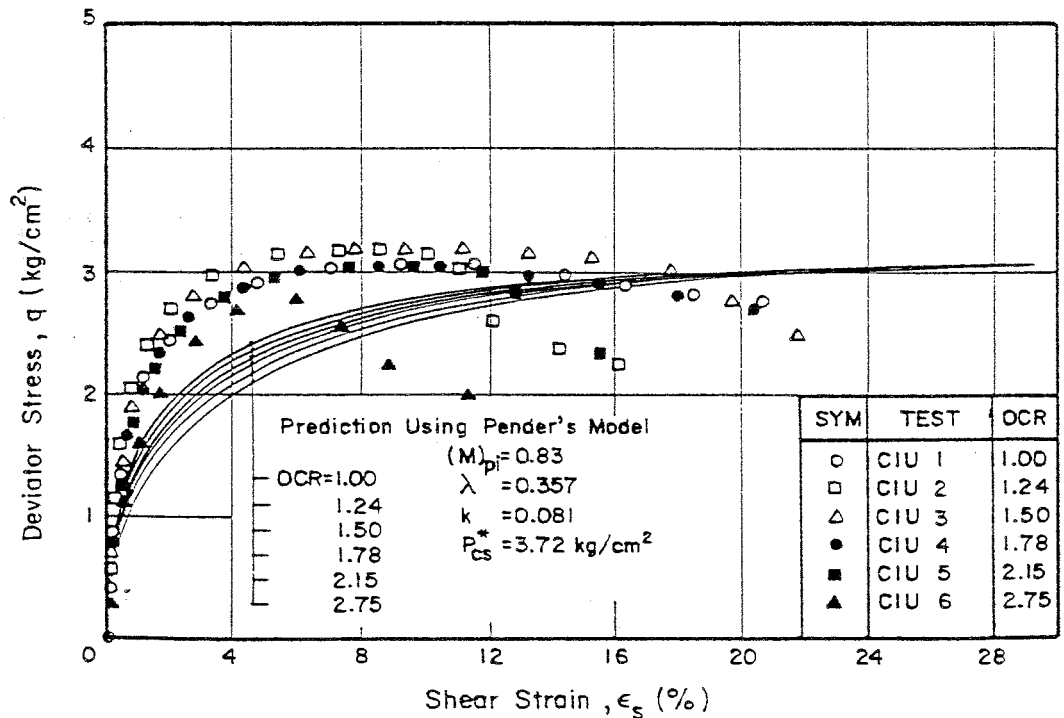


Fig. 7.21 (q , ϵ_s) Plot for Isotropically Overconsolidated Samples Compared with the Predictions from Pender's Model (Peak Stress State)

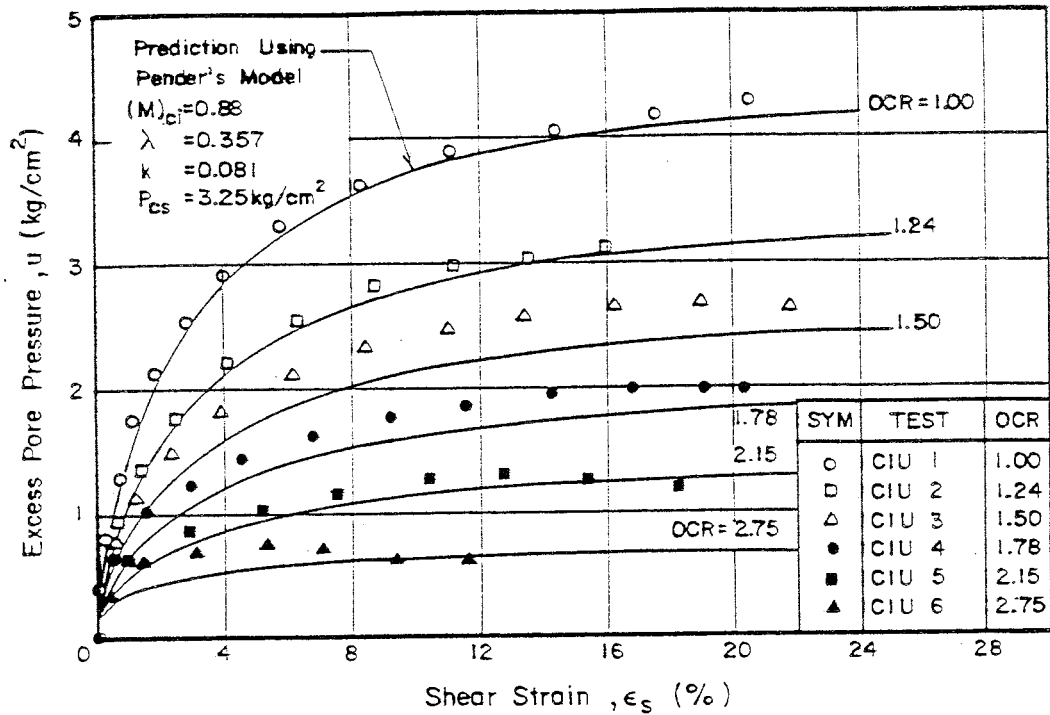


Fig. 7.22 (u, ϵ_s) Plot for Isotropically Overconsolidated Samples Compared with the Predictions from Pender's Model (Critical State)

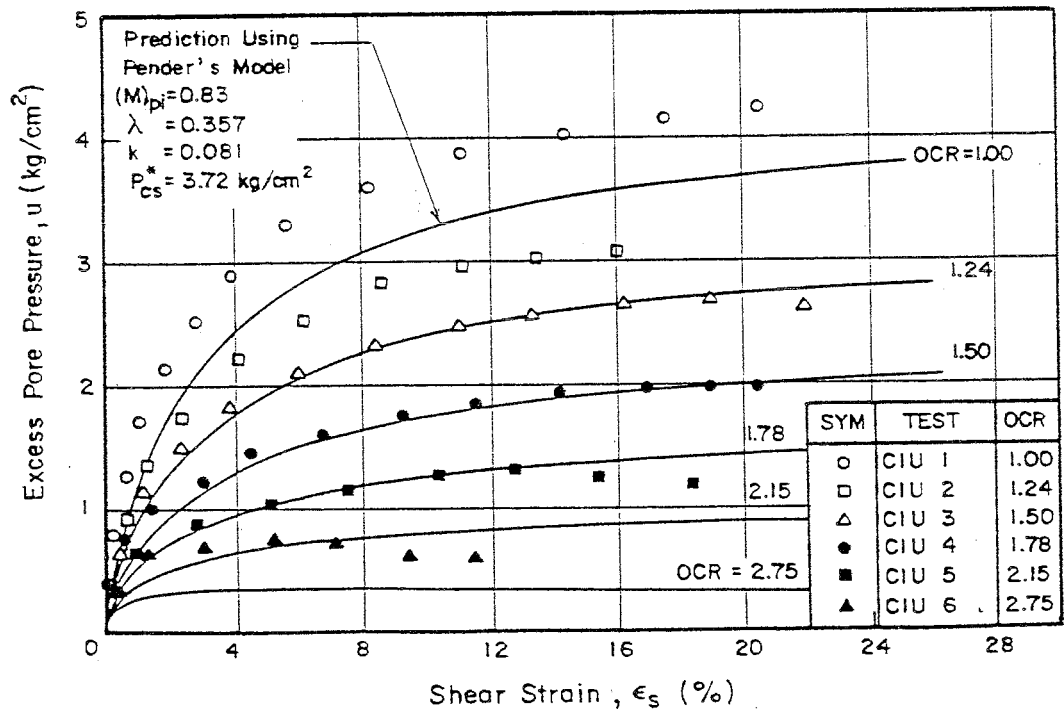


Fig. 7.23 (u, ϵ_s) Plot for Isotropically Overconsolidated Samples Compared with the Predictions from Pender's Model (Peak Stress State)

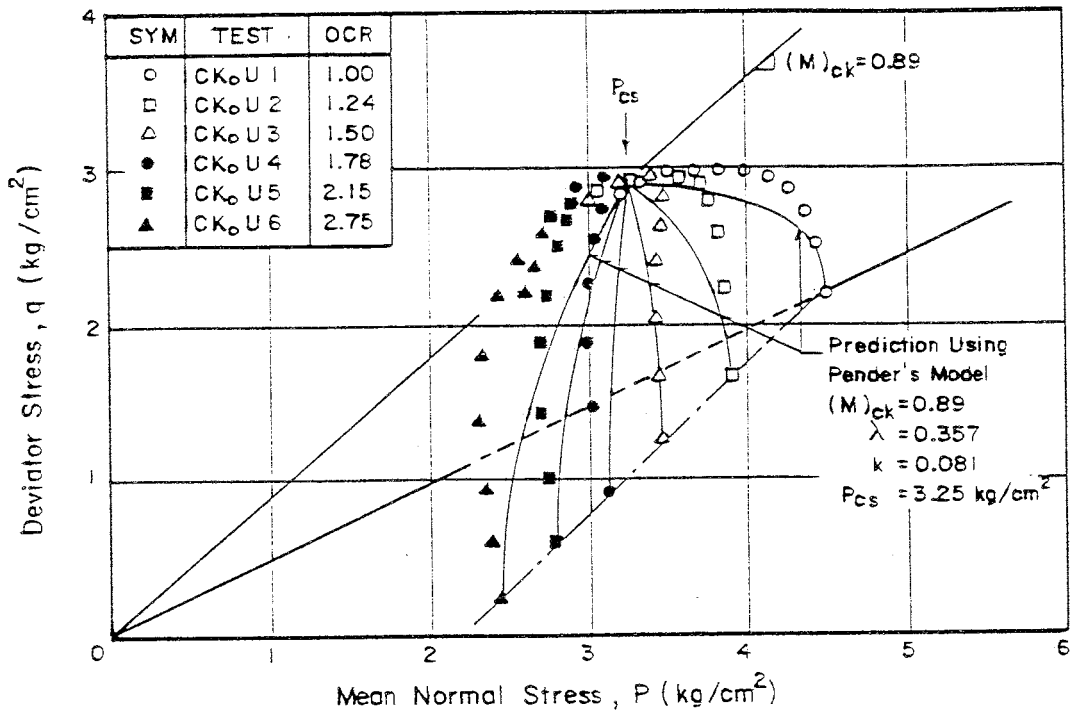


Fig. 7.24 (q, p) Plot for K_0 -overconsolidated Samples Compared with the Predictions from Pender's Model (Critical State)

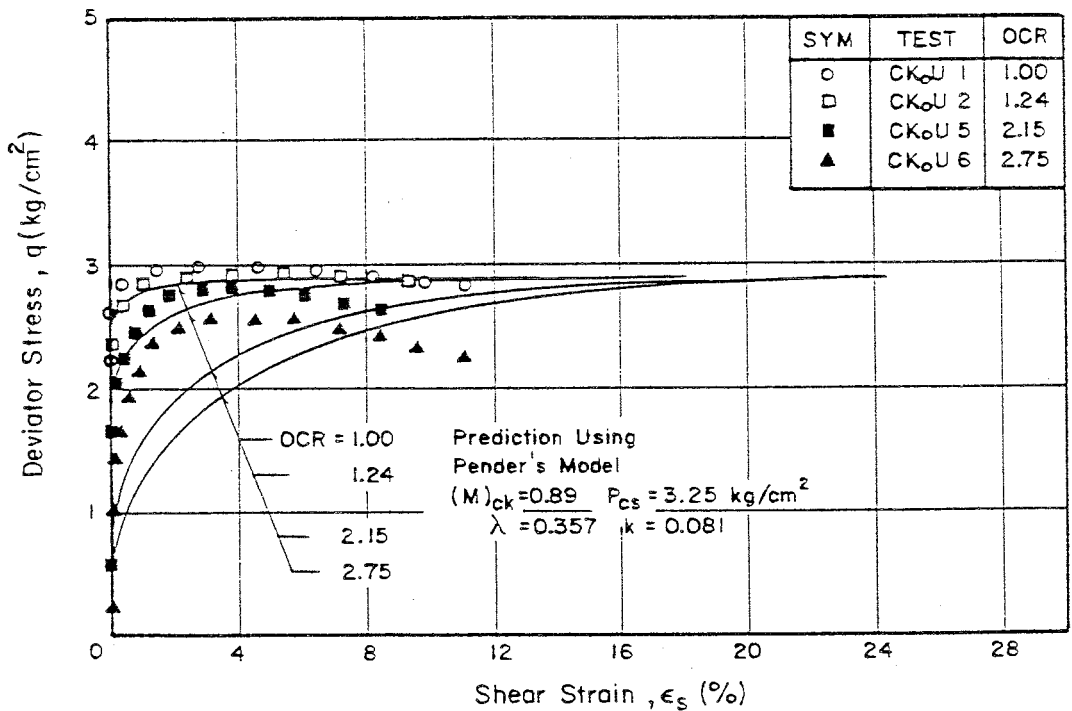


Fig. 7.25 (q, ϵ_s) Plot for K_0 -overconsolidated Samples Compared with the Predictions from Pender's Model (Critical State)

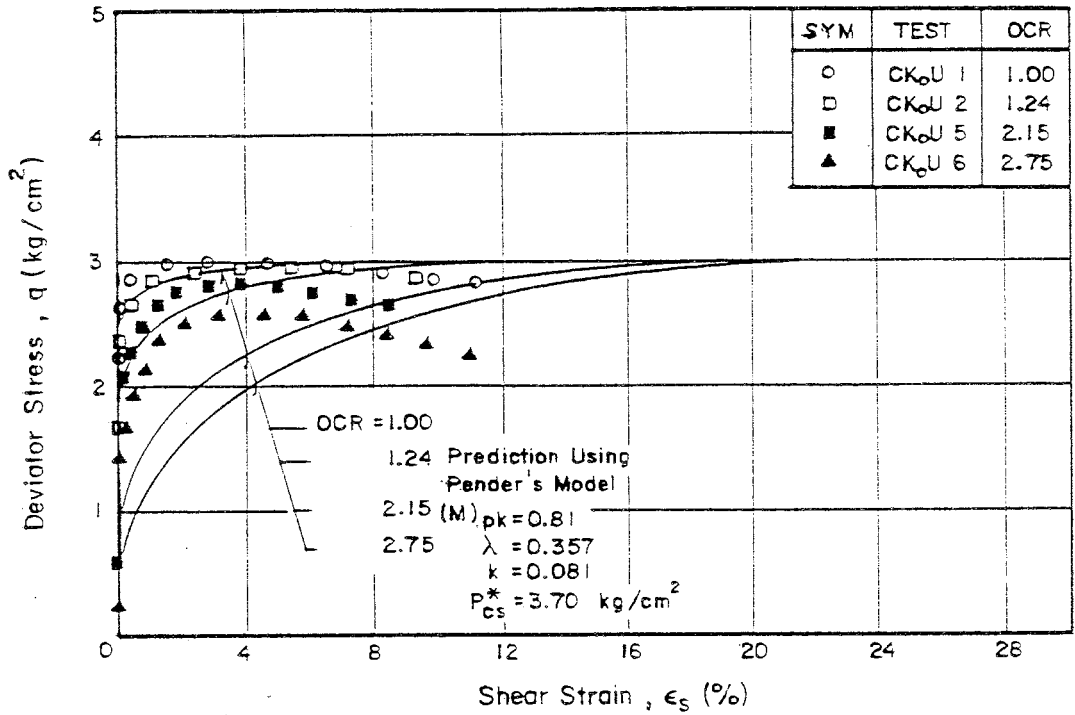


Fig. 7.26 (q, ϵ_s) Plot for K_0 -overconsolidated Samples Compared with the Predictions from Pender's Model (Peak Stress State)

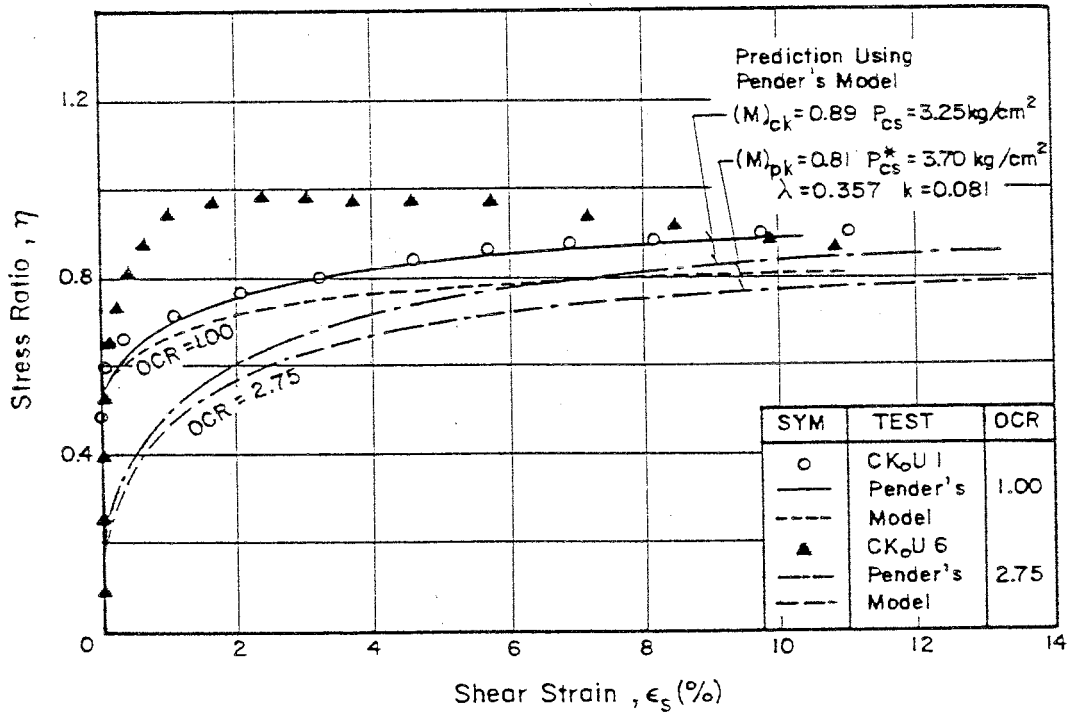


Fig. 7.27 (η, ϵ_s) Plot for K_0 -overconsolidated Samples Compared with the Predictions from Pender's Model (Critical & Peak Stress State)

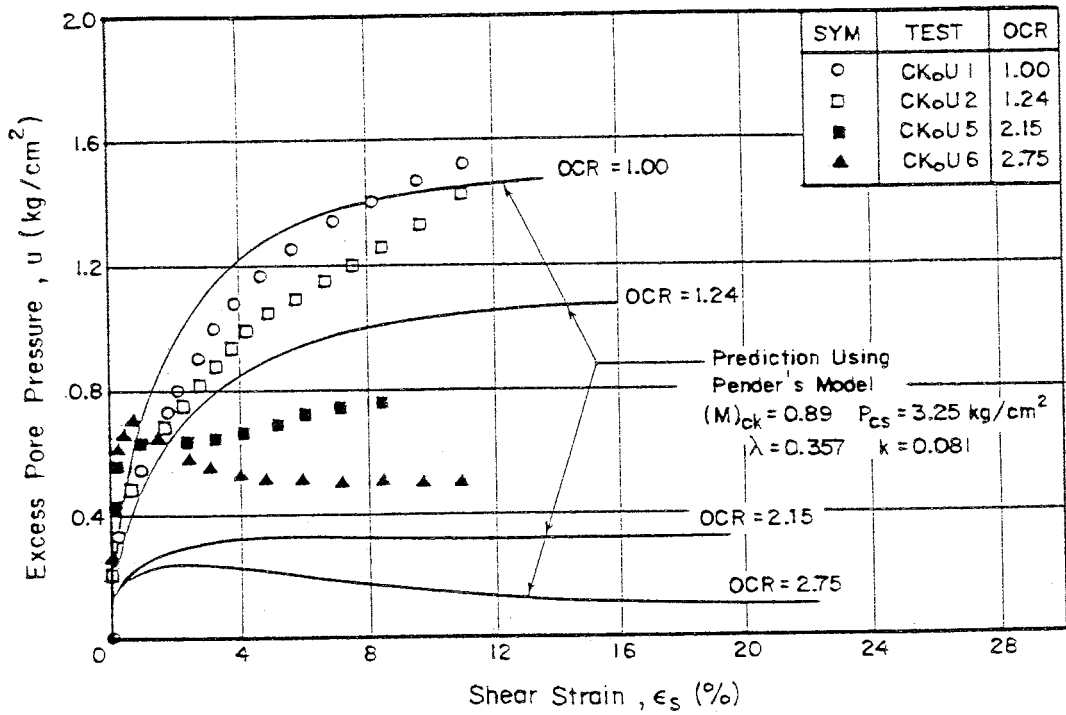


Fig. 7.28 (u, ϵ_s) Plot for K_0 -overconsolidated Samples Compared with the Predictions from Pender's Model (Critical State)

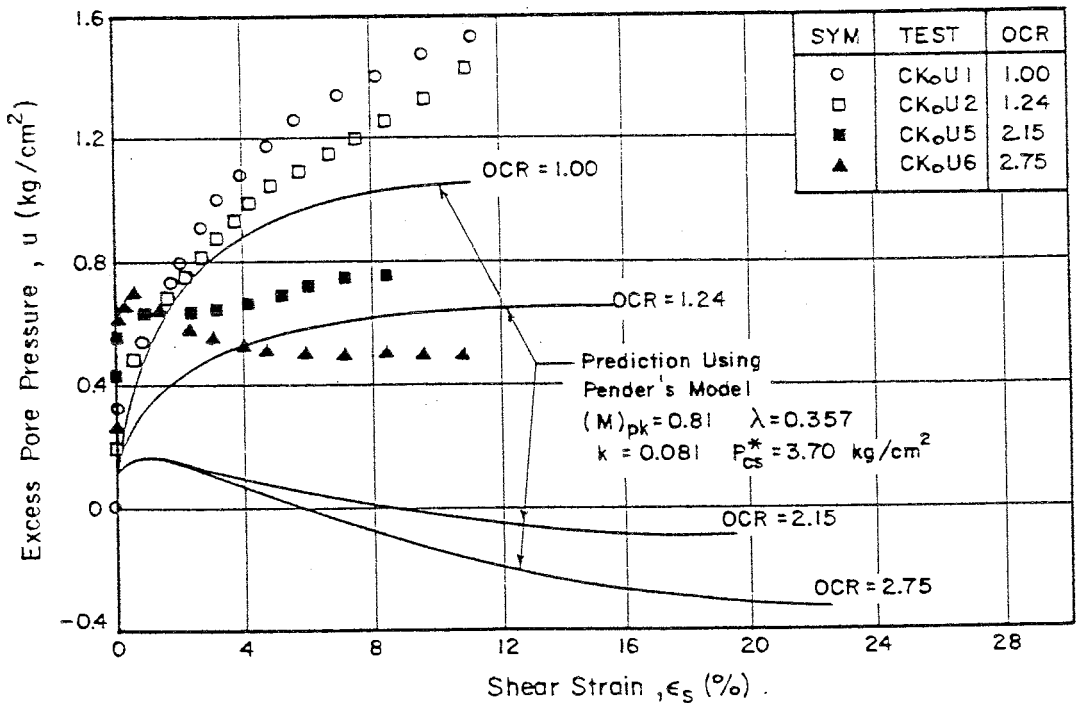


Fig. 7.29 (u, ϵ_s) Plot for K_0 -overconsolidated Samples Compared with the Predictions from Pender's Model (Peak Stress State)

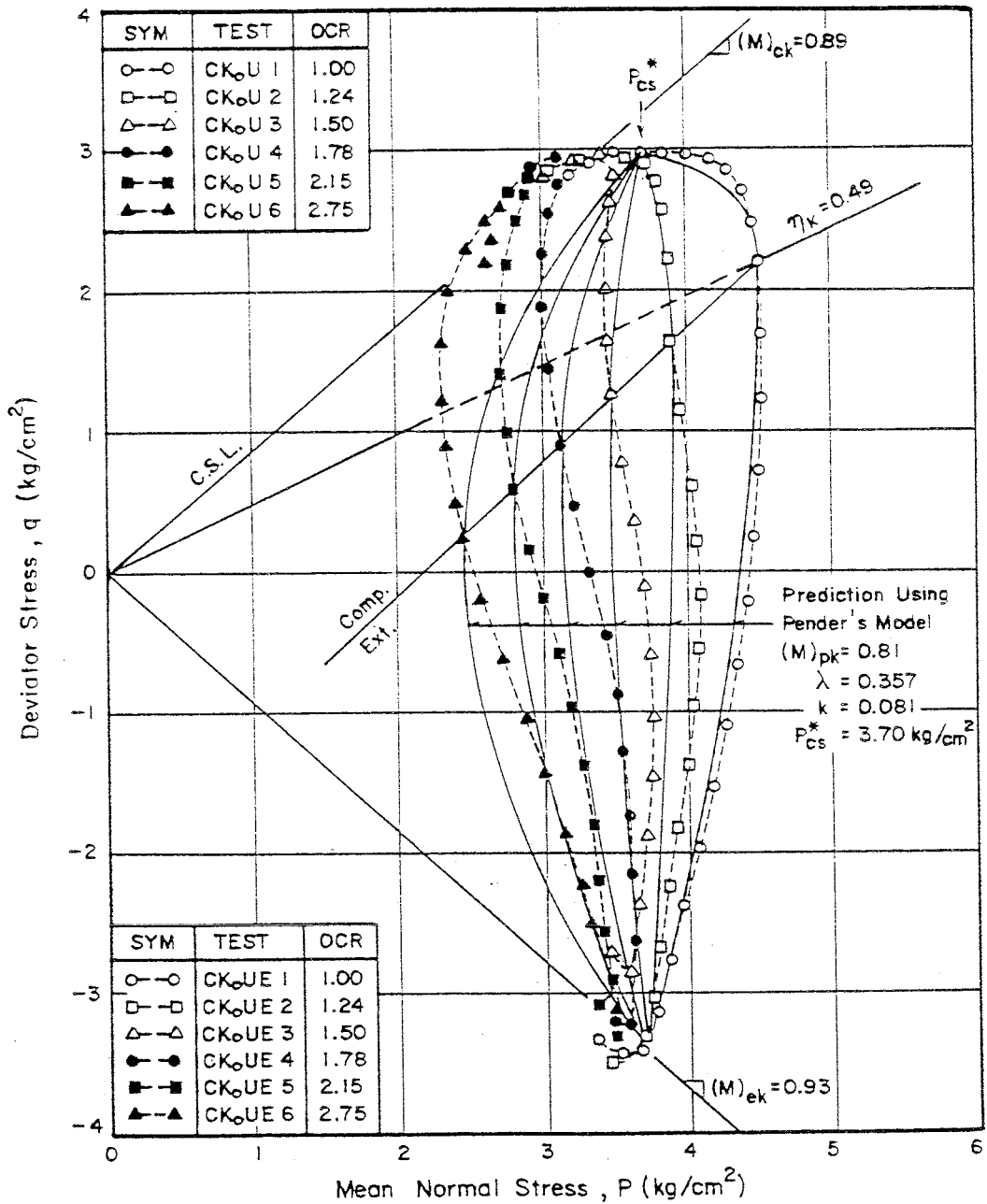


Fig. 7.30 (q, p) Plot for K_0 -overconsolidated Samples both in Compression and in Extension Conditions Compared with the Predictions from Pender's Model (Peak Stress State)

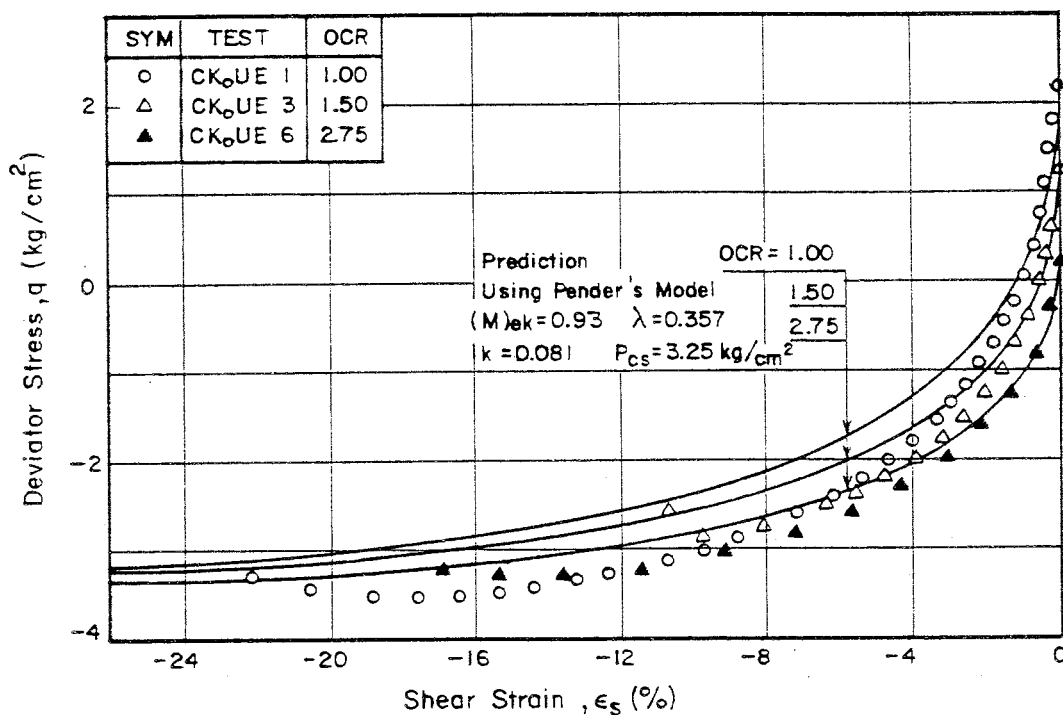


Fig. 7.31 (q, ϵ_s) Plot for K_0 -overconsolidated Samples in Extension Conditions Compared with the Predictions from the Pender's Model

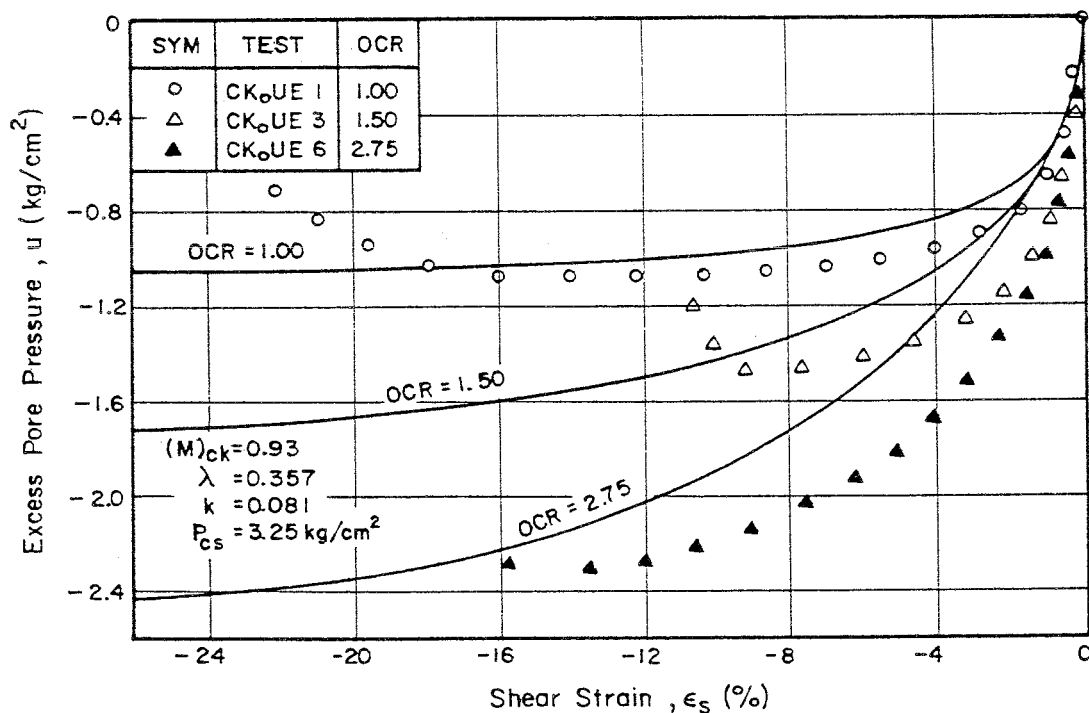


Fig. 7.32 (u, ϵ_s) Plot for K_0 -overconsolidated Samples in Extension Conditions Compared with the Predictions from Pender's Model

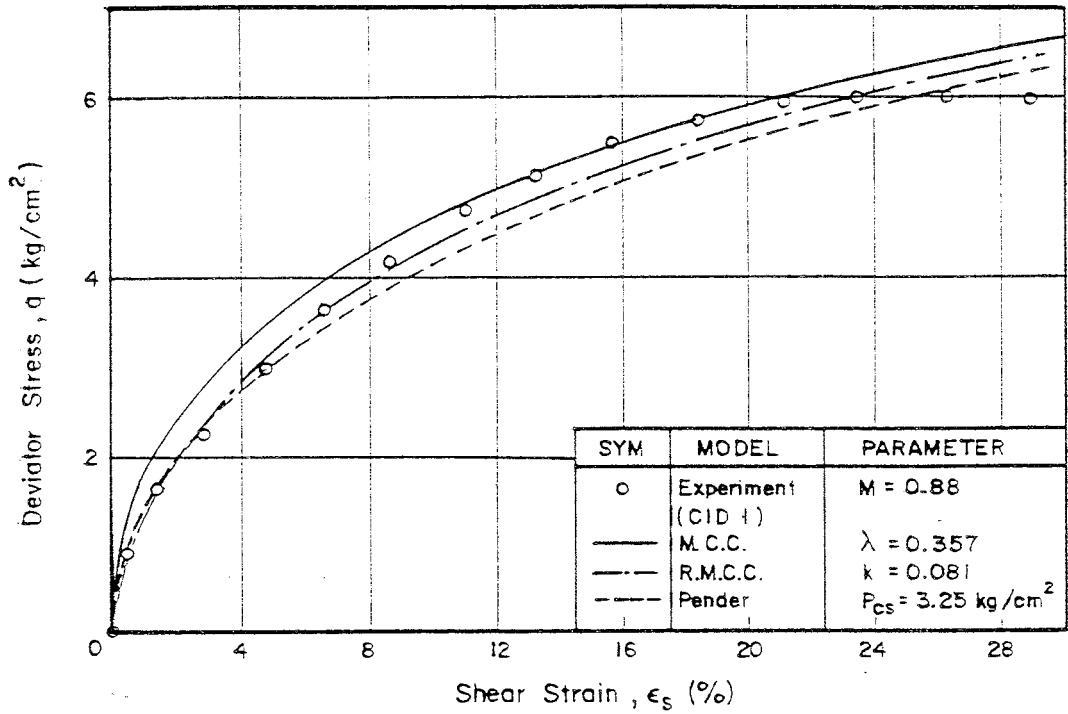


Fig. 7.33 (q, ϵ_s) Plot for CID1 Sample Compared with the Model Predictions

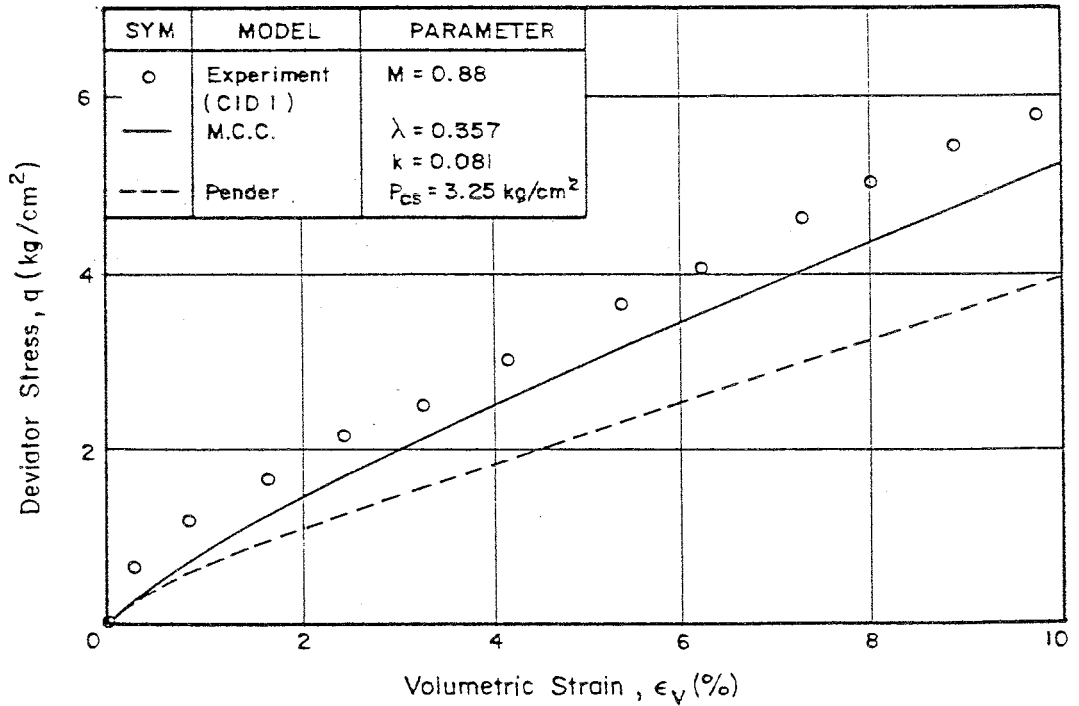


Fig. 7.34 (q, ϵ_v) Plot for CID1 Sample Compared with the Model Predictions

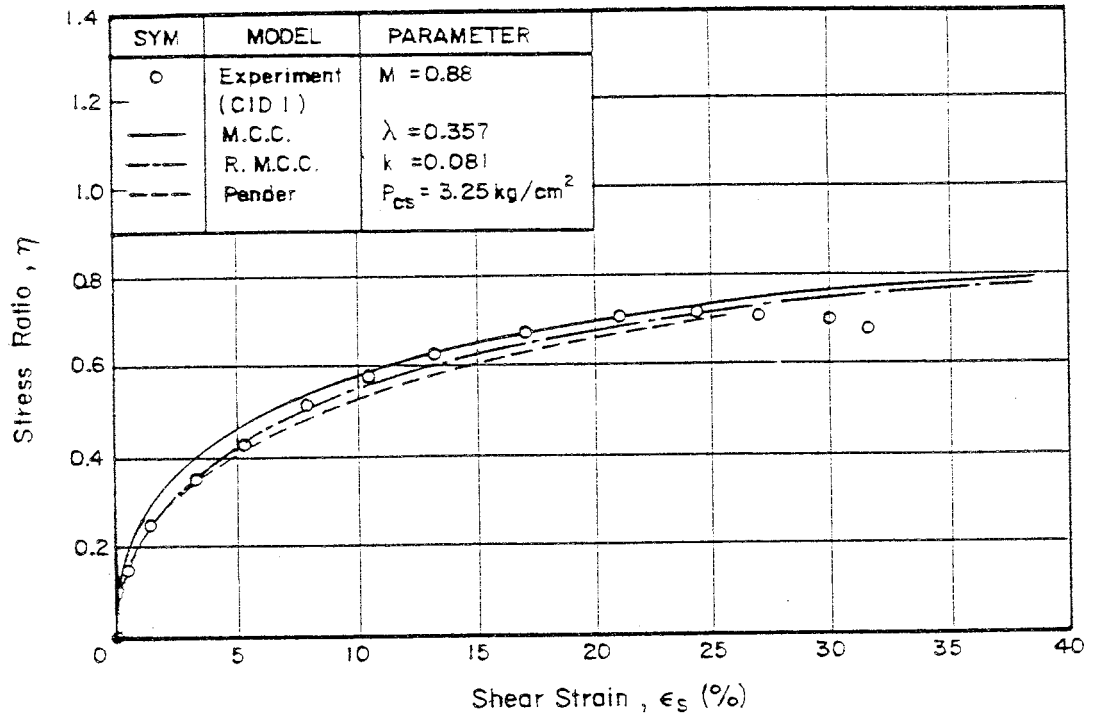


Fig. 7.35 (η, ϵ_s) Plot for CID1 Sample Compared with the Model Predictions

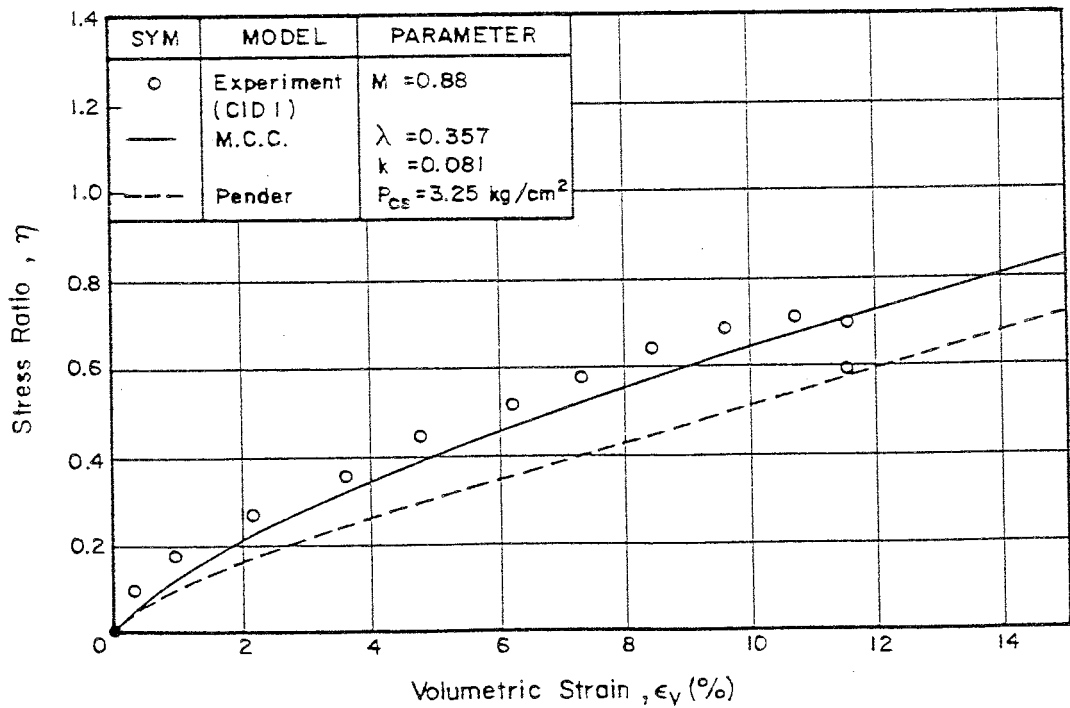


Fig. 7.36 (η, ϵ_v) Plot for CID1 Sample Compared with the Model Predictions

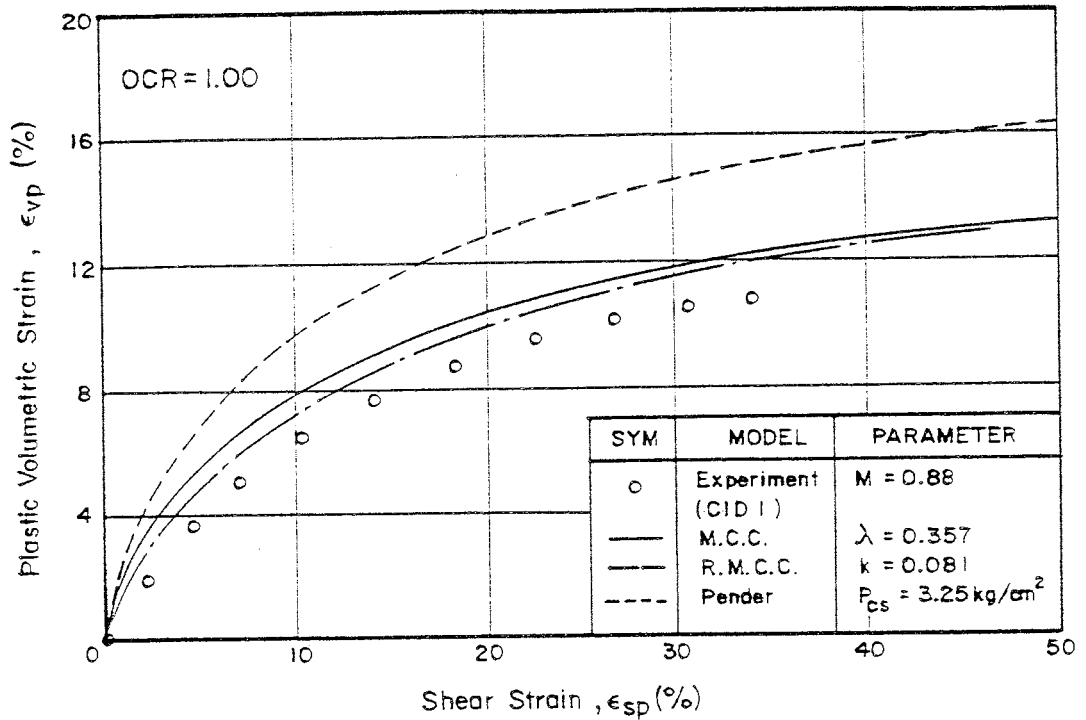


Fig. 7.37 $(\epsilon_{vp}, \epsilon_{sp})$ Plot for CID1 Sample Compared with the Model Predictions

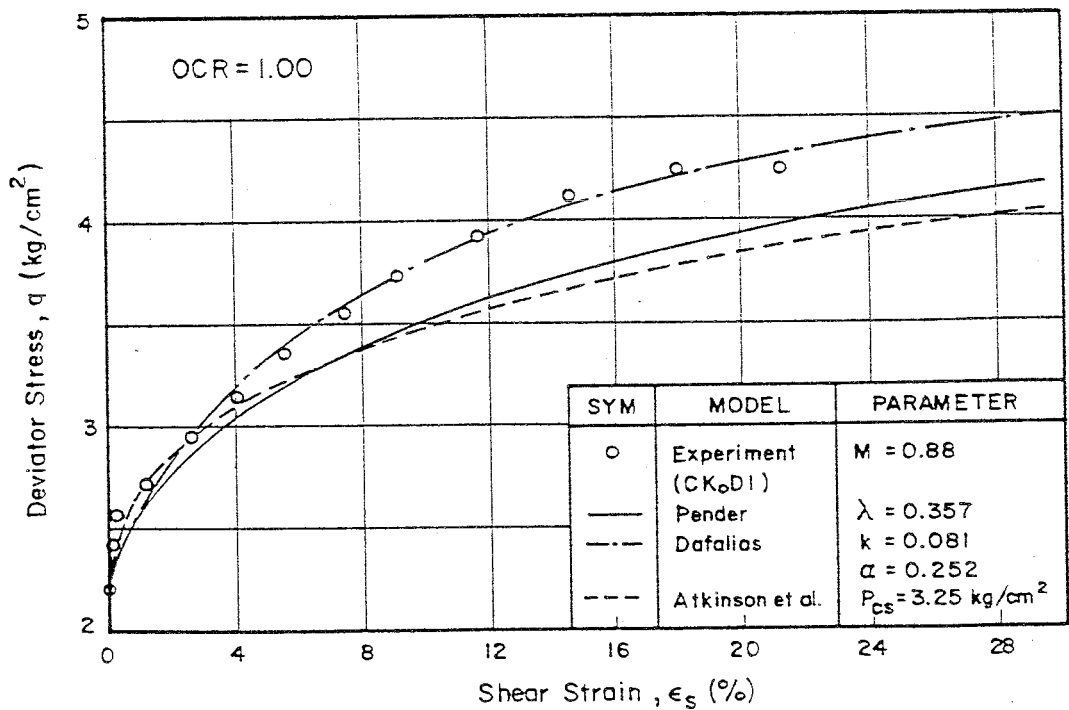


Fig. 7.38 (q, ϵ_s) Plot for CKoD1 Sample Compared with the Model Predictions

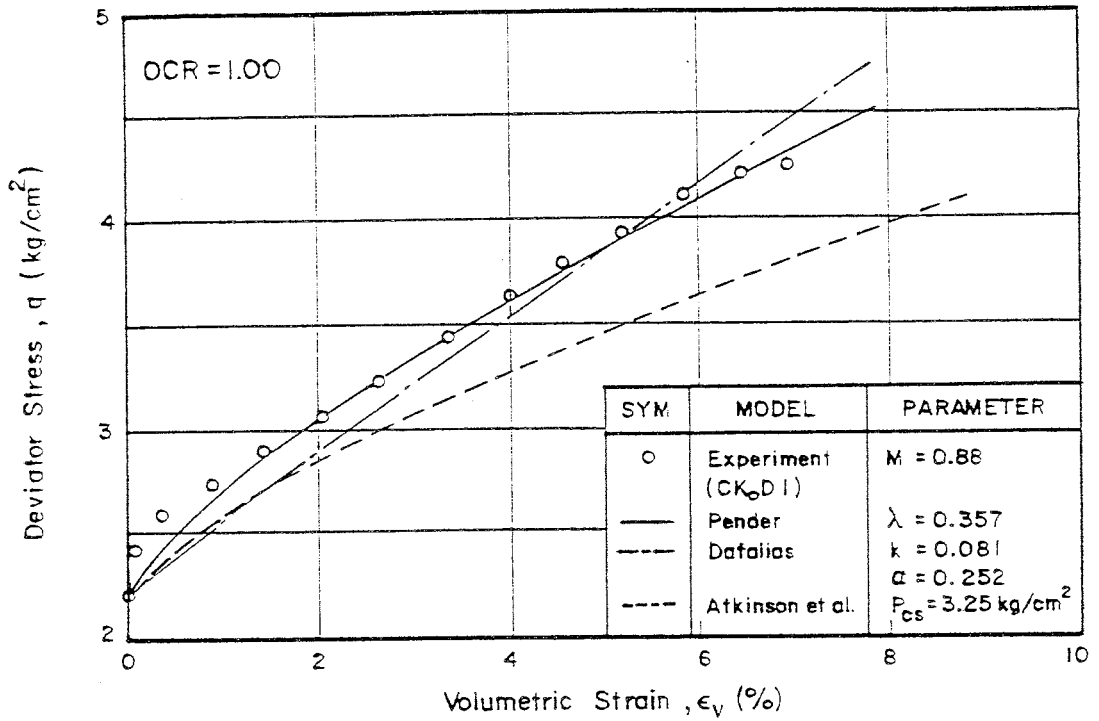


Fig. 7.39 (q, ϵ_v) Plot for CKoDI Sample Compared with the Model Predictions

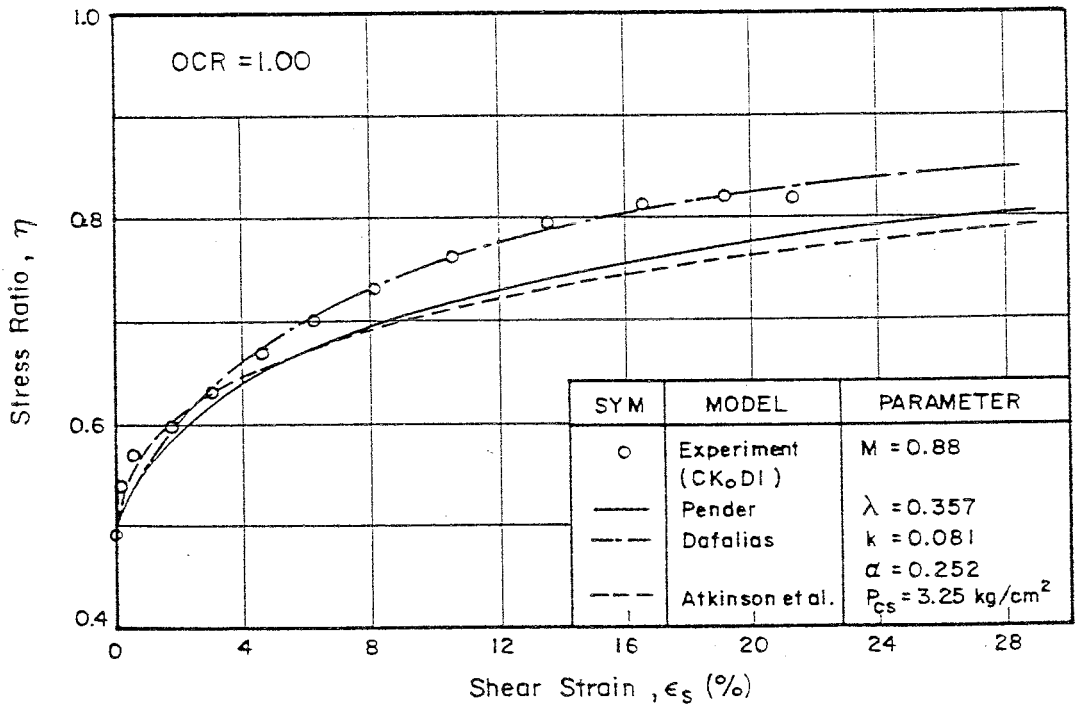


Fig. 7.40 (η, ϵ_s) Plot for CKoDI Sample Compared with the Model Predictions

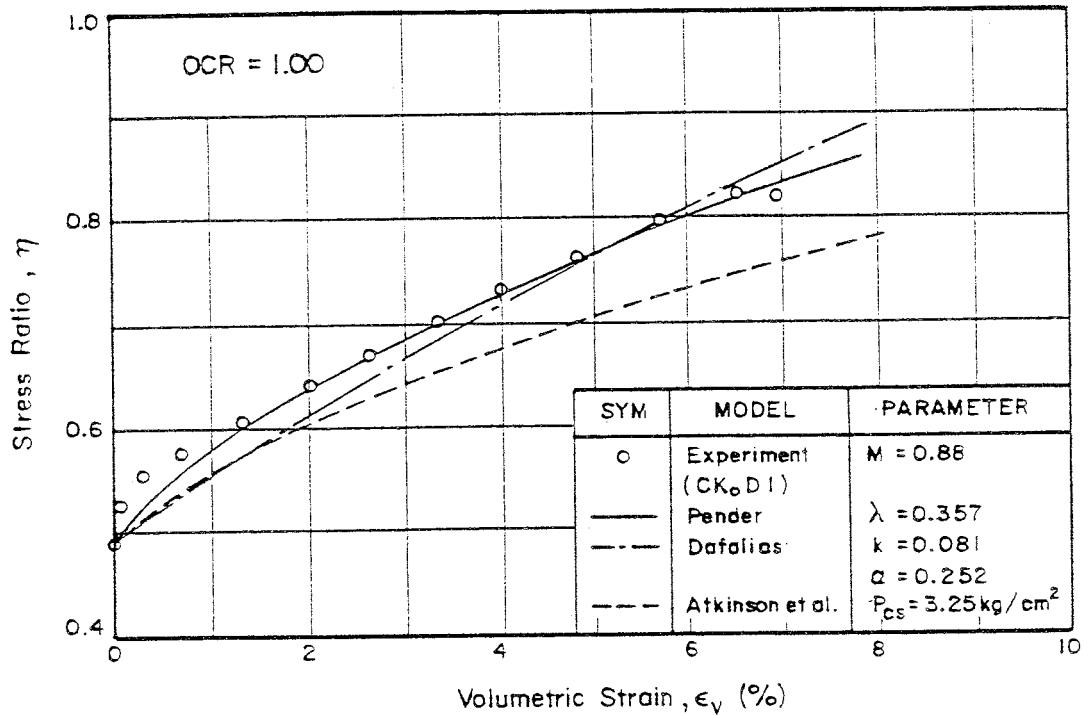


Fig. 7.41 (η, ϵ_v) Plot for CKoD1 Sample Compared with the Model Predictions

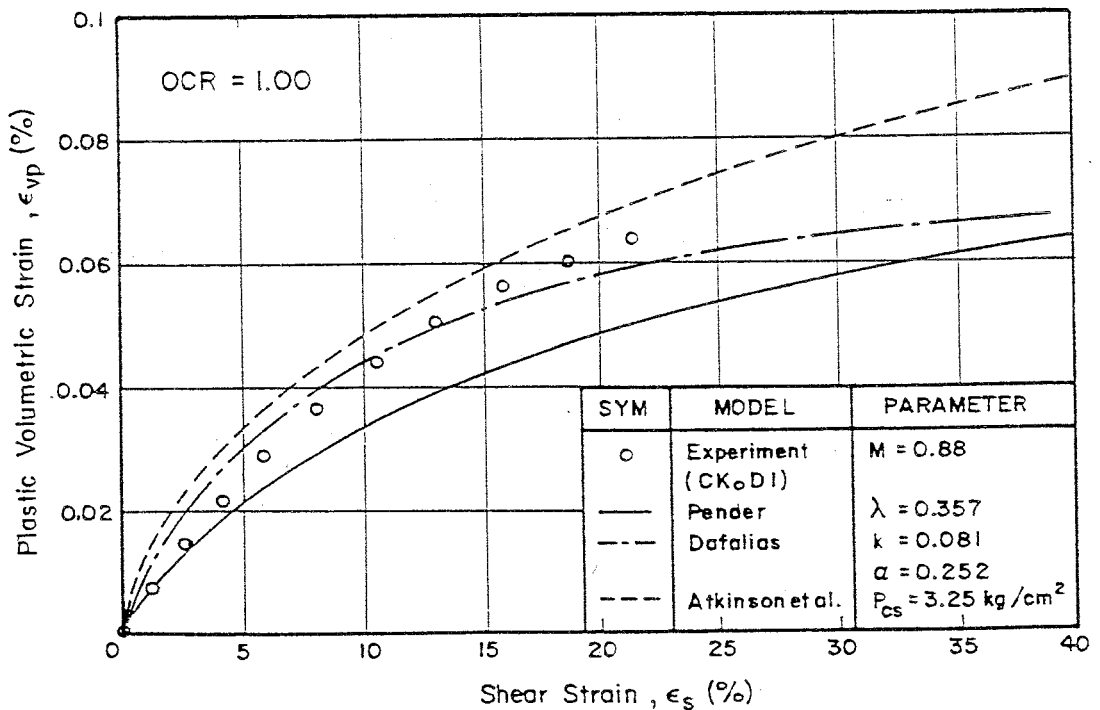


Fig. 7.42 $(\epsilon_{vp}, \epsilon_s)$ Plot for CKoD1 Sample Compared with the Model Predictions

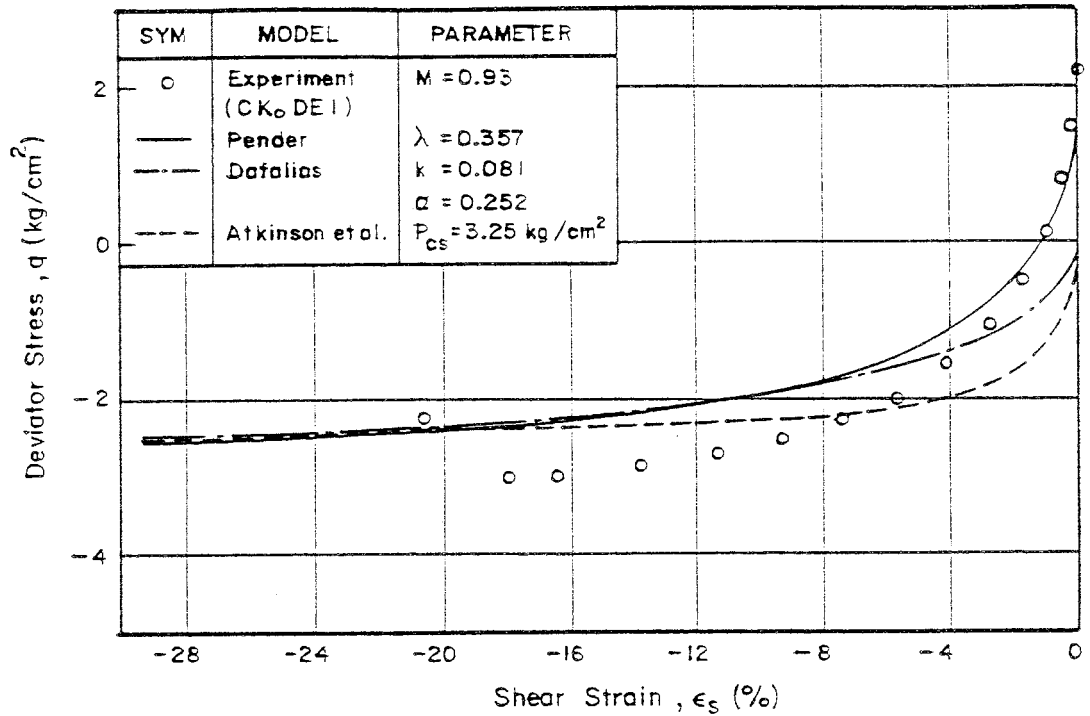


Fig. 7.43 (q , ϵ_s) Plot for CK₀DE1 Sample Compared with the Model Predictions

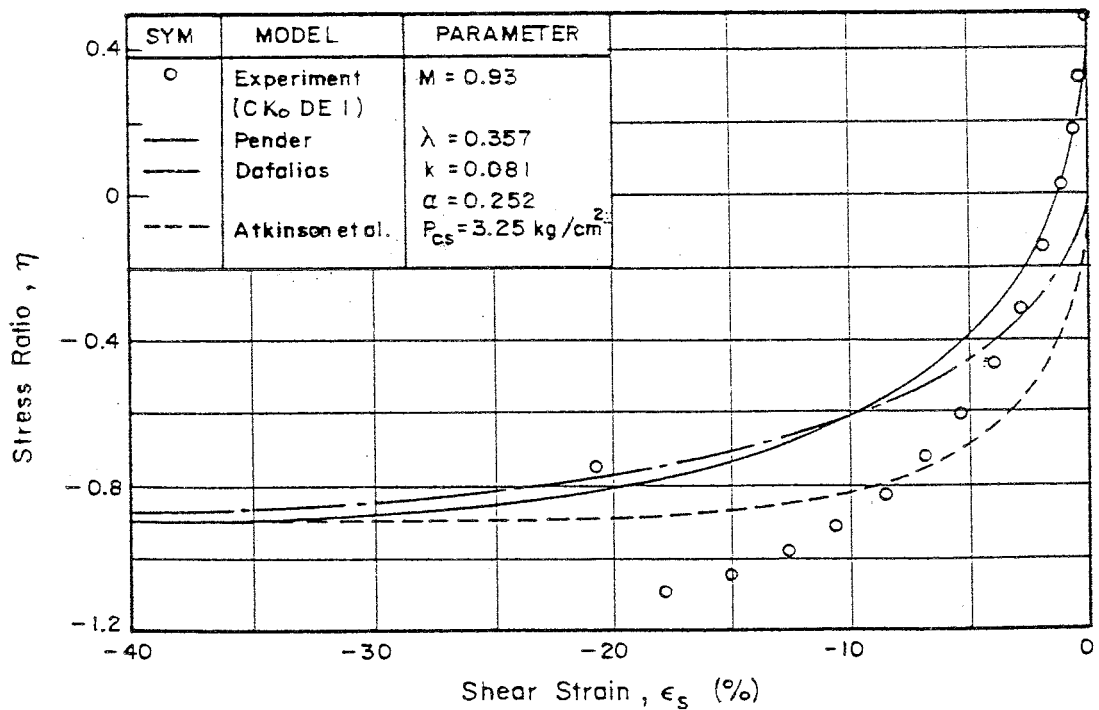


Fig. 7.44 (η , ϵ_s) Plot for CK₀DE1 Sample Compared with the Model Predictions

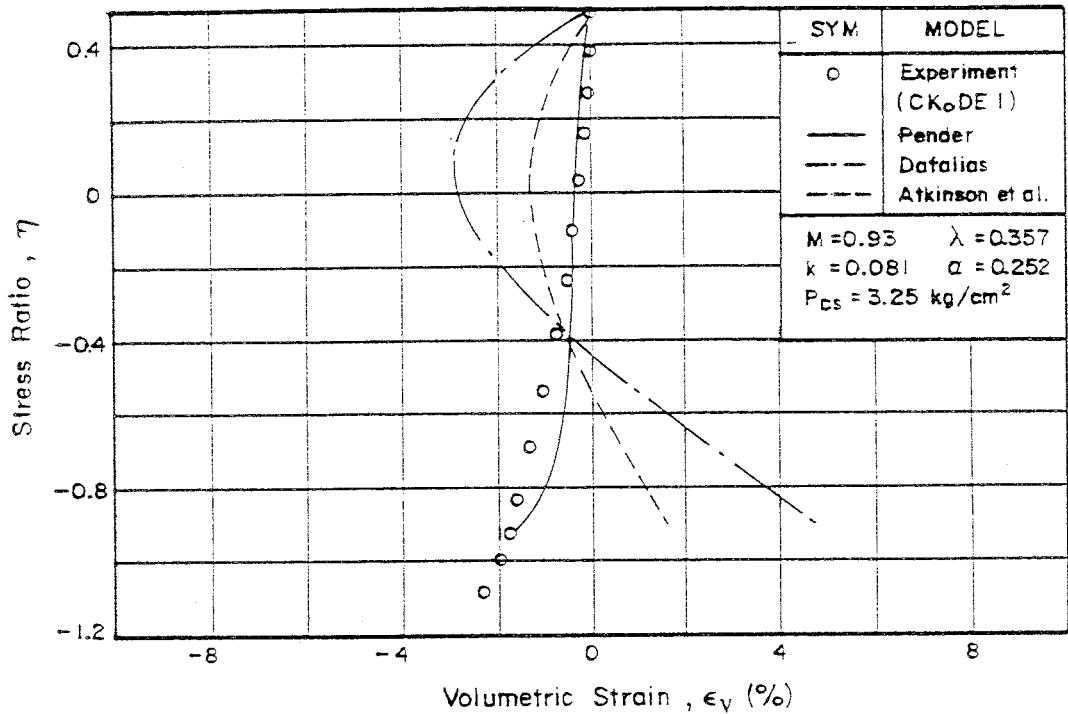


Fig. 7.45 (η, ϵ_v) Plot for CKoDE1 Sample Compared with the Model Predictions

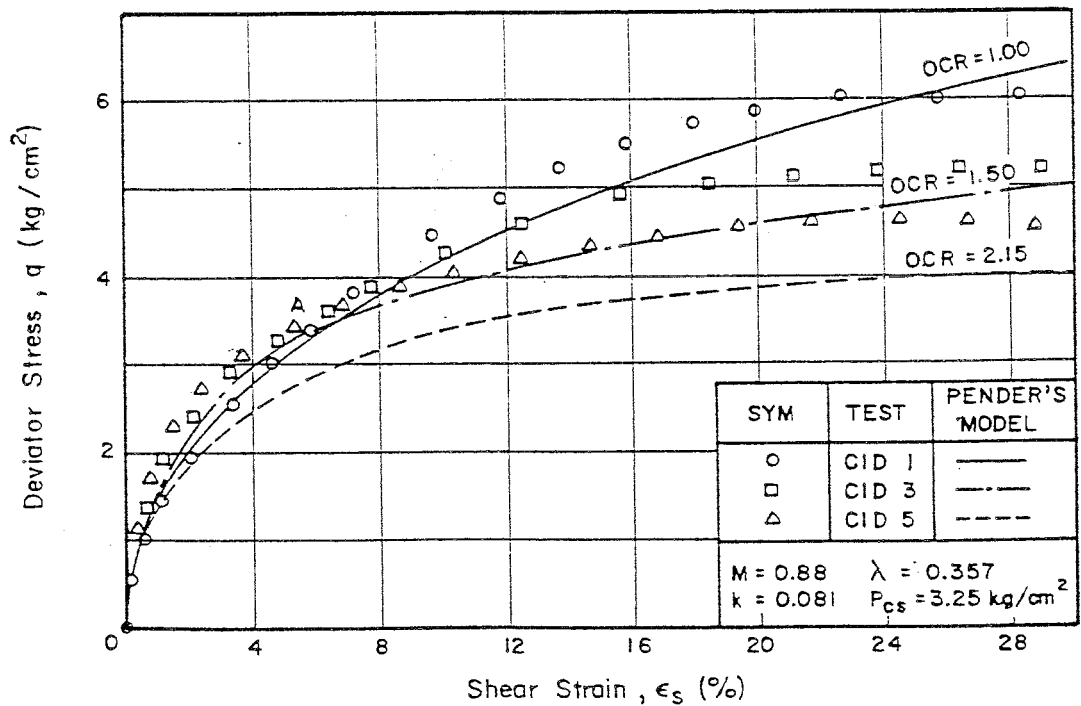


Fig. 7.46 (q, ϵ_s) Plot for Isotropically Overconsolidated Samples Compared with the Model Predictions

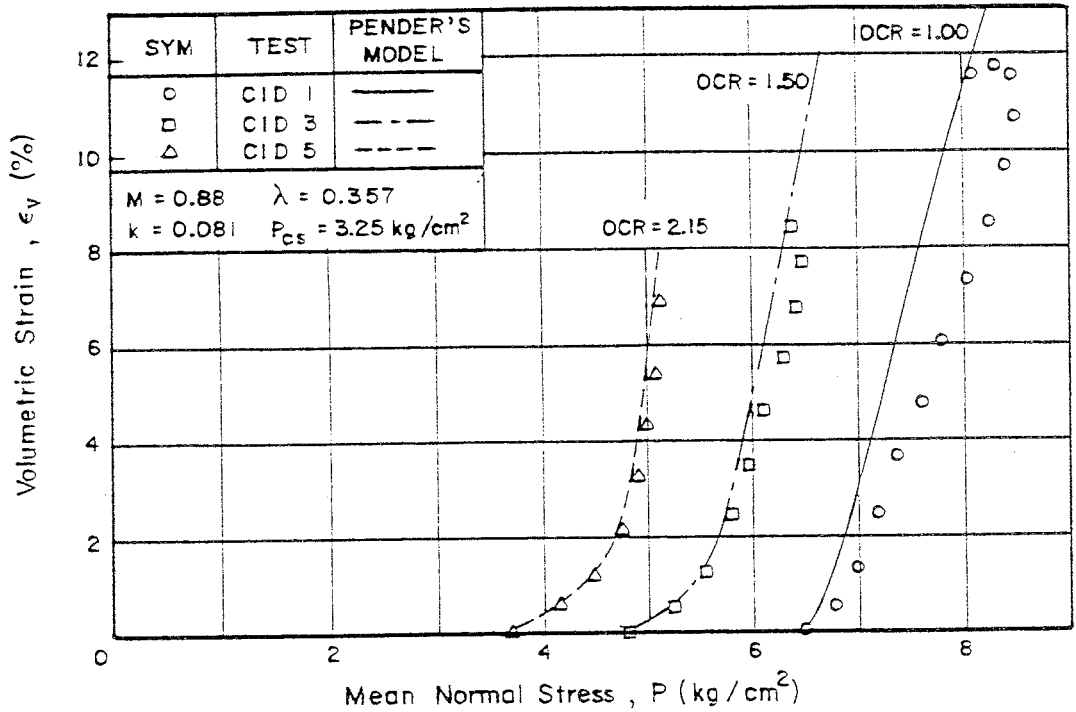


Fig. 7.47 (ϵ_v, p) Plot for Isotropically Overconsolidated Samples Compared with the Model Predictions

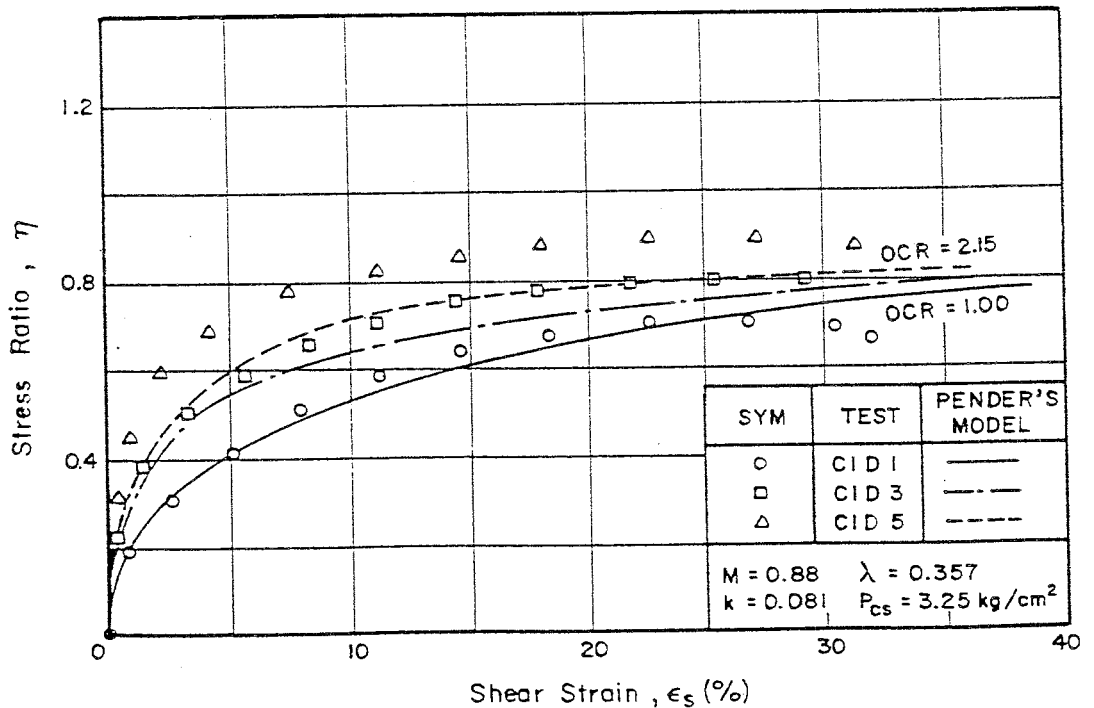


Fig. 7.48 (η, ϵ_s) Plot for Isotropically Overconsolidated Samples Compared with the Model Predictions

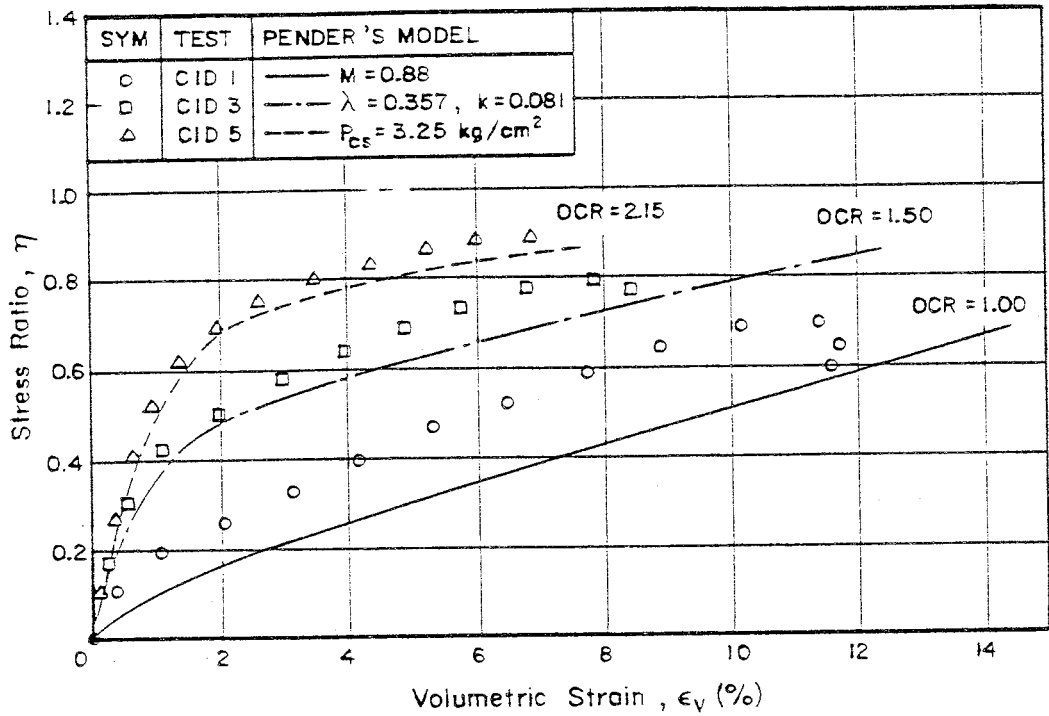


Fig. 7.49 (η, ϵ_v) Plot for Isotropically Overconsolidated Samples Compared with the Model Predictions

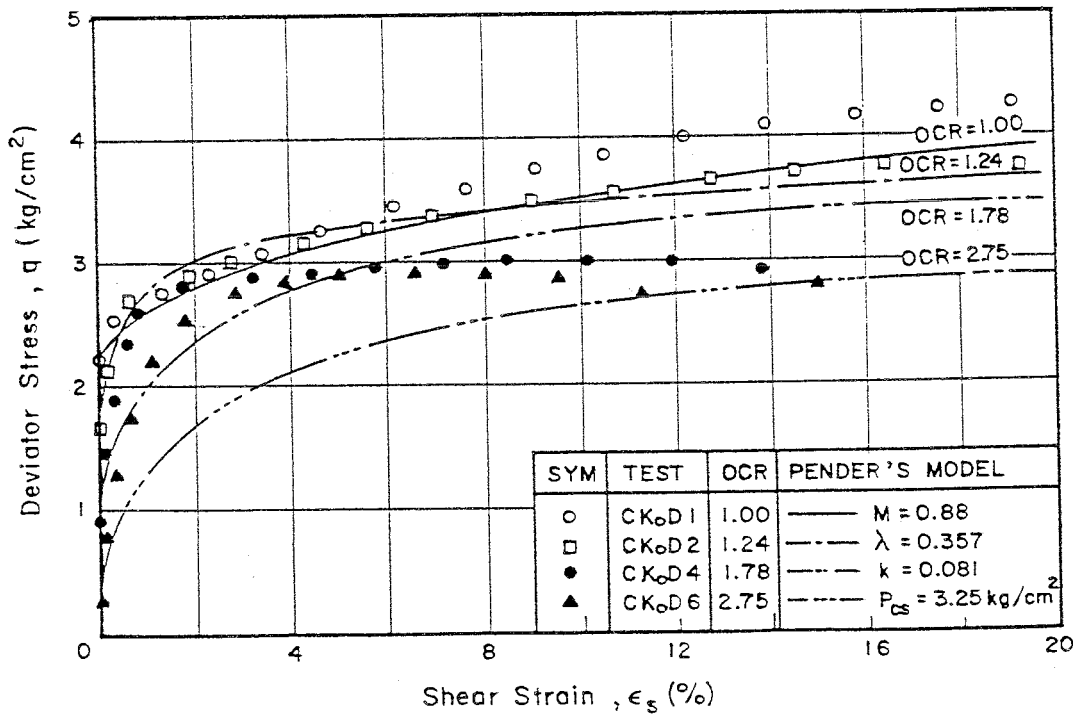


Fig. 7.50 (q, ϵ_s) Plot for CKoD Samples Compared with the Model Predictions

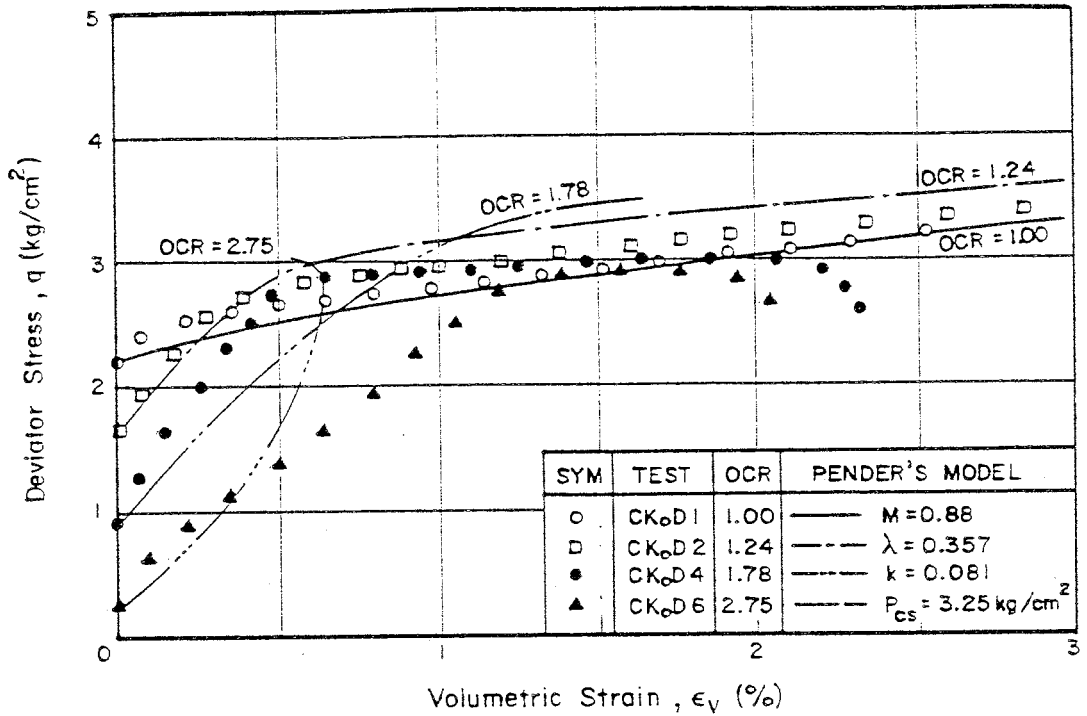


Fig. 7.51 (q, ϵ_v) Plot for CKoD Samples Compared with the Model Predictions

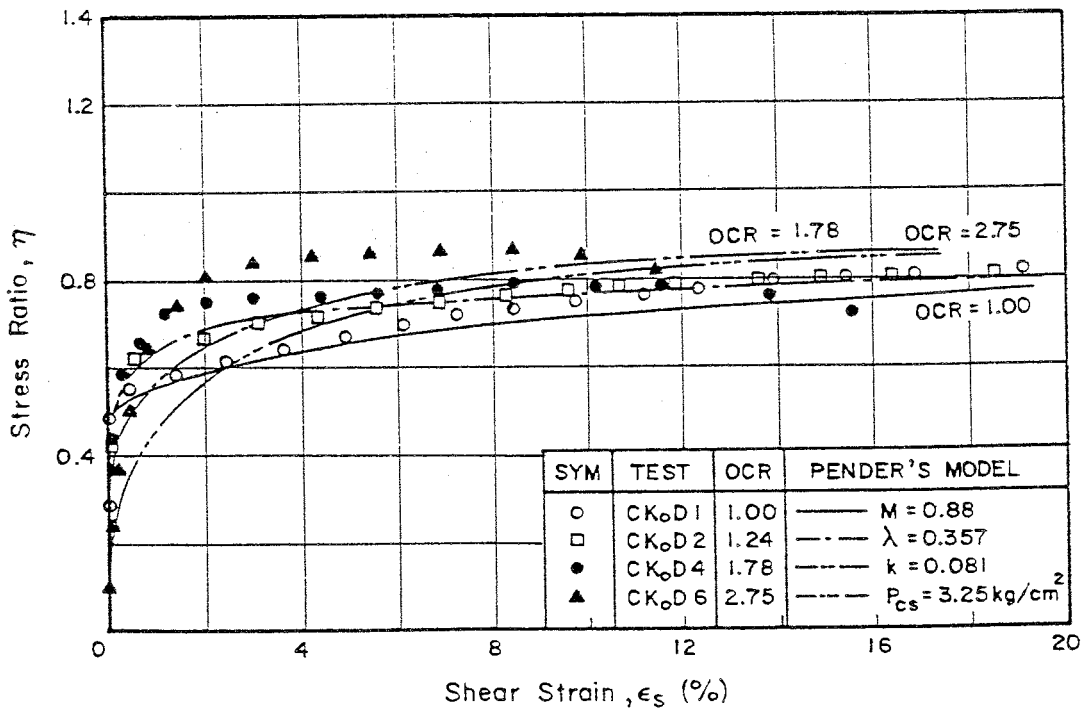


Fig. 7.52 (η, ϵ_s) Plot for CKoD Samples Compared with the Model Predictions

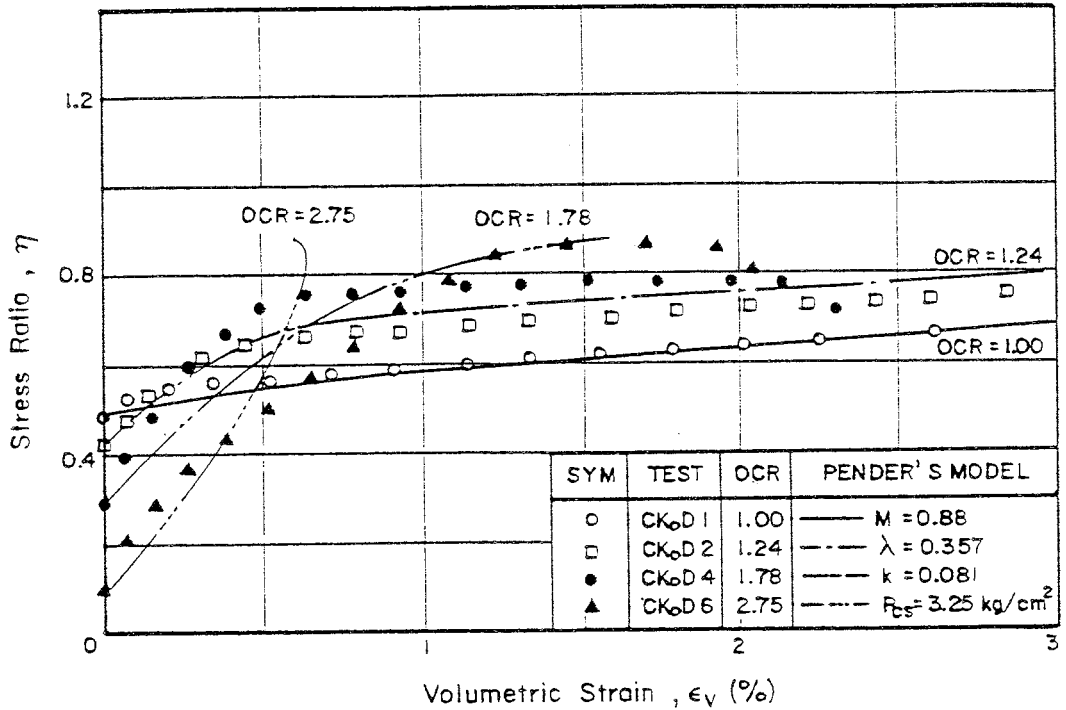


Fig. 7.53 (η, ϵ_v) Plot for CKoD Samples Compared with the Model Predictions

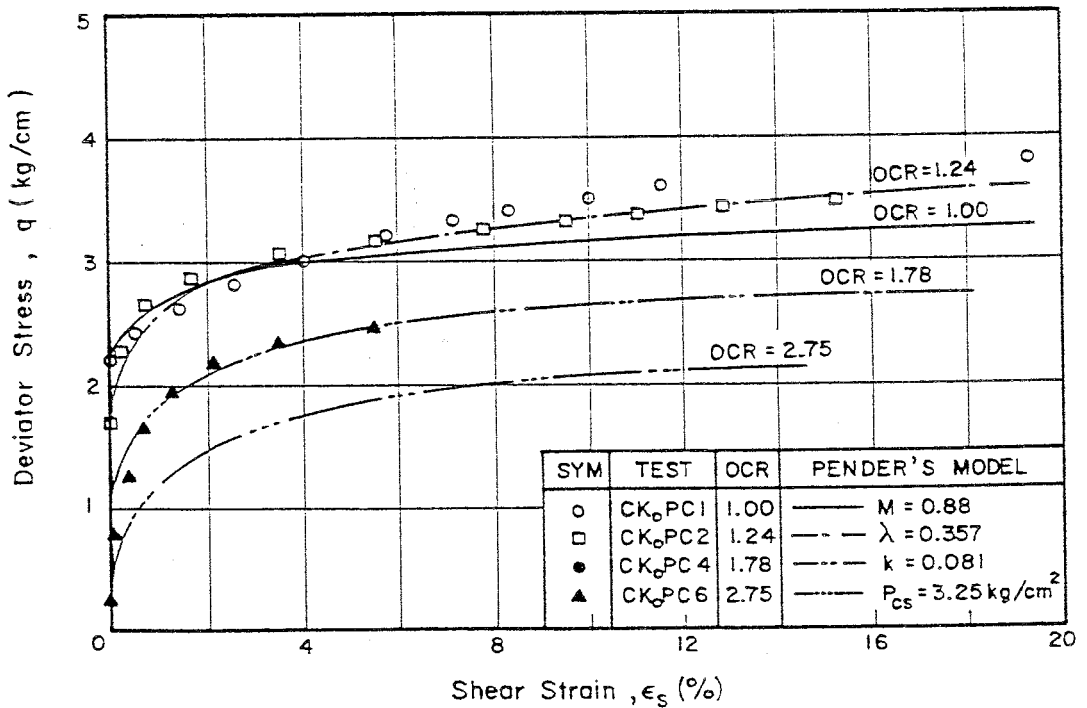


Fig. 7.54 (q, ϵ_s) Plot for CKoPC Samples Compared with the Model Predictions

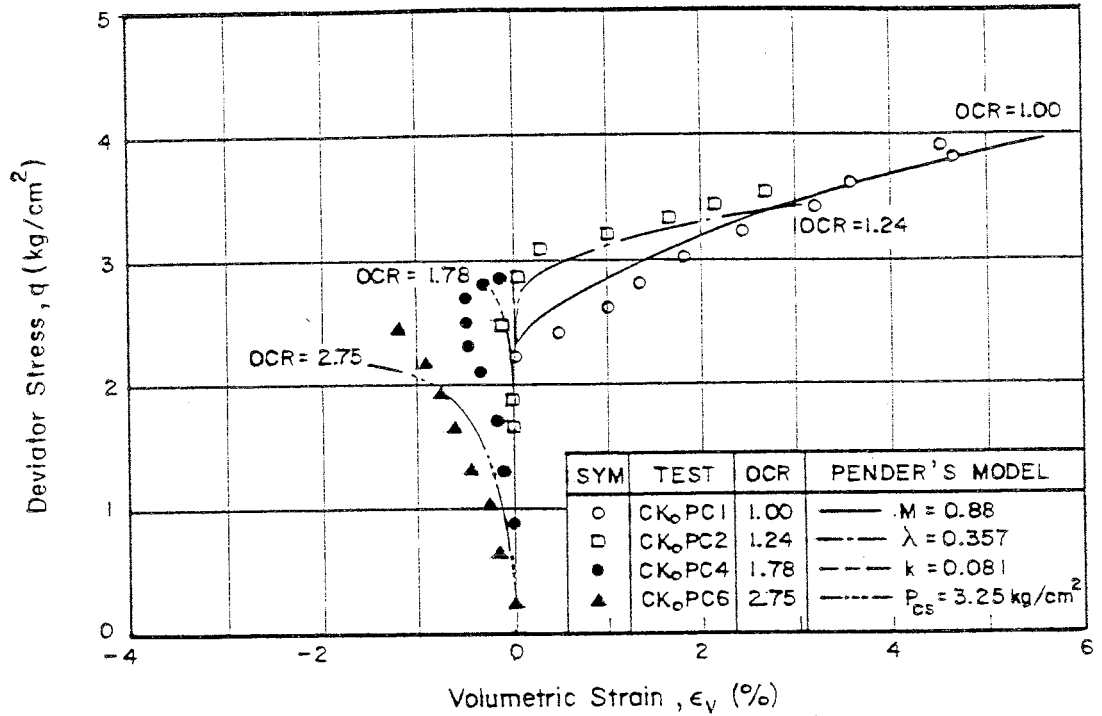


Fig. 7.55 (q, ϵ_v) Plot for CKoPC Samples Compared with the Model Predictions

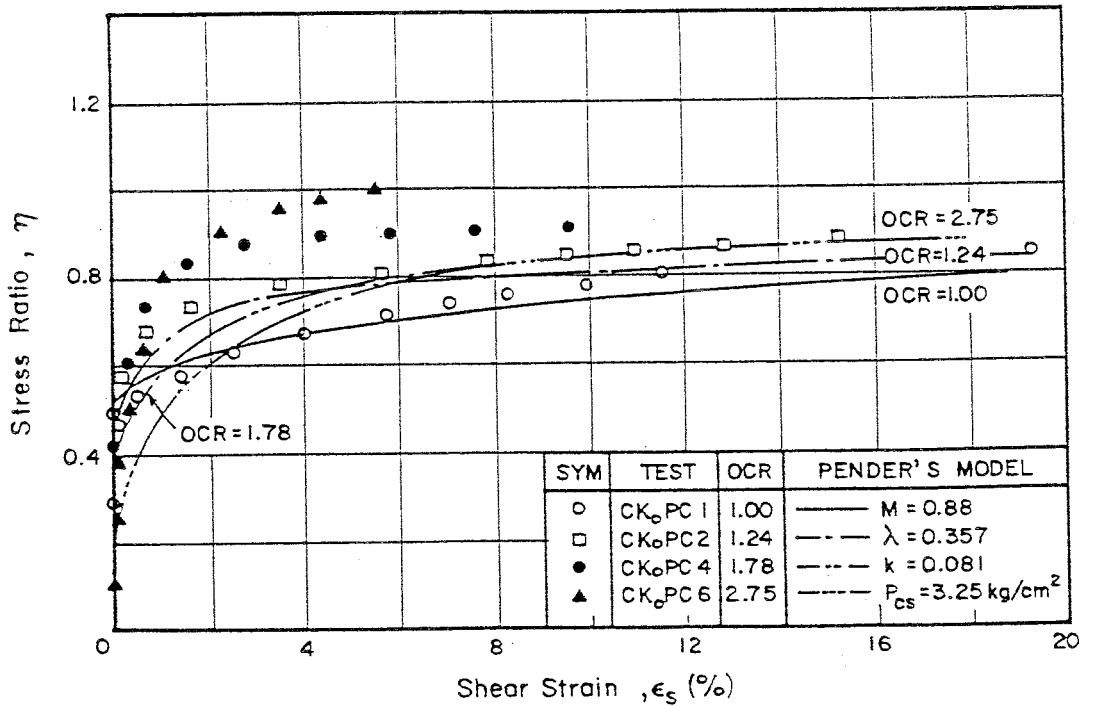


Fig. 7.56 (η, ϵ_s) Plot for CKoPC Samples Compared with the Model Predictions

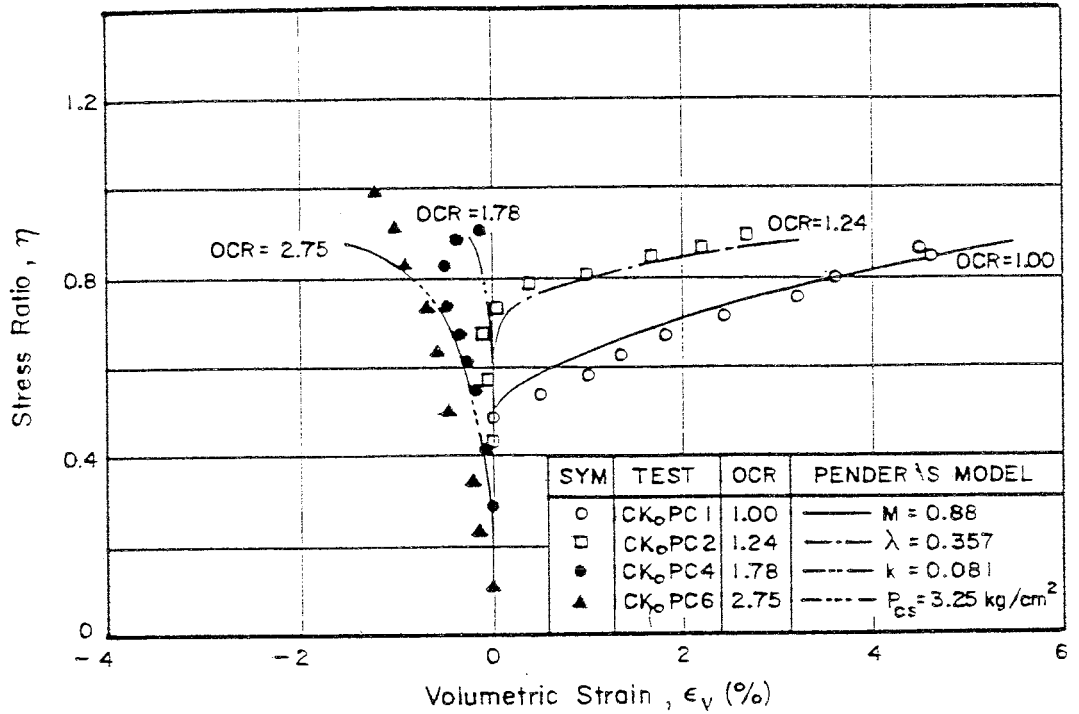


Fig. 7.57 (η , ϵ_v) Plot for CKoPC Samples Compared with the Model Predictions

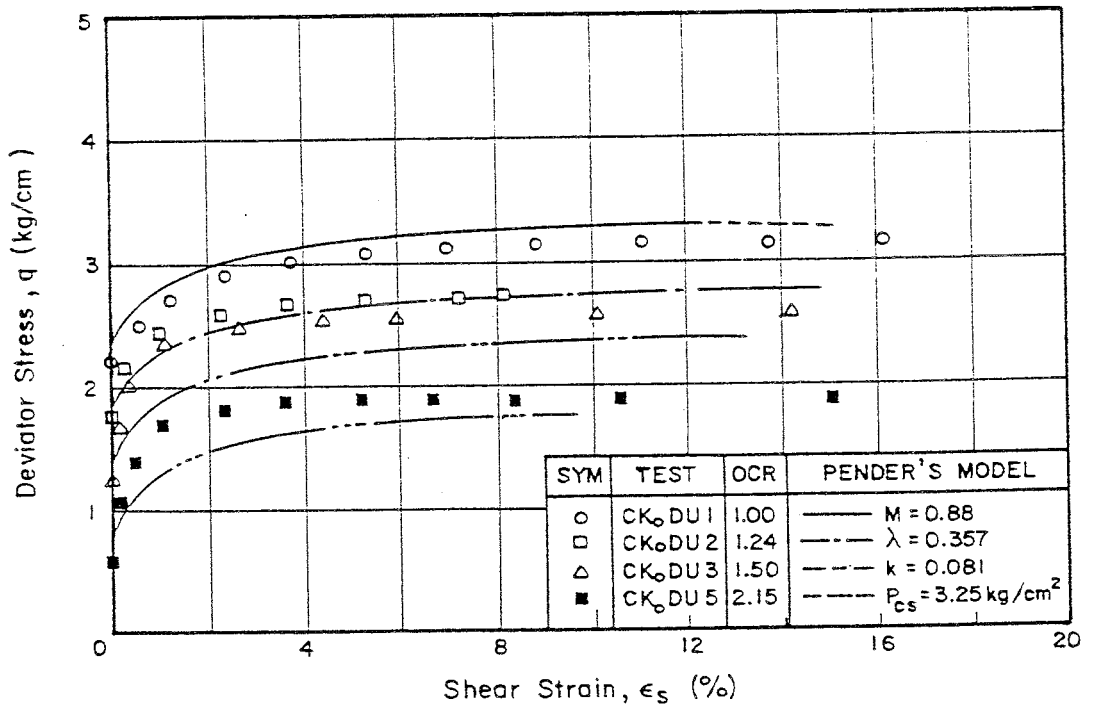


Fig. 7.58 (q , ϵ_s) Plot for CKoDU Samples Compared with the Model Predictions

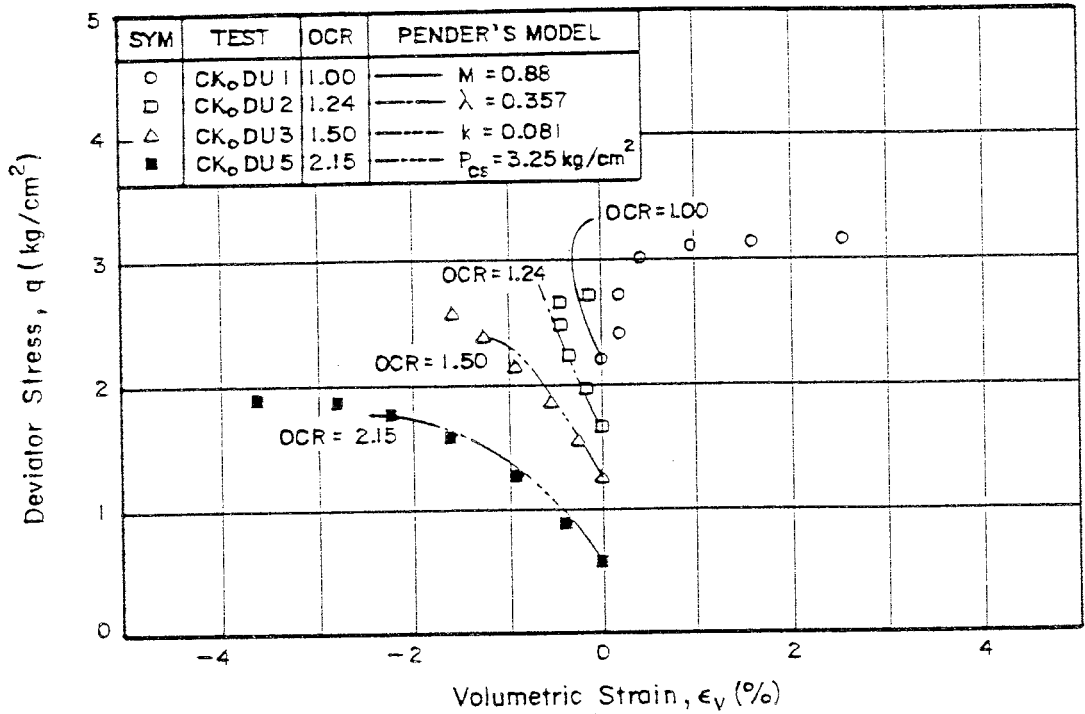


Fig. 7.59 (q, ϵ_v) Plot for CK_oDU Samples Compared with the Model Predictions

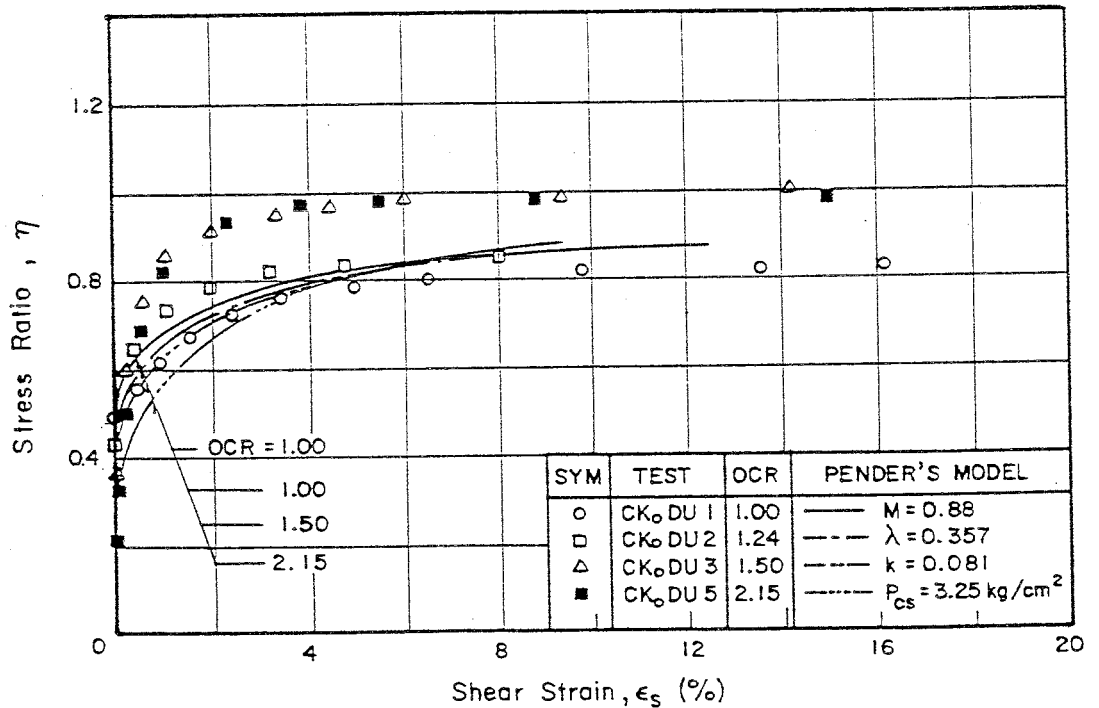


Fig. 7.60 (η, ϵ_s) Plot for CK_oDU Samples Compared with the Model Predictions

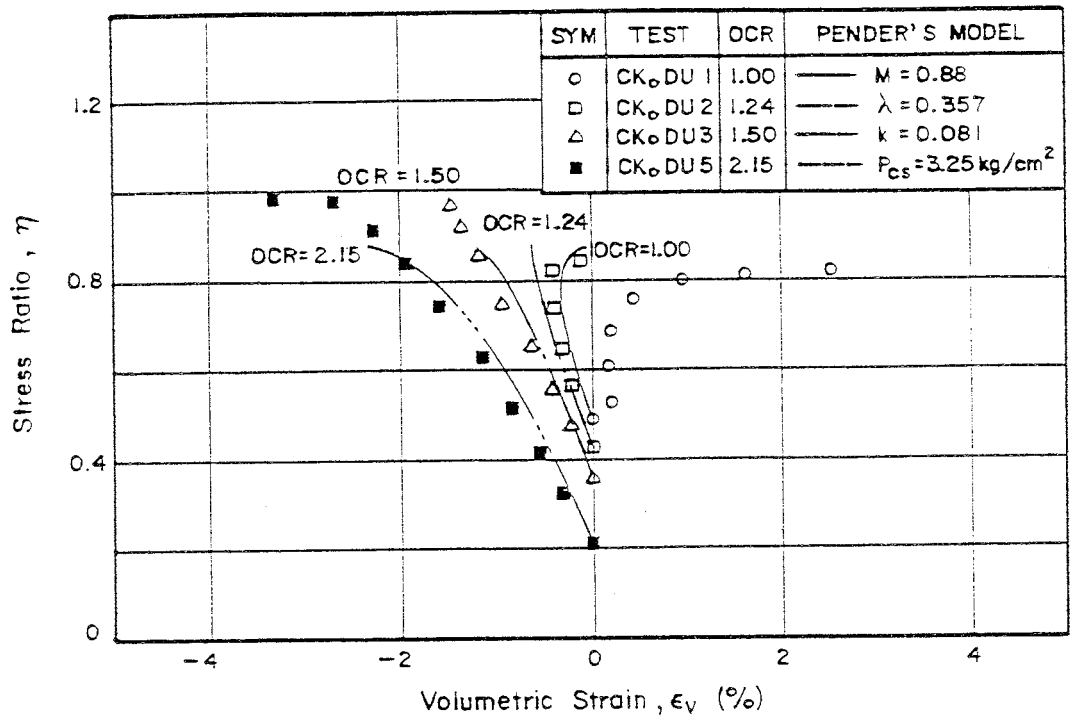


Fig. 7.61 (η, ϵ_v) Plot for CK_oDU Samples Compared with the Model Predictions

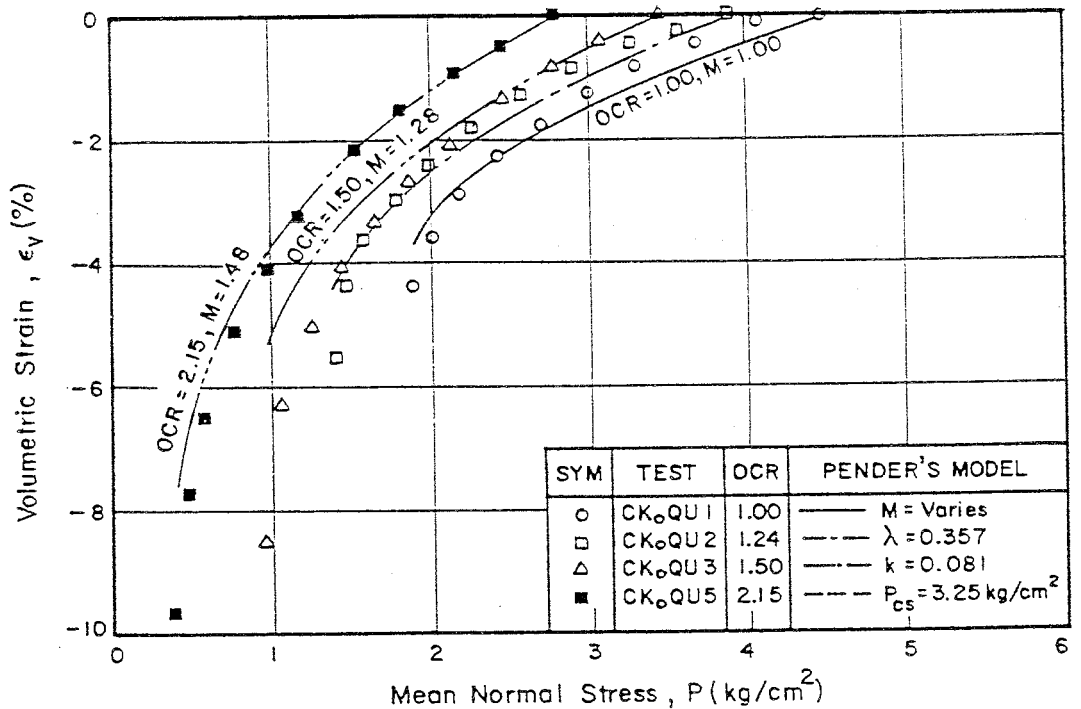


Fig. 7.62 (ϵ_v, p) Plot for CK_oQU Samples Compared with the Model Predictions

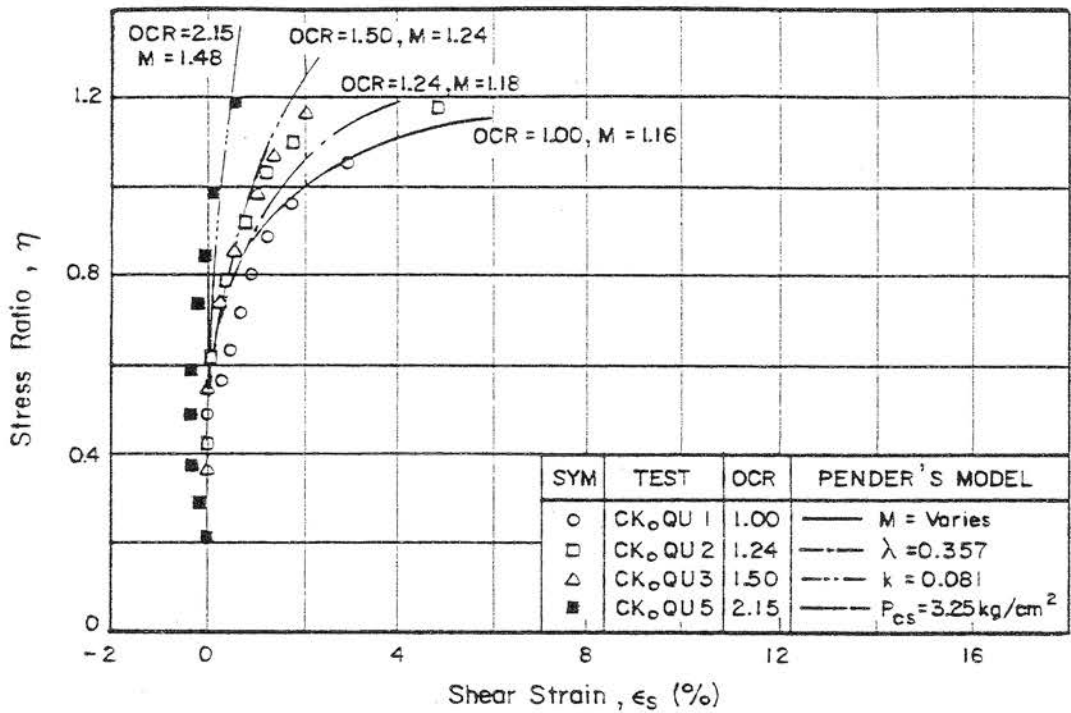


Fig. 7.63 (η, ϵ_s) Plot for CK_oQU Samples Compared with the Model Predictions

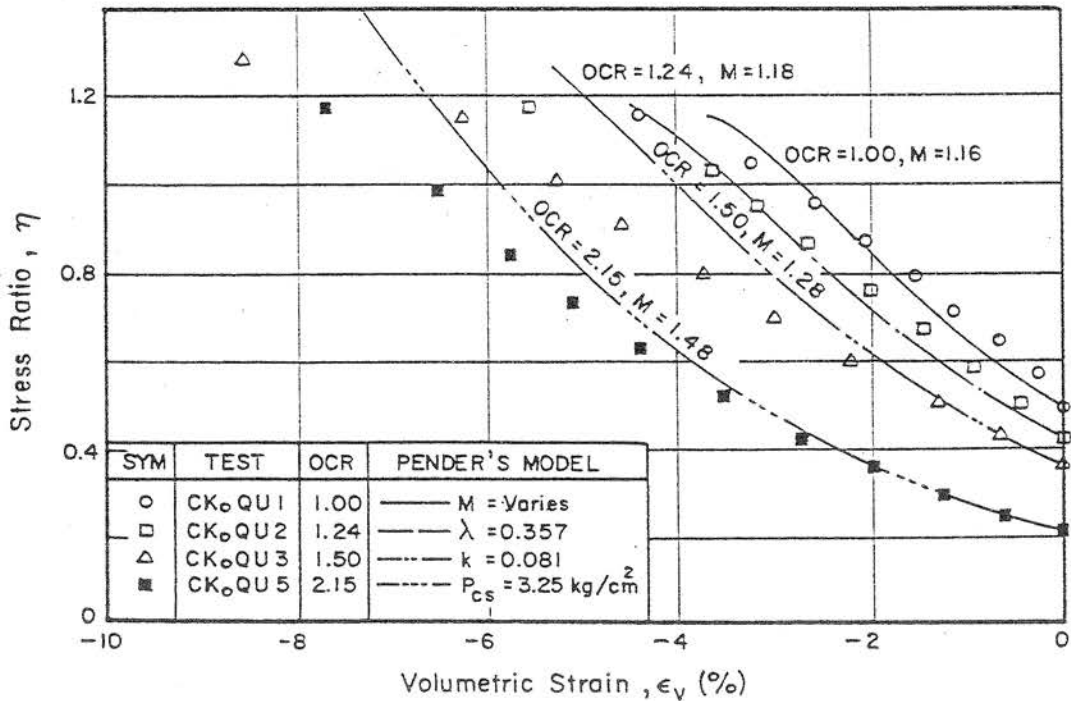


Fig. 7.64 (η, ϵ_v) Plot for CK_oQU Samples Compared with the Model Predictions

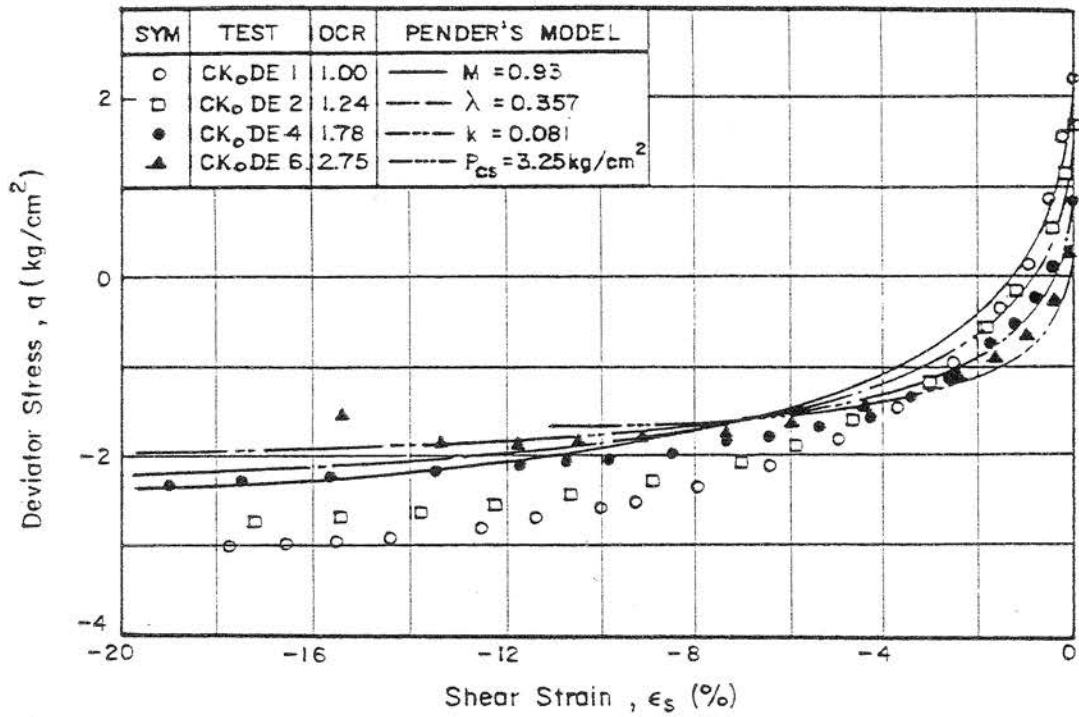


Fig. 7.65 (q, ϵ_s) Plot for CK_oDE Samples Compared with the Model Predictions

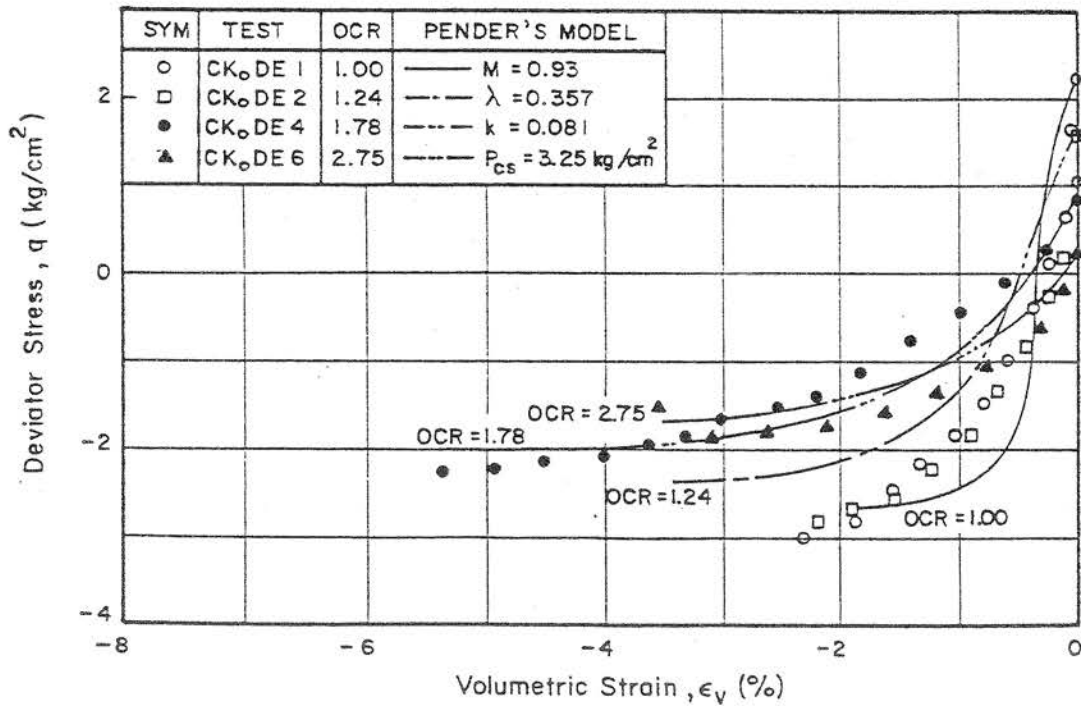


Fig. 7.66 (q, ϵ_v) Plot for CK_oDE Samples Compared with the Model Predictions

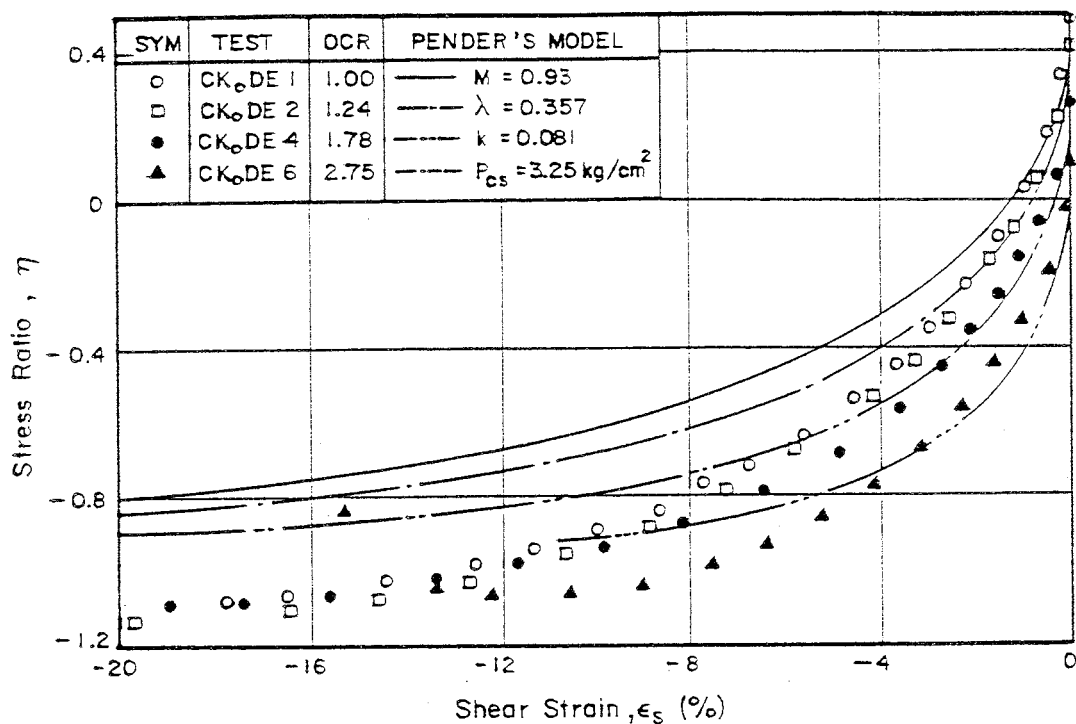


Fig. 7.67 (η, ϵ_s) Plot for CK_oDE Samples Compared with the Model Predictions

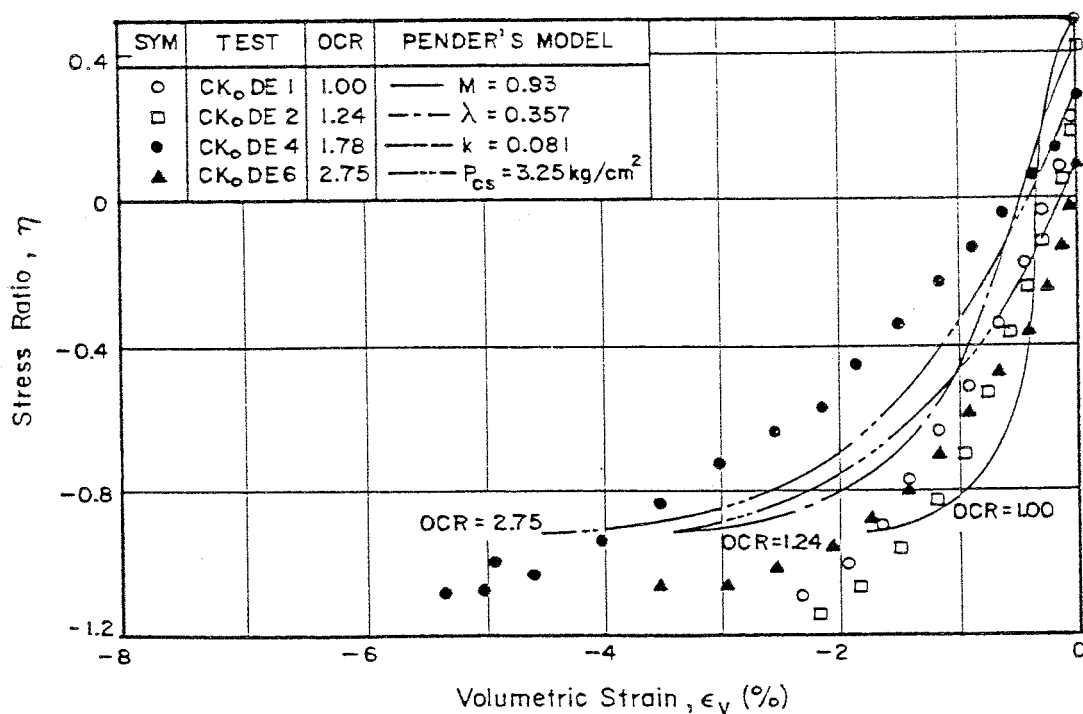


Fig. 7.68 (η, ϵ_v) Plot for CK_oDE Samples Compared with the Model Predictions

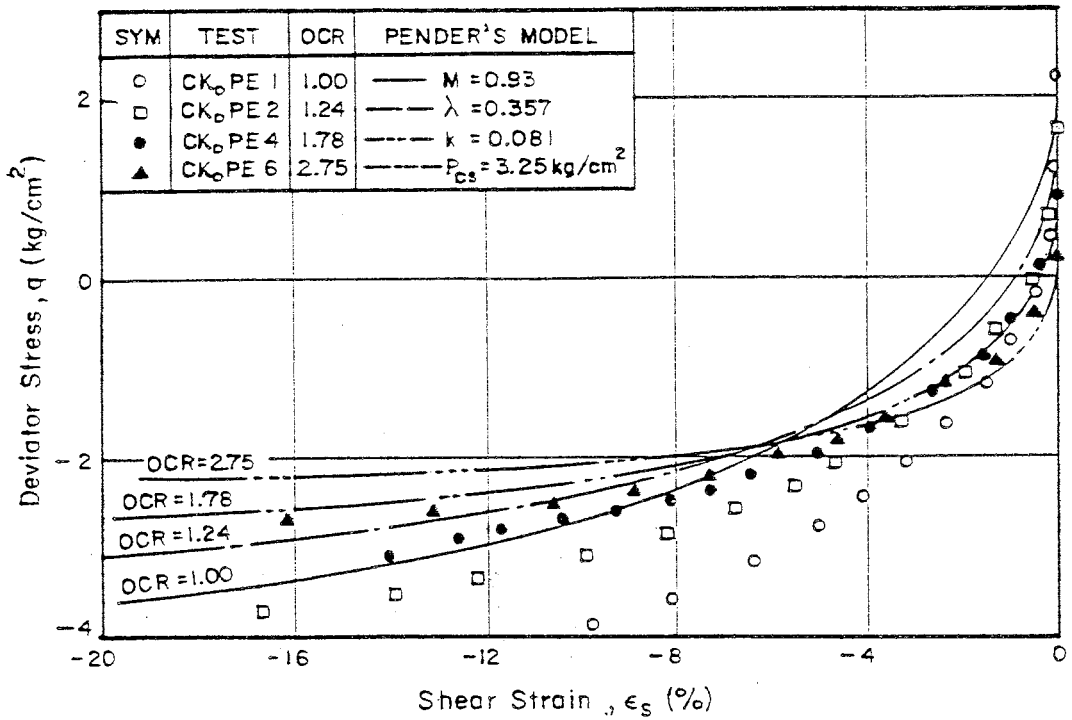


Fig. 7.69 (q, ϵ_s) Plot for CK₀PE Samples Compared with the Model Predictions

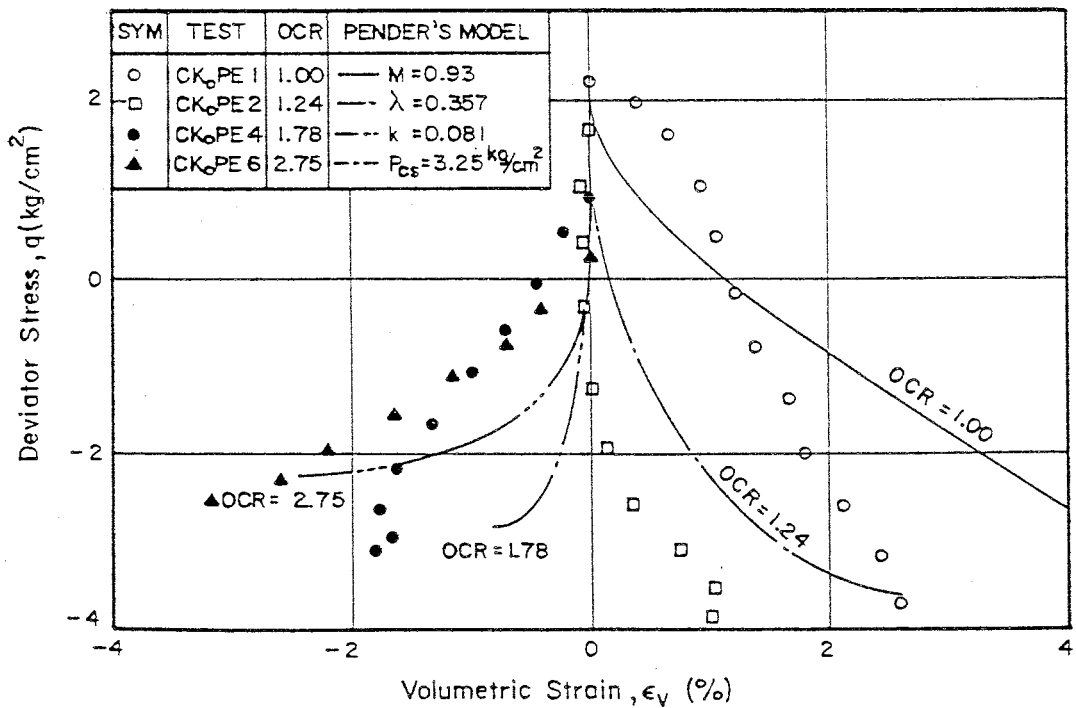


Fig. 7.70 (q, ϵ_v) Plot for CK₀PE Samples Compared with the Model Predictions

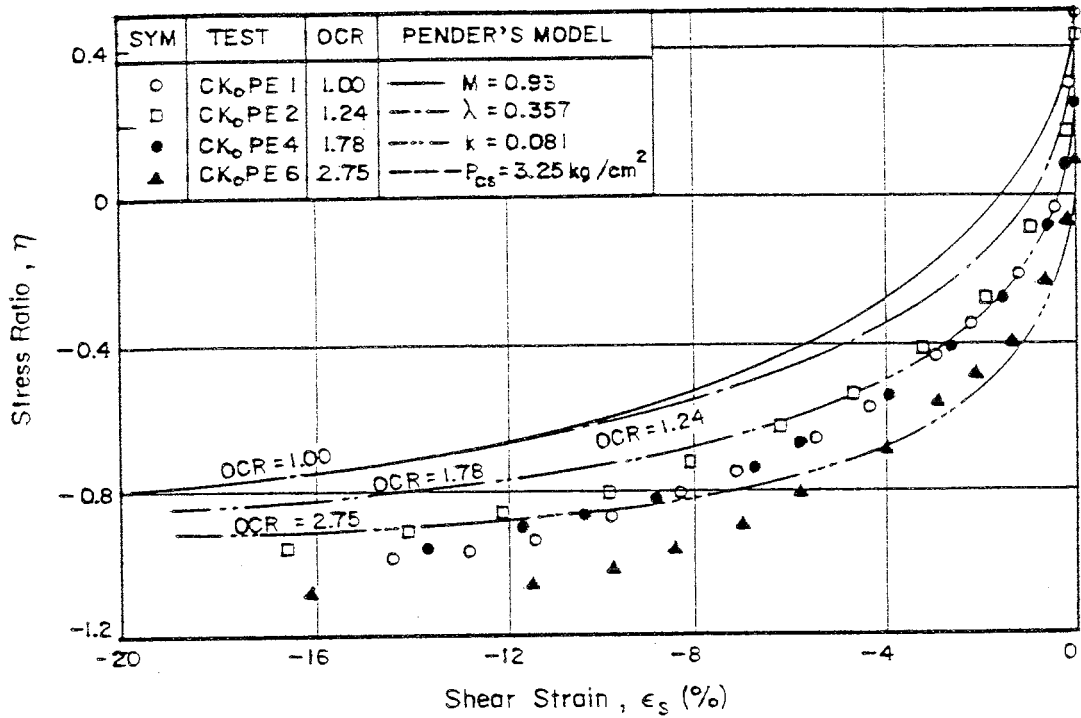


Fig. 7.71 (η, ϵ_s) Plot for CKoPE Samples Compared with the Model Predictions

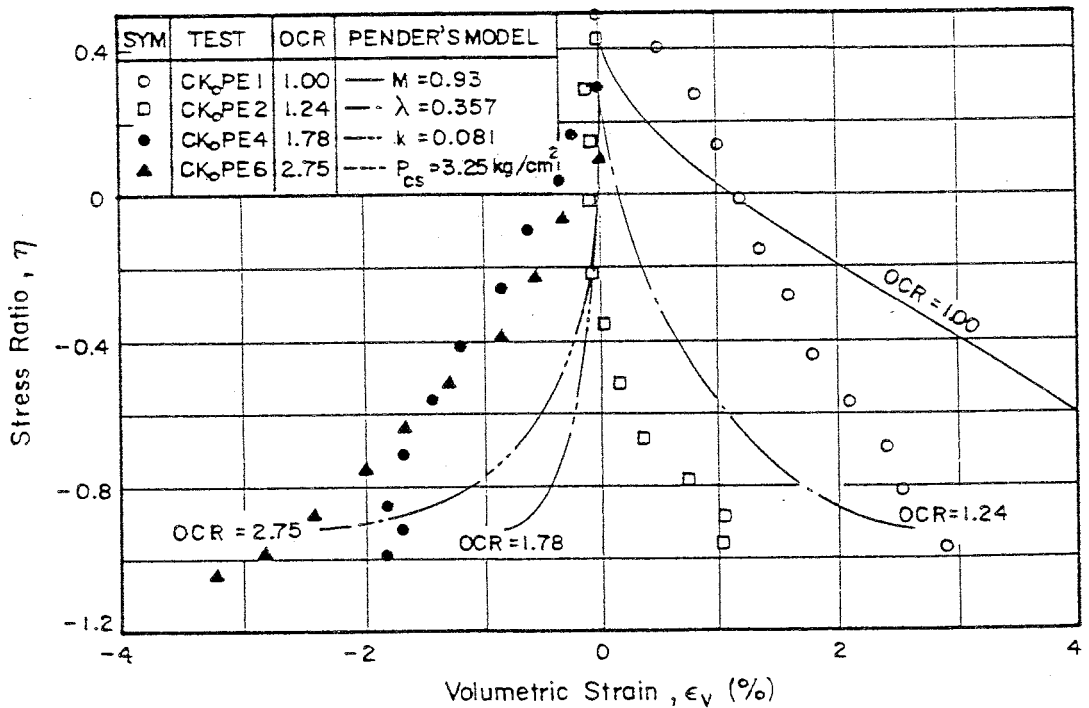


Fig. 7.72 (η, ϵ_v) Plot for CKoPE Samples Compared with the Model Predictions

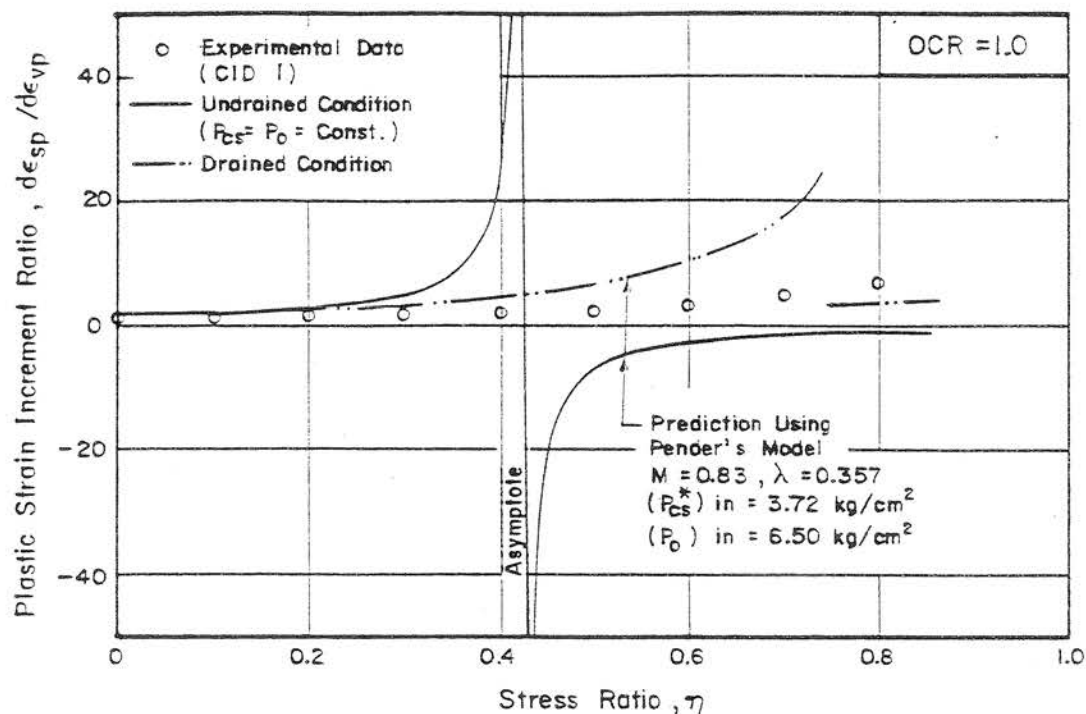


Fig. 7.73 Variations of the $(d\epsilon_{sp}/d\epsilon_{vp})$ along the CID1 Path Compared with the Predictions from Pender's Model (Wet Zone)

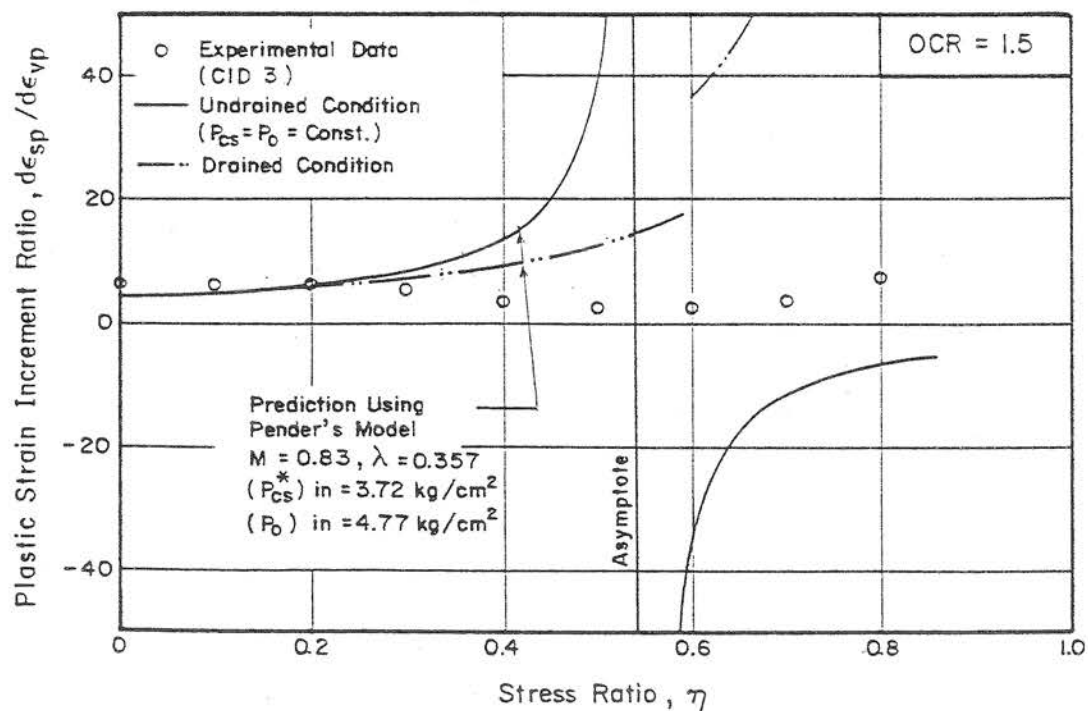


Fig. 7.74 Variations of the $(d\epsilon_{sp}/d\epsilon_{vp})$ along the CID3 Path Compared with the Predictions from Pender's Model (Wet Zone)

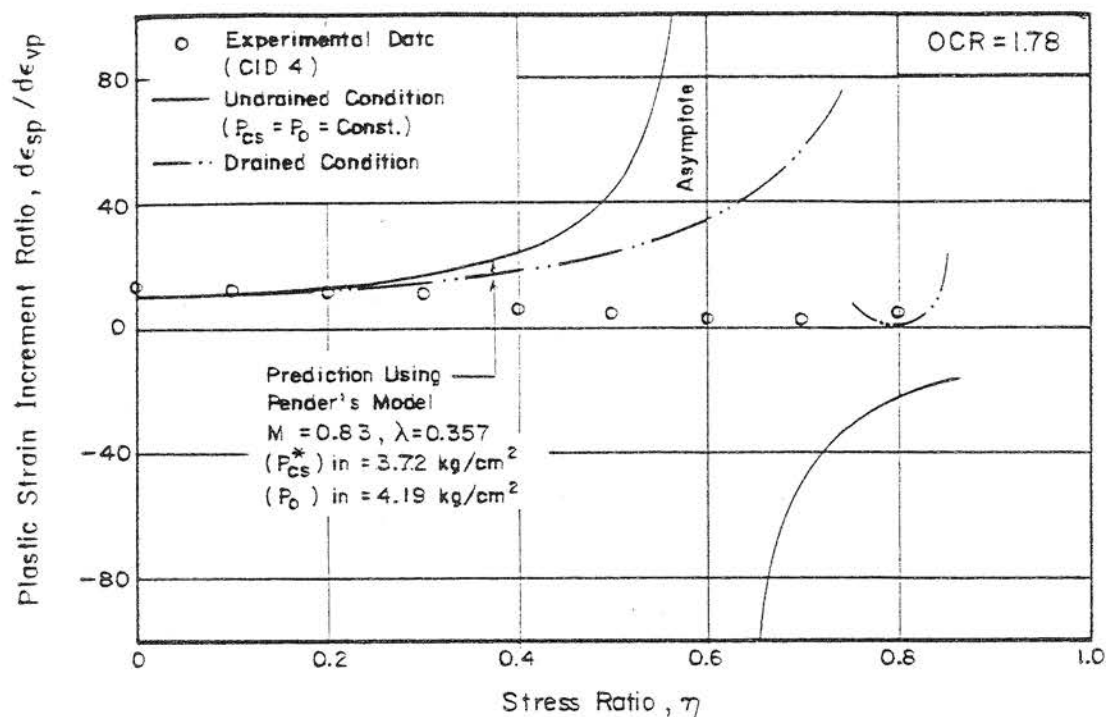


Fig. 7.75 Variations of the $(d\epsilon_{sp}/d\epsilon_{vp})$ along the CID4 Path Compared with the Predictions from Pender's Model (Dry Zone)

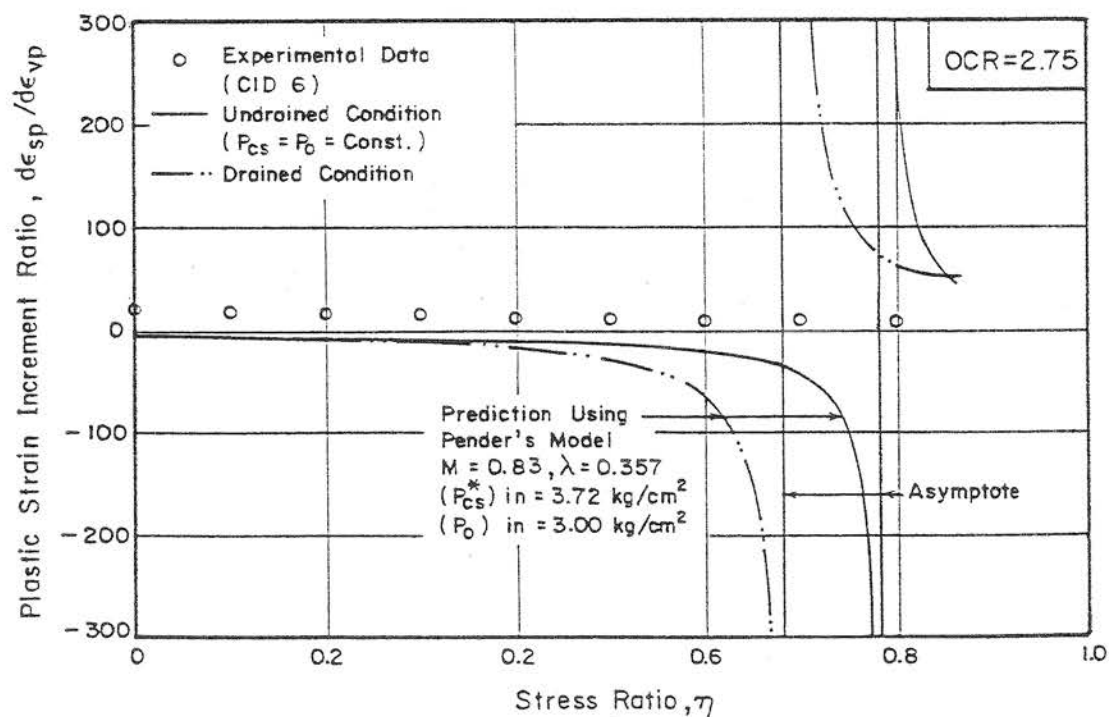


Fig. 7.76 Variations of the $(d\epsilon_{sp}/d\epsilon_{vp})$ along the CID6 Path Compared with the Predictions from Pender's Model (Dry Zone)

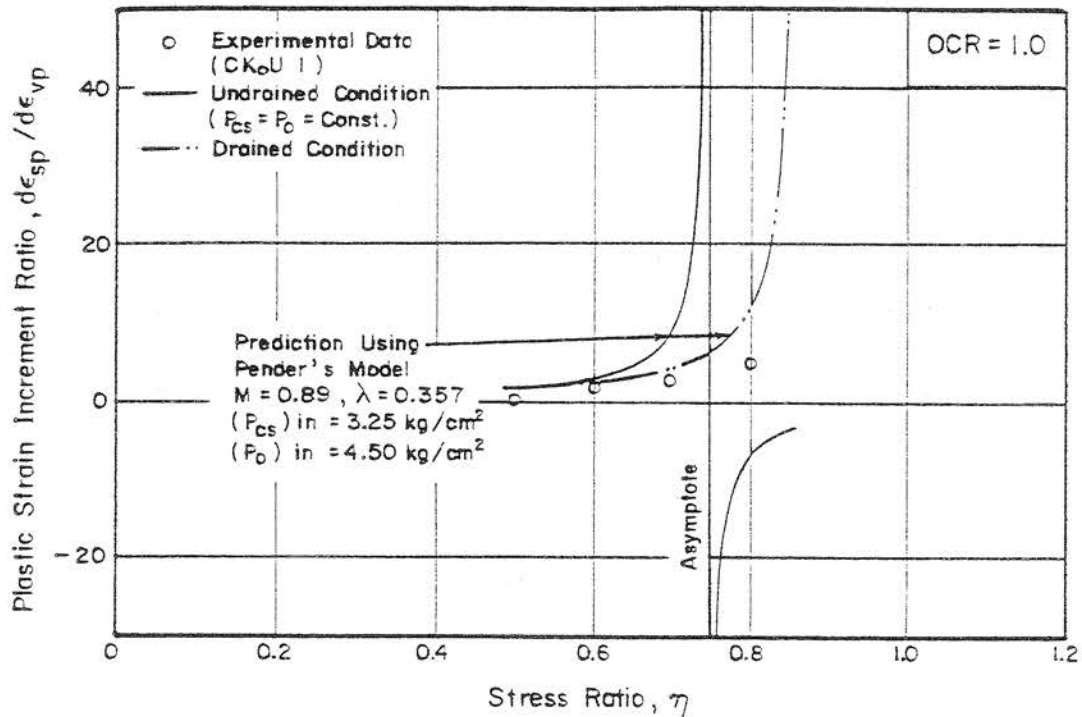


Fig. 7.77 Variations of the $(d\epsilon_{sp}/d\epsilon_{vp})$ along the CKoD1 Path Compared with the Predictions from Pender's Model (Wet Zone)

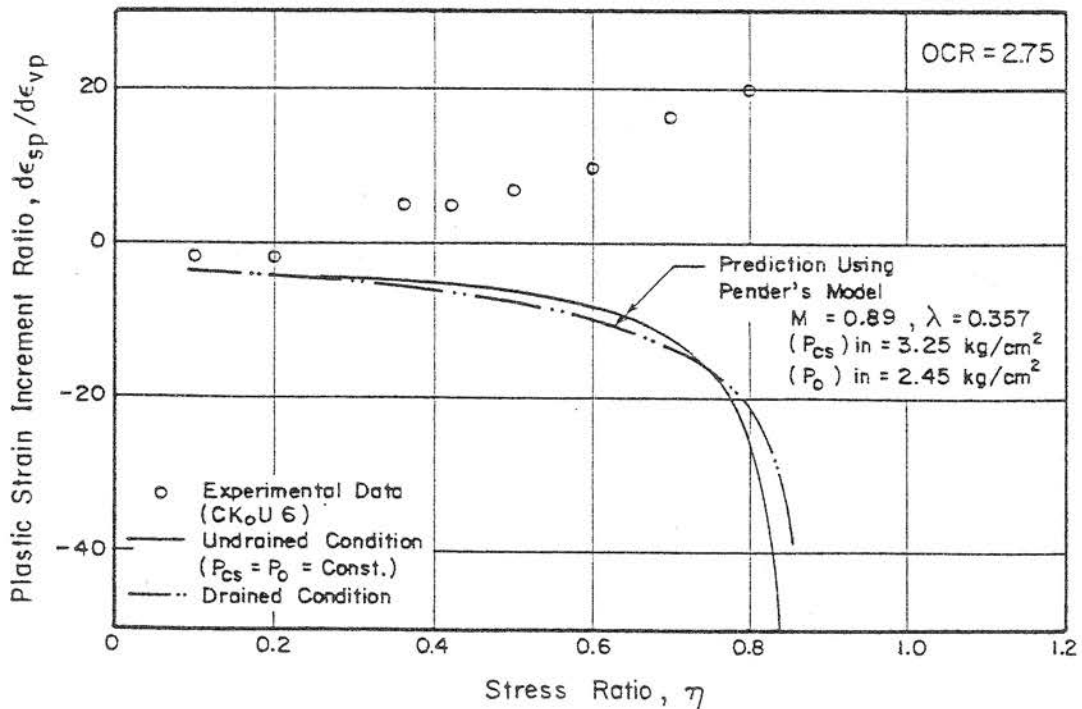


Fig. 7.78 Variations of the $(d\epsilon_{sp}/d\epsilon_{vp})$ along the CKoD6 Path Compared with the Predictions from Pender's Model (Dry Zone)

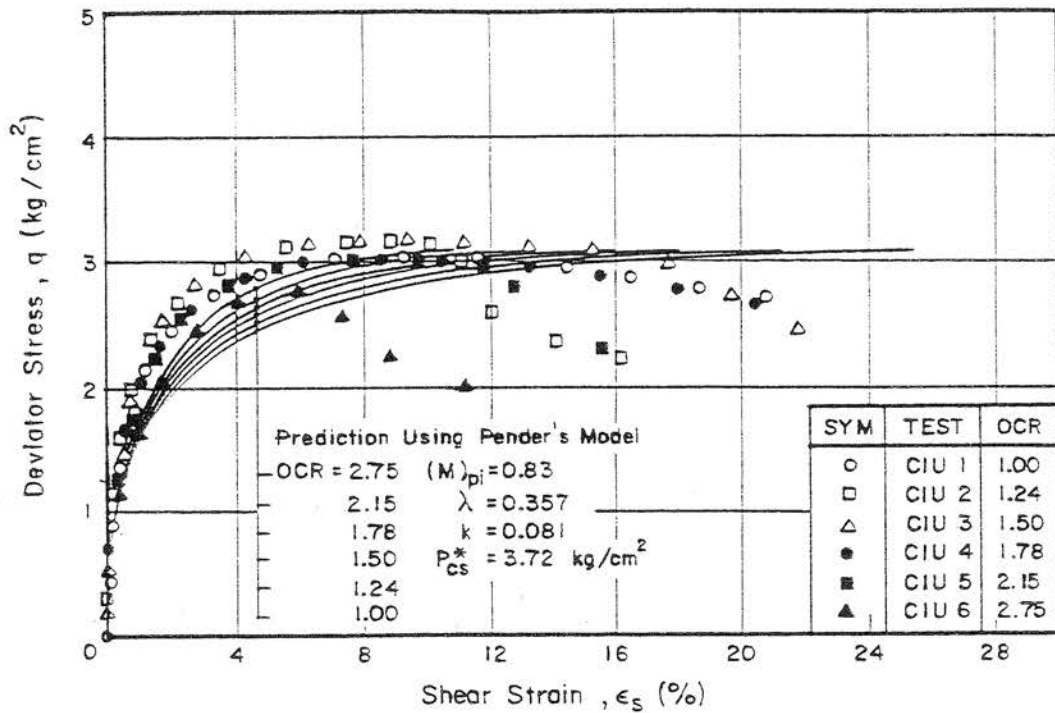


Fig. 7.79 (q, ϵ_s) Plot for Isotropically Overconsolidated Samples Compared with the Predictions from Pender's Model with Some Modifications

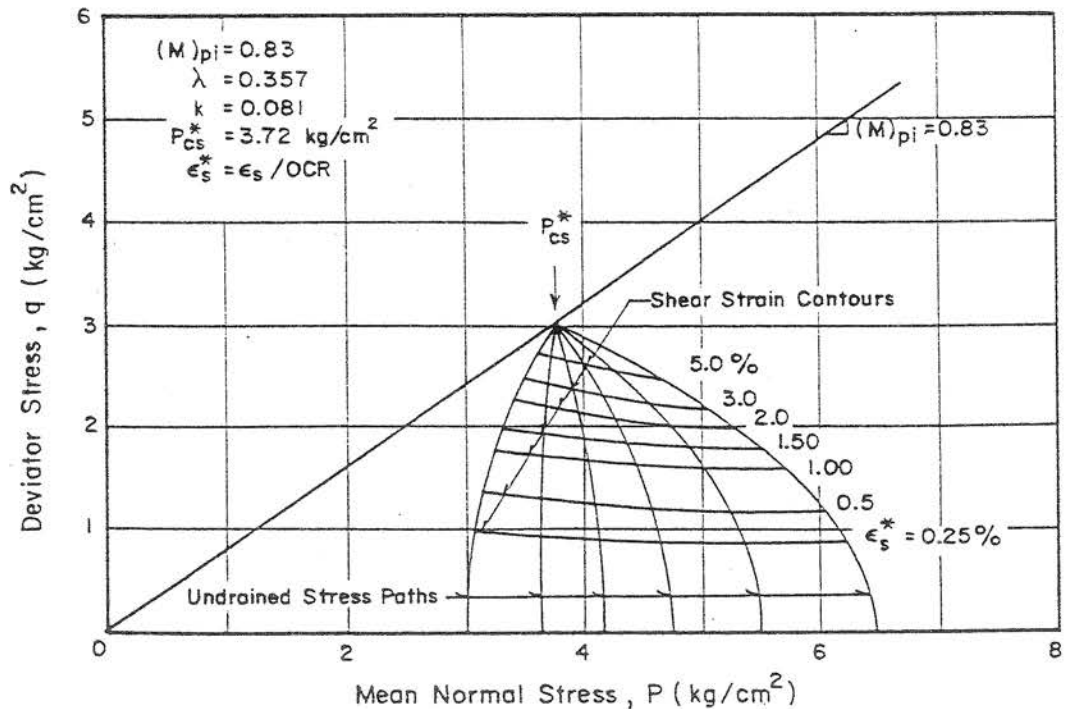


Fig. 7.80 Shear Strain Contours and Undrained Stress Paths for the Isotropically Overconsolidated Samples Predicted from Pender's Model with some Modifications

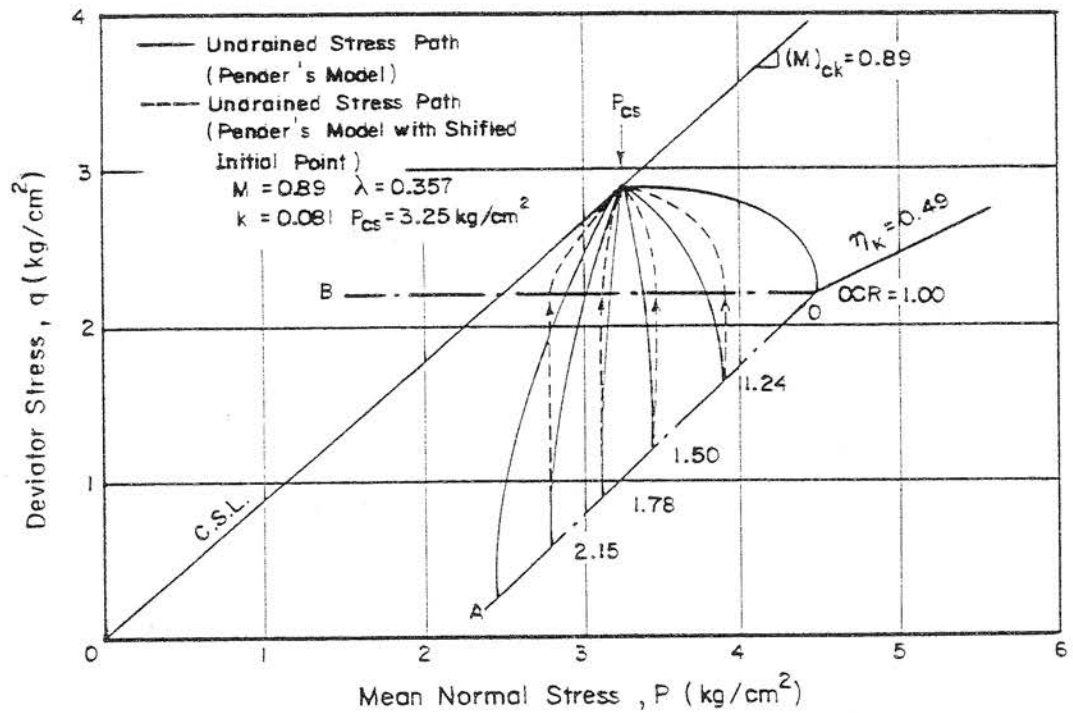


Fig. 7.81 (q, p) Plot from Pender's Model with and without Shifted Initial Stress Points

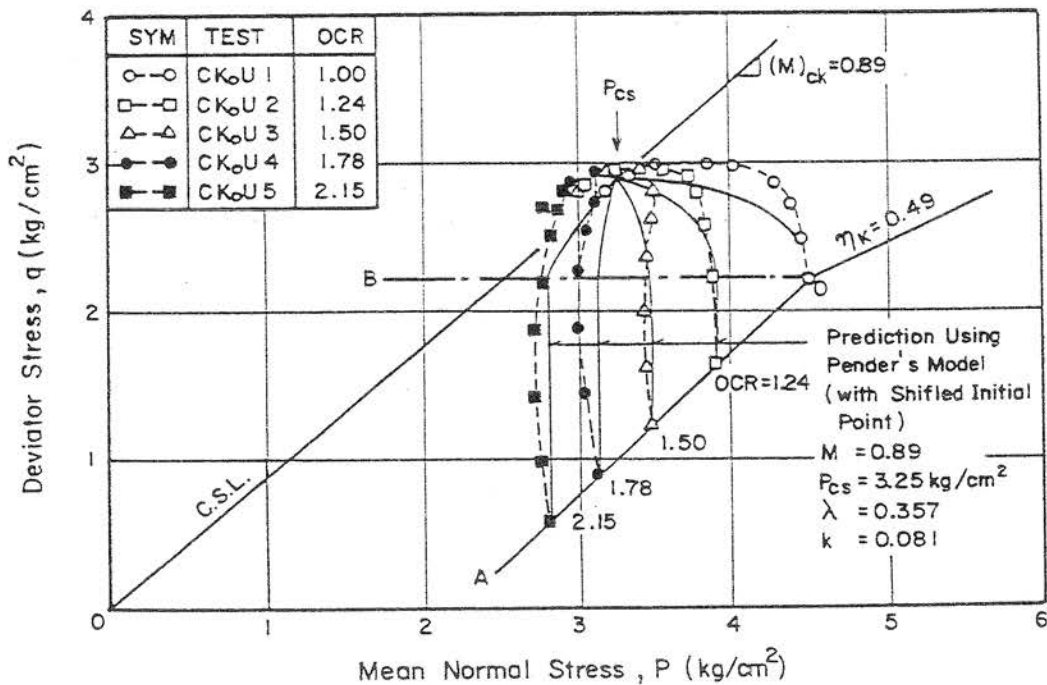


Fig. 7.82 (q, p) Plot for K_o -overconsolidated Samples Compared with the Predictions from Pender's Model with Shifted Initial Stress Points

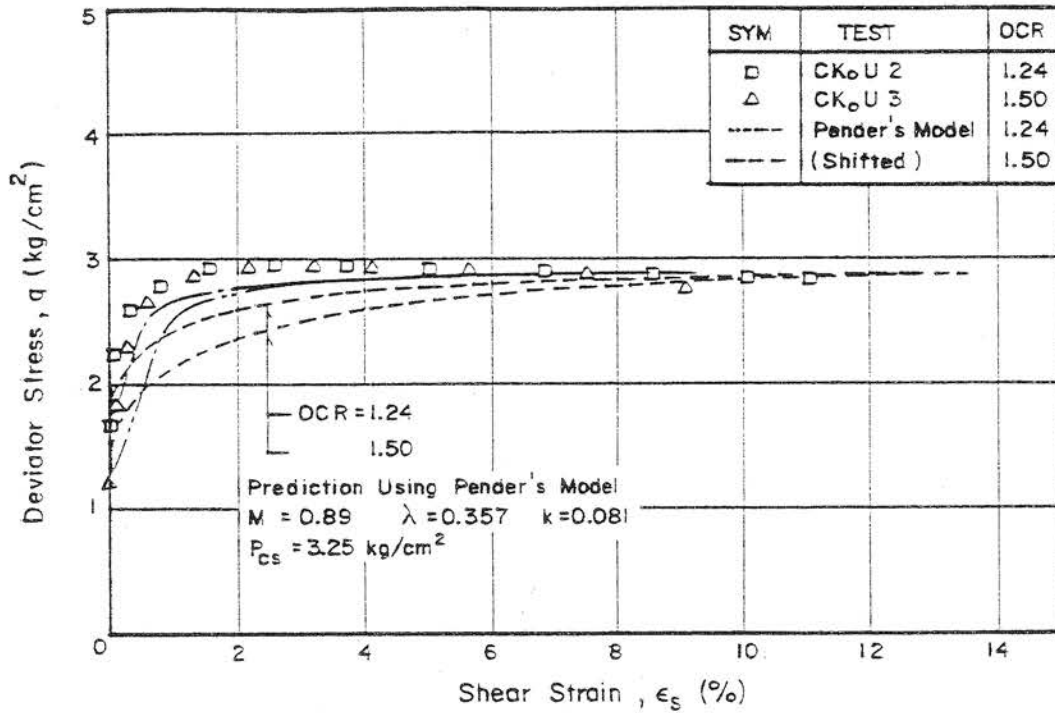


Fig. 7.83 (q , ϵ_s) Plot for K_o -overconsolidated Samples Compared with the Predictions from Pender's Model with and without Shifted Initial Stress Points (Wet Zone)

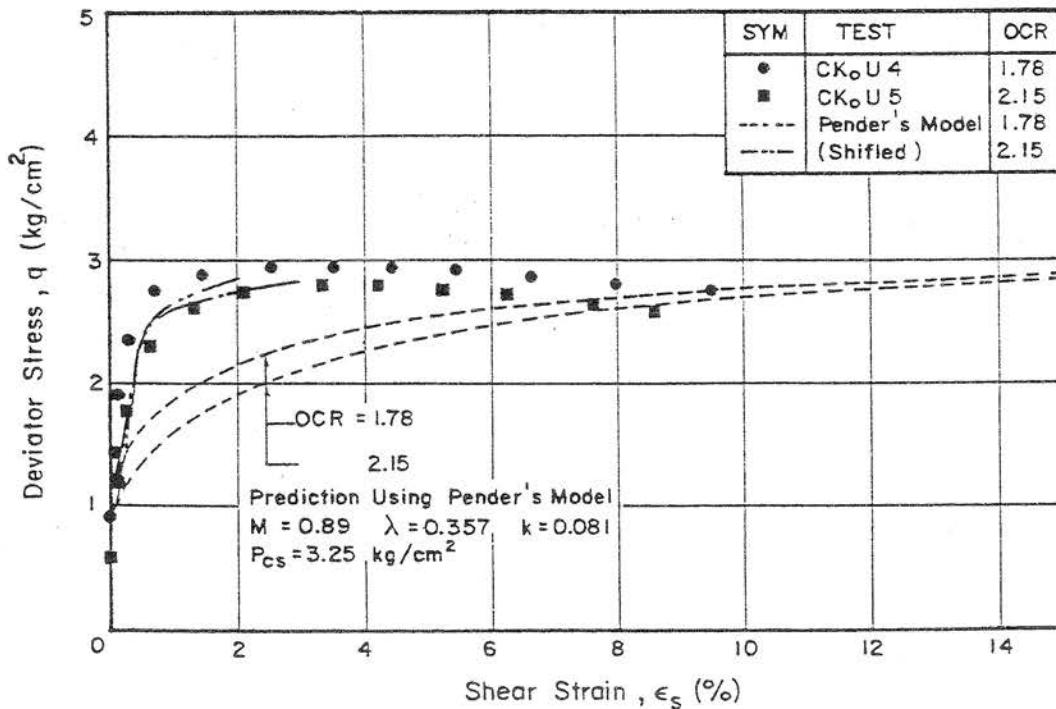


Fig. 7.84 (q , ϵ_s) Plot for K_o -overconsolidated Samples Compared with the Predictions from Pender's Model with and without Shifted Initial Stress Points (Dry Zone)

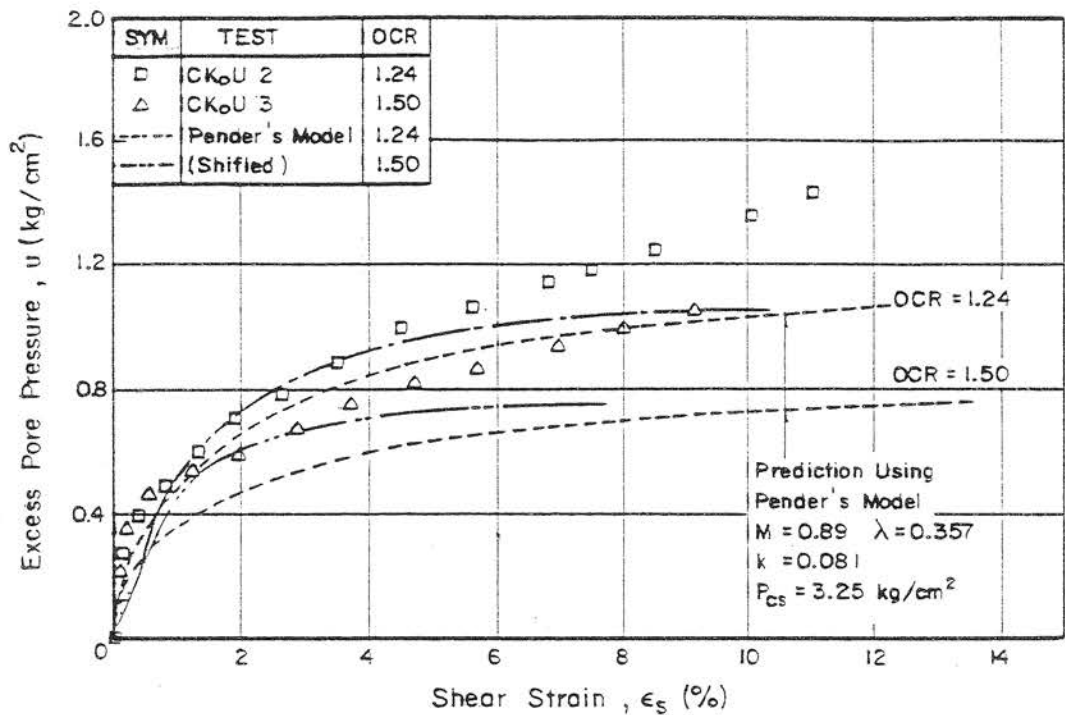


Fig. 7.85 (u, ϵ_s) Plot for K_0 -overconsolidated Samples Compared with the Predictions from Pender's Model with and without Shifted Initial Stress Points (Wet Zone)

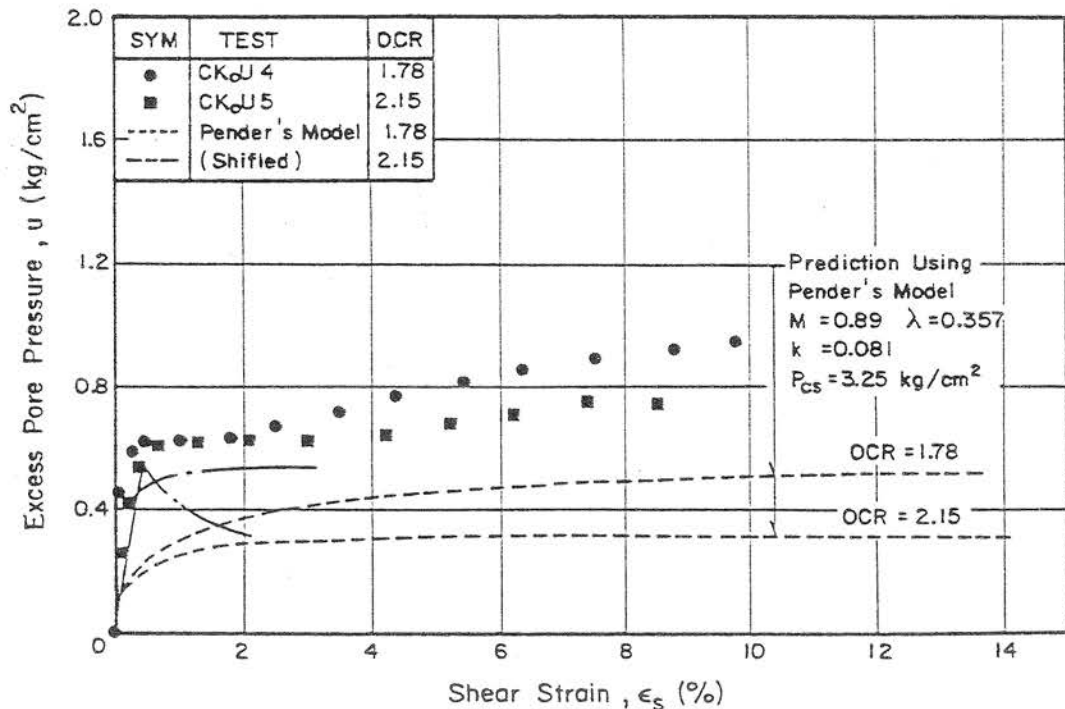


Fig. 7.86 (u, ϵ_s) Plot for K_0 -overconsolidated Samples Compared with the Predictions from Pender's Model with and without Shifted Initial Stress Points (Dry Zone)

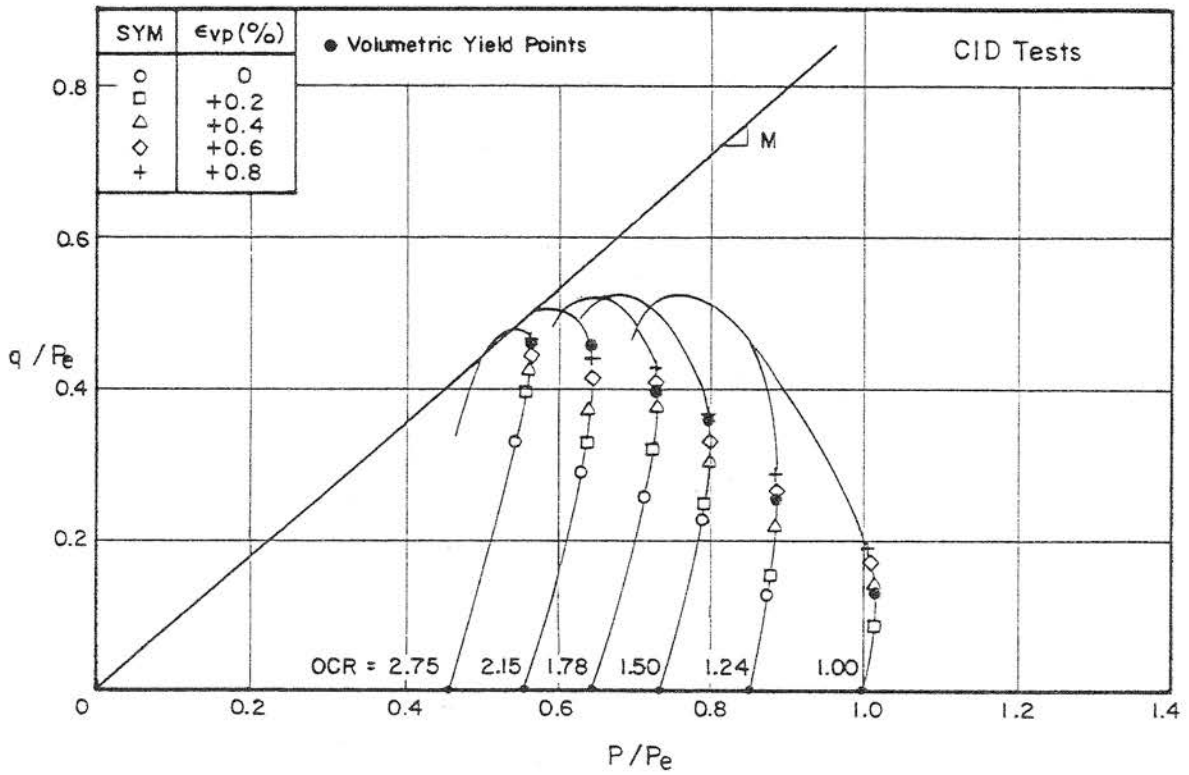


Fig. 8.1a Plastic Volumetric Strains within the State Boundary Surface from CID Tests

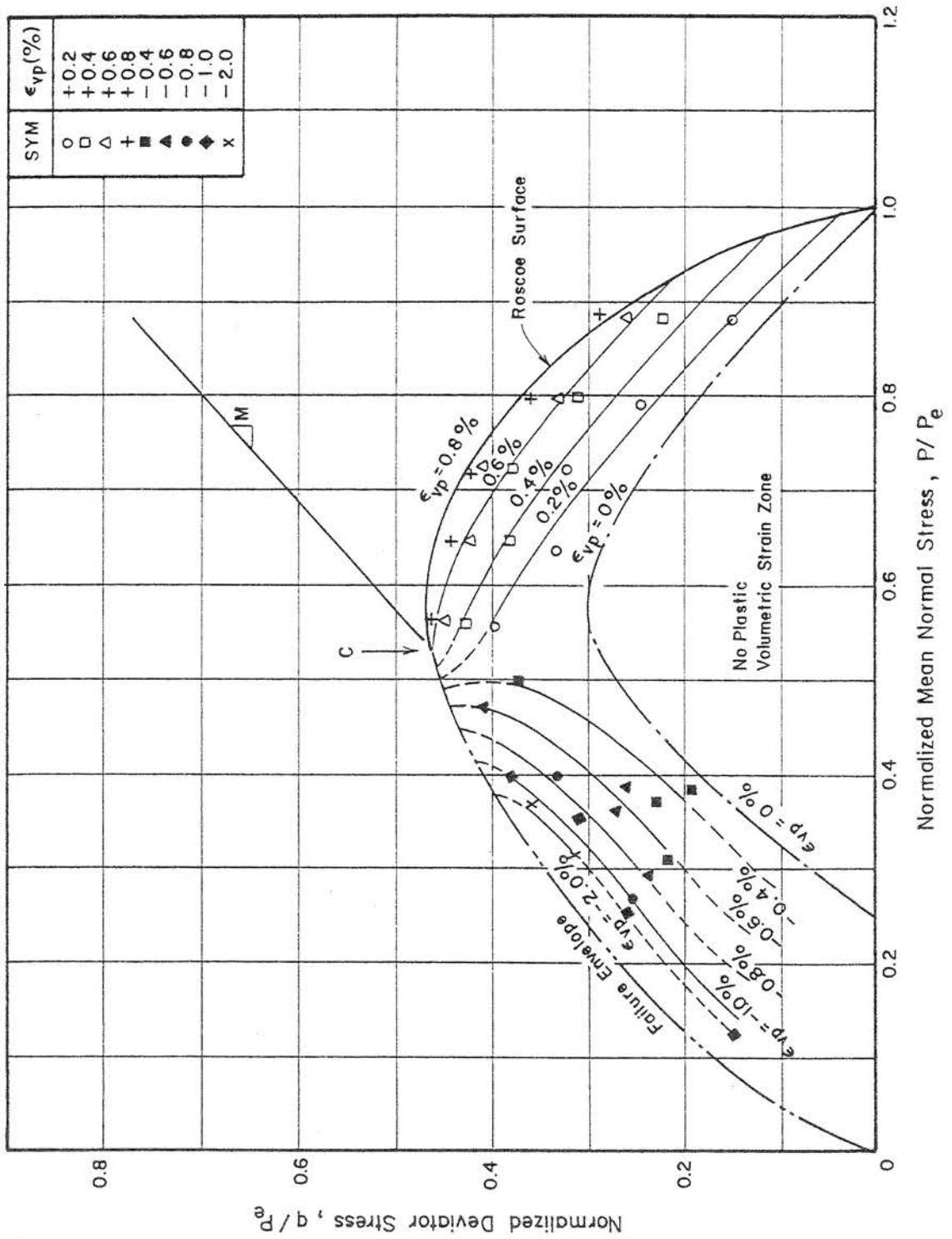


Fig. 8.1b Plastic Volumetric Strain Contours within the State Boundary Surface

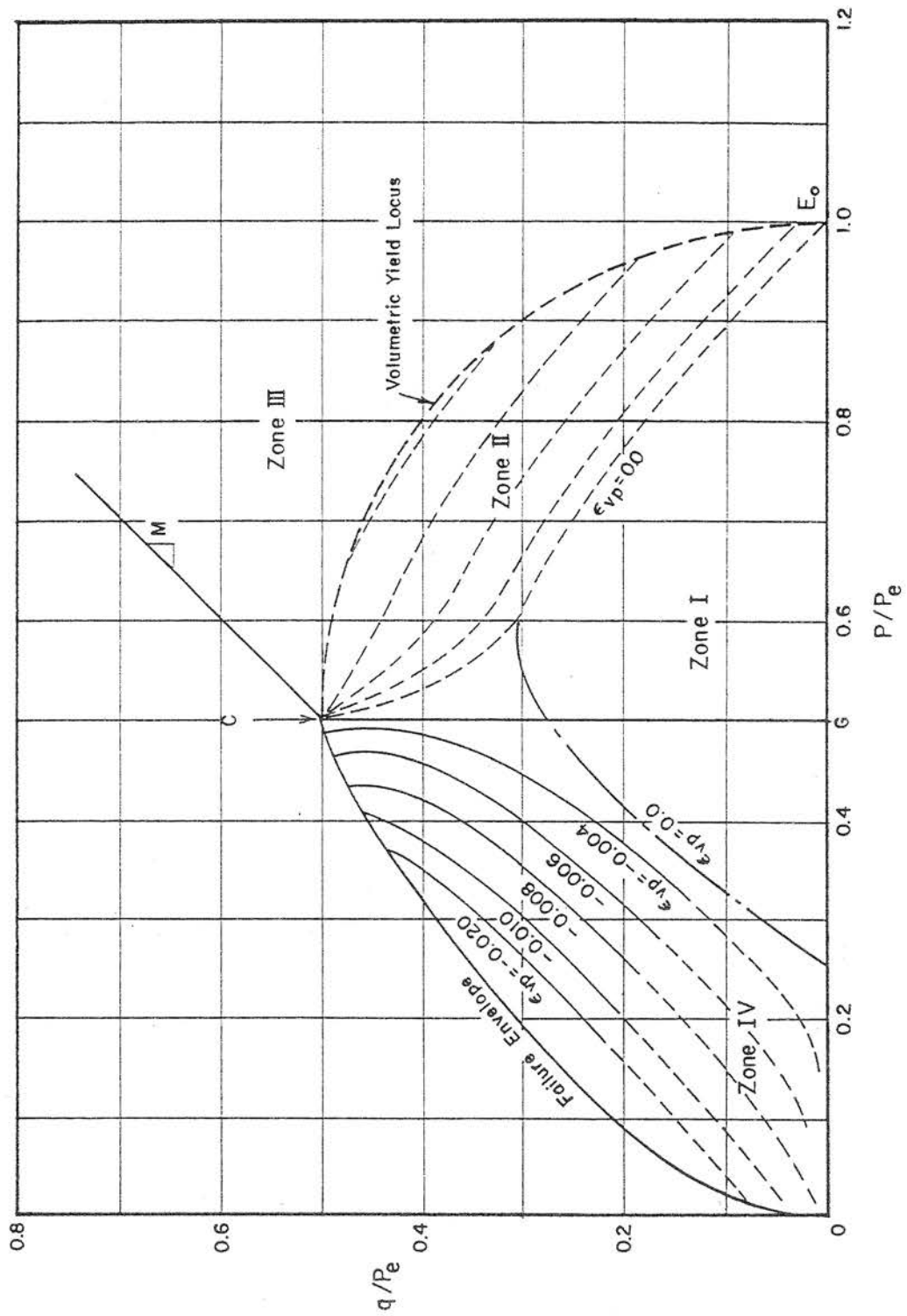


Fig. 8.2 Simplified Plastic Volumetric Strain Contours within the State Boundary Surface and the Strain Zones

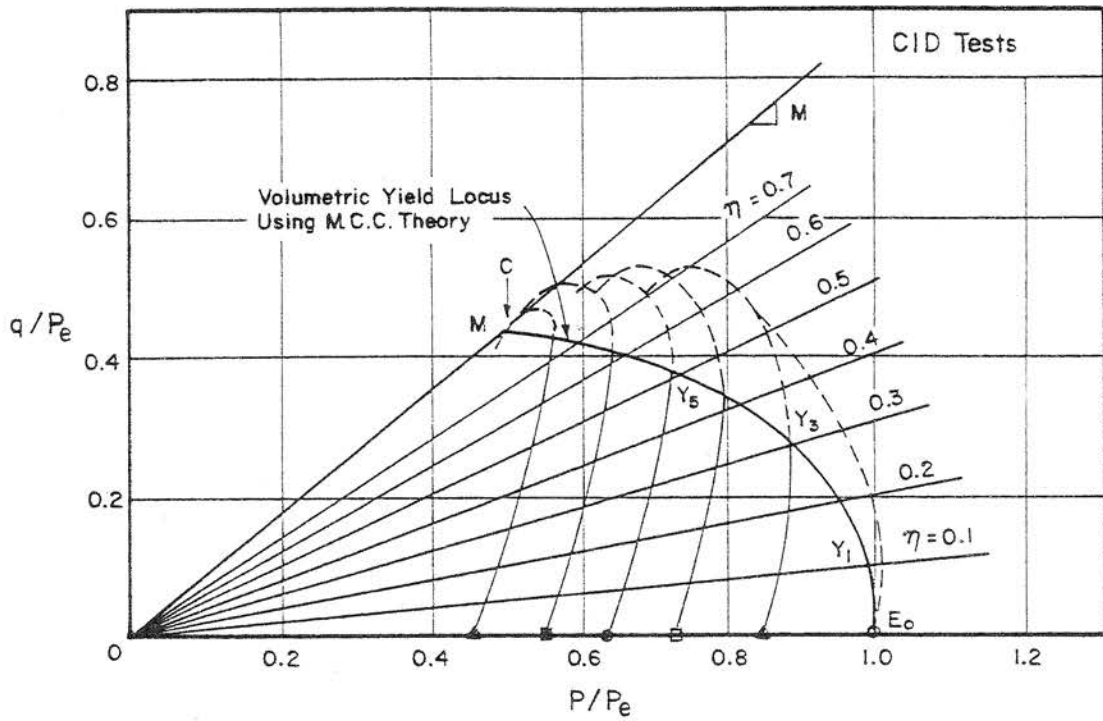


Fig. 8.3 Constant Stress Ratio Lines and Normalized Drained Stress Paths from CID Tests

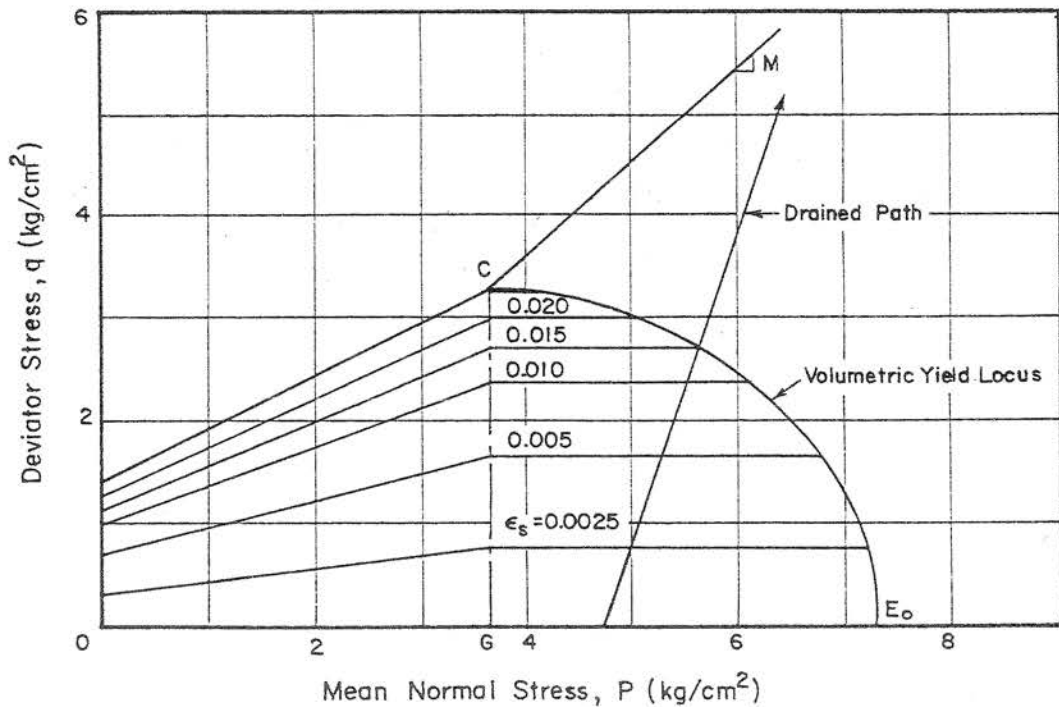


Fig. 8.4 Typical Shear Strain Contours within the State Boundary Surface and the Corresponding Stress Path

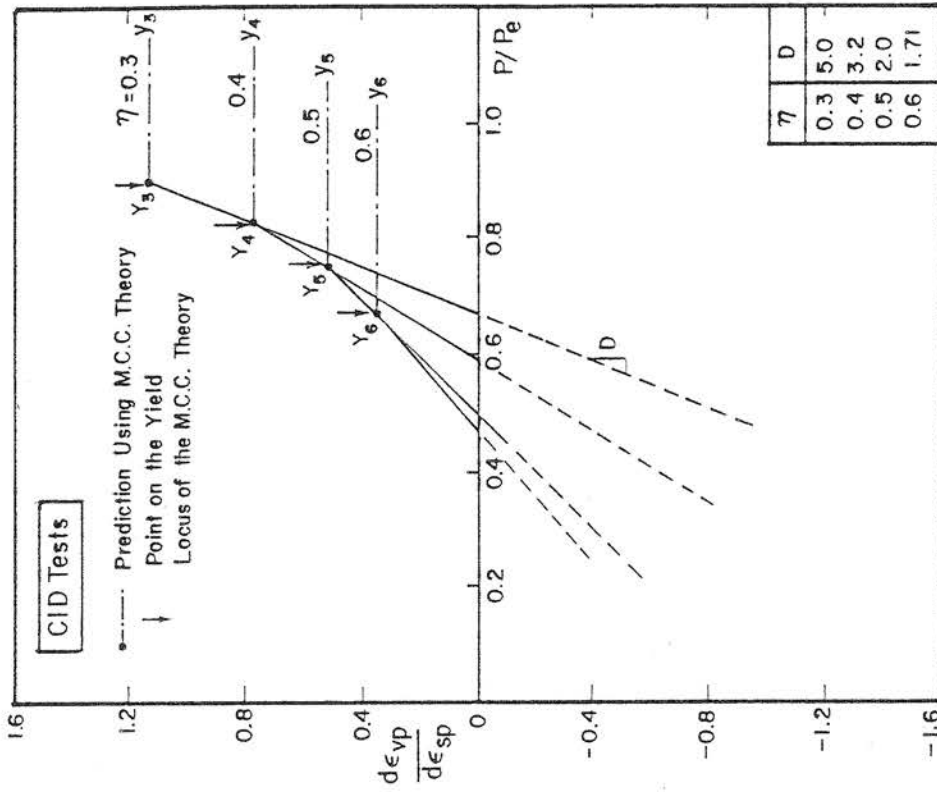


Fig. 8.6 Simplified ($\frac{d\epsilon_{vp}}{d\epsilon_{sp}}$, $\frac{P}{P_e}$) Relationship on the Constant Stress Ratio Lines from CID Tests

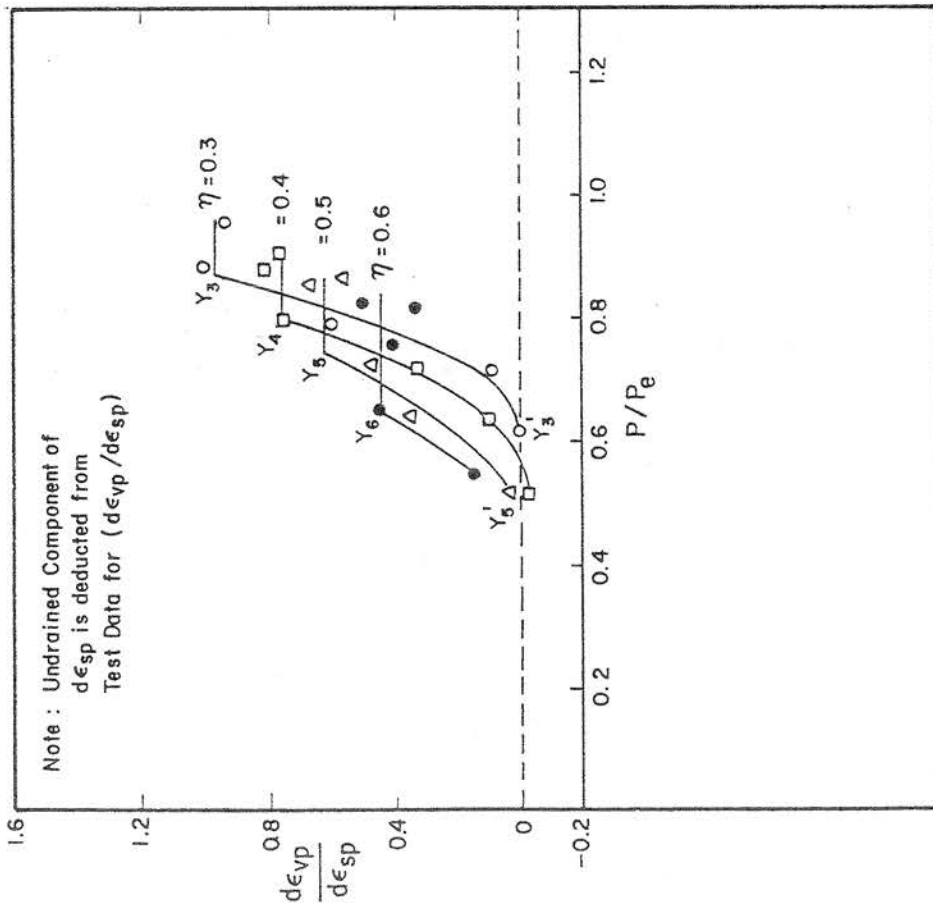


Fig. 8.5 Variation of the Dilatancy Ratio with the Mean Normal Stress on the Constant Stress Ratio Lines from CID Tests

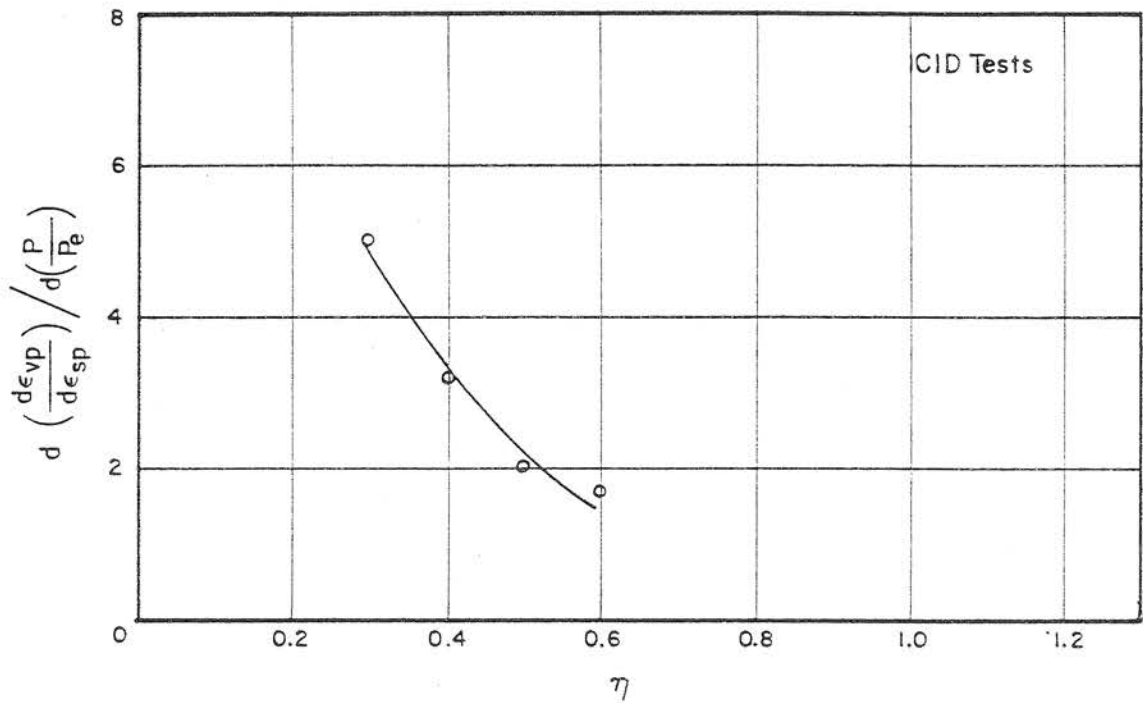


Fig. 8.7 Gradient of the $\left(\frac{d\epsilon_{vp}}{d\epsilon_{sp}}, \frac{p}{p_e}\right)$ Relationship with the Stress Ratio from CID Tests

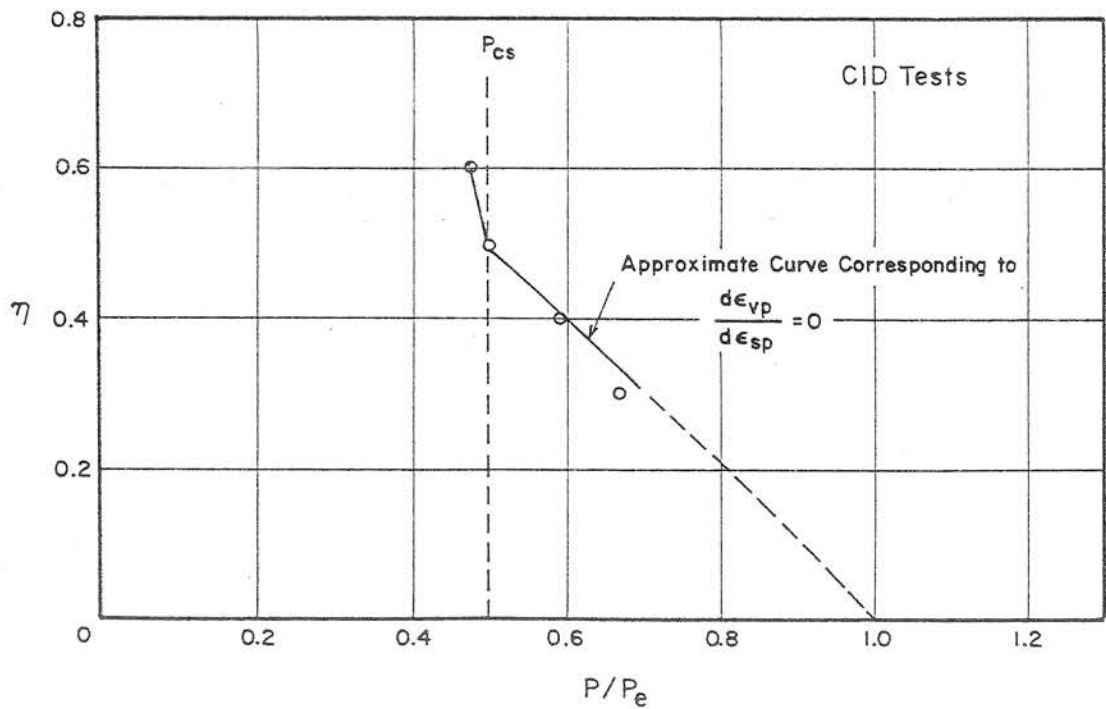


Fig. 8.8 p/p_e at Zero Dilatancy Ratio on the Particular Stress Ratio Line from CID Tests

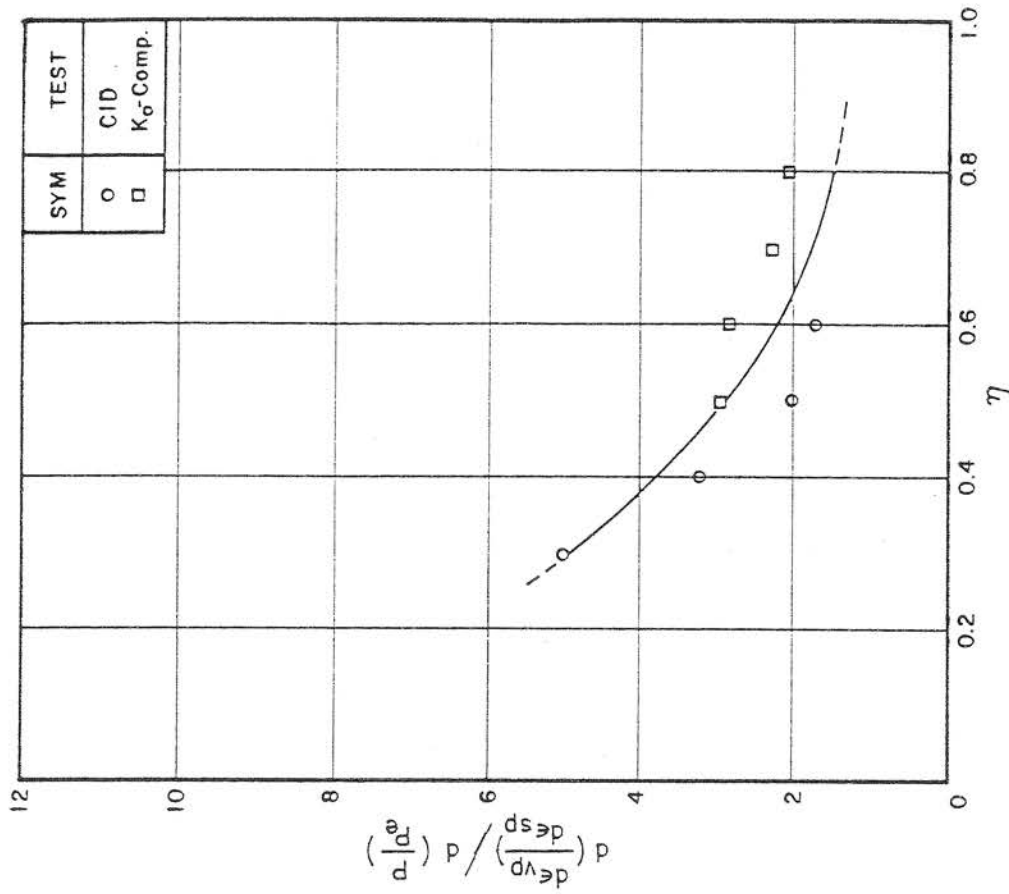


Fig. 8.9b Gradient of the $(\frac{d\epsilon_{vp}}{d\epsilon_{sp}}, \frac{p}{P})$ Relation - ship with the Stress Ratio from CID and K_σ Compression Tests

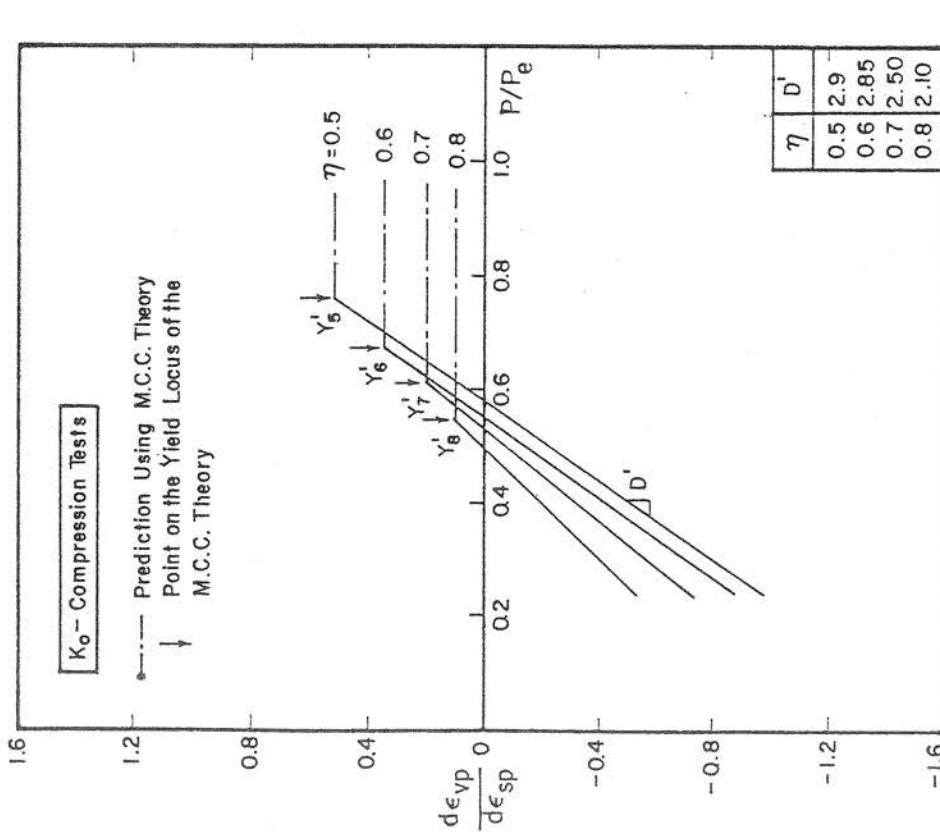


Fig. 8.9a Simplified $(\frac{d\epsilon_{vp}}{d\epsilon_{sp}}, \frac{p}{P})$ Relationship on the Constant Stress Ratio Lines from K_σ Compression Tests

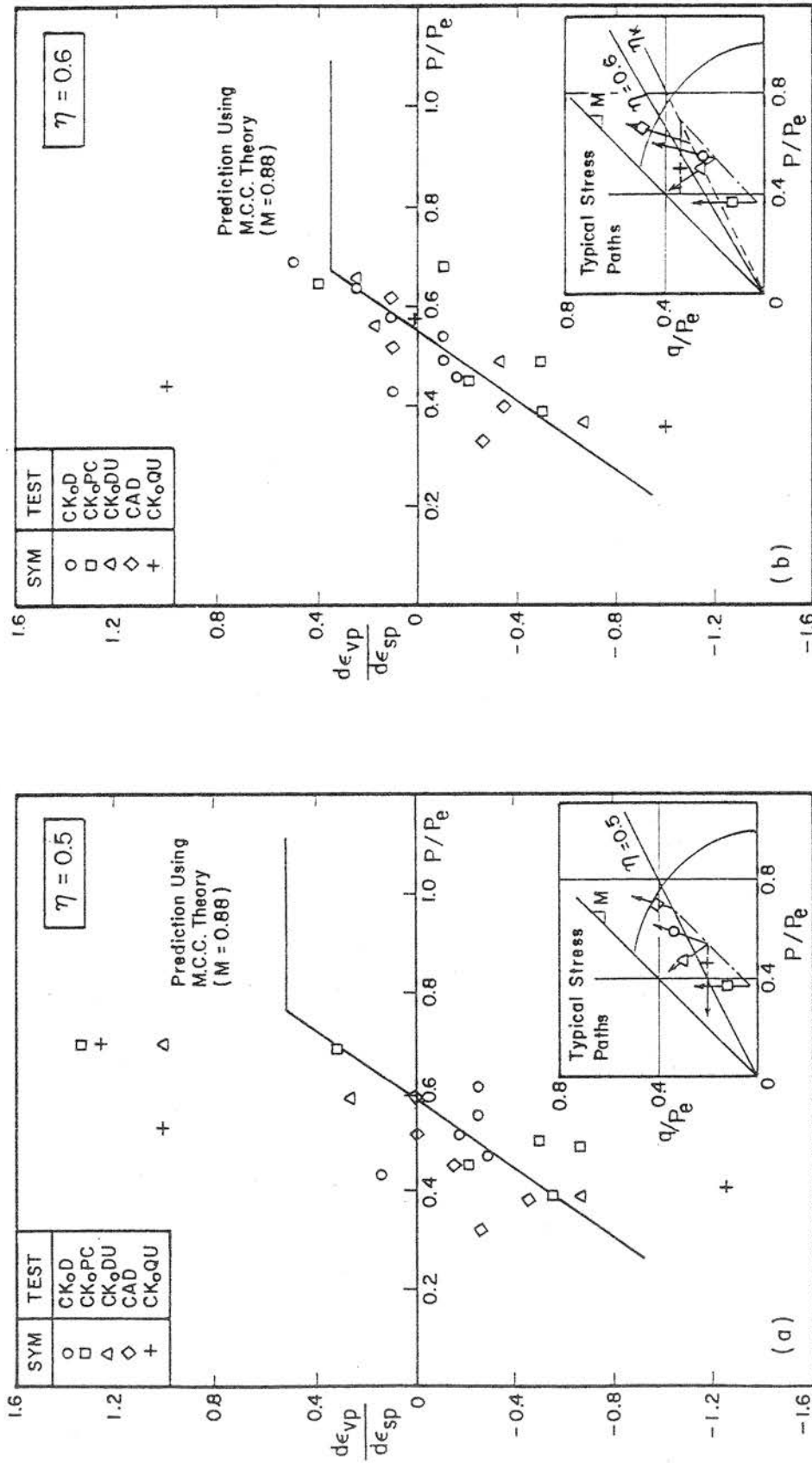


Fig. 8.10a ($\frac{d\epsilon_{vp}}{d\epsilon_{sp}}$, $\frac{p}{p_e}$) Relationship on the Constant Stress Ratio Lines from K_o Compression Tests: (a) $\eta = 0.5$, (b) $\eta = 0.6$

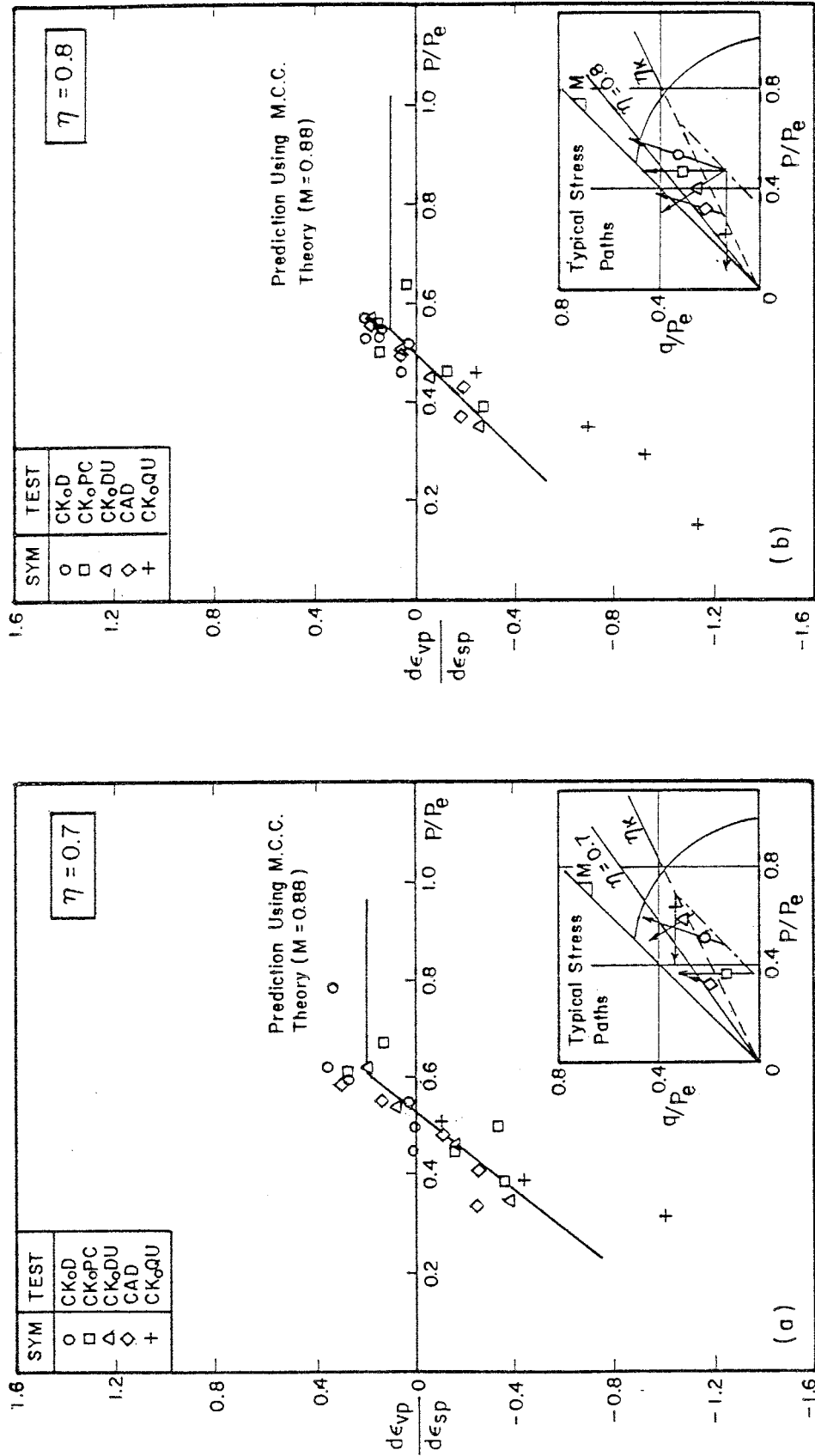


Fig. 8.10b ($\frac{d\epsilon_{vp}}{d\epsilon_p}$, $\frac{p}{p_e}$) Relationship on the Constant Stress Ratio Lines from K_0 Compression Tests: (a) $\eta = 0.7$, (b) $\eta = 0.8$

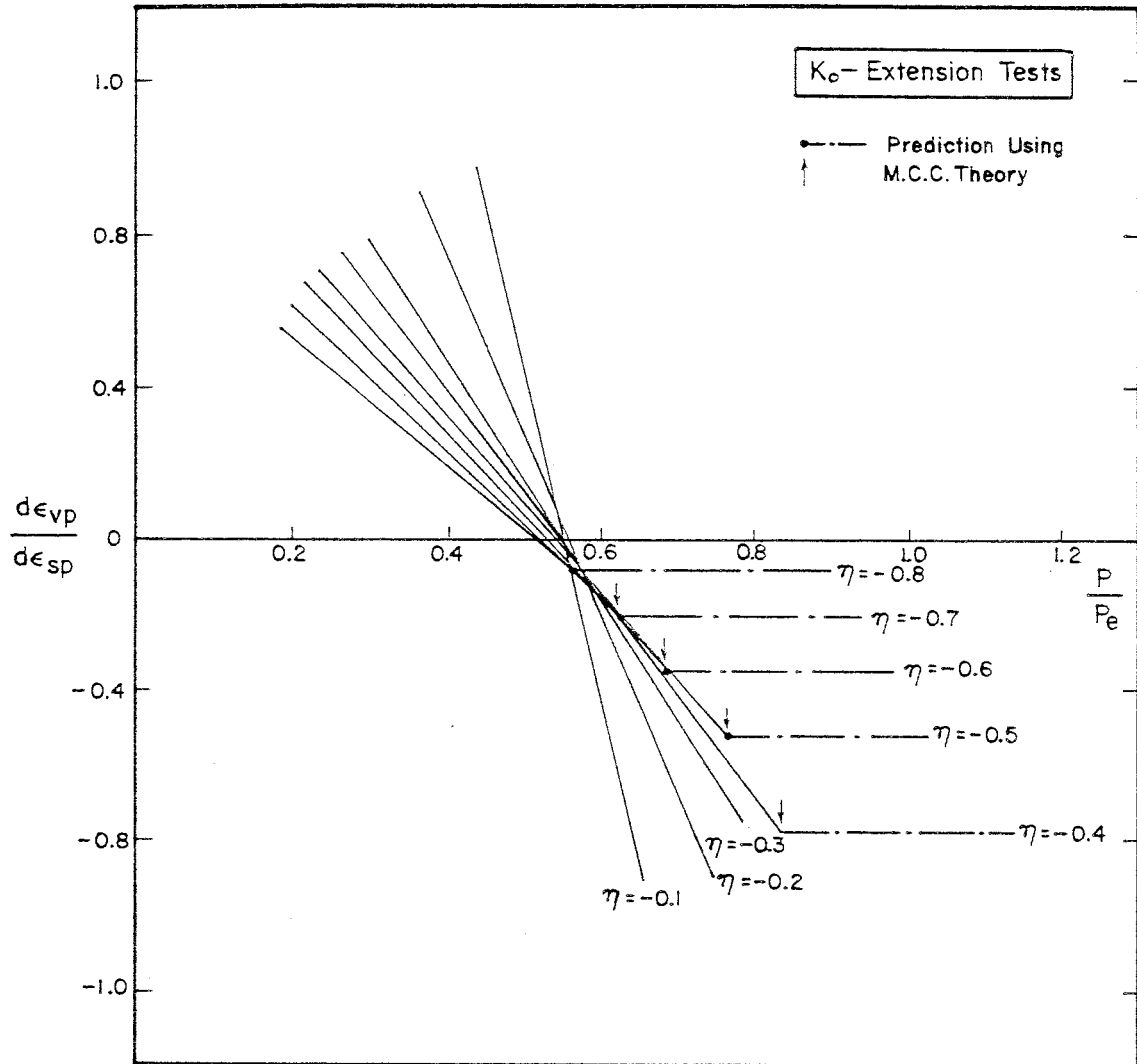


Fig. 8.11 Simplified ($\frac{d\epsilon_{vp}}{d\epsilon_{sp}}$, $\frac{p}{p_e}$) Relationship on the Constant Stress Ratio Lines from K₀ Extension Tests

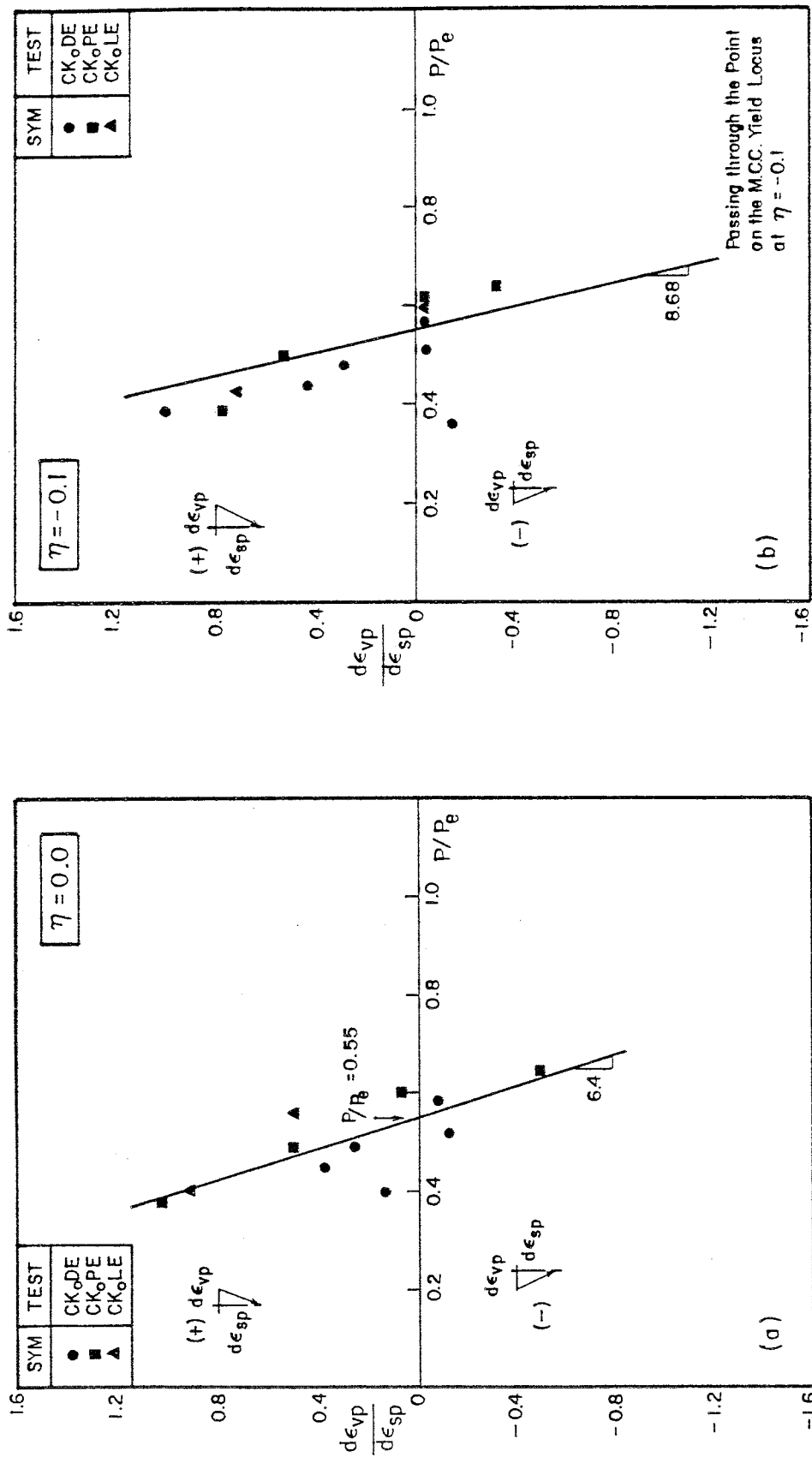


Fig. 8.12a ($\frac{d\epsilon_{vp}}{d\epsilon_{sp}}$, $\frac{P}{P_e}$) Relationship on the Constant Stress Ratio Lines

from Ko Extension Tests: (a) $\eta = 0.0$, (b) $\eta = -0.1$

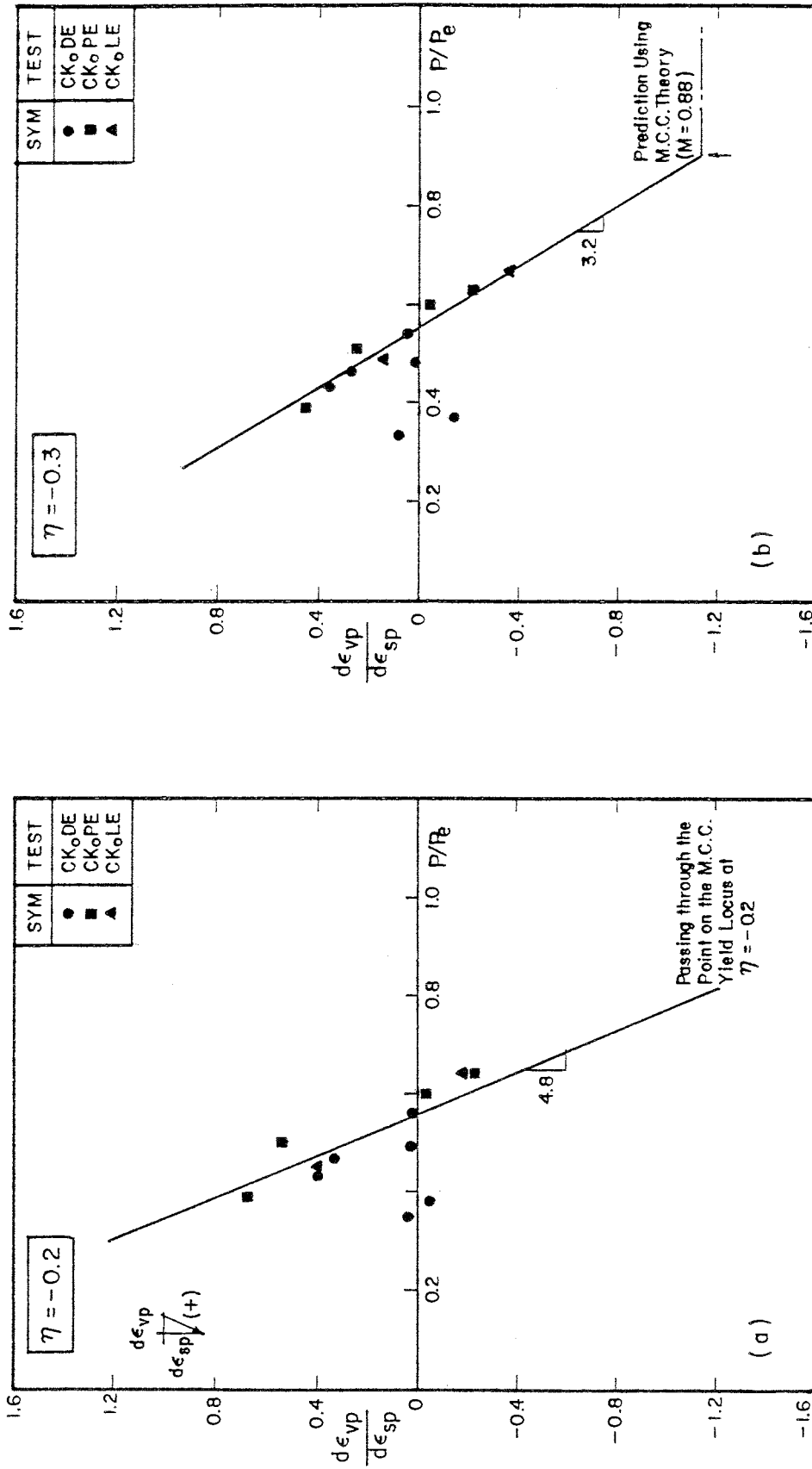


Fig. 8.12b ($\frac{d\epsilon_{vp}}{d\epsilon_{sp}}$, $\frac{P}{P_e}$) Relationship on the Constant Stress Ratio Lines

from K_o Extension Tests: (a) $\eta = -0.2$, (b) $\eta = -0.3$

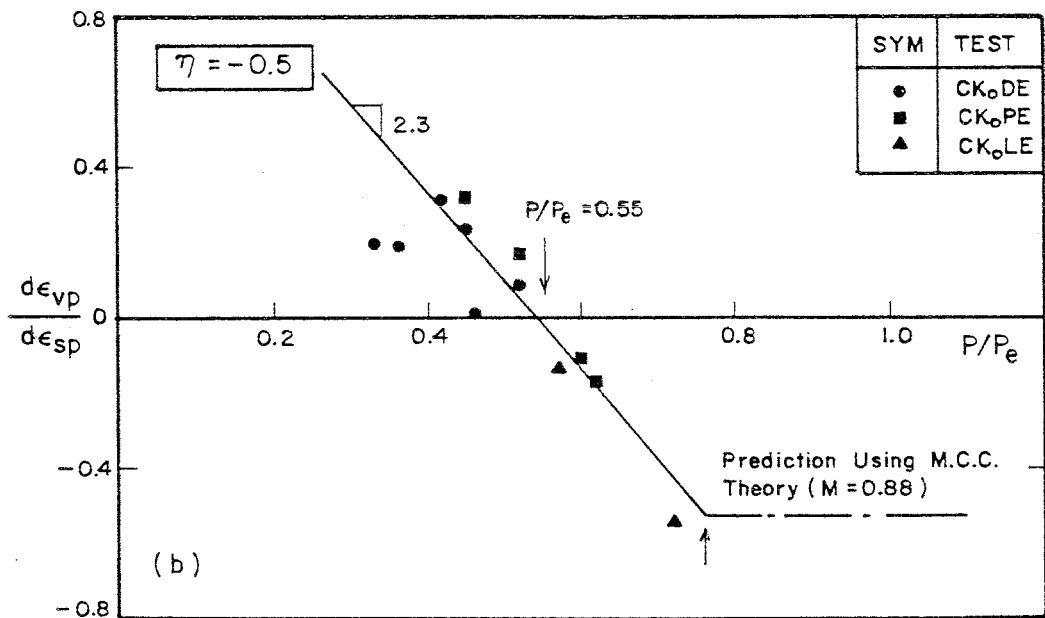
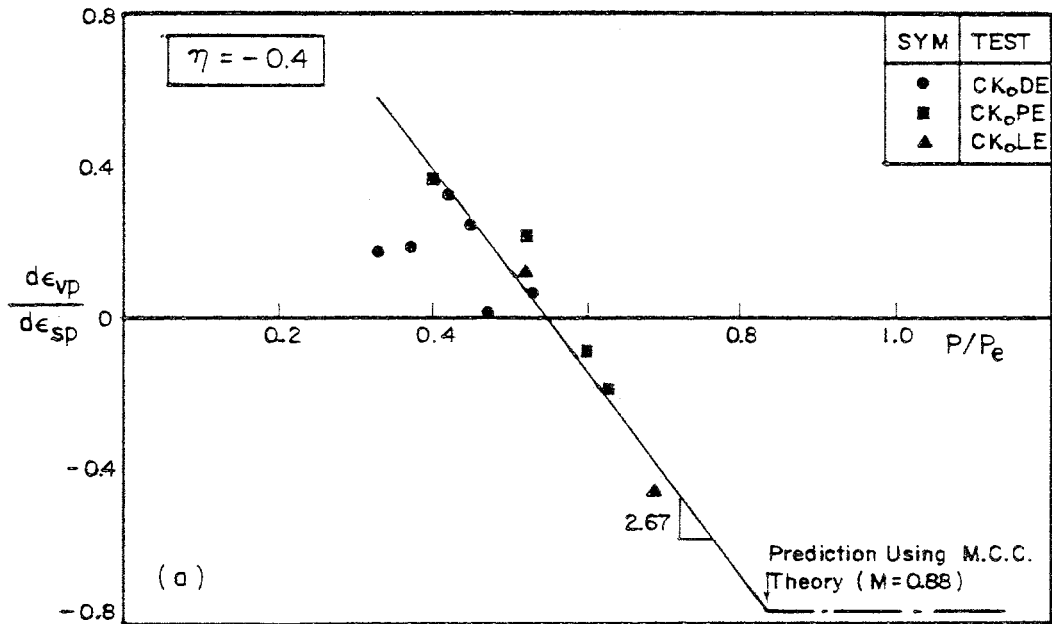


Fig. 8.12c ($\frac{d\epsilon_{vp}}{d\epsilon_{sp}}$, $\frac{P}{P_e}$) Relationship on the Constant Stress Ratio Lines from K_o Extension Tests: (a) $\eta = -0.4$, (b) $\eta = -0.5$

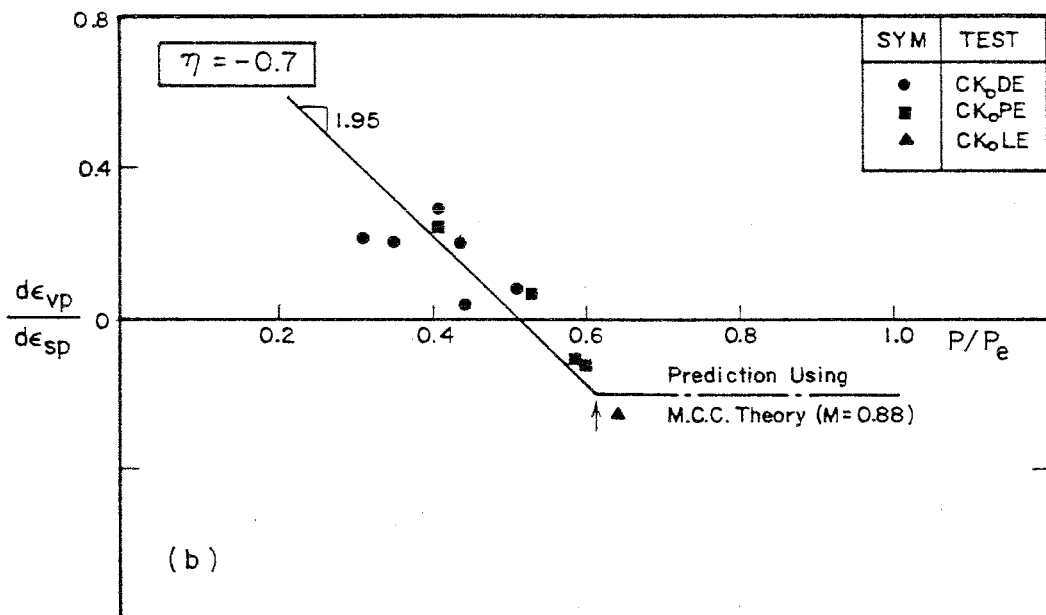
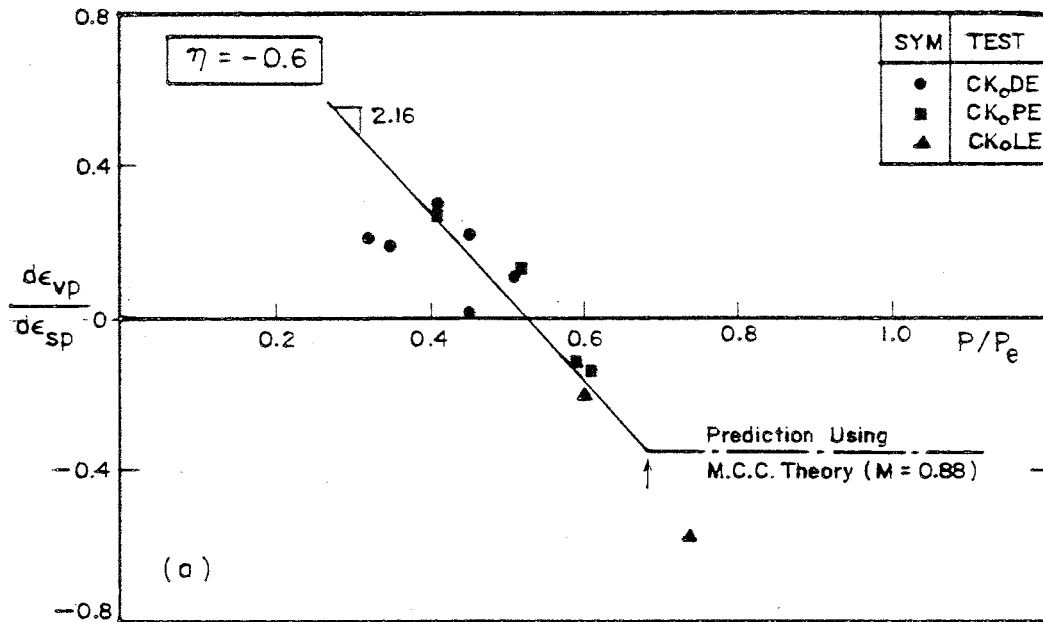


Fig. 8.12d ($\frac{d\epsilon_{vp}}{d\epsilon_{sp}}$, $\frac{P}{P_e}$) Relationship on the Constant Stress Ratio Lines from K_o Extension Tests: (a) $\eta = -0.6$, (b) $\eta = -0.7$

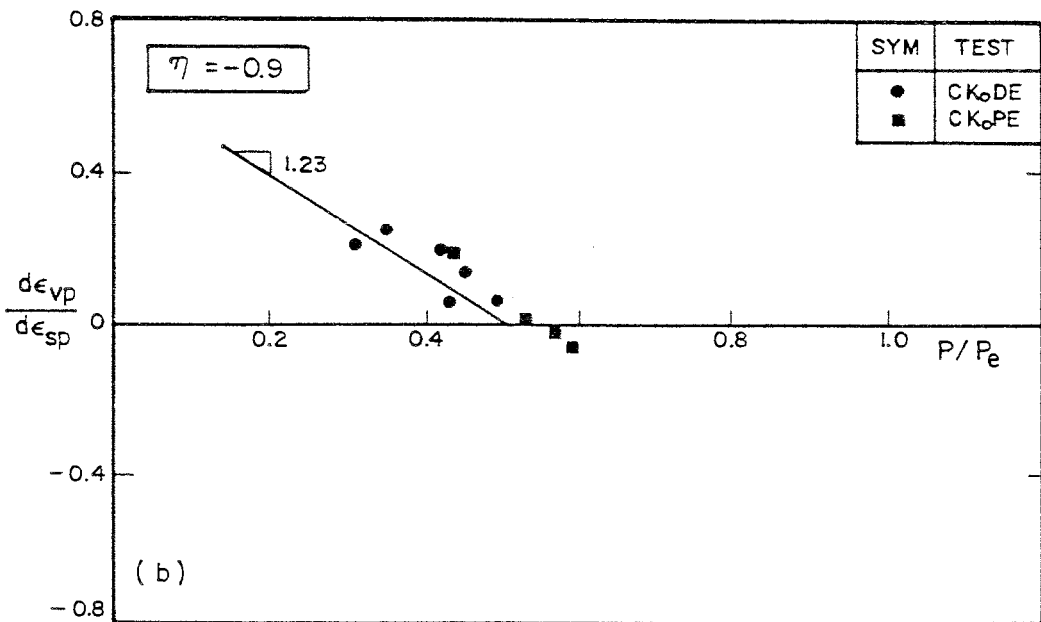
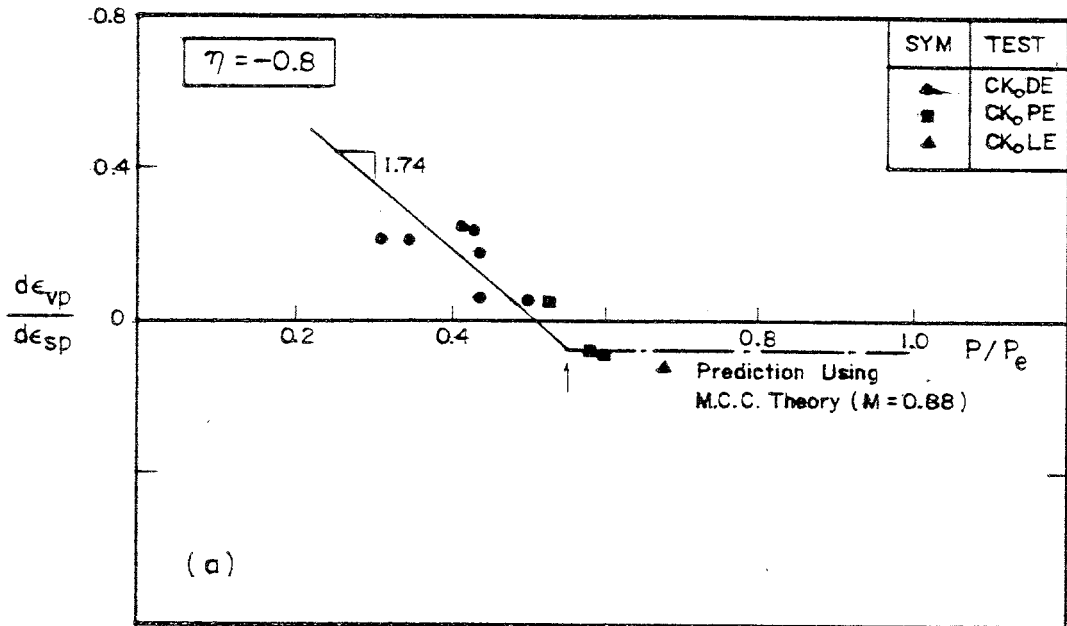


Fig. 8.12e $\left(\frac{d\epsilon_{vp}}{d\epsilon_{sp}}, \frac{P}{P_e} \right)$ Relationship on the Constant Stress Ratio Lines from K_o Extension Tests: (a) $\eta = -0.8$, (b) $\eta = -0.9$

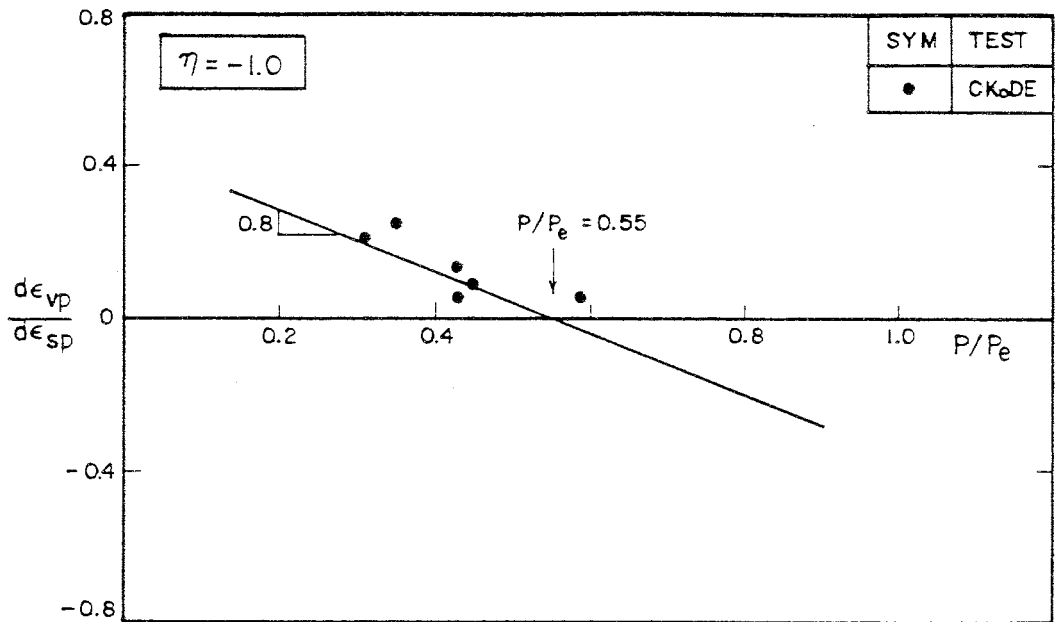


Fig. 8.12f $(\frac{d\epsilon_{vp}}{d\epsilon_{sp}}, \frac{P}{P_e})$ Relationship on the Constant Stress Ratio Line $\eta = -1.0$ from K_0 Extension Tests

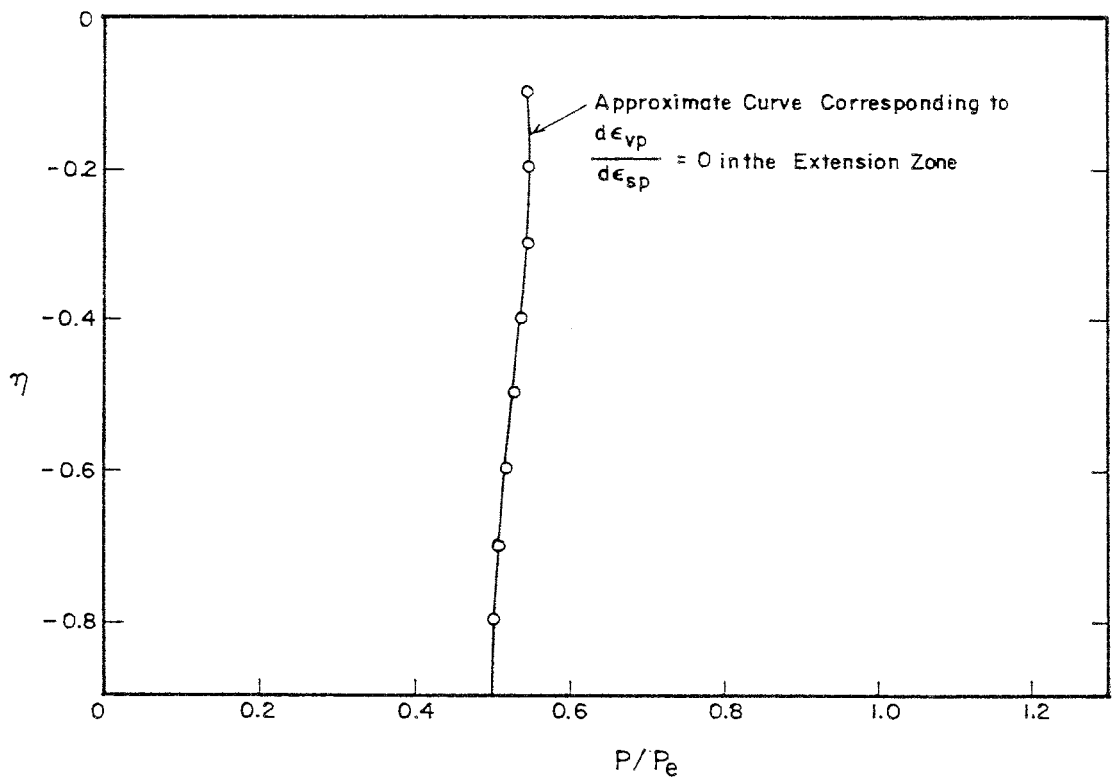


Fig. 8.13 p/p_e at Zero Dilatancy Ratio on the Particular Stress Ratio Line from K_0 Extension Tests

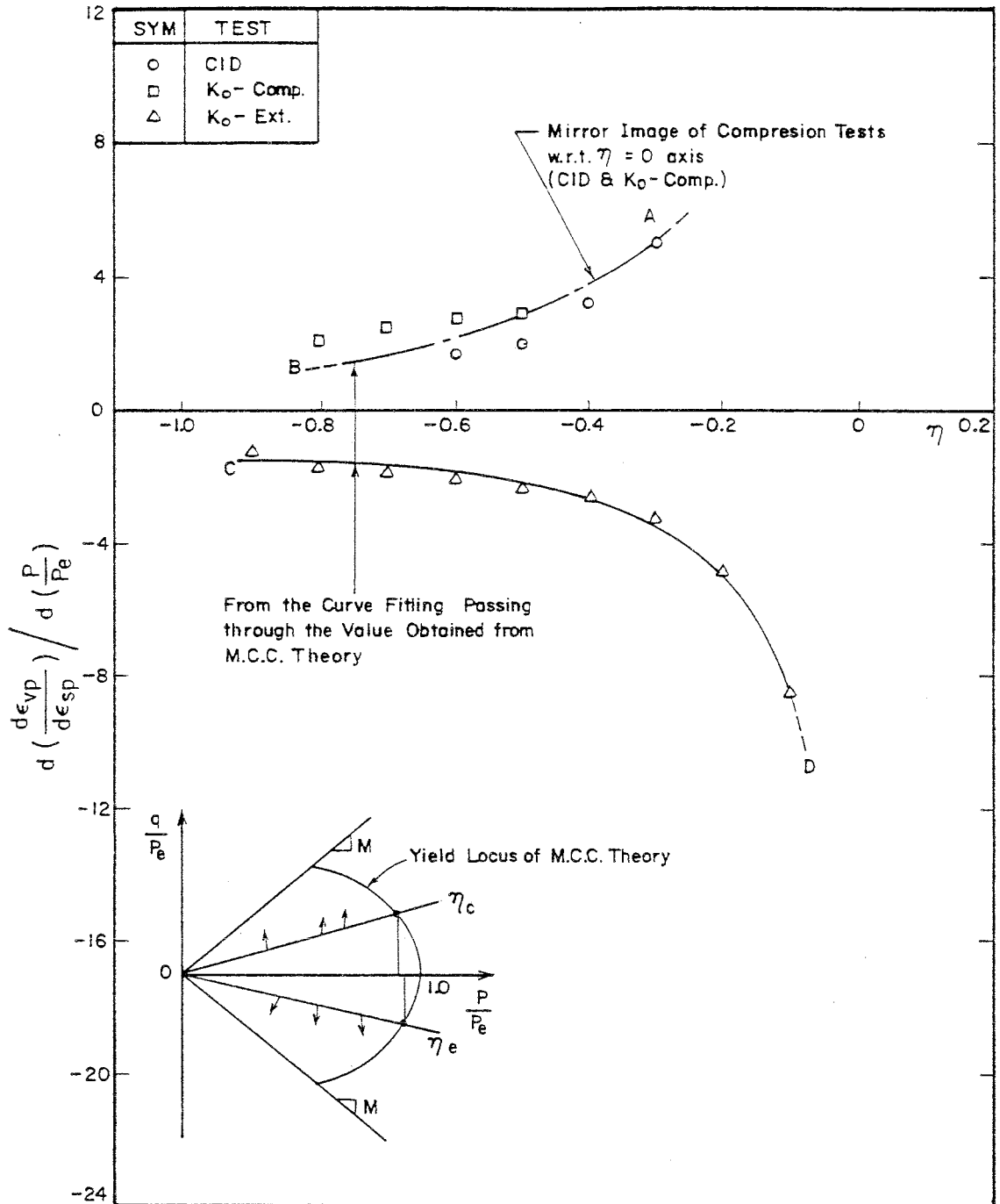


Fig. 8.14 Gradient of the $(\frac{d\epsilon_{vp}}{d\epsilon_{sp}}, \frac{p}{P_e})$ Relationship with the Stress Ratio from CID, K_o Compression and K_o Extension Tests

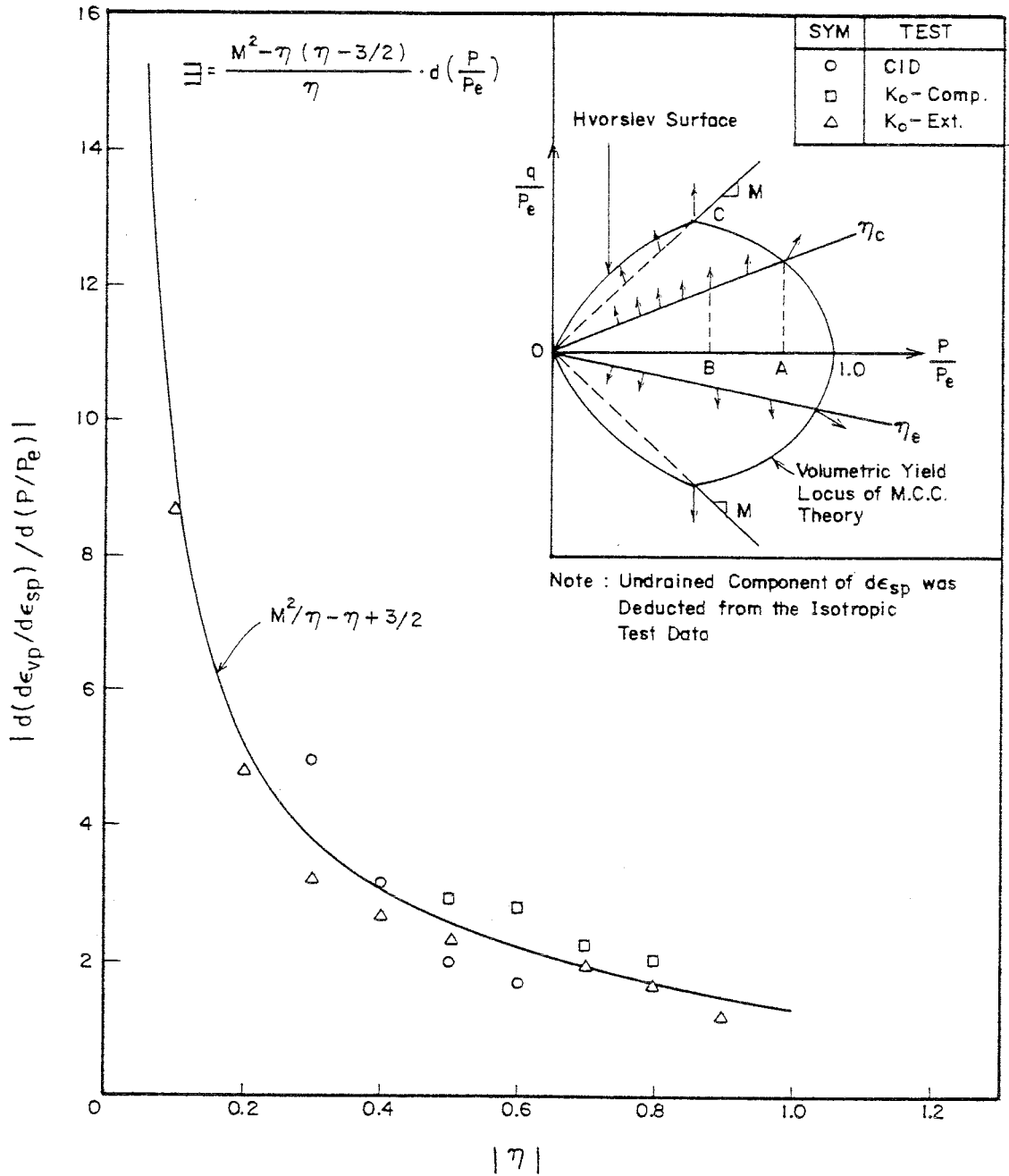


Fig. 8.15 Variation of the $\left(\frac{d\epsilon_{vp}}{d\epsilon_{sp}}, \frac{p}{p_e} \right)$ Plot with the Stress Ratio within the State Boundary Surface

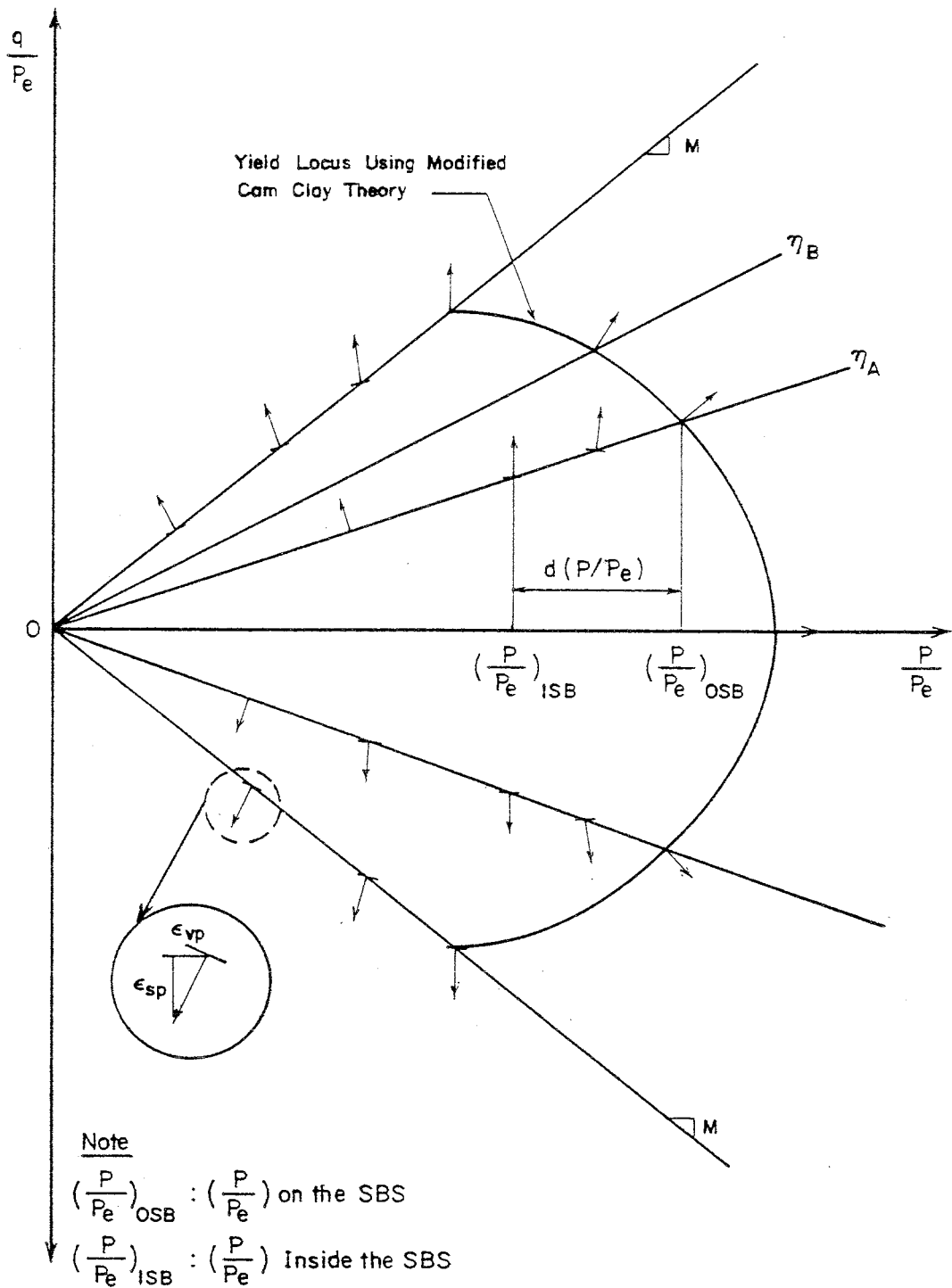


Fig. 8.15a Direction of Plastic Strain Increment Vectors and Their Locations within the State Boundary Surface

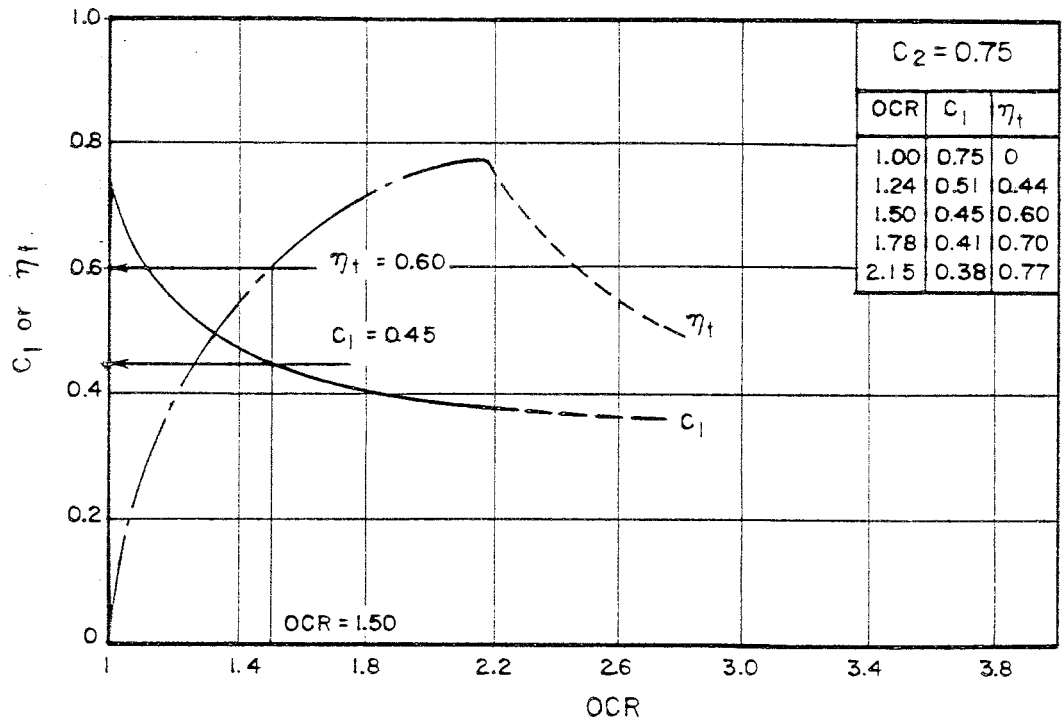


Fig. 8.18 OCR- C_1 - η_t Relationship from CID Samples on the Wet Zone

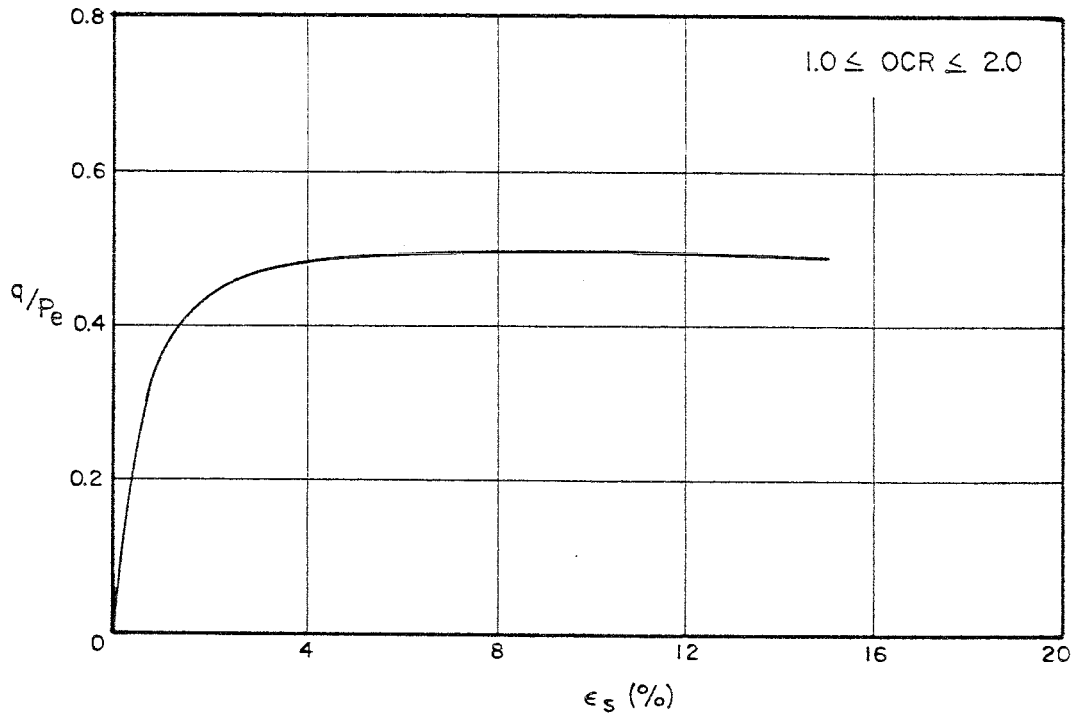


Fig. 8.19 Simplified Stress-Strain Relationship for the Samples on the Wet Zone

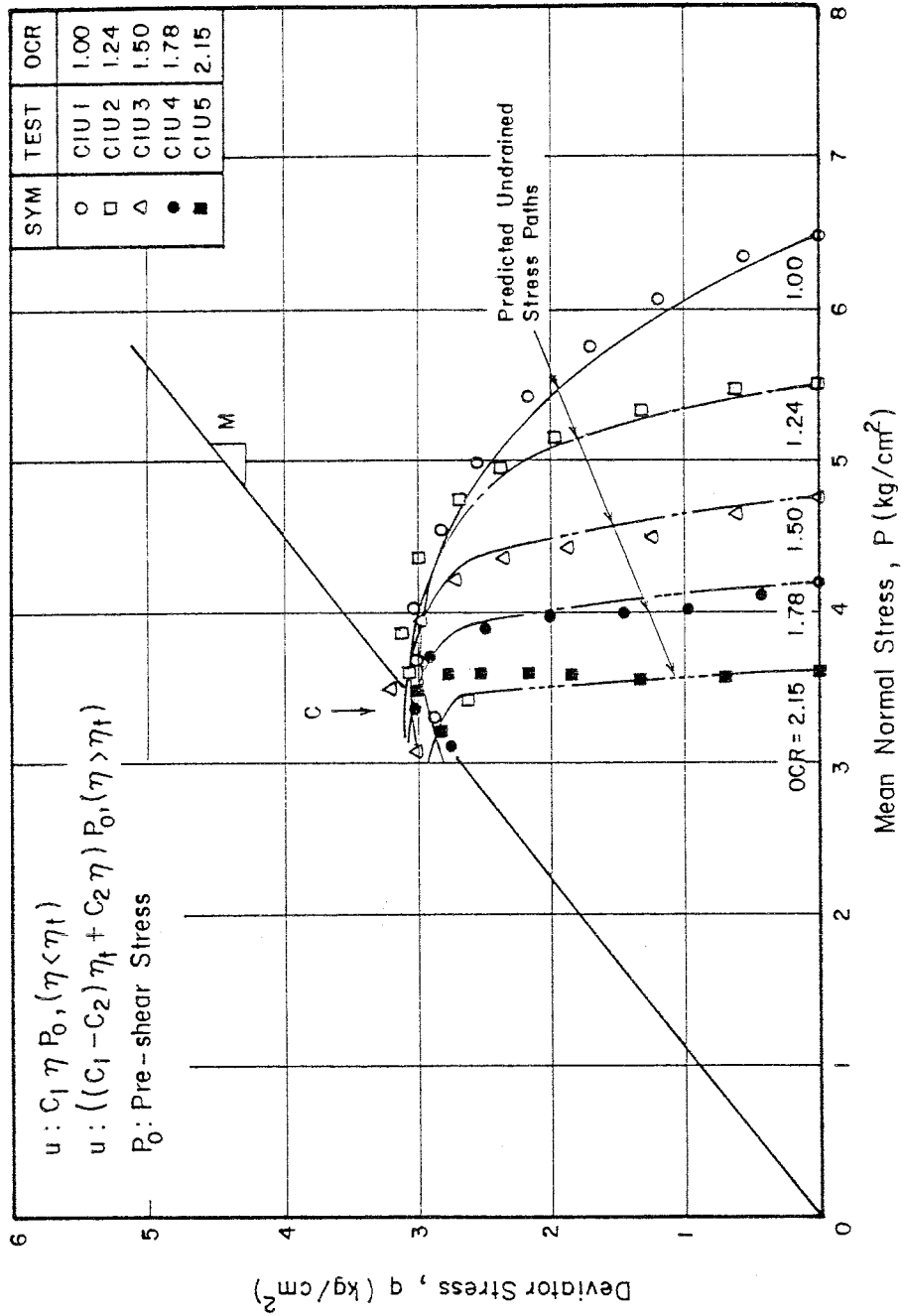


Fig. 8.20 Comparisons between the Predicted Undrained Stress Paths and the Experimental Observations from CIU Tests

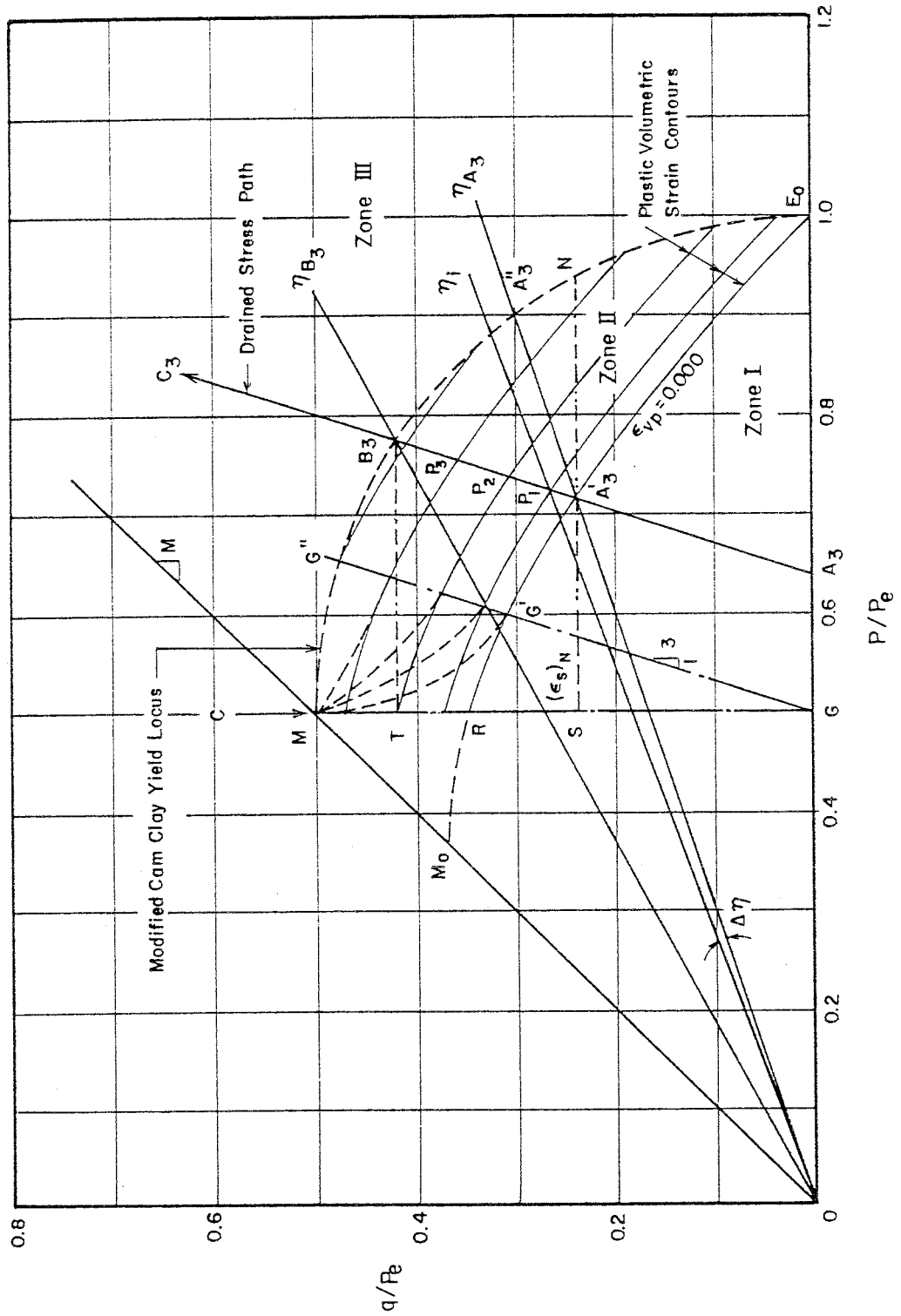


Fig. 8.21 Schematic Diagram for the Calculation of the Plastic Strains within the State Boundary Surface (Wet Zone)

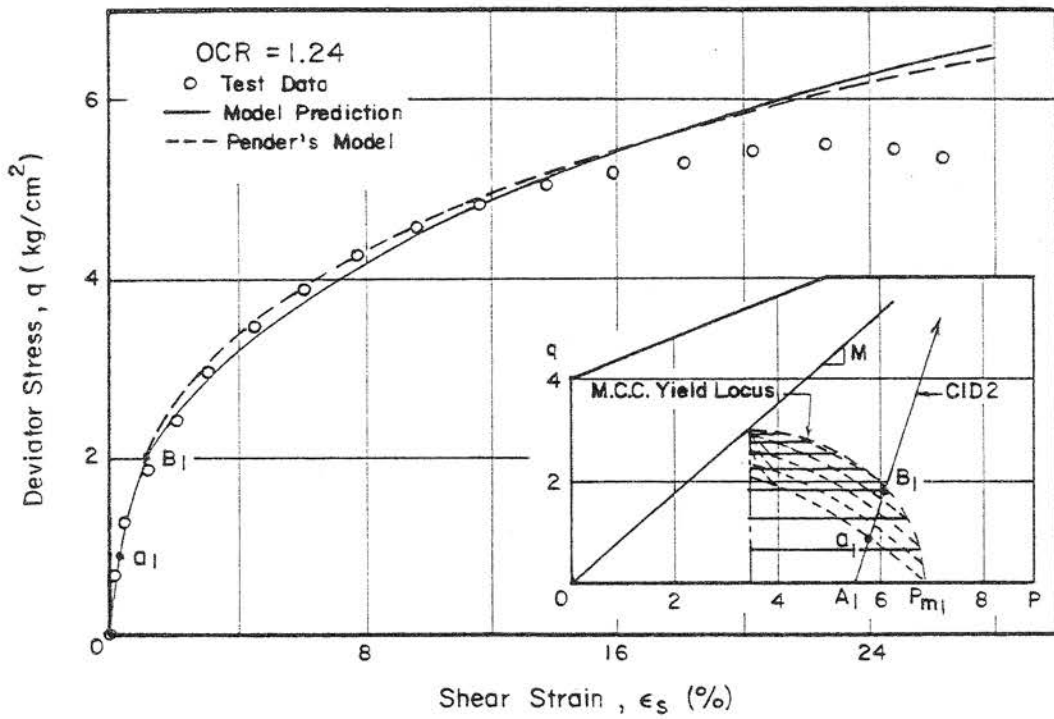


Fig. 8.22a (q , ϵ_s) Plot for CID2 Sample Compared with the Model Predictions

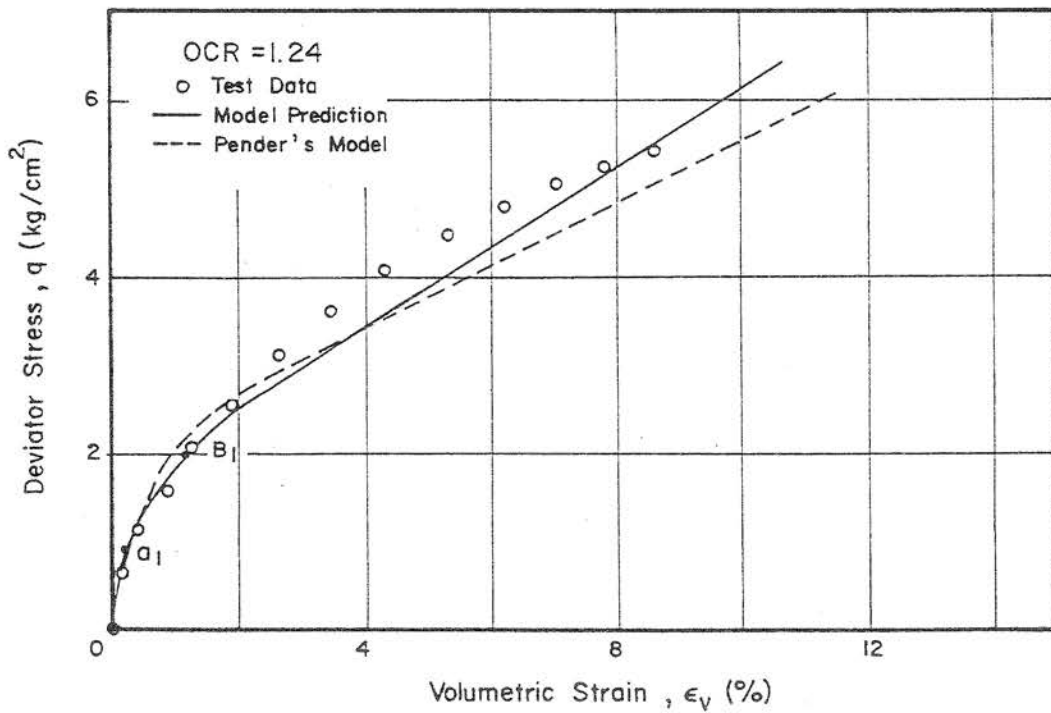


Fig. 8.22b (q , ϵ_v) Plot for CID2 Sample Compared with the Model Predictions

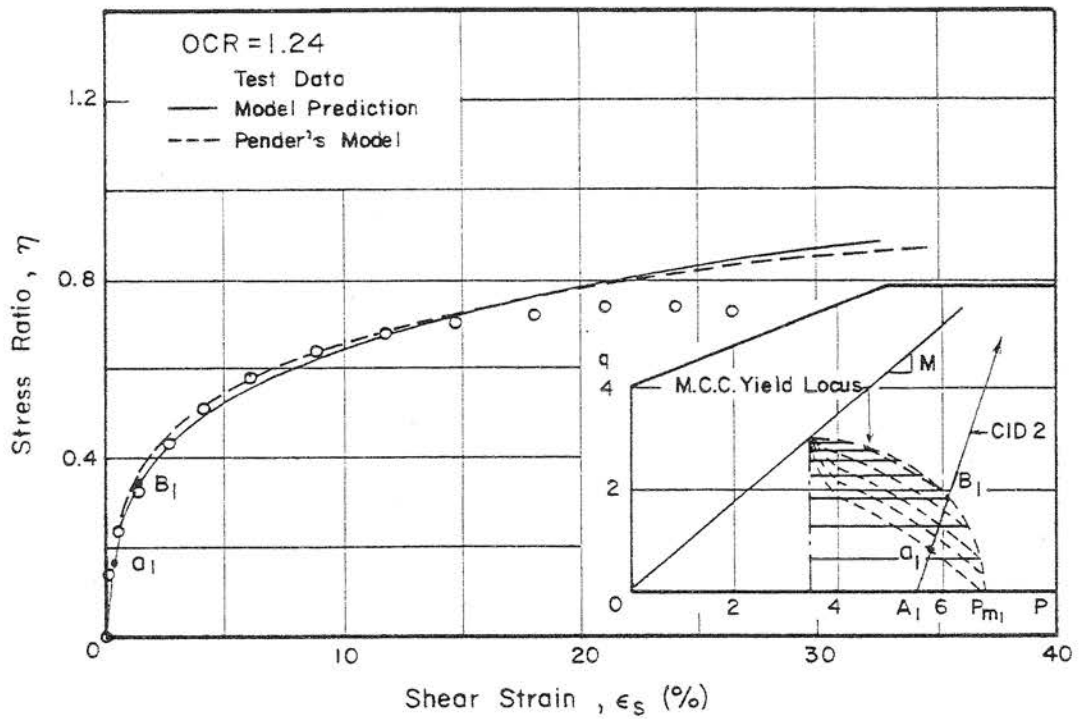


Fig. 8.23a (η , ϵ_s) Plot for CID2 Sample Compared with the Model Predictions

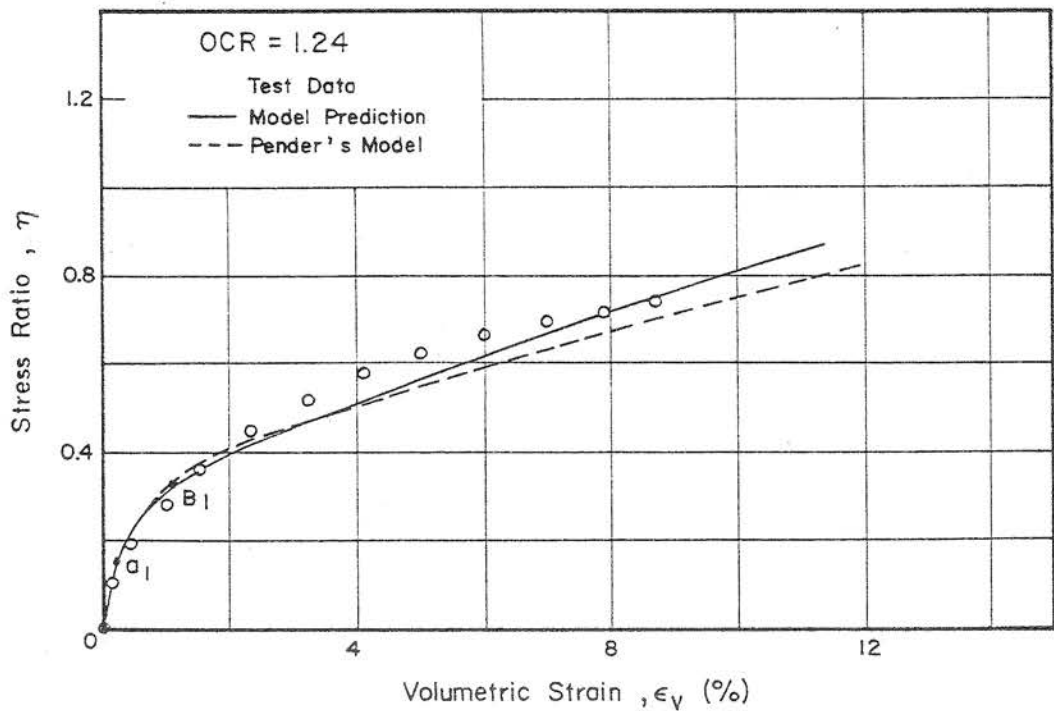


Fig. 8.23b (η , ϵ_v) Plot for CID2 Sample Compared with the Model Predictions

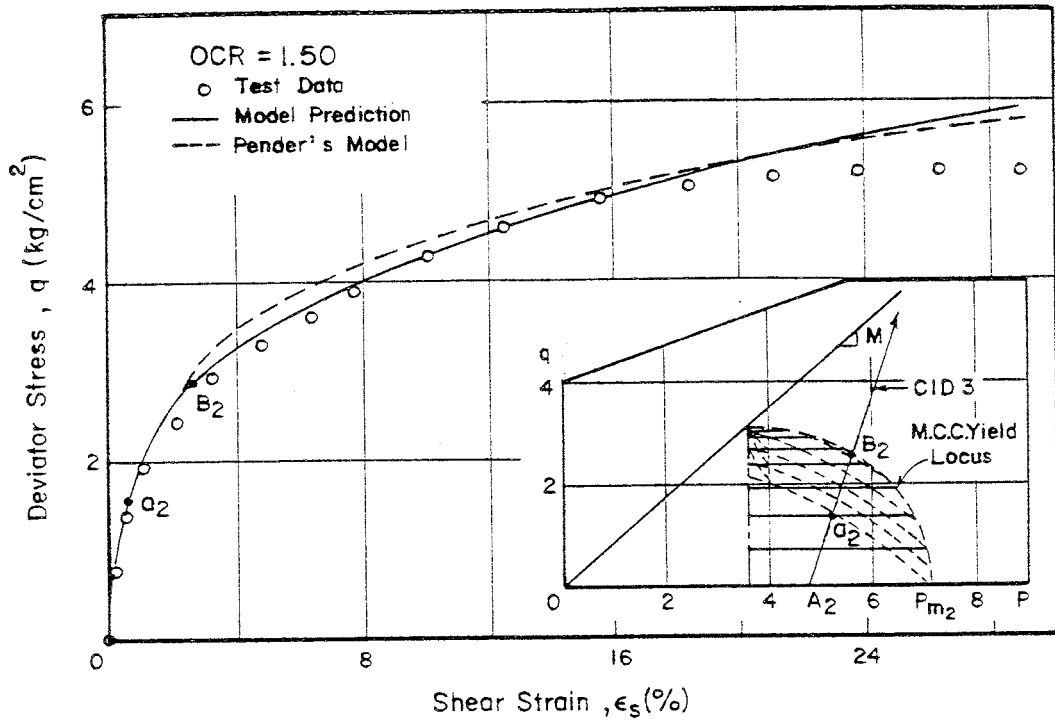


Fig. 8.24a (q , ϵ_s) Plot for CID3 Sample Compared with the Model Predictions

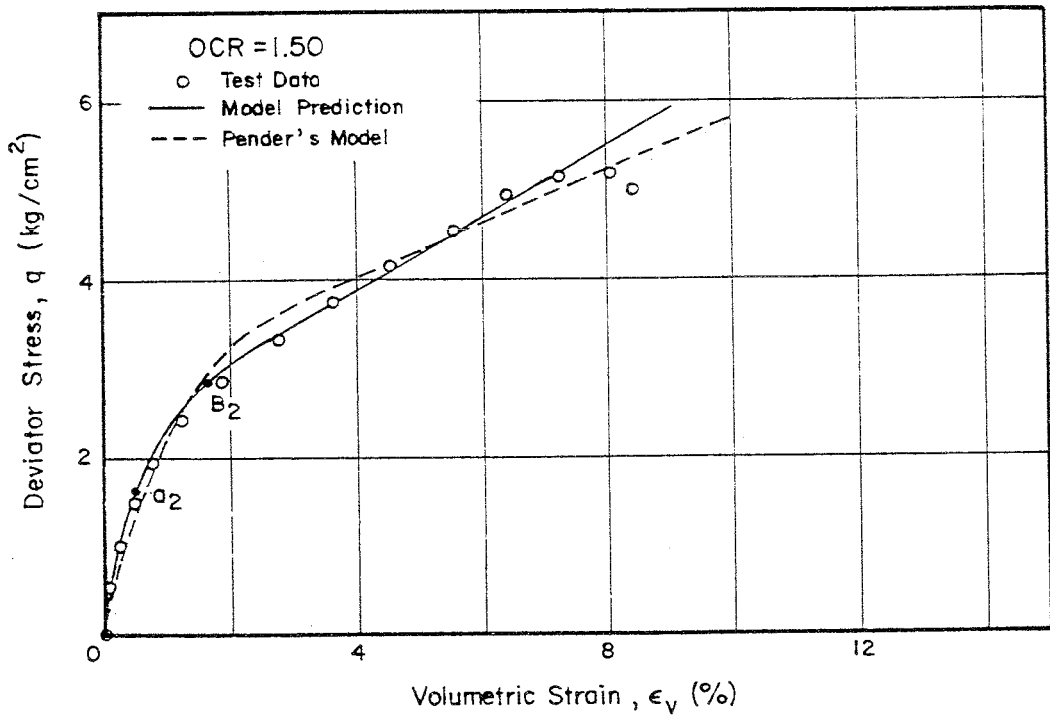


Fig. 8.24b (q , ϵ_v) Plot for CID3 Sample Compared with the Model Predictions

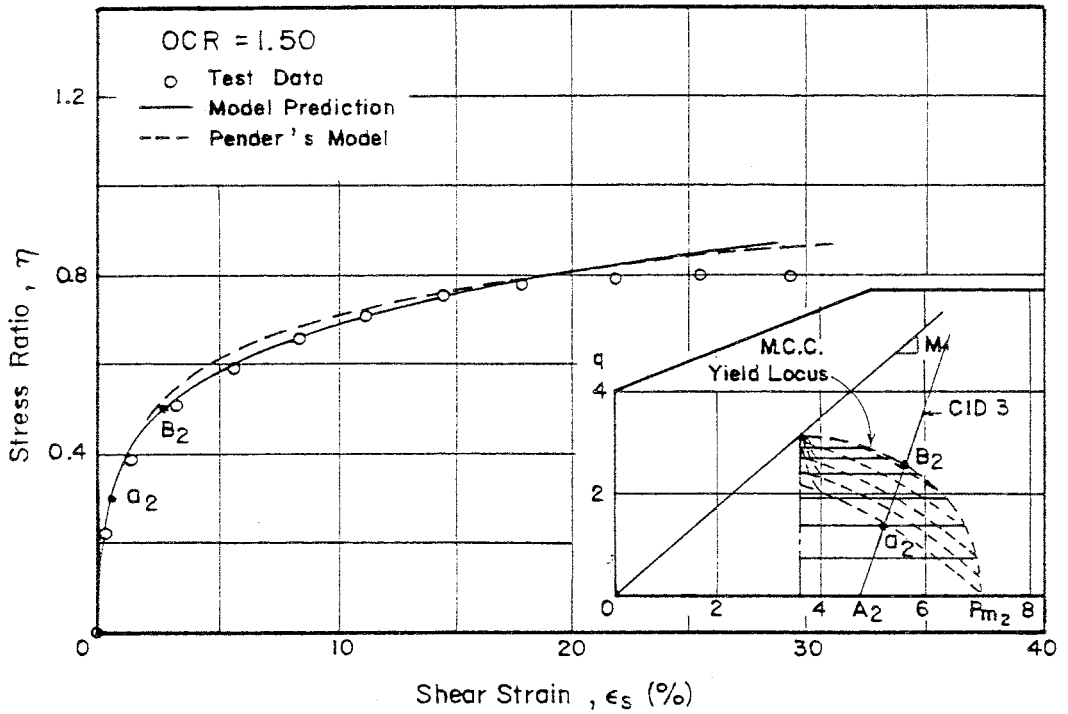


Fig. 8.25a (η , ϵ_s) Plot for CID3 Sample Compared with the Model Predictions

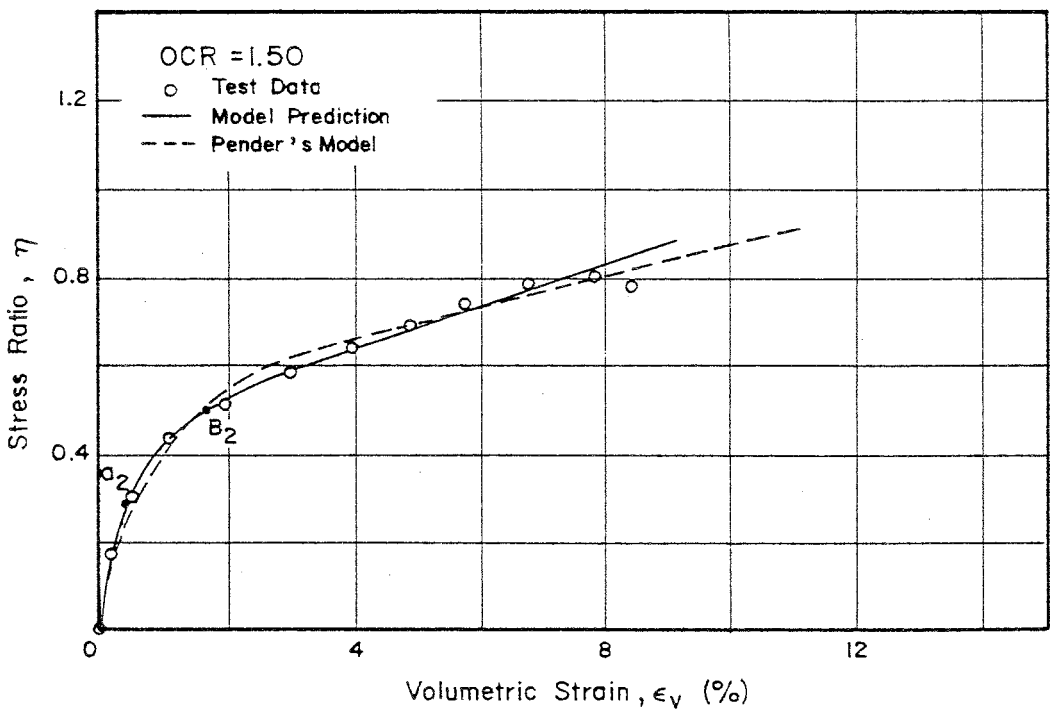


Fig. 8.25b (η , ϵ_v) Plot for CID3 Sample Compared with the Model Predictions

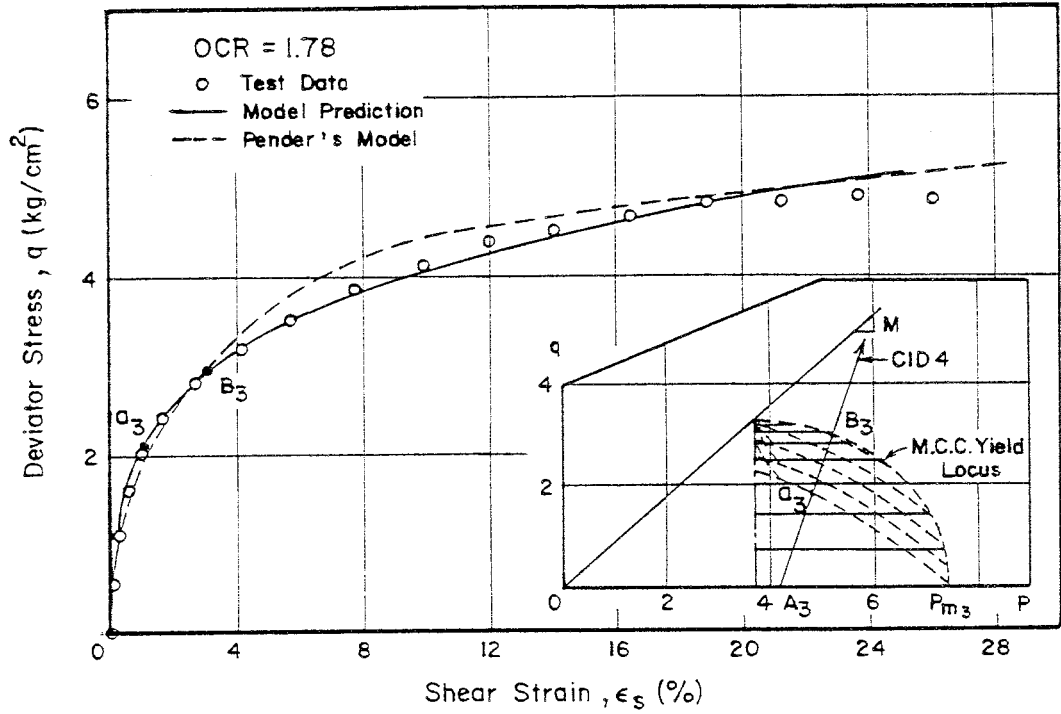


Fig. 8.26a (q, ϵ_s) Plot for CID4 Sample Compared with the Model Predictions

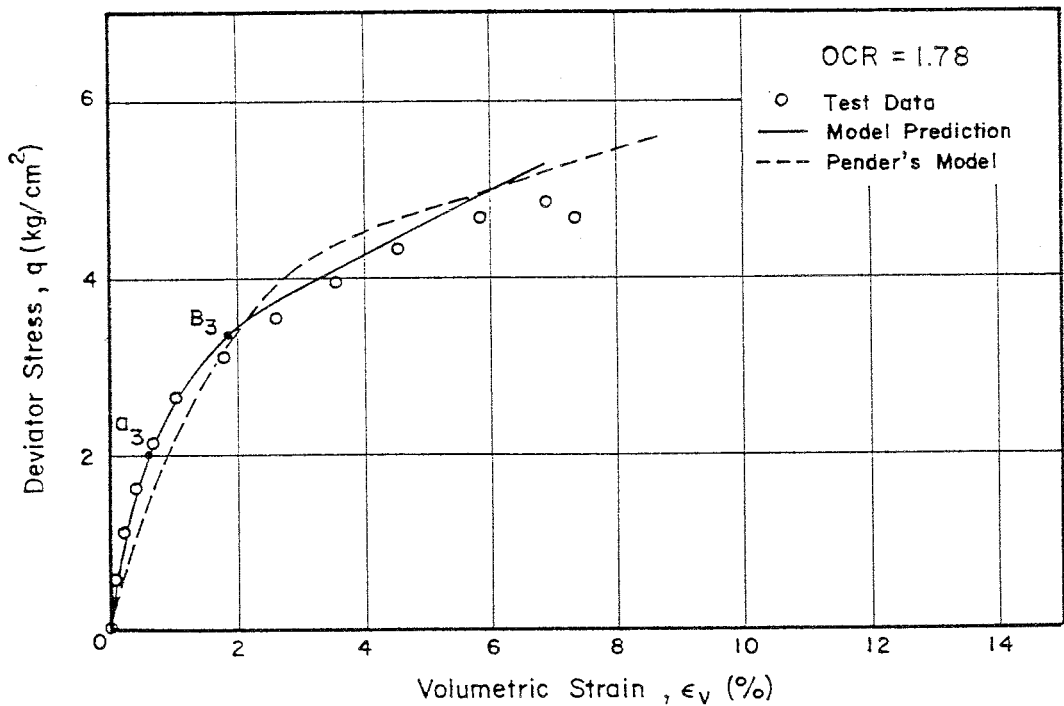


Fig. 8.26b (q, ϵ_v) Plot for CID4 Sample Compared with the Model Predictions

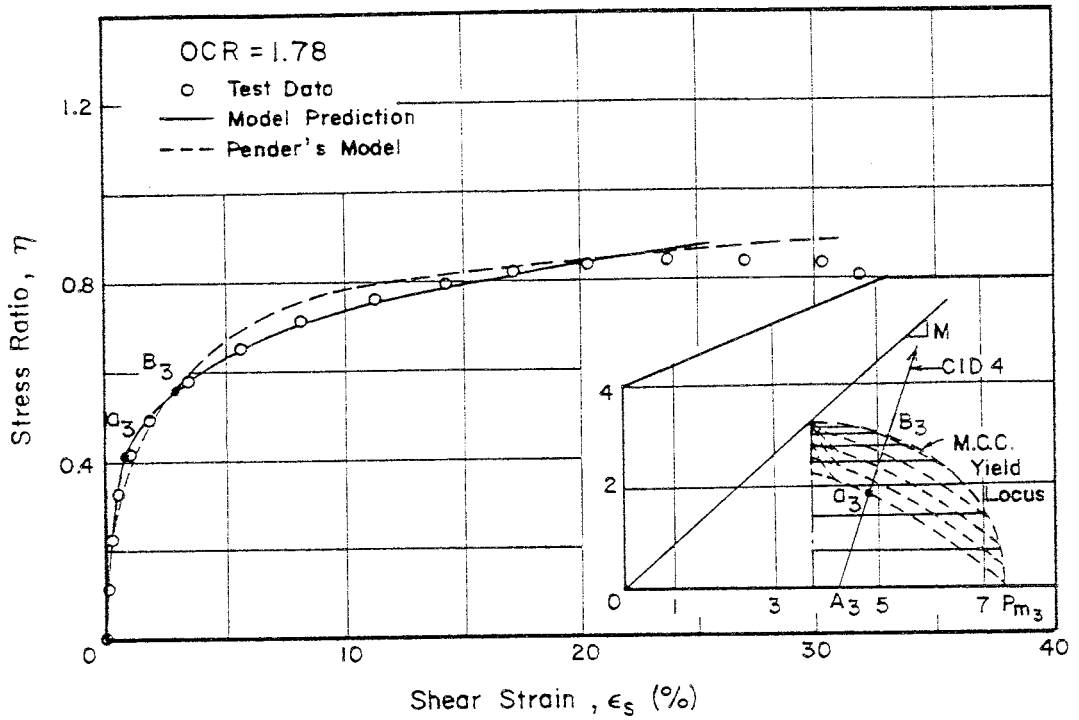


Fig. 8.27a (η , ϵ_s) Plot for CID4 Sample Compared with the Model Predictions

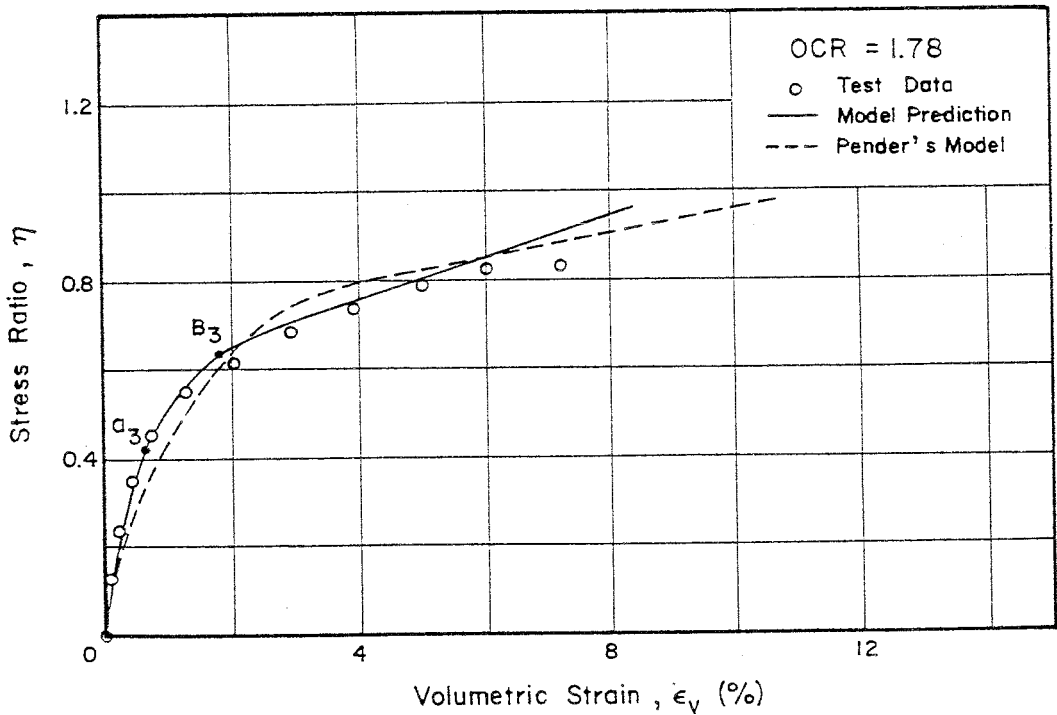


Fig. 8.27b (η , ϵ_v) Plot for CID4 Sample Compared with the Model Predictions

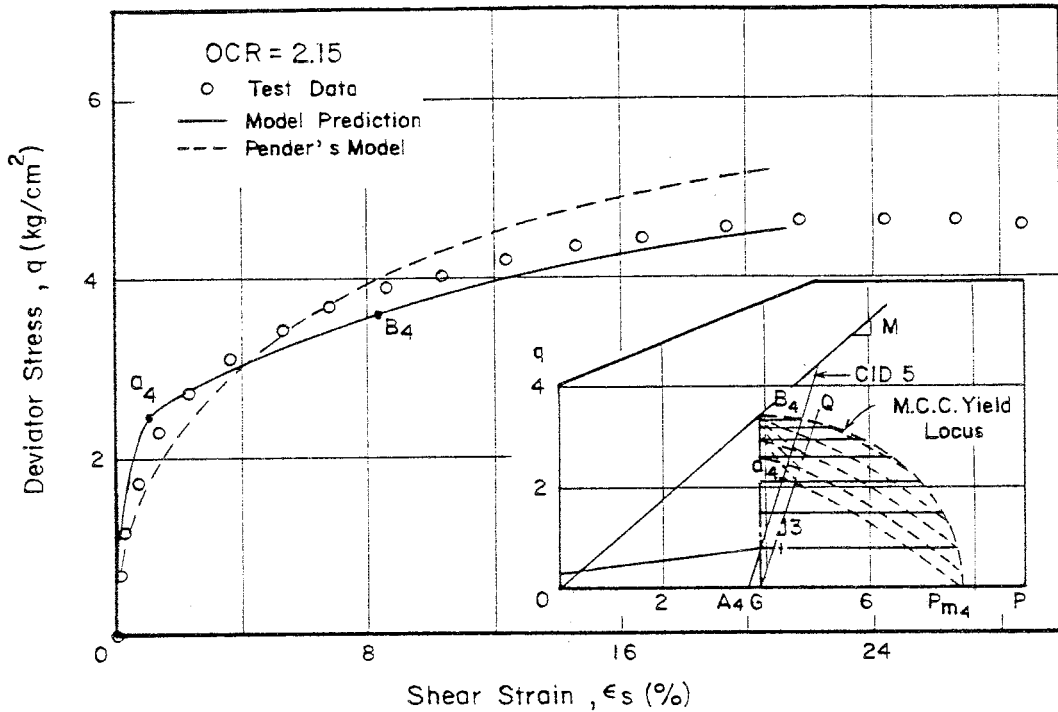


Fig. 8.28a (q, ϵ_s) Plot for CID5 Sample Compared with the Model Predictions

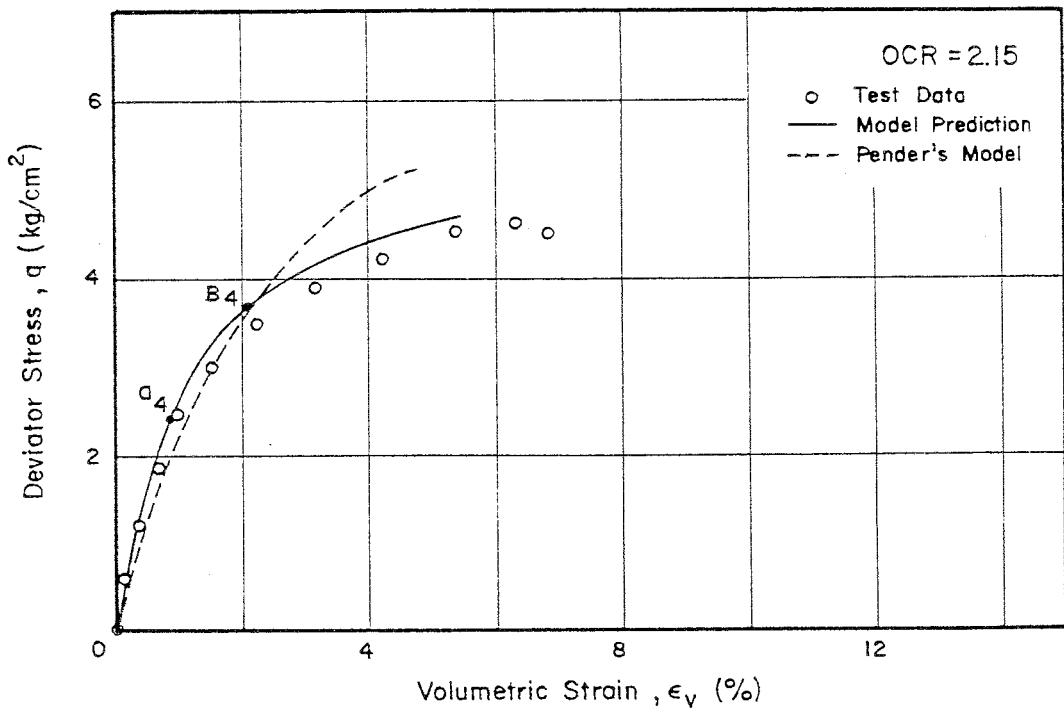


Fig. 8.28b (q, ϵ_v) Plot for CID5 Sample Compared with the Model Predictions

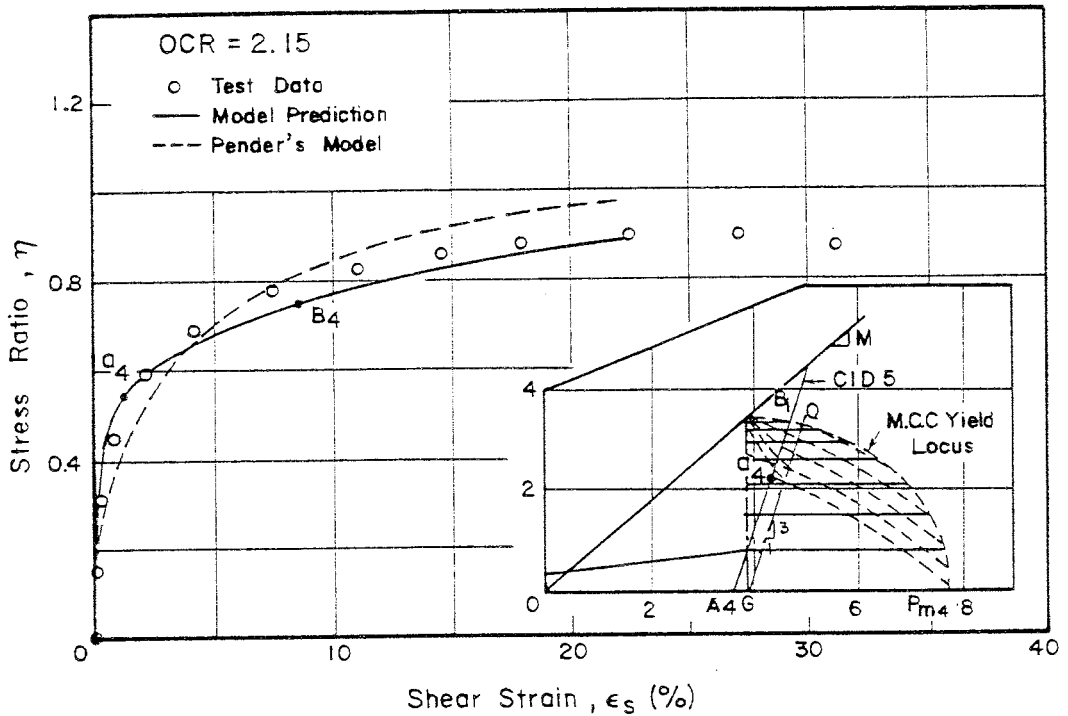


Fig. 8.29a (η , ϵ_s) Plot for CID5 Sample Compared with the Model Predictions

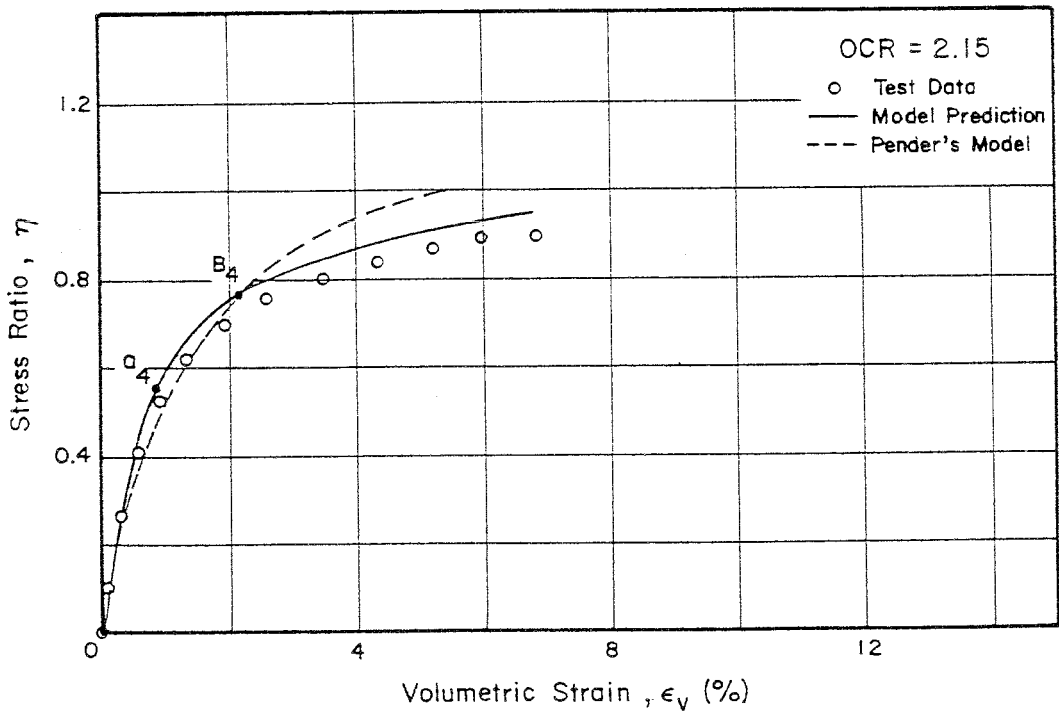


Fig. 8.29b (η , ϵ_v) Plot for CID5 Sample Compared with the Model Predictions

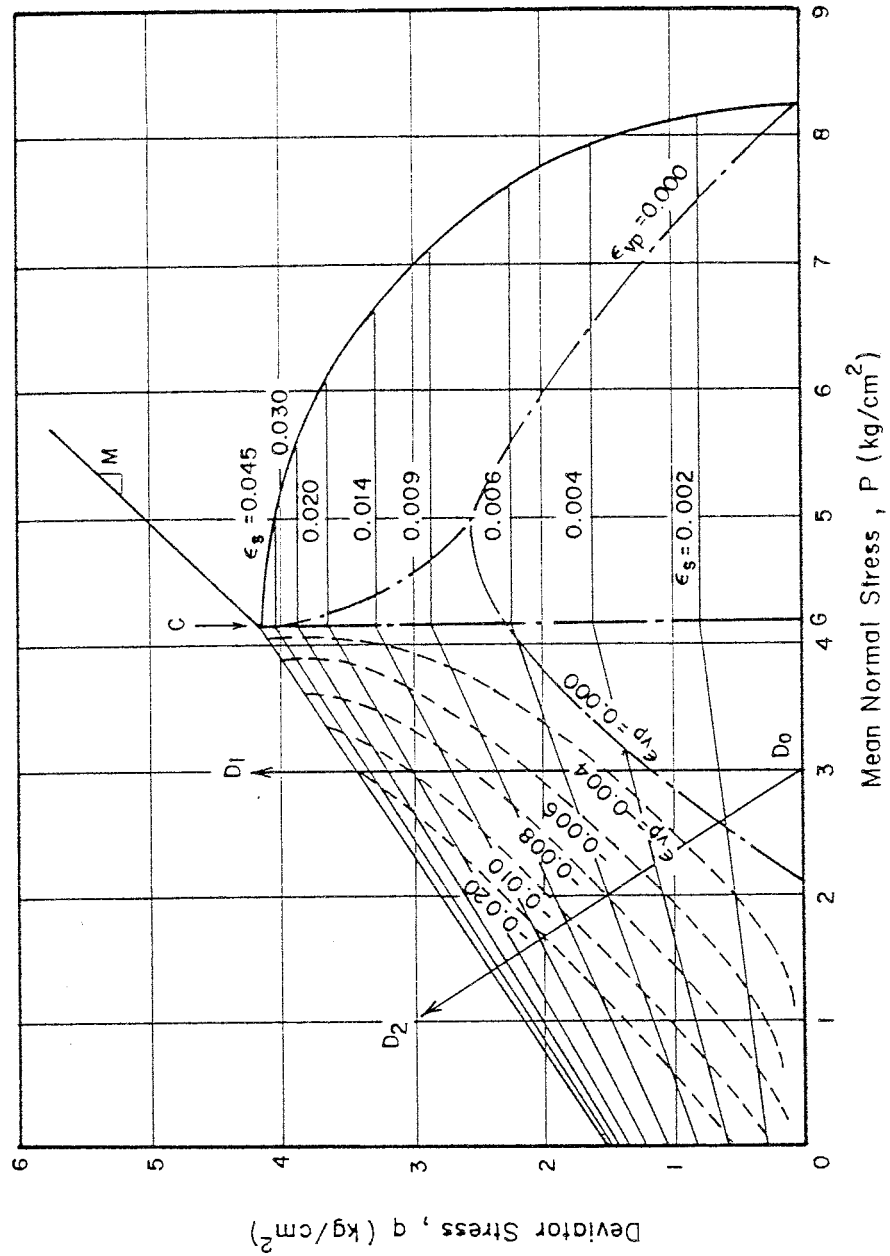


Fig. 8.30 Simplified Strain Contours on the Dry Zone and Typical Stress Paths Sheared from the Isotropic Pre-shear Conditions for the Model Comparisons

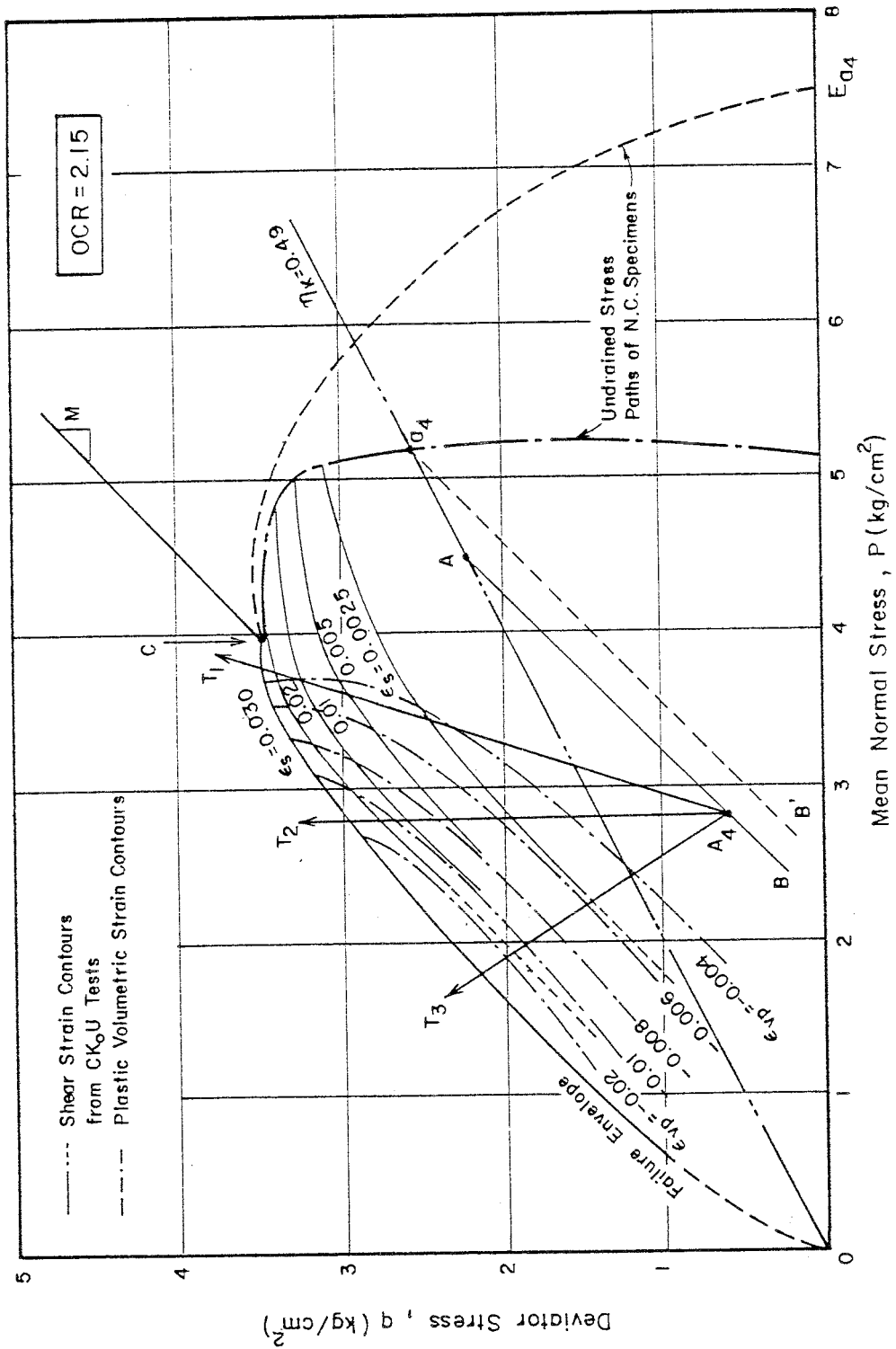


Fig. 8.31 Simplified Strain Contours on the Dry Zone and Typical Stress Paths Sheared from the K_0 Pre-shear Conditions for the Model Comparisons

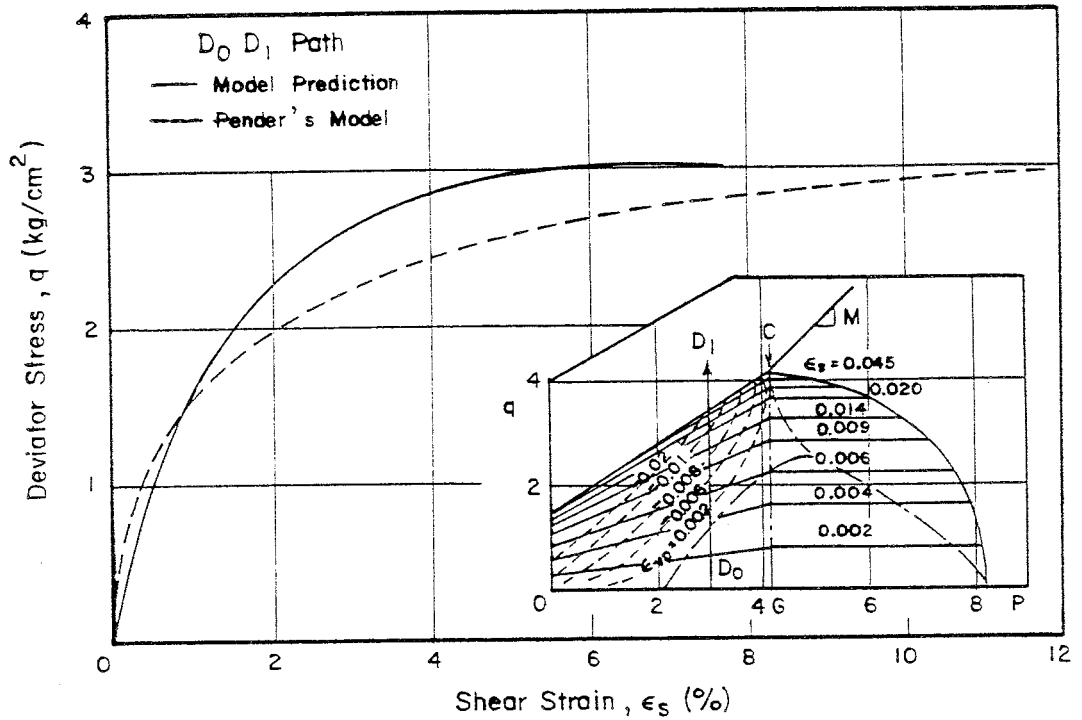


Fig. 8.32a (q, ϵ_s) Plot for the Constant p Compression Test Sheared from Isotropic Pre-shear Condition Compared with the Model Predictions (Dry Zone)

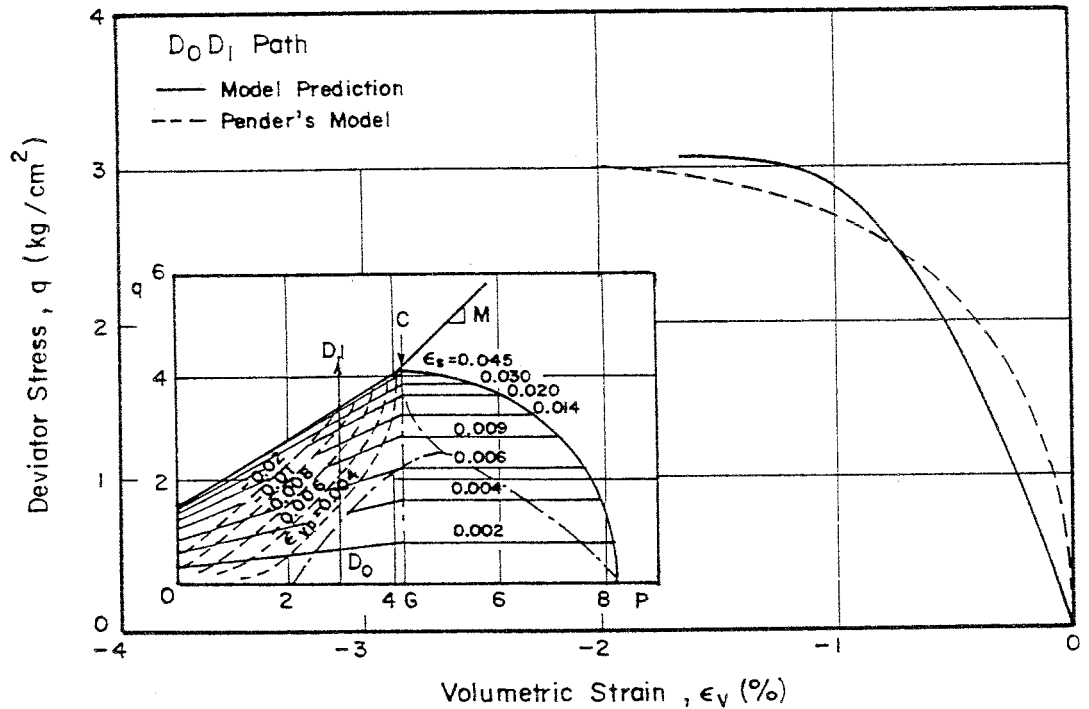


Fig. 8.32b (q, ϵ_v) Plot for the Constant p Compression Test Sheared from Isotropic Pre-shear Condition Compared with the Model Predictions (Dry Zone)

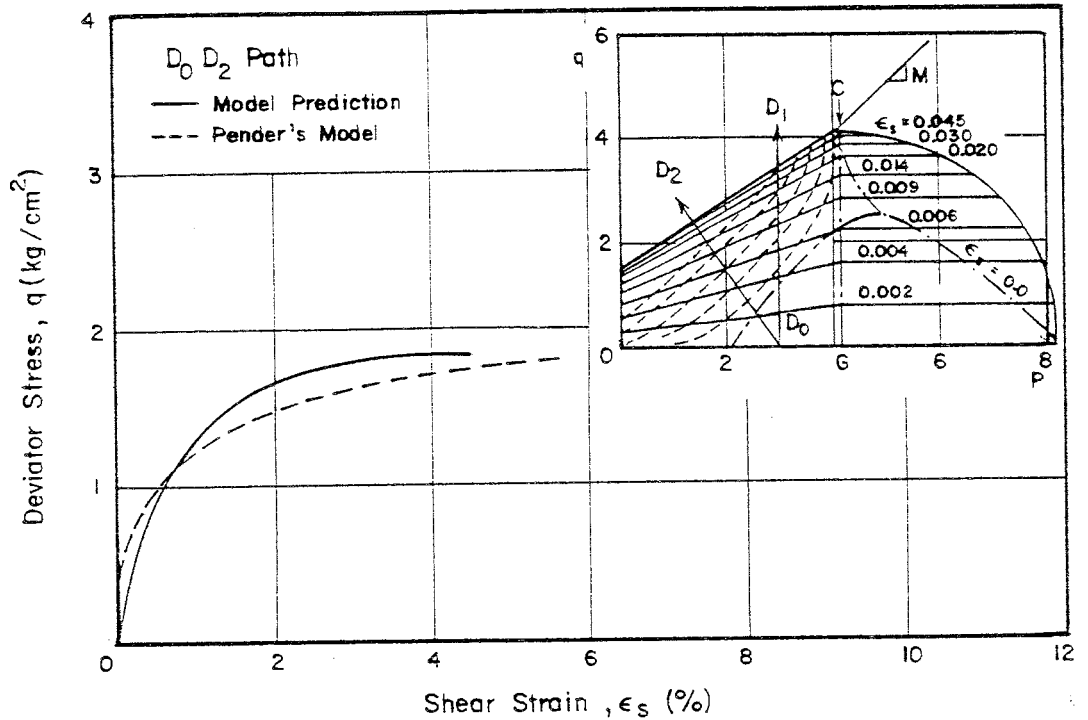


Fig. 8.33a (q , ϵ_s) Plot for the Unloading Compression Test Sheared from Isotropic Pre-shear Condition Compared with the Model Predictions (Dry Zone)

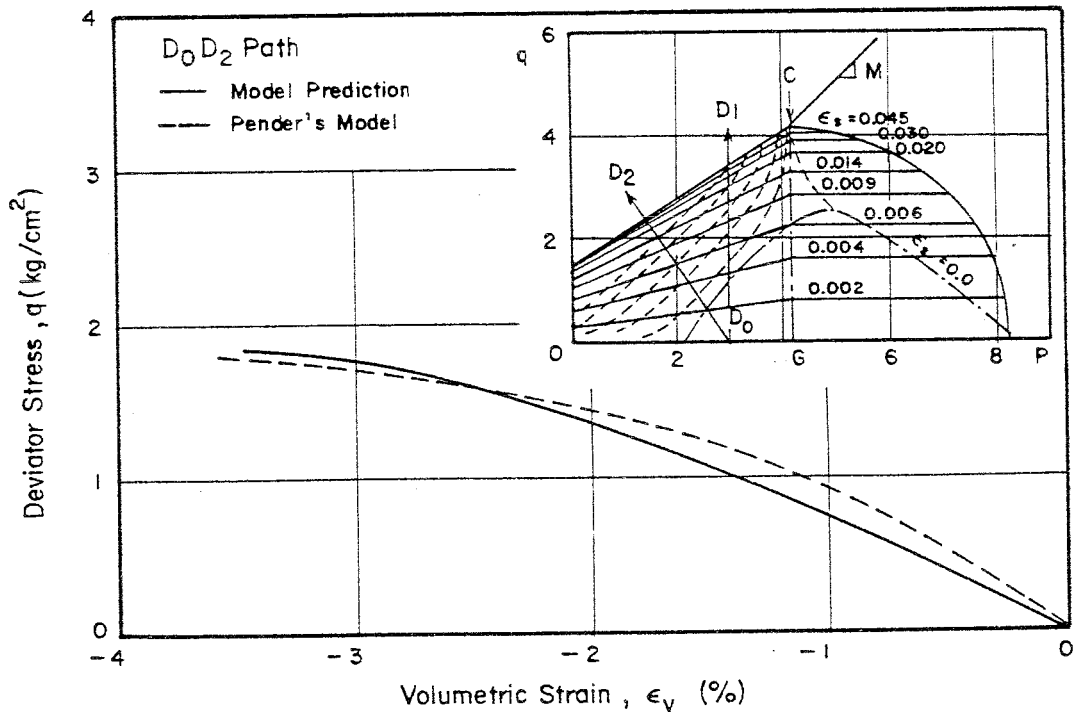


Fig. 8.33b (q , ϵ_v) Plot for the Unloading Compression Test Sheared from Isotropic Pre-shear Condition Compared with the Model Predictions (Dry Zone)

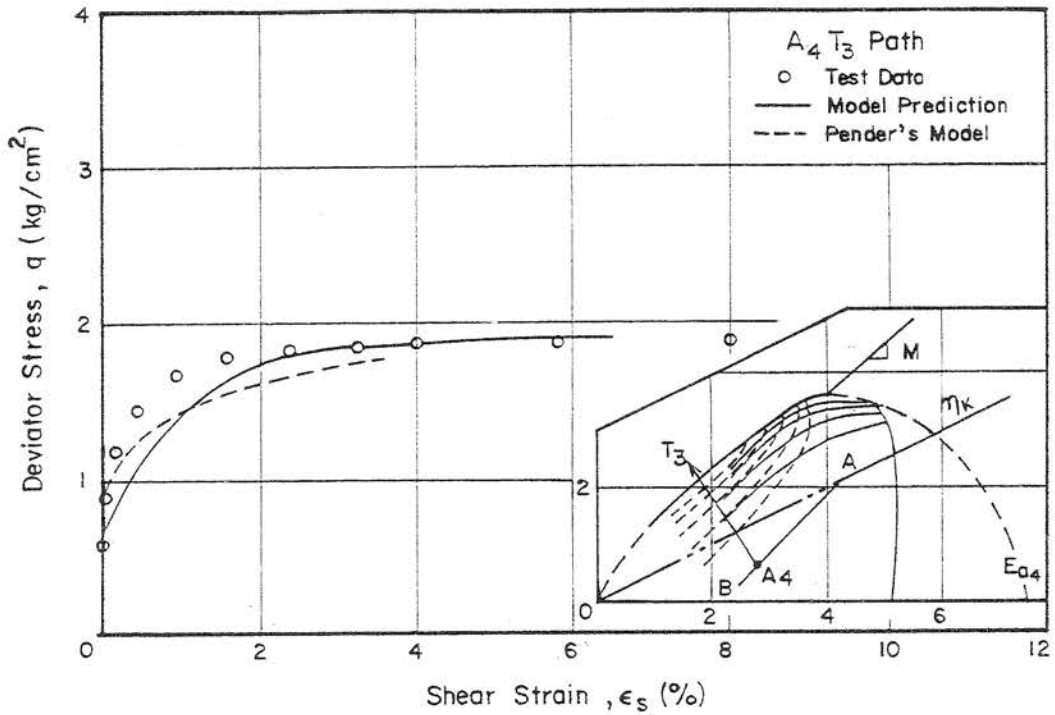


Fig. 8.34a (q, ϵ_s) Plot for the Unloading Compression Test Sheared from K_0 Pre-shear Condition Compared with the Model Predictions (Dry Zone)

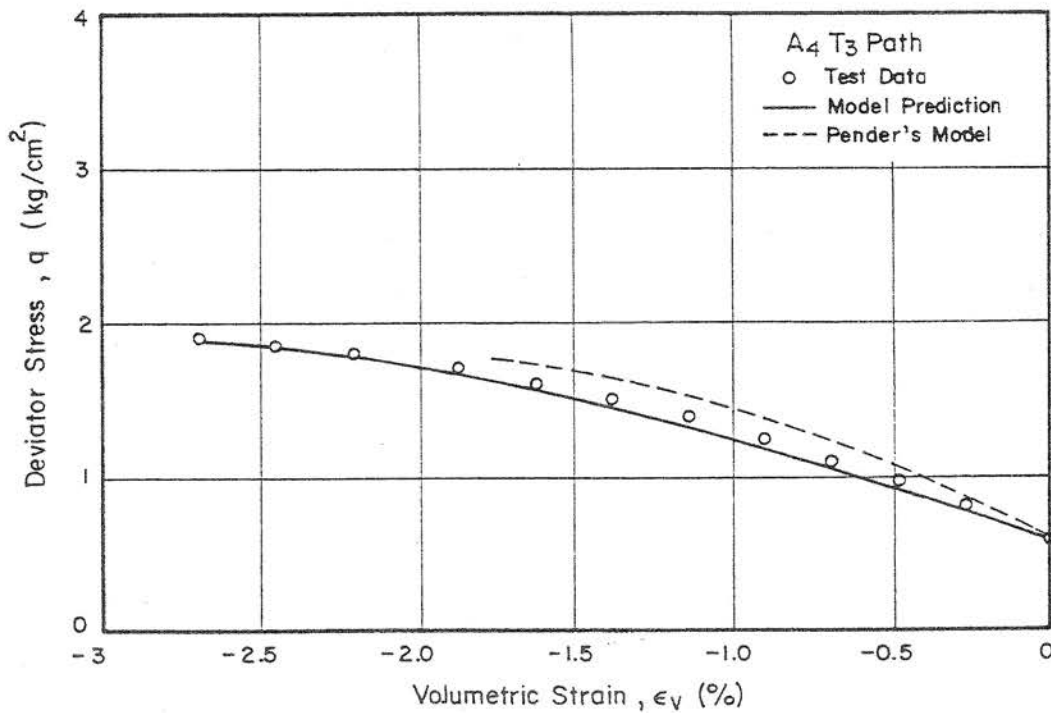


Fig. 8.34b (q, ϵ_v) Plot for the Unloading Compression Test Sheared from K_0 Pre-shear Condition Compared with the Model Predictions (Dry Zone)

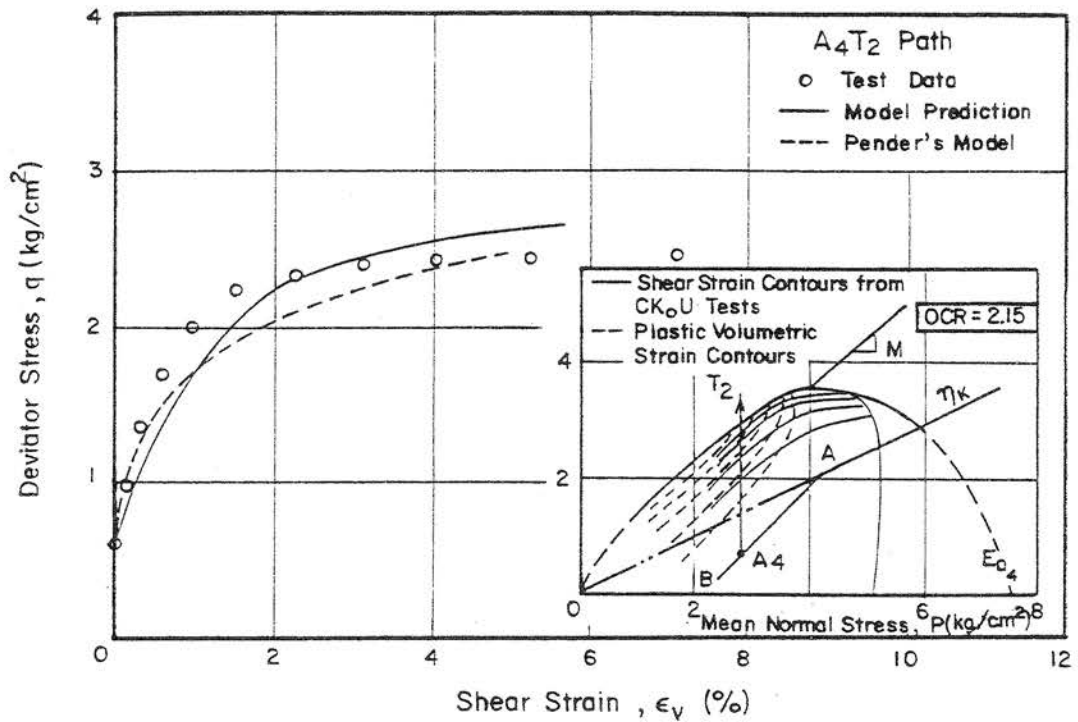


Fig. 8.35a (q, ϵ_v) Plot for the Constant p Compression Test Sheared from K_0 Pre-shear Condition Compared with the Model Predictions (Dry Zone)

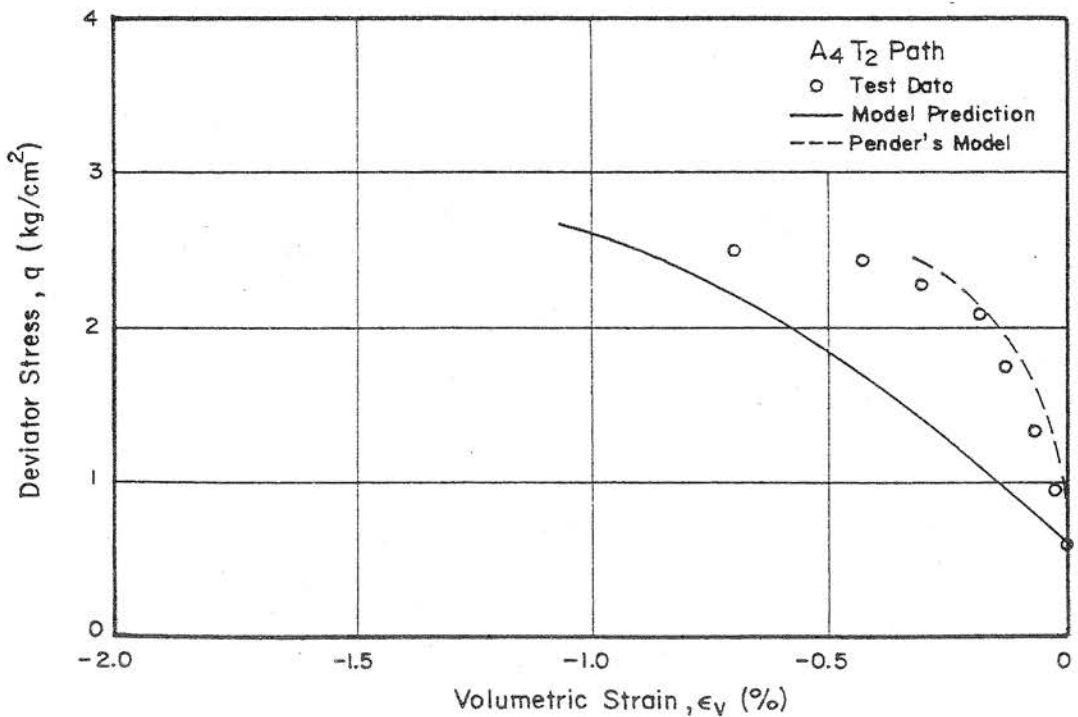


Fig. 8.35b (q, ϵ_v) Plot for the Constant p Compression Test Sheared from K_0 Pre-shear Condition Compared with the Model Predictions (Dry Zone)

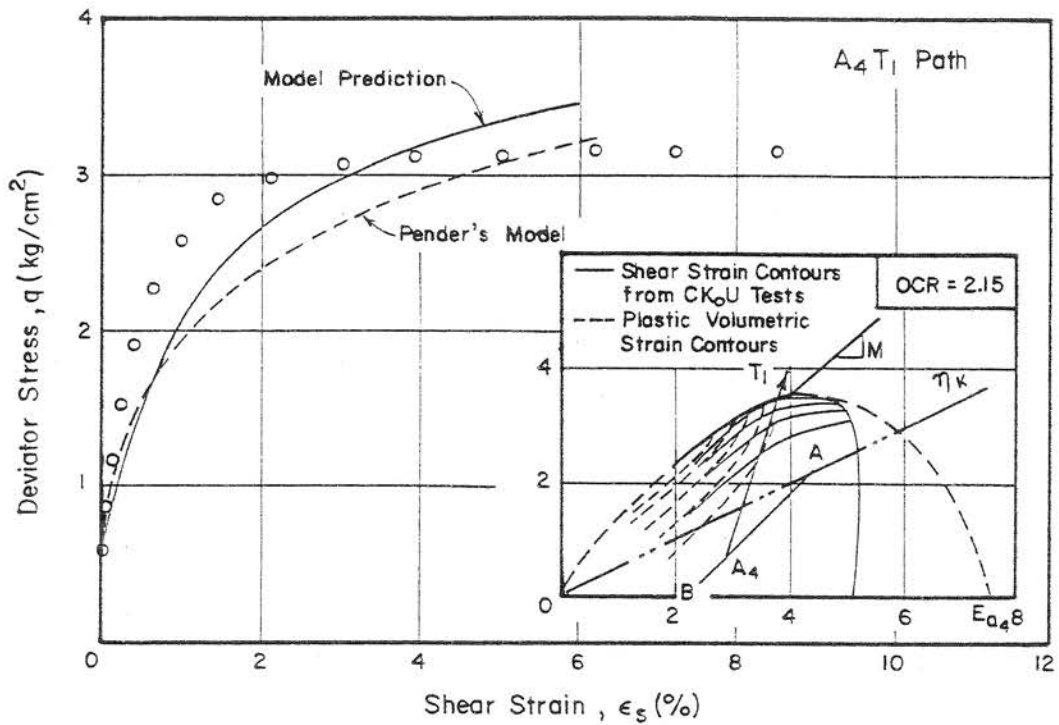


Fig. 8.36a (q, ϵ_s) Plot for the Conventional Compression Test Sheared from K_0 Pre-shear Condition Compared with the Model Predictions (Dry Zone)

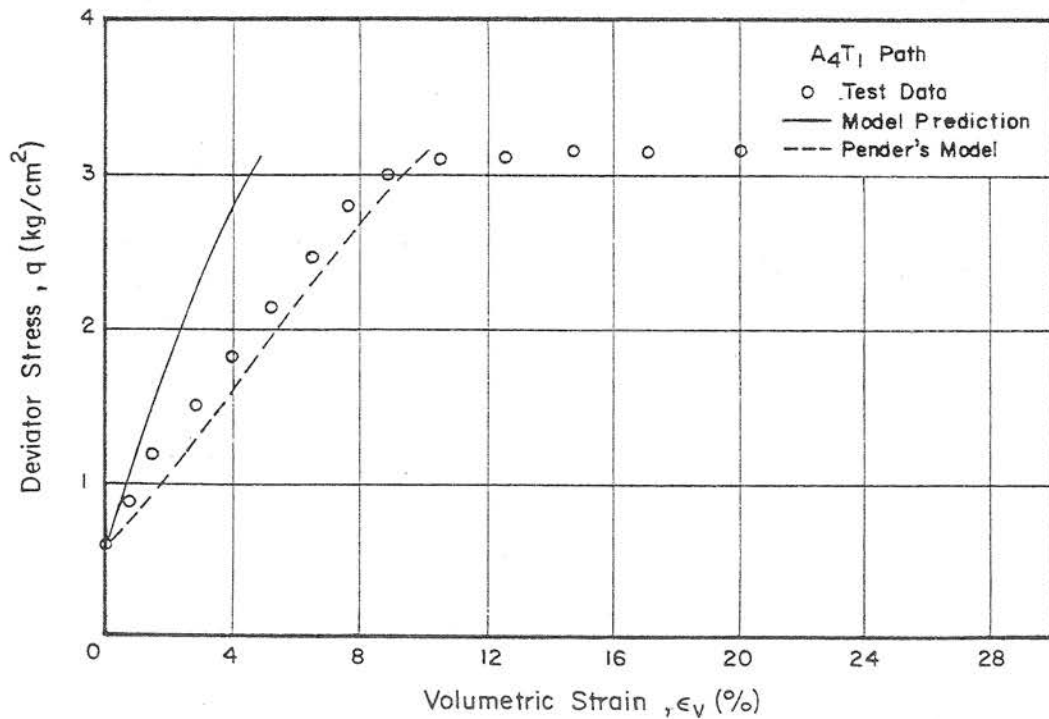


Fig. 8.36b (q, ϵ_v) Plot for the Conventional Compression Test Sheared from K_0 Pre-shear Condition Compared with the Model Predictions (Dry Zone)